Compte rendu de la

HUITIEME RENCONTRE DE MORIOND

Méribel-lès-Allues (France) 4-16 Mars 1973

VOL. II

LE POMERON

J. TRAN THANH VAN

SOUS LE HAUT PATRONNAGE DE

- INSTITUT NATIONAL DE PHYSIQUE NUCLÉAIRE ET DE PHYSIQUE DES PARTICULES
- LABORATOIRE DE L'ACCÉLÉRATEUR LINÉAIRE
- LABORATOIRE DE PHYSIQUE THÉORIQUE ET HAUTES ÉNERGIES
- LABORATOIRE DE PHYSIQUE THÉORIQUE ET PARTICULES ÉLÉMENTAIRES

PUBLICATION SUBVENTIONNÉE PAR LE CNRS

Bibliothèque

C 100/14
M
11
R73

Proceedings of the

EIGTH RENCONTRE DE MORIOND

Méribel-lès-Allues (France) March 4 - 16, 1973

VOL. II

THE POMERON

edited by
J. TRAN THANH VAN

SPONSORED BY

- INSTITUT NATIONAL DE PHYSIQUE NUCLÉAIRE ET DE PHYSIQUE DES PARTICULES
- LABORATOIRE DE L'ACCÉLÉRATEUR LINÉAIRE
- LABORATOIRE DE PHYSIQUE THÉORIQUE ET HAUTES ÉNERGIES
- LABORATOIRE DE PHYSIQUE THÉORIQUE ET PARTICULES ÉLÉMENTAIRES

AND BY THE CNRS FOR PUBLICATION

The second Session of the Eigth Rencontre de Moriond was organised by

J. Trân Thanh Vân

with the active collaboration of

A. Dar
M. Le Bellac
and C. Michael

Permanent Secretariat :
Rencontre de Moriond
Laboratoire de Physique Théorique et Particules Elémentaires
Bâtiment 211 - Université de Paris-Sud
91405 ORSAY (France)

AVANT-PROPOS

La Rencontre de Moriond qui s'est tenue du 4 au 16 mars 1973 à Méribel-les-Allues (Savoie), est la huitième d'une série commencée en 1966.

La première Rencontre a eu lieu à Moriond dans des châlets savoyards où les physiciens, expérimentateurs et théoriciens, partageaient non seulement leurs préoccupations scientifiques, mais aussi les tâches culinaires et les travaux ménagers. Elle regroupait principalement les physiciens français travaillant dans les interactions électromagnétiques. Au cours des Rencontres suivantes venait s'ajouter à la session sur les interactions électromagnétiques une session sur les interactions fortes à hautes énergies.

Le but principal de ces Rencontres est d'une part, de faire le point sur les récents développements de la physique contemporaine, et d'autre part, de promouvoir une collaboration effective entre expérimentateurs et théoriciens dans le domaine des interactions électromagnétiques et des particules élémentaires. Par ailleurs, la durée relativement longue de la Rencontre et le faible nombre des participants doivent permettre à la fois une meilleure connaissance humaine entre les participants et une discussion approfondie et détaillée des communications présentées.

Ce souci de recherche et d'expérimentation de nouvelles formes de communication, de nouveaux terrains d'échange et de dialogues, qui depuis l'origine anime les Rencontres de Moriond, nous a amenés, il y a trois ans, à susciter la création pour les biologistes de la première Rencontre de Méribel sur la Différenciation Cellulaire qui se tient en même temps et dans les mêmes locaux

que la première session de la Rencontre de Moriond. Des séminaires communs ont été organisés afin d'étudier dans quelle mesure les méthodes d'analyse utilisées en physique pouvaient être appliquées à certains problèmes qui se posent en biologie. Comme l'an passé, le film en couleurs "Le Code Génétique" réalisé et commenté par M. le Professeur Tavlitzki, a enthousiasmé les participants. Pour la première fois, un physicien s'est adressé aux biologistes : P. Sonderegger a projeté un film sur les particules élémentaires et a fait une introduction sur les lois de symétrie dans la physique des hautes énergies. Ces deux conférences ont suscité de nombreuses discussions "informelles", animées et enrichissantes entre biologistes et physiciens. Ces échanges font espérer qu'un jour peut-être, les problèmes, pour le moment si complexes, posés en biologie, donneront naissance à de nouvelles méthodes d'analyse ou à de nouveaux langages mathématiques.

La première session de la huitième Rencontre de Moriond (4-10 mars 1973) est consacrée aux interactions électromagnétiques et faibles. Une partie importante des débats porte sur le modèle des partons et les théories unitaires de Jauge.

La deuxième session (10 au 16 mars 1973) est consacrée au Pomeron et aux phénomènes asymptotiques ainsi qu'aux réactions inclusives.

M. Gourdin a accepté la tâche lourde et ingrate de coordonner le programme de la première session.

Pour la seconde session, A. Dar, M. Le Bellac et C. Michael ont participé à l'élaboration du programme et à l'organisation de la Rencontre.

Mesdames J. Jude et D. Schiff pour les Comptes-Rendus , Mesdemoiselles M.P. Cotten, Ev. Hanquart et N. Ribet pour l'orga-

nisation générale, ont dépensé beaucoup de temps et d'efforts pour la réussite de cette Rencontre.

M. et Mme Raiberti, qui nous ont accueillis si aimablement dans leur hôtel, ont su grâce à leur extrême gentillesse et leur active coopération rendre aisé le règlement de tout problème matériel et permettre aux biologistes et aux physiciens de travailler dans une atmosphère de détente et de bien-être.

Au nom de tous les participants, je les remercie de tout coeur.

J. Tran Thanh Van

FOREWORD

The Rencontre de Moriond held at Meribel les Allues (France) from March 4 to 16, 1973, was the eighth such meeting.

The first one was held in 1966 at Moriond in the French Alps. There, physicists - experimentalists as well as theoreticians - not only shared their scientific preoccupations but also the household chores. That meeting grouped essentially French physicists interested in electromagnetic interactions. At following meetings a session on high energy strong interactions was added to the electromagnetic one.

The main purpose of these meetings is to discuss recent developments of contemporary physics and to promote effective collaboration between experimentalists and theoreticians in the field of electromagnetic interactions and elementary particles. Besides, the length of the meeting coupled with the small number of participants favours better human relations as well as a more thorough and detailed discussion of the contributions.

This concern for research and experimentation of new channels of communication and dialogue which from the start animated the Moriond meetings, incited us, three years ago, to organize a simultaneous meeting of biologists on Cellular Differentiation at Meribel les Allues. Common seminars were organized to study to what extent analytical methods used in physics could be applied to some biological problems. Two beautiful color films were presented : "The Genetic Code" produced and commented by Professor Tavlitzki (Institute of Molecular Biology) and another one devoted to elementary particle

physics. P. Sonderegger (CERN) gave an introduction on symmetry laws in high energy physics. Both seminars gave rise to spirited and enriching discussions between biologists and physicists. They led us to hope that biological problems, at present so complex, may give birth in the future to new analytical methods or new mathematical languages.

The first session of the 1973 Rencontre de Moriond (March 4-10) was devoted to electromagnetic and weak interaction phenomenology and to discussions with the biologists. An important part of the program dealt with the parton model and the unified theories.

The Pomeron and related phenomena as well as multiparticle production were extensively studied in the second session (March 10 -16).

M. Gourdin accepted the heavy and ungrateful task of coordinating the program of the first session.

A. Dar, M. Le Bellac and C. Michael looked after the coordination of the different talks and the organization of the second session.

Mrs. J. Jude and D. Schiff, for the Proceedings, Misses M.P. Cotten, E. Hanquart and N. Ribet, for the general organization, all devoted much of their time and energy to the success of this meeting.

Mr. and Mrs. Raiberti, the hotel keepers, who so kindly looked after us, contributed through their hospitality and their active cooperation to the wellfare of the biologists and the physicists, enabling them to work in a relaxed atmosphere.

On behalf of the participants I thank them all heartily.

J. Tran Thanh Van





Secretariat :

COTTEN Marie-Paule, Laboratoire de l'Accélérateur Linéaire, Bâtiment 200, Université de Paris-Sud, 91405 ORSAY (France).

HANQUART Evelyne, Laboratoire de Physique Théorique et Hautes Energies, Bâtiment 211, Université de Paris-Sud, 91405 ORSAY (France).

RIBET Nicole, Laboratoire de Physique Théorique et Hautes Energies, Université de Paris-VI, Tour 16 4, Place Jussieu, 75230 PARIS CEDEX 05 (France).

PARTICIPANTS

Second Session

AMATI Danielo, Division TH. C.E.R.N., 1211 GENEVE 23 (Suisse)

BAGLIN Christian, Laboratoire de Physique Nucléaire des Hautes Energies, Ecole Polytechnique, 17 rue Descartes, 75230 - PARIS CEDEX 05 (France)

BAKER Marshall, Physics Dept., University of Washington, SEATTLE WA 98105 (U.S.A.)

BARLOUTAUD Roland, D. Ph. P.E., C.E.N. SACLAY, B.P. 2, 91190 GIF-sur-YVETTE (France)

BELLETTINI Giorgio, Istituto di Fisica, Università di Pisa, Piazza Torricelli 2, PISA (Italy)

BERGER Edmond, Division Th. CERN, 1211 GENEVE 23 (Suisse) and Argonne National Laboratory, 9700 South Cass Avenue, ARGONNE IL 60439 (U.S.A.)

BYERS Nina, Department of Theoretical Physics, Oxford University, 12 Parks Road, OXFORD OX1 3PQ (England)

CANESCHI Luca, Theoretical Study Division, CERN, 1211 GENEVE 23 (Suisse)

CARRIGAN Jr. Richard, National Accelerator Laboratory, P.O. Box 500, BATAVIA, IL 60510 (U.S.A.)

COIGNET Guy, Institut de Physique Nucléaire, Bâtiment 100, Université de Paris-Sud, 91405 ORSAY (France)

CONFORTO Gianni, Rutherford High Energy Laboratory, CHILTON, DIDCOT Berks. (England) and I.N.F.N. ROMA (Italy)

COON Darryl D., University of Pittsburgh, Department of Physics, PITTSBURGH PA 15213 (U.S.A.)

CORDIER Alain, Laboratoire de l'Accélérateur Linéaire, Bâtiment 200, Université de Paris-Sud, 91405 ORSAY (France)

COUSINOU Marie-Claude, Laboratoire de Physique Nucléaire des Hautes Energies, Tour 32, Université de Paris VI, 4 place Jussieu 75230 PARIS CEDEX 05 (France)

DAR Arnon, M.I.T. Physics 6-406, CAMBRIDGE, MA 02139 (U.S.A.) and Physics Department, Technion Israel Institute of Technology, HAIFA (Israel)

DAVIS Philip J., Laboratoire de l'Accélérateur Linéaire, Bâtiment 200, Université de Paris-Sud, 91405 ORSAY (France)

DIAS DE DEUS Jorge, Niels Bohr Institute and Nordita Blegdamsvej 17, 2100 COPENHAGEN Ø (Denmark)

DONOHUE John T., Laboratoire de Physique Théorique, Domaine du Haut Vigneau, 33170 GRADIGNAN (France)

FRIED Herbert M., Physics Department, Brown University, PROVIDENCE RHODE ISLAND 02912 (U.S.A.)

GLAUBER Roy J., Theoretical Study Division, CERN, 1211 GENEVE 23 and Harvard University, CAMBRIDGE, MA 02138 (U.S.A.)

GOLDBERG Marcel, Laboratoire de Physique Nucléaire des Hautes Energies, Tour 32, Université de Paris VI, 4 place Jussieu, 75230 PARIS CEDEX 05 (France)

GRANDPEIX Jean-Yves, Laboratoire de l'Accélérateur Linéaire, Bâtiment 200, Université de Paris-Sud, 91405 ORSAY (France)

GRISS Martin, Lauritsen Lab. of High Energy Physics, California Institute of Technology, PASADENA, CA 91109 (U.S.A.)

HALZEN Francis, Department of Physics, University of Wisconsin, MADISON WI 53706 (U.S.A.)

HENYEY Frank. S., Randall Laboratory of Physics, University of Michigan, ANN ARBOR MI 48104 (U.S.A.)

IENGO Roberto, Laboratoire de Physique Théorique et Hautes Energies, Bâtiment 211, Université de Paris-Sud, 91405 ORSAY (France)

JABIOL Marie-Antoinette, D. Ph. P.E., CEN-SACLAY, B.P. 2, 91190 GIF-sur-YVETTE (France)

KANG Kyungsik, Laboratoire de Physique Théorique et Hautes Energies, Université de Paris VI, Tour 16, 1er étage, 4 place Jussieu, 75230 PARIS CEDEX 05 and Brown University, PROVIDENCE, RI 02912 (U.S.A.)

KRISCH Alan D. Randall Laboratory of Physics, University of Michigan, ANN ARBOR, MI 48104 (U.S.A.)

KUTI Julius, Department of Atomic Physics, Roland Eötvös University, Puskin utca 5-7, BUDAPEST VIII (Hungary)

LE BELLAC Michel, Laboratoire de Physique Théorique, Université de Nice, Parc Valrose, 06034 NICE CEDEX (France)

LEITH David W.G.S., Stanford Linear Accelerator Center, P.O. Box 4349, STANFORD CA 94305 (U.S.A.)

LEROYER Yves, Laboratoire de Physique Théorique, Domaine du Haut Vigneau, 33170 GRADIGNAN (France)

LOW Francis E., M.I.T. Physics 6-406, CAMBRIDGE, MA 02139 (U.S.A.)

LUBATTI Henry J., Visual Techniques Laboratory, Physics, University of Washington, SEATTLE WA 98105 (U.S.A.)

MARTIN Alan, Theoretical Study Division, CERN, 1211-GENEVE 23 (Suisse)

MARTIN André, CERN, Division Th. 1211 GENEVE 23 (Suisse)

MEUNIER Jean-Louis, Laboratoire de Physique Théorique, Université de Nice, Parc Valrose, 06034 NICE CEDEX (France)

MICHAEL Christopher, CERN, Division Th. 1211 GENEVE 23 (Suisse)

MIETTINEN Hannu Ilmari, Rutherford Laboratory, CHILTON, DIDCOT, Berks. (England) and University of Helsinki, Siltavuorenpenger 20 b, HELSINKI 17 (Finland)

MIHUL Alexandru Mihai, J.I.N.R. (DUBNA) Head P.O. Box 79, Moscow, (U.R.S.S.)

MIHUL Mme, J.I.N.R. (DUBNA) Head P.O. Box 79, Moscow (U.R.S.S.)

NUYTS Jean, Université de Mons, Département de Physique Théorique, 19 avenue Maistriau, 7000 MONS (Belgique)

PAJARES Carlos, Laboratoire de Physique Théorique et Particules Elémentaires, Université de Paris-Sud, Bâtiment 211, 91405 ORSAY (France)

PATRASCIOIU Adrian, Laboratory for Nuclear Science, M.I.T. Physics 6-406, CAMBRIDGE MA 02139 (U.S.A.)

PETERSSON Bengt, Laboratoire de Physique Théorique et Particules Elémentaires, Université de Paris-Sud, Bâtiment 211, 91405 ORSAY (France)

PHAM Xuan Yem, Laboratoire de Physique Théorique et Hautes Energies, Tour 16, 1er étage, Université de Paris VI, 4 Place Jussieu 75230 PARIS CEDEX 05 (France)

PHILLIPS Roger J.N., Rutherford High Energy Laboratory, CHILTON, DIDCOT, Berks. (England)

PIRILA Pekka, CERN, Division Th. 1211 GENEVE 23 (Suisse)

PRENTICE Jim D. Phys. Dep. University of Toronto, TORONTO M5 S, 1A7 (Canada)

RIMPAULT Marcel, Laboratoire de Physique Théorique, Domaine du Haut Vigneau, 33170 GRADIGNAN (France)

ROY D.P. , Rutherford High Energy Laboratory, CHILTON, DIDCOT Berks. (England)

RUUSKANEN Vesa, Department of Physics, University of Jyväskylä, Nisulankatu 78, 40720 JYVASKYLA (Finland)

SALIN Philippe, Laboratoire de Physique Théorique, Domaine du Haut Vigneau, 33170 GRADIGNAN (France)

SCHIFF Dominique, Laboratoire de Physique Théorique et Particules Elémentaires, Université de Paris-Sud, Bâtiment 211, 91405 ORSAY (France)

STROLIN P. CERN, 1211 GENEVE 23 (Suisse)

STROINOWSKI Ryszard, CERN 1211 GENEVE 23 (Suisse)

TAN Chung-I, Physics Department, Brown University, PROVIDENCE, RI 02912 (U.S.A.)

TRAN THANH VAN Jean, Laboratoire de Physique Théorique et Particules Elémentaires, Bâtiment 211, Université de Paris-Sud, 91405 ORSAY (France)

WALKER James K., National Accelerator Laboratory, P.O. Box 500, BATAVIA, IL 60510 (U.S.A.)

WANG Jiunn-Ming, Institute of Theoretical Physics, State University of New York, STONY BROOK, NY 11790 (U.S.A.)

WHITE A.R., CERN, Division Th. , 1211 GENEVE 23 (Suisse)

YOKOSAWA Akihiko, Argonne National Laboratory, ARGONNE IL 60439 (U.S.A.)

















C O N T E N T S

Second Session

J. TRAN THANH VAN	"Introduction"	25
G. BELLETTINI	" Total proton-proton cross-section at the ISR"	35
P. STROLIN	"Proton-proton elastic scattering at ISR energies"	65
R.A. CARRIGAN Jr.	"Small angle proton scattering at NAL and an emerging picture of high energy processes"	79
A. MARTIN	"High Energy theorems for particle-particle and particle-antiparticle scattering and ISR data"	91
F. LOW	"Dynamics of strong interactions"	103
A.R. WHITE	"The importance of the structure of the Pomeron"	105
M. BAKER	"Reggeon theory of diffraction scattering"	125
A.D. KRISCH	"Lorentz contracted geometrical model"	157
J.K. WALKER	"The impact picture for strong interactions"	159
H.I. MIETTINEN	"Shadow approach to diffraction scattering"	193
J. TRAN THANH VAN	"Exploratory dip systematics in elastic scattering"	235
C. BAGLIN	"Elastic scattering of π^+ and K^+ mesons on protons at 10 GeV"	247
D.D. COON	"Phenomenology of proton-proton scattering at all angles"	267
H.M. FRIED	"Hadronic scattering at small and large momentum transfers"	281
F. HALZEN	"Tracing partons in hadron collisions at high transverse momentum"	289

D.W.G.S. LEITH	"Diffraction phenomena : review of the experimental situation" 319
R. BARLOUTAUD	"$Q^{\pm}$ production in $K^{\pm}p$ interactions at 14 GeV/c" 383
G. CONFORTO	"A_2 production in $\pi^- p$ collisions and Pomeron exchange"..... 401
H.J. LUBATTI	"A new model of diffractive dissociation". 411
C. MICHAEL	"Isoscalar exchange in vector meson production" 433
A. YOKOSAWA	"Review on scattering-amplitude analysis". 435
A.D. MARTIN	"Some properties of absorptive corrections" 451
F.S. HENYEY	"Impact parameter description of multiparticle and elastic scattering, with an application to the multiperipheral model". 463
K. KANG	"On the two-reggeon cut problems"..... 491
D.P. ROY	"Duality in reggeon-particle scattering".. 499
P.V. RUUSKANEN	"A nova model for diffraction dissociation with longitudinally decaying novas"..... 515
J. DIAS DE DEUS	"A model of the breaking of Hagedorn Theory and scaling at high transverse momentum".. 535
A.L.M. MIHUL	"Average quantum numbers per particle. What are they good for ?"..... 551
B. PETERSSON	"Pair production and quantum number exchange in multiparticle production"..... 553
CHUNG-I TAN	"Clusterings in hadronic production and Markovian walk"..... 563
J.M. WANG	"Production in the central region"..... 579
R. STROYNOWSKI	"A comparison of medium energy data with ISR results"..... 583
D.W.G.S. LEITH	"Conclusions for the VIIIe Moriond on the Pomeron"..... 607

INTRODUCTION

Ce n'est pas sans une inquiétude certaine que j'ai pris la décision, en mai 1972, suivant une suggestion de David Leith, de consacrer la seconde session de la huitième Rencontre de Moriond à l'étude du Pomeron, car la seule certitude que j'avais est que la nature du Pomeron (ou de l'échange du vide) est très peu connue. En effet, si dans la physique des hautes énergies, les contributions dans la voie t des pôles de Regge auxquels sont associées des résonances expérimentalement observées sont reliées, grâce à la dualité, à celles des résonances dans la voie s, les contributions du Pomeron dans la voie t ne sont pas reliées à quelque chose de bien défini dans la voie s. D'autre part, le Pomeron est-il un pôle donc factorisable ou une coupure et dans ce dernier cas, quelles sont ses principales propriétés ? Ce sentiment d'inquiétude était cependant mêlé à des espoirs sérieux car de nouvelles données expérimentales étaient attendues des anneaux de collision proton-proton (ISR), du CERN et du super accélérateur de Batavia, et j'espérais que dans la perspective des prochaines données excitantes, les théoriciens se mettraient au travail pour clarifier la nature du Pomeron.

Sur le plan expérimental comme sur le plan théorique, nos espoirs ont été comblés et ce colloque sur "le Pomeron" qui regroupe les principaux spécialistes de la question s'est révélé, grâce à tous les participants, extrêmement enrichissant et prometteur pour l'avenir.

Sur le plan expérimental, des résultats très intéressants obtenus grâce aux anneaux de collision du CERN (ISR) sur les sections efficaces totales proton-proton ont été présentés par G. Bellettini pour la collaboration Pisa-Stony Brook, et P. Strolin pour celle de CERN - Roma. Par des méthodes différentes, ils ont obtenu heureusement le même résultat : les sections efficaces totales croissent, et probablement comme une puissance du logarithme de l'énergie, alors qu'aux plus hautes énergies des accélérateurs conventionnels elles semblaient rester constantes. La pente du pic de diffraction a été étudiée en détail aux énergies de NAL ($p_L \simeq 200$ GeV) par R. Carrigan et aux énergies du ISR par Strolin. Si l'on associe le pic de diffraction à l'échange de la trajectoire du Pomeron $\alpha(t) = 1 + \alpha' t$, la pente α' qui est de 0.5 jusqu'à 200 GeV diminue à 0.2 aux énergies du ISR. A plus grand transfert, des minima très prononcés apparaissent dans les sections efficaces différentielles proton-proton (P. Strolin). Remarquons qu'à plus basse énergie, on observe aussi des minima dans les sections efficaces différentielles pion-nucleon ou anti-proton-proton (C. Baglin).

Des données sur la production diffractive de $\varrho^{\pm}$ confirment la présence du point de cross-over dans les sections efficaces différentielles des réactions inélastiques (R. Barloutaud) et celles sur la production de A_2 dans les collisions pion nucléon remettent en cause la présence d'une contribution du Pomeron à cette réaction (G. Conforto). Un exposé de revue de D. Leith sur la dissociation diffractive a permis de faire ressortir ses principales propriétés :

a) sections efficaces indépendantes (ou presque) de l'énergie.

b) égalité entre les sections efficaces de production de

particules et d'antiparticules

c) existence d'un pic vers l'avant dans la section efficace différentielle

d) conservation de l'hélicité dans la voie s (?).

Sur le plan théorique, c'est autour du Pomeron, ses couplages, ses singularités et son comportement asymptotique que les discussions ont été les plus acharnées. Se plaçant dans la perspective des sections efficaces totales croissantes, A. Martin a analysé les théorèmes asymptotiques et les conséquences physiques pour les sections efficaces élastiques et le rapport des parties réelles et imaginaires de l'amplitude vers l'avant. F. Low a résumé les différentes tentatives pour bâtir une théorie des interactions fortes comme les modèles duaux ou les modèles multipériphériques. La situtation confuse du signe de la coupure à deux Pomerons ainsi que celle de l'annulation du couplage à trois Pomerons et du couplage Pomeron Reggeon Reggeon à $t = 0$ a été clarifiée par un exposé de A. White qui a présenté une analyse de ces questions à la fois du point de vue de la voie t et de la voie s. Dans ce dernier cas, il a montré l'importance de la structure du Pomeron en fonction des états intermédiaires de la voie s.

La théorie des Reggeons de Gribov a été discutée en détail par M. Baker. Cette partie, purement formelle, a permis de faire le point de nos connaissances sur la nature du Pomeron.

Sur le plan phénoménologique, différents modèles ont été présentés pour décrire les données à hautes énergies, en particulier celles obtenues récemment aux ISR :

- le modèle géométrique et la contraction de Lorentz par A. Krisch
- le modèle de paramètre d'impact de Cheng-Wu par J. Walker

- l'utilisation des productions multiples pour calculer à travers l'unitarité, les amplitudes de diffusion élastique proton-proton par H. Miettinen.

D'autre part, une étude systématique des minima dans les sections efficaces différentielles a été proposée par J. Tran Thanh Van qui, à partir de la diffusion proton-proton, prédit les structures dans les autres réactions élastiques.

Le domaine de la diffusion élastique et inélastique à grands transferts, domaine qui n'est pas encore bien exploré sur le plan expérimental, a été étudié sur le plan théorique par différentes approches :

- le modèle dual avec trajectoires non linéaires par D.D. Coon
- le modèle de Bremsstrahlung par H. Fried
- le modèle de parton-interchange de R. Blankenbecler et al.

Une discussion phénoménologique des données expérimentales à grands moments transverses et la comparaison avec différents modèles ont été présentées par F. Halzen.

Les productions multiples et spécialement l'étude des corrélations, ont été étudiées dans une session spéciale animée par M. Le Bellac. De nouvelles données ont été présentées par G. Bellettini, R. Stroynowski et A. Mihul. Différents aspects théoriques ont été discutés par :

- Chung I Tan pour l'effet de clustering
- Dias de Deus pour la théorie de Hagedorn
- F. Henyey pour le modèle des paramètres d'impact
- K. Kang pour le lien entre les réactions inclusives et la coupure à deux P•merons.
- D.P. Roy pour la dualité

- P. V. Ruuskanen pour le modèle de nova.

Finalement, dans le domaine des réactions à deux corps, des mises au point ont été faites par A. Yokosawa, A.D. Martin et C. Michael. A. Yokosawa a présenté les résultats définitifs de l'expérience d'Argonne sur la polarisation de la diffusion pion nucleon avec échange de charge. Le désaccord persistant avec les résultats de la collaboration CERN-Saclay pose un grave problème, spécialement aux théoriciens. A. D. Martin a étudié la réaction $\pi^- p \rightarrow \pi^- \pi^+ n$ et a trouvé que les corrections d'absorption décroissent quand la masse du système ($\pi^- \pi^+$) augmente. C. Michael a résumé la situation des pôles de Regge pour les productions des mésons vectoriels.

Ce résumé un peu succint des principales contributions à la session du Pomeron montre la diversité des approches pour percer les mystères de l'échange du vide. Si ce colloque qui est un des premiers consacrés à cet aristocrate de la physique des hautes énergies, a permis de faire le point de la situation expérimentale aux très hautes énergies et de clarifier quelques problèmes fondamentaux, nous nous sommes quittés avec l'impression qu'une longue, difficile mais passionnante route s'ouvre désormais devant nous. Amis, au travail.

J. Tran Thanh Van

INTRODUCTION

It was not without a certain amount of anxiety that following David Leith's suggestion in May 1972, I decided to devote the second session of the eight Moriond Meeting to the study of the Pomeron, for the only thing I was sure of was that the nature of the Pomeron (or of the exchange of the vacuum) is little known. Contributions in the t channel of the Regge poles are related to those of the resonances in the s channel through duality, but the Pomeron contributions in the t channel are not related to something well defined in the s channel. On the other hand, is the Pomeron a pole, and therefore can it be factorized, or is it a cut and in this case, what are its main properties ? This feeling of anxiety was somewhat mitigated by some serious hopes as new experimental data were expected from the CERN proton-proton (ISR) storage rings and Batavia super accelerator and I dared hope that the perspective of these forthcoming exciting data would further motivate the theoreticians to endeavour to clarify the nature of the Pomeron.

From the experimental as well as theoretical points of view, our hopes were crowned with success and this Pomeron conference, which brought the main experts on this question together, proved to be extremely enriching thanks to all the participants.

In the experimental field, G. Belletini, of the Pisa-Stony Brook collaboration, and P. Strolin, of the CERN-Roma group, presented some very interesting results obtained from the CERN storage rings on the proton-proton total cross-sections. Fortunately, they both obtained the same results although their methods were different : the total cross sections increase,

probably as a power of the logarithm of the energy whereas they appeared to remain constant at the highest energies of conventional accelerators. The slope of the diffraction peak was studied in detail at NAL energies ($P_L \simeq 200$ GeV/c) by R. Carrigan and at ISR energies by P. Strolin. If the diffraction peak is associated with the exchange of the Pomeron trajectory $\alpha(t) = 1 + \alpha' t$, the slope α' which is constant at 0.5 up to 200 GeV reduces to 0.2 at ISR energies. At larger momentum transfers very pronounced minima appear in the proton proton differential cross sections (P. Strolin). We note that at lower energies, minima are also observed in the pion nucleon and antiproton proton differential cross sections (C. Baglin).

Data for the diffractive production of $Q^{\pm}$ confirm the presence of the cross-over point in the differential cross sections of inelastic reactions (R. Barloutaud), and those for the production of A_2 in pion-nucleon collisions brings forward again the possibility of a Pomeron contribution to this reaction (G. Conforto). D. Leith's critical review on diffractive dissociation brought out its main properties :

a) energy independent (or almost) cross sections

b) equality between cross-sections of particle and anti-particle production

c) existence of a sharp forward peak in the differential cross-sections

d) helicity conservation in the s channel (?).

From the theoretical point of view, the most lively discussions centered around the Pomeron, its couplings, its properties, its asymptotic behaviour. A. Martin analysed the

asymptotic theorems, and the physical consequences for the elastic cross sections and the ratio of the real and imaginary parts of the forward amplitude. F. Low reviewed the different attempts made to build up a theory of strong interactions, such as the dual or multiperipherical models. Al. White analysed the problem of the two Pomeron cut both from the t and s channel points of view and thus somewhat clarified the problem of the cancellation of couplings of three Pomerons and the Pomeron-Reggeon-Reggeon coupling at $t = 0$. He particularly emphasized the importance of the Pomeron structure in terms of the intermediate states in the s channel. M. Baker discussed the Reggeon theory of the Pomeron in detail.

This formal part of the session enabled us to sum up what we know on the nature of the Pomeron.

In the phenomenological field, different models were presented to describe the high energy data, particularly those recently obtained at the ISR :

- the geometrical model and the Lorentz contraction by A. Krisch

- the Cheng Wu impact parameter model by J. Walker

- the utilization of multiparticle production to calculate the proton-proton elastic amplitudes through unitarity by H. Miettinen.

Tran Thanh Van presented a systematic study of the minima in the elastic differential cross sections which, starting from proton-proton scattering, predicts the structure in the other elastic reactions.

Different approaches were suggested to explain theoretically elastic and inelastic scattering at larger momentum transfers,

which is a field not yet well explored experimentally :

- The dual model with non-linear trajectories by D.D. Coon

- the Bremsstrahlung model by H. Fried

- the Blankenbecler, Brodsky and Gunion parton interchange model.

F. Halzen discussed experimental data at large momentum transfers from a phenomenological point of view and compared the predictions of different models.

Multiparticle production and more specifically the correlation in inclusive reactions were studied in a special session animated by M. Le Bellac. G. Bellettini, R. Stroynowski and A. Mihul presented new data. Several theoretical points were raised :

- Chung I Tan discussed the clustering effect
- Dias de Deus, Hagedorn's theory
- F. Henyey, the impact parameter model
- K. Kang, the existing link between inclusive reactions and the two-Pomeron cut
- B. Petersson, the antiproton spectra
- D.P. Roy, duality
- P. V. Ruuskanen, the nova model.

Finally, A. Yokosawa, Al. D. Martin and C. Michael reviewed a few points in the two-body reaction field. A. Yokosawa presented the latest results obtained at Argonne on the polarization of pion-nucleon charge-exchange scattering. The disagreement shown with the results of the CERN-Saclay collaboration raises a serious problem, especially for the theoreticians. Al. D. Martin studied the $\pi^- p \rightarrow \pi^- \pi^+ n$ reactions and found that the absorption corrections decrease when the mass of the system $(\pi^- \pi^+)$ increases.

C. Michael summarized the Regge pole situation for vector meson production.

This short summing up of the different contributions of the Pomeron session shows the variety of approaches suggested to pierce the mysteries of the vacuum exchange. This colloquium, one of the first to be devoted to this outstanding problem of high energy physics, enabled us to review the experimental situation at high energies and to clarify a few fundamental problems. We separated with the impression that a long and difficult, but thrilling road was now opened in front of us.

Friends, let us work!

J. Tran Thanh Van

TOTAL PROTON-PROTON CROSS-SECTION AT THE ISR

G. Bellettini
Istituto di Fisica della Università, Pisa
Istituto Nazionale di Fisica Nucleare, Sezione di Pisa

Abstract: The recent ISR data on total proton-proton cross-section for centre-of-mass energy between ≈ 23 and ≈ 53 GeV are reviewed from an experimentalist's point of view.

Résumé : Les expériences récentes aux ISR sur la section efficace totale proton-proton sont discutées et analysées, surtout du point de vue d'un expérimentateur.



INTRODUCTION

Two ISR experiments[1-3] have recently found that the total proton-proton cross-section σ_T grows by $\sim$ 10% over the c.m.s. energy range from $\approx$ 23 to $\approx$ 53 GeV. I shall now review these results, with emphasis on the delicate points of the experiments and comments on the problems which deserve further study. Also a third experiment has produced data on σ_T [4], but since this data is rather old and preliminary I shall not discuss it here. In what follows, my main concern will be in establishing the facts, in order to give a feeling for the confidence level of the results. Though I shall conclude that σ_T is indeed growing with energy, and consequently a discussion on the theory would be in order, I will not have time to enter into theoretical arguments.

If two continuous beams cross each other at an angle α, the total rate of interaction R_T is connected to σ_T by (under the approximation in which the velocity of the protons $\beta \approx 1$) [5]

$$R_T = \frac{I_1 I_2}{c\, e^2\, \mathrm{tg}\, \frac{\alpha}{2}} \cdot \frac{\int \rho_1(z)\rho_2(z)\, dz}{\int \rho_1(z)\, dz \int \rho_2(z)\, dz} \cdot \sigma_T = L\sigma_T \qquad (1)$$

where c is the velocity of light and e the electron charge. At the CERN ISR, the two beams cross each other on the horizontal plane, with $\alpha \approx 15°$. $\rho_{1,2}(z)$ are the vertical distributions of current in the two beams. The luminosity L represents the overlap of the two beams at the intersection, and replaces the product of beam intensity times the number of target/cm^2 in a conventional transmission experiment. In the Pisa-Stony Brook (PSB) experiment[1,2], σ_T is measured by measuring L and R_T separately. L is measured with the Van der Meer method[6] and also with a direct measurement of $\rho_1(z)$ and $\rho_2(z)$. R_T is obtained by measuring a fraction R_M of the true rate, and correcting for the loss ΔR (which is of the order of a few per cent), mostly of elastic events: $R_T = R_M + \Delta R$.

In the Rome-CERN (RC) experiment[3], σ_T is obtained by (a) measuring the differential elastic cross-section at a single angle of about 6 mrad -- which implies measuring the elastic rate of that angle and the luminosity; (b) extrapolating to the forward direction by making use of the known[7,8] slope of the diffraction peak; (c) assuming no spin-dependence and a purely imaginary scattering amplitude at forward angles, and applying the optical theorem. In symbols

$$\frac{d\sigma_{el}}{d\Omega}(\theta) = \frac{1}{L}\frac{\Delta R_{el}}{\Delta\Omega}(\theta) \tag{2}$$

$$\frac{d\sigma_{el}}{d\Omega}(0) = \frac{d\sigma}{d\Omega}(\theta)\, e^{+|b|p_{ISR}^2\theta^2} \tag{3}$$

$$\sigma_T = \frac{4\pi\hbar}{p_{ISR}}\sqrt{\frac{d\sigma}{d\Omega}(0)}\ , \tag{4}$$

where ΔR_{el} = elastic rate in $d\Omega$, b is the forward slope parameter, and p_{ISR} the ISR beam momentum.

At the lowest ISR energies, the Rome-CERN Collaboration has also measured detailed angular distributions down to the Coulomb interference region, and deduced σ_T from a four-parameter fit to the data in terms of σ_T, b, ρ (ρ = ratio of the real to imaginary part of the strong interaction scattering amplitude) and the detection efficiency k. In symbols (disregarding the imaginary part of the order of 2% which is induced in the Coulomb amplitude in the presence of strong interactions)

$$\frac{dR_{el}}{d\Omega} = k\frac{p_{ISR}^2}{\pi\hbar^2}\left|\frac{2}{137\, p_{ISR}^2\theta^2} + (i+\rho)\frac{\sigma_T}{4\sqrt{\pi}}e^{(b/2)p_{ISR}^2\theta^2}\right|^2 . \tag{5}$$

The assumptions here are no spin dependence, and that the real part

of the strong interaction amplitude is proportional to the imaginary part. With this method one does not need to measure L. If the Coulomb term in the right-hand side of Eq. (5) gives an important contribution -- namely if the measurement is extended at angles as small as $\sim$ 2-3 mrad at the lowest ISR energies, and at even smaller angles at higher energies -- it determines by itself the normalization constant k.

A discussion on the methods used and on the results obtained by the PSB and by the RC experiments will be given in the second section.

1. THE LUMINOSITY MEASUREMENTS

1.1 The Van der Meer (V.d.M.) method

If a detector is suitably arranged in order to reveal some kind of beam-beam interactions and no background, according to Eq. (1) its rate R_M is related to the detected partial cross-section σ_M by

$$R_M = \sigma_M \cdot L = k_M \frac{\int \rho_1(z)\rho_2(z)\, dz}{\int \rho_1(z)\, dz \int \rho_2(z)\, dz} \quad . \qquad (6)$$

Notice that the only unknown in k_M is σ_M. If the detection efficiency is insensitive to small vertical displacements of the two beams, and one measures $R_M(\delta)$ as a function of the relative vertical beam displacement δ, the rate given by Eq. (6) will vary only due to the changing overlap integral $\int \rho_1(z)\rho_2(z+\delta)\, dz$. In practice one must correct for the small variations at the different δ's, during the $R(\delta)$ measurement, of I_1, I_2 which are contained in k_M. One readily obtains

$$A = \int R_M(\delta)\, d\delta = k_M \frac{\int \left[\rho_1(z)\, dz \int \rho_2(z+\delta)\, d\delta\right]}{\int \rho_1(z)\, dz \int \rho_2(z)\, dz} = k_M \ ,$$

namely a measure of A gives k_M and in turn σ_M. In this way the

detector, which is a relative luminosity monitor, is calibrated. At any later time t the machine luminosity will be given by $R_M(t)/\sigma_M$.

I shall now review the possible errors which are usually discussed in connection with the V.d.M. method. All these errors have been studied in detail by the ISR staff or by the experimental teams. None of them can be larger than a few per cent.

a) To get a good measurement of A, $R(\delta)$ should be measured at small (say about 0.25 mm) δ-intervals, and over a wide δ-range, in order to fully include the tails of the $R(\delta)$ function. At all δ's, background should be negligible or subtracted. A typical example of a V.d.M. curve taken recently at the ISR is given in Fig. 1. From this type of data, incomplete knowledge of the tails, limited statistics and resolution do not, as a rule, allow reduction of error on A to below 1%.

b) The displacement δ, as given by the ISR Control Room to the experimenters, is known only within some error. The displacement is obtained by inducing a stable orbit distortion at the crossing region. Perturbations are induced in four points, two of which are located upstream, and two downstream of the intersection. The nominal displacement, as calculated from the main program giving the beam orbits, is checked by means of various pick-up systems. There has been continuous progress in recent times both on the program operation and on the orbit measurement. Since November 1972, the quoted residual error on the displacement scale is $\lesssim 2\%$ [9]. By making use of a counter/spark chamber monitor telescope (see Section 1.2), the PSB Collaboration has also checked the displacement scale by making a separate investigation. The two beams have been moved by equal amounts both below and above the median plane, and the nominal displacement has been compared to the actually observed displacement. The results have indicated that the true scale cannot be different from the nominal scale by more than about 1.5% at all ISR energies. Work is in progress on this problem in the PSB experiment. For the time being one makes the statement, on the basis of these results, that the quoted vertical displacement scale is correct within ±2%, and that there is no energy-dependent systematic error.

c) Although no effect of this type is predicted by the machine orbit calculations, one might suspect that the beam widths are different at different displacements, being for instance wider at larger distances from the median ISR plane. A reversible perturbation of this type would not produce obvious inconsistencies in the V.d.M. curve, and would simulate larger A's than in reality, and thus larger σ_T's. This effect could also depend on energy. However, one would expect it to be stronger at higher beam intensities. In the RC experiment, results identical within the errors were obtained in two successive luminosity measurements, for which the product of beam intensities was different by a factor of ten. In the PSB experiment, during the test of the displacement scale mentioned in (b) above, the overlap distribution $\rho_1(z)\cdot\rho_2(z)$ was obtained at 15.4 and 26.6 GeV/c, at several vertical positions of both beams which were up to 5 mm apart. The distribution $\rho_2(z)$ was also measured over a 4 mm displacement range. No important variation was noticed in the width of either distribution. More detailed measurements are in progress on this problem. For the time being, we conclude that it is extremely unlikely that some big surprise will result form these measurements.

d) If the luminosity measurements are performed in all intersections simultaneously, as is normally done at the ISR, one might worry that some residual distortion from beam displacements in other areas would disturb the measurement in a given area. Effects of this type, which manifest themselves as non-reproducibility of the $R(\delta)$ curve if beam positions in other areas have changed, have been observed from time to time at the ISR. However, in the two experiments with which we are concerned, all basic calibrations leading to the quoted σ_T-values have been obtained by moving the beams only at the relevant crossing point.

e) If the stacked ISR beams are bunched, formula (1) would not be valid. Different bunching at different energies could produce any apparent energy dependence in σ_T. The radio-frequency structure of the beams disappears within a few milliseconds after the RF is switched off, and no other source of beam bunching can be easily

thought of. Measurements made by the ISR staff have found no appreciable structures up to a frequency of 100 MHz [11]. Although at the moment one cannot yet give an upper limit for the effect, one feels that it is completely negligible.

f) The nominal ISR vertical displacement scale is quoted for the central orbit. For radially displaced orbits the actual displacements are larger at smaller radii (smaller momenta) and vice versa. This can produce a difference among V.d.M. curves made for stacks of different radial positions, which can be as large as 1-2%. In the actual running conditions of the published[1,2] PSB measurement, this effect amounted to less than 1%, and was not corrected for. It is possible, however, and it will be done in future, to keep track of the radial stack position for each V.d.M. and each data-taking run, and to apply a correction to account for the effect of the difference.

Considerations (a) to (f) above lead one to conclude that, though the V.d.M. method for calibrating the relative monitors deserves further study, it is very hard to believe that it is at present subject to systematic errors larger than ±2%, and that these errors are energy-dependent. Both PSB and RC quote ±2% as the energy-independent systematic error associated with the V.d.M. method. In addition, both experiments add a ±2% error to each measured rate, to account for additional possible systematic uncertainties associated with the L-measurement.

1.2 The direct luminosity measurement of the PSB experiment

The PSB set-up comprises a scintillator counter/Čerenkov counter/spark chamber telescope which is sketched in Fig. 2. The telescope is set at 90° from the beams, on the horizontal plane towards the inside of the ISR. With two beams in the machine, it is triggered by energetic pions generated in beam-beam collisions, and with one beam in the machine it is triggered by energetic recoil protons generated in quasi-elastic scattering on protons bound in

titanium nuclei. During the single-beam runs, titanium is evaporated by heating a Ti-ball located inside the pipe below the point of intersection.

The tracks reconstructed in the telescope are projected back on the median plane of the diamond to give the vertical coordinate of the track origin. In this way, $\rho_1(z)\rho_2(z)$ is obtained in the beam-beam runs, and $\rho_1(z)$ or $\rho_2(z)$ are obtained in the single-beam Ti-runs. By knowing $\rho_1(z)$ and $\rho_2(z)$ at a given time, the luminosity can be calculated from formula (1) and the relative monitors can be calibrated. The separately measured overlap $\rho_1(z)\rho_2(z)$is used as a check.

Although this method looks appealing because one deduces L according to its own definition, there are a number of errors associated with it which up to now have been a barrier to obtaining better results than with the V.d.M. method. The background below the $\rho_{1,2}(z)$ or $\rho_1(z)\rho_2(z)$ distributions is always very small and produces errors on L which are $\lesssim 1\%$. The non-uniformity of the Ti gas is approximately taken into account in the unfolding of the true distributions, and the residual error on L is also estimated to be $\lesssim 1\%$. The statistical errors, and uncertainties in fitting $\rho_{1,2}(z)$ with analytical curves, produce an error in typical runs of $\pm 2\%$. An additional error is due to the finite resolution of the telescope, which broadens the true distributions by an appreciable amount. In order to obtain the proper $\rho_1(z)\rho_2(z)$ or $\rho_{1,2}(z)$, this resolution must be unfolded from the measured data. Multiple scattering is mainly responsible for this effect, and to a smaller extent the intrinsic spark chamber resolution and the finite horizontal beam width. These effects are calculated with the Monte Carlo method, and are checked by removing or adding material in the telescope. One finds for the half-width of the resolution function $\delta z = 0.70$ mm for pions, and $\delta z = 0.73$ mm for protons. The calculated L by means of formula (1) depends only weakly on δz, but there is an uncertainty induced on the average position of a source point of about ± 30 μ.

As a whole, owing to this and ~~to the~~ previously-mentioned uncertainties, the precision obtainable in the L measurement was limited to about ±3%. To within this precision, the luminosity data obtained with the counter/spark chamber telescope by the PSB experiment were indeed in agreement with the results obtained with the V.d.M. method, showing in particular that there is no strong energy-dependent systematic error associated with this method. This is a very important result in itself.

2. THE RATE MEASUREMENTS

2.1 The rate measurement in the Pisa-Stony Brook experiment

In the PSB experiment, the rate of beam-beam interactions is measured by a large counter-hodoscope system, which is sketched in Fig. 3. A left-right coincidence trigger is requested to signal a candidate event, and several time-of-flight distributions between left and right detectors are studied off-line in order to find out, with a few nanoseconds resolution, how many events accepted by the trigger had some left-going and some right-going track which originated at the same time at the intersection. The upper part of Fig. 4 shows an example of such TOF distributions. Within the trigger acceptance of about ±30 nsec, all but one (T_{44}) spectra include background events due to jets accompanying the two beams. The shape of the background peaks is found in runs with one beam only circulating in the ISR; the peaks are normalized to the data (dotted distributions in bottom part of Fig. 4) and subtracted. The number of the remaining events (the contributions by T_4L and T_2L are multiplied by two) gives the measured rate R_M. Since most events have high multiplicity and appear in more than one TOF, the spectra are studied one after the other in the order T_{44}, T_{42}, T_{24}, T_{22}, T_4L, T_2L, and in each spectrum all events appearing in any of the previous distributions are excluded (first histogram of the top part of Fig. 4, and histograms of the bottom part of Fig. 4). The relative rate contributed by the various TOF's is plotted in Fig. 5 as a

function of energy. The error in the total rate R_M is due to uncertainties in the background subtraction and, to a smaller extent, to the statistical error, accidentals, etc., and is in all cases of the order of 0.5%.

Although the PSB set-up covers about 90% of the solid angle, a number of beam-beam events are lost by the trigger; these can be listed as follows: a) events with no charged track in one hemisphere; b) events with some charged tracks at small angles only, inside the hole at the centre of H_3, H_4; c) events as in (b), with tracks only inside the hole in H_1, H_2 around the incoming beam (direction H_6, see Fig. 3); d) events with charged tracks only at angles larger than the edges of H_1, H_2 but still not inside L (between $\sim 30°$ and $\sim 40°$ from each beam).

Events of type (a) are very rare. Events such as $pp \to pN^*$ ($N^* \to p\pi^0$ or $N^* \to n\pi^+$) would still give, for the known low-lying isobars, one charged particle in both hemispheres. Events such as $pp \to nN^{*++}$ and $pp \to \pi^0(d\pi^+)$ or similar fancy events would not give a left-right coincidence. The cross-section for these events is $<<$ 1 mb at CPS energies and is expected to decrease rapidly with increasing energy. Check runs have been made at various energies by inserting Pb converters in front of H_1 and H_3, which allowed the trigger to be extended to nearly all photons and to $\sim$ 20% of the neutrons. These data are being analysed. Results are being found that are higher than those of normal runs by a fraction of a mb, and therefore consistent with them within the errors. We shall assume that events of type (a) can be neglected within the precision of this experiment.

Events of type (b) can be elastic or quasi-elastic. The elastic differential cross-section is well known[7,10] and can be integrated with the Monte Carlo method over the beam-beam crossing to give the rate R^{el}_{out} lost in the holes, and the rate R^{el}_{in} accepted by the trigger. R^{el}_{out} is part of the loss of type (b). It varies from about 0.5 mb to about 2.5 mb from the lowest to the highest ISR energies.

The fact that this increase is about half of the over-all increase of σ_T should not worry at all, because it does not depend on any of the questionable details of $d\sigma/dt$, but is a straightforward consequence of the strong increase of flux that any cross-section depending basically on t only would give, through a forward hole of fixed size. R_{in}^{el} is part of the measured rate R_M, and indeed within the detected events R_{in}^{el} are recognizable as elastic on the basis of simple criteria. After having removed these events, one studies the remaining ones as a function of the maximum angle of the tracks in one hemisphere, down to the inner edge of H_4. One finds distributions such as the one shown in Fig. 6, which can be integrated over the forward hole to give empirically the loss of inelastic events. This loss grows with energy, but is only $\simeq$ 0.5 mb at the highest ISR energies. In addition to R_{out}^{el}, it gives the complete loss of type (b) above.

Loss of type (c) can be estimated on the basis of the number of events having tracks, in one hemisphere, that are only around the incoming beam hole (namely, in hodoscope H_6). At all energies these events were found to be $\lesssim$ 0.2% and were neglected.

Loss of type (d) was studied by considering the number of events of the type H_2L or H_4L -- namely, having tracks at large angles on one side only -- and checking how many of these had tracks on the external counters of the L-box only. Curves such as the one shown in Fig. 7 were drawn, by means of which one could estimate with an empirical extrapolation how many events are lost in the gaps between the H_2's and L. This estimate was also checked by plotting the number of events having tracks in only the outside rings of H_2, and by extrapolating again into the region between H_2 and L. The loss was consistently found to be $\lesssim 1‰$ at all energies, and was neglected.

In Table 1 are shown the measured and the corrected cross-sections by the PSB Collaboration, relative to measurements done before the end of 1972. More recently, new data have been collected

in the same and in new (with lead converters, with asymmetric beam energies) conditions. The new data have fully confirmed the old ones.

2.2 The rate measurement in the Rome-CERN experiment

In the RC experiment, elastic events were detected by a left-right coincidence between two sets of (x,y) counter hodoscopes, as illustrated in Fig. 8. The hodoscopes were plugged inside special pots, such that after stable stacked beam conditions were reached in the ISR, they could be displaced as near as about 1 cm from the beam axis. The rate distribution over one full hodoscope, associated with a track crossing a fixed central bin in the opposite one (bin area = $\Delta x \cdot \Delta y$, with $\Delta x, \Delta y$ = width of horizontal and vertical counters), is shown in Fig. 9. The elastic rate ΔR_{el} is given by the volume of this peak, after subtraction of the flat background below it. The solid angle is $\Delta\Omega = \Delta x \cdot \Delta y$ and σ_T is obtained by applying formulas (2), (3), and (4).

The background to be subtracted is found by integrating, below the elastic peak, the flat distribution of events which is found around it, and varies from $\sim$ 3.5% at 11.8 GeV/c to $\approx$ 10% at 26.6 GeV/c. After assuming a generous error of ±15% on this subtraction, one is left with an error of $\approx$ ±1-1.5% in the measured rate. In order to make the peak in Fig. 9 as narrow as possible, the ISR are run under special conditions, such that the overlap volume of the two beams is smallest (Terwilliger scheme). The relative monitors giving L are calibrated with the V.d.M. method in normal beam conditions, since the closed orbit distortions needed for the V.d.M. scan cannot be produced when the machine works in the Terwilliger scheme. Given the large size of the monitor counters, one calculates that to within 0.5% the calibration constant k_M of the monitor found in this way is also applicable to runs taken in the Terwilliger scheme. As a check, the RC group has found that identical results were obtained from three different monitor telescopes of counters, whose dimensions varied from 20 × 20 to 40 × 50 cm^2. Experimental data collected in

the PSB experiment also support this conclusion. When applying formula (3), an energy-dependent slope parameter b is used, ranging from 11.8 $(GeV/c)^2$ to 13.1 $(GeV/c)^2$. The extrapolation factor used to deduce from the measured cross-section at θ = 6 mrad the value at θ = 0 varies from 1.10 at 11.8 GeV/c to 1.35 at 26.6 GeV/c. As the measurement is performed at a fixed angle (and thus at an energy-dependent momentum transfer), the increase with energy of this factor is, as in the PSB case, a straightforward consequence of the well-known fact that the elastic scattering cross-section depends on the momentum transfer. The effect of the dependence of b on energy, which is not very well known, is of minor importance. If one takes b = const over the entire ISR energy range, only $\lesssim$ 2% is removed out of the $\approx$ 10% increase of σ_T. It should also be noted that, when applying formula (4), all errors in $(d\sigma/d\Omega)(0)$ (in particular the errors on L) propagate only with weight $\frac{1}{2}$ on σ_T. The results obtained at the four typical ISR energies are given in Table 2. The $\frac{1}{2}$ weight with which the error on L propagates to σ_T explains the smaller quoted errors with respect to the PSB case.

At p_{ISR} = 11.8 and 15.4 GeV/c the RC Collaboration has also measured detailed angular distributions of elastic scattering, comprising about 35 points in the interval $|t| \sim 0.001$ $(GeV/c)^2$ to $|t| \approx 0.01$ $(GeV/c)^2$ [8]. For this experiment a different set of counters was used, which is illustrated in Fig. 10. The data obtained are shown in Fig. 11. Since one gets an appreciable rate from pure Coulomb scattering, one does not need -- as explained in the Introduction -- to know the machine luminosity. If one fits [see Eq. (5)] the data in terms of k, σ_T, ρ, and b (the fit, however, is very insensitive to this parameter), one gets the results given in Table 2. The agreement with data based on the V.d.M. method is excellent, but no confirmation on the effect of growing cross-sections is given, since the energy span is too small.

3. CONCLUSIONS

The combined data from the two experiments are shown in Fig. 12, together with some data at lower energies. One observes an increase of σ_T by $\sim$ 10% from $p_{ISR} = 11.8$ to $p_{ISR} = 26.6$ GeV/c. The probability that this striking phenomenon is in reality due to systematic errors in the experiments is, in my opinion, very small. In the PSB experiment, the effect is about equally due to an increase, with increasing energy, of the observed rate and of the loss of elastic events into the beam pipe. The first is an experimental fact, and the second is an obvious and non-controversial calculation. About the most delicate parameter, the luminosity, one should blame unknown, non-understood, and until now unobserved phenomena in order to simulate an energy-dependent cross-section. As far as the RC experiment is concerned, it must be observed that the method used is indirect, since it assumes that spin effects are negligible and uses the optical theorem. However, these assumptions are very well satisfied even at CSP energies, and all that we know of strong interactions leads us to believe that these assumptions at ISR energies are fully justified. As far as the real part is concerned, the RC Collaboration has measured ρ at 11.8 and 15.4 GeV/c and found an average value $\rho = 0.025 \pm 0.035$. At higher energies the plausible values of ρ are also small. In any case one finds in the data analysis that as long as $-0.05 < \rho < 0.2$, the calculated cross-section does not vary by more than 0.2 mb from that obtained by assuming $\rho = 0$. Errors in the background subtraction to the elastic rate cannot produce any uncertainty as sizeable as the observed change in σ_T. Consequently, one concludes that also this experiment provides a very strong support for the growing cross-section.

Though the picture looks complete and convincing, the novelty of the machine, the delicate nature of the experiments, and the importance of the result have led the PSB group to perform further measurements and checks. In the near future we shall see the result of this effort, which will hopefully strengthen even more our confidence in this fascinating new phenomenon.

REFERENCES

1) S.R. Amendolia, G. Bellettini, P.L. Braccini, C. Bradaschia, R. Castaldi, V. Cavasinni, C. Cerri, T. Del Prete, L. Foà, P. Giromini, P. Laurelli, A. Menzione, L. Ristori, G. Sanguinetti and M. Valdata; G. Finocchiaro, P. Grannis, D. Green, R. Mustard and R. Thun, Phys. Letters 44 B, 119 (1973).

2) S.R. Amendolia, G. Bellettini, P.L. Braccini, C. Bradaschia, R. Castaldi, V. Cavasinni, C. Cerri, T. Del Prete, L. Foà, P. Giromini, P. Laurelli, A. Menzione, L. Ristori, G. Sanguinetti and M. Valdata; G. Finocchiaro, P. Grannis, D. Green, R. Mustard and R. Thun, Total cross-section measurements at the ISR, Geneva, 15 March 1973, submitted to Nuovo Cimento.

3) U. Amaldi, R. Biancastelli, C. Bosio, G. Matthiae, J.V. Allaby, W. Bartel, G. Cocconi, A.N. Diddens, R.W. Dobinson and A.M. Wetherell, Phys. Letters 44 B, 112 (1973).

4) G. Barbiellini, M. Bozzo, P. Darriulat, G. Diambrini-Palazzi, G. De Zorzi, A. Fainberg, M.I. Ferrero, M. Holder, A. McFarland, G. Maderni, S. Orito, J. Pilcher, C. Rubbia, A. Santroni, G. Sette, A. Staude, P. Strolin and K. Tittel, presented at the International Conference on Particle Physics (unnumbered), Oxford, 1972.

5) W.C. Middelkoop and A. Schoch, AR/INT.SG/63-40, unpublished. J.M. Jauch and F. Rohrlich, Theory of photons and electrons (Addison-Wesley, Cambridge, Mass., 1955).

6) S. Van der Meer, CERN-ISR-PO/68-31, unpublished.

7) G. Barbiellini, M. Bozzo, P. Darriulat, G. Diambrini-Palazzi, G. De Zorzi, A. Fainberg, M.I. Ferrero, M. Holder, A. McFarland, G. Maderni, S. Orito, J. Pilcher, C. Rubbia, A. Santroni, G. Sette, A. Staude, P. Strolin and K. Tittel, Phys. Letters 39 B, 663 (1972).

8) U. Amaldi, R. Biancastelli, C. Bosio, G. Matthiae; J.V. Allaby, W. Bartel, G. Cocconi, A.N. Diddens, R.W. Dobinson, V. Elings, J. Litt, L.S. Rochester and A.M. Wetherell, Phys. Letters 43 B, 231 (1973).

9) P. Bryant, ISR Performance Report, ISR/MA/PJP/rh, 27-3-73.

10) U. Amaldi, R. Biancastelli, C. Bosio, G. Matthiae, J.V. Allaby, W. Bartel, G. Cocconi, A.N. Diddens, R.W. Dobinson and A.M. Wetherell, Phys. Letters 36 B, 504 (1971).

11) B. Zotter, private communication.

Table 1

Summary of results of the PSB Collaboration, prior to January 1973. The elastic and inelastic losses listed in the 5th and 6th columns are inside the outgoing beam pipe, and have been calculated as explained in the text

Beam momentum (GeV/c)	c.m. energy squared $(GeV)^2$	Equivalent lab. beam momentum (GeV/c)	Detected cross-section (mb)	Increment for elastic loss (mb)	Increment for inelastic loss (mb)	σ_T (mb)
11.8	548	291	38.66 ± 0.79	0.54 ± 0.10	0.10 ± 0.02	39.30 ± 0.79
15.4	932	496	39.93 ± 0.81	0.75 ± 0.10	0.17 ± 0.04	40.85 ± 0.82
22.6	2005	1068	40.69 ± 0.84	1.54 ± 0.15	0.34 ± 0.10	42.57 ± 0.86
26.6	2776	1480	40.53 ± 0.83	1.95 ± 0.20	0.50 ± 0.12	42.98 ± 0.84

Table 2

Summary of results of the RC Collaboration,
obtained both with forward extrapolation of $d\sigma_{el}/d\Omega$ ($\theta \sim 6$ mrad)
and L measurement with the V. d. M. method, and with the Coulomb interference method

ISR momenta (GeV/c)	c.m. energy $\sqrt{s}$ (GeV)	Equivalent lab. momentum (GeV/c)	σ_T	σ_{el}	σ_{in}
V. d. M. METHOD					
(11.8 + 11.8)	23.5	290	39.1 ± 0.4	6.8 ± 0.2	32.3 ± 0.4
(15.4 + 15.4)	30.6	500	40.5 ± 0.5	7.0 ± 0.2	33.5 ± 0.4
(22.6 + 22.6)	44.9	1070	42.5 ± 0.5	7.5 ± 0.3	35.0 ± 0.5
(26.6 + 26.6)	52.8	1480	43.2 ± 0.6	7.6 ± 0.3	35.6 ± 0.5
COULOMB INTERFERENCE METHOD					
(11.8 + 11.8)	23.5	290	38.9 ± 0.7	6.7 ± 0.3	32.2 ± 0.7
(15.4 + 15.4)	30.6	500	40.2 ± 0.8	6.9 ± 0.4	33.3 ± 0.8

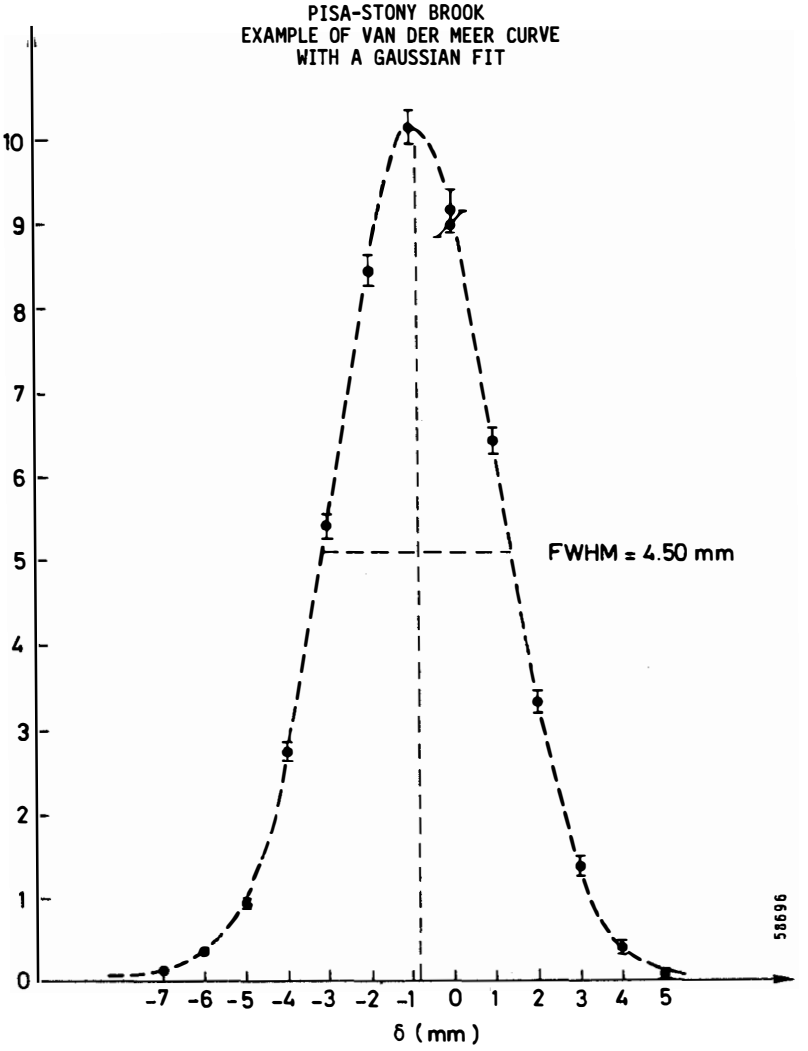


Fig. 1 Example of beam displacement curve R(δ) at p_{ISR} = 15.4 GeV/c.

PISA-STONY BROOK
SPARK CHAMBER LUMINOSITY TELESCOPE

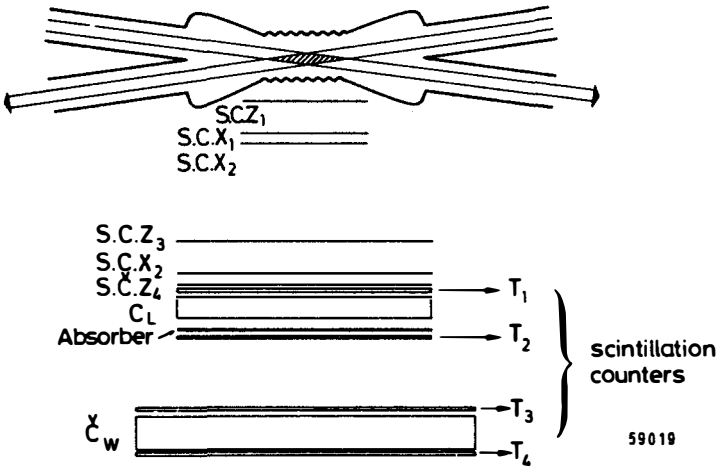


Fig. 2 Sketch of the PSB luminosity telescope. S.C., magnetostrictive spark chambers; x,z, measured horizontal or vertical coordinate; C_L, C_W, lucite and water Cerenkov counters.

PISA-STONY BROOK
LAYOUT OF THE TOTAL CROSS-SECTION EXPERIMENT
(TOP VIEW)

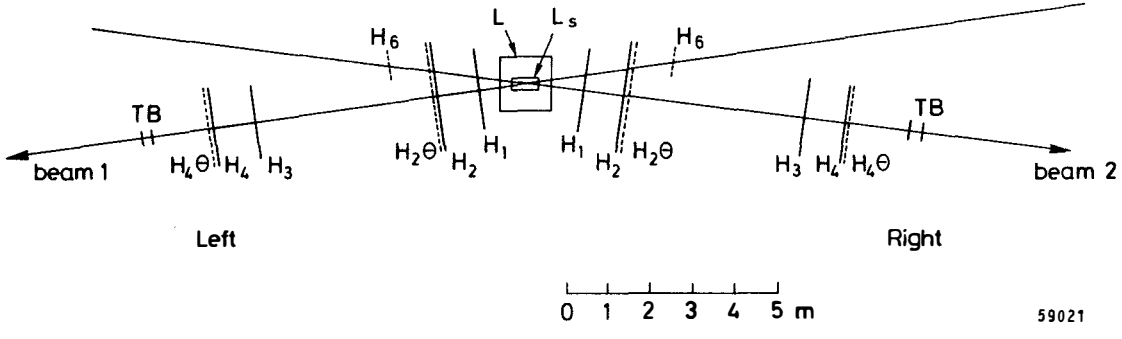


Fig. 3 Schematic layout of the Pisa-Stony Brook experiment. H_1, H_2, H_3, H_4, counter hodoscopes which are used to trigger on left-right particles in coincidence. $H_2\theta$, $H_4\theta$, H_6, counter hodoscopes measuring the production angle of the particles. TB, small counters touching the pipes, which are used in the trigger. L_S, L, large-angle counter hodoscopes, which are used both in the trigger and for track definition.

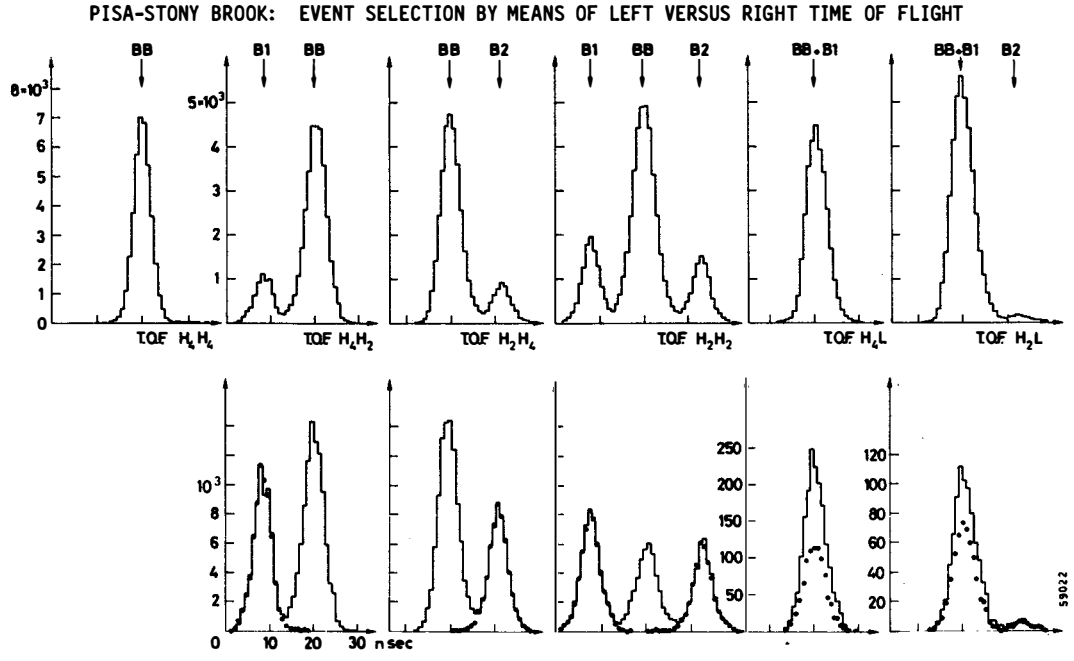


Fig. 4 Typical time-of-flight spectra between various left and right (or centre) hodoscopes. In the upper part of figure, the raw spectra are shown. BB is the signal, B1 and B2 are background events due to jets accompanying the beams. The lower part of the figure indicates the subtracted background (dotted histograms), and the residual BB signal which is left in each distribution after removing all events accepted in previously studied distributions. TOF spectra are studied in the order T_{44}, T_{42}, T_{24}, T_{22}, T_4L, T_2L.

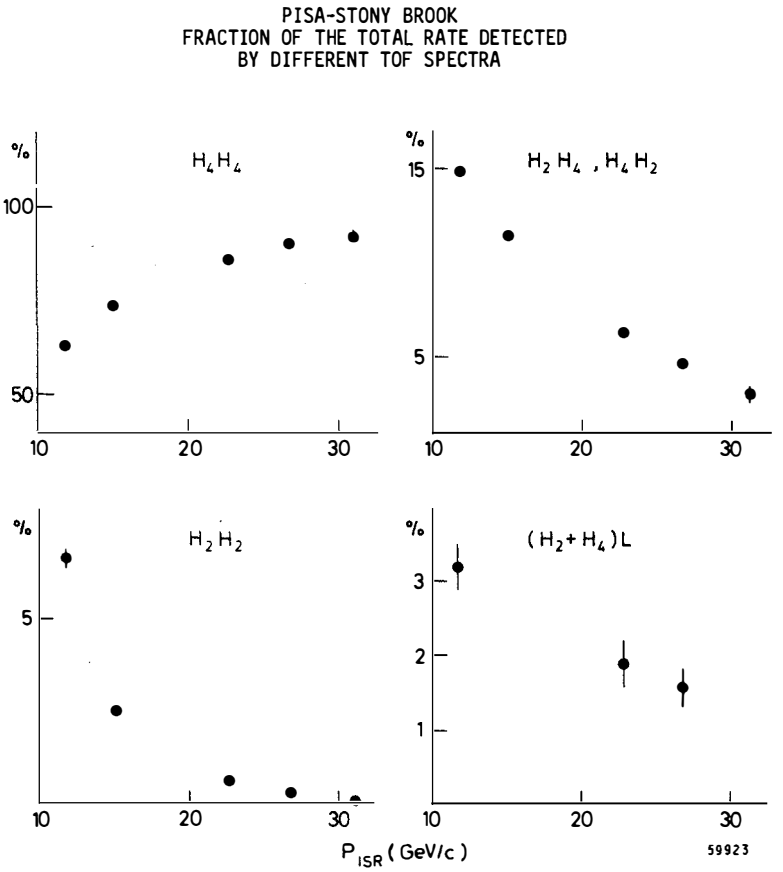


Fig. 5 Fractional rate contributed by the various TOF distributions, as a function of the ISR (equal) beam momenta. One sees that most of the rate is contributed by T_{44}, which contains only very little ($\lesssim$ 1%) background (see Fig. 4).

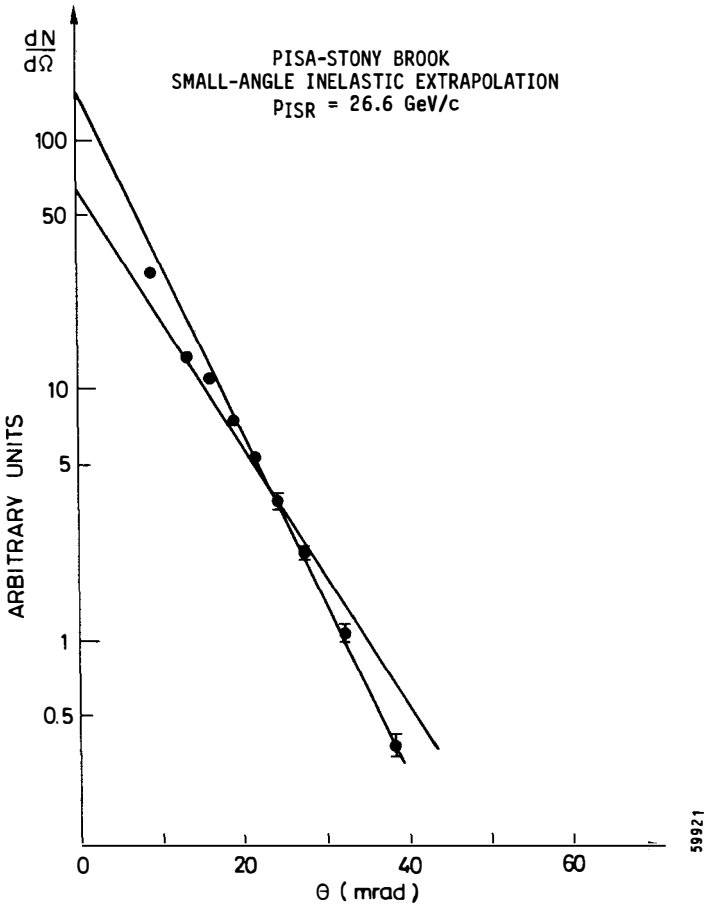


Fig. 6 Distribution of inelastic events having on one side all tracks at angles smaller than θ, as a function of θ. To small angles, the distribution extends to the inner edge of H_4. The loss is calculated by integrating this empirical function over the hole inside H_4. The two lines show the estimated size of the extrapolation error.

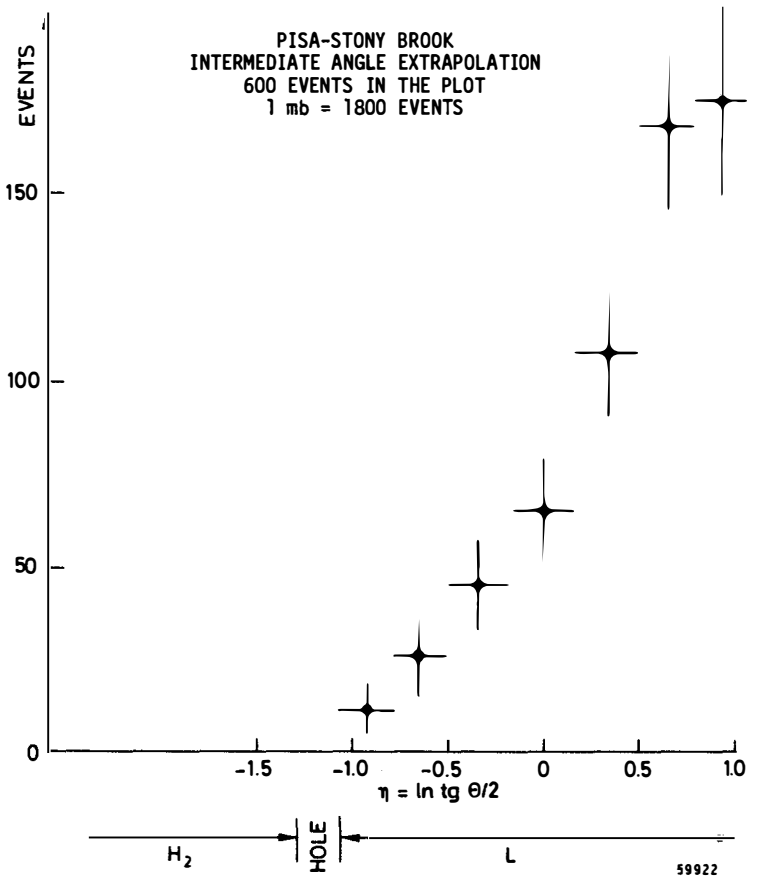


Fig. 7 Example of distribution of inelastic events of type H_2L or H_4L, plotted versus the maximum angle of the tracks in the L-box. The area below this curve, in the region between $\sim 30°$ and $\sim 40°$, gives the empirically estimated loss of inelastic events of type (d) (see text), which is found to be $\lesssim 1‰$.

CERN-ROME
LAYOUT OF TOTAL CROSS-SECTION EXPERIMENT

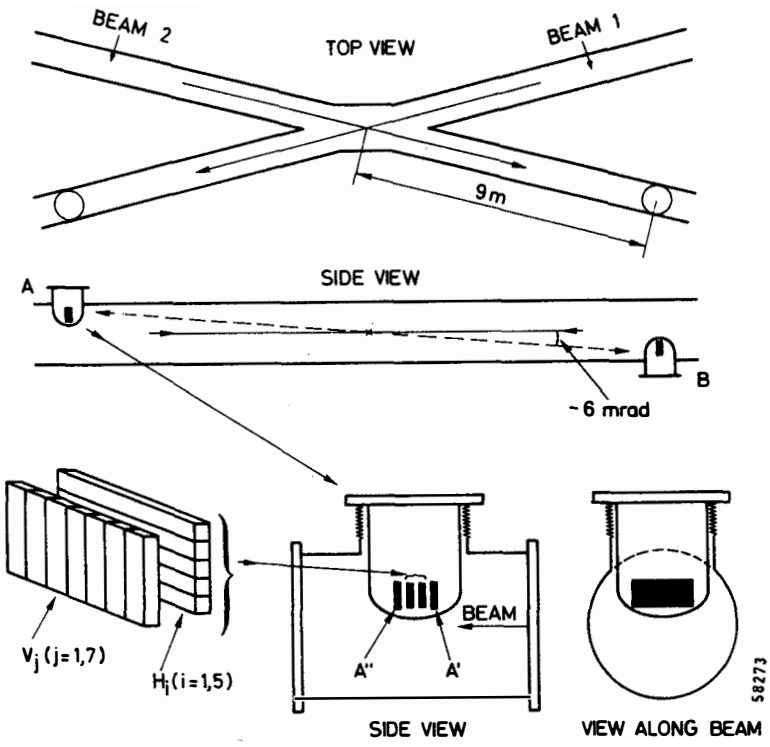


Fig. 8 Sketch of the apparatus used by the RC group for the σ_T measurement (Ref. 3).

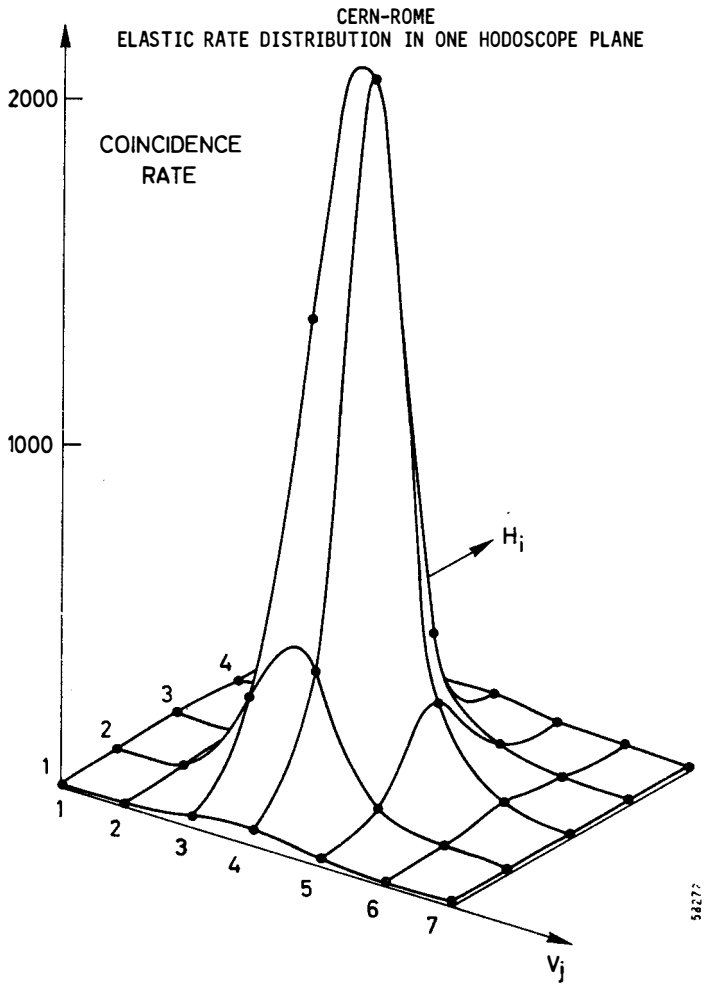


Fig. 9 Example of two-dimensional rate distribution in the RC experiment (Ref. 3), over the full area of one hodoscope pair, for a central position of the associated track in the opposite hodoscope.

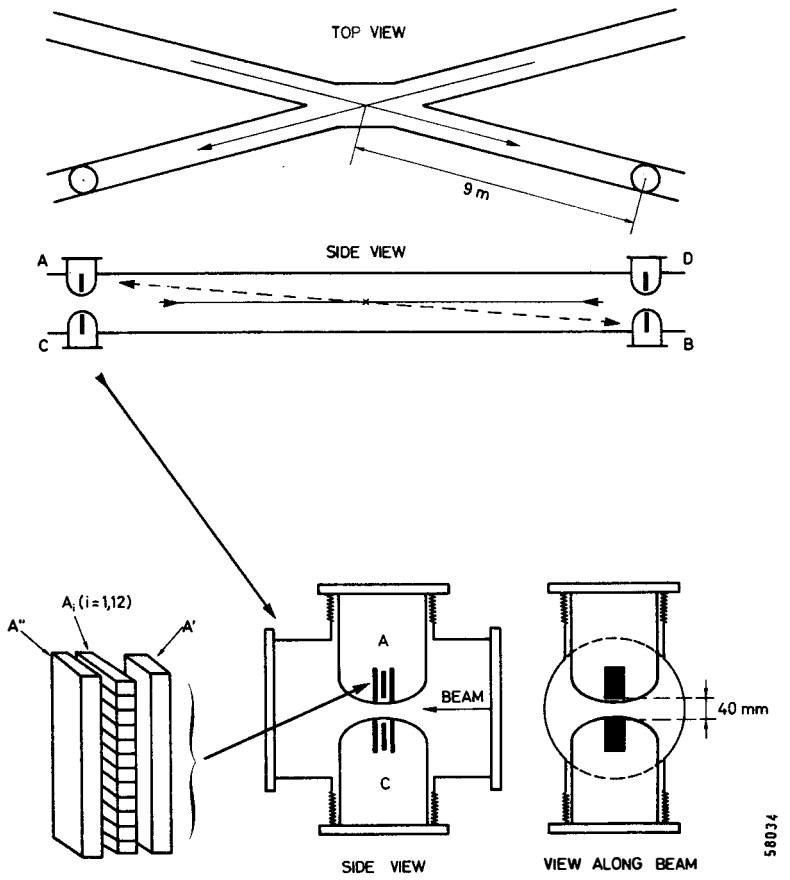


Fig. 10 Sketch of the experimental set-up used by the RC Collaboration in the elastic differential cross-section study in the Coulomb interference region (Ref. 8).

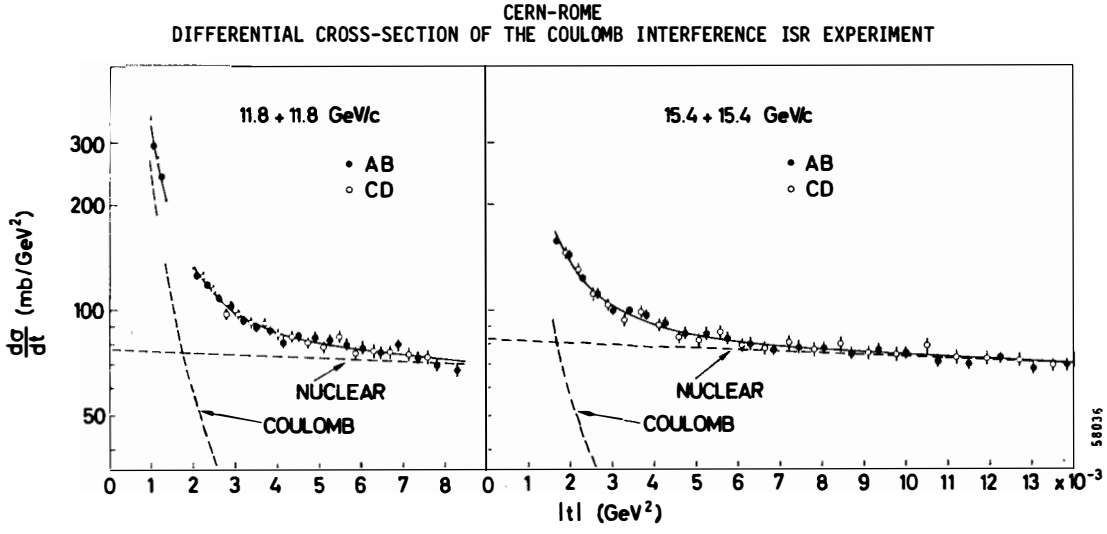


Fig. 11 Angular distributions of the RC Coulomb interference experiment at p_{ISR} = 11.8 and 15.4 GeV/c (Ref. 8). The curves show the best fit to the data in terms of formula (5) (see text).

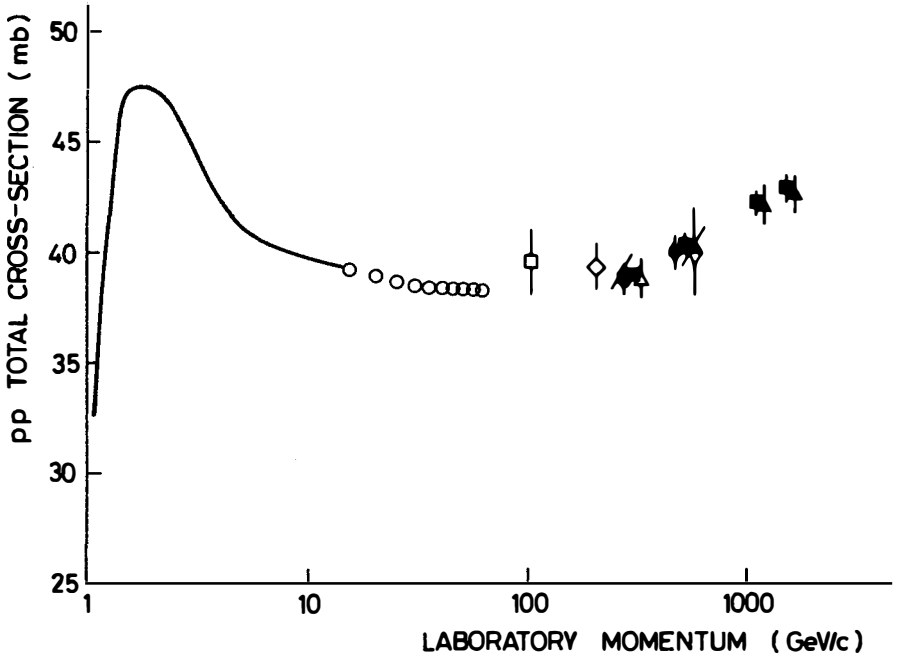


Fig. 12 Combined data from the PSB experiment (prior to January 1973) and from the RC experiment, compared to a sample of data at lower energy. ▲, PSB; △, RC Coulomb interference; ▮, RC forward extrapolation.

PROTON-PROTON ELASTIC SCATTERING AT ISR ENERGIES

P. Strolin
CERN, Geneva, Switzerland

Abstract : The experimental results obtained on proton-proton elastic scattering at the CERN Intersecting Storage Rings are reviewed in this work, with special consideration to the most recent results on large angle scattering.

Resumé : Les résultats expérimentaux obtenus aux anneaux de stockage du CERN concernant la diffusion élastique proton-proton sont l'objet de cet exposé. Les résultats les plus récents sur la diffusion à grand angle sont spécialement traités.

PROTON-PROTON ELASTIC SCATTERING AT ISR ENERGIES

P. Strolin
CERN, Geneva, Switzerland

Following the early results, almost two years ago, a number of experiments have been performed at the CERN Intersecting Storage Rings on proton-proton elastic scattering for momentum transfers up to $-t \sim 6$ GeV^2 [1-3]. Its high-energy, possibly asymptotic, behaviour — such as the shrinking of the diffraction peak, the structure taking shape at $|t| \sim 1$ GeV^2, and the very rapid drop with energy of the differential cross-section at large momentum transfers — was left open by accelerator experiments. Although some points are awaiting further investigations, the experiments at the high c.m. energies available at the ISR have brought about very significant results. The present paper primarily concerns the differential cross-section, and especially discusses the recent results on large-angle scattering[3]. The measurements of total cross-section are reported by Bellettini[4]. A review of the ISR results on small-angle scattering has been given by Amaldi[5].

Two groups have collected data on proton-proton elastic scattering at the ISR. The Rome-CERN group has in two successive phases covered scattering angles ranging from the forward diffraction peak down to the Coulomb interference region. The Aachen-CERN-Harvard-Genova-Torino group (ACHGT) has taken data on the forward diffraction peak and successively on large-angle elastic scattering.

The detector used by the Rome-CERN group for the measurement in the Coulomb interference region is represented in Fig. 1. Elastic events are identified as coincidences between scintillation counters of the hodoscope arrays A and B (C and D) viewing the interaction point along collinear directions in the c.m. system. Similar counter hodoscopes, situated further away from the ISR beams, were used in the earlier experiment for the measurement of the differential cross-section beyond the Coulomb interference.

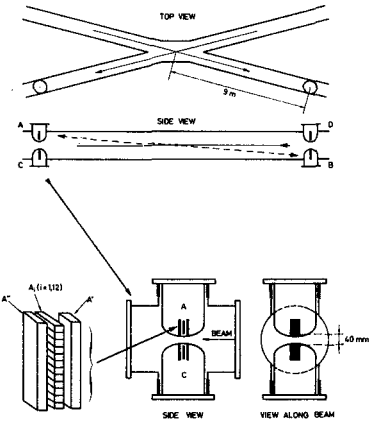


Fig. 1

The ACHGT detector consists of a double-arm magnetic spectrometer equipped with wire spark chambers having a magnetostrictive read-out (Fig. 2). The trajectories of the scattered protons are thus completely determined. Reconstruction of the interaction vertex is done with a resolution of 1.5 mm and ensures the beam-beam nature of the event. Collinearity of the two trajectories is assessed with an angular resolution 0.6 mrad. The momentum resolution of the spectrometers is 2%. The initial phase of the experiment was exclusively devoted to the study of the diffraction peak. Since this did not require magnetic analysis for background rejection, wire chamber telescopes were used instead of complete spectrometers.

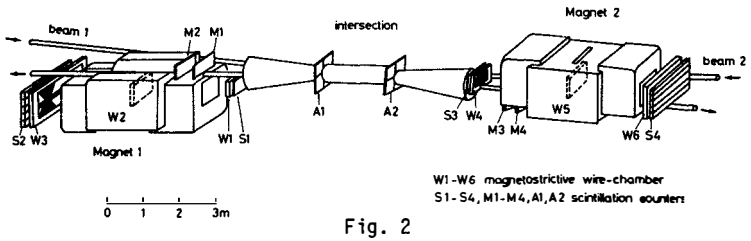


Fig. 2

A compilation of the proton-proton elastic scattering differential cross-section as a function of energy is given in Fig. 3. The ISR large-angle data of the ACHGT group[3] are characterized by a neat diffraction-like structure, with a marked dip at $-t \sim 1.4$ GeV^2, i.e. in correspondence with the shoulder observed at accelerator energies.

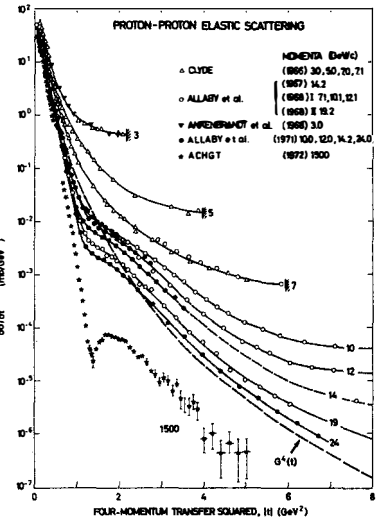


Fig. 3

Figure 4 shows the p-p differential cross-section at the beam momenta currently available at the ISR (11.8, 15.4, 22.6, and 26.8 GeV/c, i.e. $\sqrt{s}$ = 23.5, 30.7, 44.9, and 53.2 GeV) resulting from partial analysis of the ACHGT data[3]. Normalization of these curves is done relative to the ISR small-angle data. Since the spectrometers were located at a fixed angle with respect to the beam, the t-range varies with energy. In the energy range where the structure in the differential cross-section is observed at the ISR, it appears to be independent of s within experimental and normalization errors ($\sim$ 20%). This holds in particular for the position of the dip ($-t$ = 1.45 ± 0.1, 1.38 ± 0.04, and 1.37 ± 0.04 GeV^2 at $\sqrt{s}$ = 30.7, 44.9, and 53.2 GeV).

The insurgence, already at accelerator energies, of a structure around the above t-value is specially evidenced[6] by plotting $(d\sigma/dt)/d\sigma/dt)_{t=0}$ divided by the fourth power of the proton electromagnetic form factor G(t) in the spirit of Wu and Yang's paper[7]. The structure arises at about 10 GeV accelerator energies, in concomitance with a sudden change of the exponential slope at large angles as a function of $p_\perp$ [6,8,9] and of the rate of decrease of the differential cross-section at 90° as a function of momentum[10].

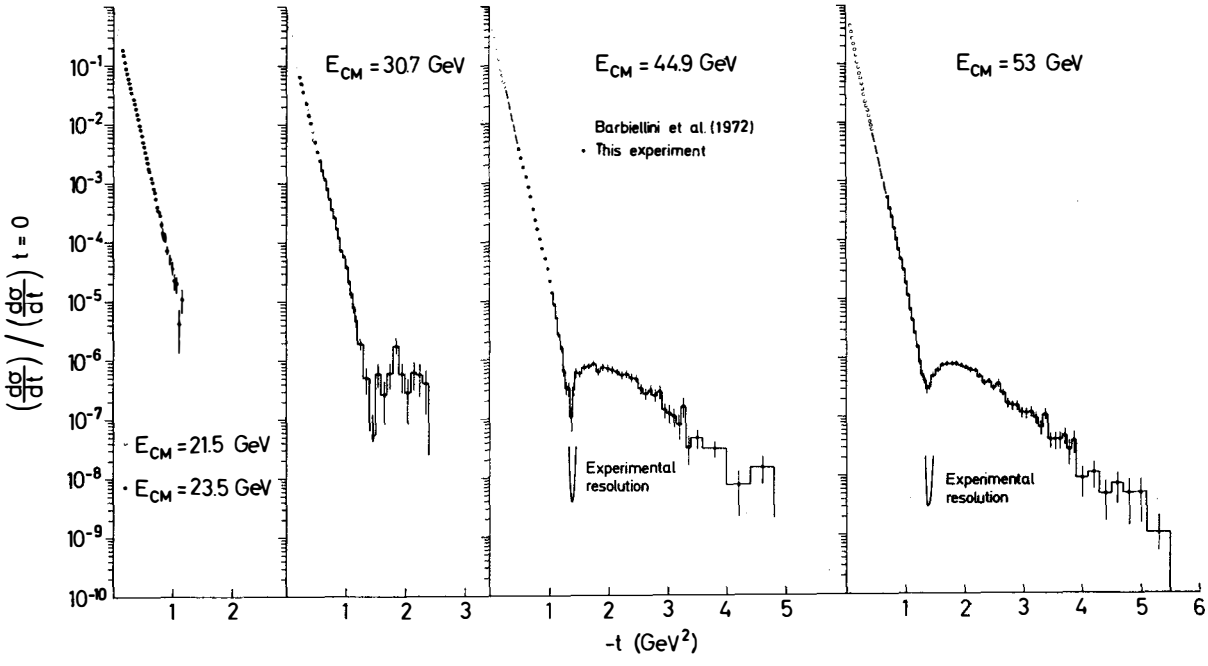

$(\frac{d\sigma}{dt}) / (\frac{d\sigma}{dt})_{t=0}$
10^{-1}
10^{-2}
10^{-3}
10^{-4}
10^{-5}
10^{-6}
10^{-7}
10^{-8}
10^{-9}
10^{-10}
E_{CM} = 21.5 GeV
E_{CM} = 23.5 GeV
E_{CM} = 30.7 GeV
E_{CM} = 44.9 GeV
Barbiellini et al. (1972)
This experiment
Experimental resolution
E_{CM} = 53 GeV
Experimental resolution
1 2
1 2 3
1 2 3 4 5
1 2 3 4 5 6
-t (GeV^2)

Fig. 4

The s-dependence at fixed t of the proton-proton elastic differential cross-section is shown in Fig. 5 [3]. A very steep dependence is observed at accelerator energies for momentum transfers beyond the diffraction peak (as s^{-10} at $-t \sim 10$ GeV^2). This led to the speculation[11] that beyond the diffraction peak elastic scattering at fixed scattering angle θ takes place with the minimal amplitude $f(s,\theta)$ allowed by analyticity and unitarity under the assumption of asymptotically constant total cross-section[12]. The ISR data indicate that this energy dependence flattens out with increasing s.

The diffraction peak at ISR energies is shown in Fig. 6 [1]. A marked steepening of the exponential slope is observed around $-t \sim 0.1$ GeV^2. Its occurrence already at accelerator energies had been inferred in a compilation by Carrigan[13] and has recently been observed[14]. A simple exponential fit $d\sigma/dt \propto \exp(bt)$ is possible for the ISR data on either side of the steepening region[1]. Fig. 7 shows the s-dependence of the slope parameter b in both exponential regions. Carrigan's paper at this meeting[15] gives the recent NAL

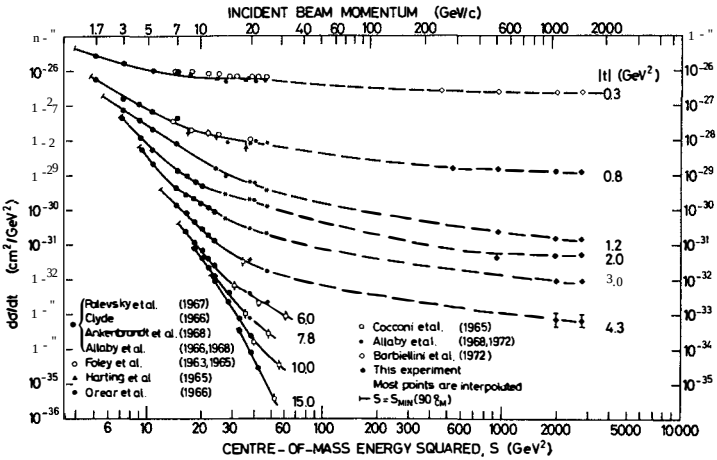
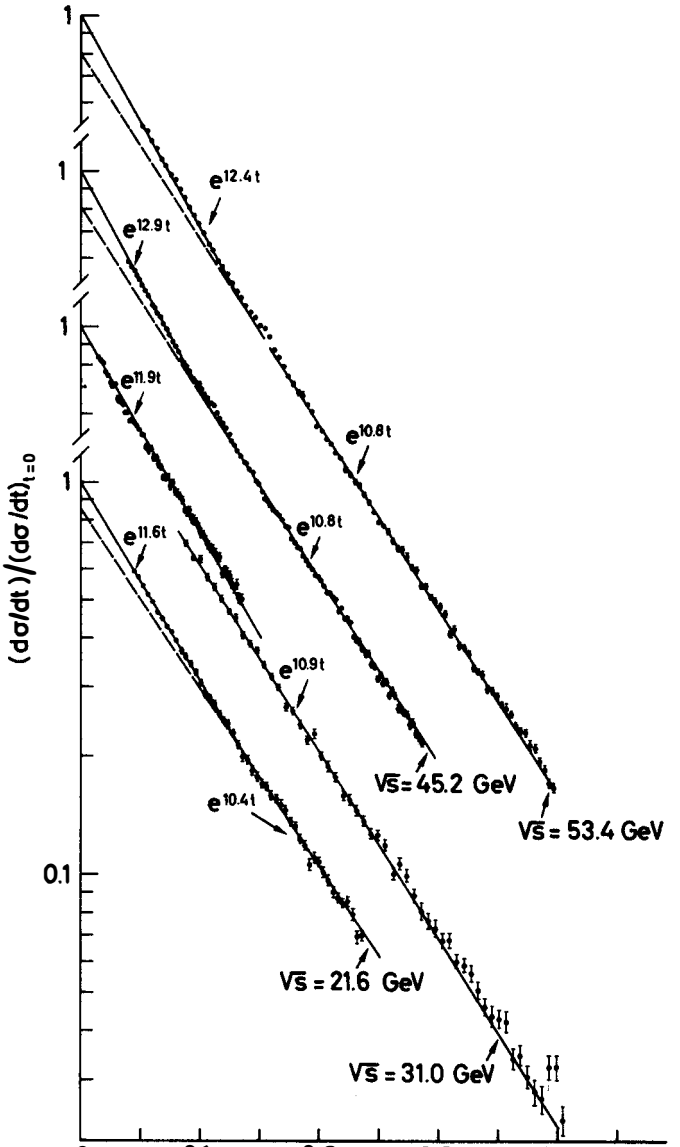


Fig. 5


1
1
1
1
0.1
$(d\sigma/dt)/(d\sigma/dt)_{t=0}$
$e^{12.4t}$
$e^{12.9t}$
$e^{11.9t}$
$e^{10.8t}$
$e^{10.8t}$
$e^{11.6t}$
$e^{10.9t}$
$e^{10.4t}$
$\sqrt{s}$ = 45.2 GeV
$\sqrt{s}$ = 53.4 GeV
$\sqrt{s}$ = 21.6 GeV
$\sqrt{s}$ = 31.0 GeV
0
0.1
0.2
0.3
0.4
$-t$ (GeV)^2
Fig. 6

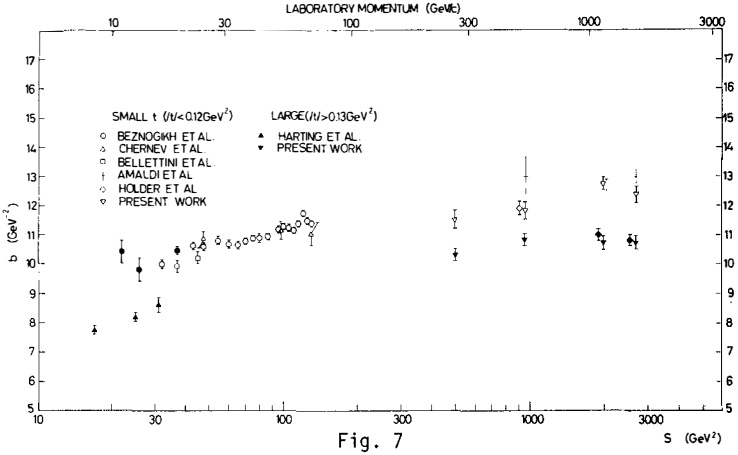


Fig. 7

measurements of the slope parameter. As also indicated by the ISR large-angle data, beyond $-t \sim 0.1$ GeV^2 the shrinking of the diffraction peak does not seem to continue at ISR energies. At smaller momentum transfers the shrinking is certainly slowed down with respect to Serpukhov energies and could even have reached saturation.

Figure 8 shows the Rome-CERN data in the Coulomb interference region ($\theta_{mrad} \sim 42/p$, i.e. a few mrad) at ISR beam momenta p = 11.8 and 15.4 GeV/c [2]. The experiment measured the proton-proton total cross-section from the optical theorem, using the Coulomb scattering for internal absolute normalization of the data, and the ratio ρ of the real-to-imaginary part of the scattering amplitude from the Coulomb-nuclear interference term. The real part was found compatible with zero value, namely $\rho = 0.02 \pm 0.05$ and 0.03 ± 0.06 at the two above momenta, respectively. Reference 15 gives a compilation of ρ as a function of s, including also the recent NAL results.

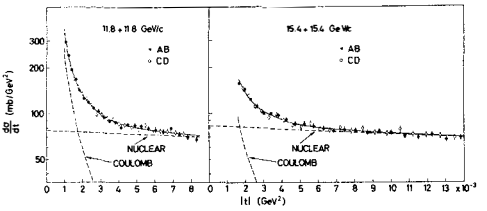


Fig. 8

Optical models[16] yield an asymptotic value for the differential cross-section and, as pointed out by Chou and Yang[16], contemplate the presence of sharp dips, in particular around the momentum transfer $-t \sim 1$ GeV^2. Elastic scattering is described as a diffractive process resulting from a local absorption of the incident wave, proportional to the overlap of two extended distributions of hadronic matter. Following Wu and Yang[7] these distributions are taken proportional to the electromagnetic charge distribution as given by the electromagnetic form factor measured in e-p scattering experiments. Figure 9 shows the results of optical model calculations by Durand and Lipes[16], where a dipole form $G(t) = (1 - t/\mu^2)^{-2}$ with $\mu^2 = 1$ GeV^2 is taken for the proton form factor. Taking a purely imaginary forward scattering amplitude, a sharp diffraction minimum is found at $-t \simeq 1.5$ GeV^2 (curve I), and this is smoothed out into a shoulder when, in accordance with accelerator data, a real part (II) is introduced. Recent calculations[17] take just the dipole fit to the electromagnetic form factor ($\mu^2 = 0.71$ GeV^2, corresponding to a proton r.m.s. radius of 0.83 fermi) and zero real part of the forward scattering amplitude, in accordance with the Rome-CERN results[2]. Apart from some differences in the height of the secondary maximum which is sensitive to the value of the total cross-section (40 mb in the figure), the agreement with the ISR data is remarkable (Fig. 10). Such models also reproduce the observed change of exponential slope by $\Delta b \approx 2$ GeV^{-2} around $-t = 0.1$ GeV^2 [18]. Carreras and White[19] have suggested a generalization of the optical model where at finite energies the interaction of hadronic matter has some degree of non-locality. The degree of non-locality and the way it vanishes asymptotically can be determined in such a way as to produce a shrinking of the diffraction peak which saturates with increasing energies.

Apart from the fact that a hadronic matter distribution according to the electromagnetic form factor is consistent with a structure of the protons in terms of constituents carrying part of electromagnetic charge and matter[18], p-p scattering could also be described in the framework of the Glauber theory[20] as scattering between composite objects[21]: the forward peak would correspond to single scattering

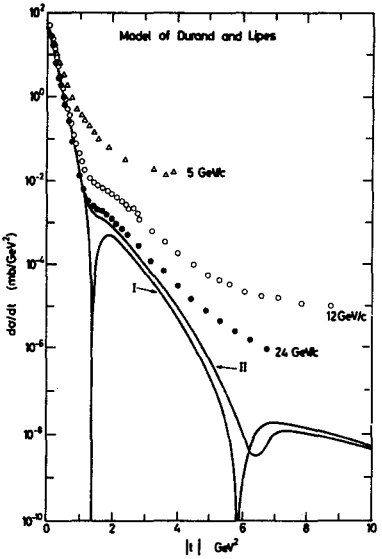


Fig. 9

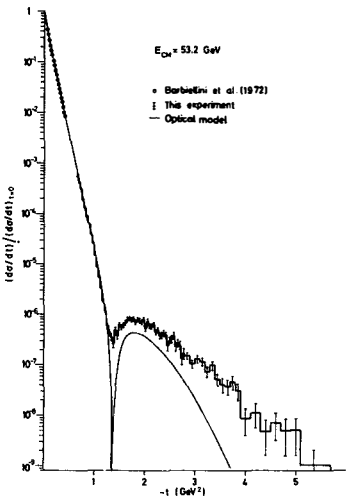


Fig. 10

whereas at larger momentum transfers one would observe the slopes characteristic of successive orders of scattering. Interference between these terms would be responsible for the observed structure, as in the case of p-d scattering. However, the large indetermination of the input of the model deprives it of insight, even with respect to the number of constituents[21].

In order to account for the energy dependence of the proton-proton differential cross-section, Chiu and Finkelstein[22] have proposed a hybrid model, where the first term of the multiple scattering series consists of a non-shrinking flat Pomeron term instead of the Pomeron with finite slope, and in addition one has a set of normal Regge poles. These then provide the energy dependence required to agree with accelerator data, while the former term, which remains alone at infinite energies, is reduced to the optical model[16] discussed above. Frautschi and Margolis[23] have instead considered the structure of dσ/dt as produced by multiple Pomeron exchanges. Because of the finite Pomeron slope the whole diffraction structure then exhibits shrinking, which does not seem to agree with experimental results.

Abarbanel, Drell and Gilman[24] suggested that the p-p scattering amplitude at large t consists of a "diffractive" tail, which dies out with increasing momentum transfer and energy, plus an energy-independent term resulting from a direct point interaction of current-current nature having the form of the fourth power of the proton electromagnetic form factor, i.e.

$$\frac{d\sigma/dt}{(d\sigma/dt)_{t=0}} = \left[a\, G^2(t) + R(s,t)\right]^2 ,$$

where a is a normalization constant independent of s and not predicted by the theory. Accelerator and ISR differential cross-sections at large momentum transfers are approximately parallel to a $G^4(t)$ (Fig. 3) so that the diffractive term R(s,t) should shrink in such a way as to produce an almost parallel displacement of the curve.

A few comments about the total cross-section, in relation to differential cross-section measurements. No rise of p-p total cross-section ($\Delta\sigma_t = 0 \pm 1.5$ mb) from $\sqrt{s} = 31$ to 53 GeV was detected in the earlier ISR experiments by the ACHGT group[25]. The rise recently reported by the Rome-CERN[26] and Pisa-Stony Brook[27] groups averages to $\Delta\sigma_t = 2.5 \pm 0.6$ mb in the same energy range and 3.9 ± 0.6 mb from $\sqrt{s} = 22$ to 53 GeV. The corresponding rise of the optical point, combined with the increase Δb of the slope of the diffraction peak[1,2], is such that the very small angle exponential differential cross-sections at $\sqrt{s} = 31$ and 53 GeV would cross each other at $-t = 2(\Delta\sigma_t/\sigma_t)/\Delta b = 0.11 \pm 0.03$ GeV^2, i.e. approximately where the second exponential slope sets in. As this slope appears to reach s-independence at ISR energies the differential cross-sections at large momentum transfers would therefore fall off one close to the other. The total elastic cross-section σ_{el} mostly resides in the very small angle region, so that from the optical theorem $\sigma_t^2 \propto b\, \sigma_{el}$. The reported increase of σ_t from $\sqrt{s} = 22$ to 53 GeV would reflect in approximately equal proportions the steepening of the very small angle slope and an increase of σ_{el}.

A saturation of the shrinking of the diffraction peak above ISR energies would then imply that a further increase of σ_t, as close to the $(\ln s)^2$ unitarity bound[28] as seems to result in the ISR energy range from the Rome-CERN and Pisa-Stony Brook's experiments, should be associated with a very steep increase of the total elastic cross-section.

REFERENCES

1. M. Holder et al., Phys. Letters 35 B, 355 (1971).
   M. Holder et al., Phys. Letters 36 B, 400 (1971).
   G. Barbiellini et al., Phys. Letters 39 B, 663 (1972).
2. U. Amaldi et al., Phys. Letters 36 B, 504 (1971).
   U. Amaldi et al., Phys. Letters 43 B, 231 (1973).
3. A. Böhm et al., Aachen-CERN-Harvard-Genova-Torino Collaboration, 16th Int. Conf. on High-Energy Physics, Batavia, 1972, and internal communication.
4. G. Bellettini, this Conference.
5. U. Amaldi, Proc. of the "Ettore Majorana" School of Subnuclear Physics, Erice, 1972.
6. J.V. Allaby et al., Nuclear Phys. B52, 316 (1973).
7. T.T. Wu and C.N. Yang, Phys. Rev. 137 B, 708 (1965).
8. J. Orear, Phys. Letters 13, 190 (1964).
9. J.V. Allaby et al., Phys. Letters 23, 389 (1966).
   J.V. Allaby et al., Phys. Letters 25 B, 156 (1967).
   J.V. Allaby et al., Phys. Letters 27 B, 49 (1968).
10. C.W. Akerlof et al., Phys. Rev. Letters 17, 1105 (1966); Phys. Rev. 159, 1138 (1967).
11. T. Kinoshita, Phys. Rev. Letters 12, 257 (1964).
    A. Martin, Nuovo Cimento 37, 671 (1965).
12. F. Cerulus and A. Martin, Phys. Letters 8, 80 (1964).
    C.B. Chiu and C.I. Tan, Phys. Rev. 162, 1701 (1967).
    R.J. Eden and C.I. Tan, Phys. Rev. 172, 1583 (1968).
13. R.A. Carrigan, Phys. Rev. Letters 24, 168 (1970).
14. D.D. Yovanovitch et al., Proc. 4th Int. Conf. on High-Energy Collisions, Oxford, 1972 (RHEL, Chilton, 1972), Vol. 2, p. 251.
15. R.A. Carrigan, this Conference.
16. R. Serber, Rev. Mod. Phys. 36, 649 (1964).
    T.T. Chou and C.N. Yang, Proc. Conf. on High-Energy Physics and Nuclear Structure, Rehovoth (1967), p. 348.
    T.T. Chou and C.N. Yang, Phys. Rev. 170, 1591 (1968); Phys. Rev. Letters 20, 1213 (1968).
    N. Byers and C.N. Yang, Phys. Rev. 142, 976 (1966).
    L. Durand and R. Lipes, Phys. Rev. Letters 20, 637 (1968).
17. B. Carreras and J.N.J. White, Nuclear Phys. B32, 319 (1971).
    M. Elitzur and R. Lipes, Carnegie Mellon preprint (1973).
    H. Moreno and R. Suaya, submitted to Phys. Letters (December 1972).

18. J.N.J. White, Nuclear Phys. B51, 23 (1973).
19. B. Carreras and J.N.J. White, Nuclear Phys. B42, 95 (1972).
20. R.J. Glauber, High-Energy Physics and Nuclear Structure (North Holland, Amsterdam, 1967), p. 315.
21. O. Kofoed-Hansen, Nuovo Cimento 60 A, 621 (1969).
22. C.B. Chiu and J. Finkelstein, Nuovo Cimento 57 A, 820 (1968); 59 A, 92 (1968).
23. S. Frautschi and B. Margolis, Nuovo Cimento 56 A, 1155 (1968); 57 A, 427 (1968).
24. H.D. Abarbanel, S.D. Drell and F.J. Gilman, Phys. Rev. Letters 20, 280 (1968); Phys. Rev. 177, 2458 (1969).
25. M. Holder et al., Phys. Letters 35 B, 361 (1971).
G. Barbiellini et al., Proc. 4th Int. Conf. on High-Energy Collisions, Oxford, 1972, and 16th Int. Conf. on High-Energy Physics, Batavia, 1972.
26. U. Amaldi et al., Phys. Letters 44 B, 112 (1973).
27. S.R. Amendolia et al., Phys. Letters 44 B, 118 (1973).
28. M. Froissart, Phys. Rev. 123, 1053 (1961).
A. Martin, Phys. Rev. 129, 1432 (1963) and Nuovo Cimento 42, 930 (1966).

SMALL ANGLE PROTON SCATTERING AT NAL and an EMERGING PICTURE OF HIGH ENERGY PROCESSES

R. A. CARRIGAN, Jr.
National Accelerator Laboratory*
Batavia, Illinois 60510 (USA)



Abstract : Preliminary small angle proton-proton scattering results from NAL are reviewed and related to other high-energy results on total cross sections, the forward real part and moderate $|t|$ scattering. It is suggested that each effect undergoes a behavior transition somewhere in the energy range from 100 to 200 GeV.

Résumé : Les résultats préliminaires de N.A.L. sur la diffusion proton-proton à petit angle sont passés en revue et reliés à d'autres résultats de haute énergie sur les sections efficaces totales, la partie réelle de l'amplitude vers l'avant et la diffusion à moyen $|t|$. On suggère que pour chaque phénomène, la dépendance en énergie subit une transition pour une énergie située dans la région 100 - 200 GeV.

SMALL ANGLE PROTON SCATTERING MEASUREMENTS AT NAL

Over the past year an extensive series of measurements of proton-elastic scattering has been underway at NAL in the internal target area of the accelerator. The experiment, the first to be undertaken at NAL, is being carried out by a collaboration of groups from Dubna, NAL, Rochester, and Rockefeller.† Parts of the work discussed here have been reported previously.[1]

The measurements have been carried out using a technique pioneered by Nikitin and his Dubna colleagues. In their approach, a target is placed directly in the circulating and accelerating beam of the accelerator. A target with an extremely small interaction length is used so that the internal beam passes through it essentially unimpeded. Both micron-thick polyethelene foils and a hydrogen gas jet with a density that is typically 4×10^{-7} gms/cm^3 have been used. Particles recoiling almost perpendicular to the beam are detected using a number of silicon solid state detectors to measure their angle and energy or energy loss. This system is capable of covering the range $0.0005 \lesssim |t| < 0.18$ GeV/c^2.

The experimental combination of a "thin" target and simple detectors results in many advantages. The experiment can run parasitically with essentially no effect on the rest of the accelerator program except for an occasional access to the equipment in the tunnel. In practice, not one but many experiments use

†The collaborators are: V. Bartenev, R. Carrigan, I-H. Chiang, R. Cool, K. Goulianos, D. Gross, A. Kuznetsov, E. Malamud, A. Melissinos, B. Morozov, V. Nikitin, S. Olsen, Y. Pilipenko, V. Popov, B. Strauss, R. Yamada, and L. Zolin.

the target. Further, these experiments can run when extraction facilities are not available.

Many incident energies can be measured during the same accelerator pulse because the accelerating beam is used. Since the recoil kinematics are essentially energy independent, there are few energy dependent systematic errors. Finally the solid state detectors constitute uncomplicated equipment by high energy standards.

In a typical run the gas jet is pulsed on twice, each time for about 250 msec (a range of 25 GeV in incident energy). The detector carriage is moved periodically to one of several angles. The complete pulse-height distribution in each detector is recorded on magnetic tape. In all cases, these pulse-height distributions show a pronounced elastic peak riding on a small background that comes from isobars, beam and gas halos, and particles originating outside the target area. Values of $d\sigma/dt$ are found by subtracting a fitted background from the elastic peak. Careful attention is paid to the measurement of the collimator sizes and the effect of nuclear interactions in the detectors.

The $|t|$ region covered extends to small enough values so that coulomb effects are pronounced. The maximum $|t|$ value is insufficient to see strong effects from the change of slope at about $|t| = 0.15$ GeV/c^2 first suggested by Carrigan.[2] In the NAL experiments, the differential cross section has been fitted to a functional form combining a simple exponential (that is, $d\sigma/dt = Ae^{bt}_{f}$) with an assumed real part and the concomitant coulomb interference. Figure 1 shows some preliminary values for b_f (the so-called forward slope parameter) measured in the NAL experiment, along with results from lower energy experiments

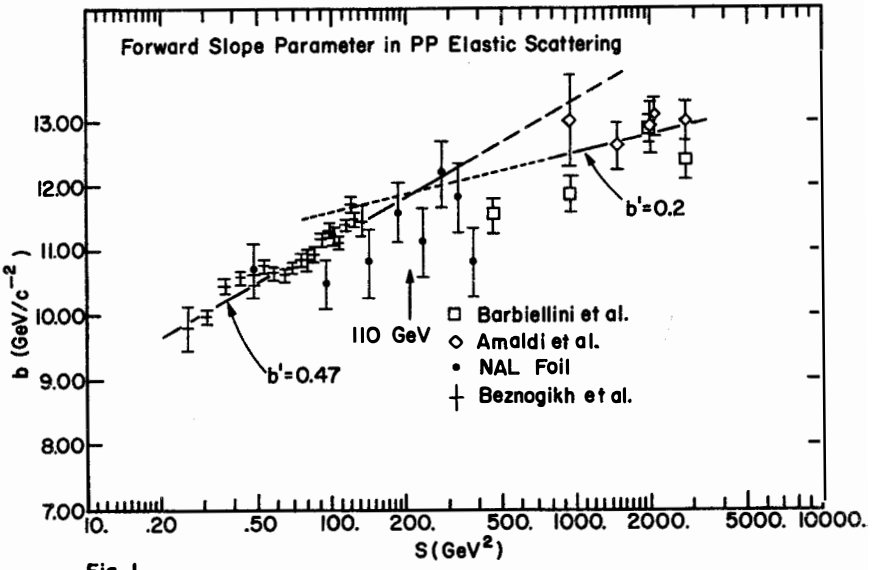

Forward Slope Parameter in PP Elastic Scattering
b (GeV/c^{-2})
13.00
12.00
11.00
10.00
9.00
8.00
7.00
b'=0.47
b'=0.2
110 GeV
Barbiellini et al.
Amaldi et al.
NAL Foil
Beznogikh et al.
10.
.20
.50
100.
200.
500.
1000.
2000.
5000.
10000.
S(GeV^2)

Fig. 1

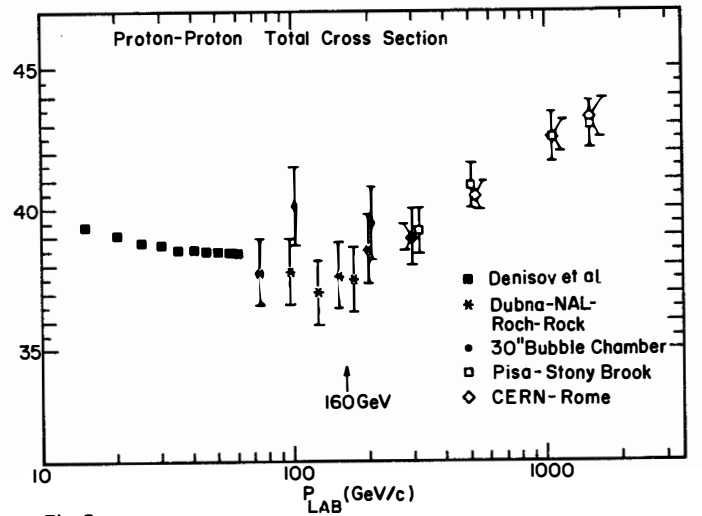

Proton-Proton Total Cross Section
45
40
35
160 GeV
Denisov et al
Dubna-NAL-Roch-Rock
30"Bubble Chamber
Pisa-Stony Brook
CERN-Rome
10
100
1000
P$_{LAB}$(GeV/c)

Fig. 2

at Serpukhov by Nikitin and his colleagues[3] and higher energy results at the ISR.[2,4]

The Dubna measurements at Serpukhov were parameterized with the expression $b_f = b_o + 2b' \ln (s/s_o)$ where $b' = 0.47 \pm 0.09$. For reference this fit is shown in Fig. 1. The NAL foil points for 200 GeV and below are also shown. Later measurements with the hydrogen jet have somewhat smaller error bars. The individual foil points are statistically compatible with the Serpukhov points while the trend of the NAL points is below the Serpukhov trend.

Above 200 GeV the situation is not too clear. Several sets of ISR measurements have been made in the region below $|t| = 0.15$ GeV/c^2 including those of CERN-Rome[4] and the Aachen-CERN-Genoa-Harvard-Turin Collaboration (ACGHT).[2] Based on the individual point error bars, the data are consistent between the two ISR experiments. However, the trend and center of gravity of the two sets of points taken alone are not consistent. Superficially, CERN-Rome shows little s dependence while ACGHT could almost be consistent with the s dependence of the data below 200 GeV. To get some feeling for the trend, the seven most recent ISR measurements above 250/GeV/c have been least squares fitted to give $b_f = 9.7 + 2 \times 0.2 \ln (s/s_o)$. This has less than half the slope of the Dubna points below 70 GeV. In any case, all of the ISR points lie below the linear extrapolation of the Dubna experiments.

Two possibilities may be considered. All of the points may lie on one straight line. This is barely possible if the Dubna absolute errors are larger than quoted and the ISR errors are taken on a point-to-point basis. A more tantalizing possibility is that the rate of change of the

slope, (that is, the shrinkage) becomes distinctly smaller somewhere between 100 and 200 GeV. Many of the present experiments are consistent with this picture.

TOTAL CROSS SECTIONS

Recently several experimental measurements of the pp total cross section have been reported. These include measurements in the thirty-inch bubble chamber at NAL[5] and several independent sets of measurements at the ISR.[4,6] The NAL internal target apparatus has also been used to measure the variation with energy of the total cross section from 48 to 196 GeV.[1] This has been done by extrapolating the small angle elastic scattering to $|t| = 0$ then using the optical theorem to obtain the total cross section. The experiment was carried out with a polyethelene foil target and a precision beam monitor. This technique gives the relative variation of the total cross section with energy. An absolute scale has been fixed by normalizing to Denisov et al.[7] at 48 GeV.

These measurements have been plotted in Fig. 2. All of the data are consistent with a picture in which the cross section falls slowly, becomes almost constant and then begins to rise again. The transition from a flat to rising total cross section appears to set in somewhere around 160 GeV.

RESULTS FROM OTHER EXPERIMENTS AT HIGH ENERGY

Some preliminary forward real part measurements have now been reported by the CERN-Rome collaboration at the ISR for equivalent laboratory energies of 300 to 500 GeV. They get positive values although their error bars bracket negative values. The NAL internal target experiment has also obtained

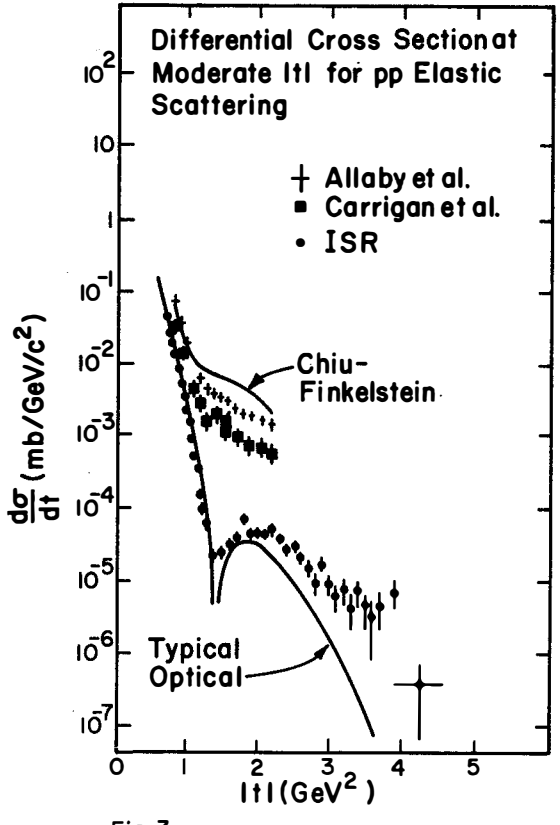

Differential Cross Section at
Moderate |t| for pp Elastic
Scattering
Allaby et al.
Carrigan et al.
ISR
Chiu-
Finkelstein
Typical
Optical
dσ/dt (mb/GeV/c²)
|t| (GeV²)

Fig. 3

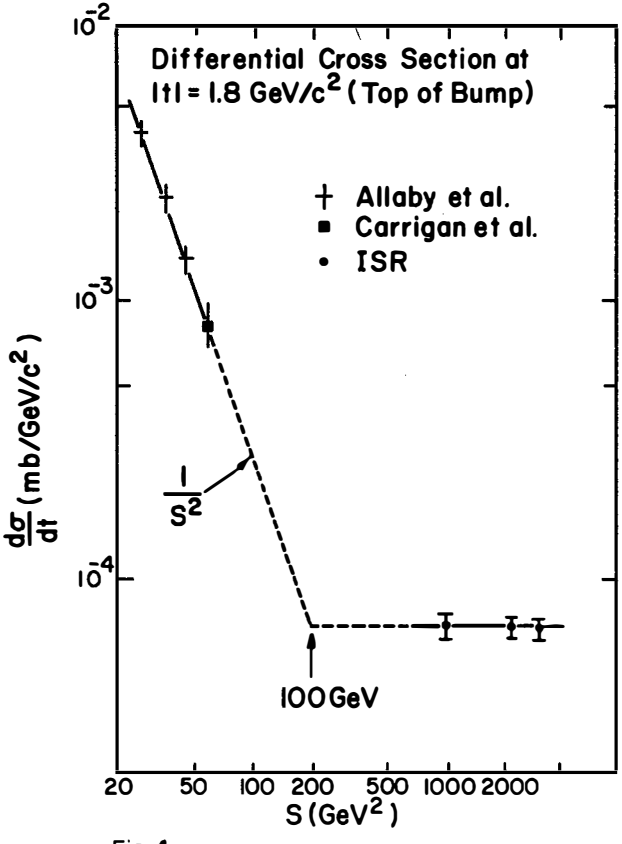

Differential Cross Section at
|t| = 1.8 GeV/c² (Top of Bump)
Allaby et al.
Carrigan et al.
ISR
1/s²
100 GeV
dσ/dt (mb/GeV/c²)
s (GeV²)

Fig. 4

forward real part values although a thorough analysis has not been completed. Suffice it to say that these measurements are consistent with the lower energy Dubna measurements and a gradually diminishing forward real part which could match the ISR points. The trend of the data indicates that the forward real part is very small, and perhaps going positive by 200 GeV.

Recently Aachen-CERN-Genoa-Harvard-Turino (ACGHT)[8] has reported beautiful ISR data in the region beyond $|t| = 0.8$ GeV/c^2. The differential cross shows a dramatic dip at about $|t| = 1.4$ GeV/c^2 followed by a bump at 1.8 GeV/c^2. Three different energies (lab equivalents of 510, 1070, and 1500 GeV) show essentially no energy dependence. The pattern of the cross section is strongly reminiscent of optical models such as Chou-Yang.[9] Earlier experiments at lower energies by Allaby et al. and Carrigan et al.[10] show a shoulder in the region where the dip appears at the ISR and a very strong energy dependence somewhat in the spirit of many Regge models. Perhaps the best existing fit is a hybrid Regge model due to Chiu-Finkelstein.[11] Both sets of data are plotted in Fig. 3.

To better illustrate the behavior, the differential cross section at $|t| = 1.8$ GeV/c^2 (at the top of the bump) has been plotted as a function of s in Fig. 4. At "lower" energies, the cross section is falling as $1/s^2$ while at ISR energies it is constant. The transition between the two regions occurs at 100 GeV.

SUMMARY OF THE SITUATION

At AGS energies, a picture of proton-proton scattering emerges in which the total cross section is falling or essentially constant, the forward peak shows some shrinkage and the

larger angles show much more s dependence. A modified Regge picture is capable of giving many of these details.

At NAL and ISR energies, the cross section is very likely rising, the forward shrinkage may be more modest, and the forward real part is small. The differential cross section reflects a diffraction pattern with very little s dependence.

It appears that each of the phenomena (σ_T, etc.) has undergone a transition and moved into a new regime at high energy. A rough approximation for the transition energy for each case is:

EFFECT	APPROXIMATE TRANSITION ENERGY
Total cross section	160 GeV
Forward real part approximately zero	200 GeV
Forward slope	110 GeV
Bump region at 1.8 GeV/c^2	100 GeV

It should be emphasized that all of these estimates are ad hoc and in some cases, based on preliminary results. It is certainly possible that the situation might be consistent with one overall transition energy.

A number of good theoretical models have been proposed which reasonably represent one or the other of the regimes. An illustration is the Cheng-Wu-Walker[12] model which seems to fit many aspects of the high energy region.

Other theoretical models, such as Chiu-Finkelstein, can potentially do even better in that they fit both regimes although with somewhat unrelated techniques used for the two regions. Perhaps some model will be found which explains both regimes on the same footing and gives a meaning to the value of the transition energy.

Future experimental interests lies in extending the measurements to other particles at NAL. Will the proton-proton high energy diffraction picture persist for other particle combinations? Will the transition energy be different in each case? (Total cross section results may already indicate this.) A particularly fascinating channel is $\bar{p}p$ where a dip at lower energies which may be Regge-like must go away, then be replaced with the pp diffraction dip at high energies. All in all, the future in hadronic physics looks exciting indeed.

*Operated by Universities Research Association Inc.,
Under Contract with the United States Atomic Energy Commission

REFERENCES

1. "Small Angle Elastic Proton-Proton Scattering from 25 to 200 GeV," V. Bartenev et al., Sept., 1972 - Contribution to the Batavia Conference (paper 802).

"Small Angle Elastic Proton-Proton Scattering from 25 to 200 GeV," V. Bartenev et al., Phys. Rev. Letters 29, 1755 (1972).

"Design, Construction and Operation of a Hydrogen Jet Target in the Main Ring of the NAL Accelerator," V. Bartenev et al., Bull. Am. Phys. Soc. DK8, 67 (1973).

"Measurement of the Slope Parameter in Small Angle pp Scattering from 30 to 300 GeV," D. Gross et al., Bull. Am. Phys. Soc. DK9, 67 (1973).

"Measurement of the Real Part of the Forward Scattering Amplitude in pp Elastic Scattering from 30 to 300 GeV," L. Zolin et al., Bull. Am. Phys. Soc. DK10, 67 (1973).

"Small Angle Elastic Proton-Deuteron Scattering from 30 to 300 GeV," R. Yamada et al., Bull. Am. Phys. Soc. DK11, 67 (1973).

"Study of Proton-Proton Interactions Using a Gas-Jet Target," V. Nikitin, Invited Talk at New York Meeting of the American Physical Society (1973).

2. R. A. Carrigan, Jr., Phys. Rev. Letters 24, 168 (1970).

G. Barbiellini et al., Phys. Letters 39B, 663 (1972).

3. G. Beznogikn et al., Phys. Letters 30B, 274 (1969), G. Beznogikn et al., Phys. Letters 39B, 411 (1972).

4. U. Amaldi et al., Phys. Letters 36B, 504 (1971), U. Amaldi et al., February, 1973 submitted to Phys. Letters (CERN-Rome).

5. J. W. Chapman et al., Phys. Rev. Letters 29, 1686 (1972); G. Charlton et al., Phys. Rev. Letters 29, 515 (1972); F.T. Dao, Phys. Rev. Letters 29, 1627 (1972).

6. S. R. Amendolia et al., February, 1973 preprint submitted to Phys. Letters (Pisa-Stony Brook).

7. S. Denisov et al., Phys. Letters 36B, 415 (1971).

8. C. Rubbia for Aachen-CERN-Genoa-Harvard-Turin Collaboration at the Batavia Conference (1972); P. Strohlin, private communication.

9. T. T. Chou and C. N. Yang, Phys. Rev. Letters 20, 1213 (1968); and Phys. Rev. 175, 1832 (1968).

10. J. V. Allaby et al., Phys. Letters 28B, 67 (1968); R. A. Carrigan, Jr. et al., Phys. Rev. Letters 24, 683 (1970).

11. C. B. Chiu and J. Finkelstein, Nuovo Cimento 57A, 649 (1968); C. B. Chiu, Rev. Mod. Phys. 41, 640 (1969).

12. H. Cheng, T. T. Wu, and J. K. Walker, to be published.

HIGH ENERGY THEOREMS FOR PARTICLE-PARTICLE AND PARTICLE-ANTIPARTICLE SCATTERING AND I.S.R. DATA *

André MARTIN

Abstract : The asymptotic theorems which constrain the elastic scattering amplitude from first principles : positivity, analyticity and unitarity are reviewed. This is done in the light of the recent I.S.R. data on total cross-sections for pp scattering which show a rise with energy, possibly like $\log^2 s$. Results for the differential cross-sections (zeros in the forward region, width of the diffraction peak, behaviour of σ_{el}) and for the ratio $\frac{\text{Re } F}{\text{Im } F}$ are given.

Résumé : Une revue est faite des théorèmes asymptotiques qui imposent des contraintes sur l'amplitude de diffusion élastique à partir des premiers principes : positivité, analyticité, unitarité. Ceci est fait à la lumière des récents résultats des I.S.R. qui indiquent une croissance avec l'énergie de la section efficace totale de la diffusion proton-proton qui pourrait se comporter comme $\log^2 s$. Les résultats concernant la section efficace différentielle (zéros vers l'avant, largeur du pic de diffraction, comportement de σ_{el}) ainsi que $\frac{\text{Re } F}{\text{Im } F}$ sont également donnés.

* Notes taken by D. SCHIFF.

The recent results from I.S.R. on total cross-sections have motivated a renewed interest in asymptotic theorems which constrain the scattering amplitude from first principles. We are in the same kind of situation as when the first Serpukhov results on $K^- p$ total cross-sections appeared and the validity of the Pomeranchuk Theorem was discussed. The subject of the present lecture is to review the general results which can be derived in presence of an asymptotic growth for the total cross-section.

1. Basic results - Froissart bound

From positivity, analyticity and unitarity [1] it is possible to derive the existence of a cut-off in the partial - wave series :

$$L_{Max} = \frac{k \log s}{2 m_\pi} \quad *$$

so that using the fact that

$$\sigma_{tot} \leq \frac{4\pi}{k^2} \sum_{o}^{L_{max}} (2\ell + 1) \qquad (1)$$

one finds the celebrated Froissart bound :

$$\sigma_{tot} \leq \frac{\pi}{m_\pi^2} (\log s)^2 \qquad (2)$$

---

* Notice the presence of m_π : $\frac{1}{2 m_\pi}$ is the maximum range of the "Yukawa tail" more and more effective with energy.

The only unknown in this inequality is the energy scale in the logarithm. A more refined result has recently been produced by Yndurain [2] and Common [3] who get a sum rule over the total cross-section which depends only on low energy parameters (and in the special case of $\pi\pi \rightarrow \pi\pi$ scattering, on no parameters at all). The factor $\frac{\pi}{m_\pi^2}$ is of the order of 60 mb to compare with .5 mb which is the coefficient of the $\log^2 s$ term obtained from a fit to total cross-section data.

2. Physical Predictions.

a) Elastic cross-sections

i) $\sigma_{tot} \sim \log^2 s$

In this case $\sigma_{el} \sim \log^2 s$. The proof goes as follows : writing Im F(s,0) as

$$\text{Im } F(s,0) \simeq \frac{1}{4\pi} s\, \sigma_{tot} = \sum_0^{L_{Max}} (2\ell+1)\, \text{Im } f_\ell \qquad (3)$$

and using Schwarz inequality :

$$\left| \sum_0^{L_{Max}} (2\ell+1)\, \text{Im } f_\ell \right|^2 \leq L_{Max}^2 \times \sum_0^{L_{Max}} (2\ell+1)\, |\text{Im } f_\ell|^2 \qquad (4)$$

which can be written :

$$\left(\frac{1}{4\pi} s\, \sigma_{tot} \right)^2 \leq \frac{1}{4\pi} L_{Max}^2\, s\, \sigma_{el} \qquad (5)$$

one finds :

$$\sigma_{el} > \frac{4 m_\pi^2}{\pi} \frac{\sigma_{tot}^2}{(\log s)^2} \qquad (6)$$

ii) $\sigma_{tot} \sim \log s$

The same type of argument leads to the conclusion that σ_{el} behaves like a constant.

b) Width of the diffraction peak.

One can define the width of the diffraction peak ΔT as given by :

$$\sigma_{el} \simeq \Delta T \times \left| \frac{F(s,0)}{s} \right|^2 \qquad (7)$$

which means that ΔT behaves like $\frac{1}{\log^2 s}$ if σ_{tot} and σ_{el} behave like $\log^2 s$. In the case where $\sigma_{tot} \sim \log s$, then $\Delta T \leq \frac{1}{\log s}$.

c) Structure of the diffraction peak

If σ_{tot} behaves like $\log^2 s$, it is convenient to introduce [3), 4)] the new variable τ:

$$\tau = t (\log s)^2 \qquad (8)$$

Auberson, Kinoshita and Martin [5)] have shown that

$$\lim_{s \to \infty} \frac{F(s,t)}{F(s,0)} = f(\tau) \qquad (9)$$

for finite arbitrarily large τ, that is for $|t| < c/\log^2 s$, where $f(\tau)$ is an entire function of order $\frac{1}{2}$. This function has an infinite number of zeros [5), 6)] close to the real axis which

accumulate around t = 0 but which might not be close enough to the physical region to produce oscillations. However S.M. Roy [7] proved that if

$$\sigma_{tot} > \frac{1}{2} \frac{\pi}{m_\pi^2} \log^2 s \qquad (10)$$

then $\frac{d\sigma}{dt}$ has necessarily a minimum (one indeed observes a diffraction minimum although .5 mb << 30 mb ?)

A most important consequence of the above considerations is that the differential cross-section cannot be fitted by an expression of the following conventional type :

$$\frac{d\sigma}{dt} \propto \exp \{ A(s)\, t + B(s)\, t^2 \} \qquad (11)$$

Examples of acceptable forms are :

$$F(s,t) = i\, s\, J_o (\sqrt{-t} \log s) (\log s)^2 \qquad (12)$$

proposed by Cheng and Wu [8]

and

$$F(s,t) = \frac{i\, s\, (\log s)^2}{(\sqrt{-t} \log s)^3} \left(1 - \frac{\sin(\sqrt{-t} \log s)}{\sqrt{-t} \log s} \right) \qquad (13)$$

proposed by Okun [9].

If $\sigma_{tot} \sim \ln s$, a behaviour

$$F(s,t) \sim i\, s \log s\, s^{\lambda t} \qquad (14)$$

is allowed, and the presence of complex zeros is not required. With the behaviour (14), one has $\sigma_{el} \sim \log s$ and $\Delta T \sim \frac{1}{\log s}$.

d) Real and Imaginary parts.

The essential tool, here, is analyticity with respect to energy $E_{lab} \cong \frac{s}{2M}$ which will be denoted by E.

We shall write the even-signature amplitude (predominantly imaginary) as :

$$F^+(E) \sim i\gamma^+ E (\log E)^{\beta^+} \qquad (15)$$

to dominant order in log E

and the odd-signature amplitude, predominantly real

$$F^-(E) \sim \gamma^- E (\log E)^{\beta^-} \qquad (16)$$

Unitarity constrains the variation domain of β^+ and β^- as indicated in the Cornille plot [10] drawn in Fig. 1.

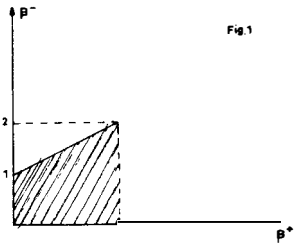


Fig.1

In particular if the real part behaves like s(log s), β^+ is necessarily equal to 0.

It is easy to see that expression (15) does not have the good crossing properties since $\log (E e^{i\pi}) = \log E + i\pi$. The correct expression is :

$$F^+(E) = i\gamma^+ E (\log E - \frac{i\pi}{2})^{\beta^+} \qquad (17)$$

and then, as first shown by Khuri and Kinoshita [11]

$$\frac{\text{Re } F^+}{\text{Im } F^+} = \frac{\pi \beta^+}{2} \frac{1}{\log E} \qquad (18)$$

In the same way, the odd signature amplitude should be written as :

$$F^-(E) = \gamma^- E (\log E)^{\beta^-} - \frac{i\pi}{2} \beta^- \gamma^- (\log E)^{\beta^- - 1} \qquad (19)$$

In the case where $\sigma_{tot} \sim \log^2 s$, which means that $\beta^+ = 2$, then

$$\frac{\text{Re } F^+}{\text{Im } F^+} = + \frac{\pi}{\log E} \qquad (20)$$

For pp scattering, one makes the additional assumption that $F^-(E)$ is negligible since $\sigma_{p\bar{p}} - \sigma_{pp}$ seems to decrease fast, and predicts :

$$\frac{\text{Re } F}{\text{Im } F} \text{ positive and equal to } \frac{\pi}{\log E} .$$

e) Pomeranchuk theorem

From the above considerations, one writes :

$$\begin{aligned} \sigma_{\text{particle}} + \sigma_{\text{antiparticle}} &\simeq \gamma^+ (\log E)^{\beta^+} \\ \sigma_{\text{particle}} - \sigma_{\text{antiparticle}} &\simeq \gamma^- \beta^- (\log E)^{\beta^- - 1} \end{aligned} \qquad (21)$$

and one shows that :

$$\left| \frac{\sigma - \bar{\sigma}}{\sigma + \bar{\sigma}} \right| < \text{const } (\log E)^{\beta^- - \beta^+ - 1} \qquad (22)$$

but from the Cornille plot, one knows that

$$\beta^- - 1 < \frac{\beta^+}{2}$$

so that

$$\left| \frac{\sigma - \bar{\sigma}}{\sigma + \bar{\sigma}} \right| < \text{const } (\log E)^{-\frac{\beta^+}{2}} \qquad (23)$$

In the particular case of pp scattering, assuming that $\sigma_{tot} \sim (\log s)^2$, one finds :

$$\left| \frac{\sigma_{pp} - \sigma_{\bar{p}p}}{\sigma_{pp} + \sigma_{\bar{p}p}} \right| < \text{const } (\log s)^{-1} \qquad (24)$$

Bourrely and Fischer [12] have made a fit to total cross-section pp data and to the pp data for the ratio Re F / Im F which will be denoted by ρ, with an expression of the form :

$$F(E) = - b_1 (M^2 - E^2)^{\frac{1}{2}} \left(1 + b_2 \log(b_3 + b_4 (M^2 - E^2)^{\frac{1}{2}}) \right) - b_5 (E - E_1)^{\frac{1}{2}} + b_6 + 2\pi f^2 \frac{1}{E - E_p} \qquad (25)$$

where $E_1 = m - 2\frac{m_\pi^2}{m}$, $E_p = m - \frac{m_\pi^2}{2m}$, $f^2 = .08$

(m = nucleon mass)

The result of the 4 - parameter fit (b_1, b_2 , b_3 , b_4) to data on σ_{pp} is shown on Fig. 2. The proton - antiproton total cross-section is fit by an extra parameter : b_5 . The best fit is also shown on Fig. 2. ρ is obtained from (25) by adjusting the substraction constant b_6 and the fit is shown on Fig. 3 : ρ becomes positive near E = 300 GeV ; for E $\simeq$ 2000 GeV, ρ takes a value of about 10 % , and for E $\simeq 2.\ 10^5$ GeV, it becomes maximum, equal to 20 % . The prediction for $\rho_{\bar{p}p}$ is given

in Fig. 3.

f) "Pomeranchuk Theorem" for elastic diffraction-peaks

Finally, let us mention that it can be proved [13], from positivity properties, that

$$\lim_{s\to\infty} \frac{d\sigma}{dt}(pp) \;/\; \frac{d\sigma}{dt}(\bar{p}p) = 1$$

and if $\Delta T \to 0$, which is the case for an asymptotically growing total cross-section

$$\lim_{s\to\infty} \Delta T(pp) \;/\; \Delta T(\bar{p}p) = 1$$

and also in this situation

$$\lim_{s\to\infty} \sigma_{el}(pp) \;/\; \sigma_{el}(\bar{p}p) = 1.$$

REFERENCES

1) A. Martin, Nuovo Cim. 42A, 920 (1966) and 44A, 1219 (1968)
L. Lukaszuk and A. Martin, Nuovo Cim. 52, 122 (1967)

2) F. Yndurain, Phys. Lett. 31 B, 368 (1970)
A.K. Common CERN preprint TH1145 (1970)

3) R.C. Casella, Phys. Rev. Lett. 24, 1463 (1970)

4) J. Finkelstein, Phys. Rev Lett. 24, 172 (1970)

5) G. Auberson, T. Kinoshita and A. Martin, Phys. Rev. D3, 3185, (1971)

6) R.J. Eden and G. Kaiser, Nucl. Phys. B28, 253 (1971)

7) S.M. Roy, Phys. Lett. 34B, 407 (1971)

8) H. Cheng and T.T. Wu, Phys. Rev. Lett. 24, 1456 (1970)

9) L.B. Okun and V.S. Popov, unpublished (1970)

10) H.Cornille, Nuovo Cim. Lett. 4, 267 (1970)

11) N. Khuri and T. Kinoshita, Phys. Rev. 140B, 706 (1965)

12) C. Bourrely and J. Fisher, CERN preprint TH1652 (1973)

13) H. Cornille and A. Martin, Phys. Lett. 40B, 671 (1972)

14) U. Amaldi et al. Phys. Lett. 43B, 231 (1973)

15) U. Amaldi et al. CERN preprint, January 1973

16) S.R. Amendolia et al. CERN preprint, February 1973

17) M. Holder et al. Phys. Lett. 35B, 361 (1971)

18) F.T. Dao et al. Phys. Rev. Lett. 29, 1627,(1972)

19) G. Charlton et al. Phys. Rev. Lett. 29, 515 (1972)
J.W. Chapman et al. Phys. Rev. Lett 29, 1686 (1972)
S.R. Denisov et al. Phys. Lett. 36B, 415 (1971)
see also a compilation :
CERN-HERA 70-2 (1970) and LBL-58 (1972)

20) Q.Y.Dumbrais, Yadernaya Fiz. 13, 1096 (1971) (English translation : Soviet J. Nuclear Phys. 13, 626 (1971))

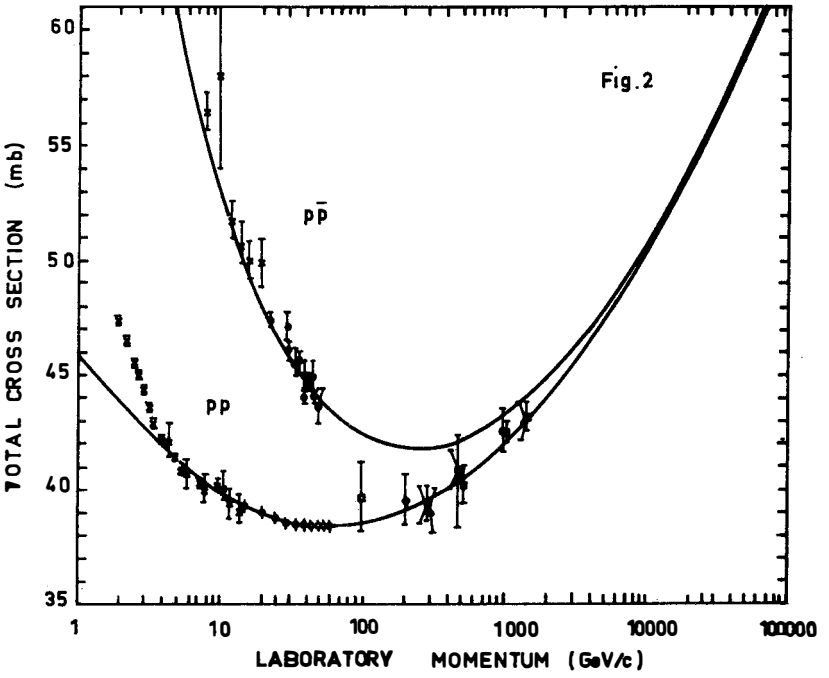
21) K.J. Foley et al. Phys Rev. Lett. 19, 857 (1967)

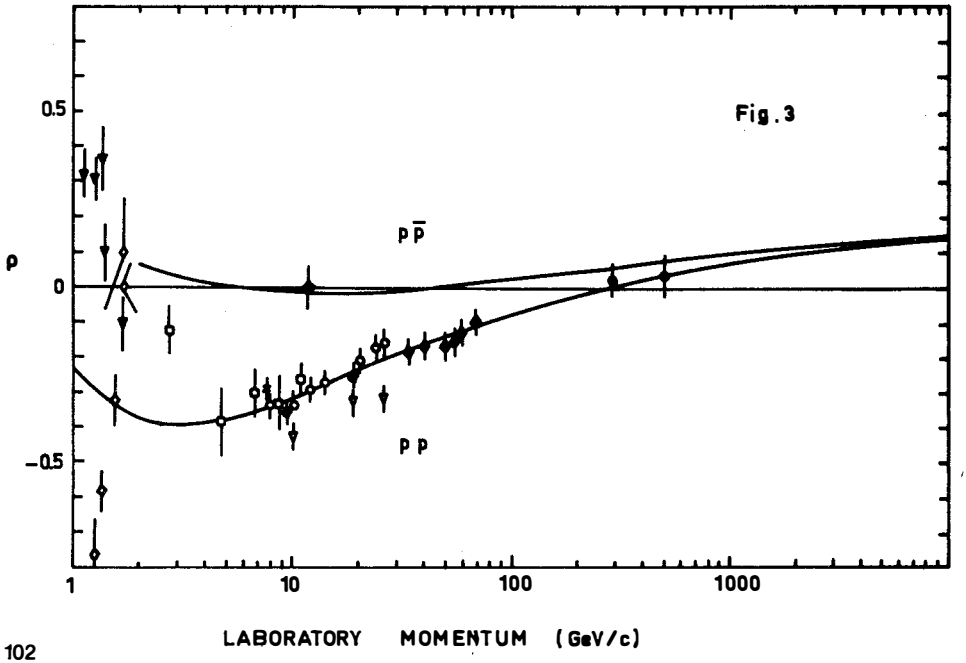
FIGURE CAPTIONS

Fig. 1 The Cornille plot [10]

Fig. 2 Plot taken from Bourrely and Fisher [12] of total pp and $p\bar{p}$ cross-sections in parametrization (25). Data taken from refs. 14 -18, 19)

Fig. 3 Energy dependence of ρ_{pp} and $\rho_{p\bar{p}}$. Data taken from refs. 14, 20, 21).


Fig.2
TOTAL CROSS SECTION (mb)
60
55
50
45
40
35
pp̄
pp
1
10
100
1000
10000
100000
LABORATORY MOMENTUM (GeV/c)


Fig.3
ρ
0.5
0
-0.5
pp̄
pp
1
10
100
1000
LABORATORY MOMENTUM (GeV/c)

DYNAMICS OF STRONG INTERACTIONS

F.E. LOW

Laboratory for Nuclear Science and Department of Physics, Massachusetts Institute of Technology, Cambridge Massachusetts.

Cet exposé a été publié dans les Comptes-Rendus de la 16ème Conférence Internationale sur la Physique des Hautes Energies. Vol. 3 P. 459.

This talk has been published in the Proceedings of the XVI International Conference on High Energy Physics. Vol. 3 p. 459.






THE IMPORTANCE OF THE STRUCTURE OF THE POMERON

A.R. White
CERN, Geneva, Switzerland

Abstract: The derivation of the two-Pomeron cut discontinuity and decoupling results for Pomeron vertices from both the t-channel and the s-channel is discussed. It is emphasized that it is essential to consider the structure of the Pomeron in terms of its s-channel intermediate states, if consistency between the s- and t-channel results is to be achieved.

Résumé : On discute l'obtention de la discontinuité de la coupure à deux Pomerons et les résultats concernant l'annulation des couplages du Pomeron à la voie s ou à la voie t. L'accent est mis sur le fait qu'il est essentiel de considérer la structure du Pomeron en termes des états intermédiaires de la voie s, pour sauvegarder la consistence des résultats de la voie t et de la voie s.

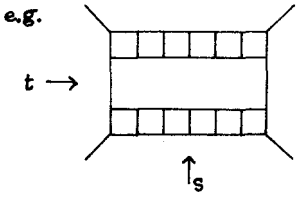


THE IMPORTANCE OF THE STRUCTURE OF THE POMERON

The whole of this talk will be based on the assumption that the Pomeron is a simple factorisable Regge pole (with intercept one) accompanied by the associated multi-Pomeron cuts which t-channel unitarity certainly requires. This is the only j-plane structure for the Pomeron which is known to be consistent with t-channel unitarity. I shall talk about both the sign of the two-Pomeron cut and the decoupling results for the Pomeron which are derived from s-channel unitarity. The common message will be that it is essential to consider the "structure" of the Pomeron in terms of its s-channel intermediate states if consistency between s-channel and t-channel results is to be achieved.

Regge cuts from t-channel unitarity

Because of its technical complexity this is a difficult subject to explain simply. It was a long time ago that Mandelstam[1] originally emphasized that the Feynman graphs which are associated with the exchange of two Regge poles, and which might be thought to give rise to Regge cuts, have a simpler intermediate state structure in the t-channel than in the s-channel.

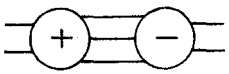


The sum over graphs of this form is associated with many s-channel states but essentially only with the four-particle state in the t-channel. More specifically since it is the asymptotic limit $s \to \infty$ with t fixed which we want to consider, we can clearly consider this limit in the neighbourhood of

the lowest intermediate state in the t-channel, which is the four-particle state. In fact it was by considering the t-channel discontinuity that Mandelstam was able to show that the set of graphs shown above does not give rise to a two-Reggeon cut but the set of graphs where the ladders are joined by non-planar couplings does.

Mandelstam's work suggested therefore that the two-Reggeon cut could be studied through the four-particle unitarity integral. In principle the asymptotic behaviour of this integral can be studied in terms of its Froissart-Gribov continuation to complex j. Not long after Mandelstam's work Gribov, Pomeranchuk and Ter-Martirosyan[2] suggested a general S-matrix approach to this problem which was based on Mandelstam's analysis. In fact I shall illustrate this approach by considering the three-particle integral

I =



in which the Reggeon-particle cut is generated. This is simpler to consider than the four-particle integral and although the Reggeon-particle cut does not contribute to the high-energy behaviour for negative t it is otherwise analogous to the two-Reggeon cut.

We consider first the partial wave projection of the integral

$$I_j(t) = \frac{1}{16(2\pi)^3 3!} \int_{4m^2}^{(t^{\frac{1}{2}}-m)^2} dt_1 \, \frac{\lambda^{\frac{1}{2}}(t,t_1,m^2)}{t} \left(\frac{t_1 - 4m^2}{t_1}\right)^{\frac{1}{2}} \times \sum_{|n|\leq j} \sum_{\ell \geq |n|} a_{j\ell n}(t,t_1)\, \bar{a}_{j\ell n}(t,t_1) \qquad (1)$$

where ℓ, n, t_1 label the angular momentum, helicity, and energy of a selected pair of the three intermediate state particles. Gribov et al. then showed that if it was assumed that the multiple partial-wave projections $a_{j\ell n}$ had Froissart-Gribov continuations to complex j, ℓ, n and that the Froissart-Gribov continuation of (1) could be obtained by performing Sommerfeld-Watson transformations on the sums over n and ℓ, then a cut would be generated as expected.

Unfortunately, subsequent investigation[3,4] of these technical assumptions suggested that this approach could not be carried through and Gribov moved back to perturbation theory to justify the construction of a Reggeon Field Theory description of Regge cuts[5]. In fact, I have now shown that these technical problems can be overcome. Ignoring odd signature contributions the continuation of (1) to complex j can be written in the form[6]

$$I(j,t) = \frac{-1}{64(2\pi)^3 3!} \int_{4m^2}^{(t^{\frac{1}{2}}-m)^2} dt_1 \, \frac{\lambda^{\frac{1}{2}}(t,t_1,m^2)}{t} \left(\frac{t_1 - 4m^2}{t_1}\right)^{\frac{1}{2}} \tag{2}$$

$$\times \sin\frac{\pi}{2} j \int \frac{dn}{\sin\frac{\pi}{2} n} \sum_{\substack{\ell-n=0 \\ \ell+n=0}}^{\infty} \frac{a(j,\ell,n)\, a^{-}(j,\ell,n)}{\sin\frac{\pi}{2}(j \mp n)} .$$

The basic points in deriving this result were the use of multiple integral representations of amplitudes to define the continuations $a(j,\ell,n)$ and the proper treatment of the helicity sum. This sum is written as a helicity contour integral with the contour in the form shown in Fig. 1.

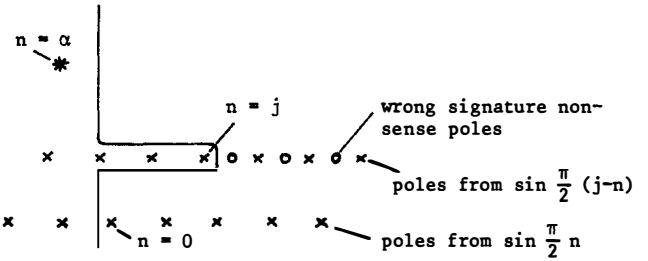


Fig. 1 Helicity contour

At even integer j the two sets of poles shown in the figure pinch the contour to give a pole whose residue is a finite sum over helicities and which is isolated by the factor sin π/2 j in (2). The proper treatment of helicity continuations and sums is also important in the development of a Sommerfeld-Watson approach to multi-Regge theory[6,7].

We can now discuss the generation of a cut in (2) [8]. A Regge pole at $\ell = \alpha$ in $a(j,\ell,n)$ will give poles in the n-plane at $n = \alpha$, $\alpha - 1$, ... in the sum over $(\ell - n)$ in (2). The amplitudes $a(j,\ell,n)$ and $\bar{a}(j,\ell,n)$ will have nonsense wrong-signature inverse square root branch-points at $j = n - 1$. The product of these will give a pole at $j = n - 1$ which can pinch with the pole at $n = \alpha$ to give a pole in the integral over t_1 in (2) at $j = \alpha(t_1) - 1$. Using $N_\alpha(j,t)$ to denote the "fixed-pole residue" of $a(j,\ell,n)$ at $j = n - 1$, $n = \ell = \alpha$ we can write the relevant part of (2) in the form

$$\sin\tfrac{\pi}{2} j \, \frac{i}{16(2\pi)^3 3!} \qquad (3)$$

$$\int_{4m^2}^{(t^{\frac{1}{2}}-m)^2} dt_1 \, \frac{\lambda^{\frac{1}{2}}(t,t_1,m^2)}{t} \left(\frac{t_1 - 4m^2}{t_1}\right)^{\frac{1}{2}} \frac{N_\alpha(j,t)\bar{N}_\alpha(j;t)}{\sin\frac{\pi}{2}\alpha(t_1)\,[j - \alpha(t_1) + 1]}$$

Now we can see that when the pole at $j = \alpha(t_1) - 1$ hits the end point of the integral at $t_1 = (t^{\frac{1}{2}} - m)^2$ there will be a singularity at

$$j = \alpha\left[(t^{\frac{1}{2}} - m)^2\right] - 1 \ . \tag{4}$$

This is the Mandelstam or Reggeon-particle cut. Further manipulation of the unitarity equations satisfied by $N_\alpha(j,t)$ gives the discontinuity across the cut in the form

$$\text{disc } a(j,t) = \tag{5}$$

$$\frac{i \sin \frac{\pi}{2} j}{8} \int_{t=(t^{\frac{1}{2}}-m)^2}^{} dt_1 \frac{\lambda^{\frac{1}{2}}(t,t_1,m^2)\delta\left[j - \alpha(t_1) + 1\right]N_\alpha(j^+,t)N_\alpha(j^-,t)}{t \sin \frac{\pi}{2} \alpha(t_1)} \ .$$

Pictorially we can represent the generation of the cut by



(6)

So the discontinuity is given in terms of the fixed-pole residue of the three-particle/Reggeon amplitude.

The generation of the two-Reggeon cut in the four-particle unitarity integral can be discussed in exactly the same way.



(7)

The discontinuity now involves the fixed-pole residue of the two particle/two Reggeon amplitude $N_{\alpha_1,\alpha_2}(j,t)$

$$\underset{\substack{\text{2 Reggeon}\\ \text{cut}}}{\text{disc}}\ a(j,t) =$$

$$-\frac{i \sin\frac{\pi}{2} j}{2^5}\int_{t_1^-}^{t_1^+} dt_1 dt_2\ \frac{\left[-\lambda(t,t_1,t_2)\right]^{-\frac{1}{2}}\ \delta\left[j - \alpha_1(t_1) - \alpha_2(t_2) + 1\right]}{t \sin\frac{\pi}{2}\alpha_1 \sin\frac{\pi}{2}\alpha_2}$$

$$\times N_{\alpha_1\alpha_2}(j^+,t) N_{\alpha_1\alpha_2}(j^-,t) \ . \qquad (8)$$

The real analyticity property of $N_{\alpha_1\alpha_2}$ gives that

$$\frac{\lambda}{t} N(j^+)N(j^-) = \left|\left(\frac{\lambda}{t}\right)^{\frac{1}{2}} N(j^+)\right|^2 \qquad (9)$$

and the sign of the imaginary part of (8) is determined to be negative.

So if $\alpha_1 = \alpha_2 =$ Pomeron we have the result that the two Pomeron cut contributes negatively to the total cross-section. It is very difficult to give a simple explanation of why the sign comes out negative except to point out that the method is clearly independent of the strength of the couplings in the theory and so is the sign. This means that the sign must be the same as that obtained from the Mandelstam graphs in weak-coupling perturbation theory. It is not possible therefore to look for a positive sign[9] from the complicated analytic continuation from positive to negative t which we have not discussed. A complete discussion of this continuation will be given in a future paper[10].

Regge cuts from the s-channel

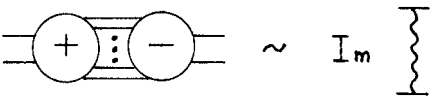
There have been many attempts to understand Regge cuts through the s-channel and the most recent are the papers by Abarbanel[11] and Chew[9] which obtain a positive sign for the two-Reggeon discontinuity. This positive sign is obtained by considering only the contributions to the two-Reggeon cut coming from multi-Reggeon production amplitudes. However, once an s-channel structure for a Reggeon is admitted a second method of generation of the cut becomes available and it is this which ultimately gives the negative sign for the cut. This point has recently been emphasized by Halliday and Sachrajda[12] in a detailed study of weak-coupling perturbation theory. Essentially the same point has been made in the past by Caneschi[13], and also by Dash, Fulco and Pignotti[14] and more recently by Blankenbecler[15] and by Neff[16]. The argument has usually been presented in terms of unitarity corrections to multi-Regge exchange changing the sign of the AFS cut[17]. Neff has phrased the argument in terms of the currently popular two-component model of particle production and this is probably the easiest to understand.

Two production mechanisms are assumed which can be pictorially represented as



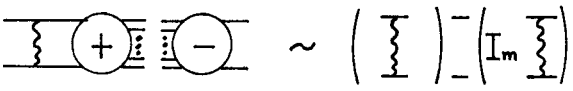
(10)

The first mechanism is some general multiperipheral "single fireball" production mechanism which builds up the constant total cross-section



(11)

where $\overline{\overline{\overline{

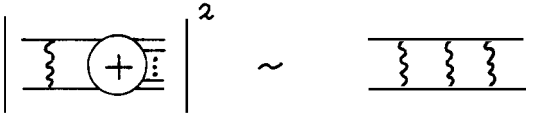


(14)

$$\equiv T\ i\ \mathrm{Im}\ T \tag{15}$$

Since the Pomeron is pure imaginary this gives a negative contribution to the two Pomeron cut. Since there are two interference terms of this sort they give exactly twice the AFS contribution and so exactly reverse the sign of this contribution.

The positivity of the total cross-section is maintained by adding



(16)

which gives a three Pomeron cut. We, therefore, see that the negative sign of the two-Pomeron cut is explicitly compensated for by the positive sign of the three-Pomeron cut.

The above argument is clearly over-simplified and incomplete but it can be made part of an iterative solution of the unitarity equations[13-15] and the reversal of the sign of the two-Pomeron cut remains. The above argument also describes in essence the way an overall negative sign emerges for the Mandelstam graphs in perturbation theory. Of course, the contribution from the two-particle intermediate state is exactly cancelled in perturbation theory and we have to consider at least the four-particle intermediate state so

that non-planar couplings of the Pomerons are allowed. However, Halliday and Sachrajda have shown that for the Mandelstam graphs the overall negative sign comes from s-channel "cuts" through the graph of the form shown in Fig. 2a which exactly reverse the sign of the contributions from cuts through the graphs of the form of Fig. 2b. Therefore cuts through a Reggeon exactly reverse the sign of contributions from cuts which leave the Reggeon untouched.

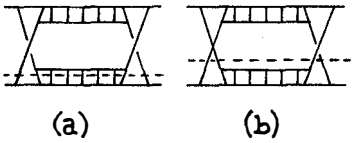


Fig. 2

So the negative sign of the two-Pomeron cut is directly related to the vital equation (11) above. This equation says simply that the Pomeron has a structure in terms of s-channel intermediate states[9]. This effect is neglected in the s-channel discussion of cuts by Abarbanel[11] and by Chew[9] and also in the sum rule treatment of cuts given by Kang, Moore and Nicolescu[18]. This is why these authors obtain a positive sign. Since it is t-channel iteration which forces a Regge pole to look something like a Feynman ladder graph and so have many s-channel intermediate states it is not surprising that it is necessary to take this structure into account to obtain consistency between the s- and t-channel.

Pomeron decoupling theorems

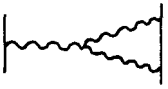
We now want to discuss the relevance of the structure of the Pomeron to the decoupling results that have been derived from s-channel unitarity expressed in the form of inclusive sum rules. The final consequence of these arguments is that a Pomeron pole with intercept

one must decouple from the total cross-section. Since the total cross-section would then be given by the two-Pomeron cut it is clear that this decoupling cannot be consistent with the negative sign cut. Since the negative sign of the cut is connected with the structure of the Pomeron it must be important to consider this structure in the decoupling arguments.

The first constraint derived from the unitarity sum rules was the triple Pomeron zero.

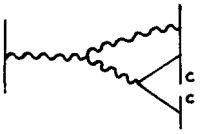
The triple Pomeron zero

If the triple Pomeron coupling $\succ$ which appears in the triple Pomeron contribution to the one-particle inclusive cross-section does not vanish when all three Pomerons have zero mass, then integrating this contribution will give a total cross-section increasing like log log s. It is therefore concluded that the zero mass triple Pomeron coupling must vanish[19]. However, once a structure is allowed for the Pomeron the situation becomes much more subtle. Pictorially the integral of the triple-Pomeron coupling can be represented as



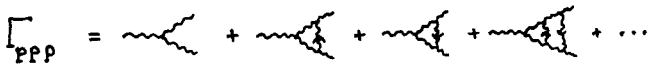
The loop integral is now analogous to that considered above for the AFS cut. This suggests that if we take account of the structure of the Pomeron then there may be cancellations analogous to the cancellation of the AFS cut that we have already discussed. In fact Halliday and Sachrajda have shown that in the Feynman ladder graph model this

contribution would be exactly cancelled by diagrams of the form (the momentum of particle c being integrated over)



where the Reggeon has been "cut open" at one end. The ladder graph model cannot give a Pomeron with unit intercept but Halliday and Sachrajda show that in general a contribution of this form will produce a negative log log s contribution to the total cross-section. Of course, if this diagram does cancel the triple Pomeron contribution then since it is non-leading relative to the triple Pomeron contribution in the internal triple Pomeron limit, it must give a negative contribution to the inclusive cross-section in some region of phase space. Again this negative contribution may be cancelled by yet further contributions-possibly associated with multi-Pomeron cuts. We can say therefore that the ladder model does not give a concrete example of how the vanishing of the triple-Pomeron coupling may be avoided but it does suggest that the structure of a Pomeron will be such as to make the whole discussion of the asymptotic behaviour of sum rule integrals highly non-uniform. As a result it is not possible to make any statement about how the sum rules are satisfied once contributions to multiparticle amplitudes are allowed which do not correspond to any simple Regge diagrams but rather to unitarity cuts through Reggeons. These contributions cannot be considered in detail without a knowledge of the structure of a Reggeon.

Although the sum rule cannot be said to require the triple Pomeron zero the zero does seem to be required by t-channel unitarity. t-channel unitarity gives the Regge cut discontinuity formulae, and these formulae can be regarded as unitarity equations governing the interaction of a Reggeon pole with its cuts. These equations can be solved using either S-matrix or field theory techniques. The zero mass triple Pomeron vertex which appears in the inclusive cross-section can be identified with the triple Pomeron vertex governing the interaction of a Pomeron pole with its cuts. In a Reggeon field theory the decoupling comes about from requiring that the bare Pomeron intercept of one not be renormalized. In this context the triple Pomeron decoupling was discovered four years ago by Gribov and Migdal[20]. Bronzan[21] has considered a model containing just sums over Pomeron ladder graphs which simply illustrates this point. In this model



where the lines represent Pomerons. The integral equation for Γ_{ppp} given by this model has an effective singular potential coming from the unrenormalized Pomeron exchange in the rungs of the ladders. This singular potential leads directly to Γ_{ppp} vanishing at the zero mass point.

From the S-matrix point of view the triple Pomeron decoupling can be understood as resulting from the collision of the Pomeron pole

and two-Pomeron cut[22]. The Pomeron amplitudes ≈O≈, ≈O≈ and ⊐O⊏ have the N/D representations[2,8]

$$\approx O \approx = \frac{1}{B(t,j) + \frac{1}{\alpha'\left(\frac{1}{4}t\right)} \log\left[j - \alpha_c(t)\right]} \tag{17}$$

$$\approx O \approx = \frac{A^{\frac{1}{2}}}{B(t,j) + \frac{1}{\alpha'\left(\frac{1}{4}t\right)} \log\left[j - \alpha_c(t)\right]} \tag{18}$$

$$\sqsupset O \sqsubset = \frac{A(t,j)}{B(t,j) + \frac{1}{\alpha'\left(\frac{1}{4}t\right)} \log\left[j - \alpha_c(t)\right]} \tag{19}$$

where A and B do not have the two-Pomeron cut at $j = 2\alpha_c(t) = 2\alpha_p(t/4) - 1$. To obtain a self-consistent Pomeron trajectory from the denominator in these equations and to obtain the negative sign for the two-Pomeron cut it is necessary[23] to have a second order CDD pole in A and B which passes through $j = 1$ at $t = 0$. This pole is arranged to give a finite Pomeron contribution to ⊐O⊏ at $t = 0$, but because $A^{\frac{1}{2}}$ appears in (18) in contrast to the A in (19) the Pomeron contribution to ≈O≈ vanishes at $t = 0$ giving the required triple Pomeron decoupling. The presence of CDD poles in the N/D representation is directly related to the singular potential that appears in the field theory approach to the problem.

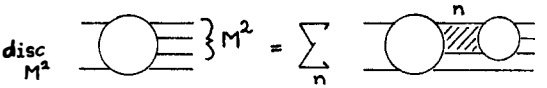
Cardy[24] has recently shown that this mechanism which produces the triple Pomeron zero also suppresses cut contributions to the inclusive triple Pomeron limit by $(\log M^2)^{-2}$ instead of the single logarithm characteristic of cut contributions to two-body processes.

Finally, we consider the implications of the triple Pomeron zero.

The Reggeon-Pomeron-particle vertex

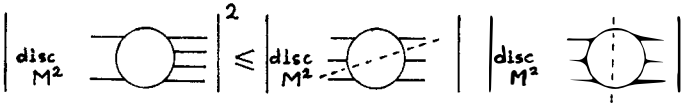
There have been two arguments given that the zero in the triple Pomeron vertex has implications for the Reggeon-Pomeron-particle vertex. The aim is to show that the vertex R–P vanishes when the Pomeron has zero mass. This result can then be continued to the particle pole on the Reggeon trajectory to conclude that the Pomeron must decouple from the total cross-section[25].

Abarbanel, Gribov and Kanchelli[26] considered the subenergy discontinuity formula



(20)

Using the Schwartz inequality together with the Mueller discontinuity formula gives



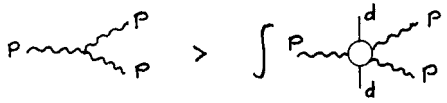
(21)

Taking the multi-Regge limit $\sum$ and choosing the quantum numbers of the particles so that the two outer exchanges are Pomerons but the central one is a Reggeon, and going to zero mass of the Pomerons, gives an inequality which can be written in the form

$$|A \text{ Disc } (R\text{–}P)|^2 \leq \left| \begin{array}{c} P \\ \diagdown \quad \diagup \; P \\ \diagup \quad \diagdown \\ P \end{array} \right| \; |B| \qquad (22)$$

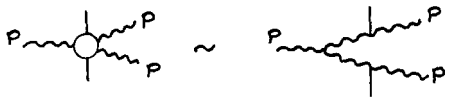
The vanishing of the right-hand side then requires the left-hand side to vanish and this appears to give the required result. However, it was shown by Moen and White[27] that taking the discontinuity of R–P removes that part of the vertex giving the total cross-section. In this case taking account of the singularity structure of the Reggeon is sufficient to weaken the otherwise strong result.

Another derivation of the vanishing of the R–P vertex has been given by Jones, Low, Tye, Veneziano and Young[28]. They consider the inclusive sum rule relating the one and two-particle inclusive cross-sections and obtain an inequality which pictorially we can represent as



(23)

The vanishing of P–P at zero Pomeron mass then requires –○– to vanish similarly. Taking the internal Regge limit so that



and using factorisation then requires ∽ to vanish. Since particle d can carry quantum numbers the internal exchange can be a Reggeon and this gives the required result. If both the amplitudes involved here contained only Regge poles so that the Pomeron contributions gave the leading asymptotic behaviour even in $t < 0$ then this result could only be avoided if non-uniformities were present at $t = 0$ which we do not expect to be the case for Regge pole amplitudes. However, once cuts are taken into account, together with the structure of

Reggeons and Pomerons, then non-uniformity of the asymptotic limits involved can again be expected to prevent this argument going through for analogous reasons to those we discussed when considering the vanishing of the triple Pomeron vertex. This has been discussed by Cardy and White in the context of the Feynman ladder graph model[10,29].

REFERENCES

1) S. Mandelstam, Nuovo Cimento 30, 1127, 1143 (1963).

2) V.N. Gribov, Y.Ya. Pomeranchuk and K.A. Ter-Martirosyan, Yad. Fiz. 2, 361 (1965); Phys. Rev. 139 B, 184 (1965).

3) Ya.I. Azimov, A.A. Anselm, V.N. Gribov, G.S. Danilov and I.T. Dyatlov, JETP (Sov. Phys.) 21, 1189 (1965), JETP (Sov. Phys.) 22, 383 (1966).
Ya.I. Azimov, Sov. J. Nuclear Phys. 10, 482 (1970).

4) I.T. Drummond, Phys. Rev. 140 B, 1368 (1965); Phys. Rev. 153, 1565 (1967).
I.T. Drummond and G.A. Winbow, Phys. Rev. 161, 1401 (1967).
G.A. Winbow, Phys. Rev. 171, 1517 (1968).

5) V.N. Gribov, JETP (Sov. Phys.) 26, 414 (1968).

6) A.R. White, Nuclear Phys. B39, 432, 461 (1972).

7) P. Goddard and A.R. White, Nuovo Cimento 1 A, 645 (1971).
J.H. Weis, Phys. Rev. D6, 2823 (1972).
H.P.I. Abarbanel and A. Schwimmer, Phys. Rev. D6 (1972).
A.R. White, CERN preprint, to appear.

8) A.R. White, Nuclear Phys. B50, 93, 130 (1972).

9) G.F. Chew, Berkeley preprint LBL 1338 (1972).

10) J.L. Cardy and A.R. White, in preparation.

11) H.D.I. Abarbanel, Phys. Rev. D6, 2788 (1972).

12) I.G. Halliday and C.T. Sachrajda, Imperial College preprint ICTP 73/18 (1973).

13) L. Caneschi, Phys. Rev. Letters 23, 254 (1969).

14) J.W. Dash, J.R. Fulco and A. Pignotti, Phys. Rev. D1, 3164 (1970).

15) R. Blankenbecler, SLAC-TN-72-13 (1972) unpublished.

16) T.L. Neff, Berkeley preprint LBL 1544 (1973).

17) D. Amati, A. Stanghellini and S. Fubini, Nuovo Cimento 25, 626 (1962).

18) K. Kang, R.W. Moore and B. Nicolescu, Paris preprint IPNO/TH/73/3.

19) H.P.I. Abarbanel, G.F. Chew, M.L. Goldberger and L.M. Saunders, Phys. Rev. Letters 26, 937 (1971).
C.E. DeTar, D.Z. Freedman and G. Veneziano, Phys. Rev. D4, 1906 (1971).
C.E. DeTar and J.H. Weis, Phys. Rev. D4, 3141 (1971).

20) V.N. Gribov and A.A. Migdal, Sov. J. Nuclear Phys. 8, 583 (1969).

21) J.B. Bronzan, Phys. Rev. D7, 480 (1973).

22) J.B. Bronzan, Phys. Rev. D6, 1130 (1972).
P. Goddard and A.R. White, Phys. Letters 38 B, 93 (1972).
I.J. Muzinich, F.E. Paige, T.L. Trueman and L.L. Wang, Phys. Rev. D6, 1048 (1972).

23) J.B. Bronzan, Phys. Rev. D4, 1097 (1971).

24) J.L. Cardy, CERN preprint TH 1625 (1973).

25) R.C. Brower and J.H. Weis, Phys. Letters 41 B, 631 (1972).

26) H.D.I. Abarbanel, V.N. Gribov and O.V. Kanchelli, Phys. Rev., to be published.

27) I.O. Moen and A.R. White, Phys. Letters 42 B, 75 (1972).

28) C.E. Jones, F.E. Low, S.-H. Tye, G. Veneziano and J.E. Young, Phys. Rev. D6, 1033 (1972).

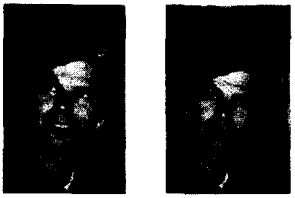
29) J.L. Cardy and A.R. White, CERN preprint TH 1596 (1972).

REGGEON THEORY OF DIFFRACTION SCATTERING

M. Baker
Physics Department, University of Washington
Seattle, Washington 98195 (USA)

Abstract: Gribov's theory of the Pomeron is reviewed and compared to the recent ISR proton-proton elastic scattering data.

Résumé : On compare la théorie de Gribov du Pomeron aux récentes données expérimentales pour la diffusion élastique proton-proton aux ISR.



The assumption of the existence of a Regge pole $\alpha(t)$ with intercept $\alpha(0) = 1$ leads to a scattering amplitude $T(s,t)$ which for large s and small t can be expressed as a series of inverse powers of $(\ell n\ s/s_0)$. In this talk I will review the arguments of Gribov[1] which lead to this series and will then discuss some work done by J. N. Ng and U. P. Sukhatme[2] in comparing this theory[3] with the high energy p-p scattering experiments at the CERN ISR.[4]

Let us consider the elastic scattering of two particles

$$p_1 + p_2 \to p_3 + p_4 \tag{1}$$

where p_i are the four momenta of the initial and final particles and where their spin has been neglected. Let $s = (p_1 + p_2)^2$ and $t = (p_3 - p_1)^2$. Then for $s \to \infty$ and small fixed t we have $t \underset{\sim}{\sim} -\vec{\kappa}^2$ where $\vec{\kappa}$ is a two dimensional space-like vector perpendicular to the incident direction. We define a scattering amplitude $T(s,t)$ normalized so that

$$\sigma_{Tot}(s) = \frac{1}{s}\ \mathrm{Im}\ T(s,0) \tag{2}$$

and

$$\frac{d\sigma(s,t)}{dt} = \frac{1}{16\pi s^2}\ |T(s,t)|^2 \tag{3}$$

Then for large s and fixed t, $T(s,t)$ can be expressed in terms of the analytically continued positive signature t channel partial wave amplitude $T(j,t)$ by a Sommerfeld-Watson integral,

$$\frac{T(s,t)}{8\pi s} = \int_C \frac{dj}{2\pi i} \left(\frac{s}{s_0}\right)^{j-1} \eta(j)\ T(j,t) \tag{4}$$

where s_o is an arbitrary scale factor,

$$\eta(j) = -e^{-i\pi j/2}/\sin\pi j \quad , \tag{5}$$

and the integral goes over a contour C in the complex j plane along a line parallel to the imaginary j axis which lies to the right of all the singularities in T(j,t).

If T(j,t) has a pole at $j = \alpha(t)$ as depicted in Fig. 1, then

$$T(j,t) \underset{j \sim \alpha(t)}{=} \frac{g_a(t)g_b(t)}{j-\alpha(t)} \tag{6}$$

where a and b label the kind of incident particles. Then

$$\frac{T(s,t)}{8\pi s} \underset{s \to \infty}{\to} g_a(t)g_b(t)\left(\frac{s}{s_0}\right)^{\alpha(t)-1} \eta(\alpha(t)) \quad . \tag{7}$$

We assume that $\alpha(0) = 1$. Then the total cross section remains constant as $s \to \infty$. For small t or $\vec{\kappa}^2$, we can expand the resulting Pomeranchuk trajectory $\alpha(t)$ as

$$\alpha(t) = 1 + \alpha' t = 1 - \alpha'\vec{\kappa}^2 \quad . \tag{8}$$

Following Gribov we denote

$$\omega \equiv j - 1 \quad . \tag{9}$$

Then $T(j,t) \equiv T(\omega,\vec{\kappa})$ and the pole formula (6) becomes

$$T(\omega,\vec{\kappa}) = \frac{g_a(\vec{\kappa})g_b(\vec{\kappa})}{\omega+\alpha'\vec{\kappa}^2} \quad . \tag{10}$$

Formula (10), as depicted in Fig. 1b, can then be interpreted as the

amplitude for the virtual production and subsequent decay of a two dimensional nonrelativistic quasi-particle of energy $-\omega$ and momentum $\vec{\kappa}$. The energy-momentum relation of a real quasi-particle is $\varepsilon_o(\vec{\kappa}) = \alpha'\vec{\kappa}^2$. The external particles a and b can then be regarded as providing sources $g_a(\vec{\kappa})$ and sinks $g_b(\vec{\kappa})$ for the quasi-particle.

The next most complicated process occurs when particles a and $\bar{a}$ each decay into two constituents each of which act as sources of Reggeons. This process is depicted in Fig. 2. In this case the $a\bar{a}$ pair acts as a source for the production of two Reggeons via the amplitude depicted in Fig. 3a. Figure 3a is the simplest example of a more general two Reggeon production amplitude which is denoted by the two particle two Reggeon vertex of Fig. 3b. The corresponding two Reggeon annihilation amplitude is denoted by the graph of Fig. 4. These vertices then lead to the generalization of Fig. 2 which is depicted in Fig. 5. Figure 5 corresponds to a process in which two Reggeons of energy $-\omega_1, -\omega_2$ and momenta $\vec{\kappa}_1, \vec{\kappa}_2$ are created by the source a with the amplitude $N_a^{(2)}(\omega_1, \vec{\kappa}_1; \omega_2, \vec{\kappa}_2)$ and subsequently decay with amplitude $\gamma(\omega_1, \omega_2)\ N_b^{(2)}(\omega_1, \vec{\kappa}_1; \omega_2, \vec{\kappa}_2)$. The factor $\gamma(\omega_1, \omega_2) = \mathrm{Im}(i\eta(j_1)\eta(j_2))$ arises due to signature and is given by

$$\gamma(\omega_1, \omega_2) = -\frac{\cos\pi(\omega_1+\omega_2)/2}{\cos\ \pi\omega_1/2\ \cos\ \pi\omega_2/2}. \qquad (11)$$

The formula corresponding to the contribution of Fig. 5 to $T(\omega, \vec{\kappa})$ is the usual formula of nonrelativistic perturbation theory for two quasi-particle intermediate states, i.e.

$$T(\omega,\vec{\kappa}) =$$

$$\int_C \frac{d\omega_1}{2\pi i}\, d\omega_2 \int \frac{d^2\vec{\kappa}_1}{\pi}\, d^2\vec{\kappa}_2\, \frac{\delta(\omega-\omega_1-\omega_2)\,\delta^2(\vec{\kappa}-\vec{\kappa}_1-\vec{\kappa}_2)}{(\omega_1+\alpha'\vec{\kappa}_1^{\,2})(\omega_2+\alpha'\vec{\kappa}_2^{\,2})} N_a^{(2)}(\omega_1,\vec{\kappa}_1;\omega_2,\vec{\kappa}_2)$$

$$\times\gamma(\omega_1,\omega_2)\, N_b^{(2)}(\omega_1,\vec{\kappa}_1;\omega_2,\vec{\kappa}_2) \quad . \tag{12}$$

The integral in eq. (12) runs over all energies $-\omega_i$ and momenta $\vec{\kappa}$ of the Reggeons consistent with energy-momentum conservation at the vertices a and b and the denominators in eq. (12) represent the free propagation of the Reggeons from a to b.

Similarly, n Reggeons can be created at a, propagate freely from a to b and subsequently be absorbed at b. The contribution of this process to $T(\omega,\vec{\kappa})$ is depicted in Fig. 6 in which each internal Reggeon line with "energy" $-\omega_i$ and momentum $\vec{\kappa}_i$ stands for the free Reggeon propagator $D^o(\omega_i,\vec{\kappa}_i) = (\omega_i + \alpha'\vec{\kappa}_i^{\,2})^{-1}$. As indicated in Fig. 7, the upper vertex of Fig. 6 corresponds to an amplitude $N_a^{(n)}(\omega_1,\vec{\kappa}_1;\ldots\omega_n,\vec{\kappa}_n)$ for the production of n Reggeons from a source determined by the scattered particle a.

Diagram 6 corresponds to a process where n Reggeons or quasi-particles are created and propagate freely until they are all absorbed by the source. We must now include the interaction between the Reggeons as depicted in Fig. 8. In Fig. 8 m Reggeons are created by the source a, propagate freely, then interact and become converted into n Reggeons, which propagate until they are absorbed by the source b. Diagram 8 then involves the new Reggeon-Reggeon

interaction vertex $\Gamma^{nm}(\omega_1', \vec{\kappa}_1'; \ldots \omega_n', \vec{\kappa}_n'; \omega_1, \vec{\kappa}_1 \ldots \omega_m, \vec{\kappa}_m)$ which is depicted in Fig. 9.

Gribov[1] has shown that the vertices Γ^{nm} are determined from an effective two dimensonal nonrelativistic Hamiltonian describing the interaction of quasi-particles. The parameters in this Hamiltonian determining the Reggeon field theory, are the bare quasi-particle spectrum $\varepsilon_o(\vec{\kappa})$ and the bare interaction among the quasi-particles. These parameters themselves are in principle determined from an underlying relativistic field theory. All the experimental information which comes from high energy low momentum transfer scattering can then be expressed in terms of the solution of the Reggeon field theory. The Reggeon theory thus selects out those properties of the fundamental relativistic theory which are relevant to high energy low momentum scattering. Such a theory might also be useful if the bare quasi-particle propagators contain more complicated singularities than poles, like in some models where the summation of simplest set of relativistic diagrams leads to cuts.[5] However, a generalization of the Reggeon calculus to such cases has not yet been developed.

The simplest example of Γ^{nm} is the triple Regge vertex $\Gamma(\omega_1, \vec{\kappa}_1, \omega_2, \vec{\kappa}_2, \omega, \vec{\kappa})$ depicted in Fig. 11 with $\omega = \omega_1 + \omega_2$, $\vec{\kappa} = \vec{\kappa}_1 + \vec{\kappa}_2$. $\Gamma(\omega_1, \vec{\kappa}_1, \omega_2, \vec{\kappa}_2; \omega, \vec{\kappa})$ is determined in terms of the "bare" triple Regge vertex $r(\omega_1, \vec{\kappa}_1; \omega_2, \vec{\kappa}_2)$ of Fig. 12 which appears in the Hamiltonian describing the interacting Reggeons. The most important effect of this interaction is to shift the spectrum. This

occurs via the diagrams of Fig. 13. The effect of such diagrams is to replace the bare Reggeon propagator $D^{o}(\omega,\vec{\kappa}) = (\omega + \alpha'\vec{\kappa}^{2})^{-1}$ Fig. 14a by the full Reggeon propagator $D(\omega,\vec{\kappa})$ of Fig. 14b. The location $\varepsilon(\vec{\kappa})$ of the singularities of $D(\omega,\vec{\kappa})$ then determines the interacting quasi-particle spectrum. Gribov and Migdal[6] showed that if for small $\vec{\kappa}^{2}$ the full Reggeon propagator has a pole at $\omega = -\alpha'\vec{\kappa}^{2}$, then the vertex $\Gamma(\omega_1,\vec{\kappa}_1,\omega_2,\vec{\kappa}_2;\omega,\vec{\kappa})$ as well as the vertices $\Gamma^{13}(\omega_1,\vec{\kappa}_1,\omega_2,\vec{\kappa}_2,\omega_3,\vec{\kappa}_3;\omega,\vec{\kappa})$ and $\Gamma^{22}(\omega_1',\vec{\kappa}_1',\omega_2',\vec{\kappa}_2';\omega_1,\vec{\kappa}_1,\omega_2,\vec{\kappa}_2)$ depicted in Fig. 15 must vanish when all the ω_i and $\vec{\kappa}_i$ are equal to zero. In particular, this means that for small ω_i and $\vec{\kappa}_i$ the vertex $\Gamma(\omega_1,\vec{\kappa}_1,\omega_2,\vec{\kappa}_2;\omega,\vec{\kappa})$ has the form

$$\Gamma(\omega_1,\vec{\kappa}_1,\omega_2,\vec{\kappa}_2;\omega,\vec{\kappa}) = a\omega + \alpha' b\vec{\kappa}^{2} + c(\omega+\alpha'\vec{\kappa}_1^{2}+\alpha'\vec{\kappa}_2^{2}) \quad . \qquad (13)$$

Equation (13) is necessary for the existence of a consistent solution to the equation for Γ if the exact Regge trajectory has $\alpha(0) = 1$. (The equation for Γ is depicted graphically in Fig. 16.)

We now turn to the calculation of the high energy limit of the scattering amplitude $T(s,t)$ which is determined in terms of $T(\omega,\vec{\kappa})$ from eq. (4). We deform the contour C in eq. (4) so as to encircle the singularities of $T(\omega,\vec{\kappa})$ in the left half ω plane. Equation (4) then takes on the form

$$\frac{T(s,t)}{8\pi s} = \int_{C} \frac{d\omega}{2\pi i} e^{\xi\omega}\left(i + \tan\frac{\pi\omega}{2}\right) \Delta T(\omega,\vec{\kappa}) \qquad (14)$$

where

$$\xi \equiv \ln s/s_0$$

and $\Delta T(\omega,\vec{\kappa})$ is the discontinuity of $T(\omega,\vec{\kappa})$ across its singularities in the negative ω plane. Because the expression for $T(\omega,\vec{\kappa})$ represented by the graphs of Fig. 8 is determined from a nonrelativistic Hamiltonian where $-\omega$ plays the role of the energy, the rules for calculating $\Delta T(\omega,\vec{\kappa})$ are analogous to the rules for calculating the discontinuity in the energy of the graphs generated by a Hamiltonian for a nonrelativistic many-body problem. That is, to calculate the contribution to $\Delta T(\omega,\vec{\kappa})$ from a given graph for $T(\omega,\vec{\kappa})$, we simply cut the diagram in all possible ways and replace all the cut Reggeon propagators by $\delta(\omega_i+\alpha'\vec{\kappa}_i^{\,2})$ leaving the uncut propagators alone. The contributions to $\Delta T(\omega,\vec{\kappa})$ in which n Reggeon propagators are cut yield the discontinuity $\Delta T^{(n)}(\omega,\vec{\kappa})$ across the N Reggeon branch cut in $T(\omega,\vec{\kappa})$. For example, $\Delta T^{(2)}(\omega,\vec{\kappa})$ is determined from the diagrams of Fig. 17. The vertices appearing in Fig. 17 are the full Regge particle vertices defined by the graphs of Fig. 17b.

The position of the n Reggeon cut occurs at the smallest value of $-\omega$ for which the mass shell conditions $-\omega_i = \alpha'\vec{\kappa}_i^{\,2}$ $(i = 1,\ldots,n)$ can be satisfied subject to energy momentum conservation $\omega = \omega_1 + \omega_2 + \ldots + \omega_n$, $\vec{\kappa} = \vec{\kappa}_1 + \vec{\kappa}_2 + \ldots \vec{\kappa}_n$. This threshold energy occurs when all the n Reggeons share the momentum $\vec{\kappa}$ equally, i.e. $\vec{\kappa}_i = \vec{\kappa}/n$. Thus

$$-\omega = n\alpha' \left(\frac{\vec{\kappa}}{n}\right)^2 = \frac{\alpha'\vec{\kappa}^2}{n} \quad . \tag{15}$$

Furthermore, the discontinuity $\Delta T^{(n)}(\omega,\vec{\kappa})$ near the threshold $-\omega = \frac{\alpha'\vec{\kappa}^2}{n}$ is determined by n Reggeon phase space. Thus from purely kinematic considerations we conclude that

$$\Delta T^{(n)}(\omega,\vec{\kappa}) \sim \frac{(-1)^{n-1}}{(\alpha')^{n-1}} C_n(\vec{\kappa})\ \theta\ (-\omega - \frac{\alpha'\vec{\kappa}^2}{n}) \left|\omega + \frac{\alpha'\vec{\kappa}^2}{n}\right|^{n-2} \qquad (16)$$

$$\text{for } -\omega \sim \frac{\alpha'\vec{\kappa}^2}{n} \quad .$$

In arriving at result (16) we have assumed that the n Reggeon amplitude defined by graphs analogous to the two-Reggeon graphs of Fig. 17b has a non-vanishing, non-singular value $C_n(\vec{\kappa})$ at threshhold. We have also replaced the n Reggeon signature factor $\gamma(\omega_1,\omega_2\ldots\omega_n)$ by $\gamma(0,0,\ldots 0) = (-1)^{n-1}$. This $(-1)^{n-1}$ factor produces oscillations in the angular distribution of scattering and reflects the destructive interference between the single scattering of Fig.1b and the double scattering off the constituents of the proton as depicted in Fig. 2.

If we insert eq. (16) in formula (14) for the asymptotic behavior of $\frac{T(s,t)}{8\pi s}$, we obtain the formula

$$\frac{T^{(n)}(s,t)}{8\pi s} \underset{s\to\infty}{\to} \frac{(-1)^{n-1}}{(\alpha')^{n-1}} C_n(\vec{\kappa})\ (i + \pi/2\ \frac{\partial}{\partial\xi}) \int_{-\infty}^{-\frac{\alpha'\vec{\kappa}^2}{n}} \frac{d\omega}{\pi} e^{\xi\omega} \left|\omega + \frac{\alpha'\vec{\kappa}^2}{n}\right|^{n-2} . \qquad (17)$$

To obtain (17) we replaced tan $\pi\omega/2$ by $\pi\omega/2$, since for $\xi \to \infty$ the main contribution to the integral comes from the region where $\omega \sim 0$. We then see that as $s \to \infty$

$$\text{Im}\ \frac{T^{(n)}(s,t)}{8\pi s} \underset{s\to\infty}{\sim} C_n(\vec{\kappa}) e^{-\frac{\alpha'\vec{\kappa}^2\xi}{n}} (-\frac{1}{\alpha'\xi})^{n-1} \quad . \qquad (18)$$

The factor $e^{-\frac{\alpha'\vec{\kappa}^2\xi}{n}}\left(-\frac{1}{\alpha'\xi}\right)^{n-1}$ in eq. (18) which was obtained from purely kinematic considerations shows that for $\alpha'\xi >> 1$, $\alpha'\vec{\kappa}^2\xi < 1$, it is sufficient to include only small values of n in the expansion of T(s,t) in the number n of exchanged Reggeons.

The estimate (16) for $\Delta T^{(n)}(\omega,\vec{\kappa})$ for $-\omega \sim \frac{\alpha'\vec{\kappa}^2}{n}$ must be modified if the n Reggeon amplitudes have singularities in ω at $\omega = 0$ for $\vec{\kappa} = 0$. The diagram (ii) of Fig. 17b does have such a singularity because of the internal Reggeon line which produces a factor $1/\omega$. This factor is, however, compensated for by the fact that

$$\Gamma(\omega_1,\vec{\kappa}_1,\omega_2,\vec{\kappa}_2) = a\omega + \alpha' b\vec{\kappa}^2 \qquad \text{at } \omega_1 = -\alpha\vec{\kappa}_1^{\,2},\ \omega_2 = -\alpha'\vec{\kappa}_2^{\,2} \qquad (19)$$

and hence $\Gamma \sim a\omega$ when $\vec{\kappa} = 0$.[8] Thus the product $D(\omega)\Gamma(\omega)g$ in diagram (ii) equals $\frac{1}{\omega} \times (a\omega)g = ag$. Hence at $\vec{\kappa} = 0$ diagram (ii) just adds a term ag to the amplitude N of diagram (i). The combination N + ag then gives the contribution of Figs. 17b (i) and (ii) to the full Regge particle vertices which determine $\Delta T^{(2)}(\omega,\vec{\kappa})$ according to Fig. 17. On the other hand the vanishing of the Regge-Regge amplitude of Fig. 15a, reduces the contribution of diagram (iii) of Fig. 17b to $\Delta T^{(2)}(\omega,\vec{\kappa})$ such that it yields a contribution to T(s,t) which is of order $1/\xi^2$ for $\xi \to \infty$.

Furthermore, the contribution to $\Delta T^{(4)}(\omega,\vec{\kappa})$ which arises from the diagram of Fig. 18 is enhanced by a factor $1/\omega^2$ over the estimate of eq. (16). This is due to the two Reggeon propagators which couple to the particles a and b. This means that the diagram of Fig. 18 produces a contribution to $T(s,t) \equiv T(s,-\vec{\kappa}^2)$ which also behaves like $1/\xi$ for $\xi \to \infty$. However the

contribution to $\Delta T^{(3)}(\omega,\vec{\kappa})$ from the diagram of Fig. 19 does not contain extra $1/\omega$ factors because $\Gamma^{13}(\vec{\omega}_i,\vec{\kappa}_i)$ vanishes. Hence, Fig. 19 generates a contribution to T(s,t) which behaves like $1/\xi^2$ for $\xi \to \infty$.

We then conclude that the dominant contributions to $T(s,-\vec{\kappa}^2)$ for $\alpha'\xi >> 1$ and $\alpha'\vec{\kappa}^2\xi \leq 1$ arise from the contributions of diagrams (i) and (ii) of Fig. 17b to $\Delta T^{(2)}(\omega,\vec{\kappa})$, which are depicted in Fig.20, as well as from the pole diagram of Fig. 1b and the four Reggeon diagram of Fig. 18.

The diagrams of Figs. 1b, 20 and 18 have singularities at $\omega = -\alpha'\vec{\kappa}^2$, $\omega = -\alpha'\vec{\kappa}^2/2$ and $\omega = -\alpha'\vec{\kappa}^2/4$, respectively. The locations of the pole at $\omega = -\alpha'\vec{\kappa}^2$ and the branch cuts beginning at $\omega = -\alpha'\vec{\kappa}^2/2$ and $\omega = -\alpha'\vec{\kappa}^2/4$ are depicted in Fig. 21. The asymptotic expression eq. (18), represents the contribution to T(s,t) coming from the tip of the cuts. Contributions to T(s,t) from the points on the branch cut which lie a distance $\sim\alpha'\vec{\kappa}^2$ from the branch point are smaller by an amount $e^{-\alpha'\vec{\kappa}^2\xi}$. For $\alpha'\vec{\kappa}^2\xi \leq 1$ this factor is not small. Furthermore the pole singularity lies a distance $\alpha'\vec{\kappa}^2/2$ from the two Reggeon branch point and produces an enhancement of the two Reggeon contribution in this region via the diagrams of Fig. 20, b, c and d. Therefore we must also evaluate these diagrams for $\omega + \alpha'\vec{\kappa}^2/2 \sim -\alpha'\vec{\kappa}^2/2$.

The expression for the discontinuity $\Delta T^{(2)}(\omega,\vec{\kappa})$ across the two Reggeon branch cutswhich are depicted in Fig. 20 contain integrations over the momenta $\vec{\kappa}_1$ and $\vec{\kappa}_2$ of the two Reggeons in the intermediate states. To evaluate this integral we set

$$\vec{\kappa}_1 = \frac{\vec{\kappa}}{2} + \vec{\kappa}'$$
$$\vec{\kappa}_2 = \frac{\vec{\kappa}}{2} - \vec{\kappa}' \qquad (20)$$

then $\omega = -\alpha'(\vec{\kappa}_1^{\,2} + \vec{\kappa}_2^{\,2}) = -\alpha'(\frac{\vec{\kappa}^2}{2} + 2\vec{\kappa}'^2)$. Hence

$$\omega + \frac{\alpha'\vec{\kappa}^2}{2} = -2\alpha'\vec{\kappa}'^2 \qquad (21)$$

Let $N(\vec{\kappa}_1,\vec{\kappa}_2) \equiv N(\omega_1,\vec{\kappa}_1;\omega_2,\vec{\kappa}_2)$ at $\omega_1 = -\alpha'\vec{\kappa}_1^{\,2}$ and $\omega_2 = -\alpha'\vec{\kappa}_2^{\,2}$. Then if we assume that $N(\vec{\kappa}_1,\vec{\kappa}_2)$ has a smooth dependence upon $\vec{\kappa}'$ and hence upon ω, we can set $\vec{\kappa}' = 0$ and use the vertex $N(\vec{\kappa}) \equiv N(\vec{\kappa}/2,\vec{\kappa}/2)$ in calculating $\Delta T^{(2)}(\omega,\vec{\kappa})$. The exponential dependence upon $\vec{\kappa}'^2$ just changes the scale of the ω integration of eq. (14) and produces a correction to $T(s,t)$ of order $(1/\alpha'\xi)^2$, which is of the same order as the neglected diagrams such as the one depicted in Fig. 19. However, we cannot set $\omega = -\alpha'\vec{\kappa}^2/2$ in Fig. 17b(ii) since that diagram contains a factor $\frac{1}{\omega+\alpha'\vec{\kappa}^2}$. This factor causes diagrams b, c and d of Fig. 20 to vary rapidly as ω goes from $-\alpha'\vec{\kappa}^2/2$ to $-\alpha'\vec{\kappa}^2$. This dependence of these diagrams produces via eq. (14) an explicit dependence of $T(s,\vec{\kappa})$ upon the variable $\alpha'\xi\vec{\kappa}^2$. There is also an unknown dependence arising from the Regge residue function $g(\vec{\kappa})$ and the two Reggeon coupling $N(\vec{\kappa})$ which appear in these diagrams. The $\vec{\kappa}$ dependence of these functions cannot be determined on general theoretical grounds and must thus be parameterized. However, even if these functions are replaced by constants, the diagrams of Fig. 20 leads to a definite energy and angular dependence of the scattering amplitude which is a consequence of the general allowable singularity

structures in the Reggeon calculus.

The explicit form for the scattering amplitude depicted by the diagrams of Figs. 1, 18 and 20 was worked out by Gribov and Migdal in Ref. 7 and the formulae used by Ng and Sukhatme to describe the ISR data are essentially the same. Ng and Sukhatme also include an exponential dependence of $g(\vec{\kappa})$ and $N(\vec{\kappa})$ on $\vec{\kappa}^2$ since they apply the theory to values of $\vec{\kappa}^2 \lesssim 2(\text{GeV/c})^2$, that is they choose

$$g(\vec{\kappa}) = g(0)e^{-R^2\vec{\kappa}^2} \quad , \tag{22}$$

$$N(\vec{\kappa}) = N(0)e^{-\beta R^2\vec{\kappa}^2} \quad . \tag{23}$$

The formulae then contain the above parameters, $g(0)$, R^2, β and $N(0)$, the slope α' of Pomeron trajectory, the Regge energy scale s_o, the triple Regge vertex parameters a and b of eq. (17) and a constant λ characterizing the five Reggeon vertex appearing in Fig. 18. The constants a, b, λ, like α', are universal and appear in all reactions. For simplicity in the preliminary analysis of p-p scattering they set $\lambda = 0$ and hence did not include the contribution of Fig. 18. They also choose the conventional scale $s_o = 1(\text{GeV/c})^2$.

Several features of this scattering amplitude are independent of the particular values of the parameters: a) the total cross section must eventually rise to a constant value because of the negative coefficient of the $\frac{1}{\xi}$ contribution to Im T(s,0) arising from the diagrams of Figs. 18 and 20. b) The imaginary part of the double scattering diagram of Fig. 2 or 20a has a negative sign and hence interferes destructively with the single scattering diagram of

Fig. 16. This results in a dip in the angular distribution at a value of $t = -\vec{\kappa}^2$ which depends upon the particular value of the parameters of eqs. (22) and (23). The real part of $T(s,\vec{\kappa}^2)$ turns out to give a negligible contribution to the differential cross section for $\vec{\kappa}^2$ in the region of the dip and hence does not fill in the dip.

c) The real part of the forward scattering amplitude approaches zero as $\xi \to \infty$ like $\frac{B}{\xi^2}$ where B is a positive constant. d) As mentioned above, the enhanced diagrams of Figs. 20b, c and d have a definite variation in $\vec{\kappa}^2$ which is pronounced for small $\alpha'\vec{\kappa}^2\xi$. Thus we might expect that the angular distribution has some structure at small angles. However, the details of the magnitude and nature of this structure depend upon the values of all the parameters of the model since all diagrams can be important in this region. Hence although the parameters can be chosen to give an excellent description of the break in the slope of the angular distribution at $\vec{\kappa}^2 \approx 1 (\text{GeV/c})^2$, this feature of the data can in no sense be considered a prediction of the theory.

I will conclude by mentioning some of the preliminary results of the analyses by Ng and Sukhatme[9] of the ISR data on elastic proton-proton scattering. Figure (22) shows the experimental differential cross section data at the highest ISR energy $s = 2776 \left(\frac{\text{GeV}}{c}\right)^2$, which corresponds to a value of $\xi = 7.92$. This cross section has the following features: (i) a diffraction peak whose slope $b \equiv \frac{d}{dt} \ln \frac{d\sigma}{dt}$ changes from an average value of $13.1 \left(\frac{\text{GeV}}{c}\right)^{-2}$ for $-t \leq .15 \left(\frac{\text{GeV}}{c}\right)^2$ to a value $10.8 \left(\frac{\text{GeV}}{c}\right)^{-2}$ for $-t \geq .15 \left(\frac{\text{GeV}}{c}\right)^2$. (ii) At $-t \approx 1.3 \left(\frac{\text{GeV}}{c}\right)^2$

there is a dip followed by a bump at $-t \overset{\sim}{\wedge} 2\ (\frac{GeV}{c})^2$. The differential cross sections at the lower ISR energies have the same characteristic features. The position of the dip remains approximately independent of energy while the height of the bump decreases slightly with increased energy. The value of b for $-t \geq .15\ (\frac{GeV}{c})^2$ decreases to $11.8\ (\frac{GeV}{c})^2$ for the lowest ISR energy $s = 548\ (\frac{GeV}{c})^2$. In Fig. (22) the results of the pp total cross section experiments[4] from the two most recent sets of measurements are plotted. The result is a cross section which increases by approximately 4 mb from $s = 548\ (\frac{GeV}{c})^2$ to $s = 2776\ (\frac{GeV}{c})^2$.

Ng and Sukhatme[9] have found that this data for $|t| \lesssim 2.2$ is well described by the Reggeon diagrams of Figs. (1b) and (20) using the following set of parameters:

$$\alpha' = .37\ (\frac{GeV}{c})^{-2} \quad , \quad a = -4.2\ (\frac{GeV}{c})^{-1}$$
$$b' \equiv b - a = -.213\ (\frac{GeV}{c})^{-1} \tag{24}$$

$$g^2(0) = 3.75\ (mb)^{1/2}\ (\frac{GeV}{c})^{-1}$$
$$R^2 = 1.54\ (\frac{GeV}{c})^{-2} \tag{25}$$
$$N(0) = 4.72\ (mb)^{1/4}\ (\frac{GeV}{c})^{-3/2} \quad , \beta = .5$$

The curves of Figs. (22) and (23) are the predictions of this theory. The parameters given in eqs. (24) and (25) yield a 4 mb rise in $\sigma_{Tot}(s)$ over the ISR energy range and correspond to an asymptotic

total cross section $\sigma_{Tot}(\infty) = 58.8$ mb. The predicted differential cross sections agree with the experimental data at all ISR energies for values of -t out to $\sim 2.2 \left(\frac{GeV}{c}\right)^2$, i.e. a little beyond the bump.

At $s = 2776 \left(\frac{GeV}{c}\right)^2$, $\alpha'\xi = 3$, and $-\alpha'\xi t \gtrsim 6$ for -t near the region of the bump. From eq. (18) we see that for these values we would expect that diagrams with three exchanged Reggeons play an important role. To evaluate the coefficients $C_3(\vec{\kappa})$ in eq. (18) we need the two particle three Reggeon vertices $N^{(3)}(\vec{\kappa})$. Since these vertices are not known a priori, we have no reason to suppose that $N^{(3)}(\vec{\kappa})$ is sufficiently suppressed relative to $N^{(2)}(\vec{\kappa})$ that Im $T^{(3)}(s,t)$ is much smaller than Im $T^{(2)}(s,t)$ at $\alpha'\xi = 3$ and $-\alpha'\xi t = 6$. For this reason we are probably stretching the theory outside its domain of applicability when we try to fit the angular distributions all the way out to the position of the bump. On the other hand, the experiments at ISR yield the best currently available data for testing Gribov's theory of diffraction scattering. For this reason Ng and Sukhatme have compared the theory with the data over a range of t for which the corrections cannot be shown to be necessarily small.

In the region of the break $-\alpha'\xi t \approx .04$, the application of the theory is on firmer grounds. However since $\alpha'\xi$ is only about 3, even in this region we cannot conclusively rule out the possibility that terms of order $(1/\alpha'\xi)^2$ are not significant. The philosophy of Ng and Sukhatme was to apply the theory in as large a region as possible to see how well it can describe the experimental data. Their work shows that the ISR pp scattering data is compatible with the Gribov

picture of the Pomeron. However since a number of the parameters are universal, high energy data from other reactions will provide more stringent tests of the theory.

In conclusion I would like to thank Uday Sukhatme and John Ng for many interesting conversations, and their invaluable help in preparing this talk. I also wish to thank Drs. C. Pajares and D. Schiff for very useful comments.

Footnotes

1. V. N. Gribov, Zh. Eksp. Teor. Fiz. 53, 654 (1967) [Sov. Phys. JETP 26, 414 (1968)].

2. J. N. Ng and U. P. Sukhatme, University of Washington preprint RLO-1388-645, to be published in Nucl. Phys. B.

3. Gribov's Reggeon calculus has been systematically applied to all high energy scattering processes in a series of papers by K. A. Ter-Martirosyan and collaborators. See, for example, K. A. Ter-Martirosyan, Yad. Fiz. 10, 1262 (1969) [Sov. J. of Nucl. Phys. 10, 715 (1970)]. K. A. Ter-Martirosyan [Lectures at the Dubna Conference on Binary Reactions, July 1971].

4. Data from Rubbia Group presented at the 16^{th} International Conference on High Energy Physics, Chicago, Illinois, Sept. 1972. G. Barbiellini et al., Phys. Letters 39B, 663 (1972). U. Amaldi et al., Phys. Letters 44B, 112 (1973). S. R. Amendolia et al., Phys. Letters 44B, 119 (1973).

5. Gribov developed the rules for the Reggeon calculus using the ϕ^3 field theory, for which the ladder graphs of Fig. 10 form the simplest set of graphs giving rise to a Regge pole. The resulting rules had such a simple interpretation that it was natural to assume they remain valid in any theory which has Regge behavior. Different relativistic field theories then give different values for the parameters of the resulting Reggeon theory.

6. V. N. Gribov and A. A. Migdal, Yad. Fiz. 8, 1002 (1968) [Sov. J. Nucl. Phys. 8, 583 (1969)].

7. The trajectories also have a small imaginary part for small $\vec{\kappa}^2$; i.e. in the presence of the interaction the quasi-particle energy $\varepsilon(\vec{\kappa}) = \alpha'\vec{\kappa}^2 + \gamma^2(\vec{\kappa}^2)^2 \ln \alpha'\vec{\kappa}^2 \pm i\pi\gamma^2(\vec{\kappa}^2)$, where γ is a constant determined by Γ^{13} and the constants a and b of eq. (13). See V. N. Gribov and A. A. Migdal, Yad. Fiz. 8, 1213 (1968) [Sov. J. Nucl. Phys. 8, 703 (1969)].

8. In the Reggeon calculus the triple Regge vertex $\Gamma(\omega_1,\vec{\kappa}_1,\omega_2,\vec{\kappa}_2,\omega,\vec{\kappa})$ is defined for all values of $\omega_1,\vec{\kappa}_1,\omega_2,\vec{\kappa}_2,\omega,\vec{\kappa}$ subject to "energy" momentum conservation conditions $\vec{\kappa} = \vec{\kappa}_1 + \vec{\kappa}_2$, $\omega = \omega_1 + \omega_2$. There are in general no "energy shell" restrictions $\omega_1 = -\alpha'\vec{\kappa}_1^2$, $\omega_2 = -\alpha'\vec{\kappa}_2^2$, $\omega = -\alpha'\vec{\kappa}^2$. For $\vec{\kappa} = 0$ we have $\vec{\kappa}_1 = -\vec{\kappa}_2$ and consequently the term $a\omega = -2a\alpha'\vec{\kappa}_1^2$ depends upon the behavior of Γ off the energy shell $\omega = -\alpha'\vec{\kappa}^2$. On the other hand inclusive cross sections in the triple Regge region determine a vertex which satisfies the conditions $\omega_1 = -\alpha'\vec{\kappa}_1^2$, $\omega_2 = -\alpha'\vec{\kappa}_2^2$, $\omega = -\alpha'\vec{\kappa}^2$, but for which there is no restriction $\omega = \omega_1 + \omega_2$. In this case for $\vec{\kappa} = 0$ we have $\omega = 0$. Hence the constant a in eq. (19) is not directly determined from inclusive cross sections.

9. J. N. Ng and U. P. Sukhatme (to be published). This work differs from reference (2) which was carried out before the rising total cross section data at ISR energies was obtained.

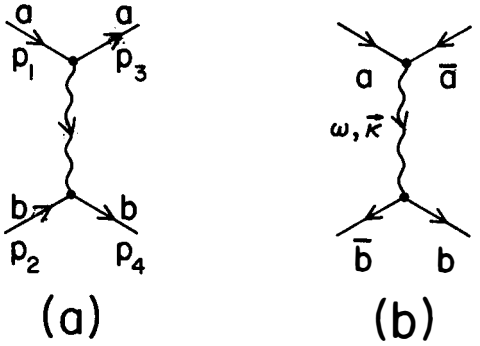


Fig. 1 Diagrams representing Regge pole exchange contributions to scattering.

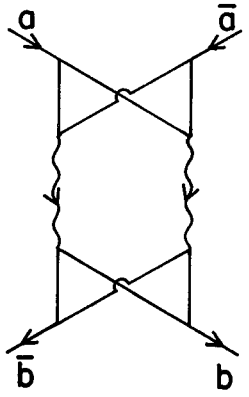


Fig. 2 Example of diagram corresponding to two Reggeon exchange contribution to scattering.

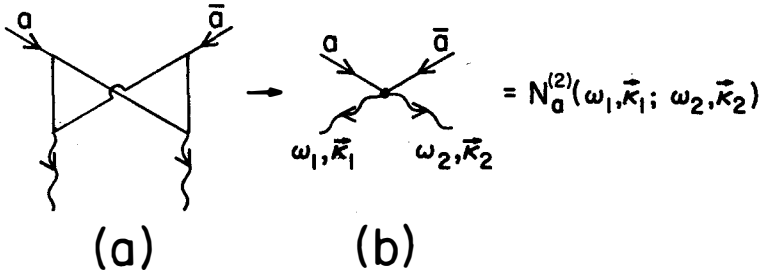


Fig. 3 Diagrams for amplitude for two particles to decay into two Reggeons.

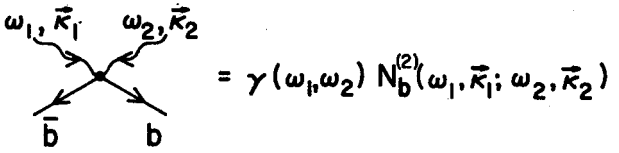


Fig. 4 Diagram for amplitude for two Reggeons to produce two particles.

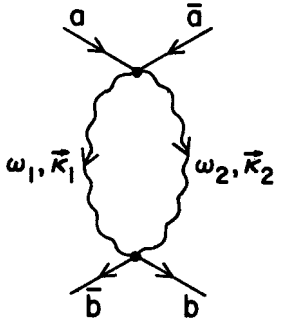


Fig. 5 Diagram representing two Reggeon exchange.

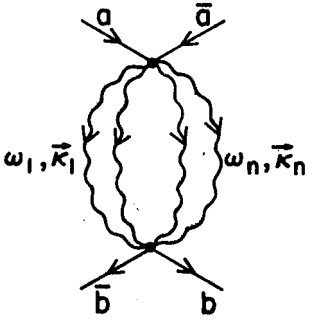


Fig. 6 Diagram representing n Reggeon exchange.

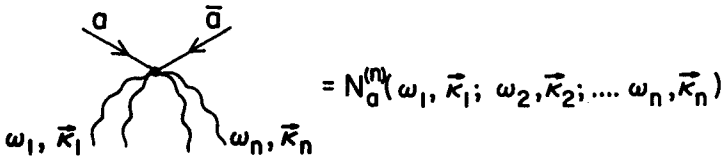


Fig. 7 Diagram representing two particle n Reggeon amplitude $N_a^{(n)}(\omega_1, \vec{\kappa}_1, \ldots \omega_n, \vec{\kappa}_n)$.

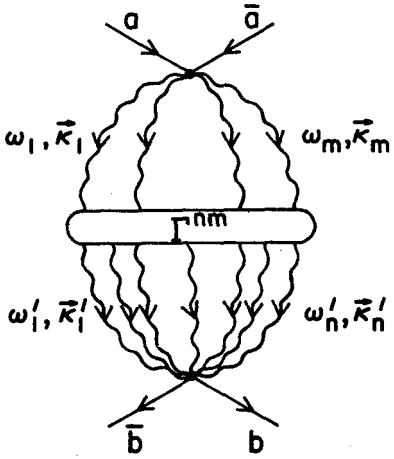


Fig. 8 General diagram representing Reggeon exchange including interaction among the Reggeons.

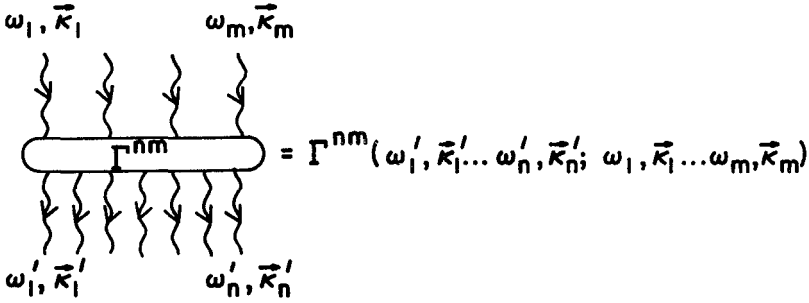


Fig. 9 Diagram representing the general Reggeon interaction amplitude.

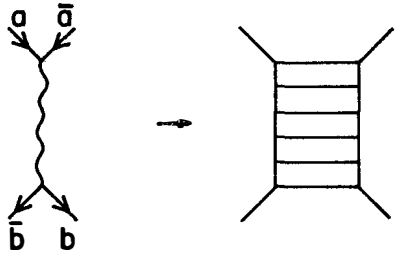


Fig. 10 Ladder diagram model for a Regge pole.

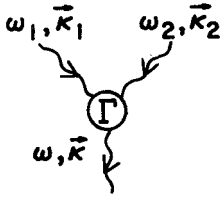


Fig. 11 Diagram representing full triple Regge vertex Γ.

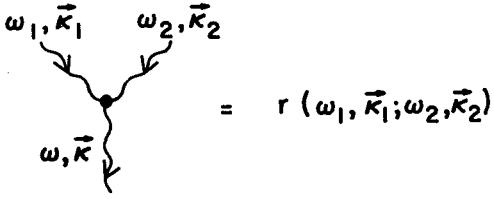


Fig. 12 Diagram representing bare triple Regge vertex r.

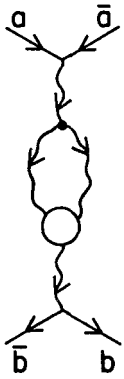


Fig. 13 Diagram representing Pomeron propagator corrections to the scattering amplitude.

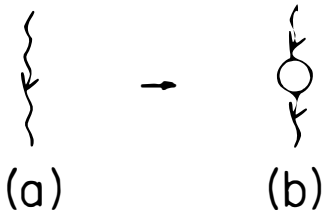


Fig. 14 Diagram representing the full Reggeon propagator.

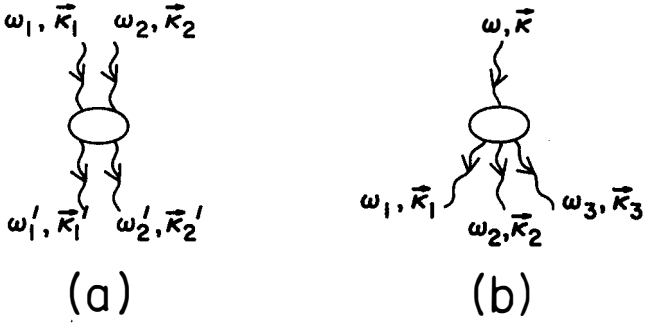


Fig. 15 Diagrams representing four Reggeon interactions.

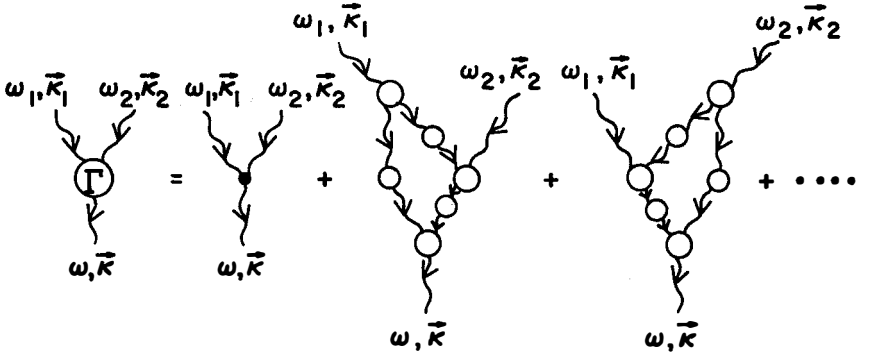


Fig. 16 Diagrams representing the integral equation for vertex function

$$\Delta T^{(2)}(\omega, \vec{\kappa}) =$$

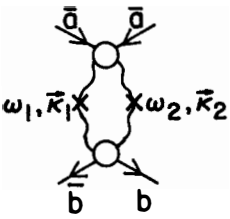


Fig. 17

where



$$= \delta(\omega_i + \alpha' \vec{\kappa}_i^2) \qquad 17a$$

and

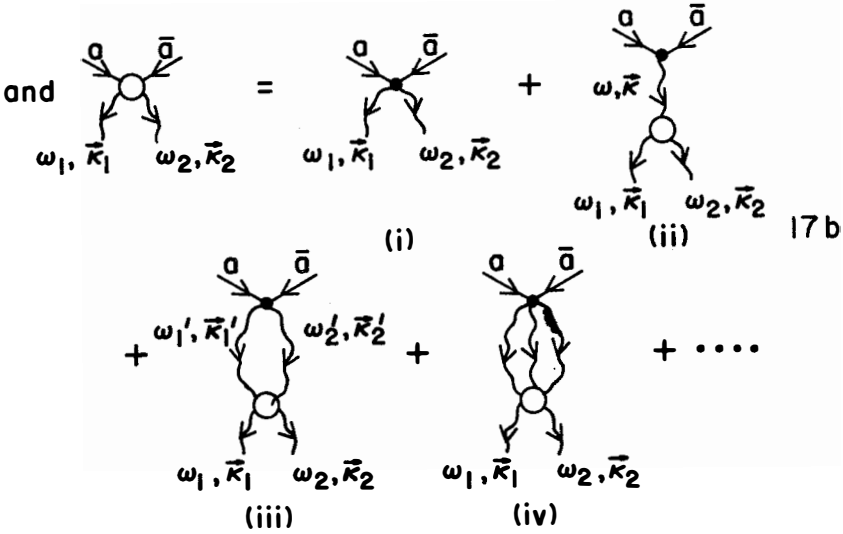


Fig. 17 Diagrams representing the equation for the full discontinuity of $T(\omega, \vec{\kappa})$ across its two Reggeon branch cut.

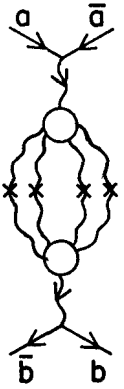


Fig. 18 Reggeon propagator contribution to $\Delta T^{(4)}(\omega,\vec{\kappa})$.

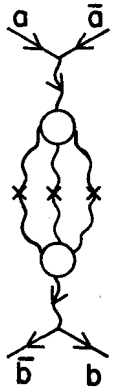


Fig. 19 Reggeon propagator contribution to $\Delta T^{(3)}(\omega,\vec{\kappa})$.

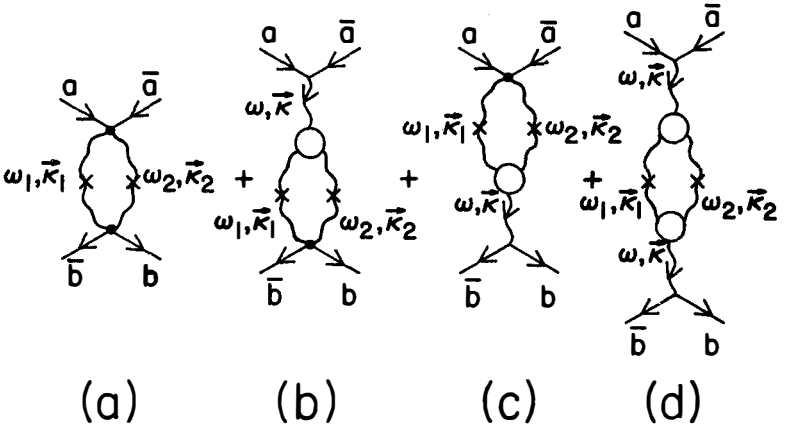


Fig. 20 Dominant contributions to $\Delta T^{(2)}(\omega,\vec{\kappa})$.

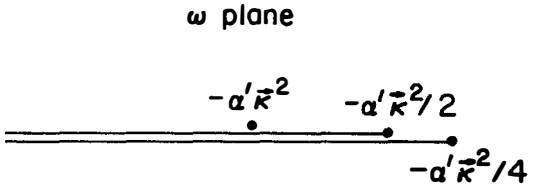


Fig. 21 Location of singularities of $T(\omega,\vec{\kappa})$ in ω plane.

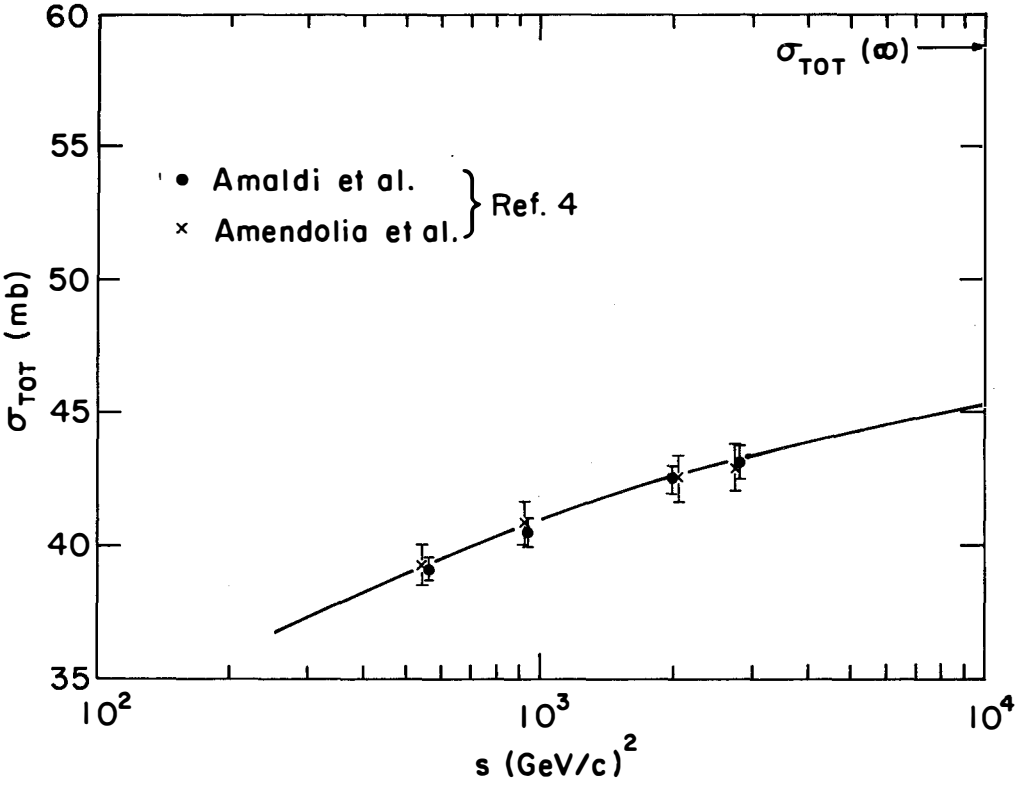


Fig. 22 Comparison of pp total cross section data at ISR energies with Gribov's theory. The data points are taken from Ref. 4.

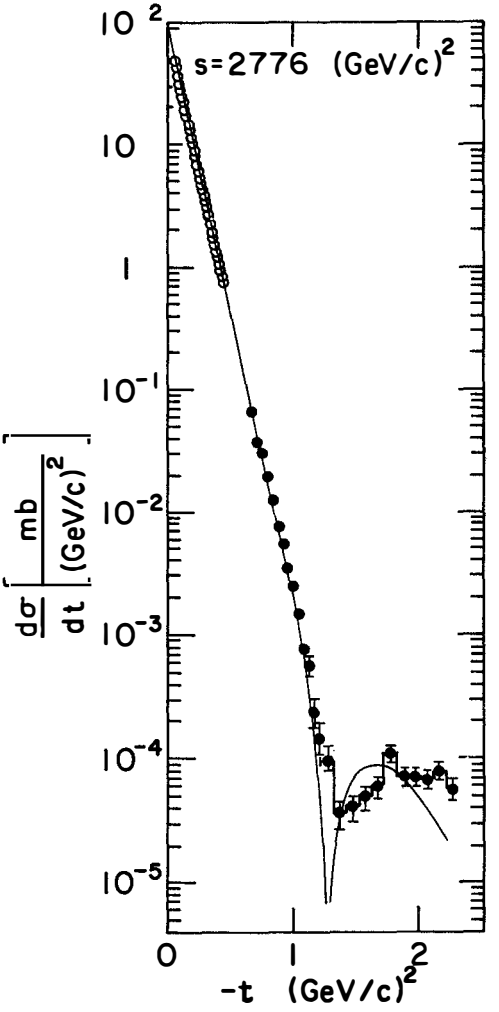


Fig. 23 Comparison of pp differential cross section data at s = 2776 $(GeV/c)^2$ with Gribov's theory. The data points are from the Rubbia group and Barbiellini et al. [Ref. 4].

LORENTZ CONTRACTED GEOMETRICAL MODEL*

A.D. Krisch
Randall Laboratory of Physics
University of Michigan, Ann Arbor Michigan 48104 (USA)

Abstract: The model assumes that when two high energy particles collide each behaves as a geometrical object which has a Gaussian density and is spherically symmetric except for the Lorentz-contraction in the incident direction. Folding the two spatial distributions together we obtain the slope (b) of the elastic diffraction peak in terms of the c.m. velocities (β_i and β_j) and the sizes (A_i and A_j) of the two incident particles. These sizes are assumed to have the experimental s-dependence of $\sigma_{tot} \propto \pi A^2$ for each reaction. The combined s-dependence of the σ_{tot}'s and the β's gives the s-dependence of the elastic slope

$$b_{ij}(s) = \frac{1}{2}(A_i^2\beta_i^2 + A_j^2\beta_j^2)\,\frac{\sigma_{tot}^{ij}(s)}{\sigma_{tot}^{ij}(\infty)}$$

This formula agrees with the experimental slope for p-p, $\bar{p}$-p, K^+-p, K^--p, and $\pi^\pm$-p elastic scattering from 3 to 1500 GeV/c, with only three parameters: $A_\pi^2 = 6.1$, $A_K^2 = 3.3$, and $A_p^2 = 10.5$ $(GeV/c)^{-2}$.

The text of the lecture will be published in Physics Letters B (April 1973).

*Supported by a research grant from the U.S. Atomic Energy Commission

Résumé : Le modèle suppose que quand deux particules de haute énergie entrent en collision, chacune d'elles se comporte comme un objet géométrique de densité gaussienne, avec la symétrie sphérique (excepté la direction incidente comme conséquence de la contraction de Lorentz). En effectuant le recouvrement des deux distributions spatiales. On obtient la pente (b) du pic de diffraction élastique en termes des vitesses dans le c.m (β_i et β_j) et de dimension (A_i et A_j) des deux particules incidentes. On suppose que ces dimensions ont la dépendence en énergie déduite par chaque réaction de la dépendance expérimentale de $\sigma_{tot}^{\pi A^2}$

La conjonction des dépendances en s des sections efficaces totales des β's donne la dépendance en s de la pente élastique.

$$b_{ij}(s) = \tfrac{1}{2}\,(A_i^2\,\beta_i^2 + A_j^2\,\beta_j^2)\;\frac{\sigma_{tot}^{ij}(s)}{\sigma_{tot}^{ij}(\infty)}$$

Cette formule est en accord avec les pentes expérimentales pour la diffusion élastique p-p ainsi que pour $\bar{p}$-p, K^+-p, K^--p, et $\pi^{\pm}$-p de 3 à 1500 GeV/c, avec seulement trois paramètres : $A_{\pi}^2 = 6.1$, $A_K^2 = 3.3$ et $A_p^2 = 10.5$ $(GeV/c)^{-2}$. Le texte de cette conférence sera publié dans Physics Letters (Avril 73).

THE IMPACT PICTURE FOR STRONG INTERACTIONS

J. K. Walker
Physics Department, National Accelerator Laboratory,
Batavia, Illinois 60510 (USA)

Abstract: A brief discussion of the general characteristics of the Impact Picture is given. This leads to a description of a phenomenological model of hadron scattering which on the one hand satisfies the impact picture at extremely high energies and on the other successfully describes the data above 20 GeV in the laboratory. In addition, many predictions on the general behavior of high energy hadron-hadron interactions are given.

Résumé : On discute brièvement les caractéristiques générales de la description en paramètre d'impact. Ceci conduit à l'exposé d'un modèle phénoménologique de la diffusion des hadrons qui d'une part satisfait à cette description en paramètre d'impact à très haute énergie et d'autre part reproduit les données pour $E_{lab} > 20$ GeV. En outre, plusieurs prédictions concernant la dépendance des interactions hadron-hadron, en général, sont données.



I. Introduction

In the last five years a profound advance has occurred in our understanding of the asymptotic high energy behavior of relativistic quantum field theories. Much of the progress in this area has been achieved by H. Cheng and T. T. Wu. They have shown that a variety of field theories have the same general feature in the limit of extremely high energies. The solution satisfies all honored physical principles such as unitarity, analyticity, and crossing symmetry.

The central question is: Does this solution apply to the strong interactions of hadrons? The test will and must come from experiments. The recent accurate measurements of proton-proton total cross sections at the ISR give strong support to the impact picture. It is, therefore, worthwhile to make a preliminary appraisal of the experimental situation at this time, when a great many new experiments will shortly be completed at the National Accelerator Laboratory, USA, and the Intersecting Storage Ring at CERN. The purpose of this paper is threefold. First, to provide an experimentalists viewpoint of the theoretical progress of the last few years in this field. As such, it embraces a lack of rigor. However, it is hoped that it provides some inspiration and understanding to experimentalists about this particular theoretical interpretation of their data. Secondly, I will report on a preliminary analysis of existing high energy data using a phenomenological model which on the one hand possesses all properties demanded by the impact picture at extremely high energies and, on the other hand, is sufficiently realistic to fit data for incident laboratory energy above 20 GeV. Finally, I will briefly present other predictions of the impact picture.

II. Theoretical Basis of the Impact Picture

Most of the theoretical effort has been devoted to a study of quantum electrodynamics with massive photons at very high energy. General features of the high energy scattering amplitudes have emerged. It has been verified that the same general features occur with scalar quantum electrodynamic field theory and ϕ^3 theory. We shall confine our attention to quantum electrodynamics.

High Energy Limit of Elastic Scattering

Consider the elastic process

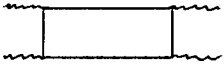
$$a + b \to a + b$$

in the limit

$$s \to \infty$$

and t fixed.

The relevant lowest order diagrams for the three processes are shown below with their corresponding dependences on energy.

Process	s^0	s	i s
e + e → e + e			
γ + e → γ + e			
γ + γ → γ + γ			

Only examples of the diagrams are shown at any given order.

At high enough order the Amplitude $\propto$ i s. Hence

$$\lim_{s \to \infty} \sigma_T \text{ is finite and non-zero.}$$

Thus cross sections tend to constants to this order in the expansion.

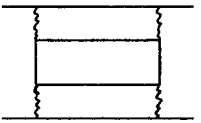
A general feature turns out to be that for the important diagrams photons are exchanged between groups of particles which may be the incident particles themselves or the ones created by them.

Higher Orders

We inquire whether if we go to still higher order are there terms that grow faster than s as $s \to \infty$. In this case the result would be

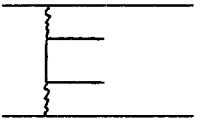
$$\lim_{s \to \infty} \sigma_T \to \infty .$$

Consider again ee - going to higher order



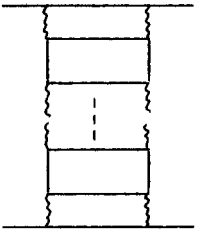
The amplitude in this case goes as i s ℓns. In general, it turns out that electron loops give s ℓns terms.

By the Optical Theorem the above diagram is related to



} the production of low energy particles in cms (in hadron physics referred to as pionization)

Given that there are diagrams that grow faster than s, a vital question poses itself: What happens after we sum all diagrams that give logarithmic factors? e.g.,



In this case, n loops lead to i $\alpha^{2(n+1)}$ s$(\ell ns)^n$.

Summing over all possibilities gives the result

$$\text{amp} \propto \frac{i\, s^{1+c}}{(\ell ns)^2}$$

where $c = \frac{11\pi\,\alpha^2}{32}$ for QED and similar results for scalar electrodynamics, ϕ^3 theory, etc. In general, c is related to a coupling constant in the theory. The exponent of the ℓns term in the denominator seems to be probably ≥ 1 in general. Thus the amplitude increases faster than s (for this class of diagrams). At first sight this is a disturbing result and appears to lead to a total cross section that rises as a power of s. This possibility would violate the Froissart bound. We will now discuss the solution to this dilemma.

We express the scattering amplitude in the impact-distance representation.

$$M(s,-\Delta^2) = \frac{is}{2\pi} \int dx_\perp\, e^{i\vec{\Delta}\cdot\vec{x}_\perp}\, D(s,x_\perp)$$

where now $M(s,-\Delta^2)$ includes contributions from ALL possible diagrams in the world.

$D(s,x_\perp)$ is defined to be the opacity at s and $x_\perp$. By a Fourier Transform we obtain

$$D(s,x_\perp) \sim s^{-1} \int d^2\Delta^2\, e^{-i\vec{\Delta}\cdot\vec{x}_\perp}\, M(s,-\Delta^2) .$$

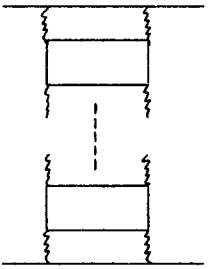
In the limit of large $x_\perp$, we replace $M(s,-\Delta^2)$ by

$$\frac{1}{-\Delta^2 - \lambda^2}$$

which is the form of the propagator for the exchange of a particle. We then obtain

$$D(s,x_\perp) \sim \exp(-\lambda\,|x_\perp|) .$$

Thus the smallest effective λ contributes most to $D(s,x_\perp)$ at large $x_\perp$. This is all consistent with our intuitive understanding. The leading diagrams of this kind are just the kind of diagrams that we have discussed and have, in addition, the s dependence given previously.



Thus at large $x_\perp$ we have the important result that

$$D(s,x_\perp) \sim \frac{s^c}{(\ell ns)^2} \; e^{-\lambda |x_\perp|} \; .$$

Now consider the case of fixed large $x_\perp$, then $D(s,x_\perp)$ increases with s.

Thus the interaction extends into larger and larger transverse distances as s increases. Thus $D(s,x_\perp)$ approaches 1, at a value of s such that

$$\boxed{\frac{c}{\lambda} \ell ns \equiv R \gtrsim |x_\perp| \; .}$$

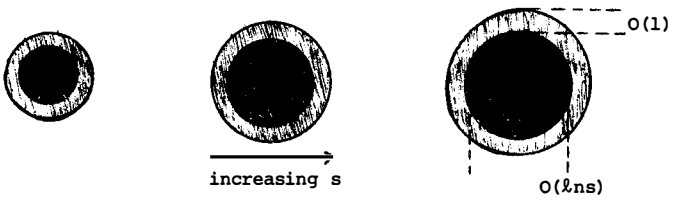
Other diagrams become important in that case.

The most general statement seems to be that

$$D(s,x_\perp)\Big|_{x_\perp \lesssim R} \longrightarrow \text{Constant} \qquad s \to \infty$$

The constant may or may not be as large as unity. However, it seems natural that for strong interactions the constant should be as large as possible, namely unity.

The picture which emerges is that a particle acts like a Lorentz contracted pancake with two regions

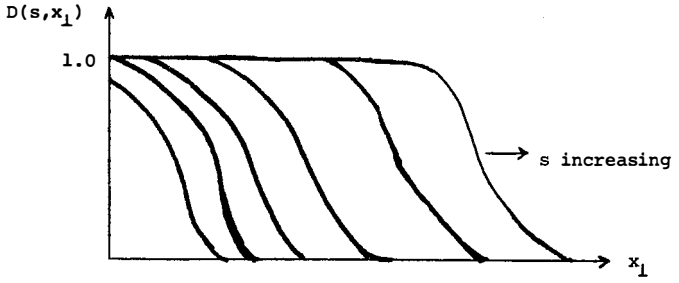


There is a gray fringe area and in the center there is a black core.

III. -1) The Phenomenological Model

In association with Cheng and Wu an effort has been made to construct a phenomenological model that possesses the above properties of the impact picture and yet at the same time is sufficiently realistic to fit the data from Serpukhov, NAL, and the ISR.

We want $D(s,x_\perp)$ to look like



The simplest form is

$$D(s,x_\perp) = 1 - \exp\left[-S(s)\ F(x_\perp^2)\right].$$

The function S(s) will be the same for all processes mediated by the Pomeron, e.g.

$$\pi + p \to \pi + p$$

and

$$p + p \to p + p\ .$$

All channel information resides in $F_j(x_\perp^2)$ for j^{th} channel. We take

$$F_j(x_\perp^2) = f_j\ \exp\left[-\lambda(x_\perp^2 + x_{oj}^2)^{1/2}\right].$$

This involves three parameters: f_j, λ, x_{oj}. λ does not depend on the channel because for large $x_\perp$

$$F_j \sim \exp(-\lambda\, x_\perp)$$

and the shape of the opacity function at the fringe should be a property of the pomeron - not of the channel.

On the basis of our experience with QED we might take

$$S(s) = \frac{s^c}{(\ell ns)^{c'}} .$$

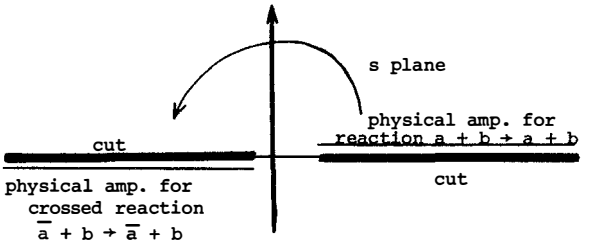
For the present, however, it is an adequate approximation to take $c' = 0$ thereby obtaining a value for an "effective" c. The asymptotic energy scale of hadron interactions is then controlled by the value of c. There is a problem with the choice $S(s) = s^c$. In this case the elastic scattering amplitudes for the two processes

$$a + b \to c + d$$

and $\bar{a} + b \to \bar{c} + d$ are not equal.

i.e. we demand that the amplitude satisfy crossing which it clearly does not with the above choice of S(s).

Consider the complex s plane.



We require that if we analytically continue the direct amplitude to the position of the other amplitude then this function should describe the crossed reaction. The choice

$$S(s) = \left[s \exp(-i\,\pi/2)\right]^c$$

achieves this.

The model then has the elastic scattering amplitudes

$$M_j(s,-\Delta^2) \text{ functions of } x_{oj},\ f_j,$$

which depend on the channel and two real constants λ and c which are common to all channels.

The differential cross section for elastic scattering in channel j is (in the limit of large s)

$$\frac{d\sigma}{dt}(j) = \left| \frac{M_j(s,-\Delta^2)}{s} \right|^2 \qquad (1)$$

where $t = -\Delta^2$.

The total cross section is related to the imaginary part of $M_j(s,0)$

$$\sigma_{total}(j) = \frac{4\pi}{s} \text{ Im } M_j(s,0).$$

[Remember that to convert from $(GeV)^{-2}$ to mb, a factor of $\frac{4.893}{4\pi}$ is needed.]

As Im M(s,0)/s is an increasing function of s, the total cross sections will rise. If total cross sections do rise indefinitely with energy, at what energy does this begin to occur? Until very recently, the data of Denisov et al. at Serpukhov for the K^+p channel, was the only case of an appreciable rise in total cross section. There is some reason to expect that an exotic channel may show asymptotic features at a lower energy than for a non-exotic channel. In order to determine the value of c, one accurate piece of data is required at very high energy. Very recently, this most important piece of information has been provided by two beautiful experiments at the ISR in the form of a total pp cross section. At lower energies we assume the increase is masked by a decreasing background. In this case we assume

$$\sigma_{total}(j) = A_j s^{-1/2} + \frac{4\pi}{s} \text{ Im } M_j(s,0). \qquad (2)$$

In order to satisfy the optical theorem, this parameter A_j should appear also in the formula for $d\sigma/dt$. However, at this stage we have concentrated on trying to take proper account only of the pomeron (or asymptotic) contribution to $d\sigma/dt$.

This completes the description of our simple model for all asymptotic hadronic processes. Later we shall generalize it to inelastic diffraction scattering without spin-parity exchange.

III. -2) Properties of the Model

The function $F_j(x_\perp^2)$ has the property that, raised to an arbitrary positive power, the two-dimensional Fourier transform is an elementary function. More precisely

$$(2\pi)^{-1} \int d\vec{x}_\perp e^{-i \vec{\Delta} \cdot \vec{x}_\perp} \left[F_j(x_\perp^2)\right]^n$$

$$= f_j^n \, n \, \lambda \left[1 + x_{oj}(\Delta^2 + n^2\lambda^2)^{1/2}\right] (\Delta^2 + n^2\lambda^2)^{-3/2}$$

$$\exp\left[-x_{oj}(\Delta^2 + n^2\lambda^2)^{1/2}\right] \qquad (3)$$

for $n > 0$.

We then obtain, after expanding $D(s,x_\perp)$

$$M_j(s,-\Delta^2) = i \, s \, \lambda \sum_{n=1}^{\infty} \frac{(-1)^{n-1} f_j^n \left[s \exp(-i\,\pi/2)\right]^{nc}}{(n-1)!}$$

$$\left[1 + x_{oj}(\Delta^2 + n^2\lambda^2)^{1/2}\right] (\Delta^2 + n^2\lambda^2)^{-3/2}$$

$$\exp\left[-x_{oj}(\Delta^2 + n^2\lambda^2)^{1/2}\right]. \qquad (4)$$

Equations (1), (2), (3), and (4) give completely the model.

Of course in this asymptotic model

$$\frac{d\sigma}{dt}(\bar{h}h) = \frac{d\sigma}{dt}(hh)$$

where h is any hadron. Since we have at the present time omitted from $d\sigma/dt$ the background terms which fall presumably approximately as some power of s, our values of $d\sigma/dt$ should be most accurate for K^+p and then less accurate in order for pp, π^+p, π^-p, K^-p, and $\bar{p}p$.

III. -3) Numerical Analysis

Our objective is to provide a reasonable numerical fit to all hadron-hadron processes at high energies $s \gtrsim 40\ \text{GeV}^2$. The fit should improve for the higher energy data.

It is worthwhile to clearly state the number of parameters in the fit. The total cross sections are parameterized in the form

$$\sigma_{\text{total}}(j) = A_j\, s^{-1/2} + \frac{4\pi}{s}\ \text{Im}\ M_j(s,0).$$

This involves six constants A_j (for the channels p, $\bar{p}$, π^+, π^-, K^+, K^-). In addition, M_j involves two parameters f_j and x_{oj} which depend on the channel but are the same for particle and antiparticle. This produces an additional six parameters. Finally, there are two parameters which are independent of the channel. The first of these λ, characterize the shape of the fringe of the interaction region. The other parameter c establishes the energy scale in asymptotic hadron dynamics.

This involves a total of 14 parameters, the six A_j help fit the total cross sections at low energies ($40 \lesssim s \lesssim 100$), thereby yielding better information on the asymptotic part of the cross section. Above $s \approx 100$ essentially all of our fits and predictions for total cross sections, elastic and inelastic diffractive cross sections, for all channels are determined by the remaining eight parameters.

Specifically the above fourteen parameters are determined from the following fourteen pieces of data:

1) At E = 20 BeV, the pp total cross section is 39.0 mb.
2) At E = 60 BeV, the pp total cross section is 38.4 mb.
3) At E = 1485 BeV, the pp total cross section is 43.2 mb. This is the crucial piece of data obtained at the ISR to which we have previously referred.
4) At E = 60 BeV, the dip in the pp differential cross section occurs at $|t| = 1.8\ (\text{BeV/c})^2$. This value is somewhat arbitrary.
5) At E = 505 BeV, the average slope, between $|t|$ of 0.14 and $0.24\ (\text{BeV/c})^2$, for $\ell n\, d\sigma/dt$ is $11.5\ (\text{BeV/c})^{-2}$ for pp elastic scattering.

6) At E = 20 BeV, the total K^+p cross section is 17.5 mb.

7) At E = 60 BeV, the total K^+p cross section is 18.3 mb.

8) At E = 60 BeV, the average slope, between $|t|$ of 0.1 and 0.28 $(BeV/c)^2$, for $\ell n\, d\sigma/dt$ is 7.4 $(BeV/c)^{-2}$ for K^+p elastic scattering.

9) At E = 47.5 BeV, the $\bar{p}p$ total cross section is 44.1 mb.

10) At E = 52.5 BeV, the K^-p total cross section is 20.3 mb.

11) At E = 20 BeV, the π^+p total cross section is 23.5 mb.

12) At E = 60 BeV, the π^+p total cross section is 23.15 mb.

13) At E = 54.2, the average slope, between $|t|$ of 0.05 and 0.53 $(BeV/c)^2$, for $\ell n\, d\sigma/dt$ is 9.5 $(BeV/c)^{-2}$ for π^+p elastic scattering.

14) At E = 60 BeV, the π^-p total cross section is 24.2 mb.

The resulting parameters are:

c	=	0.082925
λ	=	0.60071
$x_o(pp)$	=	3.8750
f(pp)	=	6.5812
A(pp)	=	47.372
$x_o(Kp)$	=	1.4295
f(Kp)	=	1.3452
$x_o(\pi p)$	=	3.8457
$f(\pi p)$	=	3.6355
$A(\pi^+p)$	=	29.220
$A(\bar{p}p)$	=	101.81
$A(K^+p)$	=	8.2543
$A(K^-p)$	=	29.384
$A(\pi^-p)$	=	40.416

III.-4) Total Cross Sections

The existing total cross section data is shown in Fig. 1. There is, in addition, cosmic ray data which shows that the proton-proton cross section is rising in the range $10^4 \lesssim s \lesssim 10^6$ GeV.

We predict on the basis of this parameterization of the data that the positive pion, kaon, and proton cross sections will all rise measurably in the energy range available at NAL. Observations of this phenomenon will be of great interest and importance.

Elastic Scattering

Figure 2 shows the predictions for the elastic scattering of protons. A break at $|t|$ somewhere between 1 and 2 $(\text{GeV/c})^2$ in the slope of $d\sigma/dt$ for proton-proton elastic scattering has been known for several years. The interesting feature of this break is that it tends to become more apparent as the incident energy is increased. This behavior is unique compared to other dips, bumps, shoulders, and structures in all channels of hadron-hadron scattering. Within the context of the impact picture, such structure in elastic differential cross sections must develop as the energy increases. This is due to the blackness of the core developing as energy increases and consequently a diffraction pattern with dips must become apparent. We predict two things; first the dip will become more pronounced as energy increases, and secondly, the position of the dip will move slowly to smaller values of momentum transfer as the energy is increased. These qualitative effects should all be observable at both the National Accelerator Laboratory and the ISR.

Recently, preliminary results on pion-proton elastic scattering at large momentum transfer have been reported by Orear et al. A distinct break in $d\sigma/dt$ occurs at $|t| \simeq 2.8$ $(\text{GeV/c})^2$. Our fit successfully predicts a dip at $|t| \simeq 3$ $(\text{GeV/c})^2$ for $s \lesssim 100$ $(\text{GeV})^2$. As the energy is increased the dip develops slightly and its position moves to smaller momentum transfer much more rapidly than in the case of proton-proton elastic scattering. Early experiments in the Meson Laboratory at the

National Accelerator Laboratory will have the accuracy and sensitivity to confirm these predictions for pion-proton scattering.

In the case of Kp elastic scattering we predict that there will be no dip in the cross section. However, we predict that the Kp elastic cross section for $|t| \gtrsim 2$ GeV^2 will be larger than the corresponding cross sections for πp and pp scattering.

We consider now the elastic scattering at small momentum transfer. We have investigated possible structure in our predicted cross section $d\sigma/dt$ for elastic proton-proton scattering in the range $0 \lesssim |t| \lesssim 0.3$. Specifically, we have fitted two straight lines to $\ell n\ (d\sigma/dt)$ to determine the value of $|t| = |t|_{break}$ such that there is an optimum fit. The result is that $|t|_{break} = 0.13 \pm 0.02$ (GeV/c)^2 in the range $10^2 \lesssim s \lesssim 10^6$. In addition, for small changes of parameters given previously this result still holds. A break at $|t| = 0.13$ in the slope of the elastic scattering cross section in proton-proton collisions therefore emerges in a rather parameter-independent way. Our model correctly gives not only the break at a reasonable place ($|t| \approx 0.13$) but also a value of Δb in the range indicated by the experimental data.

Figure 3 shows the available data for b from Serpukhov and the ISR on proton-proton elastic scattering. It can be seen that the rapid shrinkage observed at Serpukhov appears to have slowed down for $s \gtrsim 100$ (GeV)^2. We predict a continuing slow shrinkage for $s > 100$ GeV^2 in both ranges of momentum transfer.

High quality data on b from the USSR-American collaboration at NAL studying proton-proton scattering for $40 \lesssim s \lesssim 800$ and in both ranges of momentum transfer should be able to confirm these predictions.

We predict similar breaks in the πp and Kp differential cross sections. High precision (0.5%) measurements on b will be made in the Meson Laboratory of the National Accelerator Laboratory for both pions and kaons up to $s \simeq 300$ (GeV)^2. The predicted slow shrinkage and breaks should be able to be confirmed by these measurements.

III. -5) Inelastic Diffractive Scattering

Consider the scattering problem with N channels which are coupled through diffractive processes. Let the scattering matrix element be written in impact distance representation as

$$\sim s\ i \int d\vec{x}_\perp\ e^{i \vec{\Delta} \cdot \vec{x}_\perp} \left[I + a(\vec{x}_\perp) \right]$$

where $a(\vec{x}_\perp)$ is an N x N matrix and I is the unit matrix.

It is important to realize that since all diffractive processes are mediated by the same pomeron the effective "potential" involved has the same range and energy dependence. The matrix $a(\vec{x}_\perp)$ describes the scattering mediated by the pomeron and its diagonal elements represent elastic scattering. Since the pomeron is relevant to all the processes, all of the matrix elements of $a(\vec{x}_\perp)$ must be of the same order of magnitude. Since the very words "black core" mean that the diagonal matrix elements of $a(\vec{x}_\perp)$ are small there, the off-diagonal elements of $a(\vec{x}_\perp)$ must also be small there. Thus we conclude

$$a_{ij}(\vec{x}_\perp) \approx 0, \qquad i,j = 1,2,\ldots N$$

inside the core.

Outside the black core, there is a grey fringe of thickness O(1). By definition, the diagonal matrix elements of $a(\vec{x}_\perp)$ in the fringe are O(1). Therefore in the fringe we have all elements of $a(\vec{x}_\perp)$ to be O(1).

$$a_{ij}(\vec{x}_\perp) \approx O(1), \quad i,j = 1,2,\ldots N.$$

Remembering that the unit matrix I is diagonal we see that the dominant contribution to an elastic process comes from the black core. On the other hand, the dominant contribution to a diffractive inelastic process comes from the gray fringe.

Given that the radius of the black core grows as $\ell n s$ and the fringe remains of constant width, we have

$$\frac{\sigma_{\text{elastic}}}{\sigma_{\text{diffractive elastic}}} = \frac{(\ell ns)^2}{(\ell ns)} = \ell ns$$

in the limit of large s.

In terms of the previous parameterization of our model for elastic scattering the diagonal elements of $a(x_\perp)$, the simplest choice for the non-diagonal terms is

$$a_{ij}(s,\vec{x}_\perp) = C_{ij}\ S(s)\ F_{ij}\ (x_\perp^2)\ \exp\left[-S(s)\ F_{ij}(x_\perp^2)\right]$$

where C_{ij} is a real constant and $S(s)$ and $F_{ij}(x_\perp^2)$ are the same functions as defined for elastic scattering.

Using this form of $a_{ij}(s,\vec{x}_\perp)$ we obtain the matrix element for a diffractive inelastic process

$$M_{ij}(s,-\Delta^2) = i\ s\ \lambda\ C_{ij} \sum_{n=1}^{\infty} \frac{n(-1)^{n-1}\ f_{ij}^{\ n}\ \left[s \exp(-i\ \pi/2)\right]}{(n-1)!}$$

$$\left[1 + x_{oij}(\Delta^2 + n^2\lambda^2)^{1/2}\right]\ (\Delta^2 + n^2\lambda^2)^{-3/2}$$

$$\exp\left[-x_{oij}(\Delta^2 + n^2\lambda^2)^{1/2}\right].$$

There are no free parameters other than the overall normalization factor C_{ij}.

Using the previously determined parameters, Fig. 4 shows the predicted cross sections for the reactions:

$$p + p \to p + N^*(1470)$$

$$\pi + p \to \pi + N^*(1470)$$

$$K + p \to K + N^*(1470)\ .$$

In addition we show the experimental data for the reaction

$$p + p \rightarrow p + N^*(1400).$$

The calculated curve is for the reaction

$$p + p \rightarrow p + N^*(1470),$$

and we have normalized the cross section by choosing C_{ij}, for this channel equal to 0.1. The $N^*(1400)$ is shifted in mass relative to the $N^*(1470)$ which is well established in pion-nucleon phase shift analyses. The explanation for this mass shift is not clear. However, if our identification of these two structures being the same particle is correct, then, the steep slope ($b \approx 15$) observed for this reaction is accounted for in the present model. We predict a dip in the cross section at $|t| \approx 0.5$ and furthermore a slow movement of the dip position as the energy is increased. The experimental data is suggestive of a distinct change in slope at $|t| \approx 0.5$, however, there are large systematic uncertainties in the data for $|t| \gtrsim 0.5$ and the situation is unclear at this time. The figure shows that we expect the slope of $d\sigma/dt$ for

$$\pi + p \rightarrow p + N^*(1470)$$

to be significantly less than for the corresponding reaction for incident protons. In addition, there should be dip structures or breaks in these reactions which tend to move fairly rapidly as s is increased.

These three inelastic diffractive channels with no exchange of spin and parity can be studied using the very high resolution strong focusing spectrometer presently being constructed in the Meson Laboratory of the National Accelerator Laboratory.

The degree to which this model satisfies factorization can be investigated at this stage. First, we have calculated the ratios of the following reactions:

$$R(pp) = \frac{p + p \to p + p}{p + p \to p + N^{*}(1400)}$$

and similarly for the πp and Kp channels. If factorization is valid then

$$\mathcal{R} = \frac{R(pp)}{R(Kp)} = \frac{R(\pi p)}{R(Kp)} = 1.$$

Figure 5 shows the predictions of the model as a function of momentum transfer $|t|$. It can be seen that at small $|t|$ the model predicts that to within about 5 to 10%, factorization should hold. At larger $|t|$ factorization continues to be good for the πp and Kp comparison. However, in the pp to Kp comparison there is a marked increase in the extent to which factorization is broken as $|t|$ is increased. Because the differential cross sections are heavily weighted to small $|t|$ the integrated cross sections satisfy factorization to better than about 15%. In addition, we find that the s dependence of $\mathcal{R}$ is extremely weak. Thus, our model is consistent with various experimental checks which show that factorization works to about 10 or 20% for integrated cross sections. However, this model indicates that in the region of the dip which develops at $|t| \simeq 0.5$ for the pp diffraction scattering, factorization should fail rather badly.

The dashed curves are the predictions of the model in the case where we have refitted the model to all of the data given previously, however, in this case we have chosen $c' = 1$ rather than $c' = 0$. The predictions of the model are not sensitive to these choices for c'.

III. -6) Real to Imaginary Part of Forward Scattering Amplitude

The model makes predictions for these ratios for all of the elastic and diffractive inelastic processes already discussed. We recall that in the model the total cross section for a channel j such as pp or $\bar{p}p$ is given by

$$\sigma_{total}\ (j) = A_j s^{-1/2} + \frac{4\pi}{s}\ \mathrm{Im}\ M_j\ (s,o)$$

where $M_j(s,o)$ is defined earlier. Since crossing symmetry is properly taken into account in this model $M_j(s,o)$ is analytic in the upper half plane. It is thus simply a matter of extending the background term $A_j s^{-1/2}$ to complex values of s. If we neglect the masses compared with $\sqrt{s}$ then the ratio of the real to imaginary parts of the forward scattering amplitude is given by

$$\alpha = \frac{-A_{j'} s^{-1/2} + 4.893 \mathrm{Re}\ M_j(s,o)}{A_j s^{-1/2} + 4.893 \mathrm{Re}\ M_j(s,o)}$$

Here j' denotes the corresponding u channel. For example, if j is the pp channel, the j' is the $\bar{p}p$ channel.

In figures 6, 7 and 8, α is plotted in the range $10^2 < s < 10^4$ GeV^2 for pp, $\bar{p}p$, $\pi^{\pm}p$, $K^{\pm}p$. The solid lines are for the parameterization c' = 0 and the dashed lines are for the case c' = 1. The difference between the two sets of curves is quite small. Of course, both sets of curves depend sensitively on the values of the recently measured total pp cross sections at the I.S.R. Figure 1 shows the experimental data for the pp channel from Serpukhov and the I.S.R. The agreement is quite satisfactory.

For s below 100 GeV^2, it is necessary to use the experimental data at lower energies and perform the dispersion integral. For s above 10^4 GeV^2 the two sets of curves are not in good agreement. Qualitatively, all α's approach zero slowly from positive values. For the two sets of curves the value of c is quite different. For c' = 0, c = 0.08 and for c' = 1, c = 0.2. Since we expect c to be less than 1 on very general grounds both values of c are acceptable. However, the choice c' = 1 and c = 0.2 is perhaps to be preferred. Since we are dealing with strong

interactions and c is related to the coupling constant, the larger value of c appears preferably. In addition, in field theories studied so far, it appears that $c' \geq 1$, which lends support to the larger value of c. The only channel which has been experimentally investigated at high energy is once again the pp elastic. The ratio is predicted to increase from a negative value at Serpukhov energies then crosses through zero at $s < 1000$ and becomes positive. The recent data from the ISR is consistent with this behavior. At higher energies the ratio is predicted to have a broad maximum of around +0.1 in the region $10^4 \leq s \leq 10^5$ and then to fall asymptotically to zero with a $(\log s)^{-1}$ dependence.

III. -7) Ratio of Elastic to Total Cross Section

In the limit of very high s where the black core dominates in its contribution to the elastic scattering amplitude we expect

$$\sigma_{el}/\sigma_{Tot} \to 1/2.$$

On the one hand our phenomenological model of the impact picture fits this requirement, and on the other hand, it is clear from the preceding discussion that the model fits the present values of $\sigma_{el}/\sigma_{Tot} \approx 0.17$ measured at the ISR. The predicted rate of increase of this ratio, σ_{el}/σ_T from the present value of 0.17 to the asymptotic value of 0.5 is very low. For example at $s \approx 10^6$ the ratio is still not more than about 0.25. It is a fact that some functions approach their limiting values more slowly than other functions!

IV. Other Predictions of the Impact Picture

IV. -1) Pionization

In Section II we mentioned the relationship between the increase of total cross sections with energy and the production of slow particles in the center of mass system. The impact picture provides this correlation between these two phenomena in a quite precise way. There is no way out of the dilemma for the impact picture if

a) one or other of the two phenomena do not exist,

b) the s dependence of the two phenomena are not correlated.

We have previously discussed the existence of rising total cross sections. Experimentally, there is now also evidence from the ISR that pions are produced with low momentum in the center of mass system and in accord with the predicted distribution

$$\frac{d^3p}{E} f(p_\perp^2) \left[\ell ns\right]^n \times s^q$$

where q is related to c and is positive.

Figure 9 shows the data for the reaction $p + p \rightarrow \pi + \text{Anything}$. The above distribution leads to a flat distribution in rapidity as observed. Secondly, we expect a rise in the cross section for this pionization as s is increased in the range of the ISR where the total cross section begins to increase. Figure 10 shows the available data. The situation is not clear at this time as the accuracy of the data is not very good. However, a rise is suggested by the data.

The approach to the asymptotic s dependence in the central region predicted by this model is surely going to be slow. Not only is this suggested by Mueller type arguments, but more convincingly, the present data on the π^-/π^+ ratio in the central region at ISR energies is approaching 1 rather slowly. Hence it will be difficult to make a convincing comparison of the predicted and observed s dependence of pionization in the central region at available ISR energies. Clearly, a higher energy storage ring would be very useful in this regard.

There are of course many ways to saturate the Froissart bound. However, the connection between the total cross section and pionization is a key stone of the impact picture. Thus accurate data on this process is of great importance to assess the relevance of the impact picture.

Finally, in this connection, we should say that the predicted $s^q \left[\log s\right]^n$ dependence should hold for any $p_\perp$ for large enough s.

IV. -2) Pionization in Exclusive Processes

The impact picture predicts that a similar distribution

$$\frac{d^3p}{E} f(p_\perp^2) \left[\ell ns\right]^m \qquad (m \text{ negative})$$

should hold for exclusive processes with suitable quantum numbers. For example the above distribution should hold for the reaction

$$p + p \to \pi^+ + \pi^- + p + p.$$

Thus for this exclusive channel there should be a flat rapidity distribution and in addition a $\left[\ell ns\right]^m$ energy dependence. There is already some experimental evidence for both of the effects.

V. Conclusions

We have made a preliminary appraisal of the relevance of the Impact Picture for high energy hadron interactions. The conclusions at this time are the following:

1) The prediction that total cross sections rise with energy is correct for two channels and represents a major qualitative triumph for the theory. Fairly firm predictions are now given for the other channels.

2) The predicted pionization has been found to exist. The energy dependence of this process has not yet been carefully checked and may prove difficult at existing energies.

3) The predicted development of diffraction minima in the elastic scattering has been found to take place. The predicted s dependence of the position of the minima in the cross section has not yet been checked.

4) The predicted slow shrinkage in the slope parameter (b) at high energy is in good agreement with the data.

5) Predictions for πp and Kp elastic scattering have yet to be fully tested. However, the predicted first diffraction minimum in the πp case at $|t| \simeq 3$ appears to have been seen experimentally.

6) Predictions for diffractive inelastic scattering in the various

channels have been given but there is little data to confront the predictions. The little data which exists is consistent with the theory. To a good approximation factorization is predicted for these channels at low momentum transfer.

7) The predicted real to imaginary ratio for the elastic pp amplitude is consistent with the data. Predictions are given for the phase of the $\pi^{\pm}$, $K^{\pm}$ forward scattering amplitudes.

Thus there is a fairly broad agreement between the predictions of the Impact Picture and the available data on the scattering of hadrons at high energy. Many new tests have been suggested here, which when completed will subject the Impact Picture to more detailed investigation. It is extremely encouraging at this time, however, that a single consistent theoretical picture seems to be emerging which on the one hand satisfies the fundamental tenets of field theory and on the other provides a unifying view of total cross sections, elastic cross section, and inclusive reactions for all channels in hadron physics. It remains a major challenge in the near future to subject this theory to further confrontations with experimental data.

I acknowledge many stimulating discussions with Professors H. Cheng and T. T. Wu.

Figure Captions

Fig. 1 Total hadron-proton cross sections in millibarns are shown as a function of s (the square of the center-of mass energy). The curves are predictions of the impact picture with the parameterization given in the text.

Fig. 2 Proton-proton differential elastic scattering cross section $d\sigma/dt$ as a function of $|t|$ for various values of s. The solid curves are predictions of the impact picture with the parameterization given in the text.

Fig. 3 Values of the slope parameter b at small momentum transfer ($0.05 \leqslant |t| \leqslant 0.15$) and intermediate momentum transfer ($0.15 \leqslant |t| \leqslant 0.35$) are shown as a function of s. The curves are the predictions of the impact picture with the parameterization given in the text.

Fig. 4 Diffractive inelastic scattering without spin or parity exchange for the pp, πp, and Kp channels. The solid curves are predictions of the impact picture with the parameterization given in the text. The chosen values of s are those possible at the ISR and also with pion and kaon beams at the NAL and CERN II.

Fig. 5 $\mathcal{R} = \frac{R(hp)}{R(h'p)}$, where R(hp) is the ratio of the elastic to diffractive inelastic channel, is plotted versus $|t|$ for s = 100 GeV^2.

Fig. 6 Real to imaginary part of the forward scattering amplitude for the proton proton case. The solid and dashed curves are for the cases c' = 0 and c' = 1 respectively.

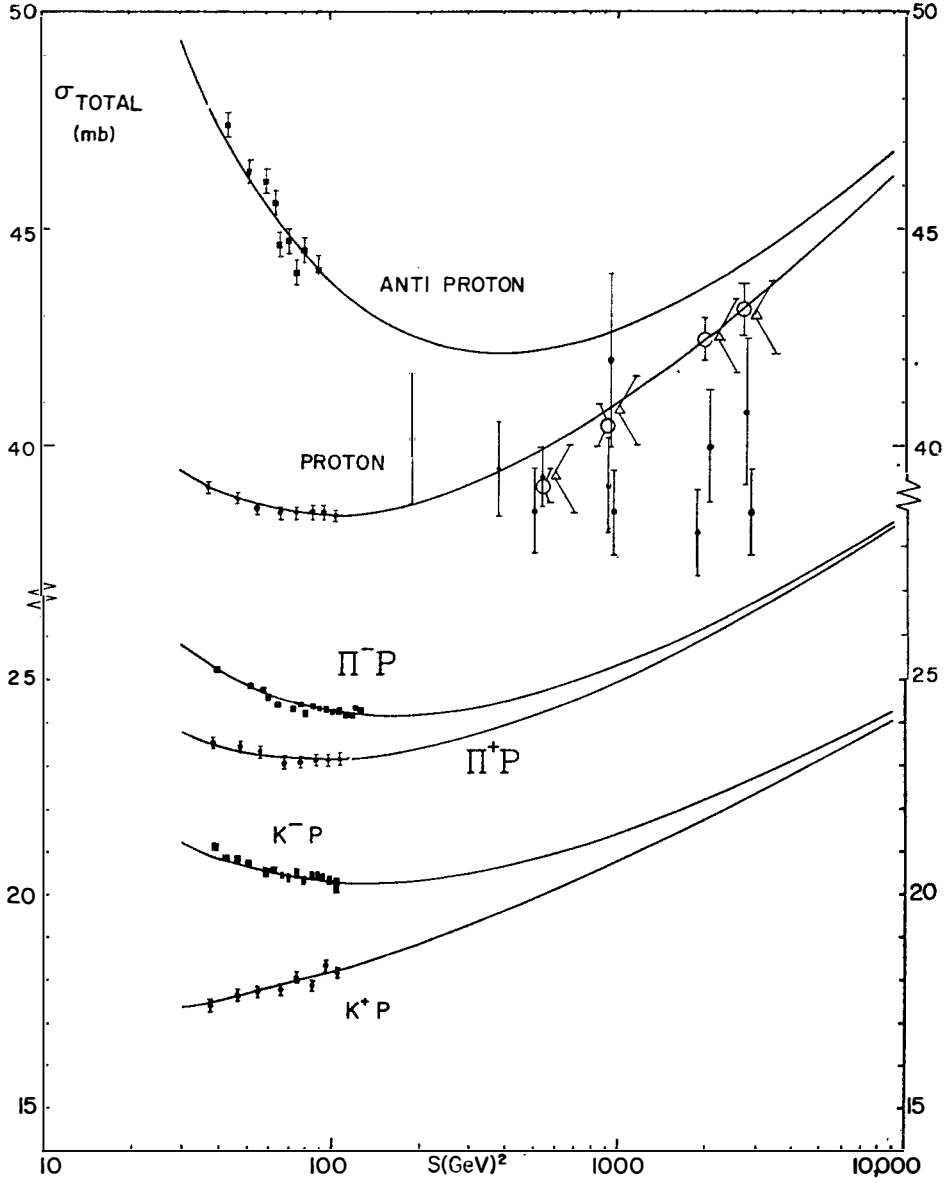
Fig. 7 Real to imaginary part of the forward scattering amplitude for the pion proton case. The solid and dashed curves are for the cases c' = 0 and c' = 1 respectively.

Fig. 8 Real to imaginary part of the forward scattering amplitude for the kaon proton case. The solid and dashed curves are for the case c' = 0 and c' = 1 respectively.

Fig. 9 Rapidity Plot in the central region for pion production in proton-proton collisions.

Fig. 10 Energy dependence of the 90 degree differential cross section for pion production in proton-proton collisions.

Fig. 1


σ TOTAL
(mb)
ANTI PROTON
PROTON
Π⁻P
Π⁺P
K⁻P
K⁺P
50
45
40
25
20
15
10
100
S(GeV)²
1000
10,000

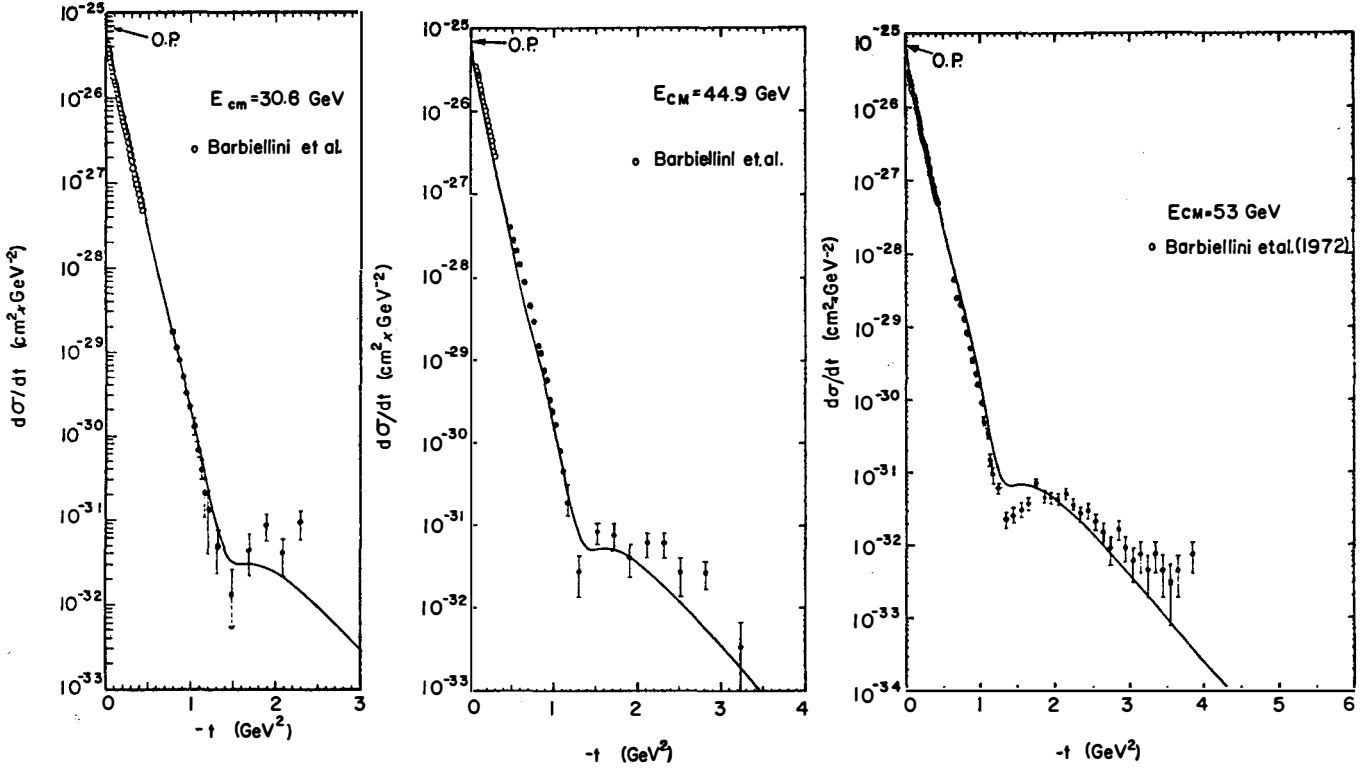

O.P.
E cm =30.6 GeV
o Barbiellini et al.
dσ/dt (cm²xGeV⁻²)
-t (GeV²)
O.P.
E CM =44.9 GeV
o Barbiellini et.al.
dσ/dt (cm²xGeV⁻²)
-t (GeV²)
O.P.
Ecm=53 GeV
o Barbiellini et.al.(1972)
dσ/dt (cm²xGeV⁻²)
-t (GeV²)

Fig. 2

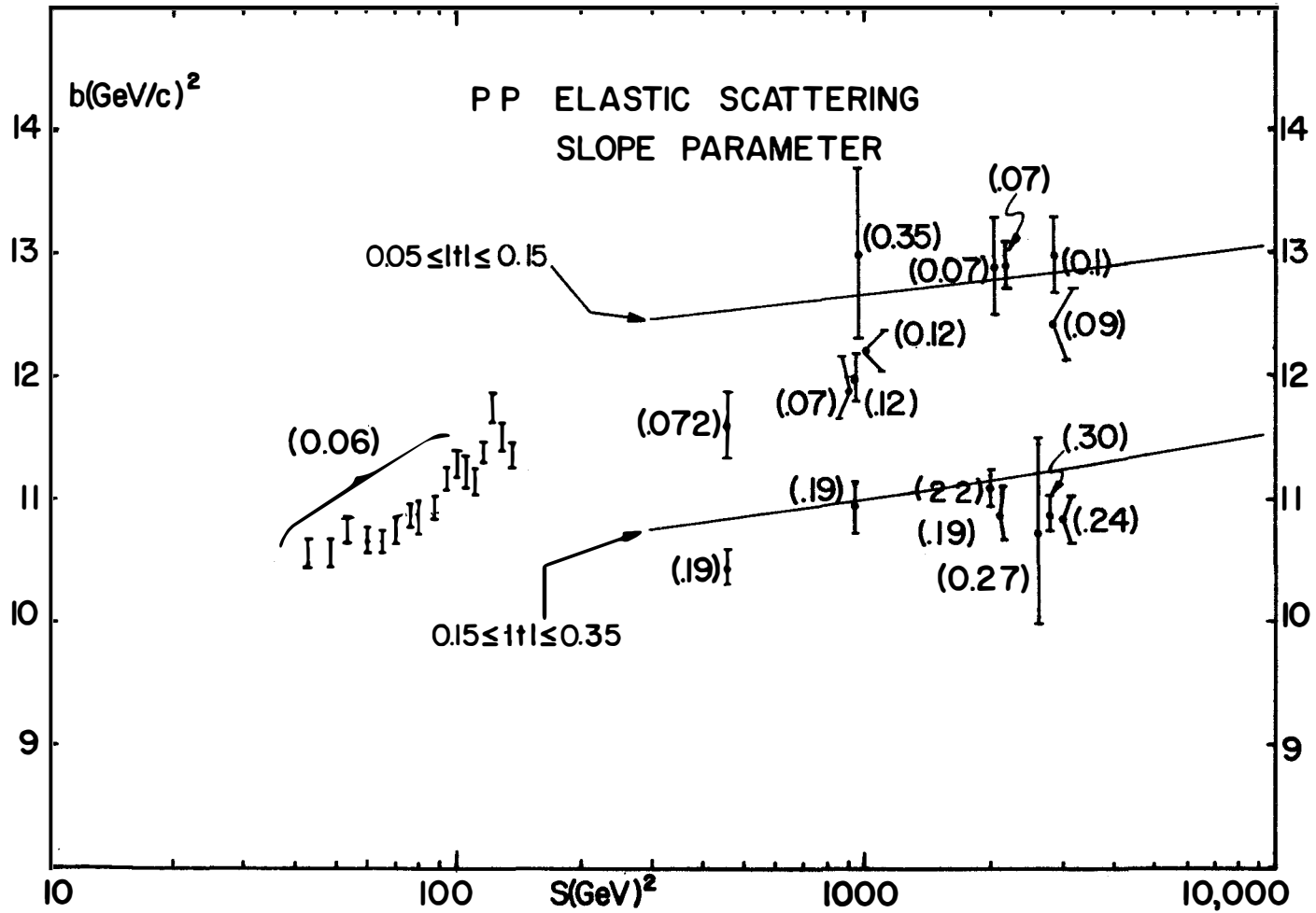

b(GeV/c)²
P P ELASTIC SCATTERING
SLOPE PARAMETER
0.05≤|t|≤0.15
0.15≤|t|≤0.35
(0.35)
(.07)
(0.07)
(0.1)
(0.12)
(.09)
(0.07)
(.12)
(0.06)
(0.072)
(.30)
(.19)
(.22)
(.24)
(.19)
(0.27)
(.19)
14
13
12
11
10
9
10
100
S(GeV)²
1000
10,000

Fig. 3

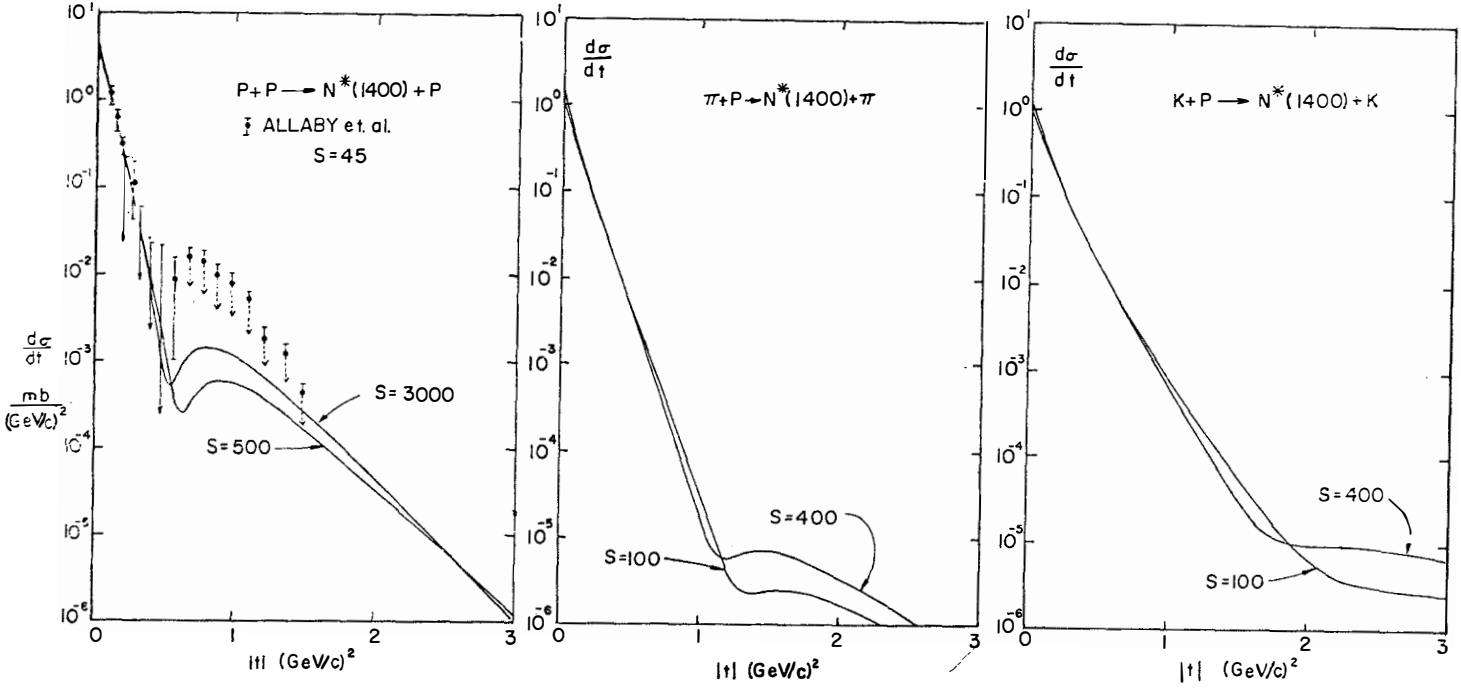

P+P → N*(1400) + P
ALLABY et. al.
S=45
S=3000
S=500
dσ/dt
mb/(GeV/c)²
|t| (GeV/c)²
π+P → N*(1400)+π
S=400
S=100
K+P → N*(1400) + K
S=400
S=100

Fig. 4

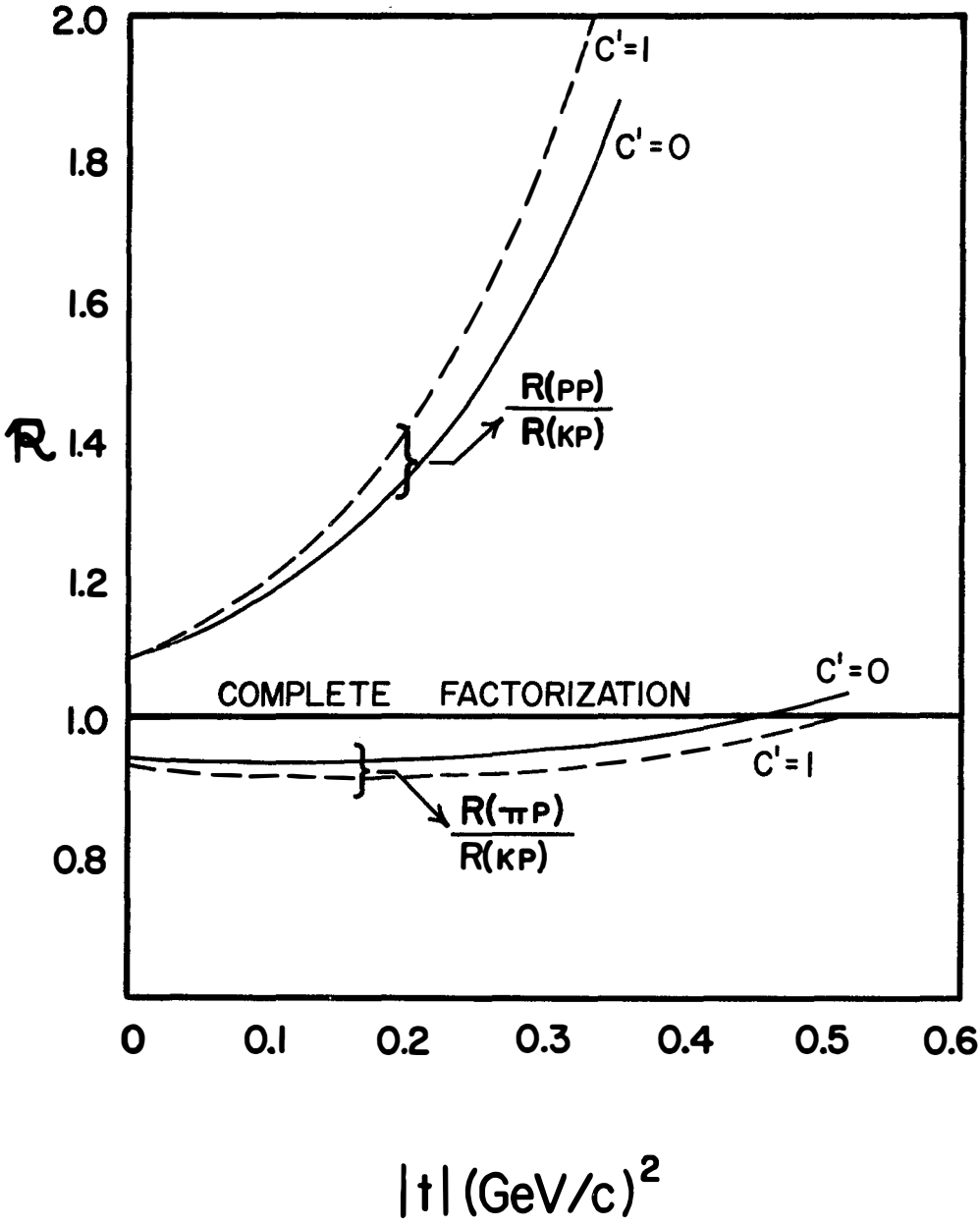

2.0
1.8
1.6
R 1.4
1.2
1.0
0.8
C'=1
C'=0
R(PP)
R(KP)
COMPLETE FACTORIZATION
C'=0
C'=1
R(πP)
R(KP)
0
0.1
0.2
0.3
0.4
0.5
0.6
|t| (GeV/c)²

Fig. 5

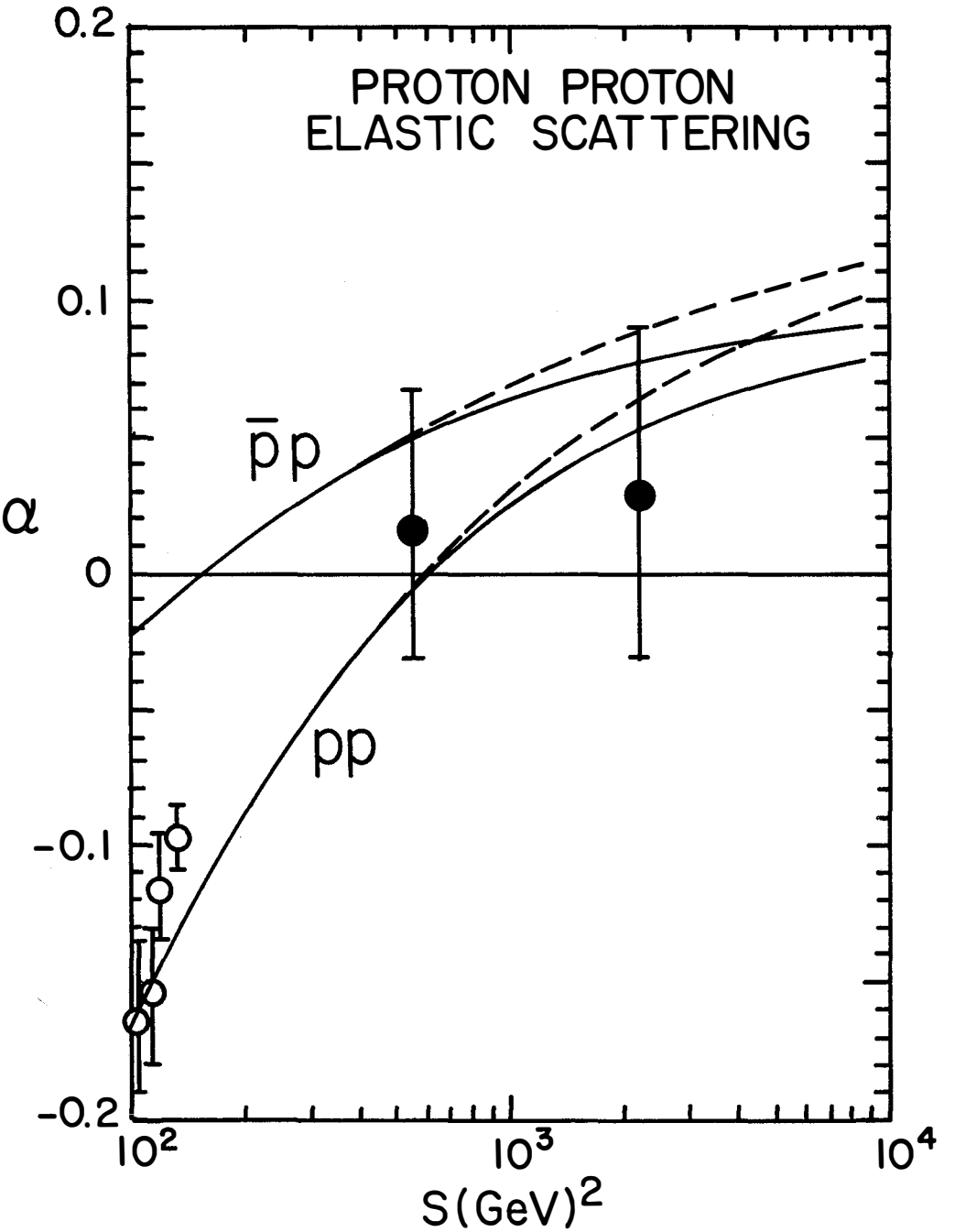

PROTON PROTON
ELASTIC SCATTERING
0.2
0.1
0
-0.1
-0.2
α
p̄p
pp
10²
10³
10⁴
S(GeV)²

Fig. 6

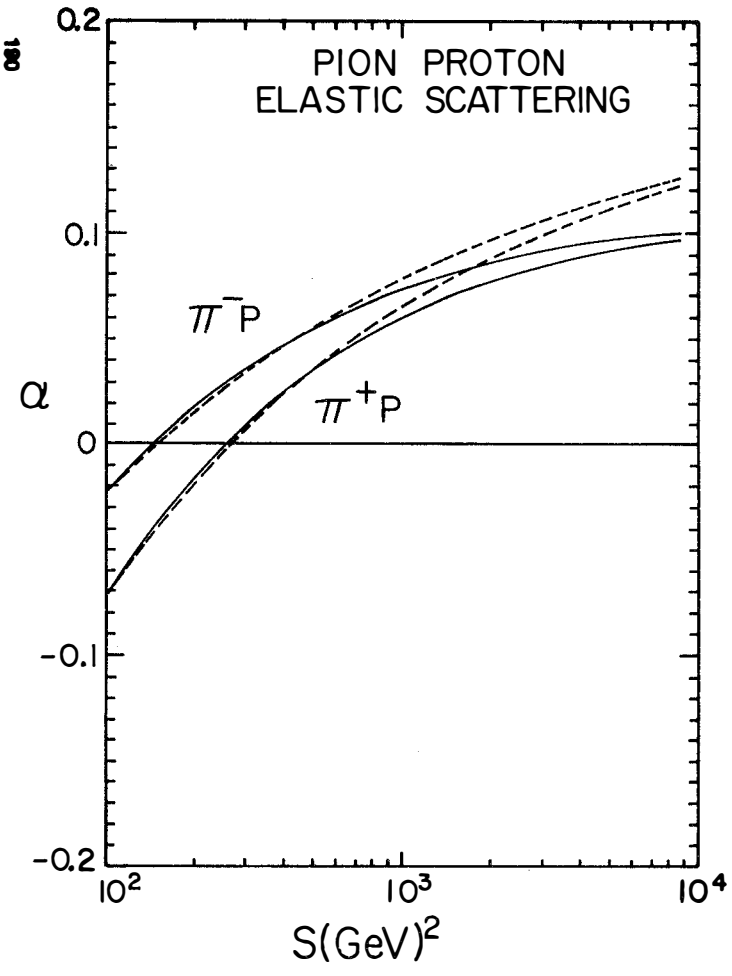

PION PROTON
ELASTIC SCATTERING
0.2
0.1
0
-0.1
-0.2
α
$\pi^- P$
$\pi^+ P$
10^2
10^3
10^4
S(GeV)^2

Fig. 7

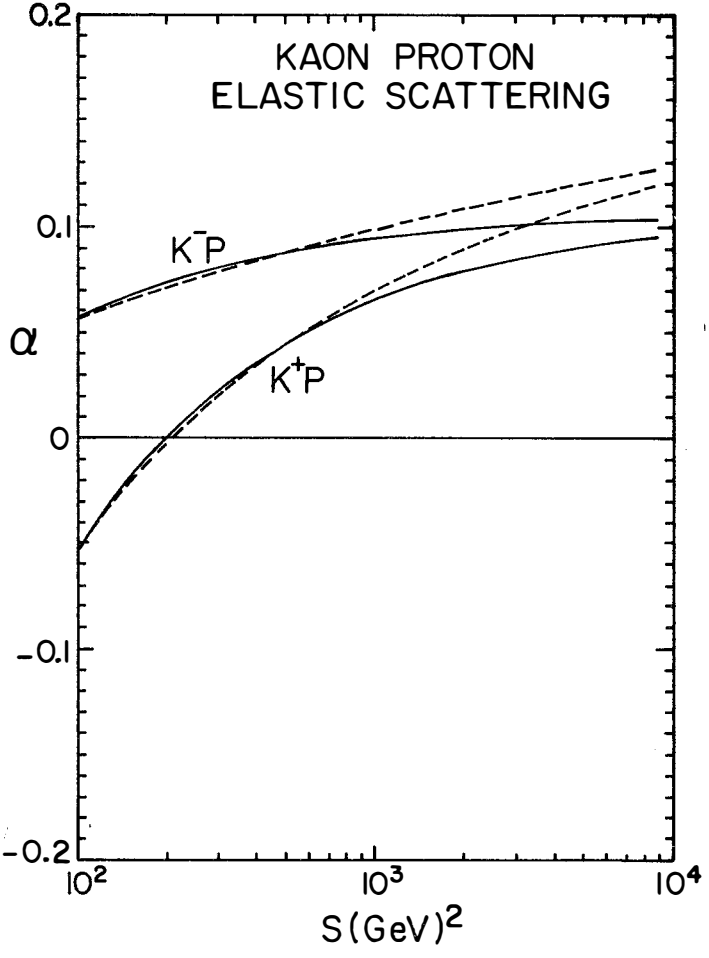

KAON PROTON
ELASTIC SCATTERING
0.2
0.1
0
-0.1
-0.2
α
$K^- P$
$K^+ P$
10^2
10^3
10^4
S(GeV)^2

Fig. 8

RAPIDITY PLOT IN THE "CENTRAL" REGION
FOR VARIOUS p_T, FOR π^+ AND π^-

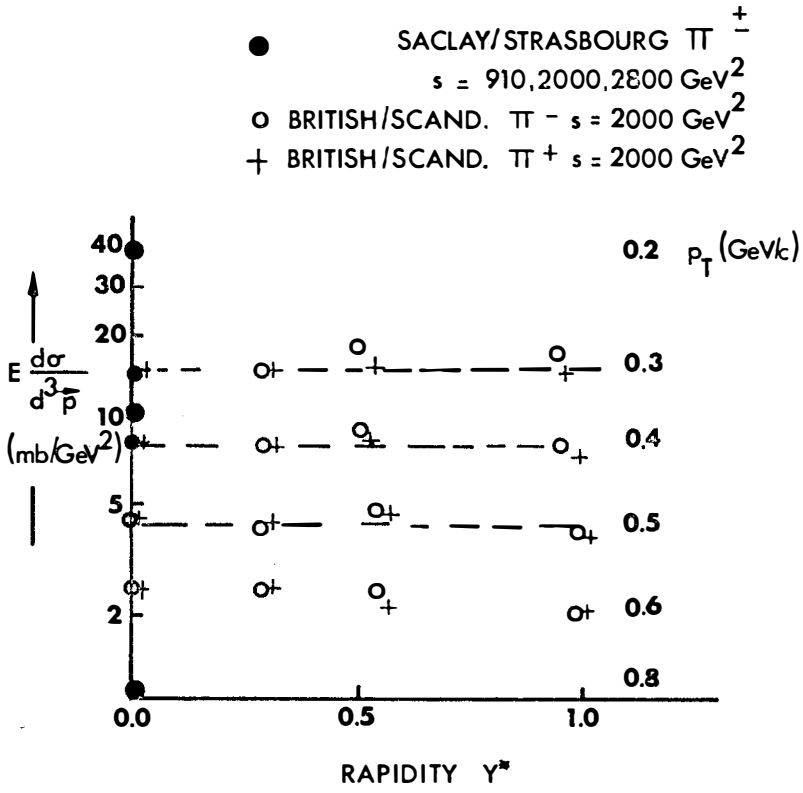


Fig. 9

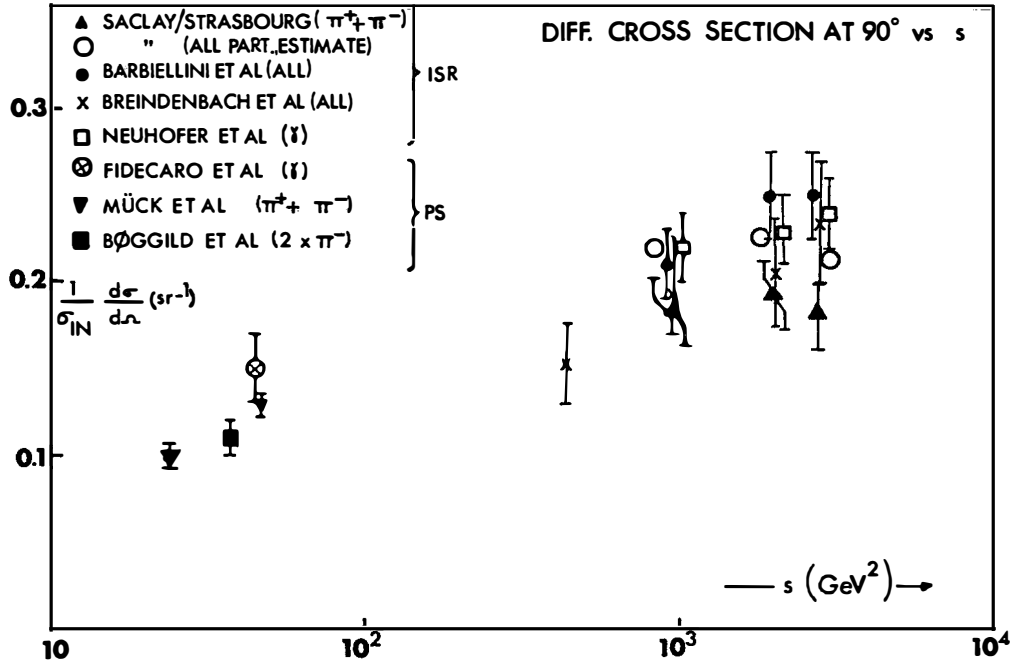

DIFF. CROSS SECTION AT 90° vs s
SACLAY/STRASBOURG (π⁺+ π⁻)
" (ALL PART.,ESTIMATE)
BARBIELLINI ET AL (ALL)
BREINDENBACH ET AL (ALL)
NEUHOFER ET AL (γ)
FIDECARO ET AL (γ)
MÜCK ET AL (π⁺+ π⁻)
BØGGILD ET AL (2 x π⁻)
ISR
PS
1/σ_IN dσ/dΩ (sr⁻¹)
0.3
0.2
0.1
10
10²
10³
10⁴
s (GeV²)

Fig. 10

SHADOW APPROACH TO DIFFRACTION SCATTERING

E.H. de Groot
Department of Theoretical Physics
Oxford University

and

H.I. Miettinen[+)]
Rutherford High Energy Laboratory
Chilton, Didcot, Berkshire

Abstract : The use of s-channel unitarity in calculating high energy elastic scattering from multiparticle production amplitudes is discussed. The important role played by the phases of the production amplitudes for this problem is emphasized. As an illustration of the s-channel techniques, a simplified analysis of high energy elastic proton-proton scattering is performed.

Résumé : On discute l'utilisation de l'unitarité dans la voie s dans le calcul de la diffusion élastique à haute énergie à partir des amplitudes de production multiple. Le rôle important, dans ce problème, des phases des amplitudes de production est souligné. On donne une analyse simplifiée de la diffusion élastique proton-proton à haute énergie comme illustration de ces techniques de voie s.



[+)] Herman Rosenberg Foundation Fellow. On leave of absence from the Research Institute for Theoretical Physics, University of Helsinki, Finland.

SHADOW APPROACH TO DIFFRACTION SCATTERING

1. Introduction
2. The s-Channel Unitarity Relation
3. Shadow Calculation of Elastic Scattering
4. Illustrative Analysis of High Energy Proton-Proton Scattering Data
5. Summary and Conclusions

1. Introduction

High energy diffraction scattering can be discussed either in the exchange channel or in the direct channel language. In the exchange picture a diffraction process proceeds via the exchange of a singularity, the Pomeron, in the t-channel of the process. This singularity has vacuum quantum numbers, its spin properties are complicated and no physical particles are known to correspond to it. Moreover, one has not the slightest idea of its physical origin. In the direct channel picture the Pomeron is an absorptive effect. It is generated as a shadow of the competition of the many inelastic channels. Its full nature and properties are not well understood in this picture either, but at least one has a framework in which to study them.

This talk is devoted to a discussion of the s-channel approach to diffraction scattering. The material is organized as follows: In Section II we briefly discuss the relation between diffraction scattering and particle production processes

provided by s-channel unitarity. The next Section is devoted to a discussion of the shadow calculation of elastic scattering and of the importance of the phases of production amplitudes for this calculation. In Section IV we illustrate the shadow techniques by performing a simplified analysis of high energy proton proton scattering. Finally, a few conclusions are drawn.

In the present discussion we concentrate to the physical ideas and neglect the technical details. A more complete discussion, as well as a detailed analysis of experimental data will be presented in a forthcoming publication.

2. The s-Channel Unitarity Relation

The basic dynamical quantity describing a collision process is the relativistic S-matrix. Conservation of probability implies that S is unitary:

$$S^+S = S\,S^+ = 1 \,. \tag{1}$$

Separating the scattered wave

$$S = 1 + iT \,, \tag{2}$$

and inserting this into (1) we get

$$i\,(T - T^+) = T^+T \,. \tag{3}$$

Sandwiching this between an incoming elastic state $|i\rangle$ and an outgoing elastic state $|f\rangle$, using the completeness relation $\sum_n |n\rangle\langle n| = 1$ and choosing suitable normalizations we get

$$(4)\quad 4\sqrt{\pi}\ \mathrm{Im}\ T_{el}(t) = \sum_{i'' = \text{elastic states}} \langle f|T^{+}|i''\rangle\langle i''|T|i\rangle \; + \sum_{n = \text{inelastic states}} \langle f|T^{+}|n\rangle\langle n|T|i\rangle \ ,$$

where we have separated the elastic intermediate states from the inelastic ones in the right hand summation. Eq. (4) is the s-channel unitarity relation. It will form the basis for the rest of our discussion.

Let us call the three terms of Eq. (4) the total, elastic and inelastic overlap functions, respectively:

$$(5)\quad \begin{aligned} \tau_{tot}(t) &= 4\sqrt{\pi}\ \ \mathrm{Im}\ T_{el}(t) \\ \tau_{el}(t) &= \sum_{i''} \langle f|T^{+}|i''\rangle\langle i''|T|i\rangle \\ \tau_{inel}(t) &= \sum_{n} \langle f|T^{+}|n\rangle\langle n|T|i\rangle \end{aligned}$$

In forward direction Eq. (4) is the well known Optical Theorem. The overlap functions are thus normalized:

$$(6)\quad \begin{aligned} \tau_{tot}(0) &= \sigma_{tot} \\ \tau_{el}(0) &= \sigma_{el} \\ \tau_{inel}(0) &= \sigma_{inel} \ . \end{aligned}$$

According to Eq. (4) the imaginary part of the elastic amplitude is built up by two parts: the second term on the right hand side gives the shadow of the inelastic channels open, the first term

that of the elastic scattering itself. Thus Eq. (4) is a non-linear integral equation for the elastic amplitude. It can be easily solved in impact-parameter space.

The unitarity relation shows that the t-dependence of elastic scattering is generated by the variation of the inelastic amplitude in a rotation, i.e. by the overlap between the production amplitudes $\langle f|T^+|n\rangle$ and $\langle f|T|i\rangle$, where $|f\rangle$ is obtained from $|i\rangle$ by a rotation of the elastic scattering angle.+) A very important observation is that the phases of the production amplitudes enter explicitly into the calculation. Thus, even if the magnitudes of the amplitudes $\langle f|T^+|n\rangle$ and $\langle n|T|i\rangle$ do not vary too much in the rotation, if the phases are rapidly varying the generated elastic amplitude will have a steep t-dependence. As we will see later, the phases play a dominant role in practical calculations.++)

Our second comment concerns the linear nature of the inelastic overlap function. If we have, for instance, two non-interfering production mechanisms 1 and 2 the overlap functions are additive:

+) This is why Van Hove called the terms (5) 'overlap functions'.[1]

++) This has been known for a long time. See e.g. the calculations of Michejda et al [2] and de Groot[3].

(7) $$\tau_{inel} = \tau_{inel}(1) + \tau_{inel}(2) .$$

The "output" of the unitarity relation, ImT_{el} is obviously not linear: $ImT_{el} \neq ImT_{el}(1) + ImT_{el}(2)$.

To solve the unitarity equation we transform it into impact parameter space. Defining the Fourier-transform

(8) $$\tilde{\tau}(x_\perp) = \frac{1}{2\pi} \int d^2\vec{p}_\perp \, e^{-i\vec{p}_\perp \vec{x}_\perp} \tau(p_\perp) \quad , \quad |\vec{p}_\perp| = \sqrt{-t}$$

and transforming Eq. (4) we get (To simplify the discussion we take the elastic amplitude to be completely imaginary for all t)

(9) $$\frac{1}{8\pi}\left[\tilde{\tau}_{tot}(x_\perp)\right]^2 - \tilde{\tau}_{tot}(x_\perp) + \tilde{\tau}_{inel}(x_\perp) = 0,$$

which can immediately be solved:

(10) $$\frac{1}{2\pi} \tilde{\tau}_{tot}(x_\perp) = 2\left[1 \pm \sqrt{1 - \frac{1}{2\pi} \tilde{\tau}_{inel}(x_\perp)}\right]$$

Notice that this equation connects the inelastic and total overlap functions at the same impact parameter. This follows from angular momentum conservation and makes the impact parameter representation very convenient for the study of unitarity effects.

The Fourier-transform $\frac{1}{2\pi} \tilde{\tau}_{inel}(x_\perp)$ measures the absorption to inelastic channels at an impact parameter $x_\perp$. Thus unitarity provides the limits:

(11) $$0 \leq \frac{1}{2\pi} \tilde{\tau}_{inel}(x_\perp) \leq 1.$$

The functional dependence of the total and elastic overlap functions on the inelastic overlap function is shown for the

negative-sign (high energy) solution in Fig. 1. When the amount of absorption is small the imaginary part of the elastic amplitude is built up mainly by the inelastic channels. However, when the absorption approaches its maximum value, the elastic overlap function increases very rapidly and provides an important contribution to the elastic amplitude. Finally, when the amount of absorption approaches the upper unitarity limit, the elastic and inelastic overlap functions become equal.

A study of the solution (10) makes it easy to understand the experimentally observed ratios of the elastic to total cross sections[1]. By (6) and (8)

$$\sigma_i = \int \underset{\perp}{x} \, d\underset{\perp}{x} \, \tilde{\tau}_i(\underset{\perp}{x}) \tag{12}$$

for i = elastic, inelastic and total, respectively. Assuming purely imaginary scattering one gets e.g. for the "Black Disc" model

$$\frac{1}{2\pi} \tilde{\tau}_{inel}(\underset{\perp}{x}) = \begin{cases} 1 & 0 \leq \underset{\perp}{x} \leq R \\ 0 & \underset{\perp}{x} \geq R \end{cases} \tag{13}$$

the ratio $\sigma_{el}/\sigma_{tot} = 1/2$. For a more reasonable shape, as e.g. a Gaussian, with nearly 100% absorption at $\underset{\perp}{x} = 0$ one will get $\sigma_{el}/\sigma_{tot} \approx 0.15 - 0.2$. This agrees well with the experimentally measured values. The small ratio of elastic to inelastic scattering follows from the strong suppression of the elastic shadow when the absorption deviates from the upper unitarity

limit.

3. Shadow Calculation of Elastic Scattering

The idea of the s-channel or "shadow" approach is to use the unitarity relation (4) to derive the elastic amplitude from a theory of particle production processes. This is - both theoretically and in practice - a very difficult program. However, even when incompletely performed, it can provide important insight into the nature and structure of elastic scattering.

The shadow calculation of elastic differential cross-section goes in four steps:

(1) To start with, one specifies a model for particle production processes. Because the phases of the multiparticle amplitudes enter explicitly into the calculations, both the absolute values and the phases of the production amplitudes must be specified. The absolute values of the amplitudes are strongly constrained by the requirement that the model must be (at least approximately) consistent with the existing multiparticle data. The phases, however, can not be directly measured in multiparticle production. They must be assumed and these assumptions can be made quite arbitrarily (the main constraint being 'the spirit of the model').

(2) At the second step one calculates the inelastic overlap function from the production amplitudes. The calculation can be performed either by using numerical methods (on a computer),

with the help of sophisticated mathematical techniques borrowed from statistical physics or with techniques especially developed for this problem[4].

(3) At the third step the inelastic overlap function is inserted into the unitarity equation and the imaginary part of the elastic amplitude is solved.

(4) Before the result can be compared with the experimental data both the real and the imaginary parts of the elastic amplitude must be known. The real part of the amplitude can be calculated - at least in principle - from the imaginary part using dispersion relations. Another way to proceed is to make an educated guess of the phase, supporting it by phenomenological and/or theoretical arguments.

The final result depends crucially on all of the four steps 1-4. This makes the full program very hard to carry out. But, as already mentioned, even when incompletely performed, it can provide useful insight into the nature and the structure of high energy elastic scattering.

The most straightforward way to simplify the approach is to skip the first two steps and to start by assuming a simple form for the inelastic overlap function (either in momentum space or in impact parameter space). The inelastic overlap function is the important link between the elastic scattering amplitude and

the particle production amplitudes which build it up, and thus it is useful to learn its properties. It also turns out that the complicated structure in both s and t of the experimentally observed elastic differential cross sections can easily be generated by inelastic overlap functions which have a relatively simple dependence on s and t.

The s-channel unitarity approach is based on the hope that the inelastic overlap function is insensitive to the details of the "input" production amplitudes and depends only on the dominant dynamical features of them. Why is it reasonable to assume that this could be the case? The answer is that the calculation of the overlap function involves n-fold phase space integrations which strongly smear the "input" information. Thus one can hope that the output depends only on the main properties of the input and all minor details of the input are washed away in the integration procedure.

Let us next do a simple but instructive exercise. To get an idea of what a realistic inelastic overlap function looks like we shall calculate an "experimental" overlap function by starting from data and performing the steps (3) and (4) in the reverse order.+) Consider the unitarity equation (4). Moving the

+) This exercise has been done earlier e.g. by Zachariasen[5] and de Groot[3].

elastic overlap function to the left hand side Eq. (4) reads

$$(14) \qquad 4\sqrt{\pi}\ \mathrm{Im}T_{el}(t) - \tau_{el}(t) = \tau_{inel}(t) \ .$$

With a reasonable assumption of the elastic phase we can solve $\mathrm{Im}T_{el}(t)$ and $\mathrm{Re}T_{el}(t)$ from the elastic scattering data. Inserting them to the left hand side of Eq. (14) and performing the loop integration we obtain an "experimental" inelastic overlap function. The results of this exercise with real data are shown and discussed in the next Section. Here we shall just do a quick mathematical calculation to give a rough idea of the answer.

Consider high energy diffraction scattering. The t-dependence of the differential cross section can well be approximated by an exponential

$$(15) \qquad \frac{d\sigma}{dt} \sim e^{At} \ .$$

A reasonable first guess of the phase of the elastic amplitude is to take the amplitude to be purely imaginary. Thus

$$(16) \qquad 4\sqrt{\pi}\ \mathrm{Im}T_{el}(t) = \sigma_{tot}\, e^{\frac{1}{2}At} \text{ and } \sigma_{el} = \frac{\sigma_T^2}{16\pi A} \ .$$

The loop integration in (14) reduces the peripherality of the input by a factor of two. Thus we get

$$(17) \qquad \tau_{el}(t) = \sigma_{el} e^{\frac{1}{4}At}$$

Combining Eqs. (16) and (17) we obtain the result

$$(18) \qquad \tau_{inel}(t) = \sigma_{tot} e^{\frac{1}{2}At} - \sigma_{el} e^{\frac{1}{4}At} \ .$$

This exercise is illustrated in Fig. 2.

From the result of our exercise we learn an important lesson. The experimental overlap function changes sign becoming negative at $t_o = \frac{4}{A} \ln \left(\frac{\sigma_{el}}{\sigma_{tot}} \right)$. Inserting typical experimental values $\sigma_{tot} = 40$ mb, $\sigma_{el} = 8$ mb we get for the position of the zero $t_o = - 0.625$ GeV^2. The existence of the zero does not depend on the assumed elastic phase and even the position of the zero is roughly independent of the phase (as long as the amplitude is dominantly imaginary in the forward direction). This observation that a reasonable inelastic overlap function is not positive definite has a direct implication for the theoretical multiparticle models. If the phases of the production amplitudes are neglected the overlap function will measure the overlap of two positive quantities and thus be a positive quantity itself. The fact that the inelastic overlap function becomes negative at moderate t-values is a direct indication of the crucial role played by the phases of the production amplitudes in building the imaginary part of the elastic amplitude.

The importance of the phases of the production amplitudes for the shadow calculation makes it necessary to get some understanding of their physical interpretation.+) We shall

+) For a deep discussion on the physical interpretation of the phases of production amplitudes see Koba and Namiki [6].

give here a very brief and superficial discussion of this problem. Our discussion is valid for a general class of statistical models including the Uncorrelated Jet Model[++].

Let us consider a simple example of a one-particle production amplitude:

[++]The transverse dynamics of the Multiperipheral Model, however, is very different from that of e.g. the Uncorrelated Jet Model. It is clear that phases, if properly taken into account, affect the results strongly also in the MPM. It is less clear, however, whether reasonable numerical agreement with the elastic scattering data can be obtained within the MPM when neglecting the phases. The calculations of Michejda et al[2] suggest that the answer is no. Michejda et al use a realistic version of the MPM (the so-called Chan-Loskiewicz-Allison model[7] and determine the parameters of the model from experimental data. When the phases are neglected they obtain for the elastic differential cross section $d\sigma/dt \sim e^{At}$ with $A \tilde{>} 1.5$ GeV^{-2}. -- For an opposite answer see the talk of Frank Henyey in these proceedings[8]. Notice, however, that the phases must be included also in the MPM is one wants the model to produce an overlap function which has zeros.

$$(19) \qquad \rho(\vec{k},\vec{\eta}) = \frac{1}{\sqrt{\pi<k_\perp^2>}}\, e^{-\frac{1}{2}\frac{\vec{k}_\perp^2}{<k_\perp^2>}}\, e^{-i\vec{\eta}\,\cdot\,\vec{k}}$$

This is an amplitude for producing one particle with the momentum $\vec{k}$. The vector $\vec{\eta}$ (a parameter) is chosen to be orthogonal to the momenta of the incoming particles. The physics of the magnitude of the amplitude (19) is clear. It corresponds to a Gaussian cut-off in the transverse momentum with a width $<k_\perp>$. To see the physical significance of the phase factor it is useful to transform the amplitude (19) into the impact parameter space:

$$(20) \qquad \tilde{\rho}(\vec{x}_\perp,\vec{\eta}) = \sqrt{\frac{<k_\perp^2>}{\pi}}\, e^{-\frac{1}{2}<k_\perp^2>\,(\vec{x}_\perp-\vec{\eta})^2} .$$

This is a Gaussian distribution in the impact parameter. The width of the distribution is related to the average transverse momentum $<k_\perp>$ by the uncertainity principle $<\Delta x_\perp> \sim \frac{1}{<k_\perp>}$. The center of the distribution is at $\vec{x}_\perp = \vec{\eta}$. The magnitude and the phase of the amplitude (19) have thus clear physical interpretations: the magnitude is related to the size and shape of the production volume whereas the phase of the amplitude is related to the average position of the volume in which the particle is produced. This observation also sheds light on the importance of the phases for the calculation of the elastic scattering. A shift of the production volume in the transverse direction corresponds to a change in the total s-channel angular momentum of the produced particles and it is exactly the total s-channel

angular momentum of the collision which determines the peripherality of the elastic differential cross section.

The phase considered above is a very simple one. However, it illustrates nicely the physics of the momentum-space phases: a phase of a production amplitude is related to the position of the production volume in x-space.

To construct a simple example of a multiparticle amplitude let us again consider the amplitude (19). Multiplying n of these amplitudes we get an amplitude for producing n-particles with momenta $\vec{k}_1,..,\vec{k}_n$. The resulting model is an example of an Uncorrelated Jet Model. Now, an interesting problem is, if one should use a different position vector $\vec{\eta}_i$ for each of the n-particles produced or e.g. to take all the $\vec{\eta}_i$'s to be the same. The physics of these two possibilities is clearly different. In the first case (uncorrelated phases) the positions in which the particles are produced do not depend on each other. In the second case (strongly correlated phases) all the particles are produced in the same average position $\vec{\eta}$. This is illustrated in Fig. 3. The accuracy at which the position(s) can be determined is in both cases given by the uncertainty principle.

When calculating the overlap function and the imaginary part of the elastic amplitude one must average over the position vectors $\vec{\eta}_i$ (the positions at which the particles are produced

are not derivable from the measurement of elastic scattering). This averaging procedure should be done with a weight function $w(\vec{n}_1,..,\vec{n}_n)$ which describes the size and density of the interaction volume. If the interaction volume is e.g. a black disc of radius R the phase-averaging procedure (for the case of the correlated phases) would give

$$\tau_{inel}(t) \sim \frac{2J_1(R\sqrt{-t})}{R\sqrt{-t}} \quad . \tag{21}$$

A more realistic interaction volume would be e.g. a black disc with smooth edges. This would give - as a first approximation - the Bessel function (21) multiplied by a smooth peripheral "modulating function" g(t) whose peripherality depends on the sharpness of the edge. A sharp edge corresponds to a flat modulating function and vice versa.

The overlap of the absolute values of the amplitudes in the rotation provides additional peripherality for the inelastic overlap function. The effect can, as a first approximation, taken to be independent of the phase factors. An illustrative result for the inelastic overlap function reads:

$$\tau_{inel}(t) = \sigma_{inel}\, f(t)\, \frac{2J_1(R\sqrt{-t})}{R\sqrt{-t}}, \tag{22}$$

where the 'modulating function' f(t) describes the combined effect of the 'opacity factor' g(t) and the factor coming from the absolute values of the amplitudes.

The inelastic overlap function (22) is a very approximate one and we have written it up only to illustrate a typical result obtained from the type of models discussed above: a Bessel function $\frac{2J_1(R\sqrt{-t})}{R\sqrt{-t}}$ associated with the production of particles in an interaction volume of radius R multiplied by a smooth peripheral 'modulating function' f(t) which receives contributions both from the shape of the interaction volume as well as from the absolute magnitudes od the production amplitudes.

Calculations done with the type of amplitudes discussed above neglecting the phase give typically much too flat elastic differential cross sections. For example, a factorizable Uncorrelated Jet Model, realistic leading particle effects included, gives for the elastic differential cross section of proton-proton scattering

$$\frac{d\sigma}{dt} \approx e^{At} , \tag{23}$$

with $A \approx 2$ GeV^{-2}, whereas the experimental value of the slope is approximately $A \approx 10$ GeV^{-2}. [2, 3, 4]. This discrepancy between the no-phase calculation and the experimental value indicates that the interaction volume is much larger than could be concluded by erroneously interpreting the inverse of the width of the transverse momentum distribution as the radius of the interaction volume. In our simple example (19) (with strongly

correlated phases) this discrepancy between the no-phase (i.e. $\vec{n} = 0$) calculation and the experimental data measures - in some sense - the viscosity of the proton. The fact that this discrepancy is numerically large can be interpreted as if only a small part of the total interaction volume is 'heated' in a single collision; the proton is of rather fragile material.

4. Illustrative Analysis of High Energy Proton-Proton Scattering Data

To illustrate the shadow approach and to emphasize some of the points discussed earlier let us now analyze some experimental data. We shall discuss elastic proton proton scattering. This for two reasons. Firstly, high energy proton-proton scattering is a good reaction to study if one wants to learn about the Pomeron. The second reason is, that now there are excellent new data from the ISR. These data display some very interesting features, including a break at small t-values ($t \lesssim -0.15$ GeV^2) and the development of a dip at $t = -1.3$ GeV^2.

To start with, let us show the results of calculating the inelastic overlap functions from the experimental data. These "experimental" overlap functions are shown in Fig. 4 for the 30 GeV/c data of Edelstein et al.[9] and the 1500 GeV/c ISR

data[+++]. The results shown have been calculated by neglecting the real part of the elastic amplitude at all t-values. At small t-values this is probably a good approximation[10] but we don't know any good arguments to neglect the real part at large t-values. However, we have repeated the calculation using several different phase assumptions including some very strongly varying phases[19]. At small t-values (up to 1 GeV^2) the results are qualitatively totally insensitive to the assumed phase and even a strong phase (e.g. Regge phase with $\alpha'_P = 1\ GeV^{-2}$) only shifts the first zero to slightly smaller t-values. The large-t results, however, are sensitive to the assumed phase.

[+++] WARNING TO THE READER. The different pieces of experimental data used to construct our "input" data are not fully consistent with each other. We have constructed the ISR data shown in the figures from the new total cross section values of Amaldi et al. and Amendolia et al.[11], from the small t-data of Barbiellini et al.[12] normalizing them to extrapolate to the optical point value of Amaldi et al. and from the large-t data of Rubbia et al.[13] presented in the Batavia Conference. The 30 GeV/c data has been normalized to an optical point value corresponding to σ_{tot} = 39.2 mb. The error-bars shown on the figures correspond to a 10% variation in the overall normalization of our "input" data plus an additional t-dependent variation within the limits obtained by multiplying quoted errors by a factor of two.

A glance at Fig. 4 tells us immediately that at small t-values the results are very similar to those of our mathematical exercise in Section 3. The position of the first zero is t_o = -0.693 ± 0.015 GeV^2 at 30 GeV/c and $t_o = -0.605 \pm 0.015$ GeV^2 at 1500 GeV/c. The fact that the zero has moved to smaller t-values with the energy increasing follows mainly from the considerable shrinkage exhibited by the data. The flatness of the differential cross section at t-values above -1.3 GeV^2 causes the total and elastic overlap functions to cross each other again (approximately at $t \approx -2$ GeV^2) and the inelastic overlap function thus gets a second zero. The position of this zero (and even the existence of it) need not be taken too seriously because of our ignorance of the elastic phase in this t-region.

Let us now try to find a simple description for the "experimental" overlap functions of Fig. 4 guided by the ideas discussed earlier. At this stage we must, however, discuss the existing knowledge of particle production processes in a bit more detail. Although the statistical type of models discussed in Section 3 might provide a suitable description for the bulk of the data there are important experimental indications that statistical models can not describe all of the data even at high energies.

The present experimental knowledge of multiparticle production suggests that there exist at least two different mechanisms of particle production: (i) a non-diffractive production mechanism which is responsible for the experimentally observed increase in the average multiplicity and (ii) a diffractive component, which depends only weakly on energy and populates primarily low mass low-multiplicity channels. At high energies the first mechanism is often referred to as 'pionization'. The main experimental evidence for this 'two-component picture' is the following. The observation of a pionization plateau at ISR as well as the behaviour of the multiplicity distributions measured at Serpukov[14] and NAL[15] strongly suggest the presence of a non-diffractive 'pionization' component. On the other hand, the observation of strong production of diffractive final states (the sizeable sharp peak close to $x = 1$ in the proton spectrum) at NAL and at ISR clearly indicates the presence of a diffractive production component[16].

Careful analyses of the shape and the energy dependence of the multiplicity distribution yield to more detailed information[17]. Several analyses of the multiplicity distributions give rather similar results for the ratio of the total amount of diffractive to non-diffractive production. This ratio is roughly 1/5. These analyses also indicate that the diffractive component contributes mainly to very low multiplicities,

$\langle n_{ch} \rangle_D \gtrsim 4$. Moreover, they show that a Poisson distribution for pairs of particles for the non-diffractive component is consistent with the present data. This last observation, as well as our intuition, clearly suggest that some simple statistical production model could well do a reasonable job for describing the non-diffractive production.

To find a model for the diffractive component is less easy. It is clear that diffractive fragmentation models of the 'Nova' - type are reasonable models for the diffractive part[18]. It is not clear to us, however, how to include realistic phases into this type of models.

An intuitive argument, however, suggests a simple description for the diffractive contribution to the inelastic overlap function. It is quite natural to associate processes leading to high multiplicity final states with a 'head-on' collision and processes leading to low multiplicity final states with a 'peripheral' collision in which the incoming particles only scratch each other. This intuitive argument is by no means necessarily correct.+) Let us, however, associate the

+) In some popular models the situation is, in fact, exactly opposite. E.g. in the multiperipheral model the 'head-on' collisions populate the lowest multiplicities whereas the highest multiplicities result from a collision in which the particles only slightly touch each other.

diffraction production with some kind of 'edge-effect', if only to see what follows[19]++). This would suggest that the contribution to the inelastic overlap function coming from the diffractive channels could be described by the formula (22) but the Bessel function $\frac{2J_1(R\sqrt{-t})}{R\sqrt{-t}}$ replaced by $J_o(R\sqrt{-t})$ (scattering from a ring instead of a disc):

(24) $\tau_D(t) = \sigma_D f_D(t)\, J_o(R\sqrt{-t})$.

The radius and modulating function in (24) could well be different from those of the 'pionization' component, but it is also quite natural to take them to be the same.

Guided by these speculations we try to parametrize the inelastic overlap functions of Fig. 4 by the formula.

(25) $\tau_{inel}(t) = \sigma_D f_D(t) J_o(R\sqrt{-t}) + \sigma_\pi f_\pi(t)\ \frac{2J_1(R\sqrt{-t})}{R\sqrt{-t}}$.

For the diffractive cross sections we have used an energy independence value σ_D = 7 mb estimated by Fialkowski[17]+): The experimental overlap function at p_{lab} = 1500 GeV/c and a description of it using the parametrization (25) are shown in Fig. 5.

++) We would like to thank Dr. R. Worden for interesting discussions on the problem of the possible 'peripherality' or 'centrality' of diffraction dissociation processes.

+) Similar estimates for the diffractive cross-section has been recently obtained by many other authors[17].

The modulating function $f_\pi(t)$ (shown in the figure) has been parametrized as a sum of two exponentials but many other simple functions would do an equally good job. The description is not a fit, we have fixed the radius R by adjusting the first zero exactly to the right place. The reason for this is that we don't want to give too much emphasis to the large-t data. An amusing fact is that the second zero of the Bessel function comes almost exactly in the right place. This result should, however, probably not be taken too seriously. The resulting descriptions for the differential cross sections at p_{lab} = 30 GeV/c and 1500 GeV/c are shown in Fig. 6. The agreement is very good, as could be guessed already from Fig. 5.

The result of our parametrization of the diffractive component is the following. We have assumed the same value for R in it as in the 'pionization' component. Thus the diffractive overlap function has its first zero already at $t \tilde{\sim} - 0.2$ GeV^2 providing a very steep contribution to the inelastic overlap function. The resulting elastic differential cross section has a break at small t-values. A comparison between experimental data and the model calculation described above is shown in Fig. 7 for small t-values. The agreement is very good.

As already stressed this explanation for the small t-break of the elastic scattering as a shadow of the two-component nature of multiparticle production is not necessarily a correct

one. It is, however, a very appealing one and, as shown above, can provide quantitative description of the small-t break essentially without free parameters.

The experimental data has shrunk quite a lot between p_{lab} = 30 and 1500 GeV/c although the shrinkage might be slowing down at ISR energies. In our parametrization this shrinkage follows from two effects. Firstly, the radius of the interaction volume has slightly grown (from 0.91 fermi at 30 GeV/c to 0.97 fermi at 1500 GeV/c). The main part of the shrinkage, however, results from the shrinking modulating function. It is not completely clear to us if this shrinkage should be attributed to a change in the shape of the interaction volume or to more complicated effects. If the size of the interaction volume is increasing, however, as suggested by the data, it would not be surprising if the sharpness of its edges is also changing.

In our parametrization the development of the diffractive minimum at $t = -1.3$ GeV^2 follows from an incomplete cancellation between the elastic (positive) and inelastic (negative) overlap functions. Thus, if the data continues to shrink, our parametrization predicts that the dip will develop to a <u>double dip</u>[+)]

[+)] This rather unconventional dip-structure follows directly from our assumption that the amplitude is purely imaginary at all values of t. A more conventional explanation for the dip would

be that the imaginary part of the elastic amplitude changes sign in the neighbourhood of $t = -1{,}3\ GeV^2$ and the zero is partially filled by the real part.

An experimental observation of such a phenomenon (at energies slightly higher than ISR) would be an extraordinary confirmation of the simple description presented above.

Let us, once more, stress the illustrative nature of the present analysis. Our numerical results should not be taken too seriously. We have, however, repeated the analysis with several different phase assumptions and these calculations show very clearly, that although the details of the results do change (e.g. the imaginary part of the elastic amplitude might well have a zero at t close to $-1.3\ GeV^2$) the basic physics remains the same. In the s-channel language the high energy proton-proton scattering is generated by absorption of a disc which has smooth edges and a radius of approximately one fermi.

As a final exercise, let us transform the experimental overlap functions into the impact parameter representation. The results are shown in Fig. 8. As already mentioned, the radius of the interaction volume has slightly increased from 30 GeV/c to 1500 GeV/c. What is even more interesting, the center of the interaction volume has become more transparent with increasing

energy. The amount of S-wave absorption is 97% at p_{lab} = 30 GeV/c and 93% at p_{lab} = 1500 GeV/c. One should, however, be very careful when interpreting this result. Our assumption of purely imaginary amplitude is probably not too good at large t-values and contributions coming from large t-values are important at small impact parameters. Moreover, this descrease of the opacity at small impact parameters could well be a 'low-energy effect'. In fact, our results of analyses of intermediate energy ISR data indicate that the decrease in the amount of S-wave absorption has happened between 30 GeV/c and the lowest ISR energy and inside the ISR energy range the amount of S-wave absorption is rather increasing than decreasing.

5. Summary and Conclusions

We would like to summarize our discussion as follows:

1. The phases of (momentum space) production amplitudes play an important role in building the elastic scattering amplitude. The experimental observation that the inelastic overlap function derived from experimental data will change sign at moderate t-values independently of the assumed elastic phase (as long as it is reasonable) we regard as a direct proof of the crucial role played by the multiparticle phases.

2. At a certain impact parameter the elastic amplitude is built by the amount of absorption to inelastic channels at the same impact parameter. This makes the impact parameter representation very suitable for the study of the unitarity relation. It might be useful to try to formulate multiparticle models directly in the impact parameter representation.+)

3. Our simple analysis of high energy proton-proton scattering should be regarded as illustrative rather than conclusive. We would, however, like to draw one conclusion from it. It shows that a simple and appealing description of the experimental data can easily be obtained when the data are analyzed in the shadow approach. Moreover, in this approach the parametrization has a direct physical interpretation. This suggests that a careful study and further development of the s-channel approach could be very useful for understanding the properties of high energy elastic scattering.

+) For an interesting discussion of the multiperipheral model using the impact parameter representation see Frank Henyey's talk in these proceedings [8].

ACKNOWLEDGEMENTS

We are grateful for Drs. R. J. N. Phillips and R. Worden for their continuous interest in our work, for many useful discussions and for critical reading of the manuscript. We thank Professor F. Henyey for useful discussions. HIM thanks the Science Research Council (Finland), the Emil Aaltonen Foundation and the Herman Rosenberg Foundation for financial support.

References:

[1] L. Van Hove, Nuovo Cimento 28, 798 (1963); Rev. Mod. Phys. 36, 655 (1964).

[2] L. Michejda, J. Turnau and A. Białas, Nuovo Cimento A56, 241 (1968); L. Michejda, Nucl. Phys. B4, 113 (1968).

[3] E. H. de Groot, Ph.D. thesis, Utrecht University (1971); E. H. de Groot and Th. W. Ruijgrok, Nucl. Phys. B27, 45 (1971).

[4] E. H. de Groot, Nucl. Phys. B48, 295 (1972); E. H. de Groot and E. M. de Jager, J. Appl. Math., to be published.

[5] F. Zachariasen, Phys. Reports 2C, 1 (1971).

[6] Z. Koba and M. Namiki, Nucl. Phys. B8, 413 (1968).

[7] H. M. Chan, J. Łoskiewicz and W. W. M. Allison, Nuovo Cimento A57, 93 (1968).

[8] F. S. Henyey, "Impact Parameter Description of Multiparticle and Elastic Scattering, with an Application to the Multiperipheral Model", Proceedings of the VIIIth Recontre-de-Moriond, Méribel-lès-Allules, 6.-16.3.1973, J. Tran Thanh Van (Edit.).

[9] Edelstein et al., Phys. Rev. D5, 1073 (1972).

[10] U. Amaldi et al., Phys. Letters 43B, 231 (1973).

[11] U. Amaldi et al., CERN preprint, January 1973; S. R. Amendolia et al., CERN preprint, February 1973.

[12] G. Barbiellini et al., Phys. Letters 39B, 663 (1972).

[13] Aachen-CERN-Genova-Harward-Turin Collaboration, Communication by C. Rubbia at the XVI International Conference on High Energy Physics, Batavia, September 1972.

[14] Soviet-French Collaboration, "Average Charged Particle Multiplicity and Topological Cross Sections in 50 GeV/c and 69 GeV/c pp Interactions", XVI Internation Conference on High Energy Physics, Batavia, September 1972.

[15] J. Chapman et al., Phys. Rev. Letters 29, 1686 (1972); G. Charlton et al., Phys. Rev. Letters 29, 515 (1972); F. T. Dao et al., Phys. Rev. Letters 29, 1627 (1972).

[16] F. Sannes et al., NAL preprint, December 1972; M. G. Albrow et al., CERN preprint, December 1972; G. Goldhaber, CERN/D.Ph.II/Phys 72-46 (1972).

[17] K. Flatkowski, Phys. Letters 41B, 379 (1972); K. Flatkowski and H. I. Miettinen, Phys. Letters 43B, 61 (1973); H. Harari and E. Rabinovici, Phys. Letters 43B, 49 (1973); W. R. Frazer, R. D. Peccei, S. S. Pinsky and C. I. Tan, University of California (San Diego) preprint UCSD-10P10-113 (1972); C. Quigg and J. D. Jackson, NAL-preprint NAL-THY-93 (1972) L. Van Hove, Phys. Letters 43B, 65 (1973).

[18] For a review see e.g. E. L. Berger, "Fragmentation Models for Particle Production", Proceedings of the Fourth International Conference on High Energy Collisions, Oxford, April 5-7, 1972, J. R. Smith (Edit.).

[19] G. L. Kane, Phys. Letters 40B, 363 (1972).
V. Barger, R. J. N. Phillips and K. Geer, Nuclear Phys. B47, 29 (1972).

Figure Captions:

Fig. 1. Solution of the s-channel unitarity equation.

2. Inelastic overlap function calculated from a differential cross section $d\sigma/dt \sim e^{At}$ assuming purely imaginary amplitude at all values of t. The values used for the total and elastic cross-sections are σ_{tot} = 40 mb and σ_{el} = 8 mb corresponding to $A = 10.2\ GeV^{-2}$.

3. Schematic illustration of particle production with strong phase correlations.

4. Inelastic overlap functions calculated from the 30 GeV/c data of Edelstein et al *[9]* and from the 1500 GeV/c ISR data *[11-13]* assuming purely imaginary amplitude at all values of t. The total and elastic overlap functions are also shown.

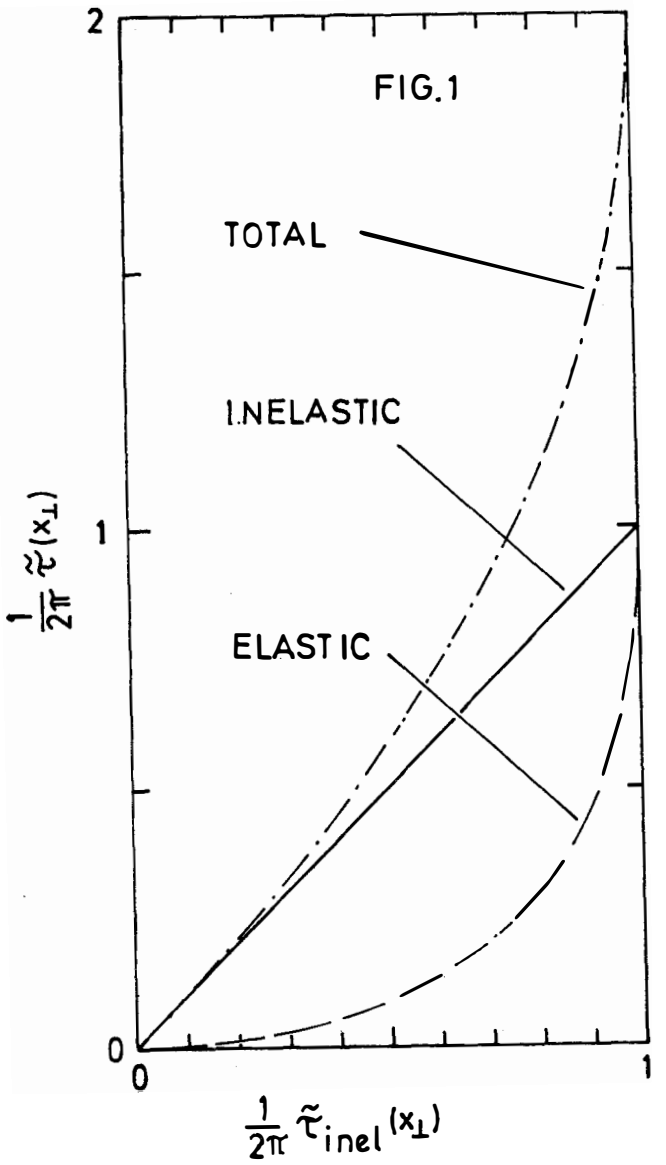
5. Inelastic overlap function at p_{lab} = 1500 GeV/c. The solid points are calculated from the ISR data *[11-13]*, for errorbars see the text. The solid curve is the two-component parametrization described in the text. The "modulating function" $f_{\pi}(t)$ is also shown.

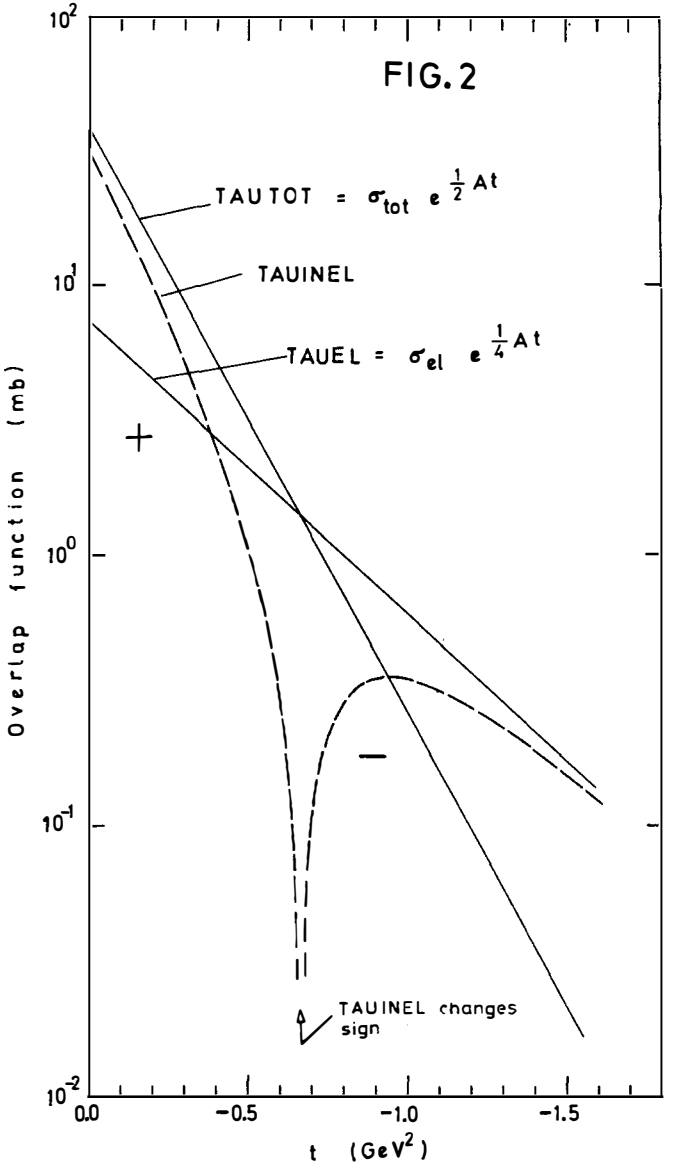
6. Elastic differential cross sections at p_{lab} = 30 and 1500 GeV/c. The solid curves are calculated from the two-component overlap function described in the text and shown in Fig. 5 for p_{lab} = 1500 GeV/c.

Figure Captions:

Fig. 7. Elastic differential cross section at small values of t at p_{lab} = 1500 GeV/c. The solid curve results from the two-component overlap function described in the text and shown in Fig. 5.

Fig. 8. Fourier transforms of the total, inelastic and elastic overlap functions calculated from the p_{lab} = 30 and 1500 GeV/c data.


FIG.1
TOTAL
INELASTIC
ELASTIC
2
1
0
0
1
$\frac{1}{2\pi}\tilde{\tau}(x_\perp)$
$\frac{1}{2\pi}\tilde{\tau}_{inel}(x_\perp)$


FIG. 2
TAUTOT = $\sigma_{tot}\ e^{\frac{1}{2}At}$
TAUINEL
TAUEL = $\sigma_{el}\ e^{\frac{1}{4}At}$
+
−
TAUINEL changes sign
Overlap function (mb)
10^2
10^1
10^0
10^{-1}
10^{-2}
0.0
−0.5
−1.0
−1.5
t (GeV^2)

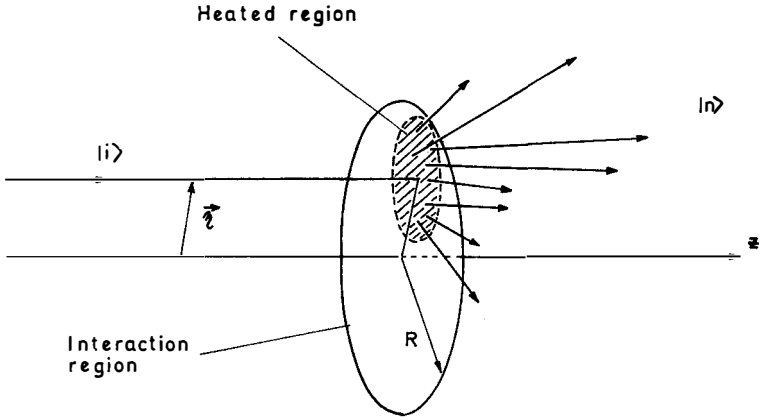


FIG. 3

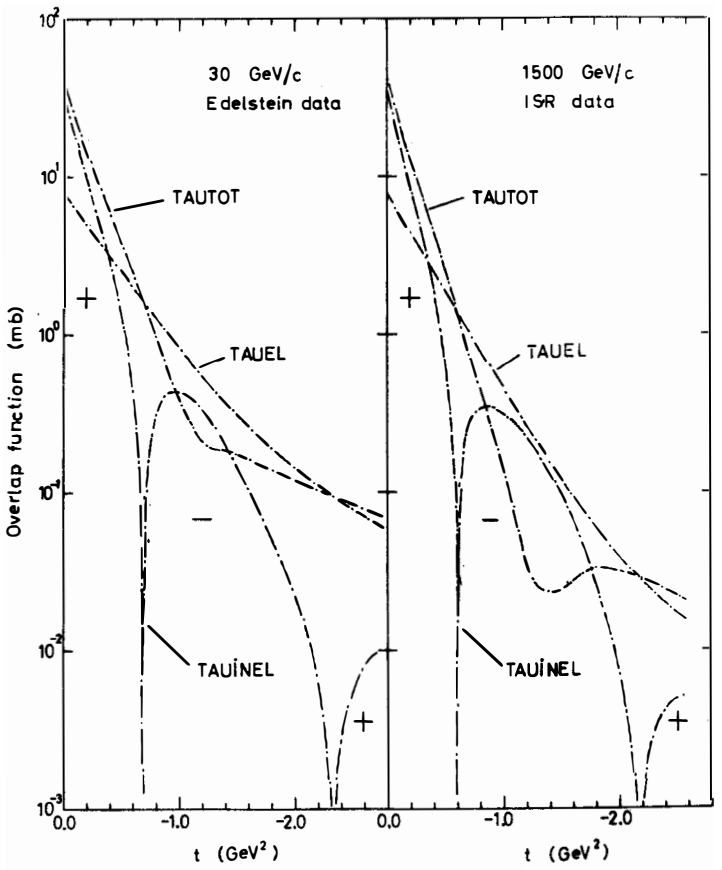

30 GeV/c
Edelstein data
1500 GeV/c
ISR data
TAUTOT
TAUEL
TAUINEL
Overlap function (mb)
t (GeV²)
0.0
-1.0
-2.0

FIG.4

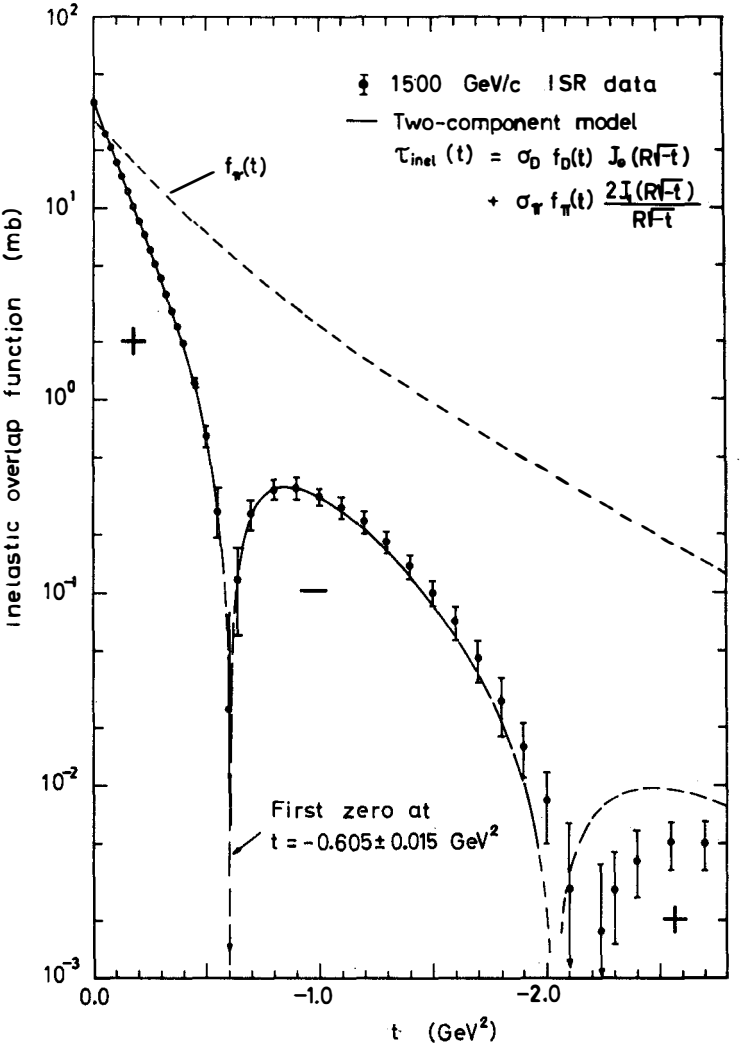

1500 GeV/c ISR data
Two-component model
$\tau_{inel}(t) = \sigma_D f_D(t) J_0(R\sqrt{-t}) + \sigma_\pi f_\pi(t) \frac{2J_1(R\sqrt{-t})}{R\sqrt{-t}}$
$f_\pi(t)$
First zero at
$t = -0.605 \pm 0.015$ GeV^2
Inelastic overlap function (mb)
10^2
10^1
10^0
10^{-1}
10^{-2}
10^{-3}
0.0
-1.0
-2.0
t (GeV^2)

FIG.5

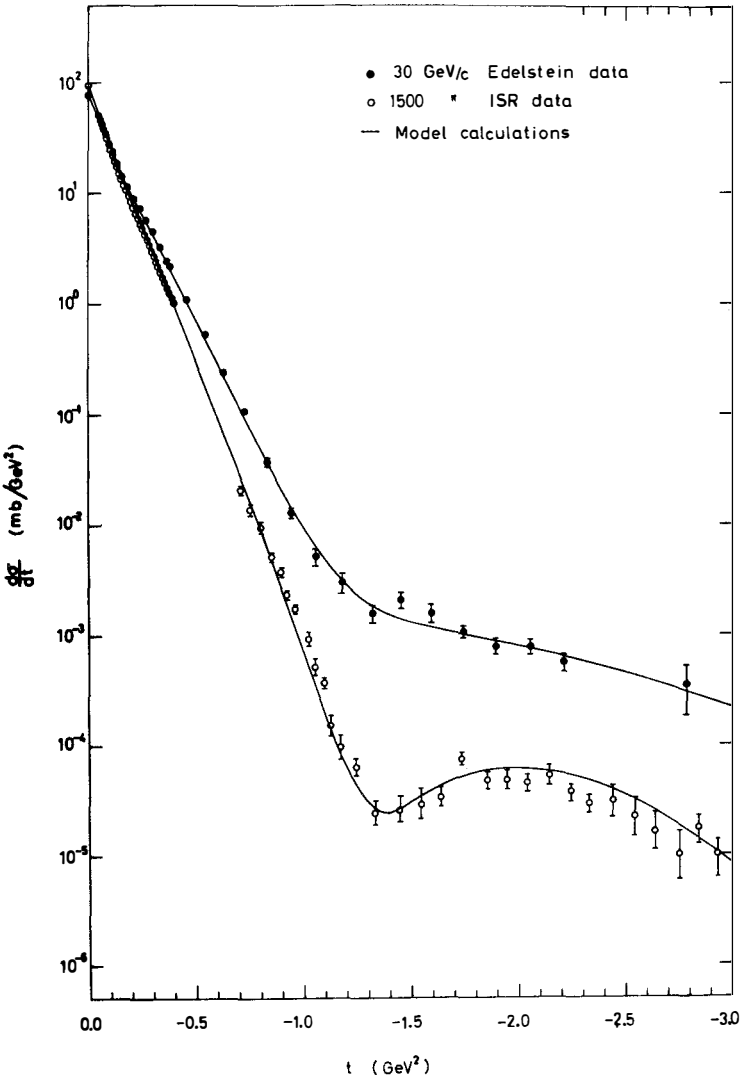

• 30 GeV/c Edelstein data
o 1500 " ISR data
— Model calculations
dσ/dt (mb/GeV²)
t (GeV²)
0.0
-0.5
-1.0
-1.5
-2.0
-2.5
-3.0

FIG.6

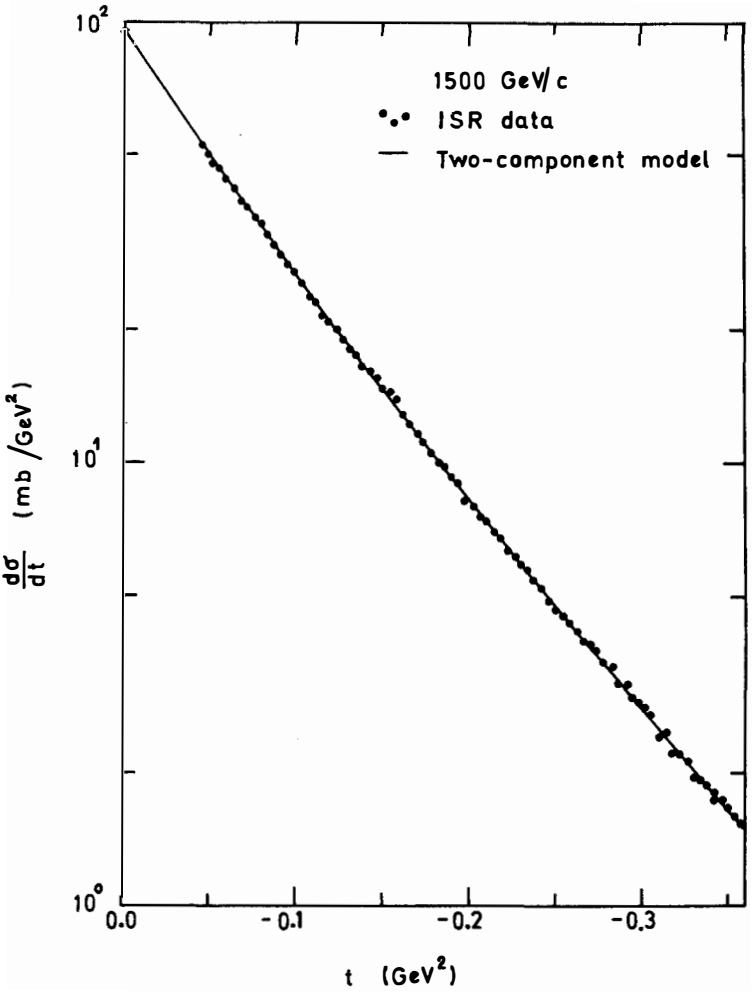
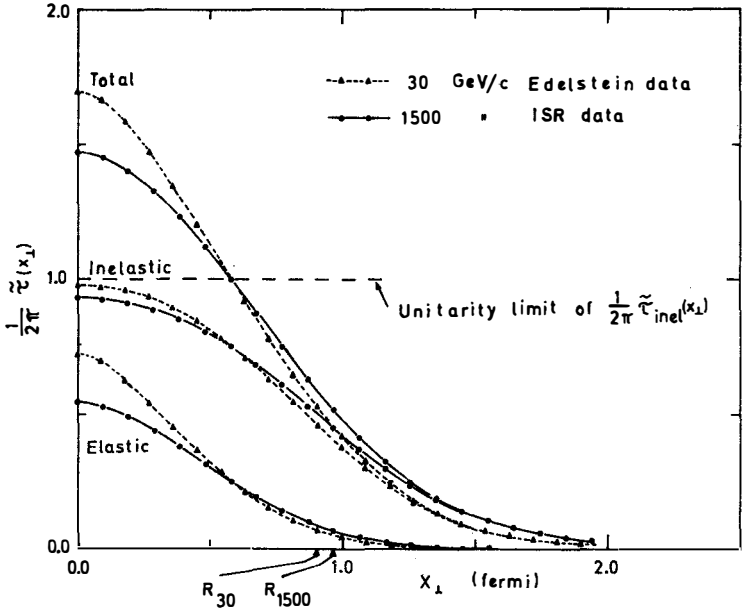

1500 GeV/c
ISR data
Two-component model
10^2
10^1
10^0
$\frac{d\sigma}{dt}$ (mb /GeV^2)
0.0
-0.1
-0.2
-0.3
t (GeV^2)

FIG.7


2.0
1.0
0.0
Total
Inelastic
Elastic
30 GeV/c Edelstein data
1500 " ISR data
Unitarity limit of $\frac{1}{2\pi}\tilde{\tau}_{inel}(x_\perp)$
$\frac{1}{2\pi}\tilde{\tau}(x_\perp)$
0.0
1.0
2.0
R_{30}
R_{1500}
$X_\perp$ (fermi)

EXPLORATORY DIP SYSTEMATICS IN ELASTIC SCATTERING

par J. Tran Thanh Van
Laboratoire de Physique Théorique et
Particules Elémentaires. Orsay.

Abstract : Regularity in the dip positions of many elastic differential cross sections is observed when the variable $X = -\sigma_{tot}^2 t$ is used. Tentative justification is presented.

Résumé : On observe que les positions des minima dans plusieurs sections efficaces différentielles élastiques sont à des valeurs fixes de $X = -\sigma_{tot}^2 t$. Une dérivation théorique est discutée.

In this paper, we will show there is a regularity in the dip position of elastic differential cross sections at high energies.

Let us first summarize the dip structure seen in elastic reactions at high energies ($p_L \geq 5$ GeV) (2 - 8)

- proton-proton : dip at $-t = 1.3$ GeV^2 (ISR Data)
- pion-proton : dip at $-t = 2.8$ GeV^2 (at 5 GeV, 10 GeV...)
- antiproton-proton : dip at $-t = .55$ GeV^2 at 5 GeV
  and at $-t = .80$ GeV^2 at 16 GeV
- kaon-nucleon : no clear dip at $-t \approx 3$ GeV^2
- proton-deuteron : dip at $-t \approx 0.3 - 0.4$ GeV^2
- pion-deuteron : dip at $-t \approx 0.5 - 0.6$ GeV^2

This erratic behaviour of dips is one of the most intriguing features of high energy elastic data.

Using the absorption model as a guide, we will show that a natural variable is $X = -\sigma_T^2 t$ where σ_T is the total cross section of the considered reaction. In fig. 1 we plot the differential cross sections of various elastic reactions at different energies versus X. The dip positions of all reactions are at the same value of X. In other words, the dip positions of different elastic reactions (or at different energies) are related by the relation :

$$(\sigma_1)^2 t_1 = (\sigma_2)^2 t_2 \qquad (1)$$

where σ_1, σ_2 are the total cross sections and t_1, t_2 the dip positions for the two reactions.

Using as input the proton-proton data with $\sigma_1 = 40$ m b and $-t_1 = 1.3$ GeV^2 we obtain the predictions given in Table I. For $\bar{p}p$ the agreements are quite good. For pion proton scattering,

in order to minimize the I = 1 contribution, we take the half-sum of $\pi^+ p$ and $\pi^- p$ scattering. The total cross section at 5 GeV is 27.5 mb and it leads to a zero in the imaginary part at $-t = 2.75\ GeV^2$ in good agreement with the experimental data. From 3 GeV to 14 GeV, the dip is predicted to move from $-t = 2.3\ GeV^2$ to $-t = 3.2\ GeV^2$. For Kp scattering, we would predict a dip around $-t = 4\ GeV^2$ at 5 GeV, which is very near of the 90° t value. Due to the absence of the backward peak, the differential cross section decreases very fast in this region and could smear the presence of an eventual dip. Data at higher energies would be useful for this reaction. For $K^+ p$ we predict a dip at $-t \simeq 6\ GeV^2$ and the results of the CERN-Paris experiment at 10 GeV will be a crucial test for this rule.

We have also tried to apply formula (1) to loosely bound nuclei as the deuteron. Surprisingly, predictions for proton-deuteron are excellent and for pion deuteron qualitatively good. For pion-helium, experimental data are available only for the low energy region ($p_L \simeq 1 - 2$ GeV). However, predictions are quite good.

Before trying to justify the formula (1) let us summarize its qualitative features.

a) For a given reaction, the dip position should move to larger (or smaller) $|t|$ value if the total cross section decreases (or increases) with the energy. Data of pion nucleon as well as anti-proton-proton scattering show clearly such a dip moves towards larger t value. The ratio of this displacing agrees quite well with the square of the total cross sections.

b) For a given energy, the dip position for different reactions is at larger (or smaller) t value if the total cross section is smaller (or larger).

Although formula (1) is mainly a phenomenological formula let us discuss the possibility to generate such a formula using the impact parameter representation.

a) With a Gaussian like distribution in the impact parameter b space, we have in the t space an amplitude which behaves as an exponential

$$\text{Im } f(b) = e^{-b^2/4A} \rightarrow \text{Im } f(t) \simeq A\, e^{A t}$$

In this case, the amplitude does not have any zero.

b) With a black dish of radius R

we have

$$\text{Im } f(t) \simeq R^2 \frac{J_1 (R\sqrt{-t})}{R\sqrt{t}}$$

$$\underset{t \simeq 0}{\rightarrow} R^2\, e^{R^2 t/8}$$

Dip structure is expected at fixed values of $R^2 t$ or $\sigma_T t$ as the total cross section is proportional to R^2.

Careful examination of the effective elastic amplitude shows that the reality is between these two preceding cases :

In $\pi^- p \rightarrow \pi^o n$, Martin and Stevens [9] have tried to find the effective elastic amplitude which is needed when ρ Regge pole exchange is given. Fig. (2) shows their result compared to a gaussian Pomeron in the b space. The main difference in the two curves is for small b.

In proton-proton scattering, same results emerge from the various versions of the eikonal model [10].

How could we systematize such an effect which seems to be

present in many elastic reactions ?

In the following, we will use a particular function for unitarizing the gaussian Pomeron Born term. This function which should produce the effect shown in Fig. (2) must have properties which enable us to have simple analytical form for the amplitude and to give exploratory predictions on all elastic reactions - one possibility is that the absorbed amplitude is of this form :

$$\text{Im } f(b) = e^{-b^2/4A} \, I_o\left(\frac{b}{b_o}\right)$$

where $I_o(x)$ is the Haenkel function which has the following behaviour :

- for small x, $I_o(x) \simeq e^{x^2/4}$
- for large x, $I_o(x) \simeq e^{x}$

and b_o some scale for the transformation.

These properties of the absorption function are needed in order to obtain the absorbed elastic amplitude given in Fig. (2) from a gaussian like Pomeron amplitude.

The amplitude in the t space is now :

$$\text{Im } f(t) \simeq e^{At} \, J_o\left(\frac{A\sqrt{-t}}{2\, b_o}\right)$$

A remarkable feature of the result is the presence of zeroes in the elastic amplitude as seen in proton-proton scattering.

Assuming that the scale factor b_o is the same for all elastic reactions and the slope A proportional to the total cross sections one obtains easily the formula (1).

Let us now make some final comments :

a) In order to obtain the dip in proton-proton scattering at $-t \simeq 1.3\ (\mathrm{GeV/c})^2$ with a slope $A = 5\ (\mathrm{GeV/c})^{-2}$, we find that $b_o = 4.75\ (\mathrm{GeV/c})^{-1}$ or 0.9 fermi. It is remarkable that the scale of the transformation b_o has this universal value of about one fermi which characterizes the radius of the Regge amplitudes in the dual absorptive model.

b) Let us write the elastic amplitude as the sum of a central part and a corrective term :

$$\mathrm{Im}\ f(b) = e^{-b^2/4A} + C$$

In Fig. (3) we show the different contributions for $A = 5(\mathrm{GeV/c})^{-2}$ and $b_o = 0.9$ fermi. Comparison with the Pomeron proposed by Hartley and Kane [11] shows clearly that their edge contribution is qualitatively the same as our corrective term. Thus, our conjecture (2) could be seen as a simple generalization to all elastic reactions of the Hartley and Kane proposal.

c) In the case of a Gaussian Born term ($b_o \to \infty$ in (2))

$$\mathrm{Im}\ f(b) \simeq e^{-b^2/4A}$$

the radius is defined as $R = 2\sqrt{A}$ with A proportional to the total cross section.

After the transformation (2), the radius is slightly changed

$$R = 2\left(\frac{A}{1 - A/b_o^2}\right)^{\frac{1}{2}}$$

With the parameters determined in a), the radius increases by 10 % .

d) In the discussion on the experimental data given before, we have implicitely assumed the validity of formula (1) and (3)

for the imaginary part of the I = 0 elastic amplitude - sum of the Pomeron and Regge pole contribution. The effects of the Regge pole contribution are contained in the difference between the total cross section of particle particle scattering and antiparticle particle scattering. It is why the dip position of $\bar{p}p$ elastic scattering is predicted to be at 0.55 Gev^2 at 5 Gev, 0.8 Gev^2 at 16 Gev and 1.3 Gev^2 at infinite energy as in the case of proton-proton scattering*. However, another possibility is that formula (1) and (3) are valid only for the Pomeron part of the elastic amplitude. In this case, the dip position is only predicted for sufficiently high energy and it will be the same for particle-particle scattering and antiparticle scattering. Taking the asymptotic value of the total cross section to be 26 mb for π p and 20 mb for Kp, the dip position is predicted to be at 3. Gev^2 for πp scattering (as seen experimentally) and 5.2 Gev^2 for Kp scattering. Interference with the imaginary part of the non Pomeron contribution could change slightly these results. In this case, structure at .5 Gev^2 in antiproton proton scattering where the non Pomeron contributions to the imaginary part are important could be explained, for example, by the dual absorptive model [12].

We have shown that regularity in the dip positions of the elastic differential cross sections is observed when the variable $X = - \sigma_{Tot}^2 t$ is used. Although this observation is mainly phenomenological, a tentative to derive this feature from absorption model is presented.

---

* Let us note that in proton proton scattering, the real part due to Regge pole contributions is very important at low energies.

This work has been done last year when the author has benefitted the hospitality of Professor Drell at SLAC.

I am grateful to V. Barger and R. Blankenbecler for interesting discussions.

REFERENCES

1. J. Tran Thanh Van, Communication at the N.A.L. Batavia meeting. 6 - 13 september 1972.

2. Aachen - CERN - Genova - Harvard - Turin Collaboration. Oral communication by C. Rubbia at N.A.L. Conference and P. Strolin Proceedings of the VIIIth Rencontre de Moriond.

3. V. Chabaud et al. Phys. Letters 38 B (1972) 441.

4. V. Chabaud et al. Phys. Letters 38 B (1972) 449.

5. D. Birnbaum et al. Phys. Rev. Letters 23 (1969) 663.

6. F. Bradamante et al. Phys. Letters 32 B (1970) 303.

7. F. Bradamante et al. Phys. Letters 31 B (1970) 87.

8. M. Querrou et al. quoted by R.J. Glauber in Proceeding of the third International Conference on High Energy Physics and Nuclear Structure.

9. A Martin and P. Stevens, Phys. Rev. D 5 (1972) 147.

10. See for example S. Frautschi and B. Margolis, Nuovo Cimento 56 A (1968) 1155 or A. Capella et al. Nuovo Cimento 63 A , (1969), 141.

11. B.J. Hartley and G.L. Kane (to be published).

12. H. Harari, Phys. Rev. Letters 26, 1400 (1971).

FIGURE CAPTIONS

Fig. 1. Differential cross sections of elastic scattering as functions of $X = -\sigma_T^2 t$.

Fig. 2. Impact parameter profiles for elastic scattering.

Fig. 3. Decomposition of the conjectured elastic amplitude (———) in a central part (— — —) and a corrective part (. . . .) . Note that the corrective part has a bump for b about one fermi.

TABLE I

Predictions on dip positions and comparison with experiments

Reactions	Energy	Total cross-sections	Predicted t value	Experimental t value	Experimental references
Input	GeV	mb	GeV^2	GeV^2	
pp	1000.	40.		1.3	ACGHT Coll.[2]
Predictions					
π p	5.	27.5	2.75	2.8	V. Chabaud et al.[3]
$\bar{p}p$	5.	62.	0.54	0.5-0.55	V. Chabaud et al.[4]
$\bar{p}p$	16.	51.	0.8	0.75-0.85	D. Birnbaum et al.[5]
K^+p	10.	18.	6.5		
K^-p	10.	22.5	4.1		
pd	12.	80.	0.33	0.3 - 0.4	F. Bradamante et al.[6]
π d	9.	52.	0.75	0.5 - 0.6	F. Bradamante et al.[7]
π H e_4	2.	100.	0.2	0.2 - 0.25	CERN- Clermont[8]

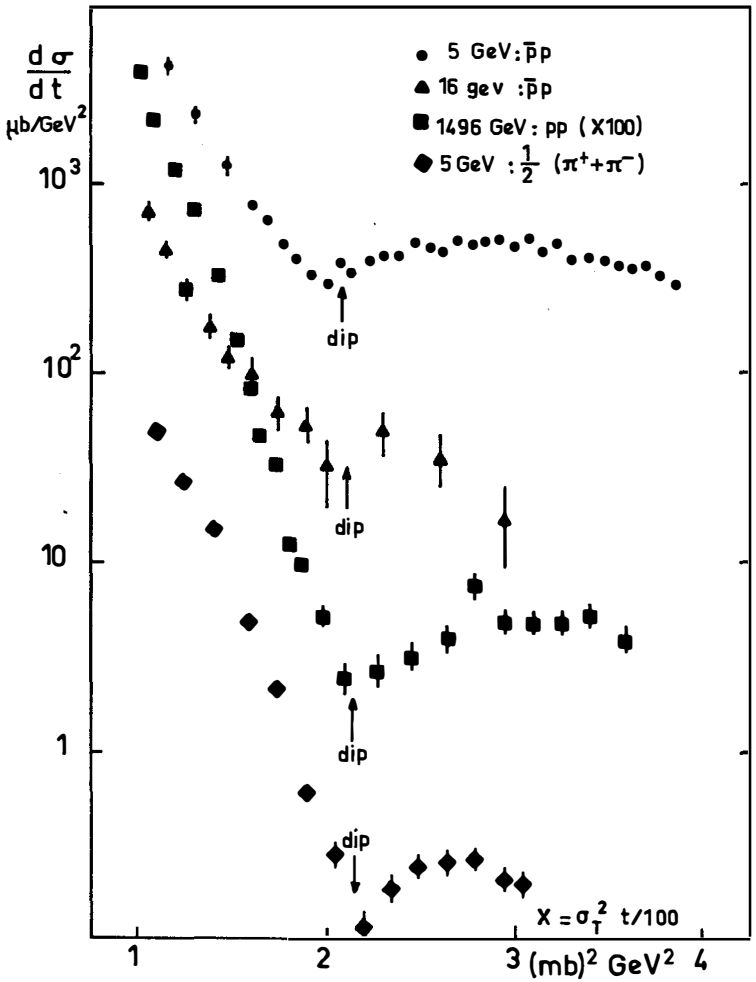

dσ/dt
μb/GeV²
10³
10²
10
1
5 GeV: p̄p
16 gev : p̄p
1496 GeV: pp (X100)
5 GeV : 1/2 (π⁺+π⁻)
dip
dip
dip
dip
X = σ_T² t/100
1
2
3 (mb)² GeV² 4

Fig . 1

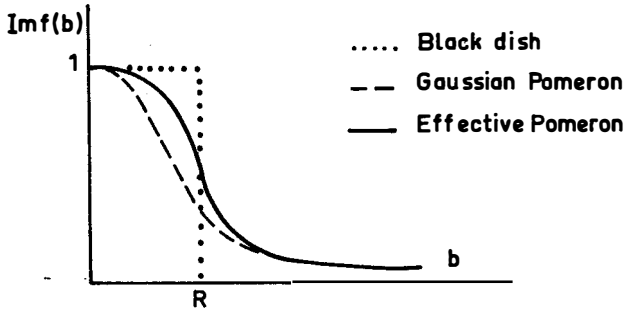

Imf(b)
1
..... Black dish
– – Gaussian Pomeron
—— Effective Pomeron
b
R

Fig. 2

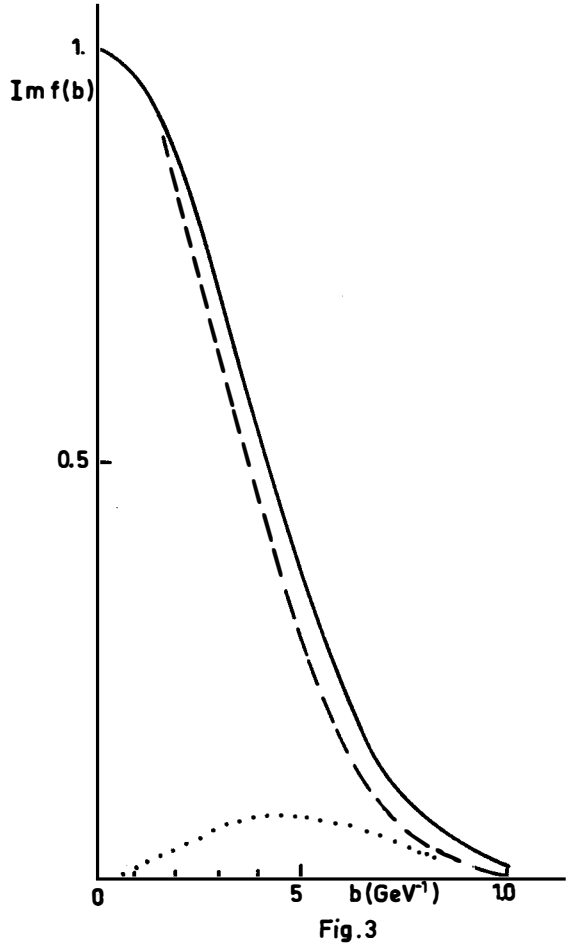

1.
Imf(b)
0.5
0
5
b(GeV⁻¹)
10

Fig. 3

ELASTIC SCATTERING OF π^+ AND K^+ MESONS ON PROTONS AT 10 GeV

C. Baglin
CERN-Ecole Polytechnique-Orsay-Stockholm Collaboration



Abstract : The angular distributions of π^+p and K^+p elastic scattering have been measured at an incident momentum of 10 GeV. Nearly the whole angular range was covered in one experimental set up. A dip is again observed in π^+p at $-t = 2.8$ GeV^2. No structure is observed in K^+p in either the forward direction up to $-t = 2$ GeV^2 or in the backward direction up to $-u = 2$ GeV^2. In the 90° c.m. region the differential cross section is approximately 2 nb/GeV^2 for both reactions. Results from other experiments above 10 GeV are summarized. Some theoretical explanations are sketched for the observed (or not observed) forward peak structures, and for the energy behaviour of the large angle region.

Résumé: Les distributions angulaires des diffusions élastiques π^+p et K^+p ont été mesurées par un moment incident de 10 GeV. Presque tout l'intervalle angulaire a été exploré avec le même apareillage. On observe un dip dans π^+p à $t = -2.8$ GeV^2. Pour K^+p, on n'observe aucune structure ni vers l'avant jusqu'à $t = -2$GeV^2, ni vers l'arrière jusqu'à $u = -2$GeV^2. Dans la région $\theta_{cm} = 90°$, la section efficace différentielle ext approximativement égale à 2mb/GeV^2 pour les deux réactions. On résume également les résultats d'autres expériences au-dessus de 10 GeV. On donne les grandes lignes de quelques explications théoriques pour les structures observées (ou non) du pic vers l'avant et par la dépendance en énergie à grand angle.

The results of measurements of π^+p and K^+p elastic scattering at 10 GeV presented here, are part of our experimental program designed to measure $\pi^{\pm}p$, $K^{\pm}p$ and $\bar{p}p$ elastic scattering at various energies. We are mainly interested in the wide angle and backward regions. Our results at 5 GeV, which have been published previously (1) are summarized in figure 1. The main features are the K^-p and $\bar{p}p$ backward peaks, the smooth U-like angular distribution of K^+p, the V-like distribution of K^-p and $\bar{p}p$ with its much lower minimum, and the dips at $-t=2.8$ and $-t=5$ GeV^2 in $\pi^{\pm}p$.

The present 10 GeV experiment used a slightly different apparatus shown in figure 2. The main difference is that we had only one analysing magnet (instead of two in the 5 GeV experiment); consequently no momentum measurement was available in the range $7 \lesssim -t \lesssim 10$ GeV^2. The lower and upper limitsof our acceptance were $-t=0.5$ and $-t=17.5$ GeV^2 respectively. The incident beam contained 78% p, 20.6% π^+ and 1.4% K^+. Details on the apparatus and the data analysis method have been described in ref. (1,8). All three prong events reconstructed from the beam hodoscope and spark chamber data were submitted to a two constraint kinematical fit at the vertex. The elastic events were extracted by a cut-off on the difference Δp between the momentum value given by the fit and that by the spectrometer for the particle going forward in the lab. system, followed by another cut-off on the χ^2 value given by the fit. Figure 3 shows a distribution of χ^2 versus Δp for large c.m. angle π^+ events. The background from inelastic events

was estimated from an extrapolation of the clearly inelastic events into elastic region (1). The correction thus applied ranged from 5% for regions with large cross sections to 15% for the smallest cross sections. The data were corrected for beam hodoscope and spark chamber efficiencies (typical chamber efficiencies were .90 $\pm$ .04 for each telescope). Finally the efficiency correction for trigger counters, veto counters, beam Cerenkov counters and fast triggering logic was estimated to be 18%.

From the data of 5×10^6 triggers recorded on magnetic tapes, the analysis selected 65000 elastic $\pi^+ p$ events and 120000 elastic $K^+ p$ events. The results are summarized in figures 4-9. The error bars are statistical, and do not include a possible systematic error which we estimated to be $\pm$ 20%.

$\pi^+ p$ elastic scattering exhibits the following features :

For $|t|$ less than 2 GeV^2, the differential cross-section shows a smooth decrease, with a break around $-t=.7$ GeV^2 (figure 4). At 5 GeV this break was more pronounced; and we had a dip at lower energy (figure 5). References to experimental work below 10 GeV are given in ref. (1).

The dip at $-t=2.8$ GeV^2 is also less pronounced at 10 GeV (figure 5) than at 5 GeV. In recent results at 14 GeV this dip is not observed (2). In the case of $\pi^- p$ elastic scattering, the dip, which is also present

at 3.5, 5, and 10 GeV, seems to have developed into a shoulder at 22 GeV (3). No such structure is shown in charge exchange data (4).

In our data at 5 GeV a dip was observed at $-t=5$ GeV^2. Presently at 10 GeV we have at most a small shoulder, if any, for this t-value (figure 5).

For large $|t|$ and $|u|$ the cross-section flattens out at a value of about 2nb/GeV^2 around 90° c.m. ($-t\approx 7.$ and $-t\approx 11$ GeV^2). Compared to our data at 5 GeV this corresponds to a decrease of the 90° c.m. cross section by a factor of 100, i.e. according to s^{-7} : much faster than the $S^{-2.5}$ dependence of the backward peak cross section, ascribed to baryon exchange (figure 6).

Comparison with data of ref. (5) shows that the π^+p and π^-p angular distributions at 10 GeV are very similar. Figure 10 shows the general behaviour of $\pi^{\pm}p$ elastic scattering above 10 GeV (2,3,4,6).

For K^+p elastic scattering we notice the following behaviour :

The forward differential cross section has a very smooth decrease (Fig. 7). At 5 GeV (1) we had a small change of slope at $-t=.9$ GeV^2 which is no more observed at 10 GeV. Also shown in figure 7 are K^-p cross section data from ref. (6).

Cross overs occur at roughly the same t-values as at 5 GeV, but the magnitude of the cross section difference in the region between the cross over points has

decreased by above a factor 2 (i.e. S^{-1}) Fig. 8

The complete angular distribution is shown in figure 9, apart from the very forward/backward directions, and the region 7. < -t < 10. GeV^2 which were not covered by our apparatus. The same smooth U-like shape is observed at 5 and 10 GeV. In the large $|t|$, large $|u|$ region ($-t \approx 14.\ GeV^2$) the differential cross section is about $3nb/GeV^2$. It is of the same order as the 10 GeV $\pi^{\pm}p$ cross sections, but two orders of magnitude lower than the 5 GeV K^+p cross section (i.e. S^{-7} decrease).

A backward peak is observed (Fig. 9). Comparison with our data at 5 GeV indicates a decrease of $d\sigma/du$ as S^{-4} for small $|u|$.

Theoretical interpretations:

The $\pi^{\pm}p$ and K^-p elastic scattering differential cross sections show a large variety of structures at various values of t and with various energy behaviours, as we noticed above; in contrast the K^+p data show a very smooth angular distribution. Remarkable theoretical progress has been achieved towards a good qualitative explanation of this complicated experimental situation. Let us give a few examples which we choose quite arbitrarily. The dip at $-t=.6\ GeV^2$ appears in $\pi^{\pm}p$, K^-p and $\bar{p}p$ elastic scattering; but not in K^+p and $\bar{p}p$, that is for reactions which have no resonances in the s-channel. Following H. Harari ( ) we write the imaginary part of the forward elastic scattering amplitude as $\text{Im}\, A(s,t) = R(s,t) + P(s,t)$. The first term

represents the single Regge (or Regge-Pomeron cut) exchanges, which are dual to the resonance contribution in the s-channel; P(s,t) is the diffractive part (Pomeron exchanges) which is dual of the non-resonant background, and supposed to be structureless for t not too large. The concept of duality led H. Harari to assume that every single prominent s-channel resonance of angular momentum ℓ produces the dip at fixed t by itself; as a consequence these resonances should satisfy the relation $\ell \alpha \sqrt{s}$ i.e. R(s,t) is dominated by the peripheral partial waves, and is proportional to $\exp(at)$ $J_o(r\sqrt{-t})$. At energies of a few GeV, R^2 is negligible with respect to P^2 and P.R. thus $d\sigma/dt \sim P^2 + 2P.R.$ A dip at the minimum of $J_o(r\sqrt{-t})$ ($-t \approx .6$ GeV^2) is then predicted in the reactions for which R can be $\neq 0$ such as $\pi^{\pm}p$, K^-p and $\bar{p}p$. Cross overs in $K^{\pm}p$ cross sections will appear at t-values for which $J_o(r\sqrt{-t}) = 0$. Finally the amplitude of the oscillations of $\{d\sigma/dt\ (K^+p) - d\sigma/dt(K^-p)\}$ between the cross over points, as well as the depth of the dip, will decrease with increasing energy, since R(s,t) decreases relative to P(s,t). Another wide class of elastic scattering structures, including the dip at $-t=2.8$ GeV^2 in $\pi^{\pm}p$ has been parametrized by J. Tran Thanh Van at this meeting : the term P(s,t) above is responsible for these structures which are then expected to remain fixed when s increases. According to J. Tran Thanh Van, P(s,t) should be proportional to $\exp(At)$ $J_o(A\sqrt{-t}/2bo)$ where A/bo is an universal constant. At sufficiently high energy, when P(s,t) dominates, dips are thus expected at constant values of $\sigma_{tot} \times \sqrt{-t}$, where σ_{tot} is the total asymptotic cross

section of the elastic process. The predicted t-values are in agreement with the experimental measurements of several reactions, including $\pi^{\pm}p$, $\bar{p}p$ and pp. The observed smooth distribution of $K^{\pm}p$ is explained, since the dip should appear at large t, ($\gtrsim$ 5. GeV^2) where the experimental resolution is very poor. Finally predictions concerning the large $|t|$, large $|u|$ region have been presented at this meeting by H. Fried in the frame of the vector meson'gluon model. The shapes of the angular distributions shown in figure 1 are explained, as well as the S^{-7} energy dependence of $\pi^{\pm}p$ differential cross sections around 90^{o} c.m. Very similar predictions have been obtained from the parton model by J.Gunion et al.(7) (Fig.10). However owing to the low precision of the $\pi^{\pm}p$ experimental data at large angle, the agreement with the predicted angular behaviour around 90^{o} c.m. is not very meaningful. It seems that theory and experiment have or less reached the same level of precision in πp and Kp large angle elastic scattering.

REFERENCES

(1) V. Chabaud et al., Phys.Lett. 38B(1972)441
See also C. Baglin et al., Nucl.Phys.B (1973)
to be published.

(2) R. Rubinstein et al., Cornell University preprint.

(3) P. Cornillon et al, Phys.Rev.Lett. 30(1973)403.

(4) W. Brockett et al., Phys.Rev.Lett. 26(1971)527.

(5) O. Owen et al., Phys.Rev. 181(1969)1794.

(6) C. Akerlof et al., Phys.Rev.Lett. 26(1971)1278.

(7) J. Gunion et al., Phys.Lett. 39B(1972)649.

(8) C. Baglin et al., Phys.Lett.(1973) to be published.

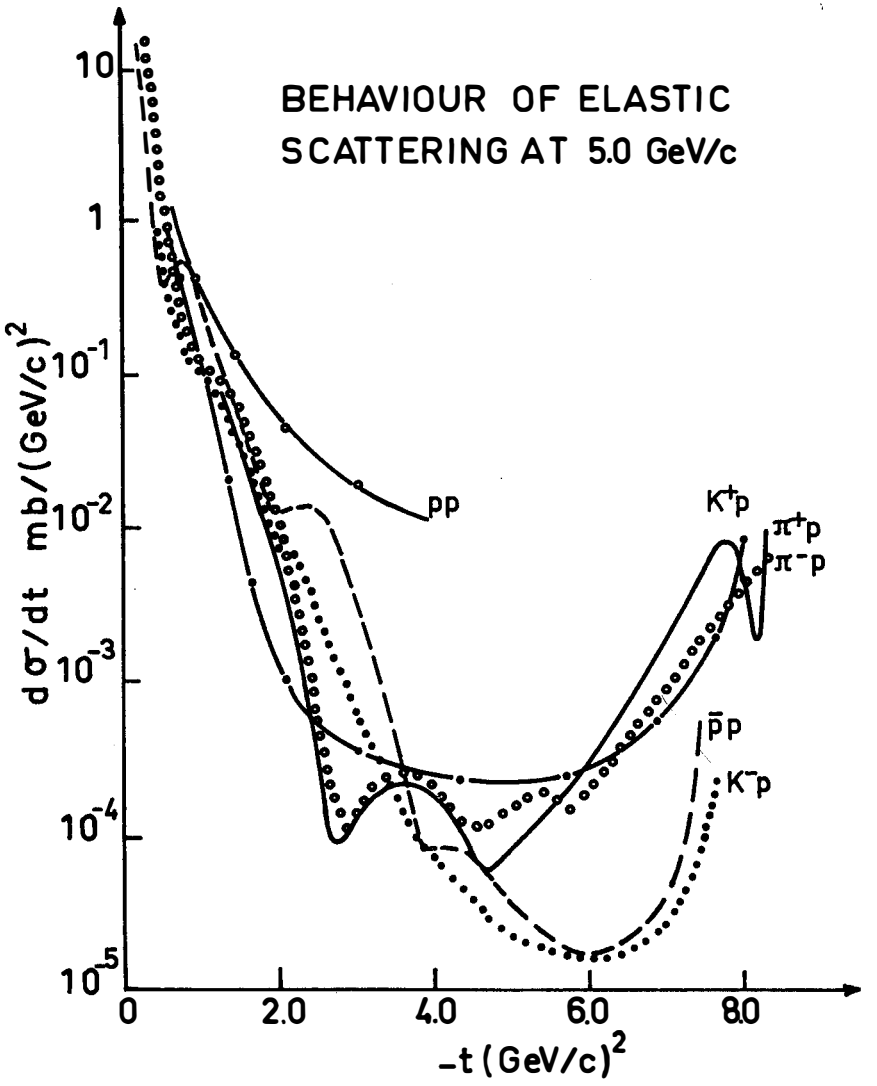
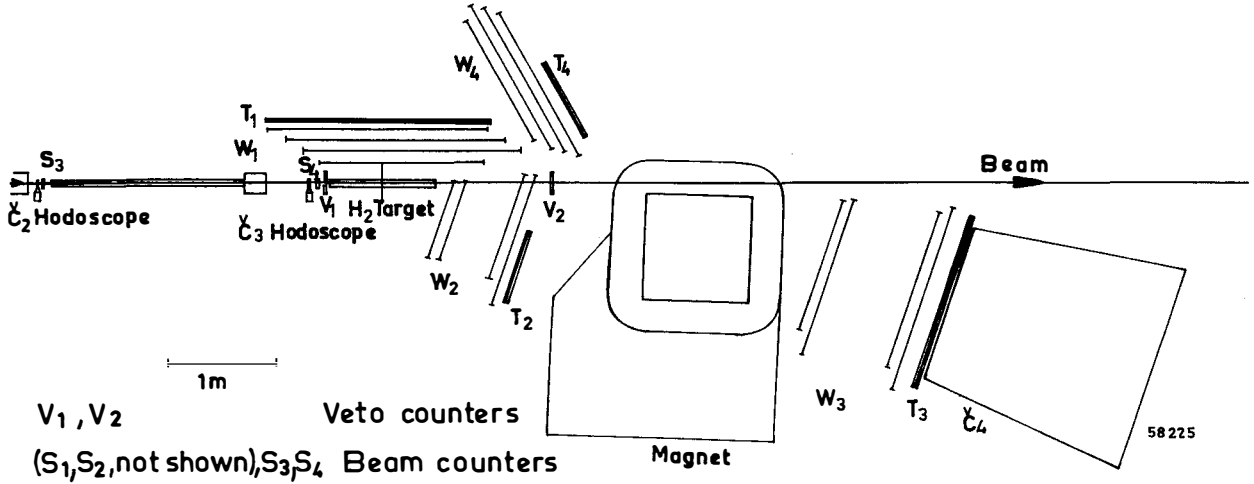

BEHAVIOUR OF ELASTIC
SCATTERING AT 5.0 GeV/c
10
1
10^{-1}
10^{-2}
10^{-3}
10^{-4}
10^{-5}
$d\sigma/dt$ mb/(GeV/c)^2
pp
K^+p
π^+p
π^-p
$\bar{p}p$
K^-p
0
2.0
4.0
6.0
8.0
$-t$ (GeV/c)^2

Fig.1



V_1, V_2 Veto counters

$(S_1, S_2$, not shown), S_3, S_4 Beam counters

$\check{C}_1, \check{C}_2$, not shown) $\check{C}_3, \check{C}_4$ Threshold gas Čerenkov counters

W_1, W_2, W_3, W_4 Wire spark chamber telescopes

T_1, T_2, T_3, T_4 Wire spark chamber trigger counters

Fig. 2

"EVENT" $= S_1 \cdot S_2 \cdot S_3 \cdot S_4 \cdot \overline{V}_1 \cdot \overline{V}_2$

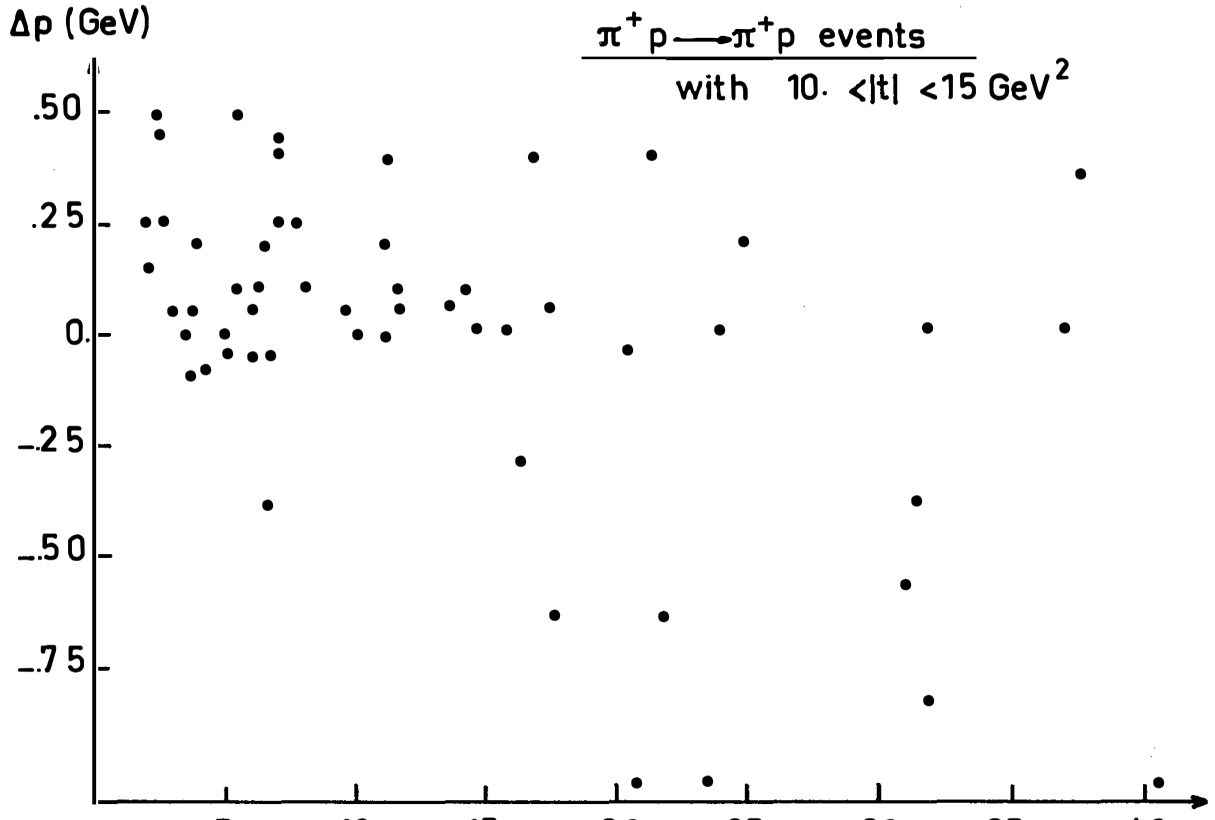

Δp (GeV)
$\pi^+ p \longrightarrow \pi^+ p$ events
with 10. <|t| <15 GeV^2
.50
.25
0.
-.25
-.50
-.75
5
10
15
20
25
30
35
40
X^2

Fig. 3

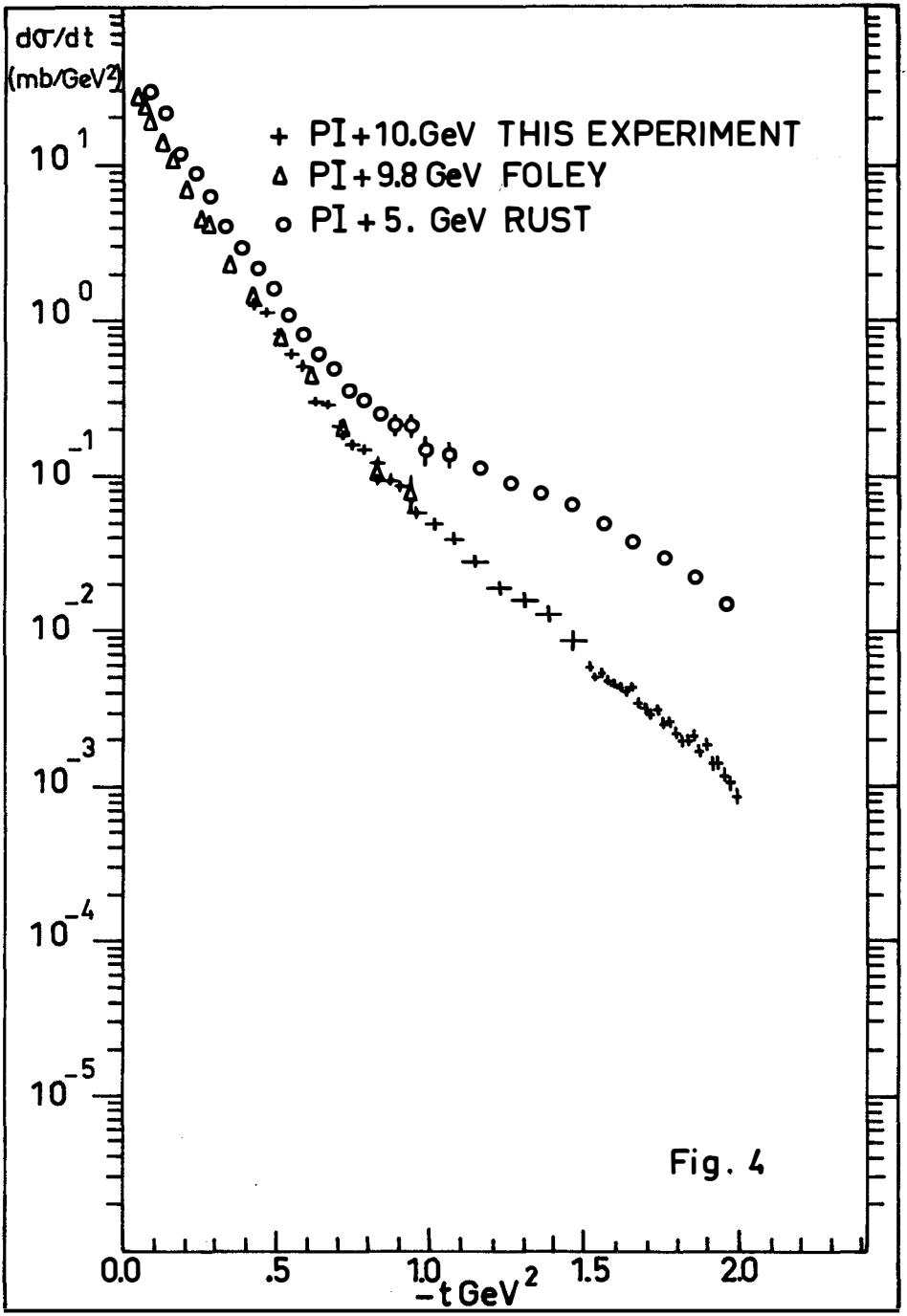
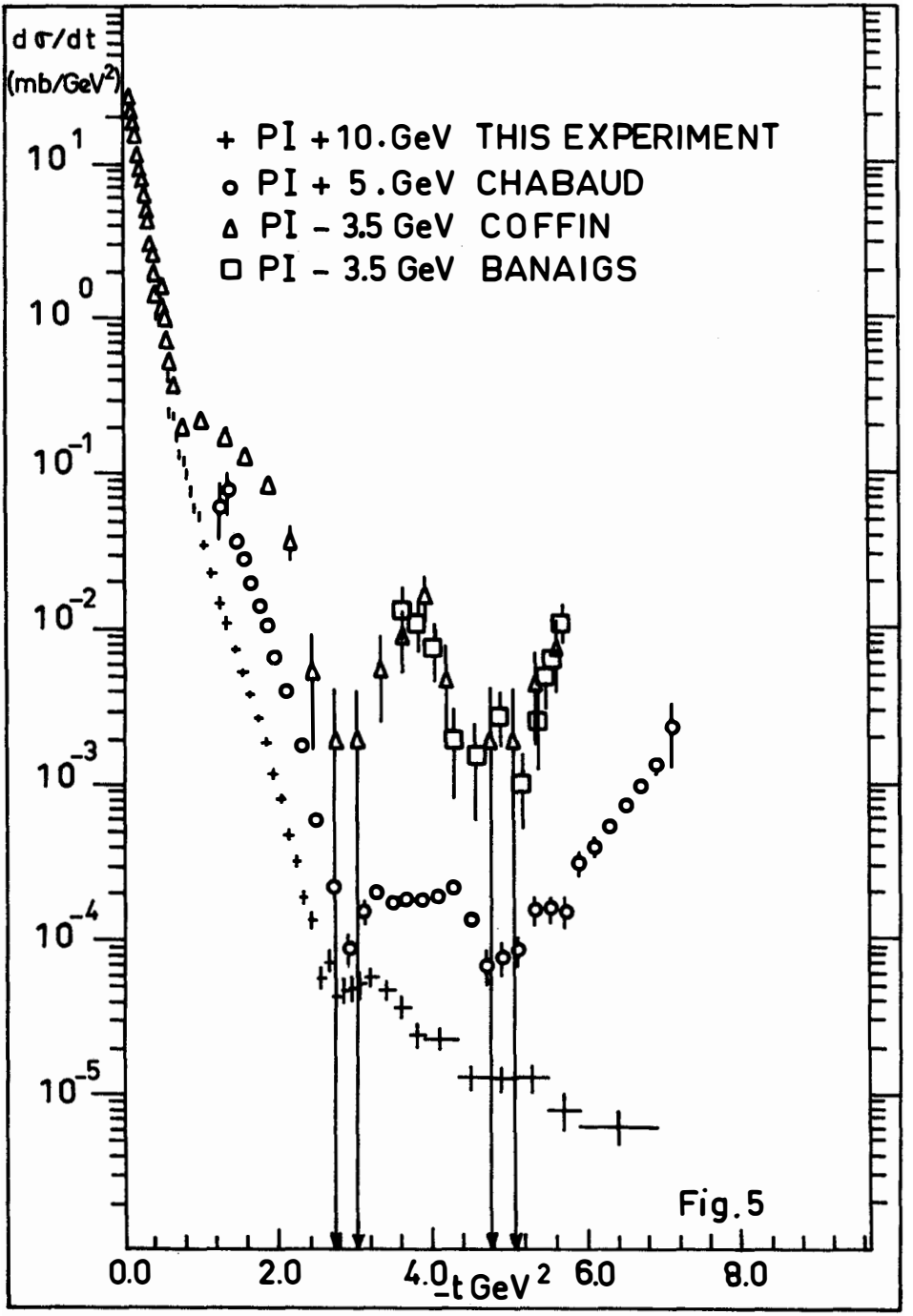

dσ/dt
(mb/GeV²)
+ PI+10.GeV THIS EXPERIMENT
Δ PI+9.8 GeV FOLEY
o PI+5. GeV RUST
10¹
10⁰
10⁻¹
10⁻²
10⁻³
10⁻⁴
10⁻⁵
0.0
.5
1.0
1.5
2.0
-t GeV²

Fig. 4


dσ/dt
(mb/GeV²)
+ PI +10.GeV THIS EXPERIMENT
o PI + 5.GeV CHABAUD
Δ PI - 3.5 GeV COFFIN
□ PI - 3.5 GeV BANAIGS
10¹
10⁰
10⁻¹
10⁻²
10⁻³
10⁻⁴
10⁻⁵
0.0
2.0
4.0
-t GeV²
6.0
8.0
Fig. 5

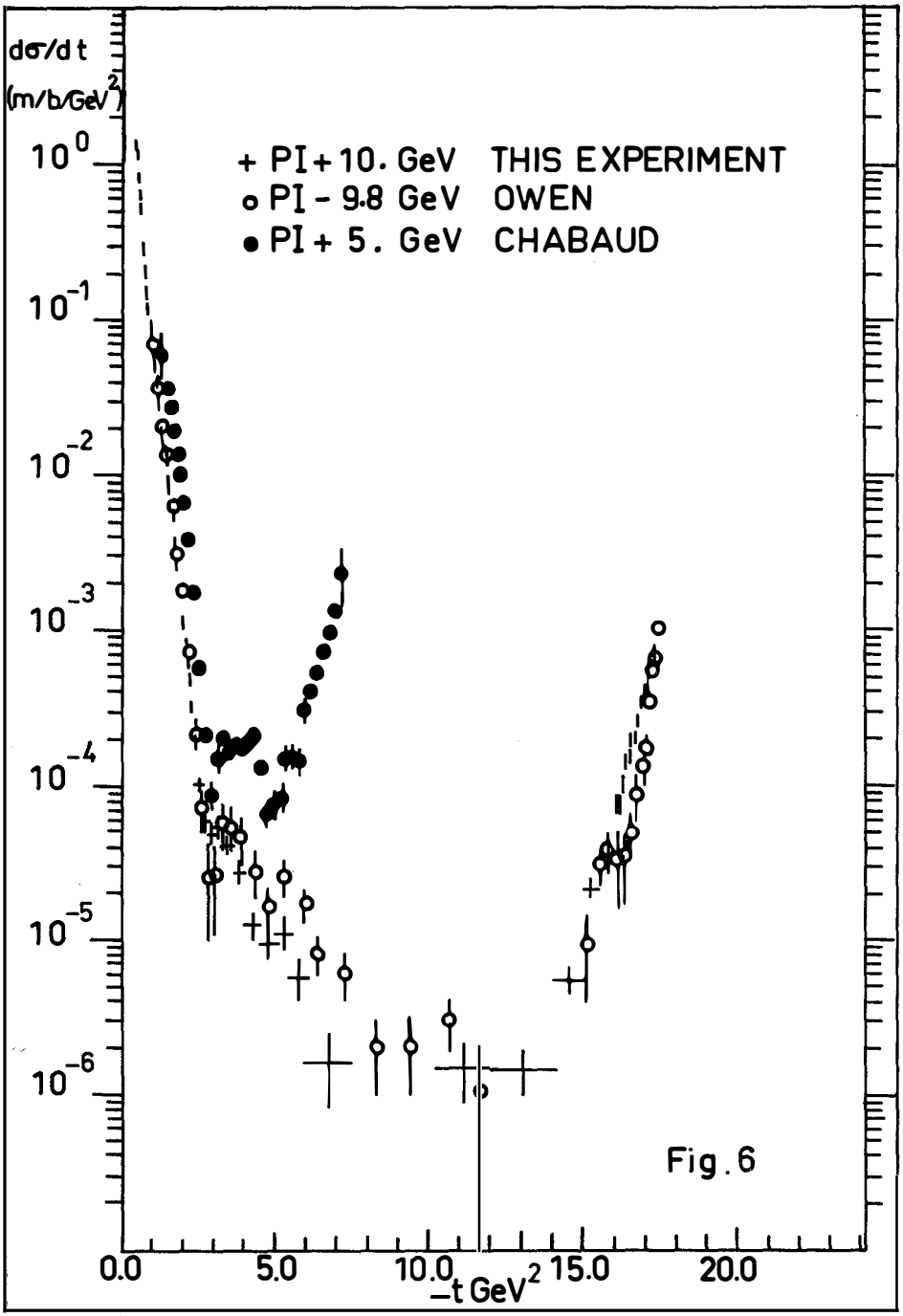

dσ/dt
(m/b/GeV²)
10⁰
10⁻¹
10⁻²
10⁻³
10⁻⁴
10⁻⁵
10⁻⁶
+ PI+10. GeV THIS EXPERIMENT
o PI- 9.8 GeV OWEN
● PI+ 5. GeV CHABAUD
0.0
5.0
10.0
15.0
20.0
−t GeV²

Fig. 6

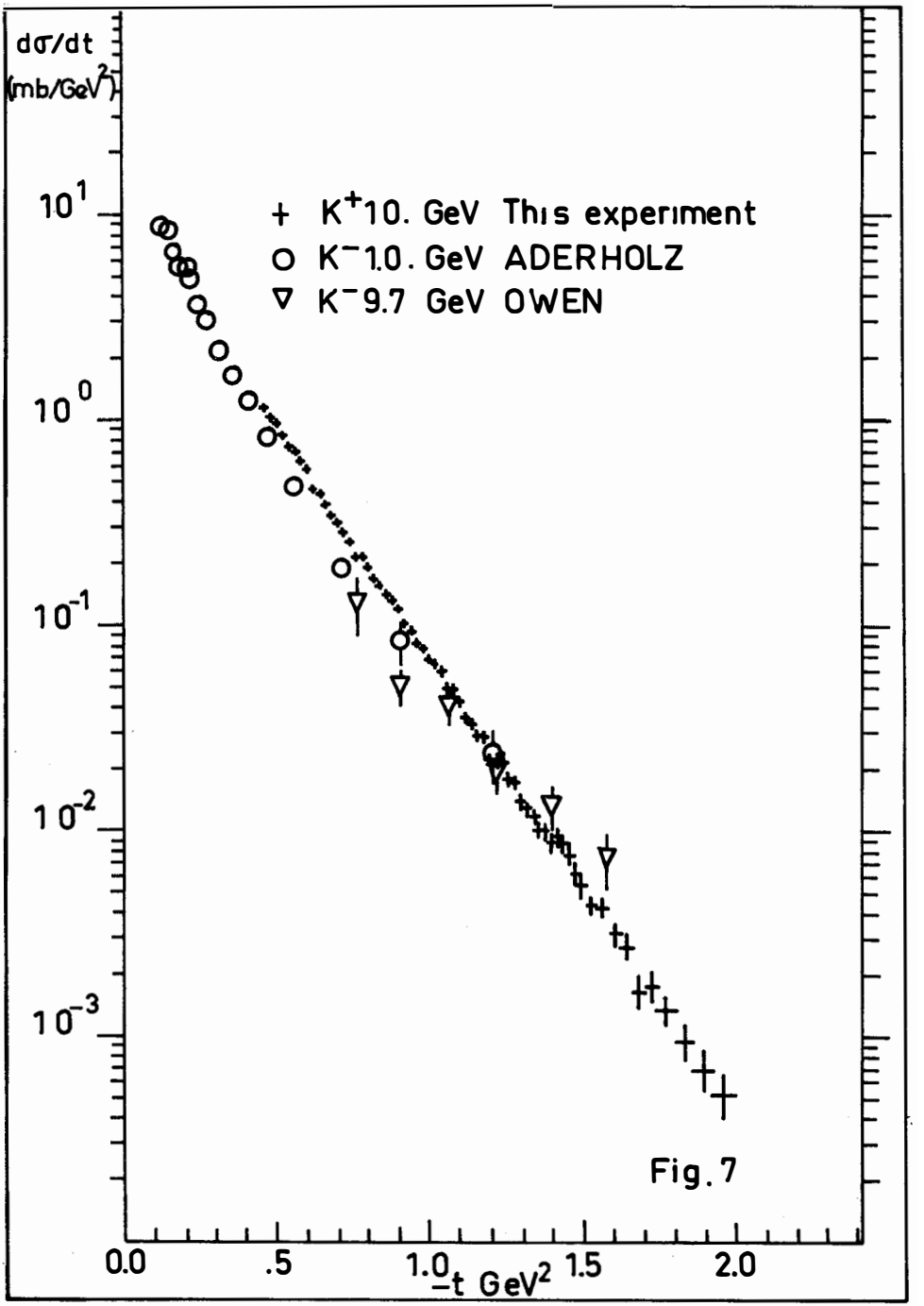

dσ/dt
(mb/GeV²)
10¹
10⁰
10⁻¹
10⁻²
10⁻³
+ K⁺10. GeV This experiment
O K⁻1.0. GeV ADERHOLZ
∇ K⁻9.7 GeV OWEN
0.0
.5
1.0
1.5
2.0
−t GeV²

Fig. 7

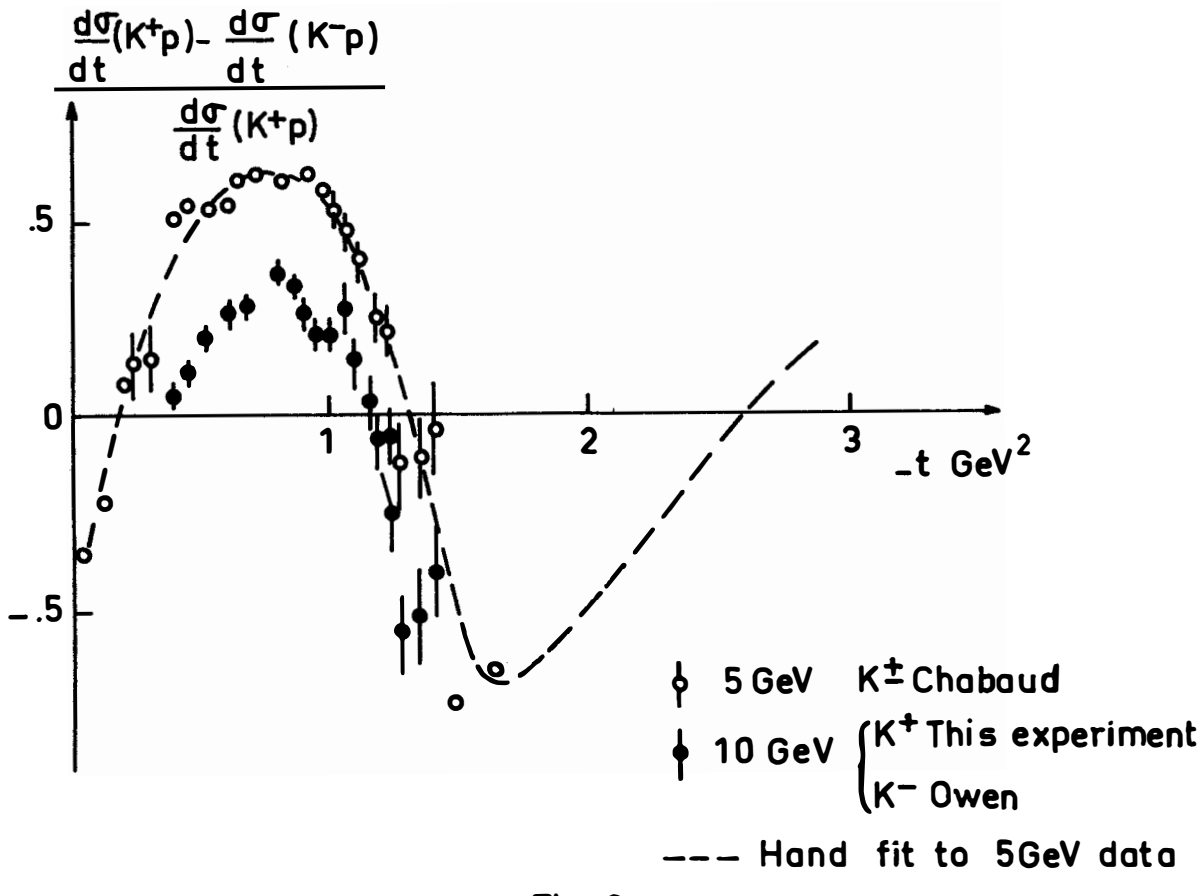
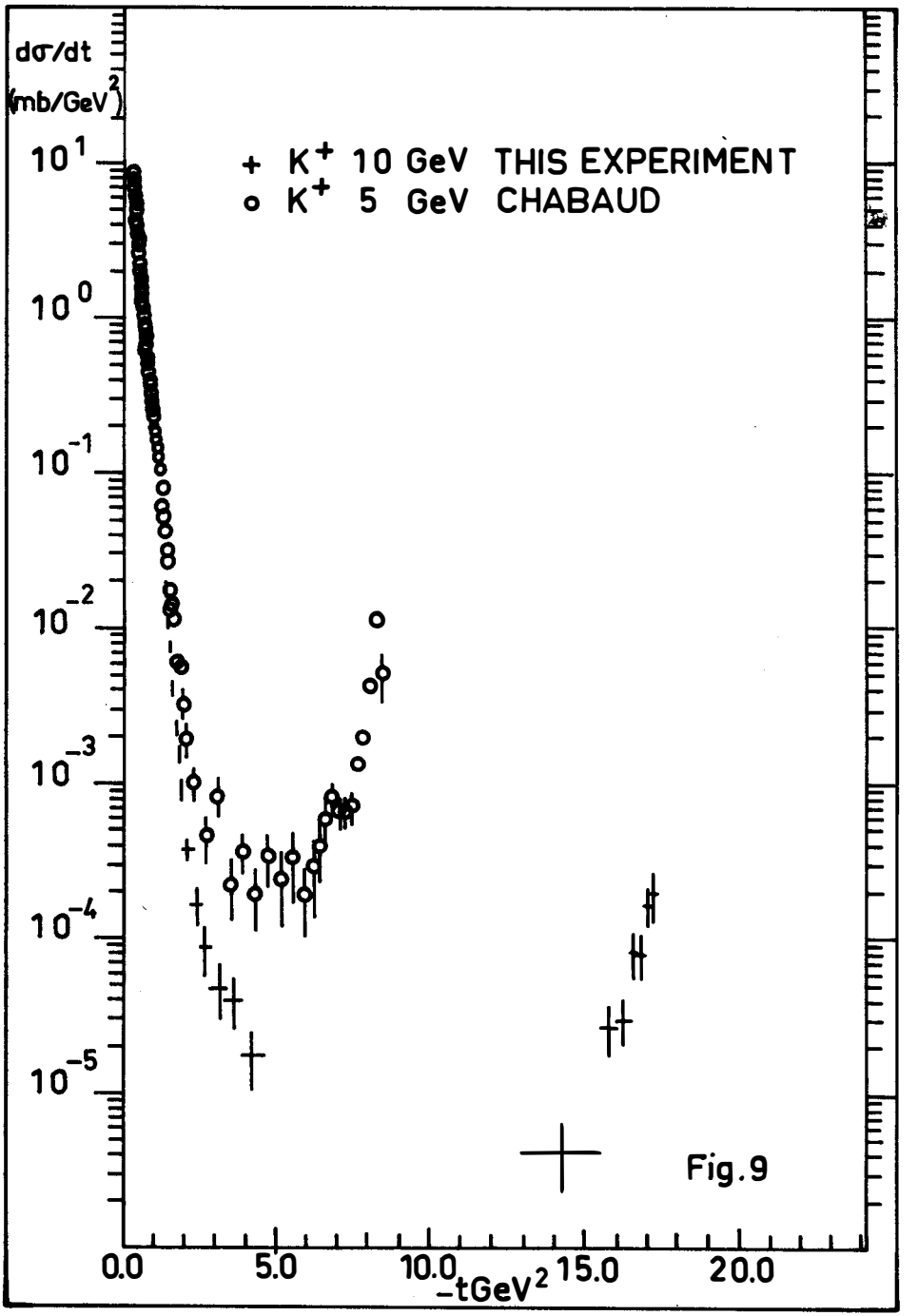

$\frac{d\sigma}{dt}(K^+p) - \frac{d\sigma}{dt}(K^-p)$
$\frac{d\sigma}{dt}(K^+p)$
.5
0
-.5
1
2
3
-t GeV^2
5 GeV $K^\pm$ Chabaud
10 GeV K^+ This experiment
K^- Owen
--- Hand fit to 5GeV data

Fig. 8


dσ/dt
(mb/GeV²)
10¹
10⁰
10⁻¹
10⁻²
10⁻³
10⁻⁴
10⁻⁵
+ K⁺ 10 GeV THIS EXPERIMENT
o K⁺ 5 GeV CHABAUD
0.0
5.0
10.0
15.0
20.0
-tGeV²
Fig.9

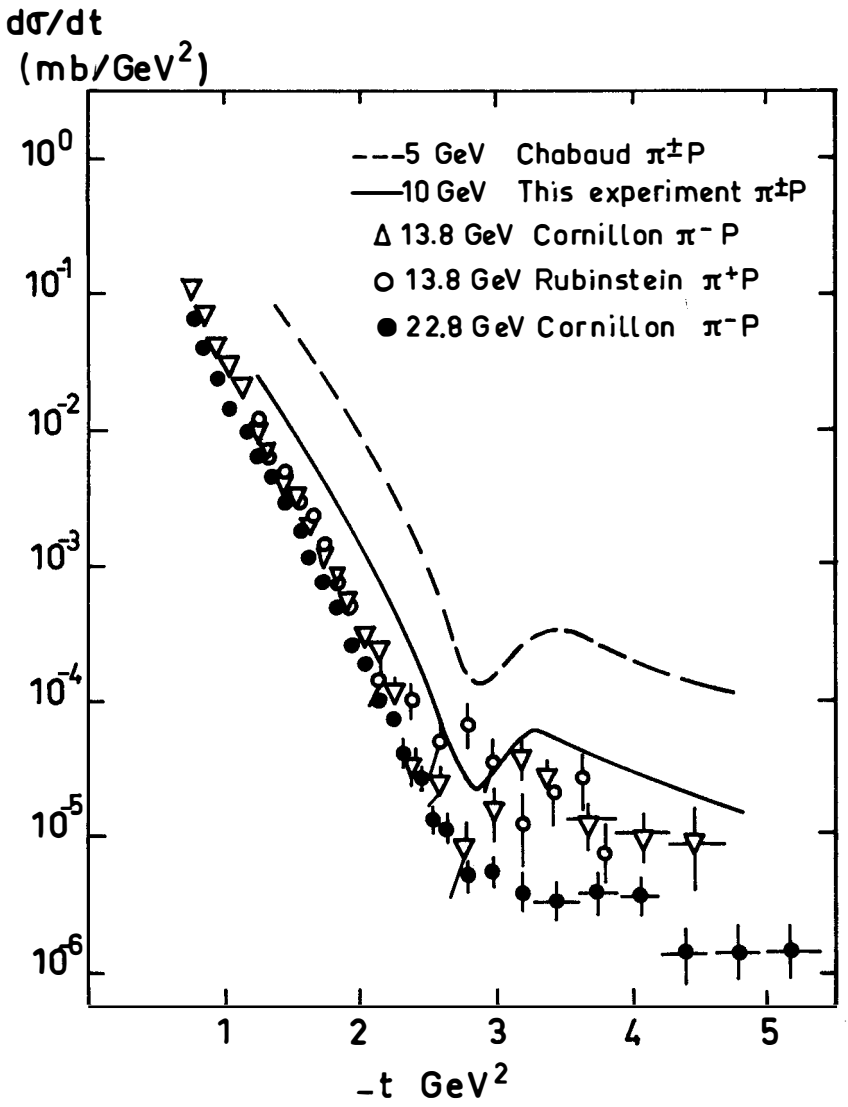

dσ/dt
(mb/GeV²)
10⁰
10⁻¹
10⁻²
10⁻³
10⁻⁴
10⁻⁵
10⁻⁶
1
2
3
4
5
-t GeV²
---5 GeV Chabaud π±P
——10 GeV This experiment π±P
Δ 13.8 GeV Cornillon π⁻P
○ 13.8 GeV Rubinstein π⁺P
● 22.8 GeV Cornillon π⁻P

Fig. 10

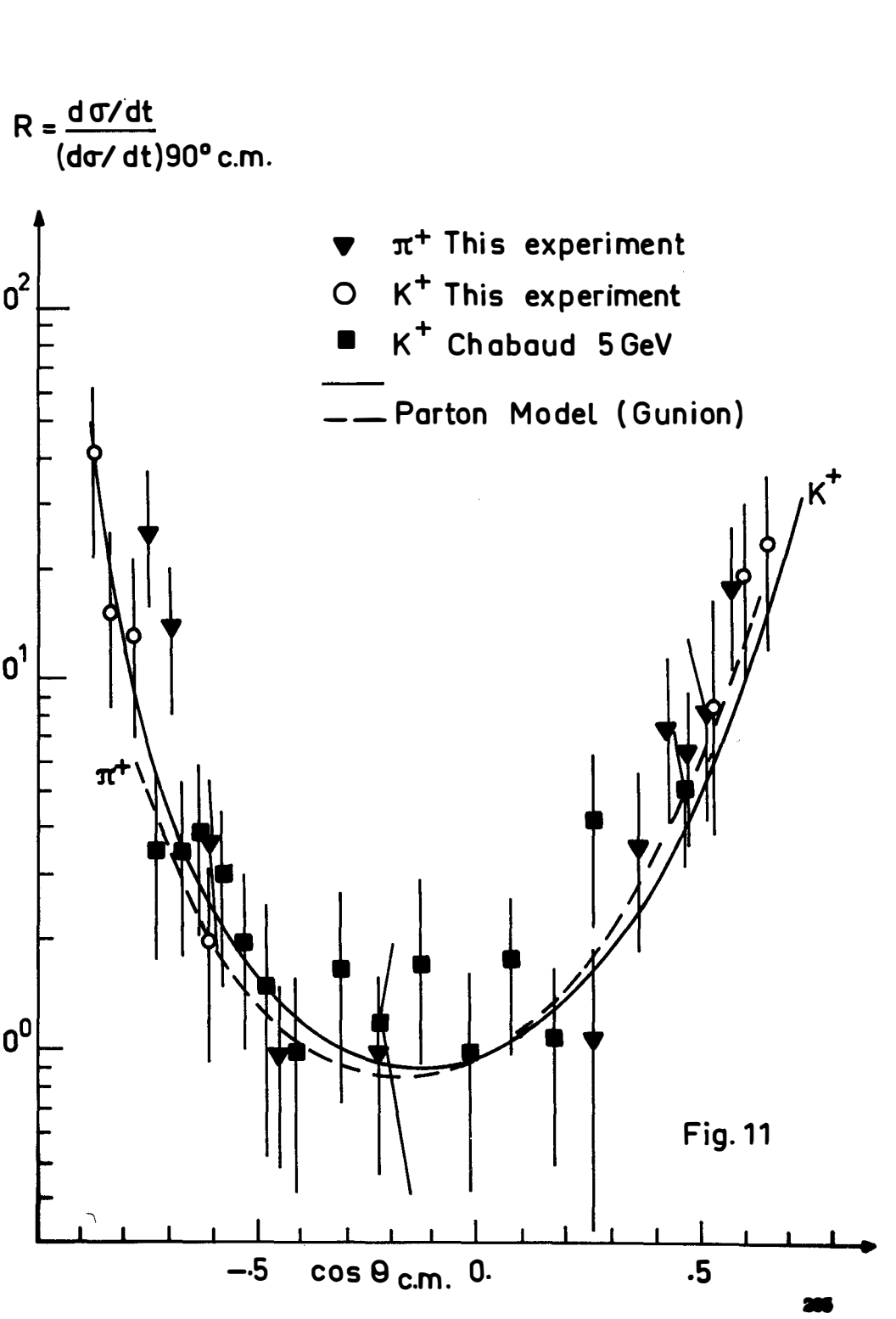

R = dσ/dt / (dσ/dt)90° c.m.
▼ π+ This experiment
○ K+ This experiment
■ K+ Chabaud 5 GeV
Parton Model (Gunion)
0²
0¹
0⁰
π+
K+
−.5
cos θ c.m.
0.
.5

Fig. 11

PHENOMENOLOGY OF PROTON-PROTON SCATTERING AT ALL ANGLES

D. D. Coon
Department of Physics, University of Pittsburgh
Pittsburgh, Pennsylvania 15260 (USA)

and

J. Tran Thanh Van
Laboratoire de Physique Théorique et Particules Elementaires
Université de Paris Sud, Bat. 211, 91 Orsay, France

Abstract: Fits have been made to the proton-proton differential cross section and the difference of the $p\bar{p}$ and pp total cross sections using a dual model of Baker and Coon. These fits tend to indicate that: (1) there is a fairly simple dominant contribution to large momentum transfer processes, (2) the range of applicability of duality and Reggeism is much larger than one might expect, (3) the Baker-Coon model has an enormous range of quantitative validity, (4) the Pomeron contribution to the $p\bar{p}$ differential cross section can be separated from the dual contribution and (5) the Pomeron contribution so extracted has a sharp diffraction minimum at the shoulder at $t = -1.2\ (GeV)^2$. The mechanism for producing the shoulder survives the test of an extrapolation from $s \gtrsim 20\ (GeV)^2$ to $s \gtrsim 2600\ (GeV)^2$ and predicts the depth of the dip at $t = -1.2\ (GeV)^2$ in the ISR data. The Pomeron contribution at conventional accelerator energies is very well approximated by an eikonalized Pomeron exchange term.



Résumé: La section efficace différentielle proton-proton et la différence des sections efficaces totales pp et $p\bar{p}$ ont été fittées en utilisant un modèle dual de Baker et Coon. Ces fits semblent indiquer que : 1) il y a une contribution dominante relativement simple aux processus à grand transfert, 2) le domaine d'applicabilité de la dualité et du Reggeïsme est beaucoup plus grand que ce que l'on pouvait attendre, 3) le modèle de Baker et Coon possède un très grand domaine de validité qualitative, 4) il est possible de séparer la contribution du Pomeron dans la section efficace différentielle de la contribution duale et 5) la contribution du Pomeron ainsi obtenue possède un minimum de diffraction accentuée, suivi d'une épaule à $t = -1.2$ $(GeV/c)^2$. Le méca,isme de production de l'épaule passe avec succès l'épreuve de l'extrapolation de $s \approx 20$ GeV^2 à $s \approx 2600$ GeV^2 et prédit la profondeur du dip à $t = -1.2(GeV)^2$ des données des ISR. La contribution du Pomeron aux énergies des accélérateurs conventionnels est très bien reproduite par l'échange du Pomeron eikonalizé.

Recently a dual model[1] with logarithmic trajectories has been found to give an excellent quantitative description of proton-proton scattering at high momentum transfer.[2] This is consistent with the idea that Pomeron exchange is not dominant in the fixed angle region. At least at presently available energies, elastic and charge exchange cross sections are of the same order of magnitude in the fixed angle region. The Veneziano model falls off much too fast to be phenomenologically useful in the fixed angle region. In contrast, the dual model with logarithmic trajectories has much slower fall off and agrees with experiment over a wide range of t and s. Only one dual term is required to fit pp data in the region $|t| > 5$ $(GeV)^2$ and $s > 18$ $(GeV)^2$. As has been noted by Barger, Geer and Halzen,[3] another Regge exchange contribution is needed to explain data in the region $s < 18$ $(GeV)^2$. We find that the addition of a second dual term provides a good description of the non-Pomeron contribution in the region $s < 18$ $(GeV)^2$.

Fits to $d\sigma/dt$ at 90° and the contribution of the dual amplitude to $d\sigma/dt$ at 19.3 GeV/c are shown in Fig. 1 and Fig. 2. In Fig. 2 we see that the dual contribution appears to be filling in a diffraction minimum to produce the shoulder at $t = -1.2$ $(GeV)^2$. This dip filling mechanism has been tested against the ISR data using parameters determined from fits to data from conventional accelerators. The results are shown in Fig. 3. The bottom of the dip is predicted remarkably well considering that we are extrapolating from $20 \lesssim s \lesssim 50$ to $s \sim 2000$. (Of course, it should

be noted that the dual model only has logarithmic dependence on s.)

The above explanation of the behavior of pp data near $t = -1.2\ (GeV)^2$ meshes very nicely with models for diffraction scattering which would have a much sharper diffraction minimum than is observed experimentally. In fact we see that the overall shape of the nondual component of $d\sigma/dt$ is very similar to what a number of authors have proposed for diffractive scattering.[4]

In order to obtain a fit at all angles, we add an eikonalized Pomeron exchange term to our two dual terms. The Pomeron Born term is taken to be proportional to the square of a dipole form factor:[5]

$$P_{BORN} = K[F(t)]^2 (E/E_0)^{1+\alpha' t}$$

where

$$F(t) = \frac{1}{(1-t)^2} ,$$

K is an overall constant, E_0 is a Regge scale factor, E is the laboratory energy of the incident proton and α' is the slope of the Pomeron trajectory, which is taken to be .1. The fit to conventional accelerator pp data which results from combining the eikonalized Pomeron Born term with two dual terms is extraordinarily good and is shown in Fig. 4.

The explicit form of the dual amplitude[1] used in the fits is

$$M(t,u) = C \frac{G(q/\tau u)}{G(q/\tau)G(q/u)} q^{\alpha(t)\alpha(u)} \qquad (2)$$

where

$$G(x) = \prod_{\ell=0}^{\infty} (1-xq^{\ell})$$

$$\tau = b - at = q^{\alpha(t)}$$

$$\upsilon = b - au = q^{\alpha(u)}$$

and a, b, C and q are real parameters. The curvature of the logarithmic trajectory $\alpha(t)$ is controlled by q which lies in the range $0 < q < 1$. The Lovelace form[6] of the Veneziano model[7] can be obtained in the limit $q \to 1$ if a, b and C are allowed to depend on q.[1] Another dual amplitude which is mathematically related to this dual amplitude has been investigated extensively.[8]

The dual amplitude in Eq. (2) has an unusual feature. At $u = b/a$ there is an accumulation point of poles as $\alpha(u) = \ell n(b-au)/\ell nq$ becomes infinite. In addition, there is a cut beginning at $u = b/a$. Thus there appears to be an ionization point and the trajectory is behaving as one would expect given a long range force between constituents. A model in which quarks interact with a long range gluon field has been proposed by Suura.[9]

Since higher lying resonances would become more and more closely spaced, one might worry about the acceptability of the meson spectrum of the model. By letting q become slightly complex in order to introduce widths, Arik[10] has obtained the general shape of the meson resonance spectrum, Fig. 5, which one would expect on the basis of the dual model. The higher lying resonances are less prominent and become indistinguishable from

the continuum. Although the ionization point is mathematically delicate, one can see from Fig. 5 that it is expected to be smooth experimentally. The dual amplitude thus has some similarity with amplitudes involving the Coulomb bound states of atomic physics. For comparison, we show the experimental photoabsorption coefficient of argon as a function of wavelength.

If one averages the imaginary part of the dual amplitude by replacing the amplitude with its large α asymptotic form using an analog of Stirling's formula, then the resonance poles are replaced by a cut and the explicit branch points of Eq. (2) are cancelled by the new branch points so that no structure is left at $u = b/a$ or $t = b/a$. This tendency of the dual model toward smooth, reasonable behavior in the physical region is due to some remarkable mathematical properties of the model and related elliptic functions. This smooth behavior in the physical region of the u-channel allows us to fit the $p\bar{p}$, pp total cross section difference. In fact, we are able to do phenomenology over a vast region of s, t space. A typical fit to the total cross section difference $\sigma_{p\bar{p}} - \sigma_{pp}$ is shown in Fig. 7.[10]

In conclusion, we observe that the dual model with logarithmic trajectories appears to work well for both positive and negative values of the kinematic invariants and points out a vast increase in the range of applicability of duality. Furthermore, by accurately parameterizing the dual component of the amplitude, we are able to isolate the Pomeron or diffractive component of pp scattering in the range $-4\ (\mathrm{GeV})^2 < t < 0$.

REFERENCES

1. M. Baker and D. Coon (to be published).
2. D. Coon, U. Sukhatme and J. Tran Thanh Van, SLAC-PUB-1171 (to be published).
3. V. Barger, K. Geer and F. Halzen, Nucl. Phys. B49, 302 (1972).
4. T. T. Chou and C. N. Yang, Phys. Rev. Letters 20, 1213 (1968); L. Durand, III and R. Lipes, Phys. Rev. Letters 20, 637 (1968); S. C. Frautschi and B. Margolis, Nuovo Cimento 56A, 1155 (1968); J. Finkelstein, Nuovo Cimento 59A, 92 (1969); A. Capella, J. Kaplan, A. Krzywicki and D. Schiff, Nuovo Cimento 63A, 141 (1969).
5. This procedure is motivated by the papers mentioned in reference 4.
6. C. Lovelace, Phys. Letters 28B, 264 (1968).
7. G. Veneziano, Nuovo Cimento 57A, 190 (1968).
8. D. Coon, Phys. Letters 29B, 669 (1969); Phys. Rev. 186, 1422 (1969); M. Baker and D. Coon, Phys. Rev. D2, 2349 (1970); D3, 2478 (1971); D4, 1234 (1971); M. Baker, D. Coon and S. Yu, Phys. Rev. D5, 1429 (1972), D5, 3108 (1972), D6, 538 (1972).
9. H. Suura, Phys. Rev. D6, 3538 (1972).
10. M. Arik, private communication.
11. R. E. Huffman, Y. Tanaka and J. Larrabee, J. Chem. Phys. 39, 902 (1963).

FIGURE CAPTIONS

Fig. 1. Comparison of 90° pp scattering data with a fit (1) using one dual term and a fit (2) using two dual terms.

Fig. 2. Differential cross section for pp elastic scattering at at $\sim$ 19.2 GeV/c. The solid and dashed lines are the dual and Pomeron contributions, respectively.

Fig. 3. ISR data at s = 2016 $(GeV/c)^2$. The dual contribution (solid line) passes just below the dip at $t \approx -1.2$ $(GeV/c)^2$. Subtraction of the dual contribution from the experimental data yields a sharp dip in the Pomeron contribution (dashed curve).

Fig. 4. Comparison of fitted curves with pp elastic scattering data. The parameters of the two dual terms contributing to this fit are chosen so that $q = .795$, $\alpha_1(0) = .8$, $\alpha_2(0) = .37$, $C_1 = .007$, $C_2 = .42$ and the $(mass)^2$ of the lowest resonance in each term is .6 $(GeV)^2$.

Fig. 5. Imaginary part of the forward dual amplitude in a resonant channel. q is taken to be .8 + .02 i in order to introduce widths and $\alpha(0) = .5$.

Fig. 6. Photoabsorption coefficient of argon as measured by Huffman et al.

Fig. 7. Comparison between the $p\bar{p}$, pp total cross section difference and the imaginary part of a dual amplitude at t = 0.

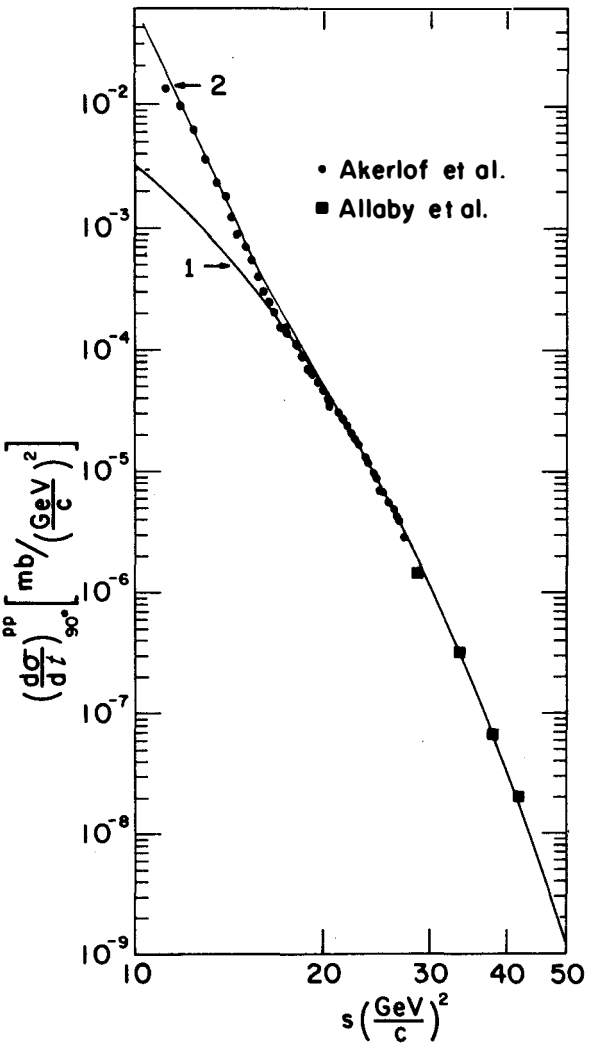

2
1
• Akerlof et al.
■ Allaby et al.
10^{-2}
10^{-3}
10^{-4}
10^{-5}
10^{-6}
10^{-7}
10^{-8}
10^{-9}
10
20
30
40
50
$\left(\frac{d\sigma}{dt}\right)^{pp}_{90°}\left[\frac{mb}{\left(\frac{GeV}{c}\right)^2}\right]$
$s\left(\frac{GeV}{c}\right)^2$

Fig. 1

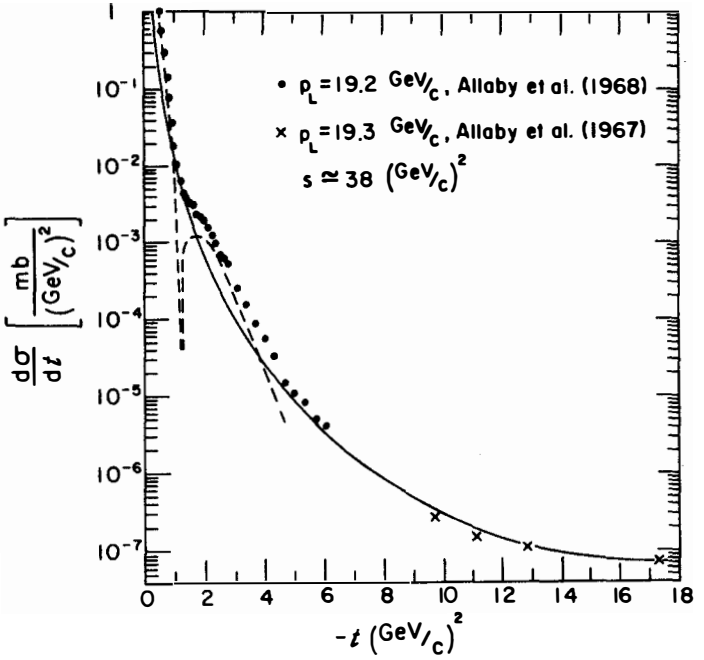

• p_L = 19.2 GeV/c, Allaby et al. (1968)
× p_L = 19.3 GeV/c, Allaby et al. (1967)
$s \simeq 38\ (GeV/c)^2$
$\frac{d\sigma}{dt}\left[\frac{mb}{(GeV/c)^2}\right]$
$-t\ (GeV/c)^2$
1
10^{-1}
10^{-2}
10^{-3}
10^{-4}
10^{-5}
10^{-6}
10^{-7}
0
2
4
6
8
10
12
14
16
18

Fig. 2

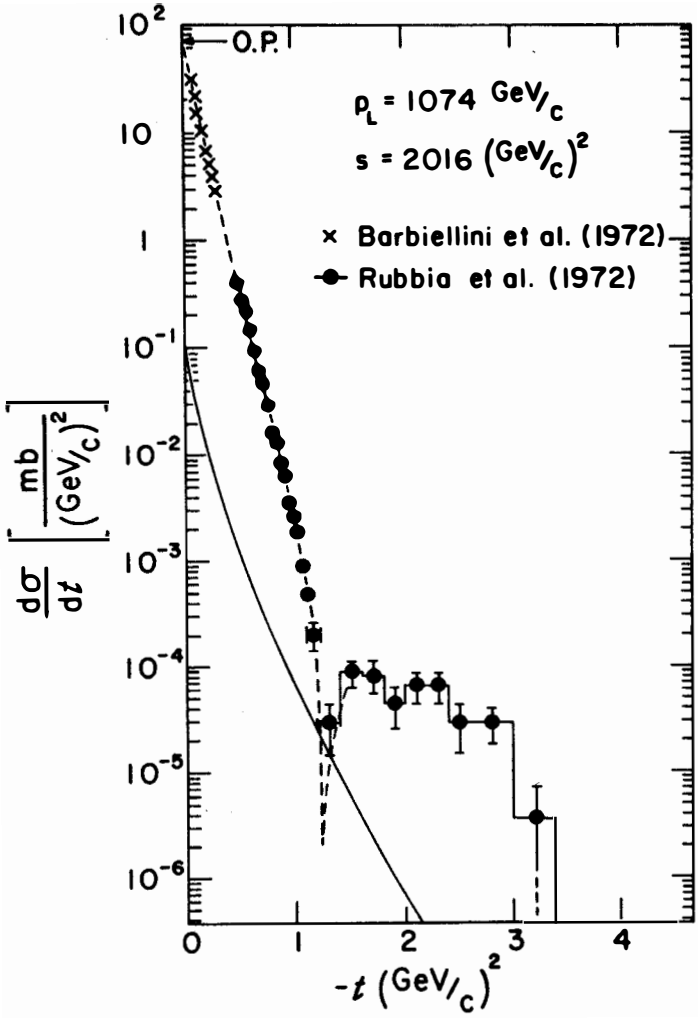

O.P.
p_L = 1074 GeV/c
s = 2016 (GeV/c)^2
× Barbiellini et al. (1972)
Rubbia et al. (1972)
$\frac{d\sigma}{dt}\left[\frac{mb}{(GeV/c)^2}\right]$
$-t\ (GeV/c)^2$

Fig. 3

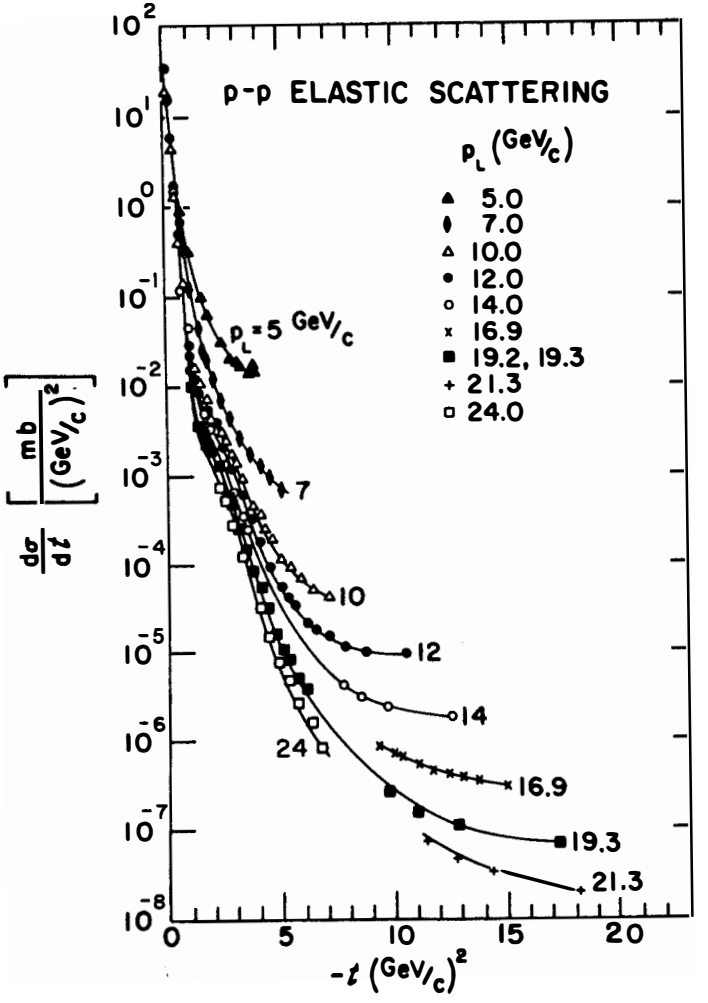

p-p ELASTIC SCATTERING
p_L (GeV/c)
5.0
7.0
10.0
12.0
14.0
16.9
19.2, 19.3
21.3
24.0
p_L = 5 GeV/c
7
10
12
14
16.9
19.3
21.3
24
$\frac{d\sigma}{dt}\left[\frac{mb}{(GeV/c)^2}\right]$
$-t\ (GeV/c)^2$
10^2
10^1
10^0
10^{-1}
10^{-2}
10^{-3}
10^{-4}
10^{-5}
10^{-6}
10^{-7}
10^{-8}
0
5
10
15
20

Fig. 4

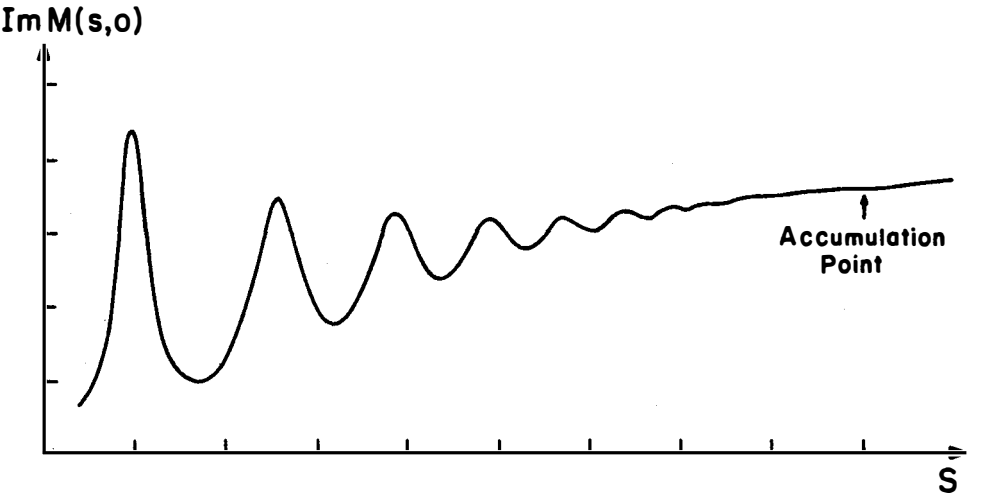

Im M(s,o)
Accumulation Point
S

Fig. 5

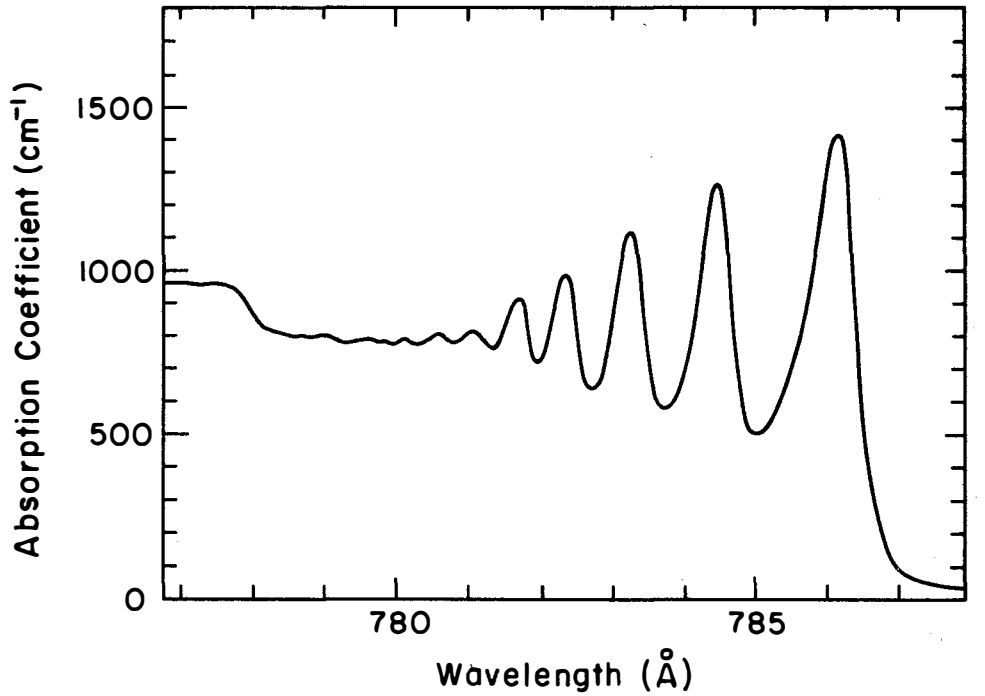

Absorption Coefficient (cm⁻¹)
1500
1000
500
0
780
785
Wavelength (Å)

Fig. 6

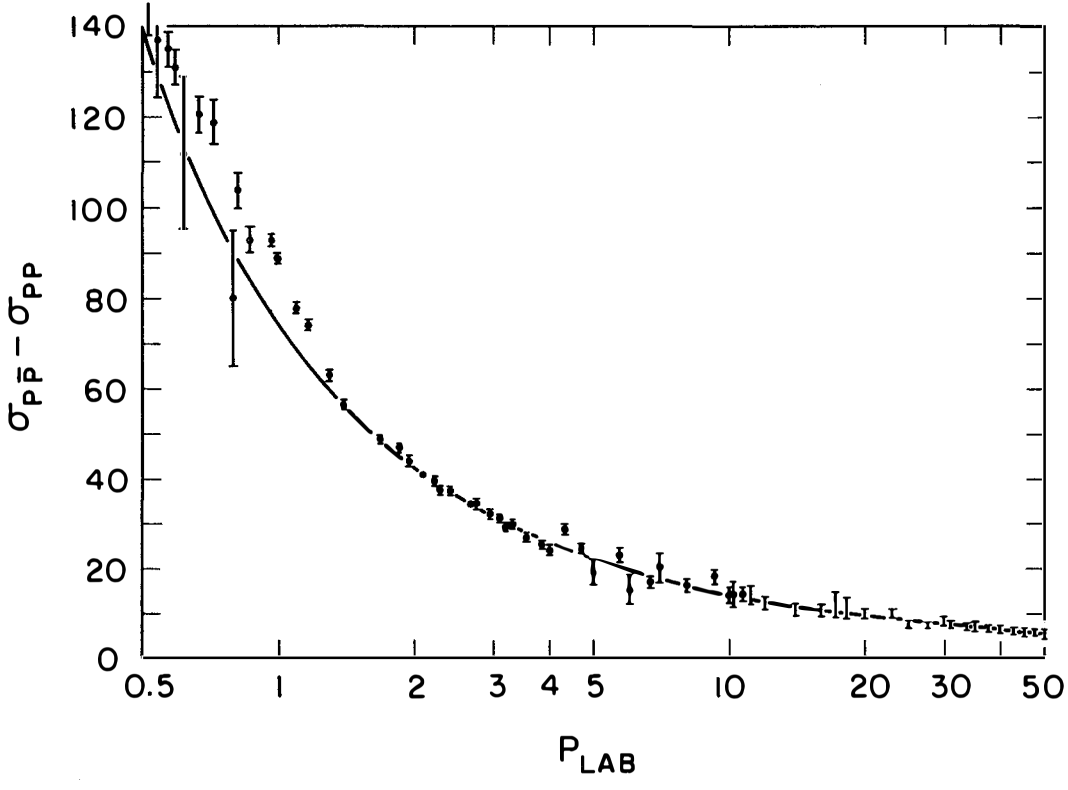

140
120
100
80
60
40
20
0
0.5
1
2
3
4
5
10
20
30
50
$\sigma_{P\bar{P}} - \sigma_{PP}$
P_{LAB}

Fig. 7

HADRONIC SCATTERING AT SMALL AND LARGE MOMENTUM TRANSFERS[†]

H. M. Fried
Department of Physics, Brown University
Providence, Rhode Island 02912 (USA)

Abstract: The nature of possible corrections to the Cheng-Wu forward-direction amplitude is examined on the basis of a complete eikonal formulation, which suggests strong cancellations away from the Froissart bound, $\sigma_T \sim \ell n^2 s$. Two models of wide-angle scattering, the interchange model and the hadronic bremsstrahlung model, are briefly discussed and compared.

Résumé : On examine la nature des corrections possibles à l'amplitude de Cheng-Wu pour la diffusion vers l'avant sur la base de la formulation complète de l'approximation eikonale qui suggère que la section efficace totale subit d'importantes cancellations à partir de la limite de Froissart, $\sigma_T \sim \ell n^2 s$.

Deux modèles pour la discussion à grand angle, le modèle d'interchange et le modèle de bremsstrahlung hadronique sont brièvement discutés et comparés.



[†]Supported in part by the U.S. Atomic Energy Commission, (Report No. COO-3130TA-279).

These remarks will be divided into two distinct categories: A) A brief but general discussion[1] of the small-angle eikonal formalism; and B) A brief report on two recent models[2,3] for hadronic scattering at large momentum transfers. With the newly reported rise of $\sigma_T(pp)$,[4] and Cheng-Wu phrases[5] filling the air, the discussion of topic A may be useful in placing that and similar calculations[6] in some sort of general (field theoretic) perspective. Items B stand as two friendly rivals in a rapidly growing field, models which purport to give a description of wide-angle hadronic processes, with each based upon a simple and intuitive (and different) framework.

A. Small-Angle Scattering

In any local, relativistic, quantum field theory, the elastic nucleon-nucleon (non-spin-flip) amplitude $T(p_1 + p_2 \to p_1' + p_2')$ at high energies and close to forward directions ($|t|/s \ll 1$) may be written in eikonal form

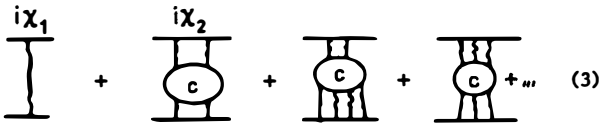
$$T(s,t) = \frac{is}{2m^2} \int d^2b \; e^{i\vec{q}\cdot\vec{b}} \left[1 - e^{i\chi(b^2;s)}\right] \quad , \tag{1}$$

with

$$\sigma_T = 2 \, \mathrm{Re} \int d^2b \left[1 - e^{i\chi}\right] \quad , \tag{2}$$

and $i\chi$ given by the sum of all connected, t-channel amplitudes (whose coordinates are set equal to and integrated over the positions of the fast nucleons' classical currents). This identification of the eikonal rests upon the validity of the eikonal limit, in which one supposes that any structure exchanged between the nucleons always involves momenta significantly smaller than those of the fast nucleons.[7]

In massive photon QED, one has the pictoral relation

$$i\chi =$$  (3)

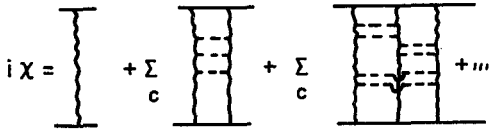
where $i\chi_1 = -i\frac{g^2}{2\pi} K_o(\mu b)$, as $s \to \infty$, and by itself defines the so-called Relativistic Eikonal Approximation.[8] In a leading-log s calculation, Cheng and Wu have estimated $i\chi_2$ in terms of the sum over tower graphs,

$$i\chi_2 = \sum_{\text{loops}}$$  $$\Rightarrow -a_1 s^{a_2} e^{-a_3 b}$$ (4)

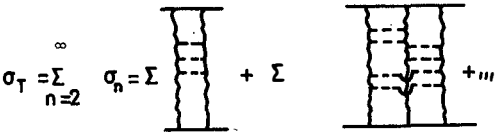
for large impact parameter b, in terms of the constants a_i, which when substituted into (2) produces $\sigma_T \sim \ln^2 s$. This arises, in the Froissart manner, because the $\int d^2b$ integral cuts off for $b = b_{max} \sim \ln s$, which condition is simply determined by the requirement $|i\chi_2| \leq 1$. The intuitive appeal of the Cheng-Wu calculation lies in their observation that for fixed s, and $b \to \infty$, one may expect that $i\chi \to i\chi_2$, since only that part of the eikonal with the smallest t-channel threshold should be important. However, the physics requires the condition $|i\chi| \leq 1$ to define $b_{max}(s)$, in which b and s must grow simultaneously; and hence the remaining contributions to the eikonal, not considered by Cheng and Wu, can play a significant role.

In the context of a special, but simple, model theory, these terms have been estimated,[1] and display strong cancellations from the Cheng-Wu result. Here, one constructs graphs from external nucleon lines, (vertical) neutral vector meson (NVM) lines, and (horizontal) "scalar pion" lines, with the eikonal given by the sum over the connected graphs (at least one pion line must connect any

NVM line to the remainder of the graph),



One may write a similar graphical expression for σ_T,



where n refers to the number of vertical NVM lines, and the sums include disconnected graphs; all non-planar "checkerboard" graphs are contained in these sums. In the approximation of assuming Regge behavior between <u>each pair</u> of NVM lines, one obtains

$$\sigma_T \underset{\sim}{\sim} -\frac{2}{m^2}\,\mathrm{Re}\sum_{n=2}^{\infty}\left(\frac{ix}{y}\right)^n y^{n^2} \quad , \tag{5}$$

where $x = g^2/4\pi$, $y = (s/\mu^2)^{\alpha/2}$, $\alpha = \frac{m^2\lambda^2}{32\pi^2}$, and λ and g are couplings of pion to NVM, and NVM to nucleon, respectively.

Two features of this result are worth noting: (a) the i^n factor (unitarity!) providing cancellations between successive real terms, and (b) the rapidly growing s-dependence $(\sim(s^{\alpha})^{\frac{1}{2}n(n-1)})$ which suggests that such cancellations are important. In the spirit of this analysis, (5) is hardly a convergent series, and some prescription must be applied in order to give meaning to the complete σ_T. One such form has been adopted[1] and produces $\sigma_T \sim s^{-\alpha/8}(\ln s)^{-\frac{1}{2}} \to 0$, indicating the possibility of complete cancellation. Regardless of whether σ_T actually vanishes as $s \to \infty$, the basic lesson to be learned from the calculation is simply that one should expect strong cancellations from the Froissart limit. If this model has any truth, once one begins to estimate the $i\chi_n$, one can not stop.

By itself, the n=2 term generates the Froissart bound, a la Cheng and Wu, while contributions of higher n provide cancellations away from that upper limit. In view of the high current interest in this question, better estimates of (5) would be most useful.

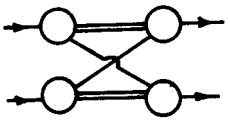
B. Wide-Angle Processes

In contrast to the very complicated forward-scattering situation, it is possible to propose relatively simple models which may be relevant to hadronic scattering at large momentum transfers. There are at least a half-dozen such theories now extant, of which two will be briefly described here. All such models display some variant of scaling, in the form of the predictions

$$\left(\frac{d\sigma_i}{dt}\right) \approx s^{-n_i} F_i(t/s) \qquad (6)$$

which relates $d\sigma/dt$ near 90^o (in the CM, $|t| \sim s/2$) to a power fall off with s and an asymptotic function of angle only; the subscript i denotes a particular scattering process.

The interchange model $(IM)^2$ uses the intuition of atomic rearrangement collisions, generalizing electron exchange to quark or parton exchange in hadronic collisions,

$T_{wA} =$  (7)

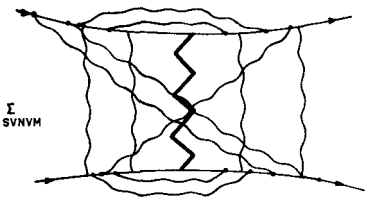
where the non-intersecting (diagonal) lines of (7) correspond to the interchanged quark/partons. Each blob represents a hadron-parton form factor whose large-variable behavior may be inferred from the experimental proton form factor, itself constructed out of the same blobs. Assuming a dipole fit for the proton's form factor, each blob should asymptotically decrease as t^{-2}; and insertion of this information into the integrals corresponding to (7) generates

the form (6) with $n_{pp} = 12$, a number which can be decreased by assuming a less rapid blob fall-off. A single normalization constant completes this two-parameter input model.

Simultaneous predictions, depending upon the sort of quark exchanged, may be made for all wide-angle processes, in particular pp, $\bar{p}p$, $k^{\pm}p$, $\pi^{\pm}p$ elastic, pion and kaon charge exchange and photopion production. Wherever measurements have been made[9] one finds, at least, qualitative agreement with the IM predictions. For example, the ratio $\left(\frac{d\sigma}{dt}\right)_{\bar{p}p} / \left(\frac{d\sigma}{dt}\right)_{pp}$ of the model at 90° and non-asymptotic energies easily reproduces the experimental ratio $\sim 2 \times 10^{-2}$. For wide-angle pp scattering at the highest available energies, the model fits the data over wide ranges of s and t as well as any two-parameter model possibly could. Further refinements have been made, and are in progress now, especially relating to inelastic processes. Clearly, the predictive power of the interchange model is very high, while present comparison with a variety of experimental data is quite favorable.

An alternate view of wide-angle scattering is provided by the hadronic bremsstrahlung model (HBM),[3] with intuition based upon soft-photon physics, in a relativistic generalization of the Schiff wide-angle potential theory scattering approximation. Here, a typical Born approximation which can in principle describe large momentum transfer processes, is modified by the exchange of multiple soft, virtual, neutral, vector mesons (SVNVM) between external hadronic legs of the particular process, thereby providing kinematical (s,t,u dependence) damping of the simple Born approximation,

$T_{WA} = \sum_{SVNVM}$



(8)

There are no infrared divergences here because the NVM are massive; one sums up that portion of every graph which would be infrared divergent were the NVM mass allowed to vanish. The model may be applied to the proton form factor, and to pp scattering, and yields a very simple, two-parameter description of these processes; one parameter sets the overall scale, and the other combines proton-VM coupling g, VM mass μ, and a (covariant!) soft-momentum cut off μ_c into the constant $\gamma \simeq \frac{g^2}{8\pi^2} \ln(1 + \mu_c^2/\mu^2)$. In terms of (6), one finds $n_{pp} = 11.2$, while the angular fit about 90^o is of the same quality as that of the interchange model.

In order to describe the scattering of other hadrons, a statement of their coupling to the exchanged SVNVM must be made; this may be done in the simplest manner by assuming that the NVM is the ω, which couples to the hypercharge current. Predictions then follow which also resemble the existing (non-asymptotic) data, although there are certain specific differences between those of the IM and the HBM (as there must be since SU(3) is violated in the amplitudes constructed by multiple ω exchange only). For example, one finds a strong similarity between KN and NN processes in the HBM, rather than between KN and πN processes of the IM. More asymptotic data, especially for πN reactions, will be needed to distinguish between these models and reality. Inelastic predictions have also been made on the basis of the HBM, some of which should shortly be put to experimental test at NAL.

References

1. R. Blankenbecler and H. M. Fried, SLAC PUB1125, (September 1972). The same physics has been discussed in the ℓ-plane by R. Aviv, R. Sugar and R. Blankenbecler, Phys. Rev. D5, 3252 (1972); and D6, 2216 (1972).
2. J. F. Gunion, S. J. Brodsky and R. Blankenbecler, Phys. Letters 39B, 649 (1972); and SLAC PUB1183 (February 1973).
3. H. M. Fried and T. K. Gaisser, Phys. Rev. 179, 1491 (1969); T. K. Gaisser, Phys. Rev. D2, 1337 (1970); and H. M. Fried, B. Kirby and T. K. Gaisser, Brown PUB274-II.
4. See the Remarks of G. Bellatini, these Proceedings.
5. H. Cheng and T. T. Wu, Phys. Rev. Letters 24, 1456 (1970).
6. S-J Chang and T-M Yan, Phys. Rev. Letters 25, 1586 (1970).
7. For an analysis of simple situations in which this is and is not true, see G. Tiktopoulos and S. Treiman, Phys. Rev. D2, 805 (1970); and E. Eichten and R. Jackiw, Phys. Rev. D4, 439 (1971).
8. M. Lévy and J. Sucher, Phys. Rev. D2, 1716 (1970); H. D. I. Arbarbanel and C. Itzykson, Phys. Rev. Letters 23, 53 (1969).
9. This includes the most recent $K_L^o p \to K_s^o p$, $\bar{K}_p^o \to \pi^+ \Lambda$, $\bar{K}_p^o \to \pi^+ \Sigma^o$ SLAC measurements, kindly communicated by D. Leith.

TRACING PARTONS IN HADRON COLLISIONS

AT HIGH TRANSVERSE MOMENTUM

Francis Halzen
Department of Physics
University of Wisconsin
Madison, Wisconsin 53706

Abstract : We discuss hadron collisions at large transverse momentum. They probe the hadrons at small distances; from this point of view we discuss :

- the phenomenological analysis of two body reactions at large angles (Secs. II and IV) and single particle inclusive reactions at large p_T (Sec.III)
- jets of large transverse momentum hadrons (Sec. IV).

Résumé : Nous discutons les collisions hadroniques à grand moment de transfert, qui constituent une investigation de la structure des hadrons à petite distance. De ce point de vue nous discutons :

- l'analyse phénoménologique des réactions à deux corps à grand angle (Secs. II et IV) et les réactions inclusives à une particule à grand p_T (sec. III).
- les jets hadroniques de grand moment transverse (Sec. IV).





I. INTRODUCTION

Deep inelastic electroproduction experiments reminded high energy physicists of the fact that complex systems often become simple in the impulse approximation. This might also be the case for collisions of hadrons, it is this belief that motivated the recent activity in the study of hadron collisions at high transverse momentum. Let me make this statement more specific. Deep inelastic electroproduction measures the inelastic form factor of the proton (Fig. 1a). The cross section depends on two variables, the energy loss of the electron $\nu=E'-E$ and the momentum transfer q^2 to the proton. For very inelastic collisions at high energies (ν, $q^2 \to \infty$ or the impulse approximation for a theorist) experiments tell us the form factor νW_2 only depends on the ratio

$$\frac{\nu}{q^2} = \frac{1}{2m_i} \qquad (1)$$

where m_i remains small when ν, $q^2 \to \infty$. Eq. (1) of course reminds us of elastic ep scattering where m_i = M (the proton mass) (Fig. 1b). This analogy leads to the picture (Fig. 1c) where we think of the inelastic interaction of the virtual photon

and the proton as a simple point interaction with a proton constituent (a parton or quark) of mass m_i. The parton carries a fraction x of the proton momentum P with

$$\frac{1}{x} = \frac{m_i}{M} \left(= \frac{q^2}{2M\nu}\right) \quad . \qquad (2)$$

The proton inelastic form factor $\nu W_2(x)$ just measures the probability of finding a parton inside the proton with a fraction x of its momentum.

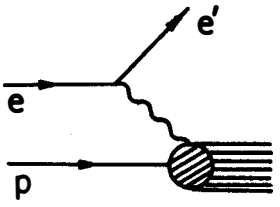


FIG. 1a

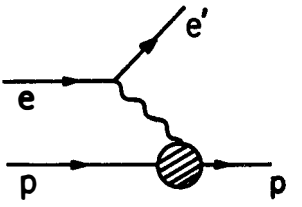


FIG. 1b

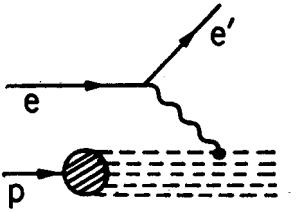


FIG. 1c

The particular simplicity of highly inelastic ($q^2 \to \infty$) high energy ($\nu \to \infty$) collisions is well known in atomic and nuclear physics. As we probe the system (proton) at small distances, we can describe the interaction as going through one of its constituents (partons), moreover we can treat those essentially as free particles (inpulse approximation). Similar and moreover phenomenologically accessible situations exist in purely hadronic interactions:

i) two body or quasi two body interactions at high energy and large angles

$$t, s \to \infty \qquad (3)$$
$$\frac{t}{s} \text{ fixed } (-\frac{t}{s} \sim \sin^2 \frac{\theta}{2})$$

ii) single particle inclusive interactions at large transverse momentum.

$$t, s \to \infty$$
$$x_1 = -\frac{u}{s},\ x_2 = -\frac{t}{s} \text{ fixed} \qquad (4)$$
$$[p_T^2 = s x_1 x_2,\ \frac{x_2}{x_1} = \tan^2 \frac{\theta}{2}] \ .$$

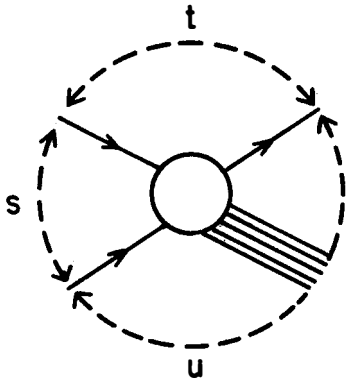


FIG. 2

Our interest in these reactions has to be contrasted with the conventional studies of two body and quasi two body collisions (t << s). They reveal the geometrical structure of hadrons. The partial wave (or impact parameter) distribution indicate that hadrons scatter"at the surface". The typical interaction radius or size of the proton is 1 Fermi and varies slowly with energy (grows as ln s?[1,2]). Production of secondary particles has been extensively analyzed in the region where it shows a sharp cut-off in transverse momentum, limiting the interaction distances again to approximately 1 Fermi.

II. LARGE ANGLE TWO BODY COLLISIONS

We first discuss the simple (but by far the most model dependent!) case of the elastic scattering of high energy protons at large angle ($-t \sim s$). Various approaches[3-8] differ in detail, but are all a simple extension of the Wu-Yang[9] idea to the parton model. A deep inelastic collision of protons is mediated by two partons carrying most of the momentum of the initial protons ($x \simeq 1$). The diagram is depicted in Fig. 3a and is determined by a form factor (Fig. 3b) and the parton-parton scattering amplitude (Fig. 3c). The form factor is, in a parton picture associated with the electromagnetic form factor of the proton,[10] (see Fig. 3b) taken to be a dipole

$$G(t) \sim t^{-2} \quad . \tag{5}$$

In the limit that one neglects all the masses in the problem (M, m_i and possible gluon masses) this picture leads to a simple scaling relation for the differential cross section at large angles

$$d\sigma/dt\ (pp \to pp) \sim s^{-d}\ F(-t/s) \quad . \tag{6}$$

The power d depends on the particular model one uses to estimate the parton-parton interaction. Assuming

that for very inelastic collisions all interactions become unimportant,[3] the interchange of constituents (partons) yields the interaction between the hadrons.

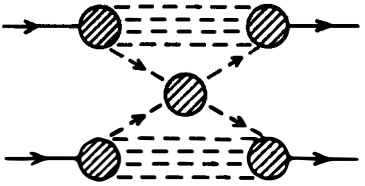


FIG. 3a

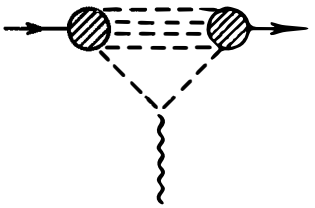


FIG. 3b

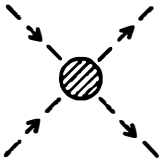


FIG. 3c

The theoretical estimates can be summarized as follows

d = 8 from a current-current contact term[11]

10 from gluon models[5,8] (or dimensional arguments in field theory[12])

12 from parton interchange[3].

Do the large angle pp data support fixed t/s scaling? To test Eq. (6) we notice it predicts a

linear dependence of $\ell n\, d\sigma/dt$ on $\ell n\, s$ at fixed t/s

$$\ell n\, d\sigma/dt = -d\, \ell n\, s + \ell n\, F(-t/s), \quad (7)$$

Eqs. (6), (7) hold in the limit that one can neglect all the masses in the problem. An empirical investigation of (7) at fixed t/s or fixed $\cos\theta$ ($\sim 1 + \frac{2t}{s}$) should therefore be equivalent; for the energy variable we can choose s, p_{lab} or any variable equal to s when one neglects masses. With the available data however the specific choice of scaling variables is unfortunately important. We therefore follow the conventional approach and search for a pair of variables for which the pp data exhibit the linearity of $\ell n\, d\sigma/dt$ versus $\ell n\, s$ of Eq.(7). The specific choice of variables exhibited in Eq. (7) shows scaling behavior for $s \gtrsim 15$ and $-t/s \gtrsim .2$. Fig. 4 represents a sample of the numerous t/s values investigated in our analyses.[5] We conclude from the same plots that

$$d = 10 \pm 0.5 . \quad (8)$$

Binning the data at fixed $\cos\theta$ we get no linear relation corresponding to Eq. (7) and a determination of d is ambiguous.[3,5,13] In view of the importance of the particular choice of scaling variable involved in this comparison it is impossible to make definite

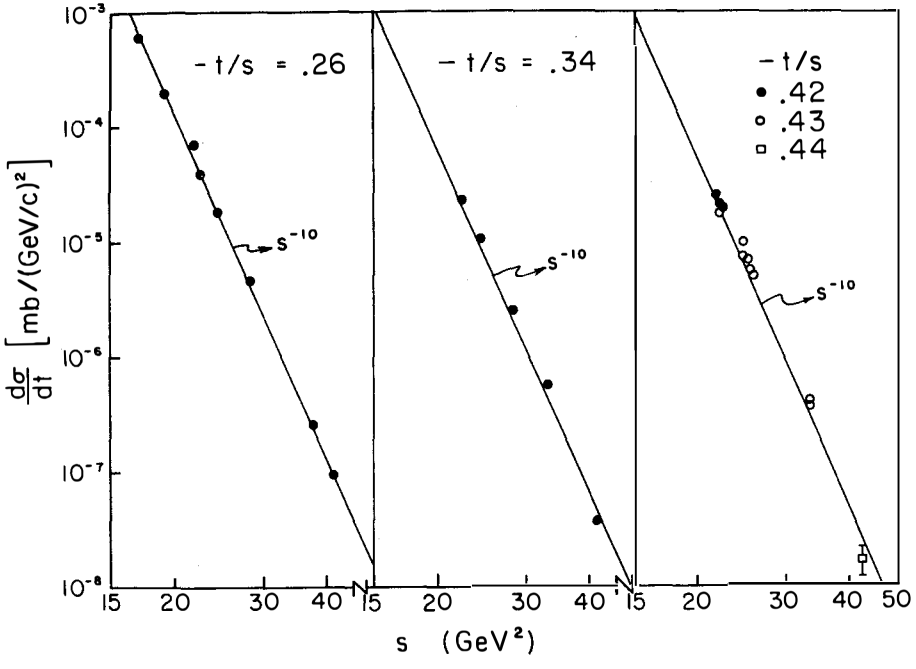

10^{-3}
10^{-4}
10^{-5}
10^{-6}
10^{-7}
10^{-8}
$\frac{d\sigma}{dt}$ [mb/(GeV/c)^2]
-t/s = .26
-t/s = .34
-t/s
• .42
○ .43
□ .44
s^{-10}
s^{-10}
s^{-10}
15 20 30 40
15 20 30 40
15 20 30 40 50
s (GeV^2)

FIG. 4

conclusions about fixed t/s scaling, it would certainly be misleading to judge the merit of different theoretical approaches solely on their specific scaling behavior in elastic scattering.

An interesting aspect of field theory models for large angle scattering is their form factor structure. If field theory is relevant to large angle scattering simple dimensional analysis suggest[12]

$$d\sigma/dt \sim s^{-2-\Sigma_i \Delta_i} \; f(\theta) \qquad (9)$$

with the form factor

$$G_i(t) \sim t^{-\Delta_i} \qquad (10)$$

i sums over the 4 particles in the two body or quasi two body collision. For pp→pp $\Delta_i=2$, assuming the dipole form of Eq. (5). This leads to Eq. (6) with d=10. If we take the π form factor to be a monopole and the photon to be pointlike (no form factor, unlike VMD models), we calculate the entries in the table below:

	d from Eqs.(9),(10)	d from parton interchange	experiment $\theta \simeq 90^o$
pp→pp	10	12	∿10
πp→πp	8	8	∿8 (ref.3)
γp→πn	7	6.5	∿7.3(ref.14)
γp→πΔ	7		∿7.3(ref.15)

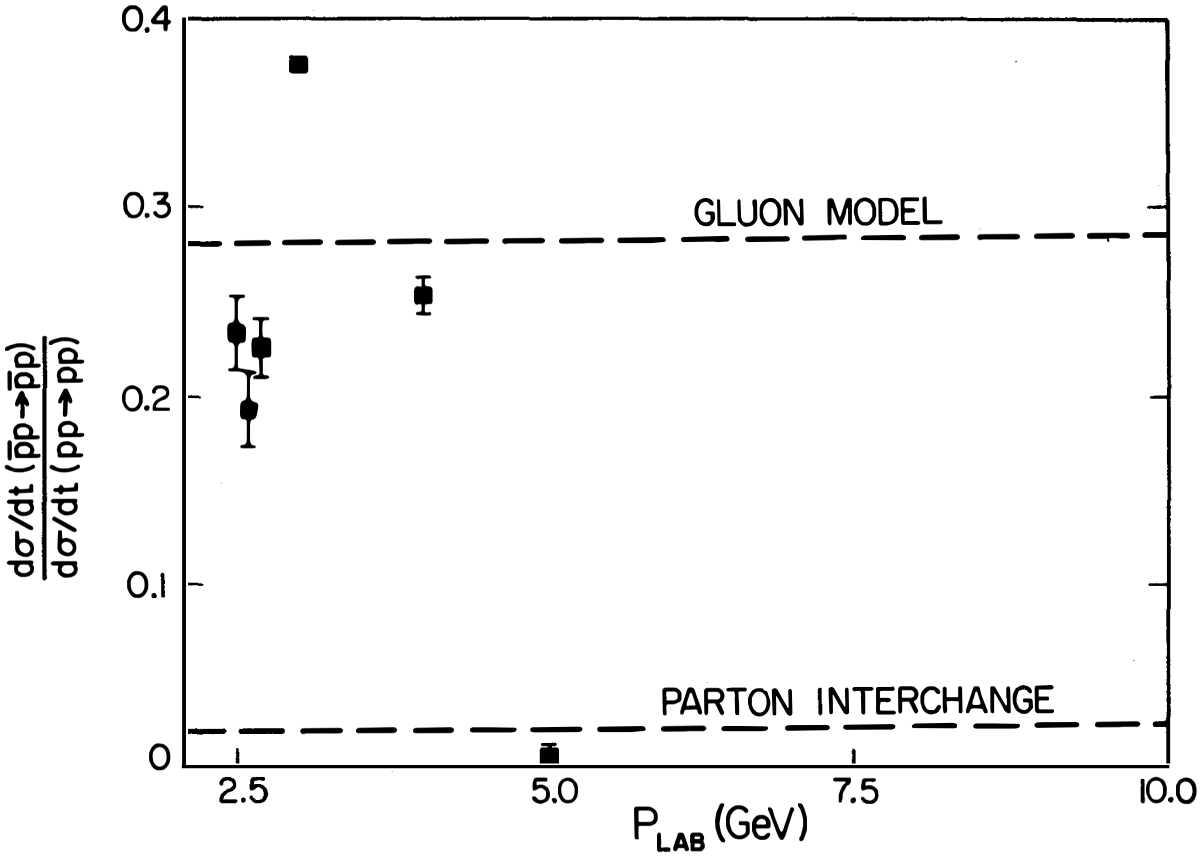

0.4
0.3
0.2
0.1
0
GLUON MODEL
PARTON INTERCHANGE
$\frac{d\sigma/dt\,(\bar{p}p\to\bar{p}p)}{d\sigma/dt\,(pp\to pp)}$
2.5
5.0
7.5
10.0
P_{LAB} (GeV)

FIG. 5

The last relation follows from

$$G_\Delta(t) = G_N(t) \qquad (11)$$

which we obtain from SU(6) or Bloom-Gilman scaling[16] for t large

$$G_\Delta(t) = G_N(t \frac{M_\Delta^2}{M^2}) . \qquad (12)$$

It is also interesting to study at 90^o the ratio

$$R = \frac{d\sigma/dt(\bar{p}p \to \bar{p}p)}{d\sigma/dt(pp \to pp)} . \qquad (13)$$

For naive gluon exchange this ratio is 5/18,[4] this value is however very sensitive to corrections to the single exchange.[8] Interchange models predict $R \simeq 1/50$. The experimental situation[17] is not clear as can be seen from Fig. 5, where we plot R at $\theta = 90^o$ as a function of incident energy.

III. INCLUSIVE INTERACTIONS AT HIGH TRANSVERSE MOMENTA

The recent data from the CERN, Columbia, Rockefeller collaboration[18] provide a striking confirmation of the ideas discussed in the preceding paragraphs. Surface collisions of hadrons lead to a strong cut-off (e^{-6p_T}, experimentally) in the transverse momentum distribution of secondary

particles. The measurements ($pp \to \pi^o$ + "anything" at $\theta = 90^o$) show however high p_T π^o events orders of magnitude above the expected (e^{-6p_T}) yield (see Fig. 6).

The scattering of protons through partons provides a natural way of populating the high p_T region.[5] The diagram can be taken from the work of Berman, Bjorken and Kogut[19] and is shown in Fig. 7.

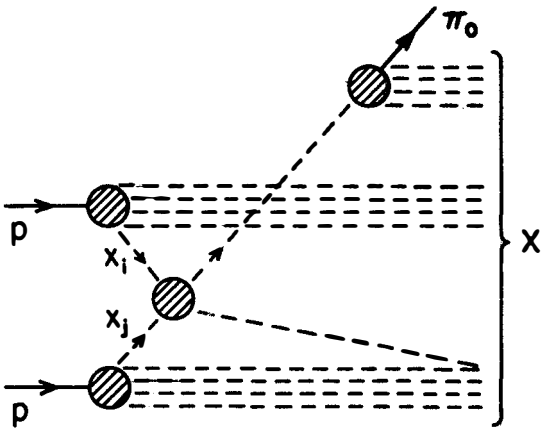


FIG. 7

The total probability of producing a π^o through a parton-parton collision consist of 3 parts (recognizable on Fig. 7)

i) the probability that the initial protons

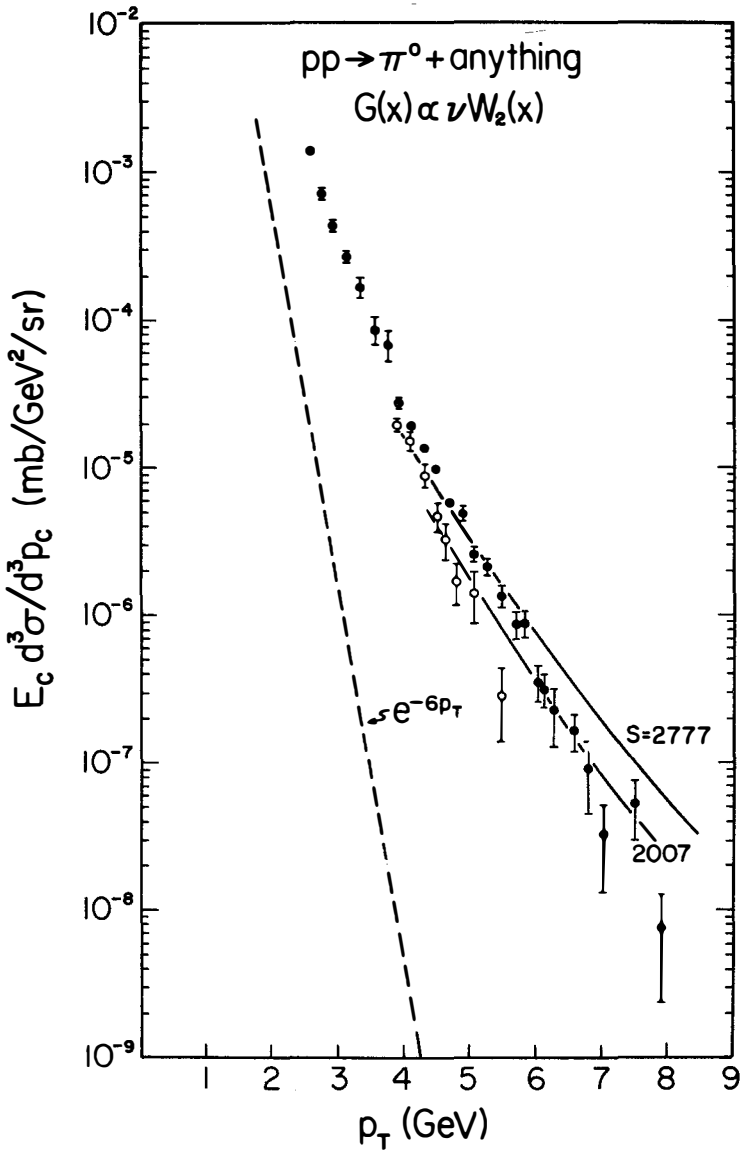

pp→π⁰+anything
G(x)∝νW₂(x)
E_c d³σ/d³p_c (mb/GeV²/sr)
p_T (GeV)
e^{-6p_T}
S=2777
2007

FIG. 6

yield partons with fraction x_i, x_j of the initial momentum. This probability is given by the proton inelastic form factor νW_2.

ii) a strong parton-parton interaction that we can estimate from elastic pp scattering, e.g. gluon model or the exchange of a vector meson; this makes it identical to one photon exchange calculations[19] except for the coupling constant.

iii) the probability that the parton i recombines in a π^o. This is described by a structure function G(x)[19] where x is the fraction of π^o momentum carried by the parton i.

The invariant cross section can be written in the simple form[5,19,20]

$$E\frac{d^3\sigma}{dp^3} \sim \frac{1}{p_T^4} F\left(\frac{p_T}{\sqrt{s}}\right) \qquad (14)$$

The structure function F is given in the appendix. To estimate the effect of diagram 7 we take $G(x) \sim \nu W_2(x)$. The cross section is normalized by the quark (parton) coupling strength $\tilde{\alpha}$ (this is the only parameter) and the result is shown in Fig. 6. It is of course no challenge to get perfect fits through small modifications of G(x).[21] A few qualitative remarks about this model estimate are listed below:

- The fall off in p_T in the parton region "is much slower than for the diffractive" ($e^{-6\ p_T}$) component. We illustrate this in Fig. 7: the p_T dependence at fixed s might be as slow as a power ! (see also ref. 22).

- The invariant cross section rises with energy at fixed p_T. The detailed energy dependence will depend on G(x). For the particular choice of G(x) considered here the parton component of the cross section is smaller than the small p_T peak at the lowest NAL energies. It grows rather fast in s making a break in p_T observable around $p_{lab} \sim 400$ GeV/c (see Fig. 9). The energy dependence slows down at ISR energies (this is seen by comparing Figs. 6 and 9, see also Fig. 10).

- Phenomenological studies of G(x) in reactions of this type open a wealth of applications of the parton model to reactions

$$\gamma N \to \text{hadron} + \text{"anything"}$$
$$e^+e^- \to \text{hadron} + \text{"anything"}$$
$$eN \to \text{hadron} + \text{"anything"}.$$

Conversely one can use these reactions to estimate expected $\pi/K/p$ ratios and particle multiplicities in general in large p_T inclusive reactions.[23]

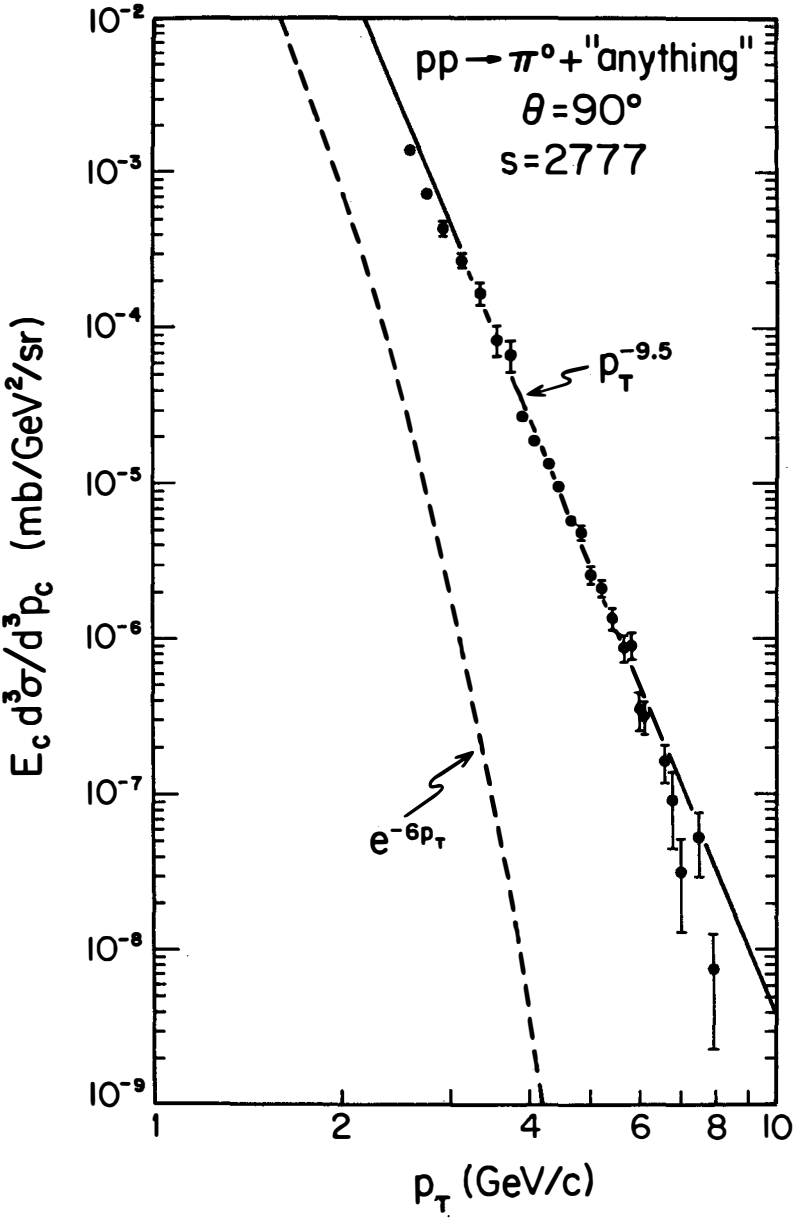

pp → π° + "anything"
θ = 90°
s = 2777
$p_T^{-9.5}$
e^{-6p_T}
$E_c\, d^3\sigma/d^3p_c$ (mb/GeV²/sr)
p_T (GeV/c)
10^{-2}
10^{-3}
10^{-4}
10^{-5}
10^{-6}
10^{-7}
10^{-8}
10^{-9}
1
2
4
6
8
10

FIG. 8

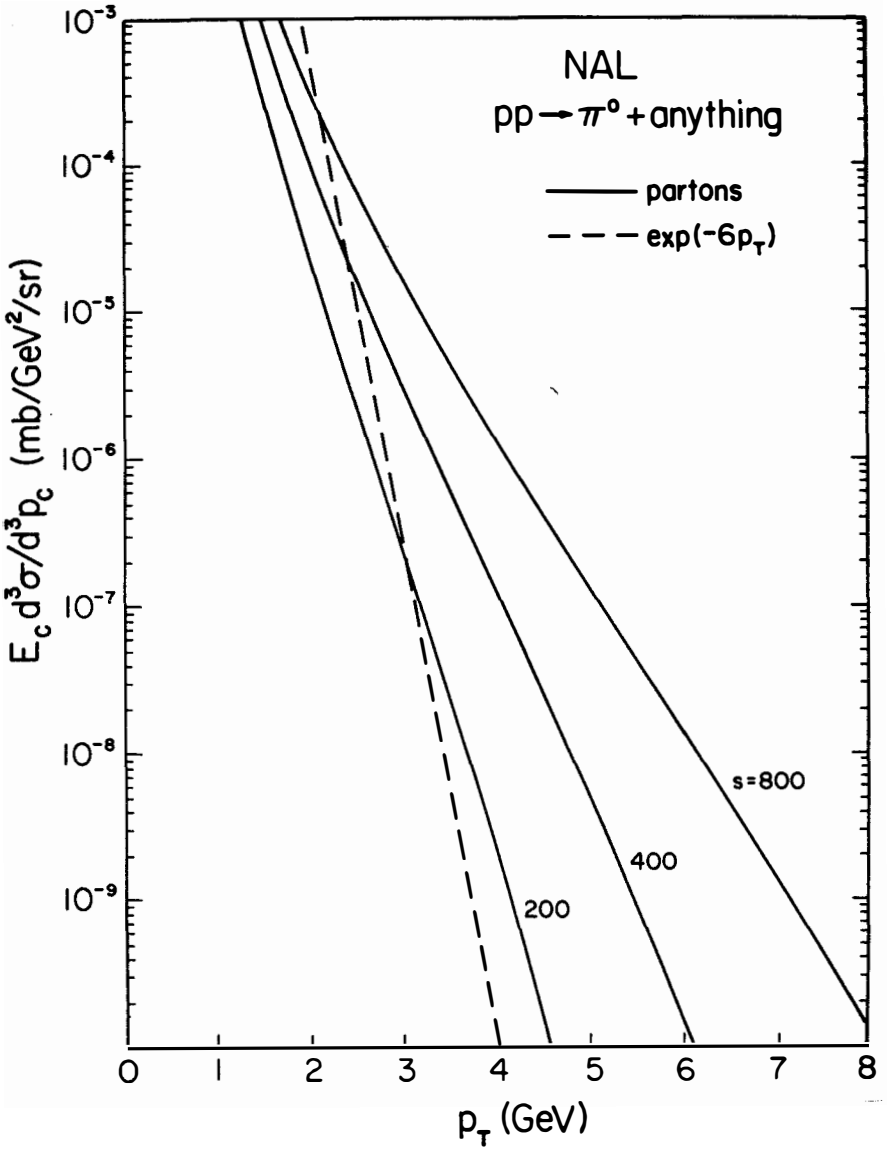

NAL
pp → π° + anything
partons
exp(-6p_T)
s=800
400
200
E_c d³σ/d³p_c (mb/GeV²/sr)
p_T (GeV)
10⁻³
10⁻⁴
10⁻⁵
10⁻⁶
10⁻⁷
10⁻⁸
10⁻⁹
0
1
2
3
4
5
6
7
8

FIG. 9

- In the Cheng Wu model the bare diffractive amplitude is $\frac{s^c}{(\ln s)^{c'}}$ with $c = \frac{11\pi}{32}\tilde{\alpha}^2$. The quark-gluon coupling in above calculation ($\tilde{\alpha} \sim 0.5$) yields $c \sim .25$. This is consistent with the value they obtained from the rising pp total cross sections.[24] Similar[20,25,26] or alternative discussions[1,27] of the ISR $pp \to \pi^o x$ data have been presented.

IV. FINAL REMARKS

It is clear from the previous discussion that one will not gain crucial insight in this approach by quantitative phenomenological discussion of p_T, s dependence. The question of rise in s at fixed p_T and the θ dependence are however very important. If inelastically scattered protons interact through parton constituents there is a well defined probability for producing partons (or quarks) at high transverse momentum. The cross section is estimated using the diagram presented in Fig. 10.

The result can be written in the form[21]

$$\frac{d\sigma}{dp_T} \sim \frac{1}{p_T^3} F_J \left(\frac{p_T}{\sqrt{s}}\right). \qquad (15)$$

The structure function F_J is given in the appendix. The proportionality constant in (15) is determined by the coupling constant $\tilde{\alpha}$ determined in the preceding paragraph. The calculated cross section at

$\theta=90°$ is shown in Fig. 10. It gives rise to a flatter distribution in p_T ($\sim e^{-p_T}$ or p_T^{-6} between $p_T=3\sim10$) than the single particle inclusive, this should make it easier to distringuish from the small p_T exponential. The cross section is definitely observable and its theoretical estimate is less model dependent than anything discussed up to now. (G(x) does not enter!) For skeptics we evaluate just the electromagnetic (one photon exchange) contribution, it is completely determined by $\nu W_2(x)$! The result is shown in Fig. 19; even this "lower limit estimate" leads to observable cross sections!

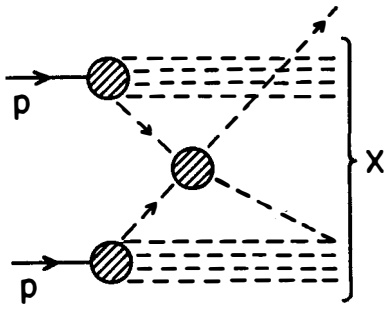


FIG. 10

Only two alternatives are present

i) we see quarks

ii) or the produced quark "dresses" itself and

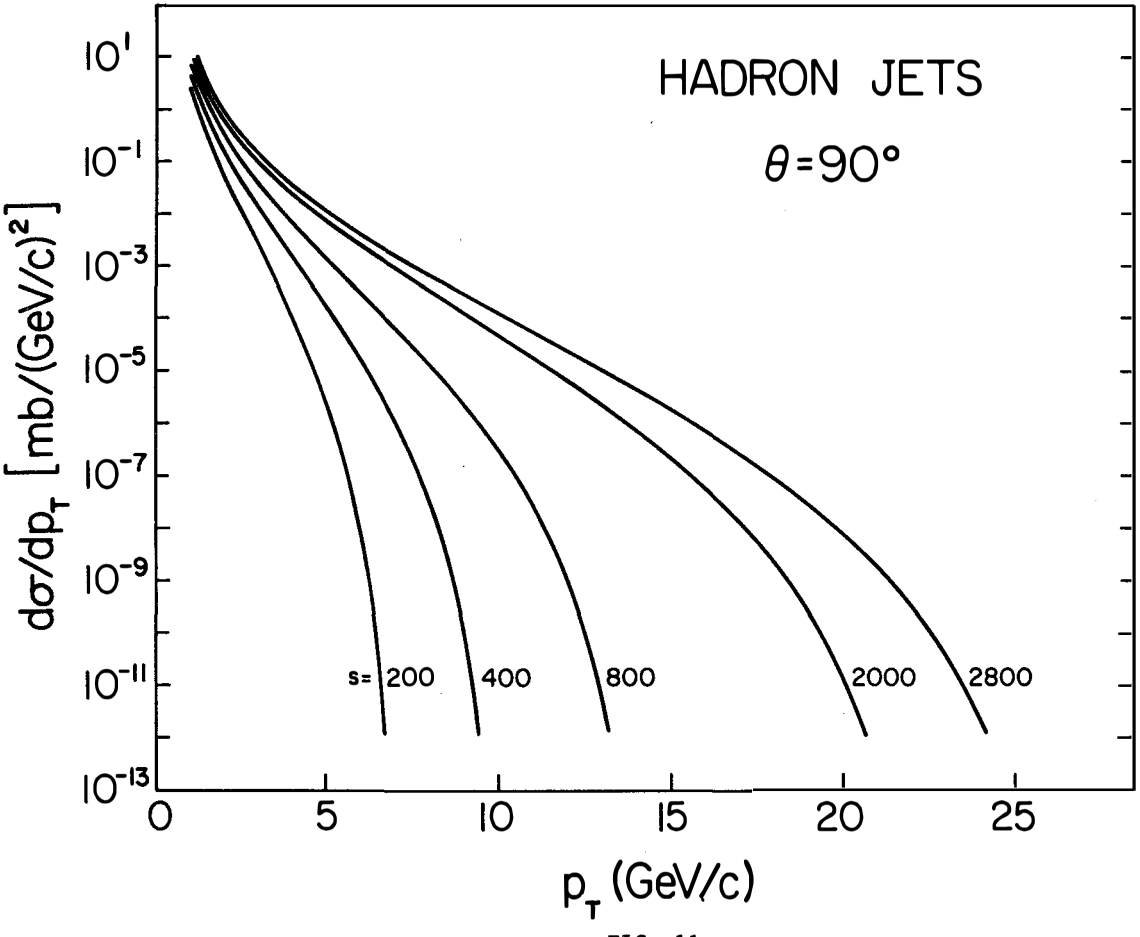

HADRON JETS
θ=90°
$d\sigma/dp_T$ [mb/(GeV/c)^2]
10^{1}
10^{-1}
10^{-3}
10^{-5}
10^{-7}
10^{-9}
10^{-11}
10^{-13}
s= 200
400
800
2000
2800
0
5
10
15
20
25
p_T (GeV/c)

FIG. 11

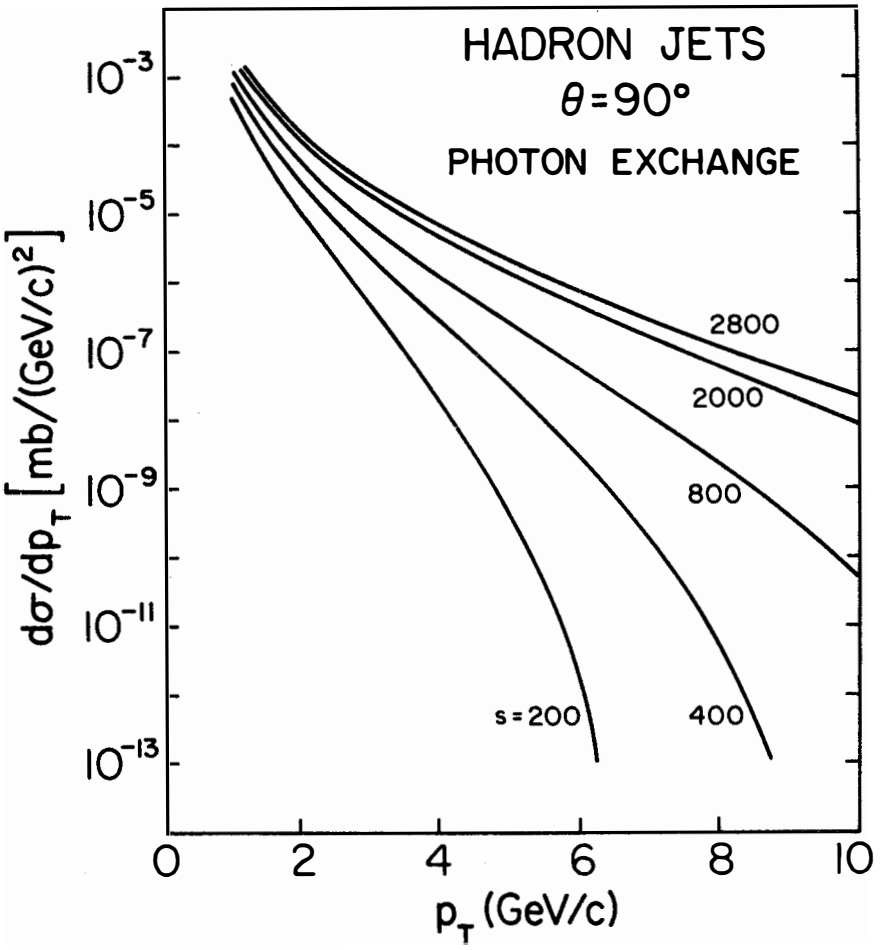

HADRON JETS
θ=90°
PHOTON EXCHANGE
2800
2000
800
400
s=200
10^-3
10^-5
10^-7
10^-9
10^-11
10^-13
dσ/dp_T [mb/(GeV/c)^2]
0
2
4
6
8
10
p_T (GeV/c)

FIG. 12

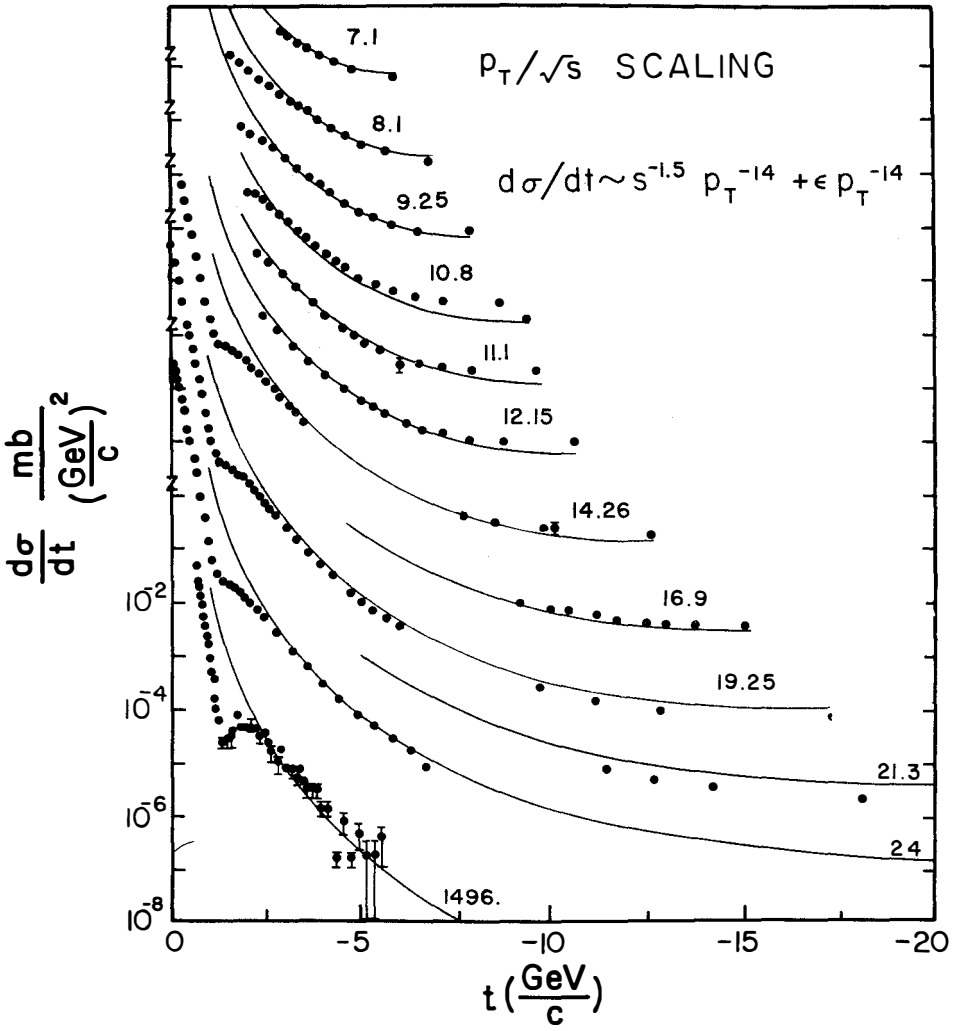

$p_T/\sqrt{s}$ SCALING
$d\sigma/dt \sim s^{-1.5}\ p_T^{-14} + \epsilon\ p_T^{-14}$
7.1
8.1
9.25
10.8
11.1
12.15
14.26
16.9
19.25
21.3
24
1496.
$\frac{d\sigma}{dt}\ \frac{mb}{(\frac{GeV}{c})^2}$
10^{-2}
10^{-4}
10^{-6}
10^{-8}
0
-5
-10
-15
-20
$t\ (\frac{GeV}{c})$

FIG. 13

is seen as a hadron jet[19] (in a small solid angle in the c.m. frame one observes paralelly moving particles with high transverse momentum[19]).

As a closing remark I come back to the scaling relation (9) for elastic scattering. Supplementing it with the phenomenological observation that, $s^2 \frac{d\sigma}{dt}$ is a function of p_T only[28] we obtain

$$d\sigma/dt \sim s^{-2}\, p_T^{-\Sigma_i 2\Delta_i} \,. \qquad (16)$$

This is a scaling relation of the same structure as those obtained for particle production. (see Eqs. (14) and (15)) Fig. 13 illustrates how indeed one can represent all the pp data outside the diffraction peak by only two powers! (For a more detailed discussion see Ref. 7 and 29).

ACKNOWLEDGEMENTS

Many people contributed to this review through comments and discussions: V. Barger, D. Coon, A.Erwin, H. Fried, J. Luthe, R. Prepost, R.J.N. Phillips but especially D. Cline.

APPENDIX

CROSS SECTION FORMULAE

We list the invariant cross sections for single particle inclusive reactions (diagram 7) and the production of hadron jets (diagram 10) at fixed angle θ. The comparison to experimental data (defined usually in kinematic variables s, p_T, θ goes in two steps:

i) transform to the new variables[19] s, x_1, x_2 by

$$x_1 x_2 = \frac{p_T^2}{s} \qquad \text{(A1)}$$

$$\frac{x_2}{x_1} = \tan^2\theta \qquad \text{(A2)}$$

ii) then the cross sections are given by a double integral that one evaluates numerically. We list these below.

Single particle inclusive (pp→c + "anything")

$$E_c \frac{d^3\sigma}{dp_c^3} = \frac{2\tilde{\alpha}^2}{p_T^4} [\, F(x_1,x_2) + F(x_2,x_1)]$$

$$F(x_1,x_2) = \iint_{\xi \leq 1} \frac{dx_i dx_j}{x_i x_j} F(x_i) F(x_j) G(\xi) \left(\frac{x_1}{x_i}\right)^2 \left(1+\frac{x_1^2}{\xi^2 x_i^2}\right)$$

$$\xi = \frac{x_i x_2 + x_j x_1}{x_i x_j}$$

$$F(x) = \frac{1}{6.84} G(x) = \nu W_2(x)$$

$$\tilde{\alpha} = 0.51 \quad \text{gluon exchange}$$

$$= 1/137 \quad \text{one photon exchange}$$

jet of high p_T hadrons produced by a quark or parton in a deep inelastic pp collision:

$$\frac{d\sigma}{dp_T} = \frac{\pi\tilde{\alpha}^2}{p_T^3} [F_J(x_1,x_2) + F_J(x_2,x_1)]$$

$$F_J(x_1,x_2) = \int_{\lambda^2}^{} \int_{\frac{\lambda^2}{x_i}}^{} dx_i dx_j F(x_i) \frac{[x_j - \frac{\lambda^2}{x_i}]^{1/2}}{x_i^3 x_j^{5/2}}$$

$$\cdot [\frac{5}{2x_j} F(x_j) N - NF'(x_j) - N'F(x_j)]$$

$$\lambda = \frac{2p_T}{\sqrt{s}}$$

$$N \equiv N(x_i,x_j,\lambda) = 16 x_i^2 x_j^2 - 12 x_i x_j \lambda^2 + \lambda^4$$

F', N' refer to derivatives $\frac{\partial}{\partial x_j}$.

REFERENCES

1. S.R. Amendolia et al., Phys.Letters (to be published) (1973).
2. U. Amaldi et al., CERN preprint (1973).
3. R. Blankenbecler, S.J. Brodsky and J.F. Gunion, Phys.Letters 39B, 649 (1972); Phys.Rev. D6, 2652 (1972), SLAC-Pub-1140 (1972), SLAC-Pub-1183 (1973).
4. D. Horn and M. Moshe, Nucl. Phys. B48, 557 (1972); CALT-68-382 (1973).
5. D. Cline, F. Halzen and M. Waldrop, Nucl.Phys.B (to be published) (1972).
6. H.W. Fried and T.K. Gaisser, Phys. Rev. 179, 1491 (1969).
7. P.V. Landshoff and J.C. Polkinghorne, DAMTP 73/4 (1973).
8. H.W. Fried (this volume); T.K. Gaisser, Phys.Rev. D2, 1337 (1970).
9. T.T. Wu and C.N. Yang, Phys. Rev. 137, B708 (1965).
10. R.P. Feynmann, Photon-Hadron Interactions, W.A. Benjamin, Inc., Reading, Massachusetts (1972).
11. H.D.I. Abarbanel, S.D. Drell and F.J. Gilman, Phys.Rev. 177, 2458 (1969).
12. W.R. Theis, Phys.Letters 42B, 246 (1972).
13. V.Barger, F. Halzen and J. Luthe, Phys. Letters 42B, 428 (1972).

14. R.L. Anderson et al., Phys. Rev. Letters 30, 627 (1973).

15. R. Prepost (private communication).

16. E. D. Bloom and F.J. Gilman, Phys. Rev. Letters 25, 1140 (1970).

17. C. W. Akerlof, et al., Phys. Rev. 159, 1138 (1967); J.V. Allaby, et al., CERN preprint (8/72); J.V. Allaby, et al., Vienna Conference (1968); C.M. Ankerbrandt, et al., Phys. Rev. 170, 1223 (1968); G. Cocconi, et al., Phys. Rev. 138, B165 (1965); K.J. Foley, et al., Phys. Rev. Letters 11, 425 (1963); J. Ginestet, et al., N.P.B. 13, 283 (1969); C. Rubbia (Paper submitted to NAL Conference), New ISR (9/72 and 1/73); E.J. Sacharidis, et al., RHEL/R186 (1970); M.G. Albrow, et al., Nucl. Phys. 37B, 349 (1972); W.F. Baker et al., Nucl. Phys. 12B, 5 (1969); V. Chabaud et al., Phys. Letters 38B, 449 (1972); O. Czyzewski et al., Phys. Letters 15B, 188 (1965); C. Daum et al., Nucl. Phys. 6B, 617 (1968); V. Domingo et al., Phys. Letters 24B, 642 (1967).

18. CERN-Columbia-Rockefeller Collaboration, contribution to the NAL-Chicago conference (1972). R. Cool (private communication).

19. S.M. Berman, J.D. Bjorken and J.B. Kogut, Phys. Rev. D4, 3388 (1971).
20. P.V. Landshoff and J.C. Polkinghorne, DAMTP 72148 (1972).
21. F. Halzen and J. Luthe (in preparation).
22. British-Scandinavian collaboration, contribution to the Vanderbilt conference (1973).
23. M. Kisslinger (private communication).
24. H. Cheng, J.K. Walker and T.T. Wu, NAL preprint (1973); J. K. Walker (this volume).
25. G. Domokos, S. Kövesi-Domokos and B.C. Yunn, Johns Hopkins preprint COO-3285-5 (1973).
26. J. Dias de Deus (this volume).
27. D. Amati, L. Caneschi and M. Testa, CERN preprint TH 1579 (1972).
28. J. Orear, Phys. Letters 13B, 190 (1964). S.S. Pinsky and J.S. Ball, Phys. Rev. Letters 27, 1820 (1971).
29. V. Barger, F. Halzen and R.J.N. Phillips (to be published).



DIFFRACTION PHENOMENA:

REVIEW OF THE EXPERIMENTAL SITUATION

David W. G. S. Leith
Stanford Linear Accelerator Center, Stanford University
Stanford, California 94305 (USA)

Introduction:

This talk is intended to be a general introduction to what we believe we know about the diffraction phenomena and, by inference, the Pomeron. The phenomena is important in many fields of physics and appears to be well understood in optics and nuclear physics experiments. An example is given in Fig. 1, where the angular distribution for α-particle scattering on Fe^{58} at 64 MeV is shown, in which the Rutherford scattering contribution has been divided out from the measured cross section.[1] The data show a clear and impressive series of diffraction maxima and minima. In high energy particle physics diffraction is also an important phenomena, accounting for ~ 30% of the total cross section, but it is not well understood. We describe diffraction in terms of two pictures -- one a geometrical model in which we discuss the scattering of particles on an absorbing disc of a given size and with a given opacity

(sometimes with edge effects taken into account) and the other a t-channel dynamical picture where we talk of particle exchange between the incident particle and the target particle (viz. Regge theory and its modifications). The exchanged particle in the case of diffraction processes is called the Pomeron. In Regge theory the energy dependence of the cross section is controlled by the trajectory properties of the exchanged particle

$$\sigma(S) \propto S^{\alpha(0)-1}.$$

Thus the flat total cross sections expected from a diffractive process are accounted for by the exchange of Pomeron with a trajectory given by

$$\alpha(0) = 1.$$

The Pomeron has quite an unusual role in particle physics, in that

-- no other pole has a trajectory with $\alpha(0)=1$;

-- there is no known particle to be associated with this trajectory, (i.e. unusual behaviour of the trajectory for $t > 0$);

-- the behaviour of the trajectory for $t < 0$, as seen in the shrinkage of the differential cross section,

$$\frac{d\sigma}{dt}(s,t) \propto S^{2\alpha(t)-2}$$

is quite different from other trajectories. The Pomeron trajectory has a rather flat t-dependence, $\alpha(t) = 1+\alpha' t$ with $0 < \alpha' < \cdot 4$ GeV^2 while other known trajectories have $\alpha' \sim 1$ GeV^2;

-- the particle behaves in scattering processes as though it carried the quantum numbers of the vacuum, whereas it behaves with respect to cross sections like a particle with spin 1.

The processes from which we learn about diffraction and the properties of the Pomeron are

(a) $A + B \to A + B$ -- the elastic scattering reaction, which is related to the total cross section through the optical theorem;

(b) $\left.\begin{matrix} A + B \to A^* + B \\ A + B^* \end{matrix}\right\}$ - inelastic scattering, in which the projectile or target is excited -- diffraction dissociation. This process was discussed by Good and Walker[2] in analogy to optical diffraction by an opaque disc. They predicted that such processes would occur, that they would proceed coherently in nucleii, and that the scattering properties would be very similar to those of the elastic reaction.

(c) $\left.\begin{matrix} A + B \to A + X \\ X + B \end{matrix}\right\}$ - inelastic, inclusive scattering. This process becomes of considerable interest at high energies.

Unfortunately, we do not have a good description of the diffraction process in particle physics, or of the Pomeron. Basically what we do have is a set of rules that allow us to identify what we mean by diffractive reaction or Pomeron exchange processes.

These rules are listed below.

-- energy independent cross sections (to factors of log S)

-- sharp forward peak in $d\sigma/dt$

-- particle cross sections equal to anti-particle cross sections

-- factorization

-- mainly imaginary amplitude

-- exchange processes characterized by the quantum numbers of the vacuum in the t-channel (i.e. I = 0, C = +1). Also, the change in parity in the scattering process follows the natural spin-parity series $(-1)^J$, or

$$P_f = P_i \cdot (-1)^{\Delta J},$$ where ΔJ is spin change.

-- the spin structure in the scattering is s-channel helicity conserving, (SCHC).

We will proceed to examine how well these rules are obeyed.

Cross Sections:

The energy dependence of total cross sections have been described in terms of two components -- a diffractive component associated with the exchange of a Pomeron, and a second component due to the exchange of other Regge trajectories. The Pomeron term gave rise to a flat contribution to the cross section, while the Regge part fell like a power of the energy. These ideas worked well for the data up to about 25 GeV/c, but do not work so well for the new data covering energies up to 70 GeV from Serpukov.

In Fig. 2 the total cross sections for $\bar{p}p$, pp, $\pi^{\pm}p$ and $K^{\pm}p$ are shown from a few GeV up through the Serpukov energy region. The data[3] may be summarized as follows:

-- $\pi^{\pm}p$, $K^{-}p$, $K^{-}n$, pp, pn total cross sections seem to have reached a plateau with little or no energy dependence;

-- $\bar{p}p$ and $\bar{p}n$ total cross sections are decreasing;

-- $K^{+}p$, $K^{+}n$ are increasing with energy in the region from 20 to 60 GeV/c;

-- the difference between Xp and $\bar{X}p$ is decreasing with energy and fits[4]

$$\Delta\sigma \propto A p_{lab}^{-n}$$

where n is given in Table 1;

-- Λp, Λn total cross sections are flat in the region (6-21) GeV/c;

-- γp, γn total cross sections have been measured up to 30 GeV. The S-dependence is very similar to that of

πN scattering. They find

$$\sigma(\gamma p) = A + Bp^{-1/2} = (97.4 \pm 1.9) + (55 \pm 5)_f E^{-1/2} + (12 \pm 2.5)_{A_2} E^{-1/2}$$

where the determination of the isoscalar (f) and isovector contributions come from comparison of the γp and γn rates;

-- The Okun-Pomeranchuk theorem, which states that the cross-sections of particles belonging to the same isospin multiplet should become equal as the energy goes to infinity, seems to be close to satisfied.

-- The Pomeranchuk theorem, which states that particle and anti-particle cross sections should be the same at asymptotic energies, seems also to be becoming satisfied. The difference in cross sections are falling as a power of the energy (see Table I) and should soon approach zero.

The situation for the pp total cross section has changed over the last few months in a very exciting way. The preliminary ISR data, and the NAL bubble chamber cross section measurements presented at Batavia[3] had large statistical and systematic errors and were quite consistent with a flat pp total cross section of 38 mb extrapolated up from the Serpukov energy region. There were, however, some indications from cosmic ray studies that the pp cross section increased at high energies, maybe even in the ISR energy region.[5]

New data from two ISR groups now show good evidence for such a rising pp total cross section, see Fig. 3. The measurements come from two very different techniques; the Bellettini group[6] measure the total cross section by counting the secondary products while the Cocconi group[7] find the total cross section by measuring the forward elastic cross section and applying the optical theorem. They measure the real part of the pp scattering amplitude at several energies to show that it is small at these energies and that its effects are negligible.

Both experiments rely heavily on measurement of the luminosity of the ISR (i.e. the number of colliding protons in the two rings per unit area). Great care has been taken in arriving at estimates of the luminosity and several different techniques for measuring it employed. Some agreement between the different methods seems to be obtained and the luminosity is claimed to be known to ~ 1-2%.

The results of the experiments agree well and show ~ 4 mb increase in the p-p cross section between (300 and 1500) GeV/c equivalent lab momentum. This observation raises many interesting questions; for example, how should we now think of asymptopia? Will the total cross section continue to rise indefinitely or will it approach an asymptotically flat cross section from below? Is the rise due to an expanding radius of the proton as the energy increases or is it due to some negative interference effect whose magnitude decreases with energy? What sets the scale for the onset of the increase; i.e. K^+p starts increasing around 20 GeV/c, p-p at

200 GeV/c -- when do $\pi^{\pm}p$, $K^{-}p$ and γp start increasing? Whatever the answers to these questions may be, and it will be a long time before we know them all, one thing is clear -- the model of a simple pole (the Pomeron) describing the high energy scattering behaviour is not going to work.

One amusing thought comes to mind -- after all these years of worrying about the $\bar{p}p$ total cross section falling with increasing energy, to meet the pp value to satisfy the Pomeranchuk theorem, we now see that it will have to turn around and also start increasing in order to catch up (or keep up) with the high energy pp cross section.

Further data on the energy dependence of cross sections for processes expected to be dominated by the diffraction phenomena are shown in Figs. 4 and 5, where the pp,[8] and $\pi^{-}p$, $K^{-}p$, and $\bar{p}p$[9] elastic cross sections are, respectively, plotted versus laboratory momentum. The characteristic flattening of the cross section as the energy increases is observed in each case. The momentum dependence of several total and elastic cross sections is given in Table 2.

The ratio of elastic to the total cross section, σ_{el}/σ_{tot}, is of interest under the assumption that we are dealing with diffraction and a geometrical picture. We have

$$\frac{\sigma_{el}}{\sigma_T} = \frac{\sigma_T^2}{\sigma_T \cdot b} = \frac{\sigma_T}{b} \propto \frac{(\text{Radius})^2}{(\text{Radius})^2} = \text{constant.}$$

i.e. at high energy one expects this ratio to be constant, and the same for particle and anti particle. Table 3 summarises data on particle-anti particle cross section ratios. It is rather incon-

clusive due to the lack of data at high energy. The one system where good data is available is for p-p scattering. Fig. 6 shows the ratio σ_{el}/σ_{tot}, for pp scattering from (1-2000) GeV/c, and demonstrates that for $p_{lab} \gtrsim 60$ GeV/c the ratio is indeed constant. This is specially interesting in the (200-1500) GeV/c region where the total cross section rises by ~ 10%; the elastic cross section increases by the same amount and the ratio stays flat.

Another interesting property of elastic scattering cross section is summarized in Table 4, where the ratios of particle to anti particle cross section are listed. It is surprising the extent to which the equality seems to be preserved, even at energies where one knows that Regge exchange process contributes substantially and therefore the process cannot be all Pomeron exchange.

Differential Cross Sections:

Let us now consider how well the "rules" and data on differential cross sections agree. The most interesting data comes from ISR studies of p-p scattering by the Rubbia group. An example of their data[10] is shown in Fig. 7. With high statistics and a precision wire spark chamber spectrometer they have studied elastic p-p scattering from (150-1500) GeV/c equivalent lab momentum.

The angular distribution is sharply forward peaked, but the data clearly show a change in the slope of the differential cross section at small t, in fact the break occurs around t = 0.13 GeV^2. The cross section is not well fit by a single exponential slope,

but fairly well described by two exponentials, e^{-at}, where $a = 12.8\ \text{GeV}^{-2}$ for $0.01 \leq t \leq 0.12\ \text{GeV}^2$, and $a = 10.8\ \text{GeV}^{-2}$ for $0.15 \leq t \leq 0.5\ \text{GeV}^2$. These observations help explain the inconsistencies between older measurements of the slope in p-p scattering cross sections made at lower energy and in different t ranges. It should be noted that this description of the data, in terms of two exponentials, is not unique and that perhaps a more continuous description would be preferable.

The overall picture of the s-dependence of the slope, b, is shown in Fig. 8.[11] The data have been fit to an exponential in two t ranges, $t < 0.1\ \text{GeV}^2$ and $0.15 < t < 0.5\ \text{GeV}^2$, from 1 GeV/c through the ISR range, (~ 2000 GeV/c equivalent lab momentum). The Serpukov data have been lowered by $\Delta b \sim 0.4\ \text{GeV}^{-2}$, which is within their quoted systematic error, and the whole data set above 30 GeV/c fit to

$$b(s,t) = b_o(t) + 2\alpha(t)\ \ell n\ \frac{s}{s_o}\ .$$

The fits are quite good and result in the following parameters:

low t region: $b_o = (7.0 \pm 1.2)$, $\alpha = (0.37 \pm 0.08)$

high t region: $b_o = (9.2 \pm 0.94)$, $\alpha = (0.10 \pm 0.06)$.

In other words, the cross section is made up of a forward region which exhibits substantial shrinkage, and a larger t region which is essentially constant in t.

As an example of other elastic data, $\pi^- p$, $K^- p$ and $\bar{p}p$ scattering cross sections at 25 and 40 GeV/c are shown in Fig. 9.[9] These data show sharp forward peaks, and when fit over the whole t

range measured, (i.e. $0.1 < t < 0.6$ GeV^2), require quadratic terms in t, (e.g. $d\sigma/dt \propto e^{at + bt^2}$).

A summary of the s-dependence of the slope for elastic scattering, as measured at $t \sim 0.2$ GeV^2, is shown in Fig. 10.[11,12] The slopes for particle and for antiparticle scattering seem to become equal at high energies with asymptotic slopes of ~ 8 GeV^{-2} for πN, $\sim 7\text{-}1/2$ GeV^{-2} for KN and ~ 11 GeV^{-2} for NN scattering. The $\pi^- p$ and $K^- p$ data show almost no shrinkage (i.e. no s-dependence of the slope), while the $\bar{p}p$ data show considerable antishrinkage up through the Serpukov region. The $K^+ p$ and p-p data show considerable shrinkage, while the $\pi^+ p$ data also shows shrinkage but much less.

Inelastic Processes; Cross sections

While we are dealing with elastic cross sections, let us consider the same information for the diffractive inelastic processes. A more complete review of this data may be found in the Batavia Conference proceedings.[13] For this discussion we will not try to answer the question of whether these inelastic processes are kinematic in origin or are dominated by resonance production, but merely observe that production of the "A_1 Region" by π's, the "Q Region" by K's and excited N*'s by N's are well defined, clearly identifiable reactions dominated by a single well defined spin-parity state.

The cross sections for these processes are quite flat as a function of energy, characteristic of diffractive processes.

For example, Fig. 11 shows the cross section for the reaction $K_L^o p \to Q^o p$ as a function of energy from (1-1/2 - 12) GeV/c from the SLAC $K^o p$ HBC experiment.[14] The energy dependence of the Q^o production cross section is found to fall as $p_{lab}^{-0.59}$. Table 5 summarizes the information for other inelastic processes and compares them to the elastic data. The inelastic processes seem to fall off a little faster than the corresponding elastic reaction, but it is not clear whether this difference is important or whether it is due to the technical difficulty of determining an "A cross section" or a "Q cross section" above the backgrounds. However, it is clear that these inelastic diffractive processes are much more like the elastic reactions than the typical Regge exchange processes where cross sections fall like $p^{-1.5}$, or faster.

These inelastic reactions also have the property that particle and antiparticle cross sections are equal. We find that:

-- the ratio of $K^o \to Q^o$ to $\overline{K}^o \to \overline{Q}^o$ in the momentum interval (4-12) GeV/c is 0.98 ± 0.08[14]

-- the ratio of $\pi^{\pm} \to A_1^{\pm}$ at 15 GeV/c is 1.00 ± 0.07,[15] 0.94 ± 0.12.[16]

The angular distributions are also sharply peaked in the forward direction with slopes comparable to, but slightly steeper than, the elastic reaction. Whether the 1-2 unit difference between elastic and related inelastic slopes is real and significant or whether it is merely a background problem will not be discussed. What is clear, is that the slopes are comparable to, and that they observe the same relationships between processes as the elastic

reactions (e.g. the slope for $\pi p \to Ap$ is greater than $Kp \to Qp$ which is less than $\bar{K}p \to \bar{Q}p$ just as $\pi p \to \pi p$ is to $Kp \to Kp$, is to $\bar{K}p \to \bar{K}p$). Data on the slope of various inelastic reaction cross sections is summarized in Table 6.

Finally, the inelastic reactions also exhibit the crossover phenomenon in the differential cross sections. The elastic process which is dominated by Pomeron exchange does, however, have some Regge exchange contribution. This additional contribution gives rise to different slopes in the cross section for particle and for antiparticle scattering. An example of this phenomena is shown in Fig. 12, where preliminary 13 GeV/c cross sections for K^+p and K^-p elastic scattering from the SLAC wire spark chamber spectrometer experiment[17] are displayed. A clear cross-over of the differential cross sections is seen for momentum transfers ~ 0.15-0.2 GeV^2. Similar behaviour is observed in $K^0p \to Q^0p$ and $\bar{K}^0p \to \bar{Q}^0p$[14] as seen in Fig. 13. The slope for the strangeness +1 and -1 processes are very similar and the crossover occurs in about the same place.

It is interesting to see how similar the elastic and inelastic (diffractive dissociation) processes are with respect to total cross section and differential cross section behaviour.

Two puzzles:

Although much of the data on angular distributions for elastic and for inelastic processes discussed above agrees well with our list of "rules", and our prejudice for diffractive reactions, there are two outstanding puzzles. (a) If all elastic

scattering reactions are dominated by Pomeron exchange why is the behaviour of the slope of the forward peak as a function of energy so different for different particles -- why does K^+p and pp shrink strongly, π^+p weakly, π^-p and K^-p essentially flat, and $\bar{p}p$ anti-shrink?

This question has been answered for the $\pi^{\pm}p$ system in a very nice analysis by Davier,[18] and for $\gamma p \to \rho^o p$ by Chadwick, Eisenberg, and Kogan.[19] In both analyses the Dual Absorption Model was applied assuming that only the Pomeron and the f^o meson contributed to the iso-scalar t-channel amplitude. The Pomeron was parameterized as a central collision process while the f^o was given a Regge energy dependence and assumed to be peripheral. The data was well fit with this amplitude and the resulting Pomeron contributions showed substantial shrinkage, in good agreement with the K^+p data.

Fig. 14 shows the K^+p slope as a function of energy as the shaded band, and the data points are the Pomeron contribution to $\pi^{\pm}p$ elastic scattering from Davier's analysis. It is interesting to see how well they agree.

Fig. 15 shows the angular distribution of $\gamma p \to \rho p$ at several energies and the fit using the above description. Also shown is the energy dependence of the slope of the Pomeron contribution to this process. Again this agrees well with the Pomeron in πN collisions as derived by Davier and with the K^+p data. It is interesting that the πN and γN data which show practically no shrinkage actually contain a Pomeron contribution which is shrinking

just like the K^+p case.

Thus we see that small admixtures of a non-diffractive amplitude may markedly change the energy dependence of the differential cross section, and that in the two cases studied in detail, the data proved to be consistent with the "same Pomeron" in all the diffractive amplitudes.

(b) We can call this the "ϕ-meson puzzle." The photoproduction of ϕ-mesons is supposed to be our best "laboratory" for studying the properties of diffraction. The ϕ-meson does not couple to hadrons and so the only contribution to the t-channel exchange should be the Pomeron. Therefore, in an unambiguous way we hope to learn of the Pomeron from the reaction $\gamma p \rightarrow \phi p$.

The cross section for this process is shown in Fig. 16, and is flat beyond threshold, or perhaps rises a little.[13] Examples of measurements of the differential cross section are given in Fig. 17[13] and the energy dependence of the slope of the forward peak is given in Fig. 18. The data is consistent with either no shrinkage on one hand, or quite considerable shrinkage if pushed to the other extreme. The Ritson group attempted to settle this question by measuring the s-dependence of the cross section at a particular t-value, $t=0.6$ GeV^2.[20] The results are shown in Fig. 19. If the shrinkage of the differential cross section is analyzed in terms of

$$\alpha(t) = \alpha(0) + \alpha' t$$

their data give $\alpha' = (-0.03 \pm 0.13)$.

This flat energy dependence is just not what we expect for the Pomeron, or at least not what we have learned from K^+p and p-p elastic scattering. One may worry about the large t value at which these measurements were made, and that the amplitude would no longer be diffraction dominated so far from the forward direction. However, in p-p scattering at similar energies quite strong shrinkage is observed at these t-values -- see Fig. 20. So we have a puzzle; what is going on in $\gamma p \to \phi p$?

We do know that the process is diffractive, in that it is almost completely natural parity exchange and that it proceeds coherently on nucleii -

(a) The Ritson group at SLAC have measured the asymmetry parameter in ϕ photoproduction with polarized photons; $\Sigma = \frac{\sigma_{\parallel} - \sigma_{\perp}}{\sigma_{\parallel} + \sigma_{\perp}}$ (with polarization $\parallel$ ($\perp$) to the decay plane of the ϕ). The experiment was performed using a diamond crystal to polarize the photon beam and by detecting both the recoil proton and the K^+K^- decay of the ϕ-meson. They found that $\Sigma = 0.985 \pm 0.12$ at 8 GeV and at $t = 0.2$ GeV^2 which is consistent with complete natural parity exchange.

(b) The above observations are supported by SLAC-Berkeley-Tufts back-scattered laser experiment. They have studied ϕ-photoproduction in the bubble chamber using the polarized photon beam and find that the decay density matrix elements and measured asymmetry at 4.8 and 9.3 GeV are consistent with pure natural parity exchange.

(c) The DESY/MIT group have studied ϕ-photoproduction from a carbon target at around 7 GeV.[24] They observed copious coherent production of the ϕ, and analysis of the decay distribution is again consistent with natural parity exchange.

However, there is one piece of evidence that although the forward $\gamma p \to \phi p$ process may be dominantly natural parity, it may not be purely imaginary as would have been expected for pure Pomeron exchange. The DESY/MIT group have measured the real part of the $\gamma p \to \phi p$ process by observing the interference between the resonant ϕ production and the Bethe-Hietler process in $\gamma C \to \phi C$, with $\phi \to e^+e^-$ at 7 GeV.[25] They report that the ϕ amplitude differs from being purely imaginary by $25^\circ \pm 15^\circ$ or, in other terms, $\left(\frac{\mathrm{ReA}_\phi}{\mathrm{ImA}_\phi}\right) = (-0.48 \pm {}^{.33}_{.45})$. This may be an indication that the $\gamma \to \phi$ process is not purely due to Pomeron exchange. Unfortunately, this is a difficult experiment and the accuracy is not good enough to draw firm conclusions:

To summarize, the ϕ photoproduction experiments provide a puzzling input on the shrinkage properties of the Pomeron. Two possible ways out of the conflict with the K^+p and pp data have been identified -- (a) that $t = 0.6$ GeV^2 is a large t for diffraction dominance and that non-leading effects may be confusing the situation, and (b) that there may be a large real part in $\gamma p \to \phi p$. Whatever the explanation, it is important to redo the Ritson experiment, studying the ϕ cross section as a function of photon energy, but at a much smaller t-value, (e.g. for $t \sim 0.1$ GeV^2).

Factorization:

If we really believed that these diffraction reactions are dominated by the exchange of a simple Pomeron, we should be able to factorize, or separate, the different vertices appearing in these processes.

For example, the three sets of reactions shown in Fig. 21 should have the same ratio independent of the nature of the incident particle. The results of this test are shown in Fig. 22, for two energies, as a function of momentum transfer.[26] Factorization is observed to hold within ~ 20%, and even seems to work as a function of t.

Two further examples of factorization tests on total cross sections are described below:

Consider the process illustrated in Fig. 23 with elastic pion and proton scattering at the upper vertex, and proton diffraction into a proton plus zero, one, two, or three pions at the bottom vertex, the ratio between cross sections of the two upper vertex processes should be the same, independent of which of the four bottom vertices they interact.

$$\text{e.g., } R_1 = \frac{\sigma(\pi p \to \pi p)}{\sigma(pp \to pp)} \text{ should equal } R_2 = \frac{\sigma(\pi p \to \pi(p\pi^o))}{2(pp \to p(p\pi^o))} \text{ etc.}$$

A paper was submitted to the Batavia Conference by the Scandinavian Bubble Chamber Collaboration[27] in which the above diffractive processes have been isolated using the Van Hove Longitudinal Phase Space (LPS) analysis.[28] The results are given in Table 7 and the agreement is surprising.

Another interesting test of factorization in diffractive processes was presented by the SLAC Streamer Chamber Group.[29] The reactions studied are given schematically in Fig. 24, where each of the diffractive contributions -- $\gamma \rightarrow \rho^o$, $\pi \rightarrow \pi$, and $p \rightarrow p$ at the top vertex, and $p \rightarrow p$ and $p \rightarrow (p\pi\pi)$ at the bottom vertex -- were isolated using the LPS analysis. If the Pomeron contribution were well behaved and factorizable, then we would expect the ratio of the cross sections for each of the top vertex process joined to both of the bottom vertex processes, to be equal. For example, we would expect $R_1 = R_2 = R_3$, where

$$R_1 = \frac{\sigma(\gamma p \rightarrow \rho^o p)}{\sigma(\gamma p \rightarrow \rho^o(p\pi\pi))}$$

and

$$R_2 = \frac{\sigma(pp \rightarrow pp)}{\sigma(pp \rightarrow p(p\pi\pi))} \quad , \qquad R_3^{\pm} = \frac{\sigma(\pi^{\pm} p \rightarrow \pi^{\pm} p)}{\sigma(\pi^{\pm} p \rightarrow \pi^{\pm}(p\pi\pi))}$$

The experimental values for R_1, R_2, and R_3 are given in Table 8 for three different energy regions. Again the agreement is surprisingly good.

In summary, the factorization assumption for diffractive processes seems to be good to $\sim$ 15-20%. It would be interesting to have some more precise tests in the (10-20) GeV/c region, to look for the breaking of the assumption that one might expect from the presence of non-leading effects, like cuts.

Quantum Numbers in Pomeron Exchange:

The "rules" for diffractive processes said that, from a t-channel point of view, the Pomeron would carry the quantum numbers of the vacuum (i.e. C = +1, I = 0 exchange). How well does the data support this assertion?

(a) I = 0 Character:

We know from amplitude analysis of elastic scattering (which we suppose to be mainly diffractive) that the dominant amplitude is the non-flip isoscalar t-channel amplitude. We also know that processes involving a change of charge in the scattering (and hence $I \neq 0$ in the t-channel) have cross sections which fall quite rapidly with energy and do not have the character of diffractive reactions.

Below we consider two examples of the I = 0 character of diffractive processes from inelastic scattering:

The reactions $\pi^- p \to N\pi\pi$ were studied at 16 GeV/c by the ABBCCHW collaboration[26] and the $N\pi$ mass spectra are shown for the various possible charge combinations (see Fig. 25). The $(N\pi)^+$ combinations, (i.e. $p\pi^0$, $n\pi^+$) which can be produced with no charge exchange and hence accessible from I = 0 exchange in the t-channel, exhibit a large low mass enhancement in the (1400-1700) MeV range. This enhancement has an almost energy-independent cross section and is related to the diffractive excitation of N^*'s. The $(N\pi)^0$ combinations (i.e. $p\pi^-$, and $n\pi^-$ respectively), which cannot be reached with I = 0 exchange, have no low mass diffractive enhancement.

A similar example is shown in Fig. 26, where 10 GeV/c $K^- p \to \overline{K}(N\pi\pi)$ reactions have been studied.[26] Again the $(N\pi\pi)^+$ mass spectrum shows a low mass enhancement associated with the diffractive production of excited N^*, while the $(N\pi\pi)^0$ spectrum shows no such structure.

Thus we see quite clearly that the observation of diffractive phenomena is closely connected with I = 0 in the t-channel.

(b) C = +1 Character:

To examine this property we compare the $K^- p \to K^-(p\pi\pi)$ data already displayed in Fig. 26 above, to data on $K_L^0 p \to K_S^0(p\pi\pi)$ of approximately the same energy, from the SLAC bubble chamber experiment.[30] The data is selected to isolate out the peripheral $p \to p\pi\pi$ reaction mechanism and the resulting $(p\pi\pi)$ mass spectrum is shown in Fig. 27. The low mass diffractive enhancement in the K^- reaction is not observed in the K_L^0 data, although these two reactions are so very similar. The difference lies in that the K_L^0 and K_S^0 are eigen states of C with opposite sign and therefore the t-channel exchange in the K_L^0 reaction must carry C = -1. This may be viewed as evidence of the C = +1 character of diffractive processes.

(c) Spin-Parity Changes:

As per our "rules" we expect that diffraction will proceed most simply with no change of spin or parity for either the target or projectile particles, but that if there is a change it will

follow the natural spin-parity sequence, viz.

$$P_f = P_i \ (-1)^{\Delta J}$$

This may be thought of as picking up angular momentum in the Pomeron-diffracting-particle scattering.

This is a phenomenological rule, whose main claim to correctness is that there are no known diffractive processes which violate it. There exists rigorous proof for the spin zero case, but there is no general theorem for the more interesting spin situations.

The main evidence for justification for this "rule" is negative in nature (as mentioned above); however, one recent confirmation of the rule comes from a bubble chamber experiment on $\pi^- n \to \pi^- \pi^- p$ at 11.7 GeV/c by the Riverside group.[31] They observe diffractive production of N^*'s decaying into $p\pi^-$ final state. The analysis is free from complications of π-π resonance effects and deals with the well understood two-body elastic decay of the N^*; (i.e. it avoids the complication of previous studies which have observed diffractive production of $N^* \to N\pi\pi$, and then applied assumptions about two-body decays into $\Delta\pi$ final states). The Riverside results show production of P_{11}, D_{13}, F_{15} N^*'s, (i.e. the correct parity sequence for our "rule") and no sign of the D_{15} state. Further, the production phase between the D_{13} and F_{15} processes was found to be 0^o, in agreement with the hypothesis of diffractive production.

On the negative side, three threats to the rule existed last year -- vector K* production by K's, tensor A_2 production by π's and axial vector B production by γ's. Each of these processes violates the natural spin-parity sequence, but claims of "diffraction-like" properties had been made. We discuss them at more length below:

(a) K*(890) Production:

At the Oxford conference data on $K^- p \to K^*_{890} p$ was reported [32] implying that the cross section, which had been falling like p_{lab}^{-2} up to 8 GeV/c actually flattened out to an almost constant value for higher energies. This was taken as evidence of Pomeron contribution to K* production.

However, new data up to 16 GeV/c is now available, [33] and the cross section seems to fall like p_{lab}^{-1} beyond 8 GeV/c and the production and decay characteristics are in good agreement with isoscalar, natural spin parity exchange. Presumably ω^o exchange takes over from π exchange at the higher energies, and this "threat" to the parity rule has disappeared.

(b) A_2 Production:

There have been suggestions for some time that perhaps the A_2 meson is produced via Pomeron exchange, thus violating our simple rule of natural spin-parity excitation in diffraction processes. Kruse, et al. [34] have submitted an analysis of A_2 production in bubble chamber data in the energy range from (5-25) GeV/c. There is also a paper from Ascoli et al. [35] on A_1, A_2, and

A_3 production at 40 GeV/c. The facts are summarized below:

i. The A_2 cross section falls off as $p^{-0.8 \pm 0.08}$ in the (5-25) GeV/c range;

ii. The relative energy dependence of A_1, A_2, and A_3 between 25 GeV/c and 40 GeV/c are essentially the same;

iii. The natural parity exchange contribution to A_2 production falls off as $p^{-0.57 \pm 0.09}$;

iv. The t-channel exchange in A_2 production is mainly isoscalar;

v. The s-dependence of the cross section implies an effective intercept, $\alpha_{eff}(0) \sim 0.7$;

vi. An analysis of the shrinkage of the $J^P = 2^+$ A_2 differential cross section yields an $\alpha_{eff}(0) \sim 0.8$.

The energy dependence and α_{eff} values quoted above are more in agreement with a strong Pomeron contribution to A_2 production than the vector, and tensor meson contributions one expected. However, we must understand at least one other fact before throwing away our current picture of Pomeron processes -- the energy dependence for the A_2 cross section as measured in the $K\bar{K}$ decay mode seems to be faster than $p_{lab}^{-1.0}$. This is a clean reaction in which to study A_2 production with very little background, and the observed momentum dependence is very much in agreement with that expected for meson exchange in the t-channel. Several experiments should be reporting new cross sections for $A_2 \rightarrow K\bar{K}$ within the near future, and we wait impatiently for their results.

(c) Photoproduction of the B-Meson:

Finally, in this section on "bogey-men", we deal with the photoproduction of the B-meson. The reaction $\gamma p \rightarrow Bp$ violates the natural spin-parity series expected in diffractive processes, yet the B signal is observed with the same strength at 2.8, 4.7, and 9.3 GeV.[36] The energy independent cross section has encouraged speculation as to the validity of the simple rules on spin couplings for the Pomeron.

However, the statistics on these observations are rather limited, each energy point having a cross section of $(1.0 \pm 0.4)\mu b$. One could accommodate quite a variety of energy dependences within these measurements. It is an important reaction and to be followed with interest, but the present results are not strong enough to call our ideas on Pomeron coupling to question -- at least not yet.

For the moment the rule seems to be obeyed.

Spin Structure in Diffractive Processes:

Our "rules" assert that diffractive processes are s-channel helicity conserving (SCHC). This hypothesis derives from the early experimental work of the SLAC-Berkeley-Tufts group on their study of ρ^o-meson photoproduction with the polarized photon beam, at 4.7 GeV.[37] They found that the diffractively produced ρ^o-meson maintained the photon helicity in the s-channel. Gilman and coworkers[38] then hypothesized that all diffractive processes

conserved s-channel helicity and showed that the present knowledge of the πN scattering amplitudes was consistent with that assumption.

New data on $\gamma p \to \rho^o p$ at 9 GeV from the S-B-T group[39], and measurements of the R, A parameters in πN[40] and NN[41] scattering by a Saclay group confirm, in the main, the early conclusions. The new experiments are discussed in more detail below.

It is interesting to note that if s-channel helicity conservation really holds, then the old "lore" that the Pomeron behaves in the energy dependence of cross-sections like a particle of spin 1, but has the couplings of a particle of spin 0, cannot be true. SCHC requires quite specific couplings in the t-channel -- in general helicities will flip and there must be quite specific relations between the t-channel spin flip and non-flip couplings.

The density matrix elements from the new S-B-T experiment[39] at 9.3 GeV are shown in Fig. 28. They confirm the dominant behaviour as being SCHC and it holds out to larger t than observed before. However, the ρ_{10} element is quite definitely non-zero as is shown more clearly in Fig. 29. It was confirmed that the effect was real and not due to a scanning bias, by rotating the plane of polarization of the incident photons with respect to the bubble chamber camera axis; no change in the result was found. Further, they find when isolating the separate exchange amplitudes that the effect belongs to the natural-parity exchange amplitude. It is also found that the magnitude of the effect does not change

rapidly with energy. All these factors imply that there is a small helicity flip amplitude, of about 15% the SCHC amplitude, which may be associated with Pomeron exchange. Results of their analysis of the helicity flip contribution are given in Table 9.

The Saclay experiment studied $\pi^{\pm}p$ scattering at 6, 16 GeV/c from a polarized proton target.[40] The recoil proton was detected in a spark chamber polarimeter. The spin rotation parameters R and A were measured. Actually good measurements of R were obtained and A found from the relation $P^2 + A^2 + R^2 = 1$, using the existing precision measurements of the polarization in p-p scattering. Rough measurements of A were taken to resolve the quadratic ambiguity in the above equation. They find A to be close to +1 as expected from SCHC.

At 6 GeV/c, an amplitude analysis was performed using all the available data on total and elastic πN cross sections, differential cross sections, charge exchange cross sections, polarization for elastic and charge exchange reactions and their own new R and A parameters. Results for the isoscalar flip and non-flip amplitudes are shown in Fig. 30. The flip amplitude has a kinematic zero in the forward direction but is certainly non zero at larger t. For the region of $t > 0.2$ GeV^2, they find the ratio of flip to non-flip amplitude to be 0.17 ± 0.2 at 6 GeV/c.

There is not sufficient πN scattering data to perform a complete amplitude analysis at 16 GeV/c but a reasonable choice of solutions gives the same ratio, at 16 GeV/c, to be 0.14 ± 0.03. That is, the πN data shows that SCHC is the dominant amplitude but

that again a small (~ 15%) helicity flip amplitude is present and that it is isoscalar and weakly s-dependent -- presumably associated with the Pomeron. It is important to remember that although the $\gamma \rightarrow \rho$ experiment and this πN experiment are both measuring 15% helicity flip amplitudes which are isoscalar and weakly energy dependent, they are not measuring the same thing; the photon experiment measures the spin structure at the meson vertex while the πN experiment measures the spin structure at the nucleon vertex.

The Saclay group also measured R, A parameters for p-p scattering at 6, 16 GeV/c, and found the parameters consistent with dominance of SCHC. There is not sufficient data to perform an amplitude analysis for p-p scattering, but it is clear that this data would be consistent with a small helicity flip amplitude.

Finally, we must consider the spin structure for inelastic processes. Table 10 summarizes recent work on this question. It shows that the vector meson photoproduction behaves very much like elastic scattering -- SCHC in the main, but with a small helicity violating amplitude. The various diffraction dissociation processes do not conserve s-channel helicity. Most of them are much more close to t-channel helicity conservation, but in general do not conserve that either. Thus, although their inelastic processes looked very much like elastic reactions from the point of view of cross section and differential cross sections, they have very different spin structure. This difference may be due to the fact that these processes are perhaps not really particle production,

but kinematic enhancements, or due to the spin change that occurs in these processes and the complex t-channel spin structure of the Pomeron.

Conclusions:

We have reviewed the data on diffractive reactions and compared them to the set of phenomenological rules developed to describe these processes. In the main, the data agrees with the rules, both for inelastic and elastic reactions. There are, however, some puzzling questions;

- the question of the $\gamma p \rightarrow \phi p$ forward slope as a function of energy,
- the small t structure in p-p scattering,
- the observation of a small helicity flip amplitude associated with the Pomeron,
- the fact that inelastic diffractive dissociation processes do not observe SCHC,
- the exchange mechanism in $\pi p \rightarrow A_2 p$ and its relation to the parity rule,
- the rising p-p total cross sections and what that implies about our definition of asymptopia,
- given that $K^+ p$ and p-p cross sections rise, when will $\pi^{\pm} p$, $\bar{p}p$, γp, etc. start to rise.

All more material for another Moriond.

TABLE 1

The values of the parameters A and n resulting from the fitting of the total cross-section differences above 3 GeV/c to the formula

$$\Delta\sigma = A\, p_{lab}^{-n}.$$

(The errors shown in the table have been evaluated taking into account statistical and systematic errors.)

Cross-section differences	A (mb)	n
$\Delta(\pi^{\mp}p)$	4.0 ± 0.3	0.32 ± 0.02
$\Delta(K^{\mp}p)$	18.1 ± 0.3	0.54 ± 0.02
$\Delta(K^{\mp}n)$	13.0 ± 0.4	0.67 ± 0.02
$\Delta(p^{\mp}p)$	63 ± 2	0.64 ± 0.02
$\Delta(p^{\mp}n)$	49 ± 7	0.61 ± 0.05

TABLE 2

Energy dependence of total and elastic cross section.

$$\sigma \propto p^{-n}$$

Particle	Experiment, n		p Range (GeV/c)
	σ (elastic)	σ (total)	
π^-	(.23 ± .03)	.05 ± .01	(10 - 65)
π^+	(.28 ± .06)	.04 ± .01	(> 10)
K^-	(.39 ± .04)	.07 ± .01	(5 - 55)
K^+	(.09 ± .03)	0 rising slowly	(5 - 20) (20 - 60)
$\bar{p}$	.46 ± .02)	.11 ± .01	(10 - 50)
p	(.26 ± .02)	.03 ± .01	(10 - 30)

TABLE 3

Ratios

σ_{el} and σ_{tot}

	p_{lab} (GeV/c)	Ratio
π^-	5.5	.188 ± .005
	55.0	.138 ± .007
π^+	7.7	.192 ± .004
	16.0	.170 ± .006
K^-	10	.140 ± .003
	40	.126 ± .014
K^+	5	.225 ± .024
	15	.196 ± .017
p	6	.294 ± .006
	60	.187 ± .008
	200	.174 ± .005
	1000	.176 ± .007
$\bar{p}$	8.0	.225 ± .012
	16.0	.185 ± .010
	40.0	.178 ± .018

TABLE 4

RATIO OF $\frac{\sigma(xp \to xp)}{\sigma(\bar{x}p \to \bar{x}p)}$

	σ_{el}(mb)	p_{lab}	
K^-	3.15 ± .08	(10 GeV/c)	.94 ± .09
	2.60 ± .3	(40 GeV/c)	
K^+	3.34 ± .3	(10 GeV/c)	
π^-	4.8 ± .1	(10 GeV/c	1.00 ± .02
π^+	4.8 ± .1	(10 GeV/c)	
$\bar{p}$	13.9 ± .3	(10 GeV/c)	1.05 ± .11
	8.0 ± .8	(40 GeV/c)	
p	11.7 ± .2	(10 GeV/c)	
	7.6 ± .3	(40 GeV/c)	

TABLE 5

Energy Dependence of Diffraction Process,
$\sigma \propto p^{-n}$ ((5-20) GeV)

Process	n
$K^o \rightarrow Q^o$	0.59 ± 0.16
$K^+ \rightarrow Q^+$	0.60 ± 0.05
$\pi^- \rightarrow A_1^-$	0.41 ± 0.11
$N \rightarrow N\pi\pi$	0.4 ± 0.6
$\pi^- \rightarrow A_3^-$	0.8 ± 0.3

For comparison, the elastic scattering energy dependence is:

Process	n
K^+p	0.09 ± 0.03
K^-p	0.39 ± 0.04
πN	~ 0.2
NN	~ 0.2

TABLE 6

Process		Slope (GeV^{-2})
$\gamma \rightarrow \rho$	~	6-8
$\pi \rightarrow A_1$	~	9-11
$\pi \rightarrow A_3$	~	8
$K \rightarrow Q$	~	5-7
$\bar{K} \rightarrow \bar{Q}$	~	8-10
$N \rightarrow (N\pi\pi)_{1400}$	~	10-11
$N \rightarrow (N\pi\pi)_{1700}$	~	5

For comparison, the elastic slopes are ~

Process		Slope (GeV^{-2})
γN	~	6
πN	~	7-9
KN	~	5-6
$\bar{K}N$	~	7-8
NN	~	9-10

Factorization Test in πN and pp Reactions

$R_1 = \frac{\sigma(\pi^- p \to \pi^- p)}{\sigma(pp \to pp)} = 0.43$
$R_2 = \frac{\sigma(\pi p \to \pi(p\pi^0))}{\sigma(pp \to p(p\pi))} = 0.46 \pm .15$
$R_3 = \frac{\sigma(\pi p \to \pi(p\pi^+\pi^-))}{\sigma(pp \to p(p\pi^+\pi^-))} = 0.35 \pm .18$
$R_4 = \frac{\sigma(\pi p \to \pi(p\pi\pi\pi)}{\sigma(pp \to p(p\pi\pi\pi))} = 0.45 \pm .15$

TABLE 8

A Factorization Test for γp , πp, and pp Reactions

	Momentum (GeV/c)		
	(6-10)	(10-14)	(14-18)
$R_1 = \frac{\sigma(\gamma p \to \rho^0 p)}{\sigma(\gamma p \to \rho^0 p\pi^+\pi^-)}$	0.053 ± 0.014	0.035 ± 0.014	0.055 ± 0.024
$R_2 = \frac{\sigma(pp \to pp)}{\sigma(pp \to pp\pi^+\pi^-)}$	0.064 ± 0.07	0.061 ± .008	0.060 ± 0.009
$R_3^+ = \frac{\sigma(\pi^+ p \to \pi^+ p}{\sigma(\pi^+ p \to \pi^+ p\pi^+\pi^-)}$		0.061 ± .006	0.063 ± 0.003
$R_3^- = \frac{\sigma(\pi^- p \to \pi^- p)}{\sigma(\pi^- p \to \pi^- p\ \pi^+\pi^-)}$		0.052 ± 0.005	0.059 ± 0.003

TABLE IX

s-CHANNEL HELICITY-FLIP AMPLITUDE RATIOS IN THIS EXPERIMENT AND IN πN SCATTERING[6] FOR $.18 < |t| < .80$ GeV^2

Amplitude Ratios*	Experimental Values of Density Matrix Elements			
	2.8 GeV	4.7 GeV	9.3 GeV	Average
Photoproduction				
$\lvert T_{01}\rvert^2/\lvert T_{11}\rvert^2 \simeq \rho^0_{00}$	-.01±.03	.07±.02	-.01±.02	.018±.012
$\lvert T_{-11}\rvert^2/\lvert T_{11}\rvert^2 \simeq \rho^1_{1-1} + \mathrm{Im}\,\rho^2_{1-1}$	.04±.05	.11±.05	-.02±.05	.04±.03
$\mathrm{Im}\,T_{01}/\lvert T_{11}\rvert \simeq 2\,\mathrm{Re}\,\rho^0_{10}$	.16±.03	.12±.03	.14±.02	.14±.016
$\mathrm{Im}\,T_{-11}/\lvert T_{11}\rvert \simeq \rho^0_{1-1}$	-.06±.03	-.05±.03	-.10±.02	-.08±.02
πN Scattering				
$\lvert F^0_{+-}\rvert/\lvert F^0_{++}\rvert$ Isospin 0 Exchange		6 GeV/c		.15±.02

*The nucleon helicities in the photoproduction amplitudes listed are $\frac{1}{2}\frac{1}{2}$ (or $-\frac{1}{2}-\frac{1}{2}$).

Table X

Reaction	P_{lab} (GeV/c)	Group	Paper	Analyzer	SCHC	TCHC
$\gamma \to \rho^0$	2.8, 4.7, 9.3	Ballam et al.	307, 411	Azimuthal and polar angle of π.	Yes (They report a possible 2% flip contribution.)	No
	(2.7 - 4.0)	Gladding et al.	206	Same	Yes ($t < .5$ GeV)	No
	(4 - 6)	Struczinski et al.	325	Same	Yes	No
	(9 - 16)	Bulos et al.	349	Same	Yes	No
$\gamma \to \omega$	2.8, 4.7, 7.3	Ballam et al.	411	Same	Yes	No
$\gamma \to \phi$	2.8, 4.7, 7.3	Ballam et al.	411	Same	Consistent	No
$\pi \to A_1$ $\pm$	8.16	ABBCH	390	LPS selection, and polar angle of π.	No	No
$\pm$	16	ABBCCHLVW	169	Azimuthal study, normal to 3π and polar angle of π.	No	No
-	40	Antipov et al.	442		No	Slight Violation
-	4.5	Beketov et al.	833	Normal to 3π plane.	No	Yes
$\pi^- \to A_3^-$	(5 - 2.5)	Ascoli et al.	341	π^+ polar angle	No	Yes (but not very strong)
$K \to Q$ -	10	ABBCCHLVW	169	Azimuthal study, and normal to plane and π polar angles.	No	No
-	14.3	Barloutaud et al.	371	Normal to $K\pi\pi$ plane, and polar angles of π.	No	No
0	(4 - 12)	Brandenburg et al	347	Normal to $K\pi\pi$ plane.	No	Yes (but not very strong)
1400	10, 16	ABBCCHLVW	169	Azimuthal study, and normal, and polar.	Data Insensitive	
1700	10, 16	ABBCCHLVW	169	Same	No	Yes
$p \to p\pi\pi$ All	8, 16	ABBCH	390	LPS and polar angles of π.	No	Yes
All	25	Chapman et al.	452	Azimuthal	No	No
1600	11.6	Oh et al.	260		No	Yes

Figure Captions

1. Differential elastic scattering cross-section for 64 MeV α-particles on Fe^{58}, divided by the Rutherford scattering cross-section, as a function of the C of M scattering angle.
2. Energy dependence of the total cross-sections of $\pi^{\pm}$, $K^{\pm}$, $p^{\pm}$ in hydrogen.
3. Energy dependence of the total p-p cross-section through the Serpukov, NAL and ISR energy regions.
4. Energy dependence of the p-p elastic cross-section.
5. Energy dependence of $\pi^{-}p$, $K^{-}p$ and $\bar{p}p$ elastic cross-sections.
6. The ratio of elastic to total p-p cross-sections as a function of energy.
7. Differential cross section for elastic p-p scattering at the CERN ISR.
8. Energy dependence of the slope of the elastic p-p differential cross-section, for two regions of t--(a) $t < 0.1$ GeV^2, (b) $0.15 \leq t \leq 0.5$ GeV^2.
9. Differential cross-section for elastic $\pi^{-}p$, $K^{-}p$ and $\bar{p}p$ scattering at 25 and 40 GeV/c.
10. Energy dependence of the slope of elastic $\pi^{\pm}$, $K^{\pm}$, $p^{\pm}$ scattering in hydrogen.
11. Energy dependence of the cross-section for the process $K_L^o p \rightarrow K_S^o \pi^+ \pi^- p$, and the sub-process $K_L^o p \rightarrow Q^o p$.
12. Differential cross-section for elastic $K^{\pm}p$ scattering at 13 GeV/c.

13. Differential cross-sections for $K^o p \rightarrow Q^o p$ (squares) and $\overline{K}^o p \rightarrow \overline{Q}^o p$ (circles) over the momentum range (4-12) GeV/c.

14. Energy dependence of the slope parameter of the Pomeron contribution in--$K^+ p$ scattering shown as the shaded region, and $\pi^{\pm} p$ scattering, shown as the circles.

15. Fits to the differential cross-section of ρ^o photo-production to the sum of P and f exchange utilising Dual Absorption Model. The energy dependence of the slope parameter for the P contribution to the process is also shown.

16. Energy dependence of the cross-section for the reaction $\gamma p \rightarrow \phi p$.

17. Differential cross-section for $\gamma p \rightarrow \phi p$ at several energies.

18. The slope of the differential cross-section for $\gamma p \rightarrow \phi p$ as a function of energy.

19. The s-dependence of the differential cross-section for $\gamma p \rightarrow \phi p$ at a momentum transfer, $t = 0.6$ GeV^2. The data indicate no shrinkage of the ϕ cross-section at this value of t.

20. Differential cross-section for elastic p-p scattering at several energies, showing strong shrinkage at all values of t.

21. Schematic diagrams for elastic π^-, K^-, and $\overline{p}$ scattering and diffractive production of N*(1690).

22. Ratio of elastic cross-section to the N*(1690) production cross-section for incident π^-, K^- and $\overline{p}$ at 8, 16 GeV/c, as a function of momentum transfer.

23. A schematic of diffractive reactions studied in a test of

factorization. The ratios R_1-R_4 refer to the ratio of the cross-sections of reactions when the top two vertices (pion and proton elastic scattering) are joined successively to the bottom four vertices representing proton diffraction into a proton plus zero, one, two or three pions respectively.

e.g. $R_1 = \left[\frac{\sigma(\pi p \rightarrow \pi p)}{\sigma(pp \rightarrow pp)}\right]$

$R_2 = \left[\frac{\sigma(\pi p \rightarrow \pi p\pi)}{\sigma(pp \rightarrow pp\pi)}\right]$

etc.

24. A schematic of diffractive reactions studied in a test of factorisation. The ratio R_1, R_2, R_3 refers to the ratio of the cross-sections when each of the upper vertices ($\gamma \rightarrow \rho$, $p \rightarrow p$, $\pi \rightarrow \pi$) is connected with the two lower vertices, representing proton diffraction into a proton or a ($p\pi\pi$) system, respectively.

e.g. $R_1 = \left[\frac{\sigma(\gamma p \rightarrow \rho p)}{\sigma(\gamma p \rightarrow \rho p\pi\pi)}\right]$

$R_2 = \left[\frac{\sigma(pp \rightarrow pp)}{\sigma(pp \rightarrow pp\pi\pi)}\right]$

$R_3 = \left[\frac{\sigma(\pi p \rightarrow \pi p)}{\sigma(\pi p \rightarrow \pi p\pi\pi)}\right]$

25. Mass spectrum for ($N\pi$) in $\pi N \rightarrow \pi\pi N$ at 16 GeV/c.

26. Mass spectrum for ($N\pi\pi$) in $\bar{K}N \rightarrow \bar{K}(N\pi\pi)$ at 10 GeV/c.

27. Mass spectrum for ($N\pi\pi$) in $\bar{K}N \rightarrow \bar{K}(N\pi\pi)$ collissions--10 GeV/c K^- and (6-12) GeV/c K^0_L.

28. Density matrix elements for ρ^0 photo-production by polarised

photons at 9.3 GeV.

29. The momentum transfer dependence of the matrix element, ρ_{10}, at 2.8, 4.7 and 9.3 GeV. This matrix element indicates the presence of a spin flip amplitude.

30. The momentum transfer dependence of the flip and non flip isoscalar πN scattering amplitudes at 6 GeV/c.

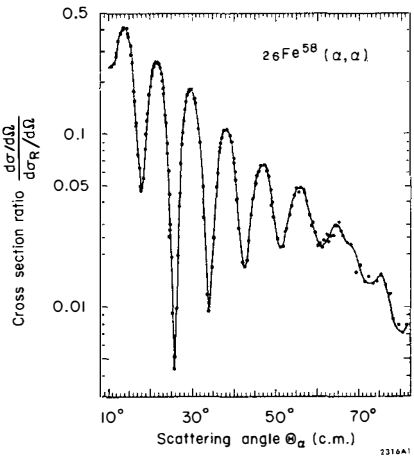


Figure 1

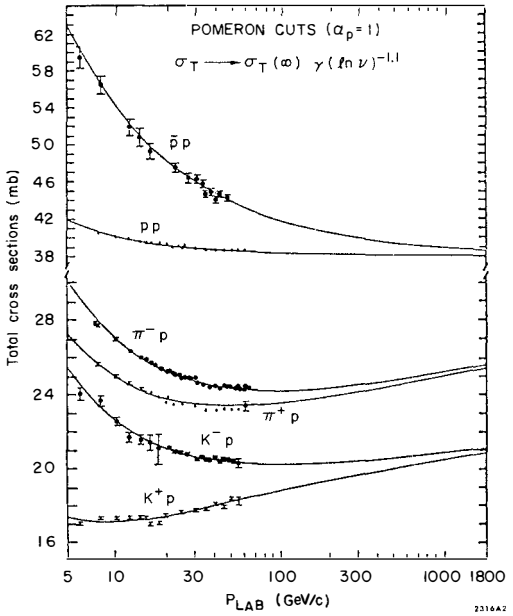


Figure 2

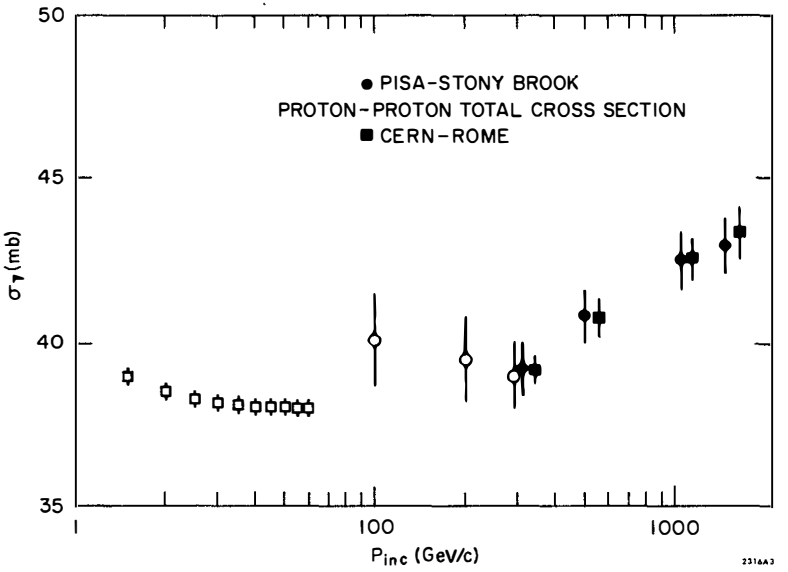


Figure 3

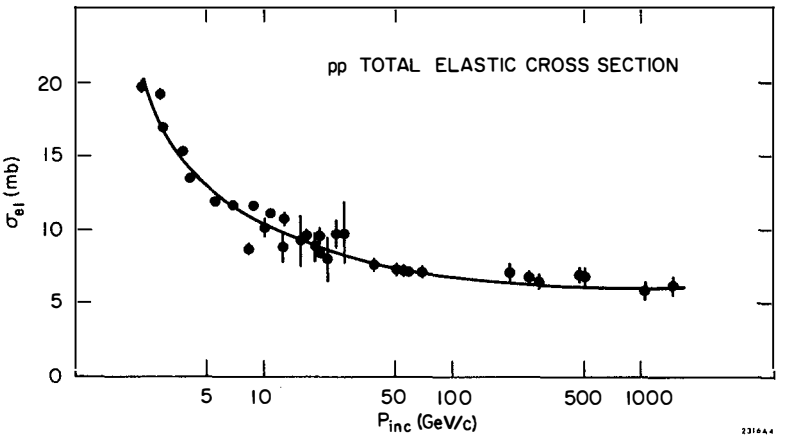


Figure 4

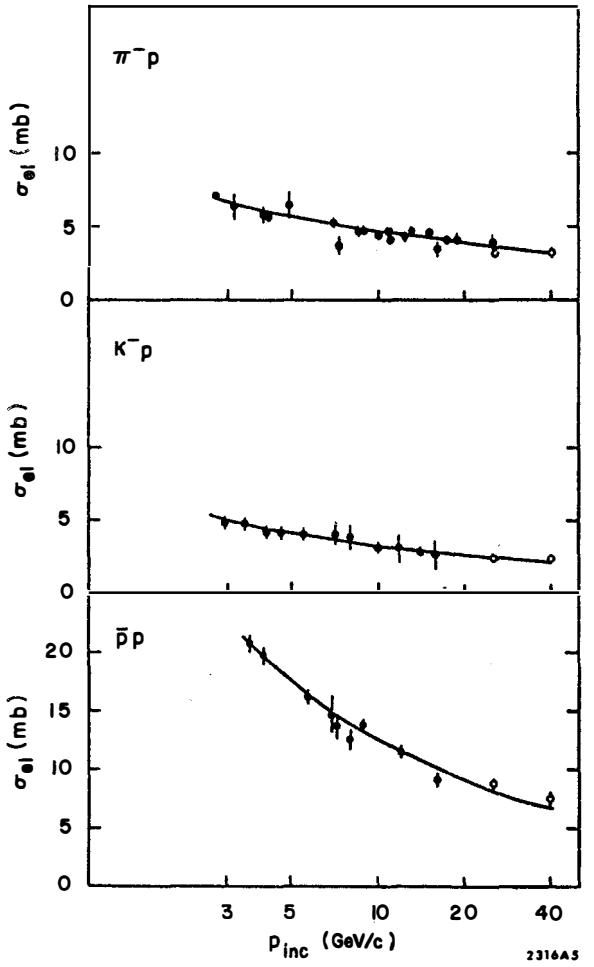


Figure 5

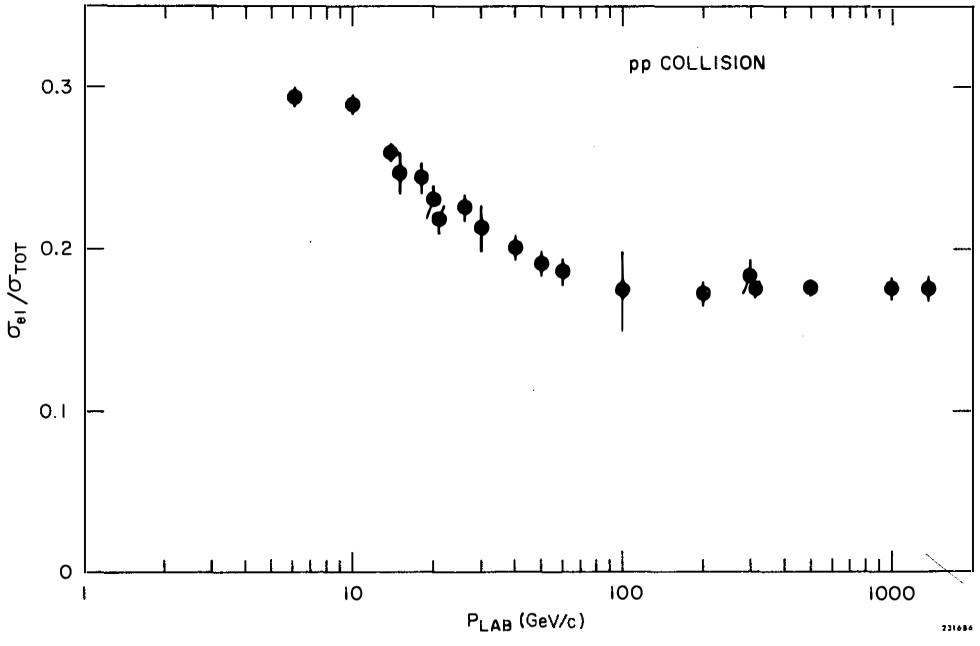

pp COLLISION
0.3
0.2
0.1
0
σ_{el}/σ_{TOT}
1
10
100
1000
P_{LAB} (GeV/c)
231686

Figure 6

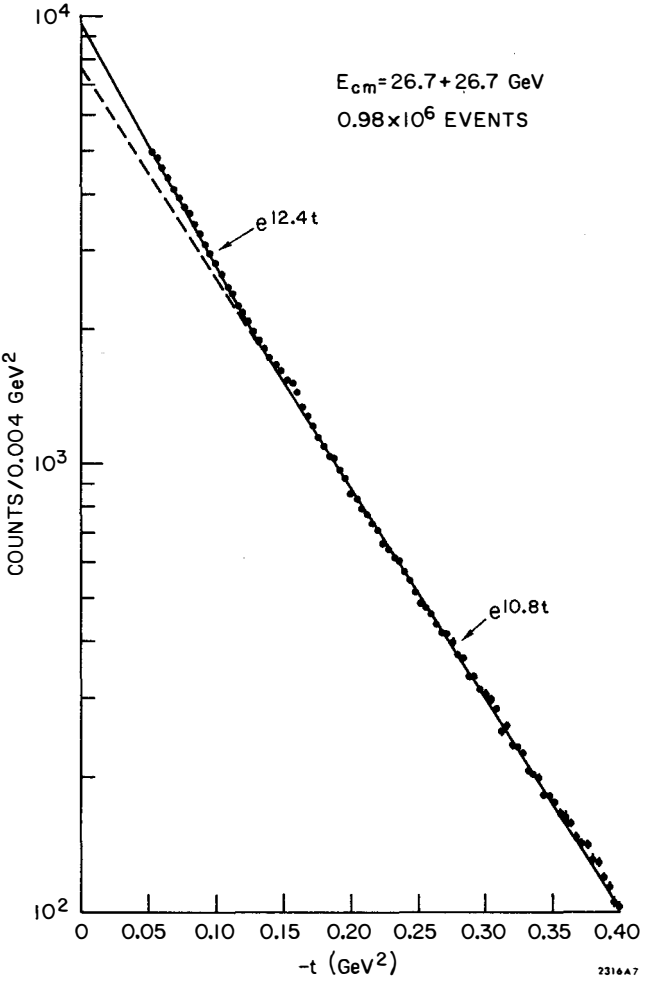

10^4
10^3
10^2
E_{cm}=26.7+26.7 GeV
0.98×10^6 EVENTS
$e^{12.4t}$
$e^{10.8t}$
COUNTS/0.004 GeV^2
0
0.05
0.10
0.15
0.20
0.25
0.30
0.35
0.40
-t (GeV^2)
2316A7

Figure 7

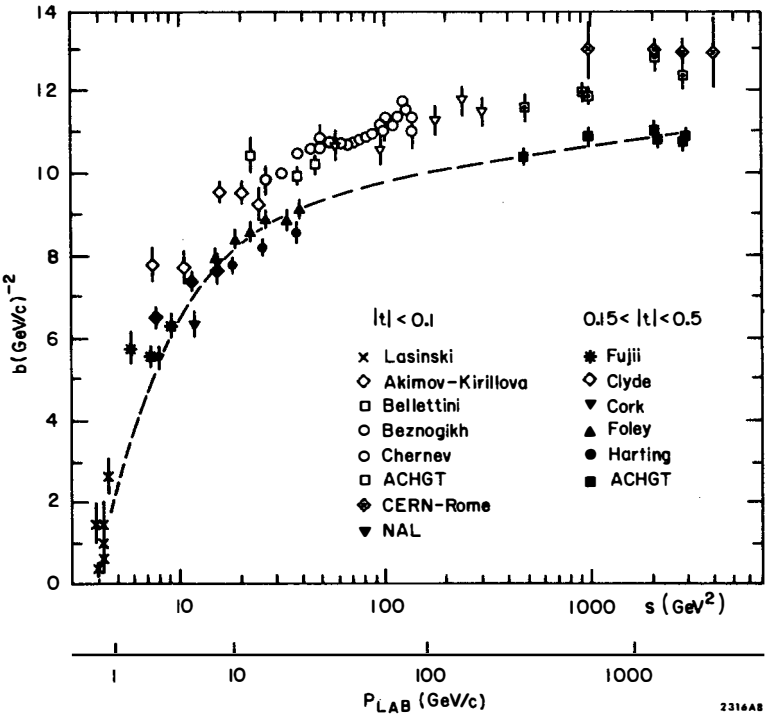

b (GeV/c)$^{-2}$
14
12
10
8
6
4
2
0
|t| < 0.1
0.15< |t|<0.5
Lasinski
Akimov-Kirillova
Bellettini
Beznogikh
Chernev
ACHGT
CERN-Rome
NAL
Fujii
Clyde
Cork
Foley
Harting
ACHGT
10
100
1000
s (GeV^2)
1
10
100
1000
P_{LAB} (GeV/c)
2316A8

Figure 8

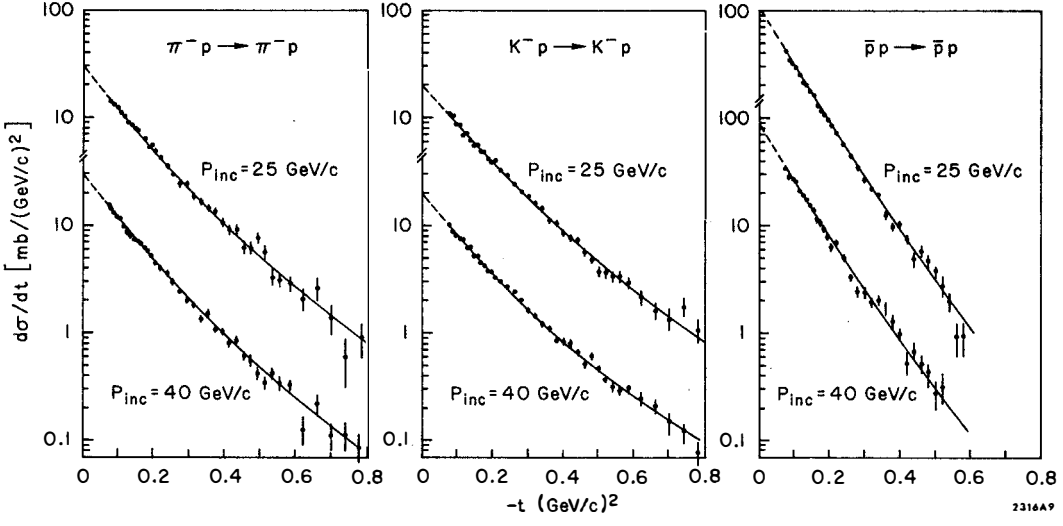

$\pi^- p \rightarrow \pi^- p$
$K^- p \rightarrow K^- p$
$\bar{p} p \rightarrow \bar{p} p$
$P_{inc} = 25$ GeV/c
$P_{inc} = 40$ GeV/c
$d\sigma/dt$ [mb/(GeV/c)^2]
$-t$ (GeV/c)^2
100
10
1
0.1
0
0.2
0.4
0.6
0.8
2316A9

Figure 9

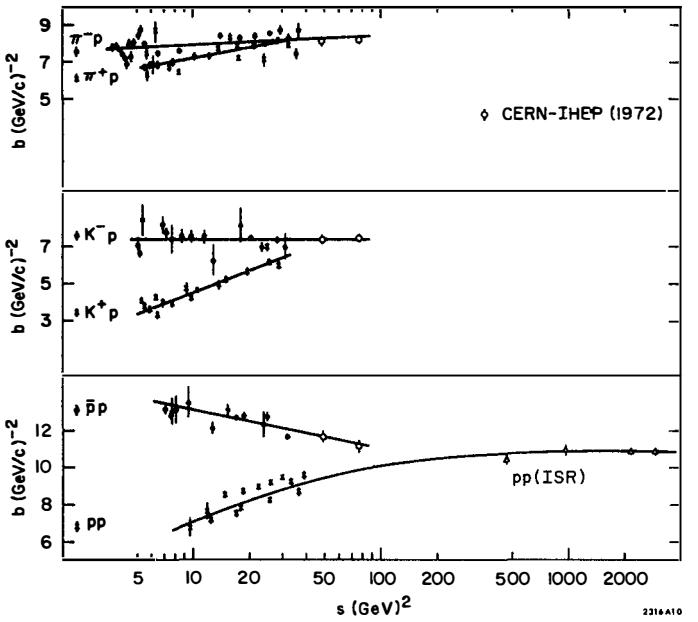


Figure 10

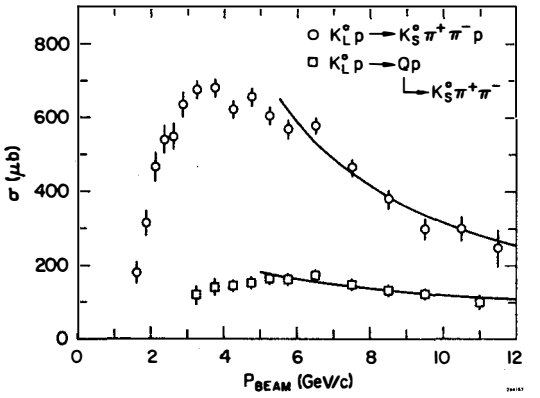


Figure 11

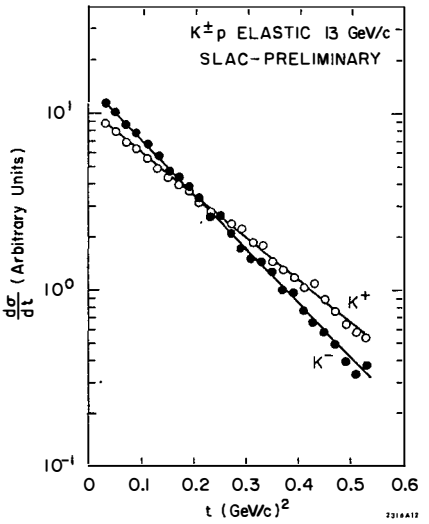


Figure 12

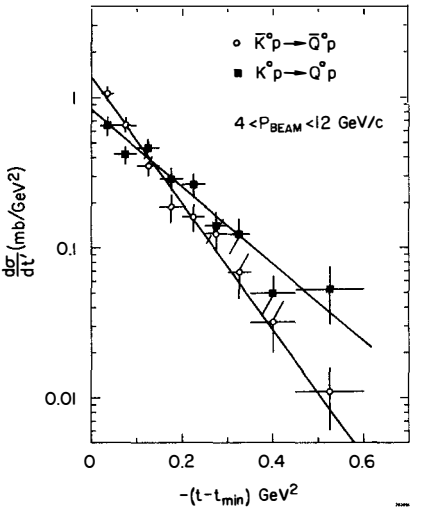


Figure 13

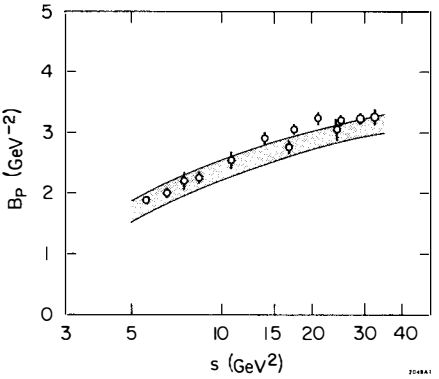


Figure 14

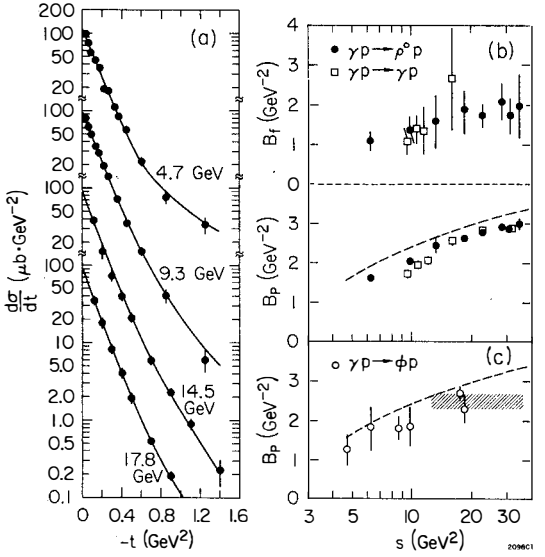


Figure 15

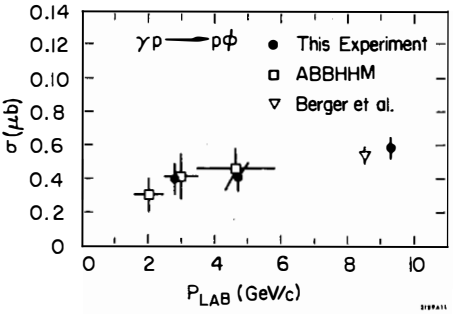

0.14
0.12
0.10
0.8
0.6
0.4
0.2
0
σ(μb)
γp → pφ
This Experiment
ABBHHM
Berger et al.
0
2
4
6
8
10
P_LAB (GeV/c)

Figure 16

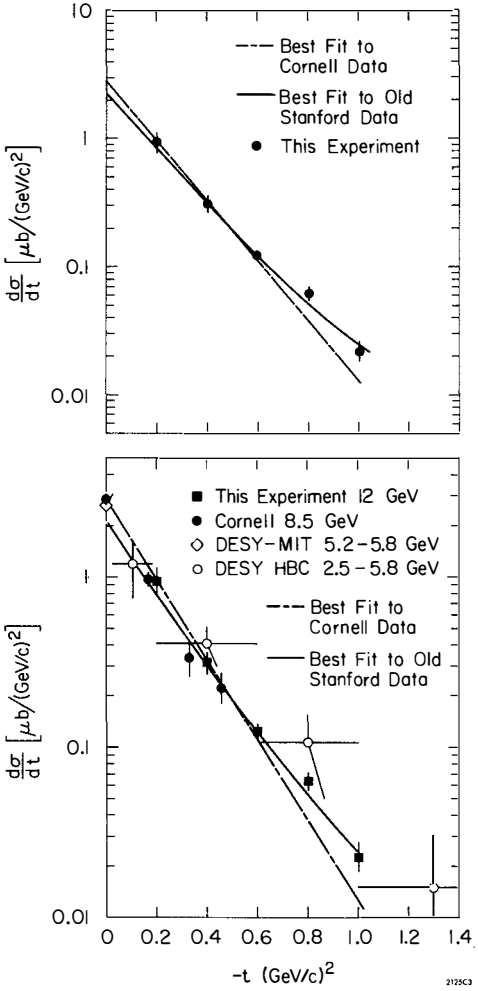

10
1
0.1
0.01
dσ/dt [μb/(GeV/c)²]
Best Fit to Cornell Data
Best Fit to Old Stanford Data
This Experiment
This Experiment 12 GeV
Cornell 8.5 GeV
DESY-MIT 5.2-5.8 GeV
DESY HBC 2.5-5.8 GeV
Best Fit to Cornell Data
Best Fit to Old Stanford Data
0
0.2
0.4
0.6
0.8
1.0
1.2
1.4
-t (GeV/c)²
2125C3

Figure 17

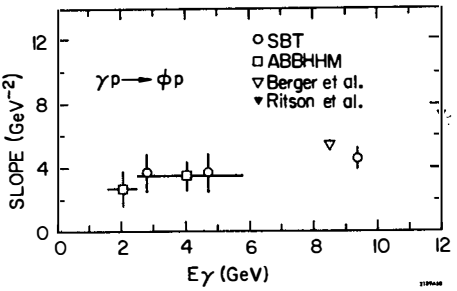


Figure 18

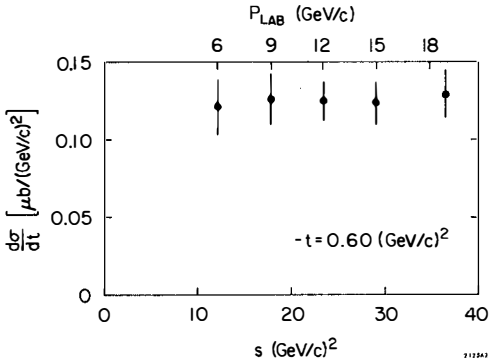


Figure 19

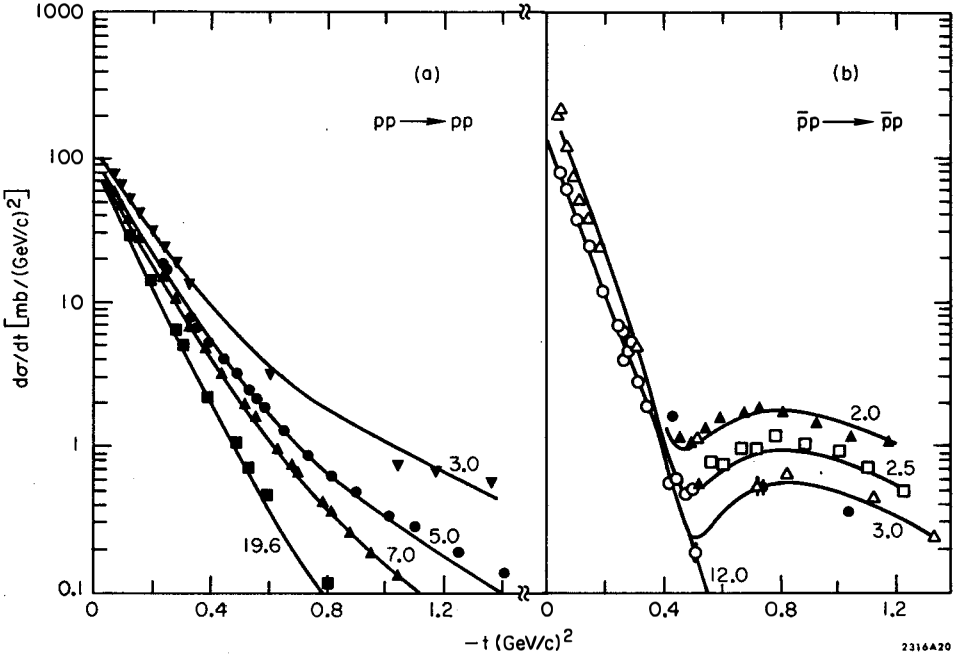

1000
100
10
1
0.1
dσ/dt [mb/(GeV/c)²]
(a)
pp → pp
3.0
5.0
7.0
19.6
0
0.4
0.8
1.2
(b)
p̄p → p̄p
2.0
2.5
3.0
12.0
0
0.4
0.8
1.2
−t (GeV/c)²
2316A20

Figure 20

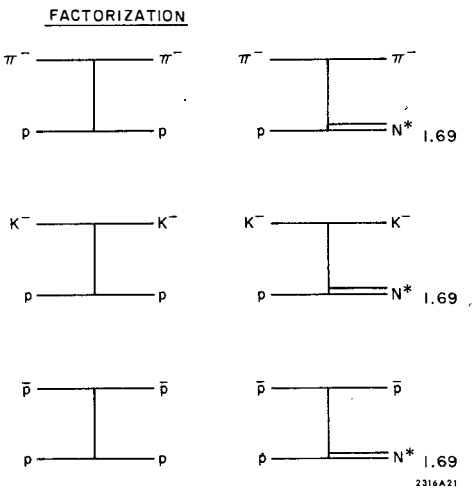


Figure 21

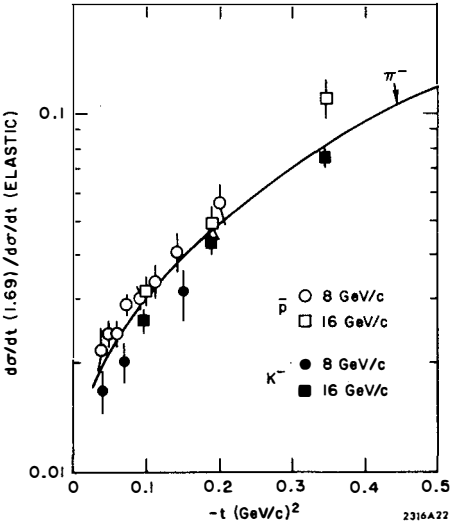


Figure 22

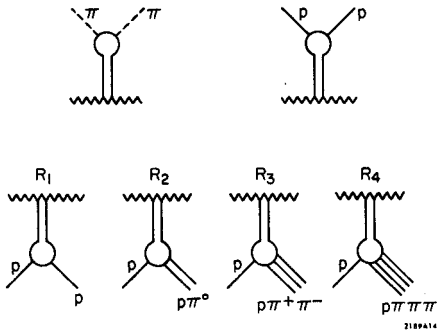


Figure 23

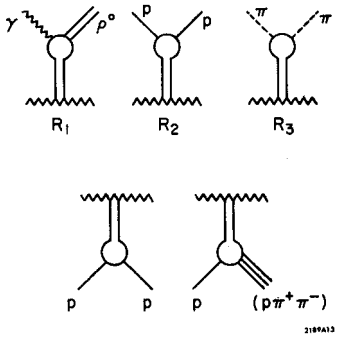


Figure 24

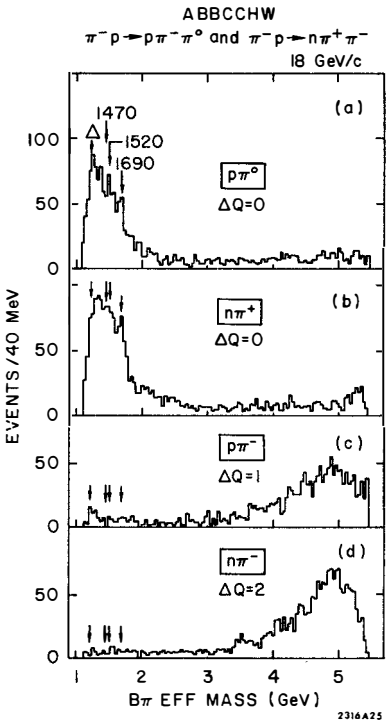


Figure 25

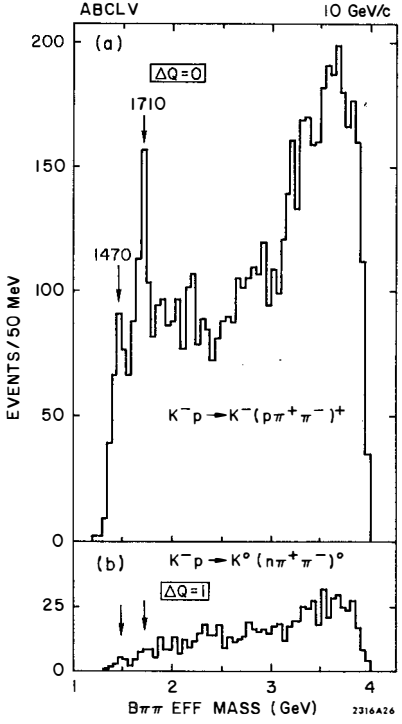


Figure 26

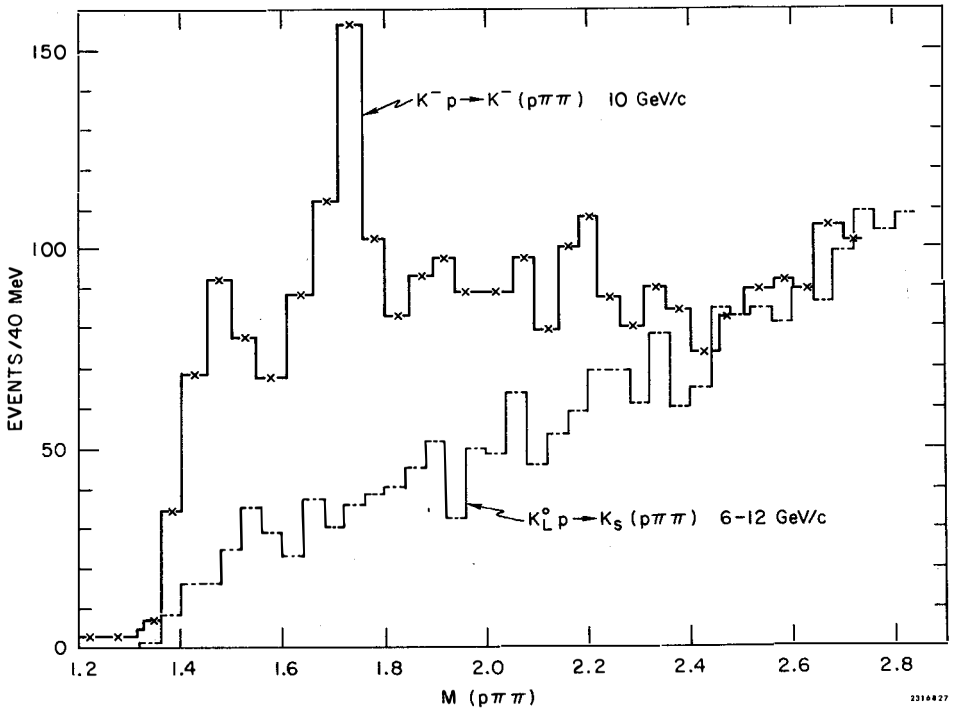

150
100
50
0
EVENTS/40 MeV
$K^- p \to K^- (p\pi\pi)$ 10 GeV/c
$K^0_L p \to K_S (p\pi\pi)$ 6-12 GeV/c
1.2
1.4
1.6
1.8
2.0
2.2
2.4
2.6
2.8
M $(p\pi\pi)$
2316827

Figure 27

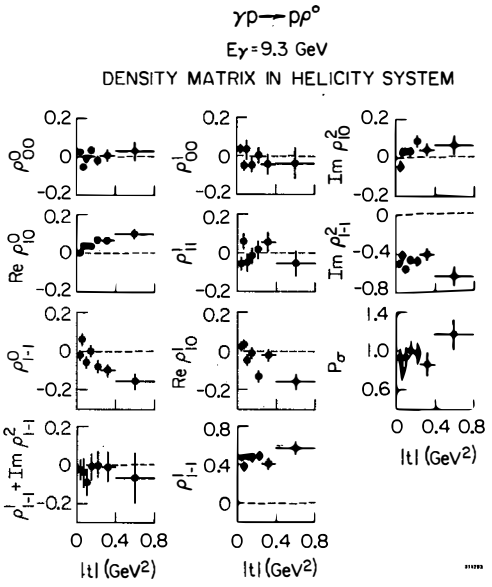

γp→pρ°
Eγ=9.3 GeV
DENSITY MATRIX IN HELICITY SYSTEM
ρ^0_{00}
ρ^1_{00}
Im ρ^2_{10}
Re ρ^0_{10}
ρ^1_{11}
Im ρ^2_{1-1}
ρ^0_{1-1}
Re ρ^1_{10}
P_σ
$\rho^1_{1-1}+\mathrm{Im}\,\rho^2_{1-1}$
ρ^1_{1-1}
0.2
0
-0.2
0.8
0.4
-0.4
-0.8
1.4
1.0
0.6
0 0.4 0.8
|t| (GeV²)

Figure 28

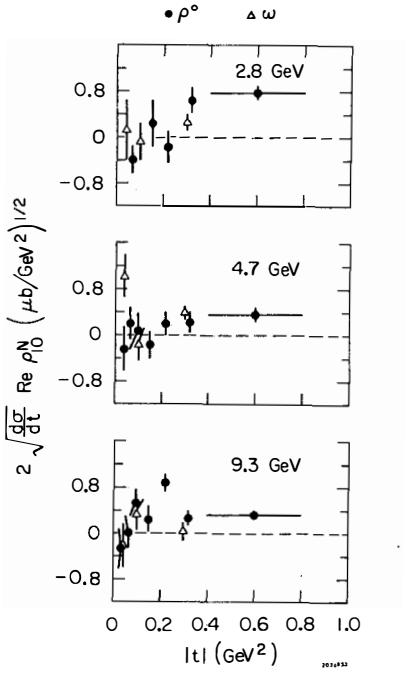


Figure 29

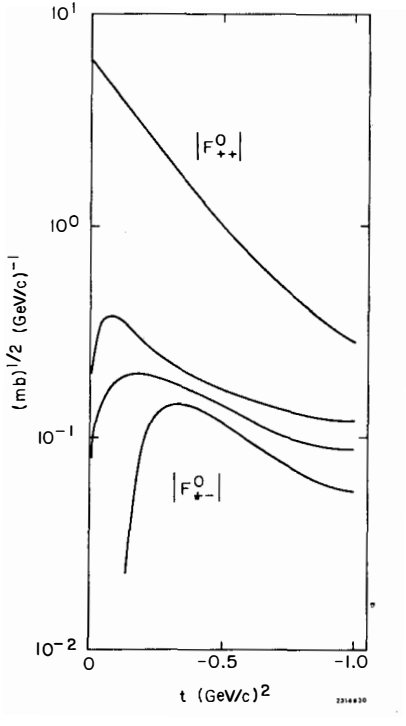


Figure 30

REFERENCES

1. F. K. McGowan, W. T. Milner, and H. J. Kim, ORNL-CPX-1, Charged Particle Cross Section Center, Oak Ridge National Lab., Oak Ridge.

2. M. L. Good and W. D. Walker, Phys. Rev. 120, 1854 (1960).

3. G. Giacomelli, XVI International Conference on High Energy Physics, Chicago-Batavia 1972 Proceedings, p. 219, Vol. 3 (1972).

4. S. P. Denisov, et al., Paper submitted to XVI International Conference on High Energy Physics, Chicago-Batavia, 1972.

5. V. V. Akiviov et al., Proceedings of 11th International Conference on Cosmic Rays, Budapest 1969.

6. S. R. Amendolia et al., submitted to Phys. Letters

7. U. Amaldi et al., submitted to Phys. Letters

8. G. G. Beznogikh et al., Paper submitted to XVI International Conference on High Energy Physics, Chicago-Batavia 1972.

9. Yu M. Antipov et al., Paper submitted to XVI International Conference on High Energy Physics, Chicago-Batavia 1972.

10. G. Barbiellini et al., Phys. Letters B39, 663 (1972), and Phys. Letters B35, 355 (1971).

11. G. Giacomelli, Rapporteur's talk at XVI International Conference on High Energy Physics, Chicago-Batavia, 1972.

12. E. Leader and M. R. Pennington, Phys. Rev. Letters 27, 1325 (1971).

13. D. W. G. S. Leith, Review talk at XVI International Conference on High Energy Physics, Chicago-Batavia 1972.

14. G. Brandenburg et al., SLAC PUB 1038 (1972).

15. ABBCH Collaboration, Paper submitted to XVI International Conference on High Energy Physics, Chicago-Batavia, 1972.

16. J. Ballam, et al., SLAC PUB 900; P. Baillon et al., Paper submitted to XVI International Conference on High Energy Physics, Chicago-Batavia, 1972.

17. R. K. Carnegie et al., Paper submitted to XVI International Conference on High Energy Physics, Chicago-Batavia, 1972.

18. M.Davier, Phys. Letters 40B, 369 (1972).

19. G. Chadwick et al., SLAC PUB 1093.

20. R. Anderson et al., SLAC PUB 1086.

21. D. R. O. Morrison, Rapporteur talk at Lund International Conference, 1969.

22. R. Anderson et al., SLAC PUB 1085.

23. J. Ballam et al., Paper submitted to XVI International Conference on High Energy Physics, Chicago-Batavia, 1972.

24. H. Alvensleben et al., Paper submitted to XVI International Conference on High Energy Physics, Chicago-Batavia, 1972.

25. H. Alvensleben et al., Paper submitted to XVI International Conference on High Energy Physics, Chicago-Batavia, 1972.

26. D. R. O. Morrison, Rapporteur talk at Kiev International Conference on High Energy Physics, Kiev, U.S.S.R. 1971.

27. S. Ljung et al., Paper submitted to XVI Internation al Conference on High Energy Physics, Chicago-Batavia, 1972.

28. W. Kittel, S. Ratti, and L. Van Hove, Nucl.Phys. B30, 333, (1971).

29. F. Liu et al., SLAC PUB 1047.

30. G. Brandenburg et al., private communication.

31. Y. Oh et al., Paper submitted to XVI International Conference on High Energy Physics, Chicago-Batavia, 1972.

32. R. Barloutaud, Rapporteur talk at the Oxford International Conference, 1971.

33. Y. Goldschmidt-Clermont, Review talk at the XVI International Conference on High Energy Physics, Chicago-Batavia, 1972.

34. U. Kruse et al., Paper submitted to XVI International Conference on High Energy Physics, Chicago-Batavia, 1972.

35. G. Ascoli et al., Paper submitted to XVI International Conference on High Energy Physics, Chicago-Batavia, 1972.

36. J. Ballam et al., Contribution to Cornell International Conference on Electron and Photon Interactions at High Energies, 1969.

37. J. Ballam et al., Phys. Rev. Letters 24, 960, 1970.

38. F. Gilman et al., Phys. Letters 31B, 387, 1970.

39. J. Ballam et al., SLAC PUB 1092.

40. A. de Lesquer et al., Phys. Letters 40B, 277, (1972); G. Cozzika et al., Phys. Letters 40B, 281 (1972).

41. J. Deregel et al., Paper submitted to XVI International Conference on High Energy Physics, Chicago-Batavia, 1972.

$Q^{\pm}$ PRODUCTION IN $K^{\pm}p$ INTERACTIONS AT 14 GeV/c

R. Barloutaud

Laboratoire de Physique des Particules Elémentaires
CEN-Saclay



Abstract : New results on the production differential cross-sections of the $Q^- \to K^0\pi^0\pi^-$ at 14.3 GeV/c are presented. The comparison to the $Q^+ \to K^0_S\pi^0\pi^+$ production differential cross sections at the same incident momentum, shows a definite cross-over. The relative amounts of C=-1 and I=1 t channel exchange amplitudes are found to be about equal in Q^- production and in K^-p elastic scattering at about the same incident momentum.

Résumé : La section efficace différentielle de production de $Q^- \to K^0\pi^0\pi^-$ a été mesurée à 14.3 GeV/c. La comparaison a la section efficace différentielle de production de Q^+ à la même énergie incidente montre un net effet de croisement. Les proportions d'amplitudes échangées dans la voie t avec C=-1 et I=1 se trouvent être sensiblement égales dans la production de Q^- et dans la diffusion élastique K^-p à des énergies incidentes voisines.

The diffractive production of mesonic systems as 3π or $K\pi\pi$, are generally assimilated to quasi elastic processes dominated by pomeron exchange and some residual Regge exchange in analogy to elastic scattering. A crucial test for the similitude of the mechanism responsible for the two processes is the accurate comparison between their cross over effects. Such cross overs have been found in the production of the 3π diffractive systems [1] and of the Q° and $\bar{Q}^\circ$ [2]. This last effect, which is especially important, has been seen for incident K° momenta averaged between 4 and 12 GeV/c. In Q production where both ω and ρ may be exchanged, the t channel amplitudes involved may a priori be different for Q^-, Q^+, Q° and $\bar{Q}^\circ$ production. In this communication, new results concerning Q^- production at 14.3 GeV/c are presented. They come from an experiment performed by the Collaboration Rutherford Laboratory, Ecole Polytechnique, Saclay [3]. In particular, the energy dependence of the Q^- production cross-section, and its differential cross section are compared with the corresponding data obtained in Q^+ production and with the results on $K^\pm p$ elastic scattering.

1. General features of reactions $K^-p \to \bar{K}N\pi\pi$

The three reactions

$K^-p \to K^-p\pi^+\pi^-$	(1)	(6093 events)
$K^-p \to K^-p\pi^-\pi^\circ$	(2)	(1781 events)
$K^-p \to \bar{K}^\circ n\pi^+\pi^-$	(3)	(583 events)

have been studied at 14.3 GeV/c in the 2m hydrogen bubble chamber. Their cross sections are respectively 750 ± 40, 620 ± 30 and 195 ± 15 μb.

At this incident momentum a good separation exists between the diffractive processes occuring at the meson and baryon vertices. This is shown in the scatter plots $M(N\pi\pi)$ versus $M(K\pi\pi)$ presented in figures 1b, e. In reaction (1) (fig. 1b) two distinct clusters correspond to these two processes, while for reaction (2) (fig. 1e) where the $N\pi\pi$ diffractive production is not allowed only the $K\pi\pi$ cluster is visible. In reaction (3) (fig. 1h) where both vertices correspond to charge exchange processes the scatter plot does not display any strong concentration. The $K\pi\pi$ projections, as well as the Chew-Low plots are also presented in figure 1 for the three reactions. The well known Q bump dominates the $K\pi\pi$ spectrum in reactions (1) and (2), while in reaction (3) only K^*_{1420} peaks at low $K\pi\pi$ masses. In order to study the production properties of the Q enhancement, the Δ has been removed from the sample ($M(p\pi^0) > 1.34$ in reactions (1) and (2) and $M(n\pi^+) > 1.34$ in reaction (3)) and the Q region has been defined as $M(K\pi\pi) < 1.5$ GeV.

2. Energy dependence of the cross-section

The energy dependence of the Q^+ and Q^0 production have been described between 2.5 and 12 GeV/c by a power-law dependence $\sigma \propto p_{lab}^{-n}$ with exponents $n = 0.67 \pm 0.07$ [4] and 0.59 ± 0.16 [2] respectively).

Using available data on reaction (1) at 3.9 GeV/c [5], 4.6 GeV/c [6], 10 GeV/c [7], 12.6 GeV/c [8] and 14.3 GeV/c (this experiment) the energy dependence of the production cross-section for five $K\pi\pi$ mass intervals below 2 GeV has been investigated. It is described by exponents n ranging between 0.3 and 0.9 (fig. 2). The average value corresponding to the Q region is 0.4 ± 0.1,

what is in reasonable agreement with the Q^+ and Q° data. The exponents n obtained from K^+p and K^-p elastic cross sections between 4 and 15 GeV/c [9] are respectively 0.10±0.10 and 0.36±0.10. This indicates a difference between the K^+p and Q^+p energy dependence, but none between K^-p and Q^-p.

One may further note that at 14.3 GeV/c the extrapolated Q^+p total cross section derived from a 12 GeV experiments [10] is equal to 216±8 μb; this is in very good agreement to the corresponding result for Q^- : 225±10 μb.

3. Cross over effects

The experimental dN/dt distributions in the Q region are presented in figure 3 for reactions (1), (2) and (3). Although the slope for reactions (1) and (2) are not exactly the same, they are definitely larger than for reaction (3) which is dominated by the production of $K^*(1420)$. An exponential function Ae^{Bt} fits very well these dσ/dt distributions up to t=-0.6 GeV^2 ; the coefficients B are 9.6±0.3, 7.9±0.5 and 5.1±1 GeV^{-2} for reactions (1), (2) and (3) respectively.

These fitted distributions have been compared to the corresponding ones for Q^+ production at 12 GeV/c [10] For the C-conjugate states $K^-\pi^-\pi^+$, $K^+\pi^+\pi^-$ and $\bar{K}^\circ\pi^-\pi^\circ$, $K^\circ\pi^+\pi^\circ$, the slope parameters B are definitely higher in the K^- reaction than in the K^+ reaction.

In order to make a quantitative comparison of the Q^+p and Q^-p differential cross section data, we have adjusted the A coefficient of the 12 GeV/c K^+p experiment to take into account the decrease of the Q^+ cross section

between 12 and 14.3 GeV/c (assumed to vary as $P_{lab}^{-0.6}$). In figure 4 we present the fitted $d\sigma/dt$ for the two pairs of line reversed reactions for the entire Q region ($1.0 < M(K\pi\pi) < 1.5$ GeV and $|t| \lesssim 0.4$ GeV^2). For each experiment the two straight lines represent the extreme values of $d\sigma/dt$ taking into account the errors on A and B. The absolute normalization error in this comparison is evaluated at $\pm$ 7 % by adding the errors on the reaction cross-sections for $K^{\pm}p \to K^{\pm}p\pi^+\pi^-$.

A definite cross-over is seen in the fitted $d\sigma/dt$ distributions for $Q^{\pm} \to K^{\pm}\pi^+\pi^-$ productions. It occurs at $|t| = 0.17 \pm 0.05$ GeV^2. The slopes of the $d\sigma/dt$ distributions for $Q^{\pm} \to K^0\pi^{\pm}\pi^0$ being closer, the cross-over position is not well determined and occurs at $|t| > 0.12$ GeV^2.

The ratio

$$r_{Q^{\pm}} = \frac{(d\sigma/dt)_{t=0} \ (K^-p \to Q^-p)}{(d\sigma/dt)_{t=0} \ (K^+p \to Q^+p)}$$

is equal to 1.28 ± 0.12 and 1.26 ± 0.14 respectively for the $K^{\pm}\pi^{\pm}\pi^-$ and $K^0\pi^{\pm}\pi^0$ decays. This ratio r and its implications for the Q production mechanism are further discussed in section 5.

4. t channel isospin decomposition of the reactions $\bar{K}N \to \bar{K}^*_{890}\pi N$

A t channel isospin decomposition of the reaction $\bar{K}N \to \bar{K}^*_{890}\pi N$ which is known to dominate the Q production has been made, by comparing the cross-sections $\sigma(1)$, $\sigma(2)$ and $\sigma(3)$ of reactions (1) (2) and (3) for a given $M(K\pi\pi)$ mass interval. The amount of Q production in the charge exchange reaction (3) measures in first approximation the

proportion of isovector exchange in the t channel. For a given $K\pi\pi$ mass interval, the ratio of the amplitudes A_1 and A_o corresponding to I=1 and I=0 exchanges, is given approximately (apter averaging over phase space and spin) by

$$\left|\frac{A_1}{A_o}\right| \simeq \sqrt{\frac{\sigma_{(3)}}{2(\sigma_{(1)} + \sigma_{(2)})}}$$

if one neglects the production of isospin 3/2 in the $K^*\pi$ system and the interference between I=0 and I=1 in the t integrated cross-sections of reactions (1) and (2).

The quantity $|A_1/A_o|$ is plotted as a function of the $K\pi\pi$ mass in figure 5. Below 1.5 GeV this ratio is approximately equal to 15±3 %. It is however important to notice that most of it comes from the 1.3-1.5 GeV $K^*(1420)$ region ; for $K\pi\pi$ masses $\leq$ 1.3 GeV, i.e. in the $K\pi\pi$ near-threshold (Q) region, the value of this ratio falls to $\sim(10\pm3)\%$(+). We may therefore conclude that the I=1 (ρ, A_2) t-channel exchange amplitude contribution to the production of the $K^*(890)\pi$ system near-threshold amounts to $\simeq$10 % of the dominant I=0 (Pomeron, ω , f^o) exchange amplitude, this assuming that the low mass $\bar{K}^o\pi^+\pi^-$ system has the same J^P as the Q^-. The I=1 exchange amplitude becomes more important ($\simeq$25 %) in the region of the 2^+ resonant $K^*(890)\pi$ system (the $K^*(1420)$ resonance) where π exchange presumably plays an important role.

(+) A similar result has been recently obtained at 12.7 GeV/c in K^+p interactions [11].

5. Comparison between the production properties of $Q^{\pm}$, Q°, $\bar{Q}^{\circ}$ and the K p elastic scattering around 14 GeV/c.

Results on the differential cross-sections for these reactions have recently become available. In particular cross-over effects have been observed in $K^{\pm}p$ elastic scattering at 13 GeV/c [12] and in $Q^{\circ}\ \bar{Q}^{\circ}$ production between 4 and 12 GeV/c [9]. In table 1 are presented for these reactions the results obtained on the position tc of the cross-over, on the values B_s and B_L of the smaller and larger slope, and on the ratio r of $(d\sigma/dt)_{t=0}$ precedently defined.

Reaction	Incident momentum (GeV/c)	tc	B_s GeV^{-2}	B_L GeV^{-2}	r	Ref.
$K^{\pm}p \to K^{\pm}p$	13	0.21±0.03	5.6	7.1	1.34	[12]
$K^{\circ}p \to Q^{\circ}p$	4-12	0.13±0.03	5.9±0.5	9.7±0.7	1.68	[9]
$\bar{K}^{\circ}p \to \bar{Q}^{\circ}p$	8-12		5.4±1	11.3±1.6		
$K^{\pm}p \to Q^{\pm}p$	14.3					[10]
$\hookrightarrow K^{\pm}\pi^{+}\pi^{-}$		0.17±0.05	7.9±0.1	9.6±0.3	1.28±0.12	and this
$\hookrightarrow K^{\circ}\pi^{\pm}\pi^{\circ}$		>0.12	6.9±0.5	7.9±0.5	1.26±0.14	exp.

All values of tc range between 0.13 and 0.21 and are compatible with $1/B_s$ which is expected if the integrated cross sections $\sigma \sim A/B$ are equal for the two processes.

As well known the Q production slopes are systematically higher than for $K^{\pm}p$ elastic scattering, but their difference ΔB as well as the ratio r are quite similar in the 13-14 GeV/c region for two processes. It seems however that ΔB is larger ($\Delta B = 5.9 \pm 1.9$ GeV/c in the 8-12 GeV/c region) for the Q°, $\bar{Q}^{\circ}$ productions This could be explained, if it is confirmed with better statistics, by the presence of I=1 t-channel exchange as

seen in the preceeding section. No data is yet available for the ratio r in $Q^o \bar{Q}^o$ production in the 14 GeV/c energy region.

The ratio r is connected to the proportion of C=-1 t-channel exchange amplitude with no helicity flip at t=0 (A_0^-) relative to the dominant C=+1 exchange amplitude (A_0^+). If A_0^+ is assumed to be purely imaginary ($\mathbb{P}$) the ratio

$$\frac{\text{Im } A^-_0}{A^+_0} = \frac{r-1}{4}$$

is about 8 % for $Q^\pm p$ and $K^\pm p$ final states. On the other hand, the ratio of I=1 over I=0 t-channel exchange in the $\bar{K}N$ elastic scattering is after averaging over t

$$\left|\frac{A_1}{A_o}\right| = \frac{1}{2}\sqrt{\frac{\sigma(K^o n)}{\sigma(K^- p)}}$$

At 14 GeV/c, this ratio amounts to $(5\pm0.7)10^{-2}$ [13, 14] which is roughly compatible with what is found in the $Q^\pm$ production at the same momentum : $(10\pm3)10^{-2}$.

All these results point to the close similarity existing between the production properties in $K^\pm p$ elastic scattering and in the diffractive production of the $K\pi\pi$ system in the Q region. This seems to indicate that the presence of non diffractive objects, such as K^*_{1420} (which is indeed known to give only a small contribution in the Q bump) or the eventual SU3 companion of the $1^{+-}B$ should not be very important in this $K\pi\pi$ region. The main contribution to the Q bump is generally interpreted in terms of a Deck type diffractive dissociation ; this in in agreement with the recent observation of the non resonant character of the 1^{++} partial wave in the corresponding 3π system

[15]. However, as already noticed [2] a simple π exchange Deck model cannot account for the observed differences in Q° and $\bar{Q}^{\circ}$ differential cross-sections. Therefore, it appears that more sophisticated theories are needed to understand all the production properties and the nature of these diffractive objects.

REFERENCES

[1] AACHEN-BERLIN-BONN-CERN-HEIDELBERG Collaboration
Phys. Letters 41B (1972) 393.

[2] G.W. BRANDENBURG et al.,
Nuclear Phys. B45 (1972) 397.

[3] RUTHERFORD-ECOLE POLYTECHNIQUE-SACLAY Collaboration
To be published.

[4] H.H. BINGHAM et al.,
Nuclear Phys. B48 (1972) 589.

[5] A. ROUGE, Private communication.

[6] A. AGUILAR-BENITEZ et al.,
Phys. Rev. Letters 25 (1970) 54.

[7] AACHEN-BERLIN-CERN-LONDON-VIENNA Collaboration
Nuclear Phys. B8 (1968) 9.

[8] T. LUDLAM et al.,
Phys. Rev. D2 (1970) 1234.

[9] Compilation of Cross-Sections :
V. K^- Induced Reactions CERN/HERA 72-2.

[10] P.J. DAVIES et al.,
Phys. Rev. D5 (1972) 2688.

[11] B. WERNER, P. SLATTERY and T. FERBEL,
Preprint UR393 from the University of Rochester.

[12] D.W.G.S. LEITH, Communication presented at the
Conference of Batavia (1972) and reported in the
G. GIACOMELLI Rapporteur's talk.

[13] R.J. MILLER et al.,
Phys. Letters 34B (1971) 230.

[14] R.J. MILLER et al.,
Rutherford Lab. Preprint RPP/H/102 (1972).

[15] G. ASCOLI, "Summary of the Experimental Situation regarding A_1, A_2, A_3 Production",
Report presented at the Batavia Conference 1972.

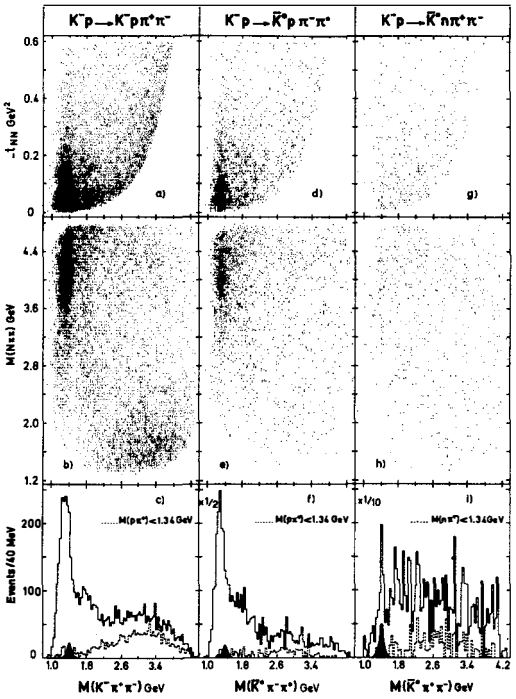


FIG. 1

For each of the three reactions (1), (2) and (3) are presented in

a, d, g) the two dimentional plots of M(Kππ) vs t_{NN} ;

b, e, h) the two dimensional plots of M(Kππ) vs M(Nππ) ;

c, f, i) the M(Kππ) mass spectra - the dotted line represents the same spectrum for Δ selected events (Δ^{++} in reaction (1), Δ^{+} in reactions (2) and (3)).

The shaded areas represent the normalized contributions of $K^{*}(1420)N$ estimated from its production in reactions $K^{-}p \to KN\pi$.

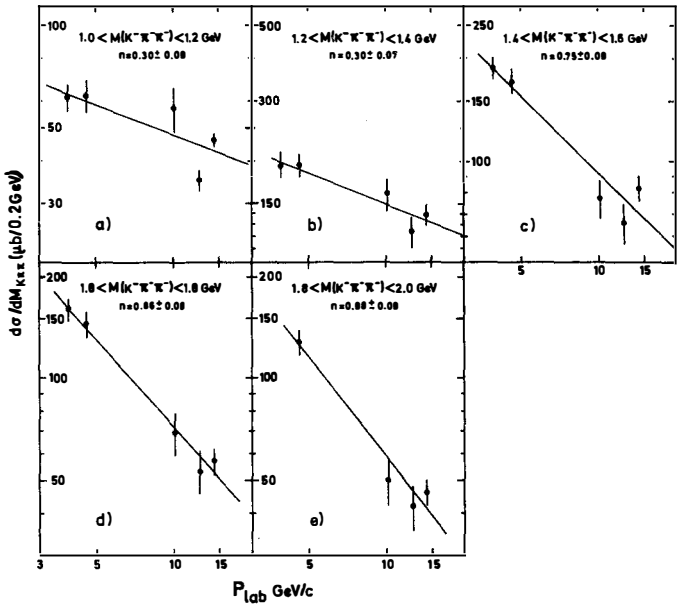


FIG. 2

Incident momentum dependence of $\frac{d\sigma}{dM(K^-\pi^+\pi^-)}$ in reaction (1) for five M(K$^-\pi^+\pi^-$) intervals between 1 and 2 GeV/c. The data come from experiments at 3.9 GeV/c [13], 4.6 GeV/c [14], 10 GeV/c [5], 12.6 GeV/c [6] and 14.3 GeV/c (this experiment), with the $\Delta^{++}(1240)$ removed. The straight lines represents fits of $\frac{d\sigma}{dM} \sim P_{lab}^{-n}$.

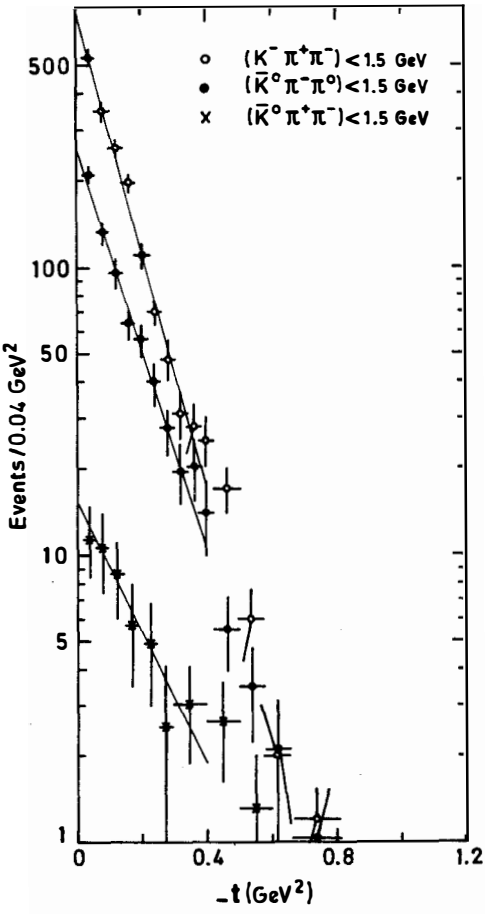


FIG. 3

dN/dt_{NN} distributions for reactions (1), (2) and (3) and for $1.0 \leq M(K\pi\pi) \leq 1.5$ GeV. Fits to Ae^{Bt} are shown for the interval $0 \leq |t_{NN}| \leq 0.4$ GeV^2.

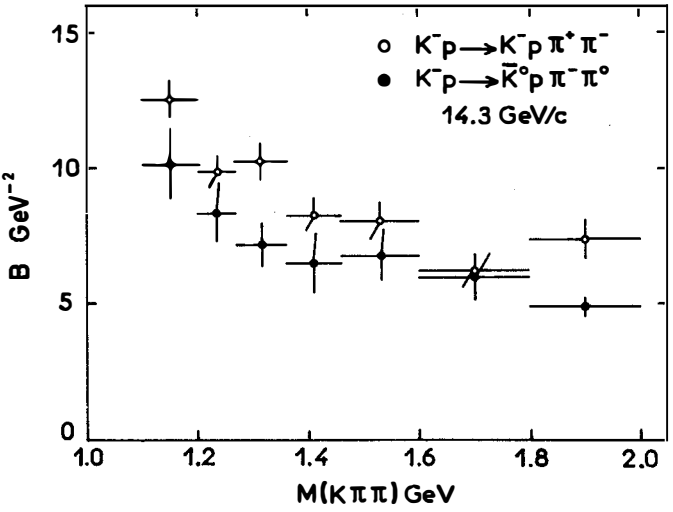


FIG. 4

Dependence on M(Kππ) of the slope of the t_{pp} distributions for reactions (1) and (2).

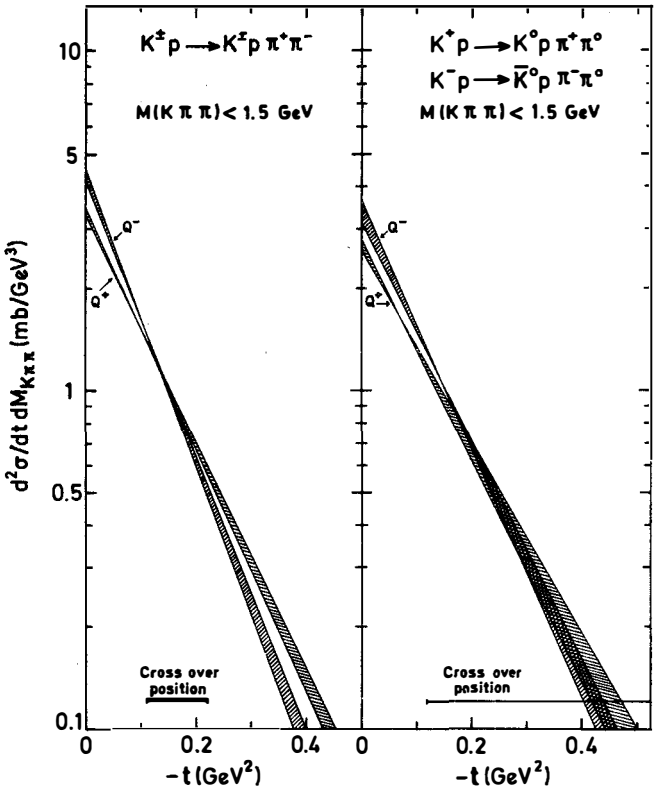


FIG. 5

$d^2\sigma/dt\ dM(K\pi\pi)$ distributions fitted as Ae^{Bt} in the $M(K\pi\pi)$ region between 1 and 1.5 GeV, for reactions $K^{\pm}p \rightarrow K^{\pm}p\pi^+\pi^-$ and $K^{\pm}p \rightarrow K^0p\pi^{\pm}\pi^0$.
The fits have been done for events with $M(p\pi^{\pm}) > 1.5$ GeV in K^- reactions and $M(p\pi^+) > 1.5$ GeV in K^+ reactions [10] in the same t_{pp} interval $0 < |t_{pp}| < 0.4$ GeV^2.
The shaded area represents the extreme values (inside 1 s.d) of the fitted parameters A and B. The absolute normalization error between the K^+ and K^- experiments is estimated at $\pm$ 7 %.

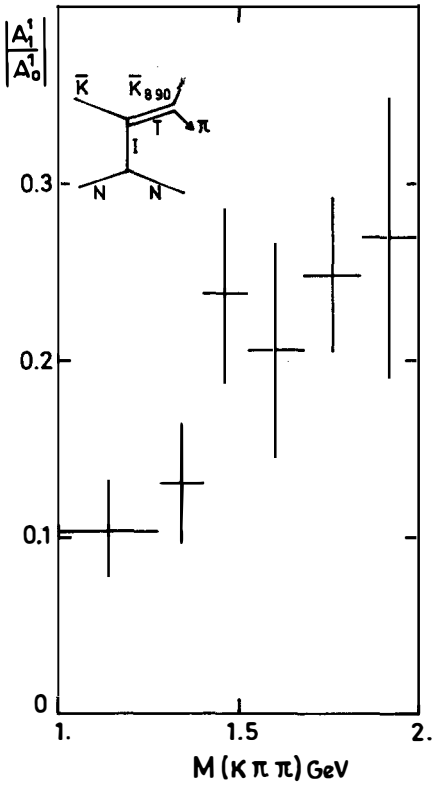


FIG. 6

Ratio of the amplitude moduli $\left|\frac{A_1^1}{A_0^1}\right|$, averaged over t_{pp}, for several K$\pi\pi$ mass intervals.

A_2 PRODUCTION IN π-p COLLISIONS AND POMERON EXCHANGE

Gianni Conforto
Istituto Nazionale di Fisica Nucleare, Sezione di Roma,
Roma 00185, Italy
and
Rutherford High **Energy Laboratory**, Chilton, Didcot,
Berkshire, U.K.





Abstract : The density **matrix** elements **obtained** in experiments studying the A_2 production from pions via the decays $A_2 \to \eta\pi$ or $A_2 \to K\bar{K}$ show that the energy dependence of the natural parity exchange component of the total cross-section is consistent with the $1/p_{inc}$ law and do not support the conclusion reached from the $A_2 \to \rho\pi$ data that some Pomeron exchange must be present in the production process.

Résumé : Les éléments de matrice densité obtenus, dans des expériences où l'on étudie la production du A_2 à partir des π, par l'intermédiaire des désintégrations $A_2 \to \eta\pi$ ou $A_2 \to K\bar{K}$ montrent que la dépendance en énergie de la composante de la section efficace totale correspondant à l'échange de la parité naturelle est compatible avec la loi $1/p_{inc}$ et contredit la conclusion obtenue à partir des données $A_2 \to \rho\pi$ qu'un peu d'échange du Pomeron est présent dans le processus de production.

A recent compilation and analysis[1] of the world π-N $\rightarrow A_2$-N, $A_2 \rightarrow \rho\pi$ bubble chamber data has found that the energy dependence of the natural parity exchange component of the total A_2 cross section is significantly weaker than (incoming π laboratory momentum $\equiv p_{inc})^{-1}$.

In terms of Regge pole phenomenology, this result is described by the value $\alpha(0) = 0.85 \pm 0.05$ obtained for the intercept of the effective trajectory. This value is substantially higher than the canonical ~ 0.5 expected on the basis of a dominating f_o exchange.

Thus the presence in A_2 production of a contribution due to the Pomeranchuk singularity P with an $\alpha(0) \sim 1$ is apparently established.

As the presence of Pomeron exchange in π-N $\rightarrow A_2$-N implies a violation of the so far rather well obeyed Gribov-Morrison selection rule[2], it is interesting to examine whether this effect is confirmed by the π-N $\rightarrow A_2$-N, $A_2 \rightarrow K\bar{K}$ or $A_2 \rightarrow \eta\pi$ data.

Because of the small branching ratios involved, the number of events available in these two channels is rather limited. On the other hand the very small amount of non-resonant $K\bar{K}$ or $\eta\pi$ background renders any background subtraction much easier and the rather involved analysis used for the $\rho\pi$ channel unnecessary.

A compilation of the total cross section data for the process $\pi^- p \to A_2^- p$, $A_2 \to K\bar{K}$ is shown in Fig.1. The data are evidently quite consistent with the $1/p_{inc}$ slope indicated in the figure.

The crucial question, therefore, is what is the energy dependence of the natural parity exchange fraction of the total cross section.

As ρ_{22} and ρ_{2-2} are both negligible[3], this quantity is given by $\rho_{11} + \rho_{1-1}$[4].

The available data, plotted as a function of p_{inc}, are shown in Fig.2.

The points at 4.5, 5-16 and 21 GeV/c come from references 5, 6 and 7 respectively. On the basis of these three points, it seems almost inevitable to conclude[8] that the energy dependence of $\rho_{11} + \rho_{1-1}$ is roughly $p_{inc}^{+0.5}$, which implies an energy dependence of the natural parity exchange component of the total cross section weaker than $1/p_{inc}$, in agreement with the results obtained from the $\rho\pi$ data.

The point at 6.0 GeV/c is still preliminary. It comes from an experiment[9] studying A_2 production from 6 GeV/c π^- via the decays $A_2 \to \eta\pi$ and $\eta \to \gamma\gamma$ in the momentum transfer range $0.27 \leq -t \leq 0.42$ $(GeV/c)^2$. Some results of this experiment have already been published[10]. The value of ρ_{11}[11] comes from the

observed distribution of the polar angle θ in the Gottfried-Jackson frame for which the apparatus has a non-uniform efficiency. A Monte Carlo calculation has been used to correct for this effect. The azimuthal angle ϕ, whose distribution yields the value of ρ_{1-1}, is instead observed with an almost uniform efficiency and no correction has been applied to data[11]. The χ^2 fit shows that this is an acceptable approximation.

Taking all experiments at their face values, there is a marked inconsistency between the 4.5 and 6.0 GeV/c results. It is unlikely that this could be due entirely to the limited t range accepted in the 6.0 GeV/c experiment as about 1/3 of the total cross-section is covered in this experiment and an unplausibly large t dependence of the density matrix elements would be necessary to explain the observed discrepancy. Since ρ_{11} and ρ_{1-1} are bound to be ≤ 0.5 and are experimentally close to this limit, any statistical fluctuation or systematic error will have an asymmetric effect in decreasing rather than increasing their values.

Even if, by splitting the blame equally between the two experiments, one takes $\rho_{11} + \rho_{1-1} \approx 0.75$, it is clear that the energy dependence of the natural parity exchange fraction of the total cross-section is much weaker than it was originally accepted.

Thus the natural parity exchange component of the total cross-section is quite consistent with the $1/p_{inc}$ dependence and any

claim for a need of Pomeron exchange in A_2 production in π-p collisions must rely on the $A_2 \to \rho\pi$ data alone.

It is a pleasure to acknowledge many fruitful discussions with E Berger, G Kane, C Michael, G Ringland, R Roberts, J Rosner and D P Roy.

Figure Captions

Fig. 1 Total cross-section for the process $\pi^- p \to A_2^- p$, $A_2 \to K\bar{K}$ as a function of the incoming π laboratory momentum p_{inc}. The dashed line indicates the $1/p_{inc}$ slope.

Fig. 2 Natural parity exchange fraction of the total cross-section for the processes $\pi^- p \to A_2^- p$, $A_2 \to K\bar{K}$ or $A_2 \to \eta\pi$ as a function of the incoming π laboratory momentum p_{inc}.

Footnotes and References

1. U Kruse et al, Batavia Conference, paper 602.
2. V N Gribov, Yad. Fiz. 5, 197 (1967), (Sov.Jour.Nucl.Phys. 5, 138 (1967)); D R O Morrison, Phys. Letters, 25B, 238 (1967).
3. For a review of the experimental evidence as well as a theoretical argument for its explanation see J L Rosner, Proceedings of the Caltech Phenomenology Conference, March 1971, p.387.
4. J P Ader, M Capdeville, G Cohen-Tannoudji and Ph Salin, Nuovo Cimento 56A, 952 (1968).
5. D J Crennel et al, Phys. Letters, 35B, 185 (1971).
6. J Lacy, thesis, University of Illinois, 1971 (unpublished).
7. K Foley et al, Phys. Rev. D6, 756 (1972).
8. C Michael, Batavia Conference, Rapporteur Talk.
9. Chicago-NAL-Toronto-Wisconsin collaboration: G Conforto, A W Key, M Kramer, R Mobley, R Prepost, D Tompkins, D Underwood and M Witherell.
10. R Prepost et al, Proceedings of the 1972 Philadelphia Conference on Meson Spectroscopy, A H Rosenfeld and K W Lai, Editors, American Institute of Physics, New York, 1972, p.379.
    A W Key et al, Phys. Rev. Letters, 30, 503 (1973).
11. A W Key et al, Bull. Am. Phys. Soc., 17, 568 (1972).

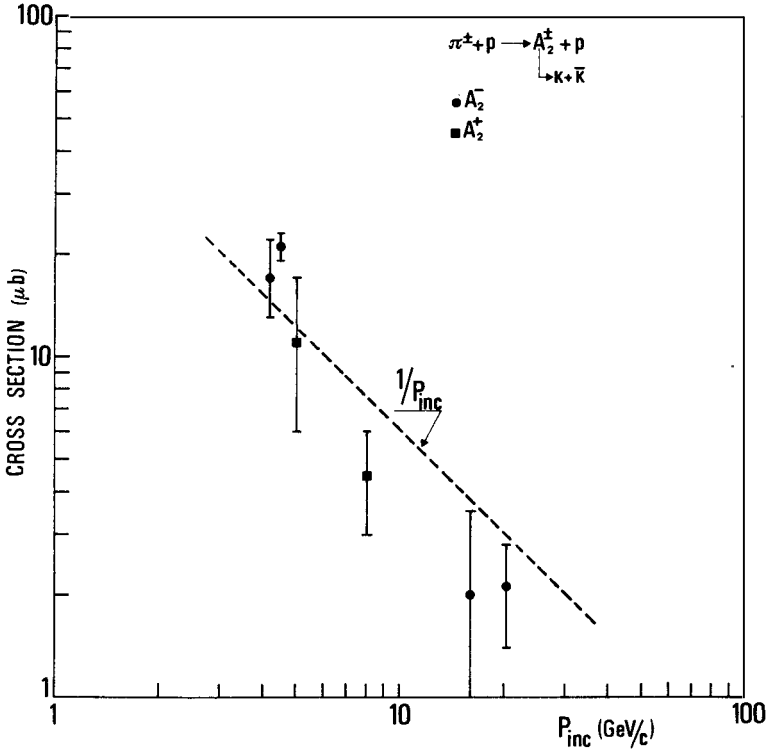

100
10
1
1
10
100
CROSS SECTION (μb)
P_inc (GeV/c)
π±+p → A₂±+p
↳K+K̄
● A₂⁻
■ A₂⁺
1/P_inc

Figure 1

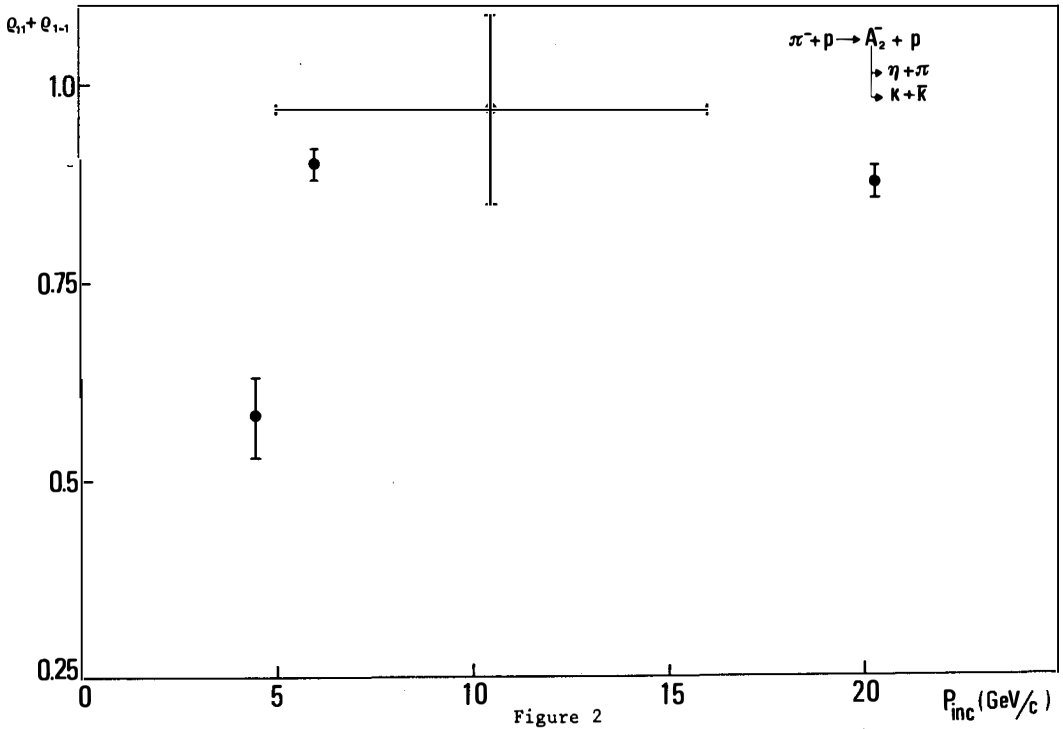

$\varrho_{11}+\varrho_{1-1}$
1.0
0.75
0.5
0.25
0
5
10
15
20
P_{inc} (GeV/c)
$\pi^-+p \rightarrow A_2^- + p$
$\rightarrow \eta+\pi$
$\rightarrow K+\bar{K}$

Figure 2

A NEW MODEL OF DIFFRACTIVE DISSOCIATION*

H. J. Lubatti† and K. Moriyasu
Visual Techniques Laboratory
Department of Physics
University of Washington
Seattle, Washington 98195

Abstract: A new model of diffractive dissociation is presented which explains most of the puzzling features of diffractive reactions. This model is based on an extension of the familiar Harari-Rosner dual quark diagrams. By introducing self-energy corrections to the bare hadron, new classes of dual diagrams are obtained.

The new diagrams which are associated with diffractive dissociation provide simple intuitive explanations for many of the experimental features of diffractive reactions. In particular, the non-resonant behavior of the well-known diffractive enhancements (e.g. the A_1 and A_3) is seen to be a direct consequence of the new diffractive diagrams. Also, by comparing the diffractive reactions $KN \to K\bar{K}\Lambda$ and $KN \to K\pi\pi N$, it is concluded that the $\bar{\lambda}\lambda$ content of the hadron is small.



Résumé : On présente un nouveau modèle de dissociation diffractive qui explique la plupart des problèmes posés par les réactions diffractives. Ce modèle est basé sur une généralisation des diagrammes de quarks duaux de Harari-Rosner. En introduisant les corrections de self-énergie pour les hadrons nus on obtient de nouvelles classes de diagrammes duaux.

Les nouveaux diagrammes qui sont associés à la dissociation diffractive fournissent des explications simples et intuitives pour beaucoup de résultats expérimentaux. En particulier, on trouve que le comportement non résonant des bosses diffractives bien connues (les A_1 et A_3) est une conséquence directe des nouveaux diagrammes diffractifs. On conclut aussi, en comparant les réactions diffractives $KN \to K\bar{K}\Lambda$ et $KN \to K\pi\pi N$, que le contenu $\bar{\lambda}\lambda$ des hadrons est petit.

*Work supported in part by NSF Science Development Grant GU-2655.

†A. P. Sloan Foundation Research Fellow.

I. INTRODUCTION:

Diffractive dissociation remains one of the most puzzling phenomenon in strong interactions. It is a manifestly inelastic process which exhibits most of the features common to elastic processes. Perhaps the most puzzling feature is that the multi-body system into which, for example, a pion dissociates has all of the characteristics of a resonance spectrum. For example, Fig. 1a shows the typical 3-pion mass spectrum obtained in the diffractive dissociation reaction

$$\pi^- d \to \pi^+ \pi^- \pi^- d. \qquad (1)$$

The well known A_1 $(\rho\pi)$, A_3 $(f\pi)$, and recently observed A_4 $(g\pi)$[1] dominate the 3π spectrum. For comparison, the di-pion mass spectrum obtained in the reaction

$$\pi^- p \to \pi^+ \pi^- n \qquad (2)$$

is dominated by the ρ, f, and g-mesons as shown in Fig. 1b. It is well known that such peaks in mass spectra are usually interpreted as resonances described by Breit-Wigner amplitudes, which have both a real and imaginary part. In fact, for reaction (2) the $\pi\pi$ scattering amplitudes have such behavior; however, as has been shown recently in a very nice analysis by Ascoli et al.[2] process (1) has a purely constant phase throughout the A_1 and A_3 mass regions. It thus becomes a central issue in strong interactions to understand the phenomenon which is causing a nonresonant amplitude in reaction (1) to peak near certain mass values.

The purpose of this talk is to present a new model within the framework of the simple quark model which can explain many of the features of diffractive dissociation. A more detailed description of this model has been presented elsewhere.[3)]

In the next section a detailed description of the salient properties of diffractive dissociation is given and the model is presented in Section III. Predictions and comparison with experimental data are made in Section IV.

II. PROPERTIES OF DIFFRACTIVE DISSOCIATION:

Most of the data on diffractive dissociation of hadrons have been obtained in what are called four-body final states in the energy range 5-20 GeV. These processes can be summarized by the following reaction sequence:

$$\begin{array}{l} X + T \to Y + T \\ \qquad\quad \big|\to X^* + \pi \\ \qquad\qquad \big|\to X + \pi \ , \end{array} \tag{3}$$

where X^* is a known resonance which decays into $X + \pi$; X can be a π, K, or N and T is the target.[†] Thus a hadron preferentially dissociates into two particles, one of which is always a pion.

[†]The only exception is when X is a nucleon; in this case, both the dissociation $N \to \Delta(1236)\pi$ and $N \to N\pi$ have been observed and have similar properties.[4)]

These reactions have the following properties which are independent of the incident particle: [5-7]

1. The observed mass distribution peaks near the $M_{X^*} + M_\pi$ threshold, which is always well above the $X\pi\pi$ threshold (examples are the A_1 $(\rho\pi)$, A_3 $(f^0\pi)$, $Q(K^*(890)\pi)$, $L(K^*(1420)\pi)$, and $\Delta\pi$ enhancements).
2. The $X^*\pi$ system is mainly in an $L = 0$ state, which implies that the system Y has unnatural parity for $X = \pi$ or K.
3. The internal quantum numbers of the system Y are identical to those of the incident particle X.
4. The integrated cross sections for such processes are rather large (e.g. $\sigma(\pi p \to A_1 p) \simeq 100\mu b$ at 15 GeV/c) and nearly energy independent (decrease like $P_{LAB}^{-0.5}$).
5. For the A_1 and A_3, the $X^*\pi$ phase is constant throughout the A_1 and A_3 mass regions, which indicates that these $X^*\pi$ systems <u>cannot</u> be resonances.[8] The absence of alternate decay modes and the inability to produce these states with comparable cross sections in charge-exchange or backward production reactions support this conclusion.
6. The A_1 and Q exhibit the cross-over phenomena observed in elastic scattering of pions and kaons.[5-7]
7. The measurement of the interaction cross section of the system Y from coherent nuclear production gives $\sigma_{YN} \simeq \sigma_{XN}$.[9]

8. The diffractive system Y does not conserve s-channel helicity in contrast to elastic scattering.

9. The differential cross section, integrated over the $X^*\pi$ mass spectrum, has an exp (bt) dependence, where the slope b has approximately the same value obtained in XT elastic scattering. For small $X^*\pi$ masses, however, the slope is $\sim$ 13-15 GeV^{-2}, which is larger than the elastic values.

The above list summarizes the important features of the diffractive dissociation of hadrons into two particles, one of which decays by pion emission. These processes are by far the most copious.

III. THE MODEL:

Attempts to explain the above features of diffractive dissociation have not been very successful. It is our feeling that a new mechanism is needed in order to understand the properties of diffractive dissociation. Reasoning from intuitive physical arguments, it is felt that diffractive dissociation should be related to the internal structure of the hadron. This is in keeping with the original suggestion of Good and Walker[10] that diffractive dissociation occurs through the interaction of the eigenstates which make up the dissociating object. A classical example is pair production where the interaction of the virtual leptons in the photon results in the materialization of an

electron-positron pair; another example is the regeneratization of K_S from K_L through the differential absorbtion of K and $\bar{K}$ in hadronic matter.

The basic notion of the new model is that the hadron is expanded in terms of virtual $q\bar{q}$ pairs as shown in Fig. 2. The basic quark model, we remind the reader, pictures the meson as a $q\bar{q}$ pair and the baryon as three quarks (qqq). In this model, we add self-energy corrections which are assumed to be SU(3) singlets with vacuum quantum numbers. It should be stressed that the expansion given in Fig. 2 is the wave function of the physical hadron as seen by a stationary observer. Thus, this point of view is very similar to that of QED.

In this picture, the greater the energy the more probable are the higher order terms. However, at any fixed energy, the higher order terms give relatively smaller contributions than those of lower order. This is due to the fact that the creation of the virtual $q\bar{q}$ pairs can be thought of as a "restoring force" which prevents the valence quarks from moving too far apart and escaping. Thus the higher order terms are smaller since they are related to the probability that the valence quarks are further apart.

The most important consequence of this model is that in addition to the usual interactions between valence quarks (VV-interactions) there also occur interactions between valence quarks and the internal $q\bar{q}$ loops (VL-interactions) and interactions between internal loops (LL-interactions); moreover, we assume that any of

these interactions can be accompanied by the "radiative decay" of one or more internal $q\bar{q}$ loops, where the resulting quarks and antiquarks then combine with the valence quarks to produce new outgoing hadrons. These radiative reactions will be denoted by VV(R), VL(R), and LL(R) according to whether the principal interaction was VV, VL, or LL. The diagramatic convention which is used for representing each class of interaction is given in Fig. 3.

It is further assumed, following Harari and Rosner,[11] that the hadronic interaction is mediated by $q\bar{q}$ or qqq exchanges. The basic rules for constructing dual quark diagrams are the same as those of Harari and Rosner:

(i) Baryons are represented by three quark lines and mesons by one quark and one antiquark line.

(ii) Quark lines do not change their identity.

(iii) The two ends of a single quark line cannot belong to the same external particle.

(iv) Those channels in which there are no quark lines crossing one another (planar) will be dual to direct channel resonances.

These rules are not sufficient for the new VL and LL interactions since they say nothing about the radiative break-up of the $q\bar{q}$ loops. It is therefore postulated that the SU(3) quantum numbers of the quarks involved in loop interactions are unchanged. This leads to the additional rule:

(v) Quark lines do not change their identity in loop

interactions even if the loop is broken by a radiative decay.

Rule (v) places a strong restriction on the radiative decay of the $q\bar{q}$ loops and allows only certain classes of VL and LL diagrams. It results in a new definition of diffractive dissociation as well as definite predictions and selection rules that can be tested experimentally.

The new classes of dual quark diagrams which result from the inclusion of $q\bar{q}$ internal loops will now be considered. The interaction between a meson and a baryon is given by the sum of terms

$$\langle M|B\rangle = \sum_{i,j} M_i B_j \qquad (4)$$

which contains all VV, VL, LL interactions, as well as radiative decays of $q\bar{q}$ loops.

The lowest (zeroth) order term in eq. (4) gives the familiar Harari-Rosner diagrams for meson-baryon scattering. These are illustrated in Fig. 4. Figure 4a has meson states in the t-channel which are dual to baryon resonances in the s-channel. Fig. 4b which is nonplanar, has the same t-channel mesons but has resonances in the u-channel and not in the s-channel. In terms of Regge-poles, this means that the exchange in Fig. 4a has a rotating phase $\exp(-i\pi\alpha(t))$ while the exchange in Fig. 4b has a purely real phase. Both diagrams can contribute to elastic or two-body inelastic scattering in lowest order.

The first-order terms M_0B_1 and M_1B_0 are the lowest order in which loop interactions can occur. According to our quark diagram

rules, an exchanged $q\bar{q}$ pair which couples only valence quarks (VV) can be in either an SU(3) singlet or octet;[†] however, because the internal loop is postulated to be an SU(3) singlet with vacuum quantum numbers only a $q\bar{q}$ exchange in an SU(3) singlet state with vacuum quantum numbers can couple a valence quark of one hadron to the $q\bar{q}$ internal loop of another. The same statement is true for LL interactions between two loops. The physical processes which result from the first-order terms M_oB_1 and M_1B_o are illustrated in Fig. 5.

The first process to consider is the interaction between two valence quarks. If there is no radiative decay, the results given in Figs. 5a and 5c can be thought of as vertex corrections to (or mass renormalizations of) the basic M_oB_o interactions of Fig. 4. When there is a radiative decay of the $q\bar{q}$ loops, the internal quarks recombine with the valence quarks and result in multi-particle production which is illustrated in Figs. 5b and 5d.

The VL interaction results in the diagram of Fig. 5e which can be recognized as the diagram which has been proposed as a representation for the t-channel exchange of the Pomeron.[12] This diagram has t-channel vacuum quantum numbers which is guaranteed by rule (v) and the vacuum quantum numbers of the $q\bar{q}$

[†]This is the usual assumption which neglects exotics. The inclusion of exotic exchanges between valence quarks should not alter any of the conclusions reached in this paper.

loop. Furthermore, it contributes pure non-resonant s-channel background to elastic scattering because it has no s-channel poles. From the point of view of the dual absorption model,[13] diagram 4e is the lowest order term in building up the elastic Pomeron. It is also interesting to note that Figs. 5a and 5e are the lowest order unitarity diagrams obtained by iterating the basic Harari-Rosner diagrams in Fig. 4 through s-channel unitarity.

The valence-loop interaction with a radiative decay leads to the new diagram, Fig. 5f, which we associate with diffractive dissociation. The physical process corresponds to the production of a three-body final state - a manifestly inelastic process - by the same VL interaction which builds up the elastic Pomeron (Fig. 5e). Hence, the t-channel (indicated by the dashed line in Fig. 5f) has quantum numbers of the vacuum. Another new, important property of this diagram is the nonplanar twist in the quark lines connecting the two outgoing mesons. This means that the amplitude for the two-meson subchannel will have a purely real phase and is therefore nonresonant.

The motivation for associating the diagram in Fig. 5f with diffractive dissociation is clear. It has the same VL interaction as elastic scattering and thus leads to the novel idea that the "elastic" Pomeron and diffractive dissociation both arise from the same source. As will be discussed in the next section, the connection between Fig. 5f and diffractive dissociation provides the strongest tests of the basic postulated of this model.

IV. PREDICTIONS AND COMPARISON WITH DATA:

A. Single diffractive dissociation of hadrons should be most probable for nonresonant two particle final states which conserve the internal quantum numbers of the incident hadron.

(i) Thus, we expect large cross sections for $\pi \to \rho\pi$, $f\pi$, $g\pi$---; $K \to K^*(890)\pi$, ρK, $K^*(1420)\pi$---, $N \to N\pi$, $\Delta\pi$--, and experimentally these states are the most copious.

(ii) All of these states are predicted to be nonresonant in lowest order, which is in agreement with the analysis of Ascoli et al.[2] for the A_1 and A_3.

(iii) $\pi \to 3\pi$, $K \to K\pi\pi$ should be suppressed since these reactions can oocur only in second order.

B. The strange quark content is preserved in diffractive dissociation; therefore, diffractive dissociation of a nonstrange hadron on a nonstrange target into strange hadrons is forbidden in lowest order.

(i) The reaction $\pi p \to (K^*(890)\bar{K})^- p$ is found to have $25 \pm 5\mu b$ [14] cross section at 7 GeV/c, which is much smaller than the cross section for $\pi \to \rho\pi$.

(ii) $\sigma(Kp \to K\phi p) \simeq 11\mu b$ at 10 and 13 GeV/c[15] which is much smaller than the case $K \to K\rho$ which is allowed.

(iii) The reactions $K^{\pm} p \to K^{\pm} (K^{+} \Lambda)$ are allowed and show the characteristics of diffractive dissociation. However, the cross sections are found to be only $\sim 10\mu b$.[16] This can be interpreted as evidence that the $\lambda\bar{\lambda}$ content of the hadron is much smaller than the $p\bar{p}$ and $n\bar{n}$ content.

C. Production of Baryon-antibaryon pairs by mesons is forbidden in lowest order. Thus, production of $N\bar{N}$, $\Delta\bar{\Delta}$, etc. by pions or $\bar{N}\Lambda$, $\bar{N}\Sigma$ by kaons is absolutely forbidden in first order. In addition, the baryon-antibaryon states which are produced in second order are predicted to be nonresonant. At 13 GeV/c, the cross section for the reaction $\pi^{+} p \to (p\bar{n})p$ is found to be $39 \pm 5\mu b$,[17] which is an order of magnitude smaller than $\pi^{+} p \to \pi^{+}\pi^{o} p$.

D. S-channel helicity is conserved in lowest order in elastic scattering and in diffractive dissociation for the undissociated hadron. Thus we predict, for example, that in the reaction $\pi N \to A_1 N$, only the nucleon helicity will be conserved. There exists no experimental data to test this prediction.

E. This model also predicts a cross-over effect for diffractive dissociation similar to that observed in elastic scattering. The diffractive diagram, Fig. 5f, can interfere with a Regge-exchange term to produce a cross-over. The interference comes from the $M_o B_1$ term with a VV(R) interaction leading to the final state shown in Fig. 5d but with a twist in the quark lines connecting the two mesons. The twist ensures that there will be maximal interference since both amplitudes have real phases in the

two-meson subchannel. Any other amplitude such as Fig. 5b, which has a large imaginary part in the two-meon subchannel, should not contribute as large an interference term.

The above prediction agrees with a recent SLAC experiment[18] on the reactions $K^o p \to Q^o p$ and $\bar{K}^o p \to \bar{Q}^o p$. The differential cross sections show a cross-over effect which is similar to that of $K^+ p$ and $K^- p$ elastic scattering. This is an important test of our model. The slope of $d\sigma/dt$ for $\pi^- p$ elastic is slightly steeper than that of $\pi^+ p$ elastic which in the Deck model would predict that the Q^o slope is steeper than that of the $\bar{Q}^o$ in contradiction to the experimental data.

F. The observation that the unstable particle cross sections $\sigma(A_1 N)$ and $\sigma(QN)$ determined from coherent production on heavy nuclei[9] are nearly equal to $\sigma(\pi N)$ and $\sigma(KN)$, respectively, can be simply understood. Because the observed hadrons result from the break up of a $q\bar{q}$ loop, it takes a certain time for the quarks to rearrange themselves and separate so that the two hadrons can interact separately. This time delay in converting the incident particle to the final diffractive state is limited by the speed of light; hence, the system will leave the nucleus before the separation occurs.† A similar phenomenon known as the Chudakov

---

†Goldhaber[20] and Feinberg[21] have proposed a similar explanation in the context of other hadron models.

effect[19] occurs for e^+e^- production. When the e^+e^- are initially produced, their wave functions overlap and they form an electrically-neutral system that does not produce ionization until they separate.

ACKNOWLEDGEMENTS

The hospitality and excellent organization created by our host, Tran Thanh Van, is gratefully acknowledged. We also wish to thank Carol Jones for the careful preparation of the manuscript.

REFERENCES

1) K. Moriyasu et al., Bull. Am. Phys. Soc. 18, 105 (1973) and VTL-HEP-19 (Feb. 1973).

2) G. Ascoli et al., Phys. Rev. D7, 669 (1973).

3) H. J. Lubatti and K. Moriyasu, "Diffractive Dissociation and Hadron Structure", VTL-PUB-11. To be published in Nuclear Physics.

4) D. Lissauer et al., Phys. Rev. D6 (1972), 1852.

5) G. L. Kane, Acta Physica Polonica B3 (1972), 845.

6) H. J. Lubatti, Acta Physica Polonica B3 (1972), 721.

7) D.W.G.S. Leith, "Diffraction Dissociation", SLAC-PUB-1141. To be published in Proceedings of XVI International Conference on High Energy Physics, Batavia, Illinois, Sept. 6-13, 1972.

8) Yu.M. Antipov et al., A_1 and A_2 Production at 40 GeV/c, AIP Conf. Proceedings, Experimental Meson Spectroscopy, 1972, (eds. A. H. Rosenfeld and K. W. Lai), (American Institute of Physics, New York, 1972), 164; Illinois-GMHS-H-ABBCH-ND-W Collaboration and CIBS Collaboration, Study of A_3 in $\pi^- p \to \pi^+ \pi^- \pi^- p$, ibid, p. 185; G. Ascoli et al., Phys. Rev. D7 (1973), 669.

9) C. Bemporad et al., Nucl. Phys. B33 (1971), 397; W. Beusch, Acta Physica Polonica B3 (1972), 679.

10) M. L. Good and W. D. Walker, Phys. Rev. 120 (1960), 1857.

11) H. Harari, Phys. Rev. Lett. 22 (1969), 562; J. L. Rosner, Phys. Rev. Lett. 22 (1969), 689.

12) P.G.O. Freund and R.J. Rivers, Phys. Letters 29B (1969), 510.

13) H. Harari, "Phenomenological Duality", Proceedings of International Conference on Duality and Symmetry in Hadron Physics, (Weizmann Science Press, Jerusalem, 1971). H. Harari, "Models for Hadronic Reactions: Duality, Absorption and Quarks", SLAC-PUB-837, (December 1970).

14) R. Diamond et al., "Properties of $K\bar{K}$ and $K\bar{K}\pi$ Systems and Diffraction Dissociation", preprint ORO-3065-26.

15) D.C. Colley et al., Nucl. Phys. B50 (1972), 1; P. Davis et al., Ibid, B44 (1972), 344.

16) D. Cohen et al., "A Study of Λ^o and $\bar{\Lambda}^o$ Final States Produced in 12.7 GeV/c K^+p Interactions", preprint UR-421, COO-305-38. T. W. Ludlam, private communication.

17) J.A. Gaidos et al., "The Reaction $\pi^+p \to (p\bar{n})p$ at 13 GeV/c", preprint COO-1428-317.

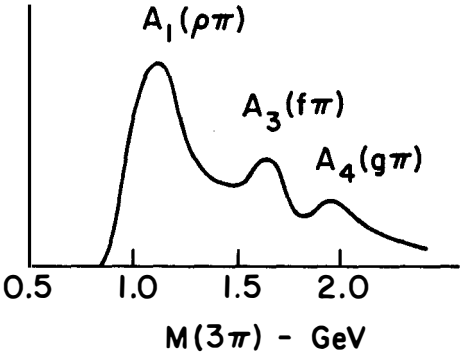
18) G.W. Brandenburg et al., Nucl. Phys. B45 (1972), 397.

See R. Barloutand in the proceedings of this conference.

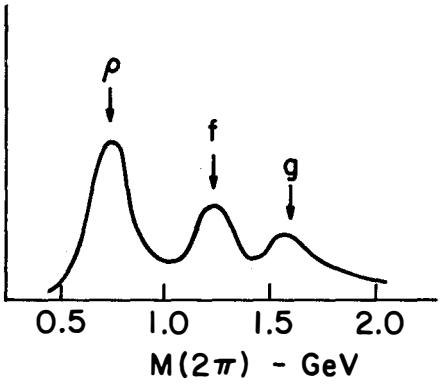
19) A.E. Chudakov, Izvestia Akademii Nauk SSSR seriä fizicheskaya 19 (1955), 650. We are grateful to Prof. J. Bjorken for pointing this out to us.

20) A. S. Goldhaber, Phys. Rev. D7 (1973), 765.

21) E.L. Feinberg, "Interaction Cross Section of Diffractionally Produced Hadrons in 'Status Nascendi'", preprint N 166, P.N. Lebedev Physical Institute, Moscow (Oct. 1972).



(a)



(b)

Fig. 1

Representative mass spectra for:

(a) A pion dissociating into 3 pions.

(b) The production process $\pi N \rightarrow \pi\pi N$.

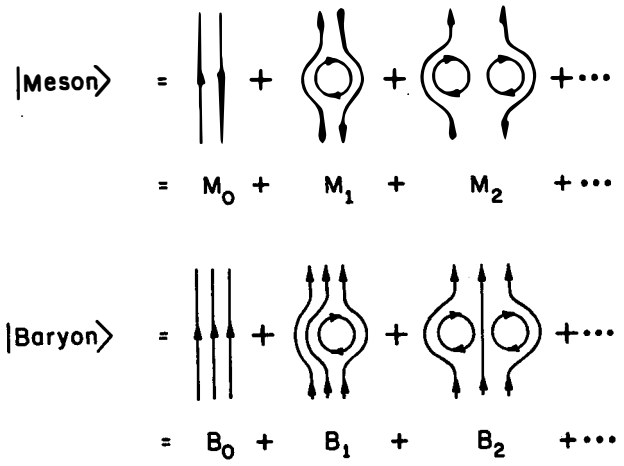


Fig. 2

Expansion of the physical hadron in terms of its self-energy corrections.

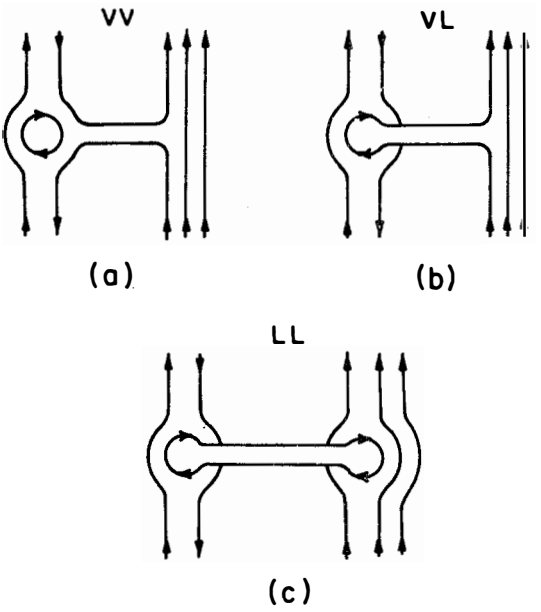


Fig. 3

Diagramatic representation of the three basic interactions between a meson and a baryon

(a) VV-interaction

(b) VL-interaction

(c) LL-interaction

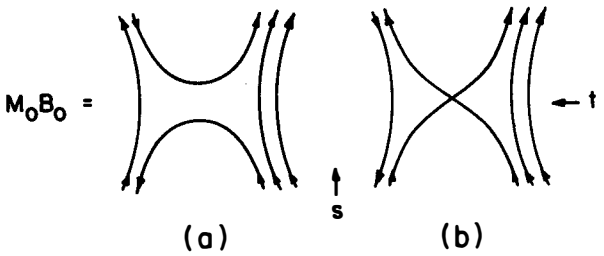


Fig. 4

Harari-Rosner dual quark diagrams for meson-baryon scattering.

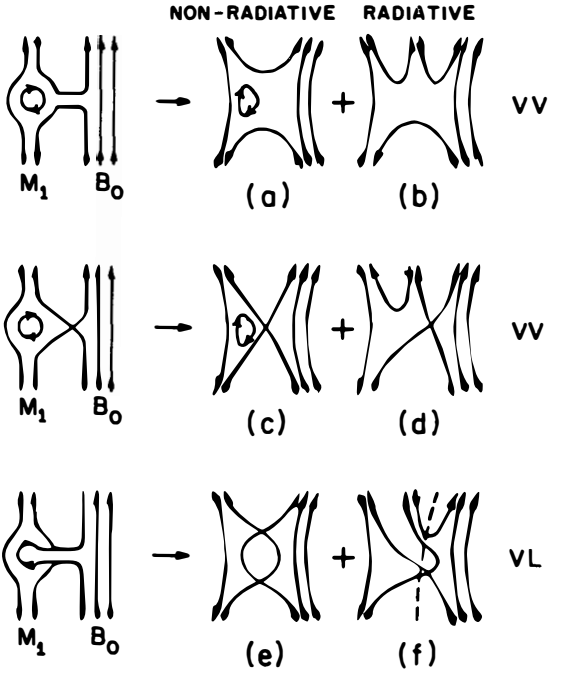


Fig. 5

The possible M_1B_o interactions.

ISOSCALAR EXCHANGE IN VECTOR MESON PRODUCTION

C. Michael

CERN - GENEVA

Abstract : The $I = 0$ exchange contributions to $K^*(888)$, $\bar{K}^*(888)$ and ρ production on nucleons are discussed. The natural parity exchange components are successfully related using SU(3) and exchange degeneracy for the ω anf f_o Regge poles. Limits on a possible Pomeron exchange component are presented.

Résumé : On étudie la contribution de l'échange $I = 0$ dans la production des mesons $K^*(888)$, $\bar{K}^*(888)$ et ρ. On montre que la composante due à l'échange de parité naturelle peut être prédite à partir de SU(3) et de la dégénérescence des poles de Regge ω et f_o. On obtient des limites pour une contribution possible due à l'échange du Pomeron.



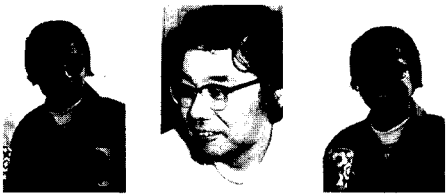
For Publication in the Proceedings on the VIII Rencontre de Moriond on Electromagnetic Interactions held at Meribel-les-Allues (France) March 10-16, 1973

REVIEW ON SCATTERING-AMPLITUDE ANALYSIS*

A. Yokosawa
Argonne National Laboratory
Argonne, Illinois 60439

Abstract: Attempts to determine πN scattering amplitudes at around 6 GeV/c have been made since results of several scattering measurements with polarized-proton targets became available. We discuss new πp charge-exchange polarization data by comparing with various theoretical models and review πN amplitude analyses.

Résumé : Des tentatives d'extraction des amplitudes de diffusion πN à 6 GeV/c ont été faites en utilisant les résultats d'expériences de diffusion sur des cibles de protons polarisés. Nous discutons les nouvelles données de l'échange de charge πp en passant en revue ces analyses en amplitudes ainsi que divers modèles théoriques.



*Work performed under the auspices of the U. S. Atomic Energy Commission

Since preliminary results of the measurements of R and A parameters[1] and of πp charge-exchange polarization[2] became available, a long-waiting crucial task to deduce πN scattering amplitudes has been attempted by several authors. In this talk, I would like, first, to compare results of new πp charge-exchange polarization data[3] obtained from ANL ZGS with various theoretical predictions, second, to review πN-amplitude analyses with an emphasis on the latest analyses[4] using the new data,[3,5] and, finally, to discuss measurements needed to improve scattering-amplitude uncertainty.

New Data and Theoretical Predictions in πp Charge-Exchange Polarization

There are numerous theoretical papers discussing πp charge-exchange polarization. Here I compare some of them with the new data.[3] With the exception of the prediction by Barger and Phillips,[6] which was made before any data in the region $|t| > 0.3$ became available, most of the predictions have perhaps been biased by the preliminary data.[2] Some of the models are actually fitted to the data whenever a preliminary stage was completed, and others stick with the consistency of their fundamental principles.

Figure 1(a) shows predictions by i) Ref. 6 (solid) based on a pole model and finite-energy sum rules, ii) Ref. 7 (dotted) using a new two-pole model, and iii) Ref. 8 (dashed) using exchange degeneracy, SU 3 symmetry, and absorption effects. Figure 1(b) shows predictions by i) Ref. 9 (solid) using ρ Regge pole plus a background term, ii) Ref. 10 (dotted) using fixed-t dispersion relation and a dual-absorption model, (a similar prediction was made by using the complex Regge-pole model[11]) and iii) Ref. 12 (dashed) using a dual-absorption model. Figure 1(c) shows

predictions by i) Ref. 13 (solid), ii) Ref. 14 (dotted), applying a Reggeized absorption model, and iii) Ref. 15 (dashed) using a new absorption model.

There is also one prediction[16] that shows a tremendous energy dependence, but if one takes 5 GeV/c of Ref. 3 and 8 GeV/c of Ref. 2, there hardly exists such an energy dependence.

Review on πN Amplitude Analysis

Ringland and Roy[17] attempted to determine the nonflip scattering amplitudes (I = 1) in πN charge-exchange scattering using the preliminary data of Ref. 2 and results of phase-shift analyses. Their conclusion is somewhat dependent on their theoretical assumptions.

The first direct analysis to determine both I = 0 and I = 1 amplitudes was performed by Halzen and Michael[18] up to $|t| = 0.625$ and then followed by Cozzika et al.,[19] who extended the analysis up to $|t| = 1.0$. Both of these papers defined amplitudes relative to H^{o}_{++}. Giffon fitted the experimental data to a certain formula and their results are in agreement with those of other authors,[18, 19] but in disagreement with the Regge model and the FESR.[20] Using methods of analytic data analysis, Kelly[21] extracted the amplitudes in the angular range $0 < |t| < 1.5$ and attempted to determine the absolute phase.

Although there is no major discrepancy among the above-mentioned papers, we observe some significant difference in determining errors in amplitude values. Here I would like to discuss the most recent analyses with an improved method of analysis using the recent data of πp charge-exchange polarization and $\pi^{\pm} p$ differential-cross-section data.

It is well known that in principle one can determine seven amplitudes algebraically from seven measurements. However,

in reality, we cannot determine amplitudes uniquely without making proper assumptions. The reliability of such assumptions naturally depends upon the accuracy of the experimental data. First, I discuss individual t-by-t analysis, and then t-dependent analysis. These two different analyses compensate each other, and their advantages and disadvantages are summarized as:

Method	Advantages	Disadvantages
t-by-t analysis	Mostly algebraic calculations and limited amount of the data fitting.	i) Eight solutions exist at each $\|t\|$ value. Therefore assume a "shortest-path" approach to determine the smoothest solution passing through each of the eight solutions at individual t. ii) Errors are not realistically calculated. iii) All the data available are not used.
t-dependent analysis	i) All the data available are used for fitting, particularly using the method of an accelerated convergence expansion. ii) Errors can be estimated realistically.	Although the t-by-t analysis gives a good clue to a proper formula to be fitted, some bias exists and a large number of parameters are involved. Some risk is involved about the uniqueness of the final solution.

We have performed two different analyses as follows:

(1) Amplitude Analysis 1 t-by-t analysis)

First we determined the seven amplitudes algebraically from seven measurements [$d\sigma$ ($\pi^+ p \to \pi^+ p$) /dt, $d\sigma$ ($\pi^- p \to \pi^- p$) /dt, $d\sigma$ ($\pi^- p \to \pi^o n$) /dt, $P(\pi^+ p \to \pi^+ p)$, $P(\pi^- p \to \pi^- p)$, $P(\pi^- p \to \pi^o p)$, and $R(\pi^- p \to \pi^- p)$, denoted by σ^+, σ^-, σ^o, P^+, P^-, P^o, and R^-, respectively], obtaining the eight solutions at each momentum transfer. These solutions were used as the starting point in a gradient search, including the additional measurements[1] of R ($\pi^+ p \to \pi^+ p$) and A ($\pi^- p \to \pi^- p$), denoted by R^+ and A^- respectively.

A "shortest-path" approach was used to determine the smoothest solution passing through each of the eight solutions at each individual t. At a given momentum transfer t_2, the distances of each solution from each of the eight at the previous momentum transfer t_1 are calculated from differences in the corresponding amplitudes at t_2 and t_1 with an appropriate metric. We define the distance between solutions as follows: Let $H_1, \ldots, H_7$ be real or imaginary parts of various helicity amplitudes; $M_{ij} = \partial^2 \chi^2 / \partial H_1 \partial H_j$ is the error matrix evaluated at a solution. Then the distance is defined to be

$$d_{12} = \sum_{i=j}^{7} \sum_{j=1}^{7} [H_i(t_2) - H_i(t_1)] M_{ij} [H_j(t_2) - H_j(t_1)].$$

In analogy to "shortest-path" constructions in phase-shift analysis, we find solutions with smoothest dependence on momentum transfer by minimizing the total distance between neighboring solutions.

The new charge-exchange polarization data[3] at 5 GeV/c and the recent σ^+ and σ^- data[5] at 6 GeV/c were used together with those data of σ^o, P^+, P^-, and R^- used in Ref. 18 and R^+ and A^- as mentioned earlier. The "shortest-path" solutions

covering the $|t|$ range from 0 to 0.625 are given in the plots of Fig. 2. The errors are taken from the diagonal elements of the error matrix and are to be used for relative comparison only. Our convention for helicity amplitudes H_{++} and H_{+-} (following Ref. 18) is such that cross section $d\sigma/dt = |H_{++}|^2 + |H_{+-}|$, in mb/ $(\text{GeV}/c)^2$.

(2) Amplitude Analysis II (t-dependent analysis)

We have done the t-dependent searches to enforce continuity by fitting the data to a particular analytic form. Our analysis differs from Ref. 2 in that we determine amplitudes up to an overall t-dependent phase. Our view is that, since the measured quantities at a given energy are unchanged if every helicity amplitude is multiplied by this phase, it is impossible to determine this phase from the data.

The right- and left-hand cuts are mapped (we call the mapping function ω) onto the edge of a unifocal elipse in the $\cos\theta_{\text{c.m.}}$ plane with $\cos\theta_{\text{c.m.}} = \pm 1$ as fixed points. We write the helicity amplitudes as products of diffractive terms and sixth-order polynomials in ω:

$$H_j = g_j \exp\{-a_j[(4m_\pi^2 - t)^{1/2} - 2m_\pi]\} \times \left[1 + \sum_{n=1}^{6} b_n^j (\omega - 1)^n\right],$$

where g_j, a_j, and b_n^j are the varied parameters and m_π is the pion mass.

The amplitudes at $P_{\text{lab}} = 6.0$ GeV/c were obtained by using all the data points (σ^+ and σ^- from Ref. 5, σ^o from the CERN compilation,[22] P^+ and P^- from Borghini et al.,[23] P^o from Ref. 4 and Drobnis et al.,[24] and R^+, R^-, and A^- from Ref. 1).

A variable metric method [25] incorporating an analytic gradient with respect to search parameters was used to obtain fits to the data.

Figure 3 shows the results at 6.0 GeV/c . (Note that new results are slightly different from those in Ref. 4) The error bands shown in this figure with respect to the best-fit values were obtained by shifting each data point in random manner about its measured value, weighting this shift by a Gaussian function of width given by the experimental error, and repeating the fitting procedure for each set of such random shifts. The fits obtained are found to be unique within the stated errors.

We note that criticism was made by Fox and Griss [26] for ACE phase-shift analyses. However, for this work we limit ourselves to fitting new data over the limited t-range where there are complete measurements. Therefore the use of the ACE method should be considered proper.

Scattering-amplitude Uncertainty versus Experimental Errors

Earlier Fox [27] examined the effect of amplitude determination with respect to experimental errors by using a method similar to our analysis I. Here we study the effect by using analysis II. We either raise or reduce the present experimental error and determine the amplitude uncertainty accordingly. Our conclusion differs from those in Ref. 27. This difference may be caused by the fact that we used all the available data. Although the details of this investigation will be described elsewhere, we outline some of the results, which are $|t|$-dependent, by averaging the entire $|t|$ region is:

Assumed experimental error in R^+ and R^-	Scattering-amplitude uncertainty					
	$RE\ H^0_{+-}$	$IM\ H^0_{+-}$	$RE\ H^1_{++}$	$IM\ H^1_{++}$	$RE\ H^1_{+-}$	$IM\ H^1_{+-}$
Half the present error	No change	Half the present error	No appreciable change		No appreciable change	
Twice the present error		Three times the present error				

Assumed experimental error in P^o	Scattering-amplitude uncertainty			
	$RE\ H^1_{++}$	$IM\ H^1_{++}$	$RE\ H^1_{+-}$	$IM\ H^1_{+-}$
Half the present error	0.8 times the present error	Half the present error		One third the present error
Twice the present error	1.2 times the present error	Twice the present error	No change	1.5 times the present error

It is also clear that a determination of R and A parameters beyond $|t| = 0.6$ is badly needed. In fact, our results of H^1_{+-} amplitude differ from those in Refs. 18 to 21 particularly at around $|t| = 0.6$. Although such difference was mainly due to the new data[3], the continuity at $|t| = 0.6$ is not well established with presently available data.

References

1. For the final version of the preliminary data, see de Lesquen et al., Phys. Lett. 40B, 277 (1972).

2. For the final version of the preliminary data, see P. Bonamy et al., Nucl. Phys. 52B, 392 (1973).

3. D. Hill et al., Phys. Rev. Lett. 30, 239 (1973).

4. P. Johnson et al., Phys. Rev. Lett. 30, 242 (1973).

5. I. Ambats et al., Phys. Rev. Lett. 29, 1415 (1972).

6. V. Barger and R. E. N. Phillips, Phys. Rev. 187, 2210 (1969).

7. E. Leader and B. Nicolescu, to be published in Phys. Rev.

8. B. Sadoulet, Proceedings of the Seventh Recontre de Moriond, Vol. 1, 207 (1972).

9. S. Kogitz and R. K. Logan, Phy. Rev. D4, 3289 (1971).

10. G. H. Ghandour and R. G. Moorhouse, Phy. Rev. D6, 856 (1972).

11. R. T. Park et al., Phys. Rev. D6, 3162 (1972).

12. J. S. Loos and J. A. J. Matthews, preprint (1972).

13. B. J. Hartley, and A. L. Kane, preprint (1973).

14. J. Anderson et al., RHCM/71/4 (1972).

15. G. A. Ringland et al., Nucl. Phys. B44, 395 (1972).

16. H. Navelet et al., XVI International Conference on High Energy Physics (1972).

17. G. A. Ringland and D. P. Roy, Phys. Lett. 36B, 110 (1971).

18. F. Halzen and C. Michael, Phys. Lett. 36B, 367 (1971).

19. G. Cozzika et al., Phys. Lett. 40B, 281 (1972).

20. M. Giffon, Nuovo Cimento 7A, 705 (1972).

21. R. L. Kelly, Phys. Lett. 39B, 635 (1972).

22. A compilation of pion-nucleon scattering data, CERN Report No. CERN/HERA 69-1, 1969 (unpublished).

23. M. Borghini et at., Phys. Lett. 31B, 405 (1970).

24. D. Drobnis et al., Phys. Rev. Lett. 20, 174 (1968).

25. W. C. Davidon, ANL Report No. 5990, 1966 (unpublished).

26. G. Fox and M. L. Griss, to be published.

27. G. Fox, 2nd International Conference on polarization targets (1971).

Fig. 1 πp charge-exchange polarization P(t) and theoretical predictions by : (a) Ref. 6 (solid),

Ref. 7 (dotted), and Ref. 8 (dashed); (b) Ref. 9 (solid), Ref. 10 (dotted), and Ref. 12 (dashed); (c) Ref. 13 (solid), Ref. 14 (dotted), and Ref. 15 (dashed).

Fig. 2 πN Amplitudes at 6. 0 GeV/c. The filled and hollow symbols represent real and imaginary parts of the amplitude. Data points are at $-t = 0.0,\ 0.125,\ 0.250,\ 0.375,\ 0.500$ and 0.625 $(GeV/c)^2$.

Fig. 3 πN amplitudes at 6. 0 GeV/c as determined from t-dependent fit shown by dark lines. The error bands are represented by shaded regions.

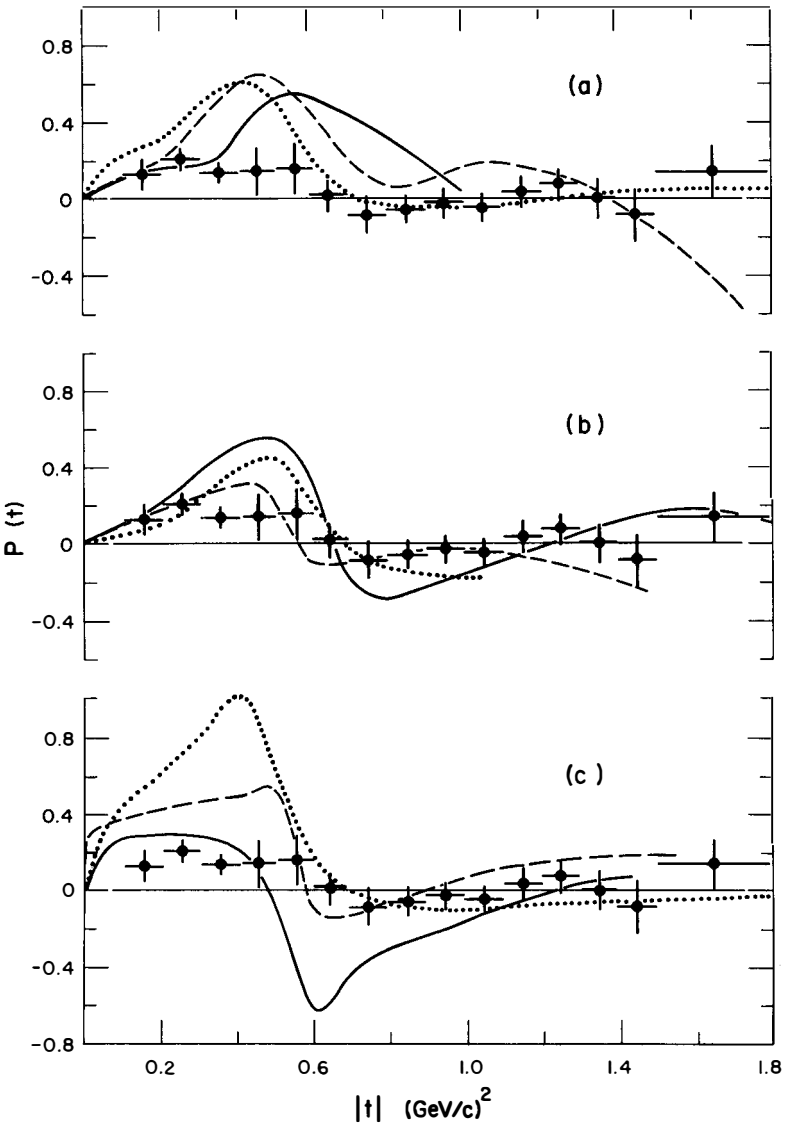


Fig. 1

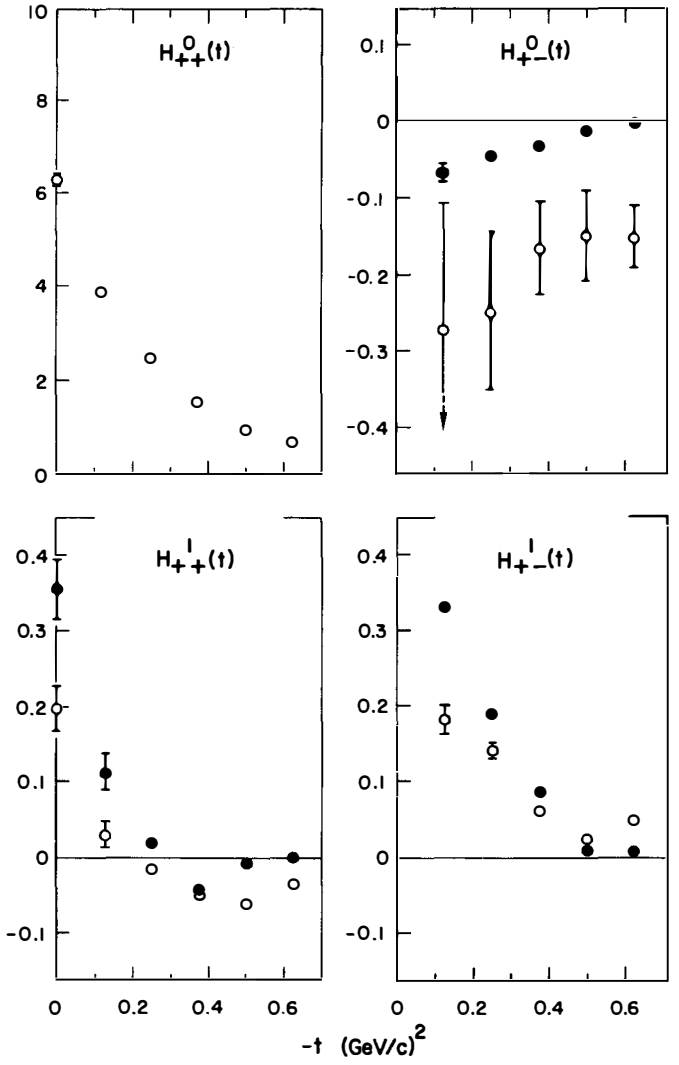


Fig. 2

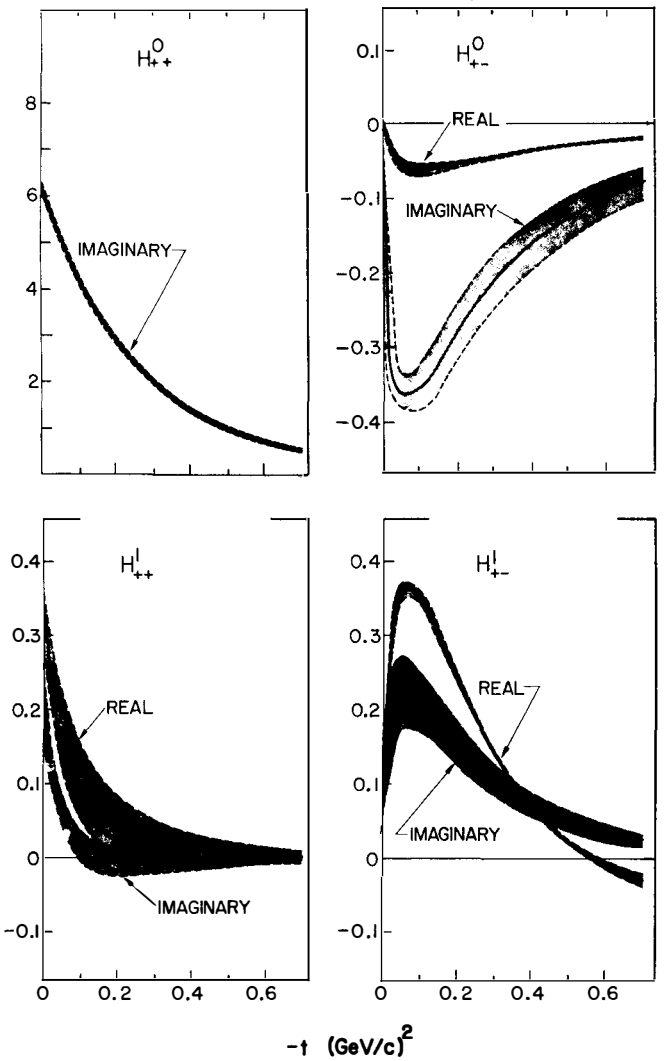

H^0_{++}
IMAGINARY
H^0_{+-}
REAL
IMAGINARY
H^I_{++}
REAL
IMAGINARY
H^I_{+-}
REAL
IMAGINARY
-t (GeV/c)^2

Fig. 3

SOME PROPERTIES OF ABSORPTIVE CORRECTIONS

A.D. Martin and P. Estabrooks
CERN - Geneva



Abstract : Absorptive corrections to Regge pole exchange are isolated in a non-flip $\pi^-p \to \pi^-\pi^+n$ reaction amplitude. The strength of absorption is found to decrease rapidly as the mass of the produced $\pi^-\pi^+$ system increases. In particular, the Williams model, which has been found to give a good fit of the small t data in the ρ region, is no longer satisfactory in the f region.

Résumé : Les corrections absorptives à l'échange d'un pôle de Regge sont déterminées dans une amplitude non-flip pour la réaction $\pi^-p \to \pi^-\pi^+n$. On trouve que les corrections deviennent moins importantes avec l'augmentation du poids du système $\pi^-\pi^+$. Le modèle de Williams, qui est satisfaisant dans la région du ρ, ne l'est plus dans la région du f.

An outstanding puzzle in the description of high energy scattering processes is the nature of absorptive corrections to Regge pole exchange. It is generally agreed that such corrections exist and several model dependent attempts at obtaining their general systematics have been made [1]. However, experimental results show that the predictive power of existing absorption models is limited. We are forced to conclude that, as yet, there is no reliable theoretically based prescription for calculating the size or structure of the absorptive effects. Amplitude analyses of spin 0 - spin $\frac{1}{2}$ scattering data tend to confirm the expectations that the absorptive corrections to Regge pole exchange are more important in helicity non-flip than in helicity flip amplitudes [2]. However, empirical estimates of their strength require an assumption about the structure of the Regge pole contributions.

Here we emphasize that the high statistics data for the reaction $\pi^- p \to \pi^- \pi^+ n$ offer an excellent opportunity for studying the phase, s, $M_{\pi\pi}$ (and to a lesser extent t and L) dependence of absorption in a much more model independent way. The variables are indicated in Fig. 1. Consider high s, small t, and a region of $M_{\pi\pi}$ where only S and P wave $\pi^-\pi^+$ production is dominant. Then the observable s channel moments of the $\pi^-\pi^+$ angular distribution can be expressed in terms of the production amplitudes as follows [3]

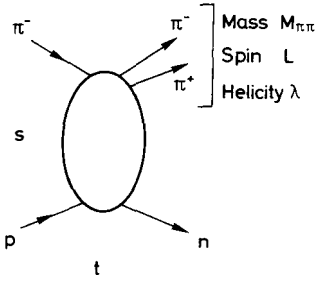


Figure 1 : Variables for the reaction $\pi^- p \to \pi^- \pi^+ n$.

$$
\begin{aligned}
\langle Y_0^0 \rangle &= |S|^2 + |P_0|^2 + |P_+|^2 + |P_-|^2 \\
\langle Y_0^1 \rangle &= 2\mathrm{Re}(S\,P_0^*) \\
\langle Y_1^1 \rangle &= \sqrt{2}\,\mathrm{Re}(S\,P_-^*) \\
\langle Y_0^2 \rangle &= \frac{1}{\sqrt{5}}\,(2|P_0|^2 - |P_+|^2 - |P_-|^2) \\
\langle Y_1^2 \rangle &= \sqrt{\frac{6}{5}}\,\mathrm{Re}(P_-P_0^*) \\
\langle Y_2^2 \rangle &= -\sqrt{\frac{3}{10}}\,(|P_+|^2 - |P_-|^2)
\end{aligned}
\qquad (1)
$$

In terms of the s channel helicity amplitudes $H^{L\lambda}_{\lambda_n\lambda_p}$ we have

$$S = H^{S}_{+-}, \quad P_o = H^{P,o}_{+-}, \quad P_- = \frac{1}{\sqrt{2}}\left(H^{P,1}_{+-} - H^{P,-1}_{+-}\right) \tag{2}$$

$$|P_+|^2 = \tfrac{1}{2}\left|H^{P,1}_{+-} + H^{P,-1}_{+-}\right|^2 + \tfrac{1}{2}\left|H^{P,1}_{++} + H^{P,-1}_{++}\right|^2 . \tag{3}$$

To order $1/s$ the amplitudes (2) arise from unnatural parity (π) exchange and Eq. (3) is due to natural parity (A_2) exchange. We have assumed that the (A_1 exchange) amplitudes

$$H^{S}_{++}, \quad H^{P,o}_{++} \quad \text{and} \quad H^{P,1}_{++} - H^{P,-1}_{++}$$

are negligible in comparison to the respective amplitudes in Eq. (2), apart from including the $O(1/s)$ contributions from π pole exchange as described in Ref. 3). The six observables of Eq. (1) determine $|P_+|$ and the magnitudes and relative phases of S, P_o and P_-. We work with s channel amplitudes since absorption is believed to be simpler in the s channel.

Before looking at the results of such an amplitude analysis we anticipate the t structure of the amplitudes and indicate how the absorptive correction can be isolated. For small t we expect the amplitudes of Eq. (2) to be dominated by π exchange and thus be of the form

$$P_o = M_{\pi\pi}\frac{\sqrt{-t'}}{t-\mu^2}, \qquad P_- = C - \frac{2t'}{t-\mu^2} .$$

For simplicity we have omitted the signature factor on the π pole terms and also slope factors of the form $\exp(bt)$. π exchange contributes equally to H^{-1}_{+-} and H^{1}_{+-}. The former is double helicity flip ($n = 2$) and so is required to vanish in the forward direction like

$t' \equiv t - t_{min}$. Hence the t' in the π pole contribution to P_-. Similarly the A_2 exchange contributions to $H^{\pm 1}_{+-}$ must vanish like t'. However, for the $n = 0$ amplitude H^1_{+-} the π and A_2 absorptive corrections need not vanish in the forward direction and so can be distinguished from the vanishing pole contributions. Hence the term C in P_-. The cross-over zeros observed in the s channel $\langle Y^1_1 \rangle$ and $\langle Y^2_1 \rangle$ moments near $-t = \mu^2$ arise from the destructive interference between C and the π pole term in P_-. There may of course be absorptive corrections to H^0_{+-} and H^{-1}_{+-} but, since they are required to vanish in the forward direction just as their respective pole contributions, they are hard to isolate.

High statistics data exist for the reaction $\pi^- p \to \pi^- \pi^+ n$ at 17.2 GeV/c. An amplitude analysis of the observed s channel moments has been performed for successive 20 MeV $\pi^-\pi^+$ mass bins in order to extract $\pi\pi$ phase shifts [4]. We find two allowed solutions for the amplitude components. A typical example is shown in Fig. 2 ; the points are the results of amplitude analyses at successive t values for the mass bin $700 < M_{\pi\pi} < 720$ MeV. Rather than showing relative phases, S and P_- have been projected into components parallel and perpendicular to P_o on the Argand plot. The amplitudes S and P_o are relevant to $\pi\pi$ phase shift analysis [4]. However, here we are interested in the properties of C, the absorptive correction to H^1_{+-}. It occurs equally in P_- and P_+.

THE PHASE OF C

The absorptive correction C can be isolated with some confidence at small t because to a good approximation the π pole contribution to P_- is determined from a knowledge of P_o

$$P^{\pi}_{-} = \frac{2\sqrt{-t'}}{M_{\pi\pi}} P_o .$$

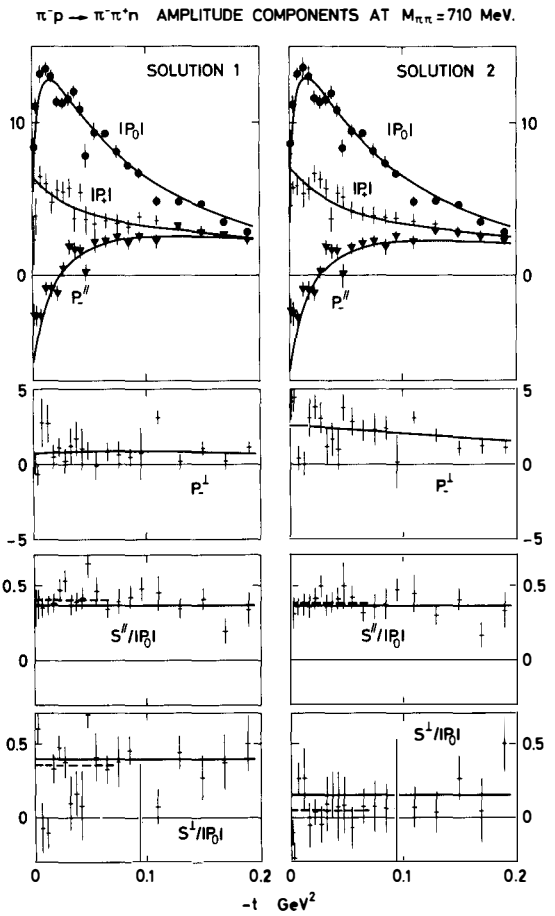


Figure 2 : The amplitude components for $\pi^-p \to \pi^-\pi^+n$ at 17.2 GeV/c obtained from the observed s channel moments for the mass bin $700 < M_{\pi\pi} < 720$ MeV, taken from Ref. 4). Solution 1 is the physical solution

Thus the absorptive correction to H^1_{+-} is

$$C^{\parallel} = P^{\parallel}_{-} - P^{\pi}_{-}, \qquad C^{\perp} = P^{\perp}_{-}.$$

The underlying assumption is that H^1_{+-} is much more affected by absorption at small t than P_o. The results for $P^{\parallel}_{-}$ show the destructive interference of the π pole and absorptive contributions. Moreover $P^{\perp}_{-}$ specifies their relative phase. From Eqs. (1) we see that only the sign of the product $S^{\perp}P^{\perp}_{-}$ is determined and from Fig. 2 we notice that the magnitude of $P^{\perp}_{-}$ differs appreciably in the two solutions. It is here that the $\pi\pi$ phase shift analysis [4] comes to our aid. For example at 710 MeV $S^{\perp}$ is found to be positive. Moreover, a comparison of the predictions of the $\pi^o\pi^o$ mass distribution with that available from $\pi^- p \to \pi^o\pi^o n$ data clearly selects solution 1 as the physical $\pi^- p \to \pi^-\pi^+ n$ amplitudes. The absorptive correction has a small positive component $C^{\perp}$. The components of P_- at the cross-over point $t \approx -\mu^2$ are sketched in Fig. 3. Such a relative phase would be obtained by the prescriptions [see for example Ref. 5)] which calculate C by convoluting a Regge P^{π}_{-} contribution with a dominantly imaginary elastic amplitude. However, absorptive corrections to A_2 exchange may also contribute to C. It is clear that reliable phase information at differing energies will be valuable for unravelling the π and A_2 absorptive corrections to C.

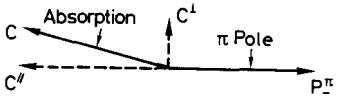


Figure 3 : the components of P_- for $-t \approx \mu^2$. P^{π}_{-} is the π pole contribution. C is the total absorptive correction to the π and A_2 contributions to H^1_{+-}.

s DEPENDENCE

Using $\pi^- p \to \pi^- \pi^+ n$ data [6] at 4.5, 6.95, 15 and 17.2 GeV/c with the produced $\pi^- \pi^+$ system in the ρ mass band we calculate and compare the s dependence of the amplitudes P_o, P_- and P_+ as described in Ref. 7). The results are shown in Fig. 4. Since C contributes equally to P_+ and P_- we have two chances to study its energy dependence at small t. However, due to the destructive interference between the π pole and C contributions to P_-, the more reliable estimate will come from P_+. The results indicate that

$$\alpha^C_{eff} \approx \alpha^\pi_{eff}$$

at small t.

$M_{\pi\pi}$ DEPENDENCE

Rather than presenting the results of the general amplitude analysis as a function of $M_{\pi\pi}$ it is sufficient to consider the following simple analysis since it contains the essential features. Assume that $\pi^- p \to \pi^- \pi^+ n$ is described by π exchange except for the replacement

$$\frac{t'}{t-\mu^2} \to \frac{t'}{t-\mu^2} - C$$

in the evasive $H^{P,1}_{+-}$ amplitude. Take C to be a real constant parameter to be determined in each $M_{\pi\pi}$ bin. Make the same replacement in the evasive amplitudes for D wave $\pi^- \pi^+$ production. Assume all amplitudes have a common slope b, that is, contain a factor $\exp[b(t-\mu^2)]$. The choice C = 1 corresponds to the Williams model [8] or Poor Man's Absorption [9]. In total we have seven parameters C, b and the magnitudes and relative phases of the amplitudes S, P_o and D_o. This simple parametrization gives a good description of all the

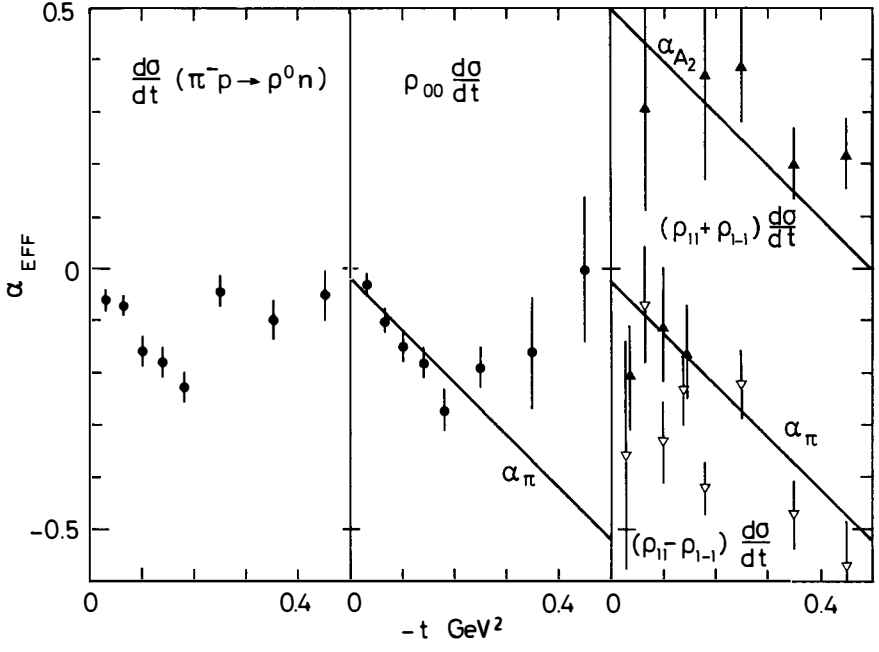


Figure 4 : The effective Regge trajectories for the various components of the $\pi^- p \to \rho^0 n$ cross-section obtained from data at 4.5, 6.95, 15, 17.2 GeV/c as described in Ref. 7). The solid and open triangles are for $|P_+|^2$ and $|P_-|^2$ respectively.

observed moments, $\langle Y_M^J \rangle$ with $J \leq 4$, in the range $0 < -t < 0.1$ GeV^2. The values obtained for C and b are shown as a function of $M_{\pi\pi}$ in Fig. 5. A surprising result is the decrease of the strength of absorption with increasing $M_{\pi\pi}$.

Ochs and Wagner [10] independently obtain this result by taking suitably weighted ratios of the experimental t channel moments $\langle Y_1^J \rangle / \langle Y_o^J \rangle$ integrated over $0.01 < -t < 0.15$ GeV^2. Moreover they observe the same tendency for all J values.

Since the $\pi^+\pi^-$ system is produced in higher spin (L) states as $M_{\pi\pi}$ increases it could be that the strength of absorption really decreases with increasing L (and not $M_{\pi\pi}$). In an attempt to check this we allowed different absorption parameters, C_P and C_D, for the evasive P and D wave amplitudes. However within the errors no systematic dependence of C on L emerged.

The decrease of absorption with increasing $M_{\pi\pi}$ is hard to understand. The conventional absorption prescription could produce such an effect if the slope b_P of the unabsorbed Regge pole amplitude increased with $M_{\pi\pi}$. Assuming the dominant S, P_o, D_o amplitudes are little affected by absorption then $b_P \approx b$, and no such trend is seen in Fig. 5.

An alternative explanation is based on the use of finite mass sum rules and duality to extrapolate the triple Regge limit to low $M_{\pi\pi}$. In this way, Hoyer, Roberts and Roy [11] predict that on average the $M_{\pi\pi}$ dependence of the resonance production cross-section is

$$\left\langle \frac{d\sigma}{dt} \right\rangle = \langle M_{\pi\pi}^2 \rangle^{\frac{1}{2} - 2\alpha_i(t)}$$

where α_i is the exchanged trajectory. As $M_{\pi\pi}$ increases they thus predict that on average :

(a) π exchange increases relative to A_2 exchange amplitudes as $M_{\pi\pi}$;

(b) antishrinkage : the slope decreases as $\log M_{\pi\pi}$.

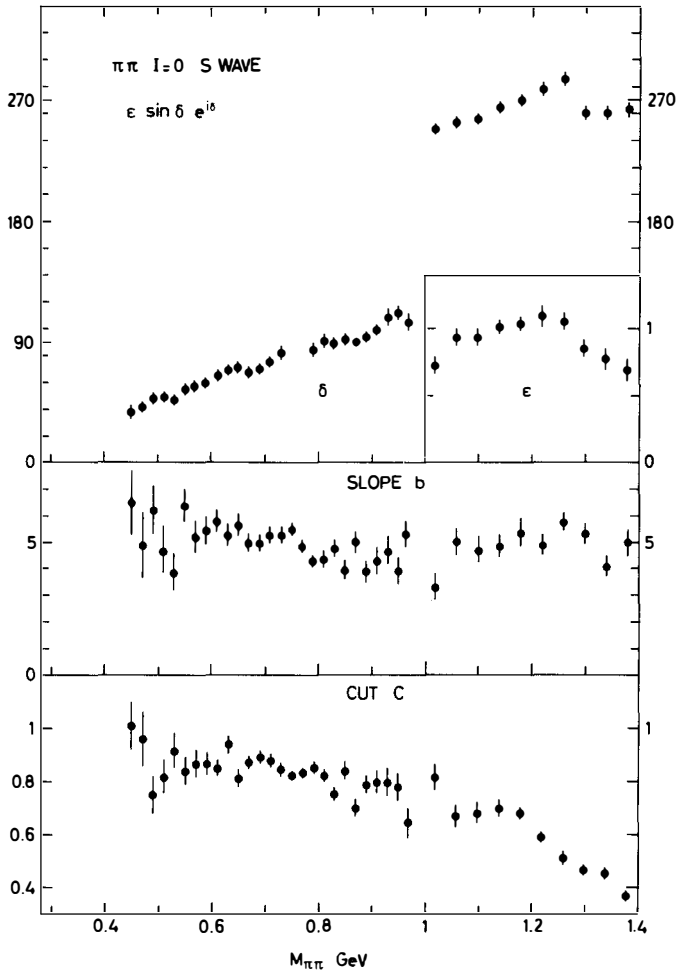


Figure 5 : The $M_{\pi\pi}$ dependence of the slope b and the absorptive correction C, taken from Ref. 4.

The $\pi^- p \to \pi^- \pi^+ n$ data at 17.2 GeV/c show definite support for (a) but not for (b). In a finite energy sum rule and Regge analysis of pion photoproduction data Worden [12] estimates that 40% of C at small t is attributable to the absorptive corrections associated with A_2 exchange. Thus noting (a), he obtains a decrease of C with increasing $M_{\pi\pi}$. However, the amount of the observed decrease, and to a lesser extent, the phase and observed s dependence suggest the explanation is more complicated.

Of course, the $\pi^- p \to \pi^- \pi^+ n$ data have other important implications of absorption, such as the indication of a dip in $\int^H_{00} d\sigma/dt$ at $-t \sim 0.5$ GeV^2 in the 4.5 and 6.95 GeV/c data which is not visible in the higher statistics 17.2 GeV/c data. However, here we prefer to emphasize how many of the empirical properties of absorption can be studied in a more model independent way.

ACKNOWLEDGEMENTS

It is a pleasure to thank Chris Michael for useful discussions and to acknowledge the collaboration of the members of the CERN-Munich experiment.

REFERENCES

1) For example :
M. Ross, F. Henyey and G.L. Kane - Nuclear Phys. B23, 269 (1970) ;
H. Harari - Ann.Phys. 63, 432 (1971).

2) C. Michael - Proceedings of the 4th International Conference on High Energy Collisions, Oxford (1972).

3) P. Estabrooks and A.D. Martin - Phys.Letters 41B, 350 (1972).

4) P. Estabrooks, A.D. Martin, G. Grayer, B. Hyams, C. Jones, P. Weilhammer, W. Blum, H. Dietl, W. Koch, E. Lorenz, G. Lütjens, W. Männer, J. Meissburger, W. Ochs and U. Stierlin - Invited talk by A.D. Martin, to be published in Proceedings of ππ International Conference, Tallahassee, Florida.

5) F. Henyey, G.L. Kane, J. Pumplin and M. Ross - Phys.Rev. 182, 1579 (1969).

6) W. Barish and W. Selove - to be published ;
J.A.J. Matthews et al. - Nuclear Phys. B32, 336 (1971) ;
F. Bulos et al. - Phys.Rev.Letters 26, 1453 (1971) ;
G. Grayer et al. - Proceedings of the 4th International Conference on High Energy Collisions, Oxford (1972).

7) P. Estabrooks and A.D. Martin - Phys.Letters 42B, 229 (1972).

8) P.K. Williams - Phys.Rev. D1, 1312 (1970).

9) G.C. Fox - Proceedings of Cal.Tech. Conference "Phenomenology in Particle Physics", p. 703 (1971).

10) W. Ochs and F. Wagner - M.P.I. Munich Preprint (February 1973).

11) P. Hoyer, R.G. Roberts and D.P. Roy - Rutherford Laboratory Preprint RPP/T/35 (1972).

12) R.P. Worden - Nuclear Phys. B37, 253 (1972) and to be published in Proceedings of Daresbury Meeting on Pion Exchange (1973).

IMPACT PARAMETER DESCRIPTION OF MULTIPARTICLE AND ELASTIC SCATTERING, WITH AN APPLICATION TO THE MULTIPERIPHERAL MODEL*

Frank S. Henyey
Randall Laboratory of Physics
University of Michigan
Ann Arbor, Michigan 48104

Abstract: Impact parameter variables are defined for a multiparticle production process. The equation of unitarity for elastic scattering is written at high energy in terms of these variables. The overall impact parameter can be expressed in terms of the impact parameters of all the produced particles. The unitarity equation becomes an "optical theorem" at each impact parameter -- diffractive scattering is given by beam depletion. These features allow this technique to give a much clearer interpretation of unitarity in any model than has heretofore been possible.

As an application of this technique, the multiperipheral model is examined. Short range order is shown to be equivalent to a random walk in impact parameter. Short range order, with an energy independent correlation length, is shown to be inconsistent with the combination of elastic and multiparitcle data.

Alternative models are suggested by use of this technique.



Résumé : Des variables de paramètre d'impact sont définies pour les processus de production multiple. L'équation d'unitarité est écrite à haute énergie en fonction de ces variables. Le paramètre d'impact total peut être exprimé en fonction des paramètres d'impact des particules produites. Cette équation devient un "théorème optique" pour chaque paramètre d'impact -- la diffraction est donnée par une soustraction d'une partie du faisceau. Grâce à ces propriétés, cette technique permet une interprétation de l'unitarité beaucoup plus claire que celles qui ont été proposées jusqu'ici et ceci pour n'importe quel modèle.

Le modèle multipériphérique est étudié à l'aide de cette technique. On montre que les corrélations de courte portée sont équivalentes à un chemin aléatoire en terme de paramètre d'impact et que les corrélations (à courte portée) dont la portée est indépendante de l'énergie sont incompatibles avec les données, si on tient compte simultanément des données de diffusion élastique et de production multiple.

Cette technique suggère l'emploi d'autres modèles.

*Work supported by the U.S. Atomic Energy Commission.

Introduction

Diffractive scattering at high energy is generally thought to be a rather direct consequence of unitarity. If a reasonably correct description of the bulk of high energy processes were to exist, one could readily calculate diffraction -- that is, the part of high energy scattering described by the "Pomeron." Only for such scattering do the contributions to unitarity dominantly interfere constructively.

However, no sufficiently good description of high energy processes exists. Most of the cross section is due to production processes, which are considerably less well understood than two-body processes. There are several competing models for these multiparticle production processes, none of which are in a sufficiently refined form to reliably calculate elastic (and other diffractive) scattering.

Until now, when a calculation based on any of these models has failed to reproduce the experimental results for elastic scattering (or when the calculation has succeeded in agreeing with some features of the data), it has not been clear whether the calculation should be taken seriously. Perhaps the failure was a consequence of some details or perhaps a consequence of general features of the model. It is the purpose of this work to remedy this defect in our ability to comprehend the

structure of unitarity for elastic scattering. We wish to understand which features of the multiparticle amplitude are important in determining elastic scattering.

There are two distinct types of features which might be important. First are those which are apparent in the data - such things as transverse momentum distributions, multiplicities, etc. These are features of the absolute square of the amplitude, since they show up in the cross section. Second are features related to the phase of the amplitude, and how the phase depends on the momenta of the particles. There is no way of deducing this phase directly from any multiparticle data. (In the case of particles with spin, relative phases between different amplitudes can be determined by polarization measurements. The unknown phase is the overall phase, which depends on the momenta of all the produced particles.)

In the case of two-body scattering at high energy, questions of unitarity and phase have profitably been studied by use of impact parameter as the relevant variable. This suggests that we attempt to understand multiparticle processes as well in the framework of an impact parameter description. The impact parameter is the transverse position of a scattering particle, that is, it is its position in a plane perpendicular to the scattering direction. Thus we will introduce a trans-

verse position, or impact parameter, for each of the produced particles. These impact parameters are, then, just the variables conjugate to the transverse momenta.

As a scattering process occurs, all longitudinal positions are occupied at some time. Therefore there is no apparent advantage in replacing longitudinal momenta. We shall use the longitudinal momentum of each particle (or its rapidity) as the longitudinal variable. We shall see that this is a fortunate choice. In contrast, in the high energy approximation in which the scattering proceeds primarily in one direction (the beam direction), only one transverse position is occupied by each particle. For this reason, impact parameter will be a useful description.

For two-body scattering there is only one impact parameter, not one for each particle. This is a result of the choice of the origin in transverse space. The origin is chosen at one particle and the impact parameter is the position of the other. We shall see that a similar phenomenon occurs for multiparticle states. In this case the arbitrariness of the choice of origin is more apparent. The choice is made to result in a slight calculational convenience; this choice, however, has absolutely no influence on the physics.

So far, our discussion has lacked precision, and has been primarily motivational. For the idea to have

real value it must be made precise, with controlled high energy approximations. Thus we next turn to the definition of impact parameter in multiparticle states, and to a calculation of unitarity for elastic scattering. Afterwards we use the result of this calculation to examine the multiperipheral model and find out whether it is in simultaneous agreement with multiparticle and elastic scattering.

General Treatment

The impact parameter $\vec{b}_j$ is defined as the variable conjugate to the transverse momentum $\vec{k}_j$. $\vec{b}_j$ and $\vec{k}_j$ are two dimensional vectors. An n-particle final state amplitude is transformed to

$$\tilde{M}(\vec{b}_j, p_j) = \int \prod_{j=1}^{n} \left[\frac{d^2\vec{k}_j \, e^{i\vec{k}_j \cdot \vec{b}_j}}{(2\pi)^2} \right] M(\vec{k}_j, p_j) \delta^2\left(\sum_{j=1}^{n} \vec{k}_j \right) \quad (1)$$

The p_j's are longitudinal momenta, and are not transformed.

The momentum conservation delta function makes this slightly different from an ordinary Fourier transform. $\tilde{M}$ is, as a result, only a function of differences of b's. A small amount of algebra establishes the inverse transformation:

$$M(\vec{k}_j, p_j) = (2\pi n)^2 \int \prod_{j=1}^{n} \left[d^2\vec{b}_j e^{-i\vec{k}_j \cdot b_j} \right] \tilde{M}(\vec{b}_j, p_j) \delta^2\left(\sum_{j=1}^{n} \vec{b}_j - \vec{B}_o \right) \quad (2)$$

$\vec{B}_o$ is completely arbitrary; since (transverse) momentum

is conserved, there is an invariance under translations $\vec{b}_j \to \vec{b}_j + \frac{\vec{B}_o - \vec{B}'_o}{n}$. In what follows we will choose $\vec{B}_o = 0$ for simplicity. With this choice it is not necessary to make explicit the dependence of the matrix element only on differences of b's; that is

$$\vec{b}_j = \vec{b}_j - \frac{1}{n} \sum_{j'} \vec{b}_{j'} \ . \tag{3}$$

We wish to compute the imaginary part of elastic scattering at all values of the impact parameter, or equivalently at all momentum transfers for which $t \ll s$. In order to do this, we introduce a set of high-energy approximations, paralleling the usual high energy approximations for two-body impact parameter. We use the rapidity $y_j = \frac{1}{2} \ell n \frac{E_j + p_j}{E_j - p_j}$ as the longitudinal variable. With this choice, if a particle is fast, its energy is almost independent of its transverse momentum, $E_j \sim p_j$ (fast particle). If, on the other hand, it is slow, it contributes little to the energy and longitudinal momentum conservation conditions (i.e. to delta functions in the unitarity equation), except in an average sense if there are many slow particles. Thus we assume $\Sigma E_j = \sqrt{s}$ and $\Sigma p_j = 0$ can be approximately written in terms of only the y_j's. Related approximations are involved in the rotation of the multiparticle state by an angle which rotates the initial state of elastic scattering to

the final state. This rotation is given by $p_j \to p_j - \frac{\vec{k}_j \cdot \vec{\Delta}}{p}$ and $\vec{k}_j \to \vec{k}_j + \frac{p_j \vec{\Delta}}{p}$ where $\vec{\Delta}$ is the momentum transfer in elastic scattering, $t \approx -\Delta^2$ and p is the incident center of mass momentum $s \approx 4p^2$, and we have assumed $\Delta^2 << p^2$. We make the approximations that the matrix element does not vary under the small shift in p_j, and that the p_j in the shift of k_j can be taken independent of variations in k_j, either because p_j is large compared to k_j and is approximately independent of k_j, or it is small and the variations of the term $p_j\vec{\Delta}/p$ as $\vec{k}_j$ is varied are small compared to a typical $\vec{k}_j$. The set of approximations we make can be shown to be good by numerical example. (Unless, for some entirely unknown reason, phases vary much more rapidly than magnitudes of amplitudes.)

These approximations allow the transverse kinematics to be separated from the longitudinal kinematics. Unitarity for the elastic amplitude can be written

$$\text{Im } M_{el}(\vec{\Delta}) = \frac{(2\pi)^4}{2} \sum_n \int \prod_{j=1}^{n} \left[\frac{d^2\vec{k}_j}{(2\pi)^2} \frac{dy_j}{4\pi} \right] M^*(p_j', \vec{k}_j') M(p_j, \vec{k}_j) \cdot$$

$$\delta^2(\Sigma \vec{k}_j) \delta(\Sigma p_j) \delta(\Sigma E_j - \sqrt{s}) \qquad (4)$$

Our approximations allow us to replace p_j' by p_j. We then transform M* and M to impact parameters $\vec{b}_j'$ and $\vec{b}_j$ respectively. We have the Fourier exponentials $e^{-i\vec{k}_j \cdot \vec{b}_j}$

and $e^{+i(\vec{k}_j + \frac{p_j\vec{\Delta}}{p})\cdot\vec{b}'_j}$. By virtue of our approximations, the only k_j dependence is in these exponentials and in the transverse momentum conservations. Thus we can do the $\vec{k}_j$ integrals explicitly, yielding delta functions of $\vec{b}_j - \vec{b}'_j$, and we can integrate the $\vec{b}'_j$'s using these delta functions. Thus M* and M are finally evaluated for the same set of coordinates. Carrying out this algebra in detail, with due regard for all the delta functions, we obtain

$$\mathrm{Im}M_{el}(\vec{\Delta}) = \sum_n \frac{(2\pi)^4}{2}(2\pi n)^2 \int \prod_{j=1}^{n} \left[d^2\vec{b}_j \frac{dy_j}{4\pi}\right] \delta(\Sigma p_j) \cdot \delta(\Sigma E_j - \sqrt{s})\, e^{i\vec{\Delta}\cdot\Sigma\vec{b}_j \frac{p_j}{p}}\, \delta^2(\Sigma\vec{b}_j)\, |\tilde{M}(\vec{b}_j, p_j)|^2. \tag{5}$$

Note again that this only depends on $|\tilde{M}|^2$, rigorously, given our high energy approximations. Finally we transform this to the impact parameter of the elastic scattering

$$\mathrm{Im}\tilde{M}_{el}(\vec{b}) = \sum_n \frac{(2\pi)^4}{2}(2\pi n)^2 \int \prod_{j=1}^{n} \left[d^2\vec{b}_j \frac{dy_j}{4\pi}\right] \delta(\Sigma p_j) \cdot \delta(\Sigma E_j - \sqrt{s})\, \delta^2(\Sigma\vec{b}_j)\, \delta^2\left(\vec{b} - \sum_{j=1}^{n} \frac{\vec{b}_j p_j}{p}\right) |\tilde{M}(\vec{b}_j, p_j)|^2 \tag{6}$$

This is the basic formula of our approach. (In the case with spin, the amplitudes must be taken to be s channel helicity amplitudes, as they are in the ordinary two particle impact parameter representation.)

This formula can be understood very simply. The longitudinal momentum and energy conservation delta functions are familiar enough. The next delta function (two dimensional) refers to the arbitrariness of the choice of origin in impact parameter space. It could just as well have been $\delta^2(\Sigma\vec{b}_j - \vec{B}_o)$. It reminds us that $\tilde{M}$ is really only a function of differences of $\vec{b}$'s. The next two-dimensional delta function is new.[1] Many people[2], guided by the multiperipheral model and their intuition have assumed either $\vec{b} = \Sigma\vec{B}_j$ or $\vec{b} = \vec{b}_1 - \vec{b}_n$, where 1 and n refer to, for example, the nucleons in pp → 2 nucleons + (n-2) pions. If the first of these is to be an approximation to the correct result, the B_j's must be taken to be differences of our b_j's: $\vec{B}_j = \vec{b}_{j+1} - \vec{b}_j$. In this case the $\vec{B}$'s are the variables conjugate to the transverse part of the multiperipheral momentum transfers: $\vec{B}_j \leftrightarrow \vec{Q}_j$, $t_j = Q_j^2$ + longitudinal part. With this definition of $\vec{B}_j$, these two common assumptions become equivalent. They represent an approximation to our result. If $p_1 \approx p$, $p_n \approx -p$, all other p's << p, then $\Sigma(p_j b_j/p) \approx b_1 - b_n$. However in the absence of a definite leading particle, our formula for $\vec{b}$ is a much better approximation.

Our expression allows a simple interpretation. It can be written as $p\vec{b} = \Sigma p_j \vec{b}_j$. Rotating by 90°, we obtain $\vec{b} \times \vec{p} = \Sigma\vec{b}_j \times \vec{p}_j$. Thus the overall impact param-

eter is given by angular momentum conservation. This is not surprising because the p_j/p factor arises from the rotation of the amplitude from the initial to final elastic scattering states. Our approximations have amounted to dropping small complicated parts of the total angular momentum.

A very important part of our result is that it is diagonal; we only need to know the absolute square of $\tilde{M}$, not its phase, in order to calculate ImM_{el}. We have an "optical theorem" at each impact parameter. Our result states that the imaginary part of elastic scattering is given by beam depletion, i.e. by the sum of all cross sections, at each impact parameter. The integral over impact parameter gives the ordinary (observable in practice) optical theorem. Unfortunately, however, impact parameter is not in practice accessible to experimental measurement. We need to know the phase in order to transform to transverse momentum.

Applications

We now turn to applications of our technique. The multiperipheral model (MPM) is an interesting example.[3] Can impact parameter help us understand the relationship between multiparticle and elastic scattering in this model?

The multiperipheral model shares a number of features with the multiparticle data, such as limited

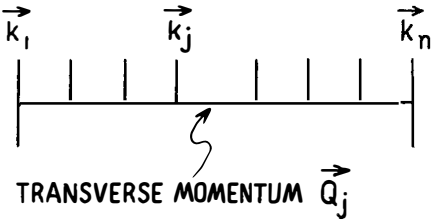


Figure 1(a). The multiperipheral model with the shortest range order possible. $\vec{Q}_j$ is a transverse momentum transfer.

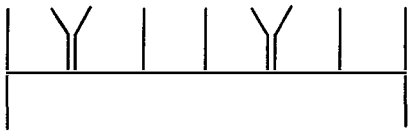


Figure 1(b). A modified multiperipheral model with correlations (clustering). Shown is a process with 6 steps, but with multiplicity minus one equal to 8.

transverse momentum, a spread of longitudinal momenta, etc. We will take these features from the data, so as to use as few details of the model as possible, and also so as not to allow the model to fit elastic scattering by means of a failure to fit multiparticle scattering.

There is, however, one feature of the MPM which is somewhat independent of the multiparticle data, and which distinguishes the MPM from other models which fit multiparticle data equally well. This feature is short range order.

We will first study the model with the shortest range order possible. This model is shown in Fig. 1(a). The amplitude is assumed to factorize into a product of functions of the momentum transfers t_j. Each t_j is given by a function of the p_j's minus Q_j^2, where $\vec{Q}_j$ is the transverse momentum transfer of the j'th link in the multiperipheral chain. There is supposed to be no further dependence of the amplitude on transverse momenta. For simplicity of calculation we take the dependence to be exponential in t_j, corresponding to a gaussian in Q_j although as we go along, it is easily seen that the results are insensitive to the functional form of the amplitudes' dependence on Q_j.

We wish to define variables $\vec{B}_j$ conjugate to the $\vec{Q}_j$. By momentum conservation $\vec{Q}_j$ is given by

$$\vec{Q}_j = \sum_{j'=1}^{j} \vec{k}_j \tag{7}$$

This allows us to relate $\vec{B}_j$ and $\vec{b}_j$. We require, in order for $\vec{Q}_j$ and $\vec{B}_j$ to be conjugate, that

$$\prod_{j=1}^{n} \left[d^2\vec{b}_j \; e^{-i\vec{k}_j \cdot \vec{b}_j} \right] \delta^2(\Sigma\vec{b}_j) = K_n \prod_{j=1}^{n-1} \left[d^2\vec{B}_j \; e^{-i\vec{Q}_j \cdot \vec{B}_j} \right] \tag{8}$$

This equation is solved (uniquely) by

$$\vec{B}_j = \vec{b}_j - \vec{b}_{j+1} \tag{9}$$

and the proportionality constant is $K_n = 1/n^2$.

We can also write the overall impact parameter in terms of the $\vec{B}_j$'s:

$$\vec{b} = \sum_{j=1}^{n-1} \chi_j \vec{B}_j \; . \tag{10}$$

From the condition

$$\vec{b} = \sum_{j=1}^{n} \frac{p_j}{p} \vec{b}_j \tag{11}$$

we obtain

$$\chi_j = \sum_{j'=1}^{j} \frac{p_{j'}}{p} \tag{12}$$

Equation 9 represents a very important feature of the MPM. The natural variable is not the impact parameter $\vec{b}_j$ but the impact parameter <u>step</u> $\vec{B}_j$. The short range order assumption is that the amplitude has the form

$$M_n = Z_n(p_j) \prod_{j=1}^{n-1} F(\vec{Q}_j) \; ; \; \left(M_n = Z_n \prod_{j=1}^{n-1} e^{-R^2 Q_j^2/2} \right) \tag{13}$$

where the first equality in this and following equations is the general result, while the second is for a gaussian distribution. This transforms to

$$\tilde{M}_n = Z_n \prod \tilde{F}(\vec{B}_j) \quad ; \qquad \left(\tilde{M}_n = Z_n \prod e^{-B_j^2/2R^2}\right) \tag{14}$$

(uninteresting factors are included in Z_n). Thus the impact parameter steps are independent. A set of independent steps is the definition of a random walk. Thus we have derived the important result that the MPM is equivalent to a random walk in impact parameter.

There are two consequences we can draw from this result. We assume $\vec{b}_{j-1}$ and $\vec{b}_{j+1}$ are held fixed. Then the uncertainty in $\vec{b}_j$ depends only on the step size ($\Delta\vec{b}_j \sim R$) and not on the number of steps. The root mean square (rms) transverse momentum, $\sqrt{\langle k_j^2 \rangle}$, is related by the uncertainty principle to the rms step size. The precise result is

$$\frac{d\sigma}{dk^2} \sim \int d^2\vec{q} \left| F\left(\vec{q} + \frac{\vec{k}}{2}\right) F\left(\vec{q} - \frac{\vec{k}}{2}\right)\right|^2$$

$$\left(\frac{d\sigma}{dk^2} \sim e^{-R^2k^2/2}\right) \tag{15}$$

From multiparticle data, the average transverse momentum is about 350 MeV/c, and the rms transverse momentum is about 430 MeV/c. We can therefore solve for the step size

$$R^2 \geq 10.9(\text{GeV/c})^{-2} \tag{16}$$

We have written this as an inequality, as in general

the uncertainty principle is an inequality. In what follows we shall take it to be an equality, since any other case is less interesting. More importantly, however, guided by the data, we will take R to be independent of energy in the region of interest.

As a second consequence of the random walk, we know that the rms value of $\vec{b}_1 - \vec{b}_n$ is proportional to the square root of the number of steps taken. The number of steps is n-1, where n is the multiplicity. Thus

$$\langle(\vec{b}_1 - \vec{b}_n)^2\rangle = (n-1)\ R^2 \ . \tag{17}$$

The rms impact parameter is related to $(\vec{b}_1 - \vec{b}_n)$ by

$$\langle b^2\rangle = \langle\chi^2\rangle\langle(\vec{b}_1 - \vec{b}_n)^2\rangle \tag{18}$$

where

$$\langle\chi^2\rangle = \sum_{j=1}^{n-1} \chi_j^2/(n-1) \tag{19}$$

and the χ_j are given by equation 12. We now can calculate elastic scattering by use of equation 5. Before we do this we make a slightly imprecise calculation. We assume for this imprecise version that multiplicities different from the average multiplicity don't matter. In this case, the elastic scattering resulting from a random walk should be gaussian: $\mathrm{Im}\tilde{M}_{el} \sim e^{-b^2/\langle b^2\rangle}$. This transforms to $\mathrm{Im}M_{el} \sim e^{\langle b^2\rangle t/4}$. Putting in our expression for $\langle b^2\rangle$, we get

$$\mathrm{Im}M_{el} \sim e^{\langle\chi^2\rangle\langle n-1\rangle R^2 t/4} \tag{20}$$

We have already calculated the minimum value of R. $\langle n \rangle$ can be taken from data. At P_{LAB} = 100 GeV/c, $\langle n \rangle \approx 10$. $\langle \chi^2 \rangle$ can also be estimated from data as explained below. The result is $\langle \chi^2 \rangle = .6$. From Equation 20, the slope works out to be $\langle \chi^2 \rangle \langle n-1 \rangle R^2/4 = 15$ GeV^{-2}.

We must check to see whether equation 20 needs improvement, and calculate the value of $\langle \chi^2 \rangle$. If neutral particles could be seen, $\langle \chi^2 \rangle$ could be directly calculated from data. Since this is not possible, $\langle \chi^2 \rangle$ must be estimated. The value we obtain is completely insensitive to details.

The curves we show have been calculated from the following model of the combination of data and short range order:

1) Each step is gaussian with $R^2 = 10.9$, as we have calculated.

2) Each event is replaced by one in which the rapidities are equally spaced. The first and last particles (nucleons) have transverse mass 1 GeV/c^2; all other particles (pions) have transverse mass 390 MeV/c^2 (slightly larger than the 350 MeV/c transverse momentum).

3) Multiplicities have a Poisson distribution in n-2.

4) $\langle n \rangle = 10$ at $P_{LAB} = 100$ GeV/c.

From these assumptions, $\langle \chi^2 \rangle$ is about .6 at 100 GeV/c (and rises slowly with energy). Extreme bounds

on $\langle\chi^2\rangle$ are that leading protons have average energy fraction $\approx .6$, which gives $\langle\chi^2\rangle > .36$, and $\langle\chi^2\rangle$ is rigorously less than 1. The calculated value is intermediate between these limits, and very insensitive to the details of the assumptions.

We compare these results with the "overlap function," i.e., that part of the imaginary part of elastic scattering excluding the contribution of elastic scattering itself to unitarity. This is because elastic scattering is much larger (being Pomeron exchange) than calculated as a multiparticle process in the MPM. In order to extract the imaginary part and to calculate the overlap function from the elastic data it is necessary to make some assumption about the phase of elastic scattering. The result is not sensitive to any reasonable choice of this phase. For definiteness the parameterization of Kane[4] is used in Figures 2 through 4.

The comparison between the MPM and overlap function is shown in Figure 2. The MPM gives much too large a slope. From equation 20, the curve should be a straight line of slope 15. One can easily see that equation 20 is entirely adequate. This slope is to be compared to that of about 5 for the data. (The cross section, with slope 10, is the square of the amplitude.) Thus this extreme short range order model must be rejected. Our result is quite general and holds for <u>any</u> model satisfy-

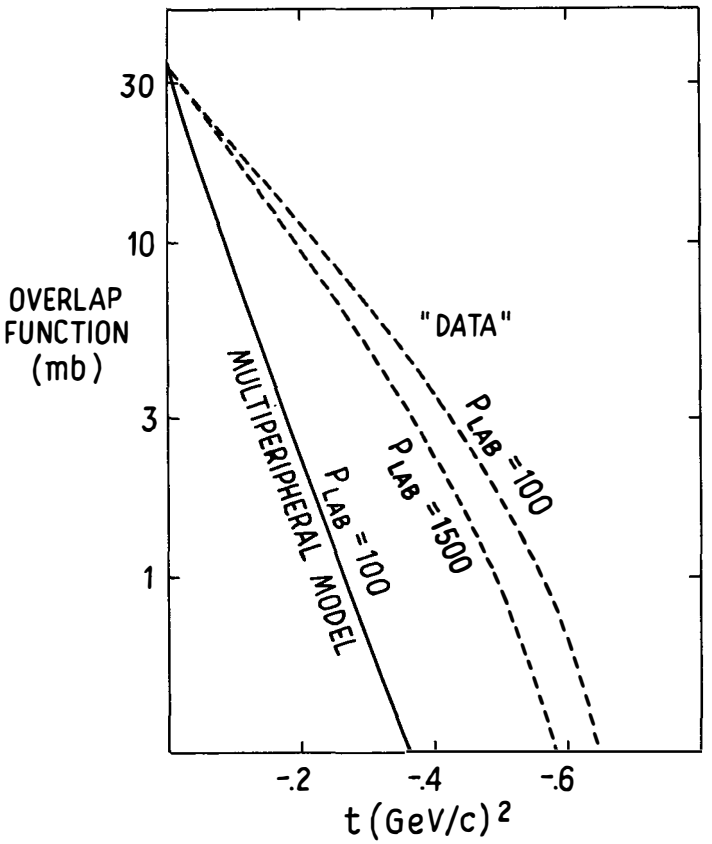


Figure 2. A comparison of the multiperipheral model with the shortest range order possible, and the overlap function extracted from elastic scattering data. The overlap function is the sum of all inelastic contributions to the imaginary part of the elastic scattering amplitude.

ing equation 13, regardless of details.

It turns out, however, that the slope is very sensitive to clustering or correlations. This comes about for two reasons. First, the number of steps is smaller, so the random walk does not get as far. Second, the step size R might be smaller. Each particle has only a share of the transverse momentum of a cluster, plus a modest amount from the decay of the cluster. Thus the rms transverse momentum of a cluster, 1/R, can be significantly larger than 430 MeV. With an average cluster size somewhat less than two particles (the amount less depends on the details of calculating R), the 100 GeV "data" can easily be fit, as shown in Figure 3.

But, if we assume that the average cluster size, $\langle N\rangle/\langle n-1\rangle$, (where $\langle N\rangle$ is the average number of steps) and the average step size R are energy independent we can calculate elastic scattering at any energy. $\langle\chi^2\rangle$ is constant or slightly rising with energy, and the multiplicity is rising. Therefore the model exhibits shrinkage. The results at the highest ISR energy are shown in Figure 4. The curve is most sensitive to $\langle n\rangle$ but in any case it is much steeper than the data. The excessive shrinkage can also be exhibited by plotting an effective Regge trajectory. This is done in Figure 5, and is compared to the effective trajectory of the data.

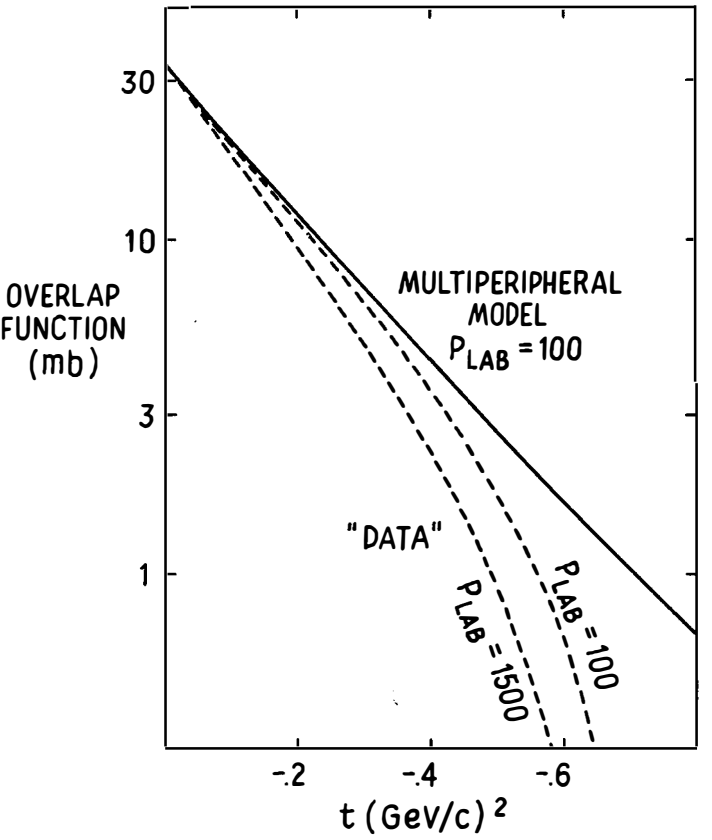


Figure 3. A modified multiperipheral model with correlations (clustering). The correlation length is chosen to give a fit at P_{LAB} = 100 GeV/c, as shown in this figure.

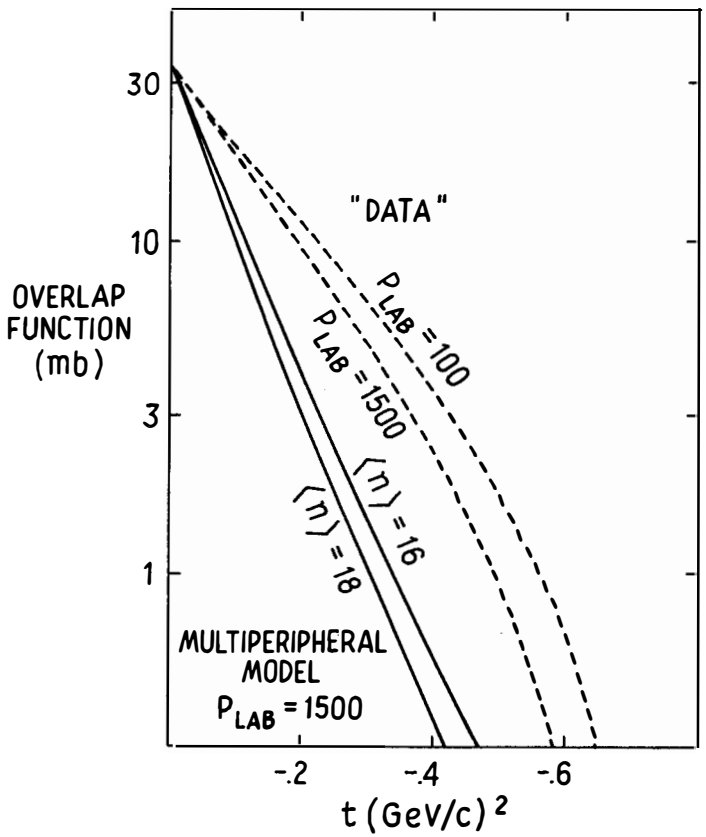


Figure 4. The modified multiperipheral model at ISR energy. The amount of clustering is determined by the fit at 100 GeV shown in Figure 3.

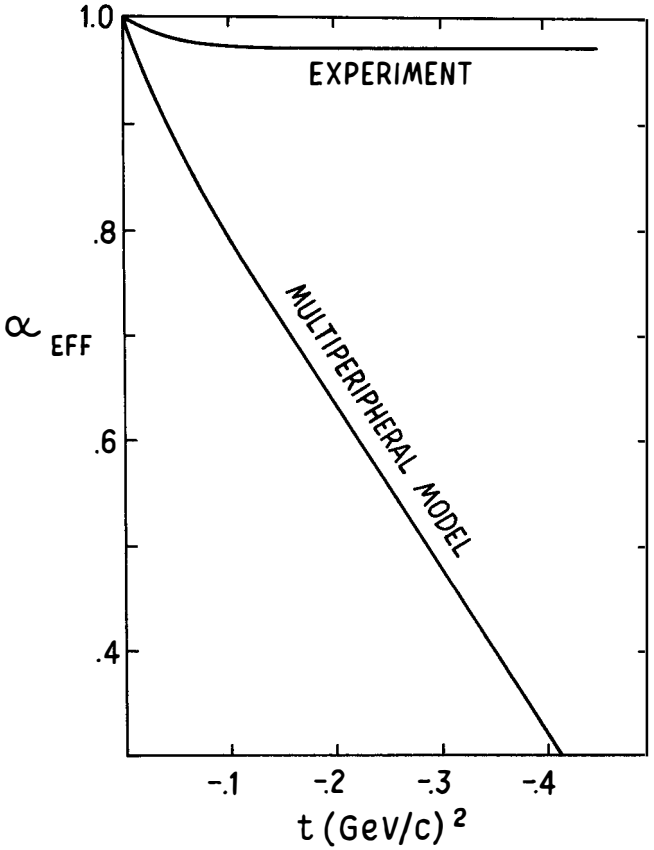


Figure 5. The effective Regge trajectory, giving the energy dependence between P_{LAB} = 100 GeV and 1500 GeV. The slope of the multiperipheral model trajectory is four times larger than the experimental trajectory, and continues to fall, while the experimental trajectory flattens out.

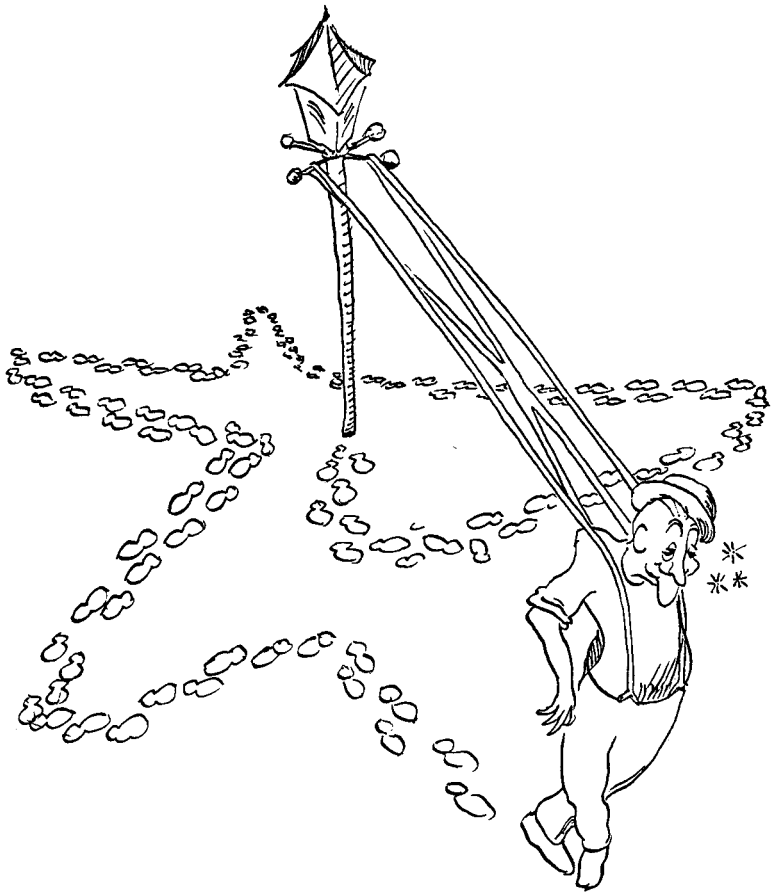
Elastic unitarity has been added in order to calculate the MPM curve. It is readily apparent that the Multiperipheral model completely fails to describe the data.

There are two ways out of this dilemma. One can assume that the ISR energies are still low energy and that the cluster size or correlation length is still growing fast enough to compensate for the increase in average multiplicity. With this assumption, one has given up any real distinction between the multiperipheral model and other models (except for the philosophical framework). Alternatively, one can reject the MPM, and assume long range order. Then the amplitude will depend on impact parameter as well as on the step in impact parameter. Even a modest cutoff in impact parameter can control the excessive shrinkage of the MPM.

One can easily verify that the uncorrelated jet model[5] goes too far in this latter direction. The slope is much too flat (unless $\langle b_j \rangle$ is a factor of three larger than required by the uncertainty principle and the data for $\langle k_j \rangle$) and there is only a minor amount of energy dependence from kinematical effects. The uncorrelated jet model cuts the impact parameter off too sharply.

The use of impact parameter can suggest new models for multiparticle and elastic scattering. As an example (shown in Figure 6),

Figure 6: A model intermediate between the multiperipheral and uncorrelated jet models. The overall impact parameter is prevented from becoming too large when the number of random walk steps is large.



a model intermediate between the MPM and uncorrelated jet models should be able to fit both multiparticle and elastic data. The amplitude in such a model might be given by $\tilde{M} \sim \prod_{j=1}^{n} F(b_j) \prod_{j=1}^{n-1} G(B_j)$. Such a model, however, lacks the elegant theoretical justification of those models which fail to fit data. Perhaps the possibility of it being roughly correct may compensate for that defect. Perhaps other models will be suggested by the interplay of multiparticle and elastic data. The use of impact parameter should facilitate such a development.

Summary

The use of impact parameter is a valuable technique for multiparticle processes at high energy, just as it is for two-body processes. The definition of impact parameter, and a calculation of elastic unitarity have been presented. Unitarity is diagonalized by using impact parameter, resulting in an "optical theorem" at each impact parameter. That is, only the absolute squares of the amplitudes need be known to calculate unitarity for elastic scattering. The overall impact parameter has been calculated, and is given by angular momentum conservation, $\vec{pb} = \Sigma p_j \vec{b}_j$.

This technique can be used to study models, and extract the features of the models which are important in determining the calculated elastic scattering. We have

examined the multiperipheral model in some detail by use of this technique. The multiperipheral model (as well as other models) is unable to simultaneously fit elastic and multiparticle data. The calculated elastic slope shrinks much too fast because of the rate of increase of average multiplicity with energy.

The use of impact parameter can suggest new models which are able to fit both types of data. As an example, we proposed a model intermediate between the extremes of the multiperipheral and uncorrelated jet models.

Acknowledgments

I would like to thank J. Van der Velde for discussions concerning the high energy multiparticle data, G. Kane for conversations on various aspects of this work, and D. Sivers for a discussion of the uncorrelated jet model.

References

1. Similar expressions have been given by R.C. Hwa, Oregon preprint, January 1973 and by G. Calucci and R. Jengo, Lett. al Nuovo Cimento 5, 373 (1972).
2. See, for example, L. Caneschi and A. Schwimmer, Nucl. Phys. B44, 31 (1972).
3. For a review of the multiperipheral model, see, for example, A. Pignotti, talk presented at the Symposium on High Energy Interactions and Multiparticle Production, Argonne National Laboratory, November 1970.
4. G.L. Kane, Phys. Lett. 40B, 363 (1972); and talk at Argonne symposium, March 1973.
5. For a review of the uncorrelated jet model, see, for example, T.W. Ruijgrok, Proceedings of the III International Colloquium on Multiparticle Reactions, Zakopane, June 1972.

ON THE TWO-REGGEON CUT PROBLEMS

K. Kang
Division de Physique Théorique, I.P.N., Paris
and
Brown U., Providence

Abstract : The two-Reggeon cut problem is reviewed in the light of recent developments concerning the notion of two-Reggeon irreducibility.

Résumé : Nous examinons le problème de la coupure générée par l'échange de deux reggeons, au vu des développements récents de la notion d'irréductibilité liée à cet échange.



During the last year, we have seen a remarkable development in the two-Reggeon cut problem in that the program suggested by Gribov, Pomeranchuk and Ter-Martirosyan[1] has now been carried through and perhaps a little beyond. The program suggested by GPT is that the Reggeon cut structure, in particular, the unitarity-like form of the discontinuity equations in complex angular momentum obtained by perturbation theory[2] can be expected to emerge from a "Reggeon field theory", similar to the Lippman-Schwinger equation in two-dimensional non-relativistic quantum mechanics in which the energy variable is replaced by the angular momentum of the Reggeon. This GPT program is advanced mainly by two inspiring pieces of work, one by White[3] and the other by Abarbanel[4].

White[3] has carried out the GPT program directly from the unitarity relation in the t channel where the Reggeons are to be exchanged. Namely, the discontinuity across the two-Reggeon cut is approached by considering first the partial wave projections of the t channel discontinuity of the two-body amplitude T_{22} across the four-particle cut and then by analytically continuing the relation in the angular momentum plane to complex j by using his earlier results[5] of the Froissart-Gribov continuation of the partial wave amplitudes to complex angular momentum and helicity. Finally, the formula is continued down to $t < 0$ to obtain the cut contributions to the asymptotic behaviour in the physical s channel. In this way, he obtains a detailed structure for the two-Reggeon cut discontinuity in angular momentum.

On the other hand, Abarbanel[4] has shown that such S matrix-like equations can be derived from s channel unitarity by assuming that the production amplitudes T_{2n} in the intermediate summation can be decomposed into a piece containing $(s_{ij})^{\alpha(t_{ij})}$ with a factorizable Reggeon $\alpha(t_{ij})$ for the dependence of the subenergy s_{ij} and another piece of non-Regge behaviour in s_{ij}. He proceeds from the unitarity relation with the notion of two-Reggeon irreducibility and then

diagonalizes these equations by using $SO(2,1)$ projections of the Reggeon amplitudes to show that the two-Reggeon cut discontinuity has the same form as that of GPT.

From these two works, we can now say that the discontinuity formula at issue is entirely expressible through the S matrix without recourse to perburbation diagrams and the cut discontinuity expression in the angular momentum plane is consistent both with direct and cross-channel unitarity. However, on the closer examination, these two authors disagree on the sign of the cut discontinuity ; while Abarbanel's cut has a positive discontinuity, White obtains a negative sign in accordance with the majority opinion of the Regge cut school.

The sign of the cut is not a new problem[6]. But the persistence of such different signs from the two works has been indeed the source of renewed interest in the two-Reggeon cut problem. Chew[7] points out that Abarbanel's decomposition of the discontinuity relation using the notion of two-Reggeon irreducibility corresponds physically to the ordering of high-energy events according to the number of "fireballs" in rapidity and the resulting integral equation has a kernel whose analyticity properties near the cut branch point is simple. He then argues for the positive sign by studying the relationship between the triple Pomeron coupling and the cut discontinuity through the Finkelstein-Kajantie mechanism[8] as $\alpha_p(0) \to 1$. On the other hand, Blankenbecler[9] and more recently Neff [10] argue that the unitarity correction to the multi-Regge exchange diagram to keep the complete amplitude within the unitarity bounds gives the dominant Regge cut contribution to the unitarity sum and in particular can change the sign of the cut.

In fact, the possibility of finding the cut through unitarity as absorptive corrections to the production amplitudes T_{2n}, i.e.,

$$T_{2n} = (S_{22})^{1/2} M_{2n} (S_{nn})^{1/2} \qquad (1)$$

has been shown before by Caneschi[11] and Dash, Fulco and Pignotti[12]. The work of Neff is essentially in the same spirit as that of these works. But he uses the concept of a rapidity space decomposition of T_{2n} in the s channel guided by the two-component descriptions of experiment, namely a combination of short range correlation and some small diffractive mechanism. Such two-component picture would then cause a part which lacks factorization and therefore has a non-scaling contribution. Essentially, the strength of this part is restricted by demanding the production amplitude T_{2n} to be unitary. In other words, the two-component picture says that the production amplitude can be written as $T_{2n} = T_{2n}^{10} + T_{2n}^{11}$ where the superscripts denote the number of rapidity gaps in the initial and final states. These elements are then requires to satisfy the unitarity relation

$$\text{Im}\, T^{i\,j}_{n\,m} = \sum_{k,\ell} T^{*\,i\,k}_{n\,\ell}\, \rho^{k}_{\ell}\, T^{k\,j}_{\ell\,m} \qquad (2)$$

where ρ^{k}_{ℓ} is the k gap projection of the ℓ body phase space. In this scheme, the original ABFST program[13] would be then T^{10} is precisely multiperipheral and T^{11} purely pole-behaved. However, in order to take unitarity into account for T^{10} and T^{11}, Neff uses the unitarization method of Baker and Blankenbecler[14]. This method gives the solutions of (2) as

$$T^{ij} = \tilde{M}^{ij} + T^{i1}\, I^{1}\, \tilde{M}^{1j} \quad (i,j = 0,1) \qquad (3)$$

with

$$\tilde{M}^{ij} = M^{io}\,(1 - I^{o}\, M^{oj})^{-1} \qquad (4)$$

where M^{10} is the given "Born" term such as the multiperipheral chain and I^{i}_{ℓ} is a real analytic function of s having imaginary part ρ^{i}_{ℓ} on the physical s cut. When (3) is inserted into (2), the dominant cut term in the absorptive part of T^{11}_{22} comes from the terms like $i(M^{*10}\, \rho^{0}\, M^{01})_{2n}\, \rho^{1}_{n}\, M^{11}_{n2}$ which gives a negative contribution for the Pomeron exchange as M^{11}_{n2} is then purely imaginary. Clearly the Abarbanel decomposition does not take into account the unitarity for T^{10}_{2n} and T^{11}_{2n} and therefore it will be extremely interesting if some long range correlation can be incorporated

into his decomposition without spoiling factorization property. What seems to be needed is to define the consistent mechanism to represent Reggeons in terms of the s channel structure.

Recently, we have shown that[15] the notion of the two-Reggeon irreducibility can be very simply understood from the non-forward inclusive type sum rule[16] for the discontinuities for the reactions $a + b \to a' + b'$ and $a + b + \bar{c} \to a' + b' + \bar{c}$,

$$\text{Disc}_s\, T_{22} = \int dp_c \frac{E_c}{E_a + E_b} \text{Disc}_{M^2}\, T_{33} \qquad (5)$$

where $$M^2 = (p_a + p_b + p_{\bar{c}})^2 = (p_{a'} + p_{b'} + p_{\bar{c}})^2$$

and $$dp_c = d^3p_c \Big/ \left[(2\pi)^3\, 2E_c\right]$$

If we assume the short range correlations only, then the two-Reggeon reducible part comes only from the phase boundary region which is defined by $1 - \varepsilon \le x_c < 1$ where $x_c = 2p_{c\parallel}/\sqrt{s}$ and ε is small and positive. The cut obtained from (5) has the form

$$\text{Disc}_s\, T_{22} = I(s,t) \qquad (6)$$
$$+ \frac{1}{2(2\pi)^3} \int dt_1\, dt_2 \frac{\theta(-\lambda(t,t_1,t_2))}{\sqrt{-\lambda(t,t_1,t_2)}} (s)^{\alpha_{b\bar{c}}(t_1)+\alpha_{b'\bar{c}}(t_2)-1} \tilde{N}^{(t,t_1,t_2)}_{\alpha_{b\bar{c}},\alpha_{b'\bar{c}}}$$

where $I(s,t)$ has the term having $s^{\alpha_{aa'}(t)}$ dependence and $\tilde{N}_{\alpha_{b\bar{c}},\ \alpha_{b'\bar{c}}}$ is the fixed pole residue in the t channel of $\tilde{T}_{22}$ representing the process $a + \alpha_{b\bar{c}} \to a' + \alpha_{b'\bar{c}}$ at the point $\alpha_{aa'}(t) - \alpha_{b\bar{c}}(t_1) - \alpha_{b'\bar{c}}(t_2) + 1 = 0$. The partial wave projection of (6) leads to the same form as the one obtained by Abarbanel

$$F(\ell,t) = g(\ell,t) + \frac{1}{2(2\pi)^3} \int dt_1 dt_2 \frac{\tau(t,t_1,t_2)\tilde{N}_{\alpha_{b\bar{c}}\ \alpha_{b'\bar{c}}}(t,t_1,t_2)}{\ell - \alpha_{b\bar{c}}(t_1) - \alpha_{b'\bar{c}}(t_2) + 1} \qquad (7)$$

where $\tau(t,t_1,t_2) = \theta(-\lambda(t,t_1,t_2))/\sqrt{-\lambda(t,t_1,t_2)}$ and $g(\ell,t)$ denotes the remaining (moving pole) contributions of (6). The expression (7) should be compared with Eq. (33) of Ref. 4), and shows a linear dependence on the fixed pole residue in the crossed-channel of Reggeon-particle scattering. One can similarly obtain the cut expressions of the discontinuities of the Reggeon-particle and Reggeon-Reggeon scattering amplitudes by calculating the contributions to (5) of the inclusive discontinuities for (Reggeon + b + $\bar{c}$ → → Reggeon + b + $\bar{c}$) and (Reggeon 1 + Reggeon 2 + $\bar{c}$ → Reggeon 1 + Reggeon 2 + $\bar{c}$) respectively near the respective phase space boundary regions. Then one obtains two more equations similar to (7), which together with (7), can be regarded as a coupled set of matrix elements of a formal operator equation as in Ref. 4). The same conclusions as Ref. 4) can then be reached for the cut discontinuity, i.e., the cut discontinuity is positive and is depending on the product of two fixed pole residua.

If the negative dut is indeed the right answer, one will have to relax the short range force dominance and modify the above analysis by including a low multiplicity diffractive production process that will contribute to the phase space boundary region. The presence of the latter type process would shadow the high multiplicity short range process and would amount to giving an s channel structure to the Reggeons. It will be extremely interesting to study then if indeed the negative sign follows from the inclusive sum rule and to see to what extent the scaling and factorization properties are to be disturbed.

ACKNOWLEDGEMENTS

I would like to thank A.R. White for discussions which have helped substantially the preparation of this talk. Also I would like to acknowledge R.W. Moore and B. Nicolescu for the pleasant collaboration and R. Vinh Mau for the warm hospitality extended to me in his Division in Paris. Finally, I would like to thank the CERN Theoretical Study Division for the kind hospitality.

REFERENCES AND FOOTNOTES

1) V.N. Gribov, I. Ya. Pomeranchuk and K.A. Ter-Martirosyan, Phys. Rev. 139B, 184 (1965) ; Soviet J. Nuclear Phys. 2, 258, (1966).

2) S. Mandelstam, Nuovo Cimento 30, 1113, 1127 and 1143 (1963) ; J.C. Polkinghorne, J. Math. Phys. 4, 1396 (1963).

3) A.R. White, Nuclear Phys. B50, 93, 130 (1972). See also his lecture in this Proceedings for historical background as well as details of the GPT program.

4) H.D.I. Abarbanel, Phys. Rev. D6, 2788 (1972).

5) A.R. White, Nuclear Phys. B39, 432, 461 (1972).

6) See for example, J. Finkelstein and M. Jacob, Nuovo Cimento 56A, 681 (1968).

7) G.F. Chew, Phys. Rev. D7, 934 (1973).

8) J. Finkelstein and K. Kajantie, Nuovo Cimento 56, 659 (1968) ; Physics Letters 26B, 305 (1968).

9) R. Blankenbecler, SLAC Preprint SLAC-TN-72-13 (1972)(unpublished).

10) T.L. Neff, Phys. Letters B 43, 391 (1973.

11) L. Caneschi, Phys. Rev. Letters 23, 254 (1969).

12) J.W. Dash, J.R. Fulco and A. Pignotti, Phys. Rev.D1, 3164 (1970).

13) L. Bertocchi, S. Fubini and M. Tonin, Nuovo Cimento 25, 626 (1962) D. Amati, A. Stanghellini and S. Fubini, Nuovo Cimento 26, 896 (1962).

14) M. Baker and R. Blankenbecler, Phys. Rev. 128, 415 (1962).

15) K. Kang, R.W. Moore and B. Nicolescu, Paris preprint IPNO/TH/ 73/3 (1973). Such possibility is also observed by S-H.H. Tye and G. Veneziano, CERN preprint TH. 1552 (1972).

16) G. Veneziano, Phys. Letters 36B, 397 (1971) ; Phys.Rev.Letters 28, 578 (1972) ; C-I Tan, Phys. Rev. D5, 1476 (1972).

DUALITY IN REGGEON-PARTICLE SCATTERING*

D. P. Roy
Rutherford High Energy Laboratory



Abstract: The Dolen-Horn-Schmid type Duality ansatz is extended to the Reggeon-particle amplitude, which is directly related to the inclusive cross-section in the resonance region $M^2 << s$. The ansatz relates the resonance production cross-section $d\sigma/dt$ (ab $\overset{\alpha}{\rightarrow}$ cdj) to the resonance mass M_j^2 in terms of the exchanged trajectory α. These duality relations agree remarkably with a large number of resonance production data.

Résumé : L'ansatz relatif à la dualité du type Dolen-Horn-Schmid est généralisé à l'amplitude Reggeon-particule qui est directement reliée à la section efficace inclusive dans la région des résonances $M^2 << s$. Cet ansatz permet de relier la section efficace de production des résonances $\frac{d\sigma}{dt}$ (ab $\overset{\alpha}{\rightarrow}$ cdj) à la masse M_j^2 des résonances en termes de la trajectoire échangée α. Les relations ainsi obtenues comme conséquences de la dualité, sont en remarquable accord avec un grand nombre de données sur la production des résonances.

*This work was done by P. Hoyer, R. G. Roberts and myself.

INTRODUCTION

We have studied a simple extension of the Dolen-Horn-Schmid type of duality relation to the inclusive case.[1]

Let us recall the Finite Energy Sum Rule for the two-body amplitude f, i.e.

$$\int_0^N \nu^{2n} f(\nu)\, d\nu \sim g\, N^{\alpha+1+2n} \qquad (1)$$

Since the approximate equality is expected to hold for several moments (n = 0, 1, 2..), one expects it to be satisfied semi-locally, i.e.

$$\langle f(\nu)\rangle \sim g\, \langle \nu\rangle^{\alpha} \qquad (2)$$

This is the famous Dolen-Horn-Schmid relation. Together with the Two-Component duality hypothesis of Harari and Freund it reads

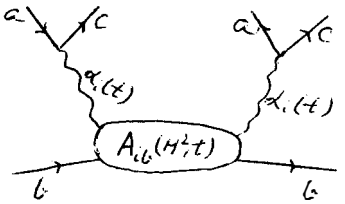
$$\langle f(\nu)\rangle^{\text{res, B.G.}} \sim g\, \langle \nu\rangle^{\alpha_{R,P}}, \qquad (3)$$

i.e., the leading Regge and Pomeron exchange average the resonance and background contributions in the low energy region.

Let us proceed to the inclusive reaction $ab \to cX$. In the region of low missing mass M^2 of X, the cross-section is dominated by the leading Regge exchange in the $a\bar{c}$ channel. More precisely

$$s\frac{d\sigma}{dtdM^2} \xrightarrow{s>>M^2,t} F(t)\, s^{2\alpha_i(t)-1}\, A_{ib}(M^2,t) \qquad (4)$$

as shown in the following Mueller diagram.



Thus the inclusive cross-section in the low missing mass region, provides a direct measure for the forward Imaginary part of the Reggeon-particle amplitude $A_{ib}(M^2,t)$.

In some models, like the dual resonance model and the perturbation theory, the Reggeon-particle amplitude is seen to share the normal analyticity properties of a two-body amplitude.[2] Moreover, in any scaling theory it has the Regge asymptotic behaviour

$$A_{ib}(M^2,\ t) \xrightarrow{\text{large } M^2} (M^2)^{\alpha_{R,P}(0)-2\alpha_i(t)} \qquad (5)$$

On the basis of these properties, it has been suggested that the Reggeon particle amplitude should satisfy a Finite Mass Sum Rule[3] analogous to eq. (1).

Again the approximate equalities are expected to hold for several moments. Thus it is reasonable to assume, following

the Dolen-Horn-Schmid procedure, that it holds semi-locally.

$$\langle A_{ib}(\nu,t)\rangle \sim g_{R,P}^{(t)} \langle\nu\rangle^{\alpha_{R,P}(0)-2\alpha_i(t)} \tag{6}$$

where $\nu = \frac{1}{2}(M^2-m_b^2-t) \simeq \frac{1}{2}(M^2)$ (7)

The extension of the two-component duality hypothesis to the Reggeon-particle case is fairly unambiguous, so long as i is not a Pomeron. Thus the non-diffractive resonance and background production cross-section are expected to satisfy the duality relations

$$\left\langle s\frac{d\sigma^{res,\ B.G}}{dtdM^2}\right\rangle \sim G_{R,P}(t)\ s^{2\alpha_i(t)-1}\ \langle\nu\rangle^{\alpha_{R,P}(0)-2\alpha_i(t)} \tag{8}$$

with $\alpha_{R,P}(0) = \frac{1}{2}, 1$.

This is evidently a very powerful relation for the resonance production data. It predicts how the production cross-section for ab → cdj should vary with the mass of the produced resonance M_j^2. As usual in the duality game, the averaging is to be done over a typical M^2 interval of 1 GeV^2.

MESON-MESON CHANNELS

Let us consider some specific examples. The processes

$$\pi^- p \to n\ (\rho^o,\ f,\ g^o..) \tag{A}$$

$$K^- p \to n\ (K^*,\ K^{**}...) \tag{B}$$

are known to be dominated by π exchange at small t. Therefore the cross-section is predicted to increase with resonance mass as

$$\frac{d\sigma}{dt} \sim \langle\nu\rangle^{\alpha_R(0)-2\alpha_\pi(t)} \qquad (9)$$

The Reggeon-particle channels for (A) and (B) are $\pi^+\pi^-$ and π^+K^-, each of which has an exotic cross channel. Therefore one expects the duality relation to hold both for even and odd moments. Fig. 1 shows a comparison of the experimental cross-sections for (A) with the duality prediction for the zeroeth (i.e. eq. 9) and first moments. Fig. 2 shows a similar comparison for (B).

Next consider the f, ω exchange contributions to

$$\pi^- p \to p(\pi^-, \rho^-, A_2^-, g^- ..) \qquad (A')$$

$$K^- p \to p(K^-, K^{*-}, K^{**-} ..) \qquad (B')$$

Since the direct and crossed Reggeon-particle channels are now identical, one expects duality relations to be valid for the odd moments only, i.e.

$$\left\langle \nu_{res} \frac{d\sigma}{dt} \right\rangle \sim \langle\nu\rangle^{\alpha_R(0)+1-2\alpha_{f,\omega}(t)} \qquad (10)$$

The f, ω contributions to the elastic scatterings are evaluated from the standard Barger-Phillips fits. For the rest, the iso-scalar exchange is isolated by taking the difference

$$\frac{d\sigma}{dt}(A') - \tfrac{1}{2}\frac{d\sigma}{dt}(A)$$

and

$$\frac{d\sigma}{dt}(B') - \tfrac{1}{4}\frac{d\sigma}{dt}(B)$$

and f, ω is assumed to be the dominant isoscalar exchange. (i.e. we neglect a possible diffractive contamination in A_2 as a first approximation).

The results are compared with the duality prediction (10) in Fig. (3). I should remark that for the π-induced reaction the agreement is only qualitative. Firstly the subtraction of A' from A produces large error bars in the data points and secondly one is forced to work only at 8 GeV/c (where one has data on both A and A') which is rather low for g production. Nonetheless, the overall agreement for the four processes considered above is rather impressive.

Two significant corrolaries follow from the duality relation (8). (1) The ratio of π to f, ω exchange is predicted to increase linearly with the resonance $(\text{mass})^2$.

$$\left\langle \frac{\pi\text{-exch.}}{f,\omega\text{-exch.}} \right\rangle \sim \langle M^2_{res} \rangle^{2\alpha_{f,\omega}(t) - 2\alpha_{\pi}(t)} \sim \langle M^2_{res} \rangle \qquad (11)$$

Thus the ratio of π to f,ω exchange should increase by a factor of 5 when we go from ρ to g production, and by a factor 3 from K^* to K^{**} production. We see from Fig. (4) that these predictions are almost in quantitative agreement with data.

(11) For a given Regge exchange the production cross-section should show a logarithmic anti-shrinkage with increasing resonance mass.

$$\left\langle \frac{d\sigma}{dt} \right\rangle_{\text{Fixed } s} \sim e^{-2\alpha'_i . t . \ell n \langle M^2_{res} \rangle} \qquad (12)$$

The agreement is reasonable for the f,ω exchange cross-section (Fig. (5)), although the largest data is admittedly poor. It is hard to extract the π-exchange cross-section at large t.

So far we have been looking at duality in meson-meson channels. It is possible to extend the analysis to meson-baryon and baryon-antibaryon channels by studying backward resonance production - i.e. the baryon exchange reactions. Unfortunately the backward production data is restricted to rather low energies (3-6 GeV/c). Some of the qualitative predictions are, nonetheless, borne out by these data remarkably well.

MESON-BARYON CHANNELS - Consider the forward and backward production of baryon resonances, e.g.

$$nK^- \xrightarrow{K^* \text{exch.}} \pi^- Y_j^* \qquad (C)$$

and

$$K^- n \xrightarrow{N \text{ exch.}} \pi^- Y_j^* \qquad (C')$$

The Reggeon-particle amplitudes for these and all the subsequent reactions to be considered here have exotic cross-channels and therefore we shall consider duality relation for the zeroeth

moment.

We have

$$\left\langle \frac{d\sigma}{dt}(C) \right\rangle \sim \langle M^2_{res} \rangle^{\alpha_R(0)-2\alpha_{K^*}(t)} \qquad (13)$$

and

$$\left\langle \frac{d\sigma}{du}(C') \right\rangle \sim \langle M^2_{res} \rangle^{\alpha_R(0)-2\alpha_N(u)} \qquad (14)$$

Thus at fixed s, the forward peak is predicted to go down, and backward peak to come up with increasing resonance mass.

The above predictions are compared with the data for (C) and (C') in Fig. (6). These data points may have only qualitative significance, as they are obtained by interpolating several experiments in the 4-6 GeV/c range. However, the suppression of the forward peak and enhancement of the backward peak with increasing resonance mass can be seen even from a single set of data (e.g. Fig. 6 of ref. 4).

BARYON-ANTIBARYON CHANNELS - Finally consider the backward production of meson-resonances. There is counter data at 16 GeV/c for

$$p\bar{\pi} \xrightarrow{\Delta \text{ exch}} p(\bar{\pi}, \bar{\rho}, \bar{A_1}, \bar{A_2}, \bar{g}), \qquad (D)$$

and the associated background[5]. The background is expected to rise linearly with M^2, i.e.

$$\frac{d\sigma}{du}^{B.G.} \sim \langle M^2 \rangle^{1-2\alpha_\Delta(u)} \sim \langle M^2 \rangle \qquad (15)$$

for $\alpha_\Delta(-2) \sim 0$. This is indeed the case as we see from Fig. 7.

This has been noted by several authors[6] and contrasted with a much slower rise of background in forward production (as expected from the fact that the meson trajectories are higher than α_Δ).

For the resonance production cross-section we have

$$\left\langle \frac{d\sigma}{du}(D) \right\rangle \sim \langle M^2_{res} \rangle^{\alpha_R(0)-2\alpha_\Delta(u)} \qquad (16)$$

If these resonances were dual to a normal Regge exchange ($\alpha_R(0) = \frac{1}{2}$), the cross-section should increase linearly with Mres. On the other hand the duality diagram prescription[7] suggests that the normal di-quark resonances in baryon-antibaryon channel, should be dual to exotic exchange with a low effective $\alpha_R(0)$. In this case $\frac{d\sigma}{du}(D)$ should go down with M_{res}. The data seems to clearly favour the latter alternative as we see from Fig. (7). The effective $\alpha_R(0)$ calculated from this figure is $\sim -\frac{1}{2}$, in contrast to the value $\sim +\frac{1}{2}$ obtained from the forward production data for the same set of resonances.

We have studied two more backward production processes

$$pK^- \xrightarrow{N \text{ exch.}} \Lambda(\pi^o, \eta, \rho^o, \omega, f, A^o_2) \qquad (E)$$

and

$$p\pi^- \xrightarrow{Y \text{ exch.}} \Lambda(K, K^*, K^{**}) \qquad (F)$$

for which data is restricted to the 4.5 GeV/c range. The effective $\alpha_R(0)$ for each case turns out to be in the range $-\frac{1}{2}$

to $-\frac{3}{2}$.

CONCLUDING REMARKS - Study of Reggeon-particle amplitude from the resonance production data, enhances the scope of duality analysis enormously. Firstly a single high statistics experiment around 10 GeV/c is adequate to do a complete test for one channel (several channels for a bubble chamber experiment). This is because the dispersion variable here is the missing mass. For particle particle scattering the analogous variable was energy, so that one had to combine data from several experiments to get a significant energy range. Secondly, many more Reggeon-particle channels are experimentally accessible than particle-particle channels. Thirdly Reggeon-particle scattering probes a significant kinematic region which was inaccessible to particle-particle scattering. For instance the conventional meson resonances in baryon-antibaryon channel were inaccessible in particle-particle scattering. But we have succeeded in probing them in Reggeon-particle scattering and in providing a phenomenological answer to their dual property, which has been a long standing controversy.

REFERENCES

1. P. Hoyer, R. G. Roberts and D. P. Roy, Rutherford Preprints, RPP/T/35 (To be published in Nucl. Phys.) and RPP/T/43 (To be published in Phys. Lett.)

2. P. V. Landshoff, Nucl. Phys. B15, 284 (1970); C. E. de Tar and J. H. Weis, MIT Preprint CTP 218 (1971).

3. J. Kwiecinski, Lett. Nuovo. Cim. 3, 619 (1972); M. B. Einhorn, Preprint UCRL-20688 (1971); P. Oleson, Preprint CERN-TH-1376 (1971); A. I. Sanda, Phys. Rev. D6, 280 (1972); M. B. Einhorn, J. Ellis, J. Finkelstein, Phys. Rev. D5, 2063 (1972).

4. S.A.B.R.E. Collaboration, Nucl. Phys. B33 161 (1971).

5. E. W. Anderson et. al., Phys. Rev. Lett. 22, 1390, (1969).

6. M. Bishari and H. J. Yesian, Phys. Lett. 38B, 312 (1972). J. Randa, Urbana Preprint (1972).

7. J. L. Rosner, Phys. Rev. Lett. 22, 689 (1969).

FIGURE CAPTIONS

1. Experimental $\nu^{0,1}_{res.} \frac{d\sigma\pi}{dt}(\pi p \to n(\rho^o, f, g^o))$ compared with the duality prediction $(\nu)^{\frac{1}{2},\frac{3}{2}-2\alpha_\pi(t)}$.

2. Experimental $\nu^{0,1} \frac{d\sigma\pi}{dt}(K^- p \to n(K^*, K^{**}))$ compared with the duality prediction $(\nu)^{\frac{1}{2},\frac{3}{2}-2\alpha_\pi(t)}$.

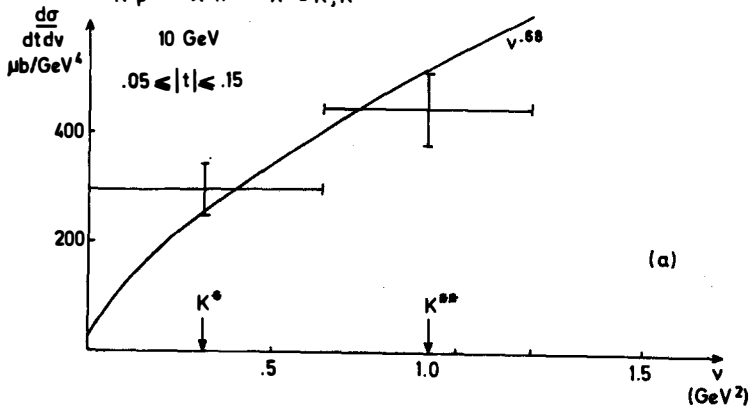
3. Experimental $\nu \frac{d\sigma}{dt}^{f,\omega}$, for $K^- p \to nX^-$ and $\pi^- p \to nX^-$ compared with the duality prediction $(\nu)^{\frac{3}{2}-2\alpha_{f,\omega}(t)}$.

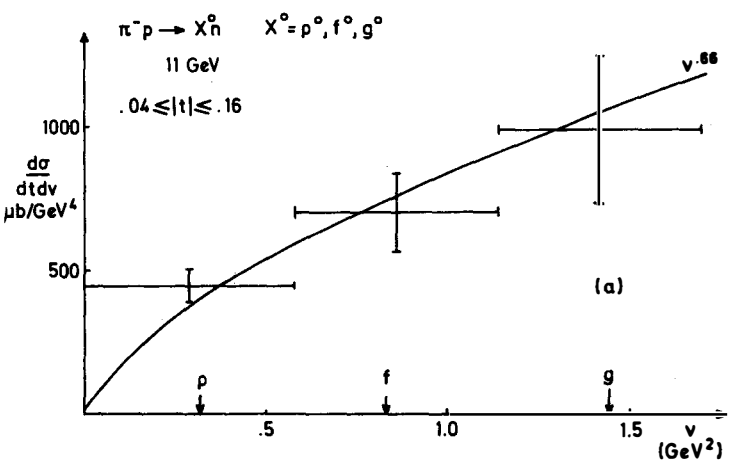
4. The ratio of π to f-ω exchange contribution. Duality predicts this to be proportional to ν_{res}.

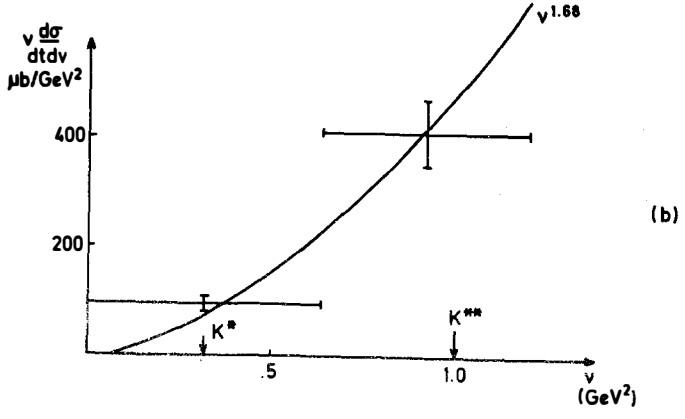
5. Anitshirnkage in $\frac{d\sigma}{dt}^{f,\omega}$ from K^* to K^{**} production; compared with the duality prediction.

6. Forward and backward Y^* production cross-sections, as a function of the $Y^*(\text{mass})^2$. The solid lines are the duality predictions of eqs. (13) and (14).

7. Resonance and background contributions to the backward cross-section $\frac{d\sigma}{du}(p\pi^- \to pX^-)$. They correspond respectively to $\alpha(0) = 1$ and $\alpha_R(0) = -\frac{1}{2}$ in eqs. (15) and (16).


dσ/dtdν μb/GeV⁴
10 GeV
.05 ≤ |t| ≤ .15
ν^-.68
400
200
K*
K**
.5
1.0
1.5
ν (GeV²)
(a)


π⁻p → X⁰n X⁰ = ρ⁰, f⁰, g⁰
11 GeV
.04 ≤ |t| ≤ .16
ν^-.66
1000
500
dσ/dtdν μb/GeV⁴
ρ
f
g
.5
1.0
1.5
ν (GeV²)
(a)


ν dσ/dtdν μb/GeV²
ν^1.68
400
200
K*
K**
.5
1.0
ν (GeV²)
(b)

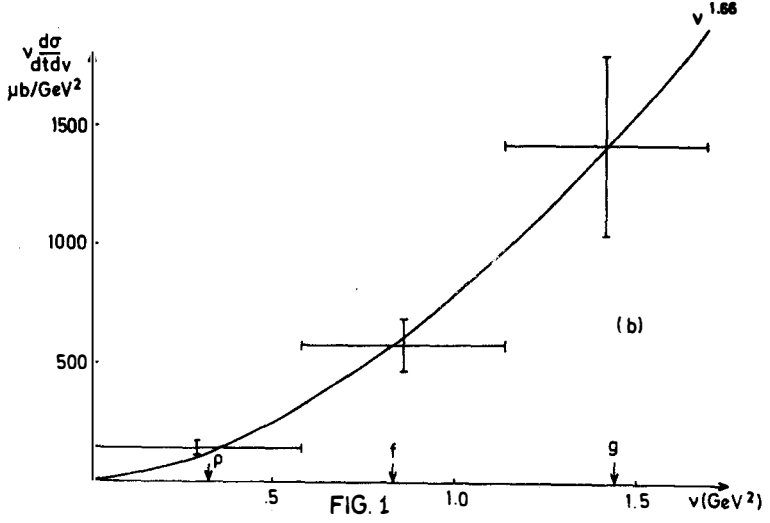
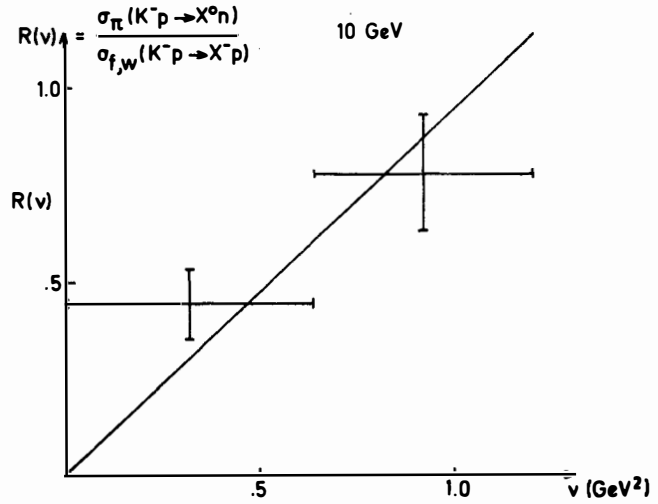
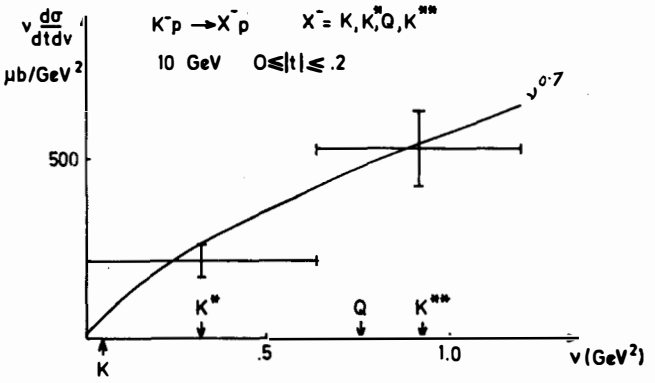
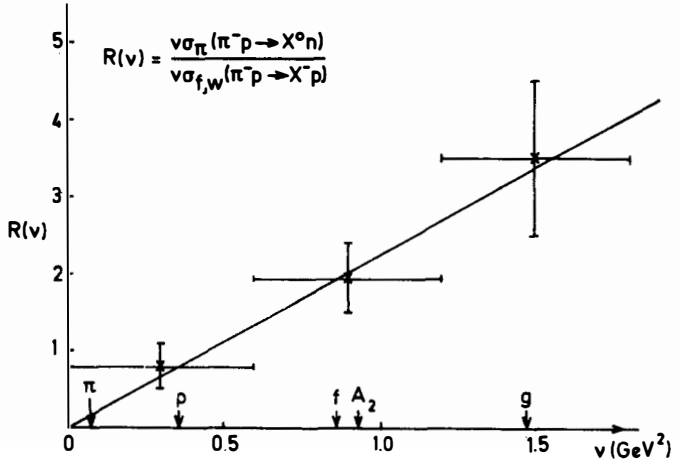

ν dσ/dtdν μb/GeV²
ν^1.66
1500
1000
500
ρ
f
g
.5
1.0
1.5
ν(GeV²)
(b)

FIG. 2

FIG. 1


R(v) = σπ(K⁻p → X°n) / σf,w(K⁻p → X⁻p)
10 GeV
R(v)
1.0
.5
.5
1.0
ν (GeV²)


ν dσ/dtdν
μb/GeV²
K⁻p → X⁻p X⁻ = K, K*, Q, K**
10 GeV 0 ≤ |t| ≤ .2
ν^0.7
500
K*
Q
K**
K
.5
1.0
ν (GeV²)


R(v) = νσπ(π⁻p → X°n) / νσf,w(π⁻p → X⁻p)
R(v)
5
4
3
2
1
π
ρ
f
A2
g
0
0.5
1.0
1.5
ν (GeV²)

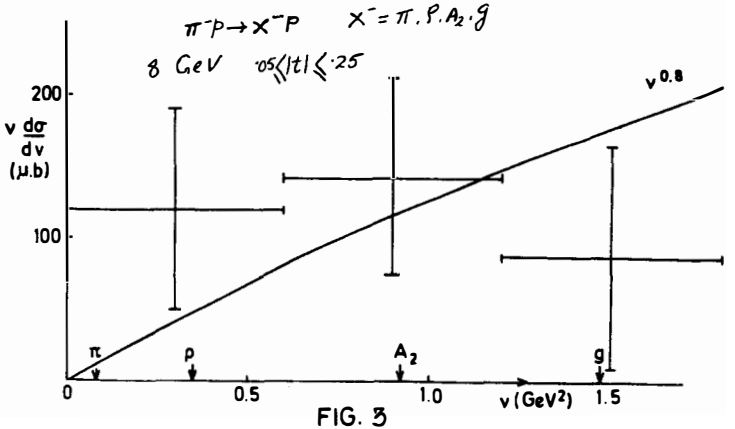

π⁻P → X⁻P X⁻ = π, P, A2, g
8 GeV .05 ≤ |t| ≤ .25
ν dσ/dν
(μ.b)
200
100
ν^0.8
π
ρ
A2
g
0
0.5
1.0
ν (GeV²)
1.5

FIG. 3

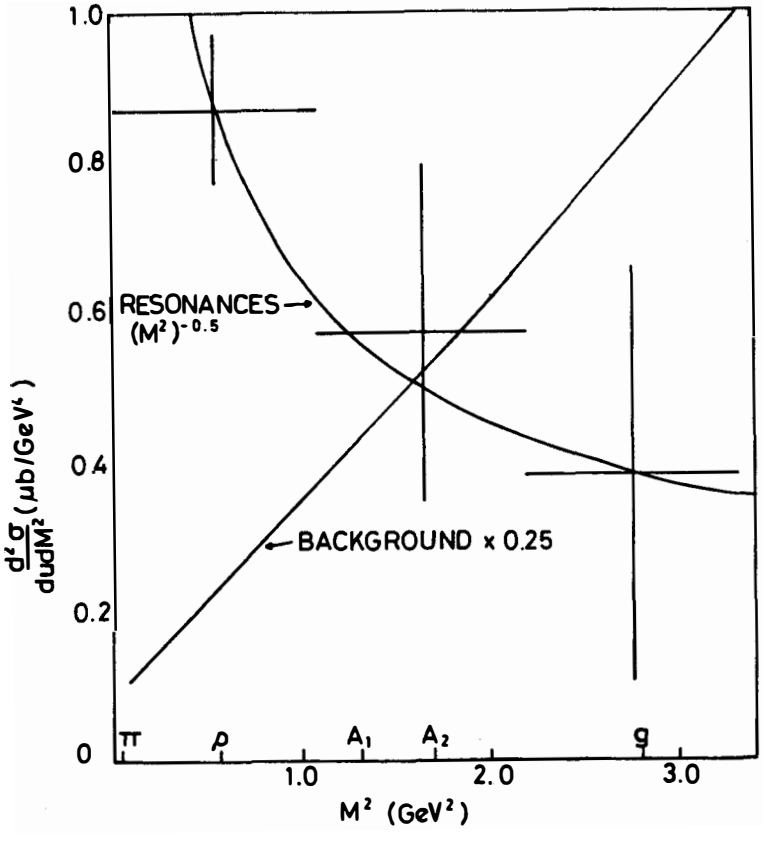

1.0
0.8
0.6
0.4
0.2
0
RESONANCES
$(M^2)^{-0.5}$
BACKGROUND x 0.25
$\frac{d^2\sigma}{dudM^2}$ (μb/GeV⁴)
π
ρ
A_1
A_2
g
1.0
2.0
3.0
M^2 (GeV²)

FIG. 6

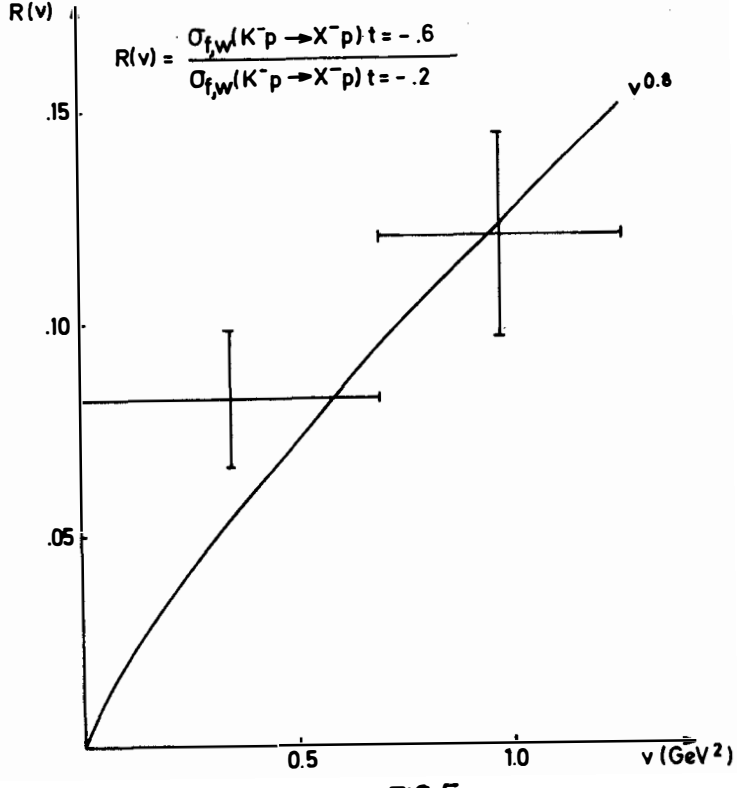

R(v)
$R(v) = \frac{\sigma_{f,w}(K^-p \to X^-p)\, t = -.6}{\sigma_{f,w}(K^-p \to X^-p)\, t = -.2}$
$v^{0.8}$
.15
.10
.05
0.5
1.0
v (GeV²)

FIG.5

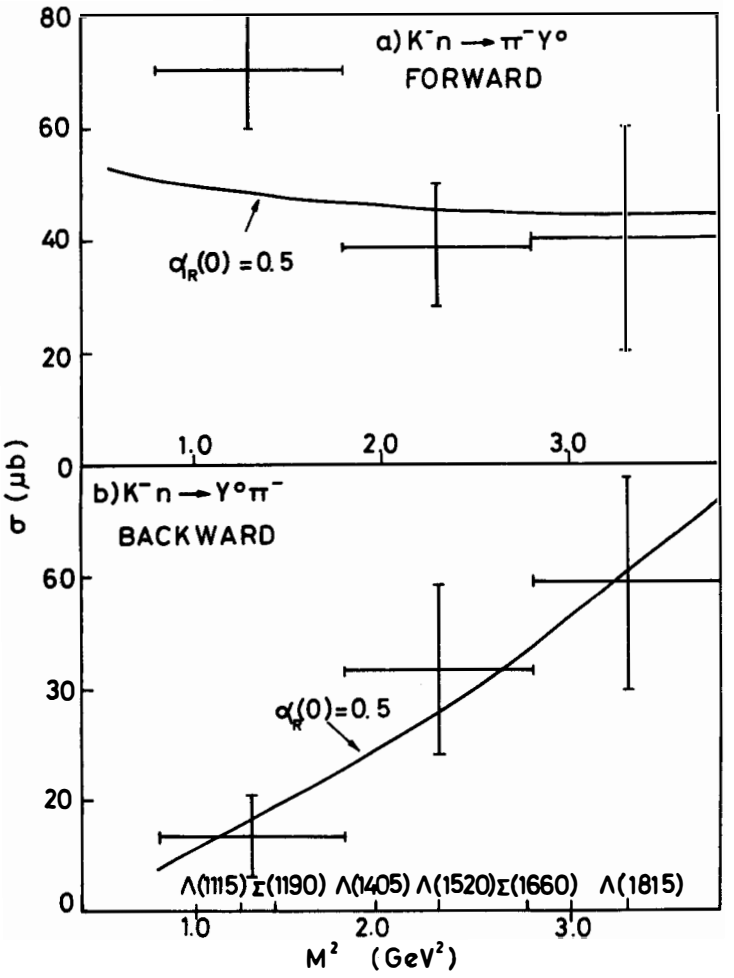

a) K⁻n → π⁻Y°
FORWARD
$\alpha_{I_R}(0) = 0.5$
b) K⁻n → Y°π⁻
BACKWARD
$\alpha_{I_R}(0) = 0.5$
σ (μb)
Λ(1115) Σ(1190) Λ(1405) Λ(1520) Σ(1660) Λ(1815)
M² (GeV²)

FIG. 7

A NOVA MODEL FOR DIFFRACTION DISSOCIATION WITH LONGITUDINALLY DECAYING NOVAS

K. Kajantie
Department of Physics, University of Helsinki,
Siltavuorenpenger 20 B, Helsinki 17, Finland
and
P.V.Ruuskanen
Department of Physics, University of Jyväskylä,
Nisulankatu 78, 40720 Jyväskylä 72, Finland



Abstract : A model for diffractive events in high energy hadron collisions is constructed and the charged particle multiplicity distribution following from this is calculated. The model is a nova-type model in which the excitation spectrum of the nova behaves like M^{-2} for large M and in which the nova decays longitudinally in its rest frame. These features are motivated by simple multiperipheral arguments. Implications of the results on multiperipheral and uncorrelated jet model descriptions of the pionization component are discussed.

Résumé : Un modèle pour les événements diffractifs dans les collisions hadroniques à haute énergie est construite et la distribution en multiplicité des particules chargées correspondante est calculée. Le modèle est un modèle du type nova dans lequel le spectre d'excitation des novae se comporte comme M^{-2} à grand M et la nova se désintègre longitudinalement dans son système au repos. Ces caractéristiques sont justifiées par des arguments simples multiphériques. On discute les implications sur les descriptions de la composante de pionization par le modèle multiphérique ou des jets non-corrélés.

One of the most clear experimental indications of diffractive dissociation at high energies is the leading particle effect as observed, for instance, in the proton-proton collisions at CERN ISR [1,2]. The fact that the peak in the inclusive x-distribution of protons at $s \approx 1000$ GeV^2 extends from $x \approx 1$ to values $x \approx .9\text{-}.95$ indicates that dissociation with masses up to 7-10 GeV ($M=(1-x)\cdot s$) is still appreciable. In terms of an excitation type of picture this means that the excitation spectrum must have a long tail as a function of the excitation mass.

On the other hand there seems to be fairly good indications from the analysis of multiplicity distributions [3-6] that the multiplicities associated with the energy independent part of the cross section are much lower than the overall multiplicities. These considerations lead to the two-component picture [3,7] of the inelastic collisions. There is, at least roughly, a diffractive energy independent part with $\langle n_{ch} \rangle \approx 3\text{-}4$ and a pionization part with $\langle n_{ch} \rangle \propto \log s$ giving the observed increase of the average multiplicity.

In this talk we present a simple model [8] which incorporates in a qualitative way both features mentioned above.

In constructing the model we use multiperipheral ideas as a guide. In the same spirit we could use e.g. the uncorrelated jet model [9]. (See also Frazar and Snider, ref. 10.) A diffractive event will then be one in which there is one and exactly one Pomeron exchanged, the exchange of several Pomerons being forbidden by unitarity [11]. The two halves of the multiperipheral diagram separated by the Pomeron exchange can then be taken to represent a Pomeron-proton collision which we will describe phenomenologically by a nova-type model [12] as illustrated in Fig. 1. This is done by specifying the excitation spectrum $\rho(M)$ of the excitation of the proton to a nova of mass M and the subsequent decay of the nova. The multiperipheral ideas then imply that $\rho(M) \sim M^{-2}$, since only the ordinary Regge poles contribute to the Pomeron-proton collision (the vanishing of triple Pomeron coupling [13]). The assumed multiperipheral nature of the Pomeron-proton collision, however, implies also that the nova decays so that only the transverse but not the longitudinal momenta are limited. This is the feature we need in order to use the nova model to describe diffraction in the two-component picture where diffraction contributes to the low multiplicities only.

We define the model in the following way:

1. Excitation spectrum. As stated above, the excitation spectrum for large masses is assumed to behave like M^{-2}. As long as we are considering high energies ($s \gtrsim 500$) the detailed form of $\rho(M)$ close to the threshold ($M \lesssim 2.5$ GeV) is not very important since it essentially does not affect other quantities than the x-distribution of the protons and there it can not be experimentally resolved at the moment. The shape, which we have used at low masses is shown in Fig. 2 and is that introduced on the basis of low energy data [14] in ref. 15. It should be noted that the area below $\rho(M)$ at the low mass end is important since it mainly determines the 2-prong cross section. The double dissociation is calculated by assuming factorization[8,15]. The normalization is fixed at 303 GeV/c to be:

$$\sigma^D = 2\sigma^D(1) + \sigma^D(2) = 7.5 \text{ mb} . \qquad (1)$$

where $\sigma^D(1)$ is the cross section for the dissociation of one of the protons and $\sigma^D(2)$ is the double dissociation cross section.

The t-dependences of the nucleon-Pomeron-nucleon and nucleon-Pomeron-nova vertices are taken to be

$$\exp(at) \quad , \quad \exp[A(M)t] \ ,$$

respectively, where $a = 4.6\ \text{GeV}^{-2}$ and $A(M) = 0.7\ \text{GeV}^{-1} \cdot (M\text{-}1\text{GeV})^{-1}$ [15]. The shrinkage of the Pomeron observed in elastic scattering is also included in a simple approximate way, as explained in point (c) below.

2. Nova decay. To make a numerical calculation for the multiplicity distribution with limited transverse but not longitudinal momenta we assume a chain decay where at each step the momentum distribution of decay pion is

$$f(p_T) = \frac{B}{\pi} e^{-Bp_T^2} \qquad (2)$$

where p_T is the component of the decay momentum perpendicular to the motion of the decaying nova. The parameter $B = 7\ \text{GeV}^{-2}$ corresponds to $\langle p_T \rangle \approx .3$ GeV. The multiplicity distribution is not very sensitive on the value of B since in the decay of heavier masses the energy of the decay is mainly determined by the longitudinal component of the decay momentum. Charges are specified statistically [15] so that the initial nova and final nucleon have $I = 1/2$ and the intermediate novas can have $I = 3/2$ or $1/2$.

The multiplicity cross sections σ_n^D have been calculated without any approximations by using a Monte Carlo program [15,16]. Results are given in Table 1 and Figs. 3 and 4.

In order to gain more insight from the results we consider the model from a different point of view which allows us to derive an approximate analytic expression for σ_n^D. First, we neglect double dissociation and charges and then we can write (ch. ref. 17.)

$$\sigma_n^D = 2 \int dM \rho(M) D(n-1,M) \ , \qquad (3)$$

where $n \geq 3$ is the total number of final state particles, including neutrals. $D(n_d,M)$ is the multiplicity distribution in the dissociation of a proton into a group of particles with effective mass M, normalized by

$$\sum_{n_d=2}^{\infty} D(n_d,M) = 1 \ , \qquad (4)$$

since $\sigma^D = \Sigma \sigma_n^D$.

The form of $D(n_d,M)$ is determined by the decay distribution of the nova. To approximate it, we apply the uncorrelated jet model to that part of the process

which corresponds to the "Pomeron-proton" collision. Then the average multiplicity $\langle n_d \rangle$ is [8]

$$\langle n_d \rangle \simeq 2\lambda \log M + b \ , \qquad (5)$$

where b is related to the cut-off parameter B and λ to the total inelastic Pp cross section $\sigma_{Pp}(M)$ by

$$\sigma_{Pp}(M) \simeq (M^2)^{\lambda-2}/\langle n_d \rangle \ . \qquad (6)$$

Our assumption that only one Pomeron can be exchanged implies that $\sigma_{Pp}(M)$ can not be a constant but must decrease. In fact, the behaviour $\rho(M) \sim M^{-2}$ corresponds to the value $\lambda = 3/2$.

By making the further approximation that all events with a given mass M correspond to the average multiplicity $\langle n_d \rangle$ and assuming that both charges of the nucleons (for the dissociated proton) and all charges of the pions are equally probable one gets the following expression for the prong cross section [8]:

$$\sigma^{D}_{2n^-+2} = \frac{3\rho_o}{\lambda} \exp\left[-n^- - \frac{1}{3}\right] \exp\left[-\frac{am_N^2}{s^2} \exp\left(4n^- + \frac{4}{3}\right)\right] \qquad (7)$$

where n^- is the number of negative pions in the final state. The second exponential factor comes from the

t_{max}-effect. The form $\rho(M) = \rho_o M^{-2}$ has been used to derive this expression and thus it is valid only when $n^- \geq 1$ since the events with $n^- = 0$ come mainly from the threshold region where the form of $\rho(M)$ is different. The calculation for double dissociation is very similar and the result, in particular, contains the most important factor $\exp(-n^-)$ of (7). The main change is a multiplicative factor n^- which emphasizes larger multiplicities (note that double dissociation contributes only when the number of particles ≥ 4).

We now comment on the numerical results and the analytical formula (7).

(a) According to this model the diffractive charged particle multiplicity (n) is concentrated in small values of n and essentially vanishes for $n > 8$. Analytically the dominant factor in the distribution is $\exp(-n^-)$ which arises from the fact that the novas decay longitudinally. Numerical results are in reasonable agreement with numbers obtained from two-component fits to data [4,6].

(b) For larger values of n^- the second factor in eq. (7) cuts off the distribution above $n^- = \frac{1}{2}\log\left(\frac{s}{m_N\sqrt{a}}\right)$. Due to its double exponential

character it acts essentially like a θ-function. In excitation mass the cut-off is at $M^2 = \frac{s}{m_N\sqrt{a}}$; ($t_{max} \simeq -\frac{m_N^2}{s^2} M^4$). The energy dependence of the cut-off is seen in Fig. 3 as an increase of the 6- and 8-prong cross sections.

(c) As a further effect which probably will change the details of the model, but for which we lack sufficient information, one can mention the shrinkage of the (effective) Pomeron. The energy dependence of σ^D in Table 1 can be somewhat changed depending on the assumptions about the shrinkage. In calculating the numbers in Table 1 we have simply taken the shrinkage proportional to the elastic shrinkage as given by the effective Pomeron slope $\alpha_P' = .4$ [18]. This means that the numbers obtained from the Monte Carlo program have been multiplied by the factor $1/(6.4+2\alpha_P' \text{ logs})$, before applying the normalization condition (2). Especially for the double dissociation the effect could be larger and thus the increase of σ^D with energy, which is mainly due to the increase of double dissociation [19], could be negligible.

(d) The model as presented here contains several parameters which are fixed rather arbitrarily (e.g. we have set $b = 0$ in (5)). However as long as we keep the M^{-2}-tail for $\rho(M)$ and the longitudinal decay

of the novas the multiplicity distribution σ_n^D is not essentially changed. In order to be able to be more specific one has to consider the momentum distributions and the pionization component. As an example, the x-distribution of protons is shown in Fig. 5 near $x = 1$, where the throughgoing protons give the dominant contribution. The form M^{-2} of the excitation spectrum gives a (nonscaling) x-distribution $d\sigma/dx \sim s^{-1/2}(1-x)^{-3/2}$. The experimental shape of the leading particle peak is much wider but as shown by the solid line in Fig. 5 the predicted shape crucially depends on the background which is used. Here the background is taken to be $\sim(1-x)\cdot x^2$ which follows from an uncorrelated jet model calculation with leading protons.

If it is found that the leading proton peak also contains a scaling component, the excitation spectrum of $\rho(M)$ has to be modified to include a M^{-1} part as well. From the numerical point of view a moderate M^{-1}-term would not change drastically the multiplicity cross section considerations at the energies up to 300 GeV/c. The distribution would become somewhat broader and there is actually some indication for the need of this e.g. in Fig. 5a, which shows that the predicted 6-prong cross section is too small as it is for all five energies [20,21] which we

have considered. The broadening of σ_n^D would also make the predicted dip at 1500 GeV/c, which is shown in Fig. 5b, less prominent. Asymptotically the average diffractive multiplicity $\langle n_{ch} \rangle^D$ would eventually grow logarithmically [10].

Finally we will consider the implications for the pionization component. The aforementioned multiplicity predictions of Fig. 5 were calculated by assuming that the pionization part is of the Poisson shape. Thus we subtracted the calculated diffractive cross sections σ_n^D from the data and fitted a Poisson distribution to the remaining part. The average numbers of negative particles $\langle n^- \rangle^P$ for the Poisson distributions are given in the Table 1. It is observed that the average charged multiplicity $\langle n \rangle^P$ of the pionization component increases rather rapidly as a function of s : according to Table 1 $\langle n^- \rangle^P \sim 1.1 \log s - 3.2$. This is natural in the framework of a two-component theory, in which $\langle n \rangle = p_1 \langle n \rangle^P + p_2 \langle n \rangle^D$ with $p_1 \sim 3/4$. Since experimentally [22] for $p_{lab} > 100$ GeV/c, $\langle n \rangle \sim A \log s$ (s in GeV^2), where A is at least 1.5 we obtain

$$\langle n \rangle^P \sim 2 \log s \ , \qquad (8)$$

where the coefficient is more likely larger than 2.

It seems reasonable to assume that π^+, π^- and π^o are all created in equal numbers. The result (8) then indicates that the overall average multiplicity for the pionization grows like $\langle n_{all} \rangle^P \sim 3 \log s$. A coefficient for the logarithmic growth which is $\gtrsim 3$ can not be achieved in the simplest version of the common models to describe pionization. Consider first the uncorrelated jet model [9], where the matrix element is $\prod_1^n f_i(p_{Ti})$. The resulting average multiplicity and inelastic cross sections are then given by Eqs. (5) and (6). (M^2 is replaced by s). The value $\lambda = 2$ corresponding to $\langle n_{all} \rangle \sim 2 \log s$ is obviously a maximum value of λ because σ_{inel} would otherwise increase like a power of s. Thus the conclusion is that the matrix element must be a function of s or that the pions are not produced independently. The first possibility is easy to achieve; for instance, a factor s^{-p} will appear directly in the expression (6) for σ_{inel} (as for any other cross section type of quantity) but will not affect eq. (5). In the second case the modifications would not be as straightforward and in either case the model would loose some of its simplicity.

The implications for the multiperipheral model are analogous. Assuming that all the produced particles

are pions and that only one trajectory with intercept $\alpha < 1$ is exchanged it is easy to show [23] that the s-dependence of σ_{inel} and $\langle n_{all} \rangle^P$ is given by

$$\sigma_{inel} \sim s^{\lambda-2\alpha-2}$$

$$\langle n_{all} \rangle^P \sim \lambda \log s . \qquad (9)$$

The constancy of σ_{inel} requires

$$\alpha = 1 - \frac{1}{2}\lambda$$

which with $\lambda \gtrsim 3$ implies a negative value for the effective intercept. This reflects the fact that in order to produce many pions, small s_i-regions must be favored so that the consecutive pions can be close to each other in the multiperipheral chain; thus the low effective intercept. This , however, seems like using brute force to make the multiperipheral model accommodate large multiplicities and does not look very realistic. A more natural way is to let the pions come closer by some other mechanism, for instance, by forming resonances, but again the simplicity of the model is lost.

Table 1

Calculated diffractive charged particle cross sections (in mb) and the average diffractive charged multiplicity. The last column gives the value of $\langle n^- \rangle^P = m$ if the charged multiplicity distribution of the pionization component (obtained by subtracting the numbers in this Table from measured cross sections) is fitted by a Poisson: $\sigma^P_{2n^-+2} = \sigma_o \, m^{n^-} e^{-m}/n^-!$. At 50 GeV/c the amount of double dissociation is 17% of the total, at 303 GeV/c 27%.

P_{lab}	σ_2^D	σ_4^D	σ_6^D	σ_8^D	σ_{10}^D	σ^D	$\langle n^- \rangle^P$	$\langle n \rangle^D$
50	2.81	2.61	0.47	0.048	0.001	5.94	1.83	3.25
69	2.91	2.78	0.62	0.073	0.005	6.38	2.19	3.34
102	2.88	2.94	0.78	0.12	0.007	6.74	2.62	3.45
205	2.84	3.15	1.08	0.25	0.033	7.36	3.39	3.68
303	2.79	3.20	1.15	0.30	0.049	7.50	3.82	3.76

References

1. M.G. Albrow et al., CERN preprint, August 1972.
2. M.G. Albrow et al., Nucl. Phys. B54, (1973) 6.
3. K. Fialkowski,Phys. Lett. 41B (1972) 379.
4. K. Fialkowski and H.I. Miettinen, Phys. Letters 43B (1973) 61.
5. L. Van Hove, Phys. Letters 43B (1973) 65.
6. C. Quigg and J.D. Jackson, NAL preprint NAL-THY-93 (1972).
7. A. Bialas, K. Fialkowski and K. Zalewski, Nucl. Phys. B48 (1972) 237.
8. K. Kajantie and P.V. Ruuskanen, Phys. Lett, to be published.
9. E.H. de Groot, Nucl. Phys. B48 (1972) 295.
10. W.R. Frazer and D.R. Snider, NAL preprint, NAL-Pub-73/15/THY.
11. J. Finkelstein and K. Kajantie, Phys. Lett. 26B (1968) 305.
12. M. Jacob and R. Slansky, Phys. Rev. D5 (1972) 1847.
13. H. Abarbanel et al., Phys. Rev. Lett. 26 (1971) 937.
14. U. Amaldi et al., Phys. Lett. 34B (1971) 435.
    J.V. Allaby et al., CERN preprint, contribution to the Oxford conference (April 5 - 7, 1972).
15. P. Pirilä and P.V. Ruuskanen, Nuovo Cimento, to

be published.

16. P. Pirilä and P.V. Ruuskanen, University of Jyväskylä preprint, Report No.2/1973.
17. R. Hwa, Phys. Rev. Lett. 26 (1971) 1143, Phys. Lett. 42B (1972) 79.
18. M.G. Albrow et al., CERN preprint, December 1972.
19. A.N. Diddens, Total Cross-Sections and Elastic Scattering at High Energies. Contribution to the Oxford Conference (April 5 - 7, 1972).
20. V.V. Ammosov et al., Phys. Lett. 42B (1972) 519, J.W. Chapman et al., Phys. Rev. Lett. 29 (1972) 1686, G. Charlton et al., Phys. Rev. Lett. 29 (1972) 515.
21. F.T. Dao et al., Phys. Rev. Lett. 29 (1972) 1627.
22. M. Jacob, High Energy Collisions, XVI International Conference on High Energy Physics, Batavia, 1972.
23. See, eg., H. Harari, Phys. Rev. Lett. 29 (1972) 1708.

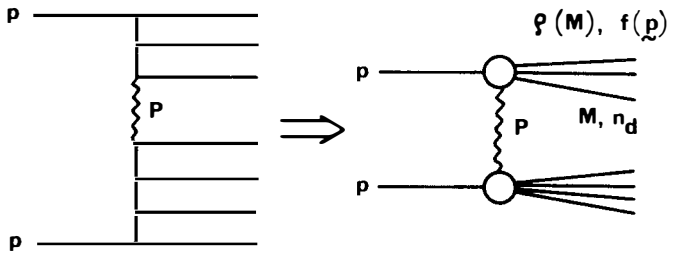


Fig. 1 - Transformation of multiperipheral diagram with single Pomeron exchange to a diffractive excitation process characterized by excitation spectrum ρ(M) and a decay distribution f(p); n_d is the number of particles into which the proton dissociates, M the mass of the nova. Only the double dissociation diagram is shown, single excitation diagrams are obtained if the Pomeron exchange is either the highest or the lowest.

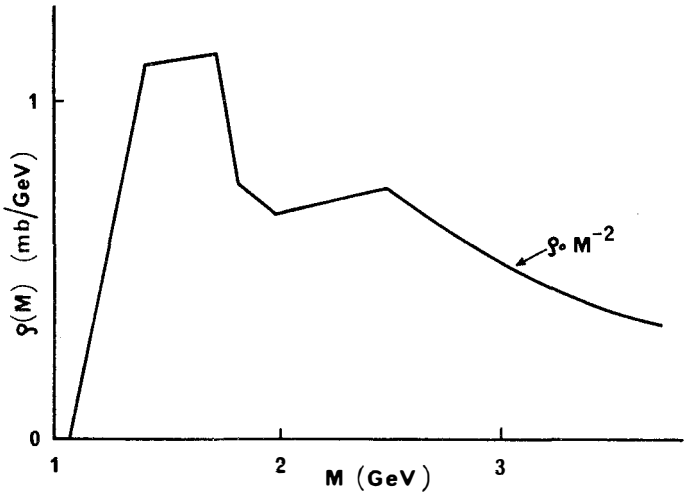


Fig. 2 - The proton excitation spectrum, the scale is fixed at 303 GeV/c.

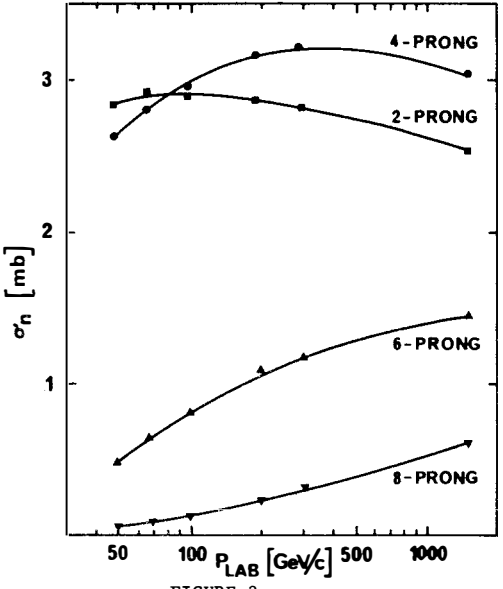


FIGURE 3

The energy dependence of the prong cross sections as predicted by the model. The increase of 6- and 8-prong cross sections is due to the opening up of the phase space and the decrease of 2- and 4-prong cross sections due to the shrinkage.

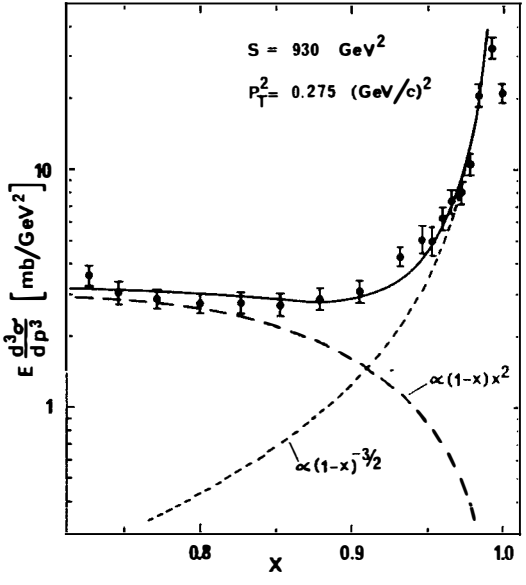


FIGURE 4

The x-distribution of the protons near x = 1. The form $(1-x)^{-3/2}$ corresponds to the excitation spectrum $\rho(M)\propto M^{-2}$ and the $(1-x)x^2$ term is a jet model prediction. Solid line is the sum of these terms. Data are from ref. 2.

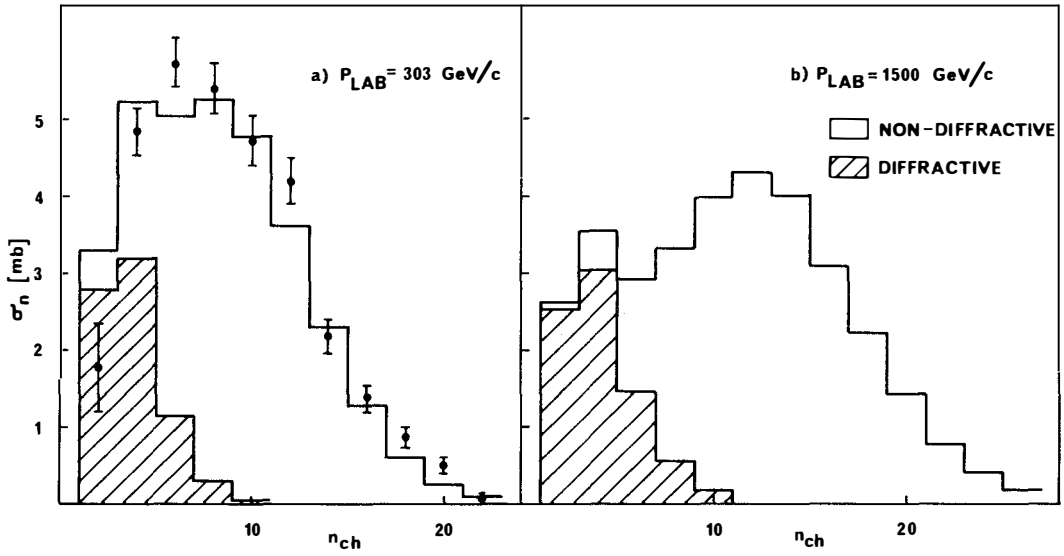


FIGURE 5

The calculated multiplicity distributions at a) 303 GeV/c and b) 1500 GeV/c. The open circles are data of ref. 21.

A MODEL OF THE BREAKING OF HAGEDORN THEORY AND SCALING AT HIGH TRANSVERSE MOMENTUM

J. M. Dethlefsen
J. Dias de Deus
H. B. Nielsen
The Niels Bohr Institute, University of Copenhagen,
Copenhagen, Denmark



Abstract : It is argued that the parton model suggests a deviation from the exact Hagedorn thermodynamic model. This in turn leads to a deviation for the large transverse momentum inclusive spectrum from the Planck spectrum expected from the Hagedorn theory. We are taking a model in which fireballs are produced by collisions of partons in the beam and in the target. These fireballs then decay under successive emission of pions, say, with a decreasing temperature. Good agreement with ISR data is obtained.

Résumé : Nous suggérons que dans le modèle des partons le modèle thermodynamique de Hagedorn ne peut pas être exact. On arrive à une déviation dans le spectre inclusive à grand moment transverse du spectre de Planck de la théorie de Hagedorn. Nous utilisons un modèle dans lequel des boules de feu sont produites par des collisions de partons dans le faisceau et dans la cible. Ces boules de feu émittent successivement des pions et la température décroit en même temps. Nous obtenons un bon accord avec les donnés des ISR.

Recently transverse momentum distributions around 90° have been obtained at the ISR[1,2]. The most striking features of these distributions are the following: i) A flattening of the distributions starting around 2 geV. ii) In the region where this flattening occurs, the inclusive cross section is growing with increasing C. M. energy so that scaling is violated.

By the flattening off we refer to that the form $\exp(-6p_{\perp})$ that fits the distribution so well below 2 geV falls far below the data points at larger transverse momenta. Such a deviation is presumably incompatible with the Hagedorn thermodynamical model[3] in which there is an absolute highest temperature of hadronic matter. If we namely assume that all the transverse momenta are originating from the thermal motion of the hadron matter, it is difficult to imagine how the spectrum can have a component flatter than the Planck function corresponding to the Hagedorn temperature T_H.

So these data suggest a breakdown of the Hagedorn theory at large transverse momenta.

Now, the essential input in Hagedorn theory is the Bootstrap, which gives rise to the form

$$e^{m/T_H} \qquad (1)$$

of the level density of the hadron. In dual model, which is also a bootstrap model, the level density[4] is again of the form (1), and the transverse spectrum[5] is of the form $\exp(-4\alpha' p_{\perp}^2)$ which is even worse than the Hagedorn prediction.
One could then guess, that in the "right" model, the bootstrap condition is not fulfilled.

In parton model the hadron is thought of as being composed of infinitely many strongly interacting constituents. If we want to avoid the Bootstrap, these constituents cannot be hadrons, but must be something else: Partons.

We now reformulate the parton model (specifically the model of ref. 6) and show that it leads to a level density deviating from that of eq. 1.

Because of the strength of the internal coupling of hadron matter the decomposition of a hadron into partons may not be meaningfull, unless we look at the hadron from a very rapidly moving inertial frame: the infinite momentum frame. In this frame the interaction between partons may be treated in a perturbative way, at least over a finite interval of time.

In zero order then, the partons are considered as being free particles. In next order, the partons suffer harmonic oscillator forces. We may treat the hadron as being composed of infinitely many free harmonic oscillators, the excitations of which are the phonons, building up the entire hadron spectrum. Finally we may simulate the higher order terms in the coupling by postulating a statistical coupling among the oscillators. When the oscillators are in statistical equilibrium among themselves the hadron is called a "fireball".

The probability of finding that a certain oscillator k in the fireball is in a definite state having a certain value H_k of the internal hamiltonian is given by

$$e^{H_k/T_{osc}} \qquad (2)$$

where T_{osc} is the oscillator temperature.

In the model which we are going to use, namely the string model, the total internal hamiltonian

$$H = \sum_k H_k \tag{3}$$

is equal to the mass square of the hadron. Keeping the total external momentum P fixed, and using the formula

$$E = \sqrt{p^2 + m^2} \simeq p + \frac{m^2}{2p} \tag{4}$$

we see that the probability of finding a definite state of the fireball with a total energy E, is given by

$$e^{-E/T_p} \tag{5}$$

where

$$T_p = T_{osc} / 2p \tag{6}$$

is the fixed momentum temperature. Formula (5) tells us that the energy of the fireball is canonically distributed. Therefore, when energy is transferred to a fireball at fixed momentum P, entropy is changed according to the formula

$$dS = dE / T_p \tag{7}$$

Because of the invariance of entropy the connection betweem the oscillator temperature and the rest system temperature T_H is then given by

$$T_{osc} = 2 m T_H \tag{8}$$

Notice that the fixed momentum temperature transforms according to the law of Planck. Further notice that a fireball is completely described by its mean mass or its rest temperature or its entropy. This in contrast to say black body radiation, where one must specify one more variable like the volume. The reason for this difference is that the density $\rho(\omega)$ of oscillators per frequency interval is fixed by the longitudinal momentum distribution of the partons and the slope of the leading Regge trajectory.

We calculate $\rho(\omega)$ in the string model suggested by Kraemmer, Nielsen and Susskind[6]. In this model the hadron is made up of an infinite but discrete chain of partons. (See fig. 1). The string is parametrized by the variable θ running from 0 to π. The topology of the string is chosen in such a way that the total momentum P of the string is evenly distributed over the string.

Requiring the speed of sound c to be constant over the string one can show that the law of dispersion of the phonons is given by

$$\omega = \frac{2C}{a(\theta)} \sin\left(\frac{K(\theta)\, a(\theta)}{2}\right) \tag{9}$$

where $a(\theta)$ is the inverse of the density of partons at the point θ. Around this point each of the partons take up a fraction

$$x = \frac{a(\theta)}{\pi} \tag{10}$$

of the total momentum. The number of partons having a fraction of total momentum between x and x + dx is then given by

$$\frac{2}{\pi}\,\frac{d\theta}{dx}\,\frac{dx}{x} \equiv F(x) \tag{11}$$

where $F(x)$ is the structure function νW_2 measured in deep inelastic electron proton scattering.

We are now able to express the density $\rho(\omega)$ in terms of the structure function, finding

$$\rho(\omega) = \frac{1}{c}\int_0^{c/\omega} F(x)\,dx \tag{12}$$

The integral of equation (12) is simply the proportion of the string in which the distance πx between neighbouring partons is less than c/ω. The idea is that this part of the string, is the one in which waves with frequency ω are allowed to run, as can be seen from the law of dispersion (9). The exact value of the constant factor of the upper limit c/ω of the integral is adjusted so that the total number of harmonic oscillators should be equal to the number of partons in the special case $F(x) = \delta(x-\epsilon)$.

The lowest oscillator mode must have mass square $1/\alpha'$ since it is this mode which builds up the leading Regge trajectory. The wavelength of the lowest mode is twice the length of the string. This gives

$$c = 1/\alpha' \tag{13}$$

We are now able to calculate any extensive thermodynamical quantity of the hadron e.g. the mean mass square:

$$m^2 = \int d\omega\, \rho(\omega)\, \frac{D\,\omega}{e^{\omega / T_{osc}} - 1} \qquad (14)$$

Here D = 6 is the effective number of degrees of freedom per parton. From formula (8) and (14) we can now calculate the Hagedorn temperature as a function of the mean mass. (See Fig. 2). At very high energies

$$T_H \simeq \frac{1}{8\,D}\, \frac{m}{\mathrm{Log}\, m/m_\pi}\, \frac{1}{F(0)} \qquad (15)$$

the level density of the hadron, which is equal to the exponent of the entropy then asymptotically grows like

$$e^{(\mathrm{Log} \frac{m}{m_\pi})^2 4\,D\,F(0)} \qquad (16)$$

that is, much slower than predicted by dual model and Hagedorn theory.

Now let us turn to the question of how to connect the model for the level density with the inclusive distributions in hadron hadron collisions.

If we believe in duality, we are free to choose between an s-channel or a t-channel description of the collision. Let us choose an s-channel description. Then the collision process may be divided up into two parts:

1) When the two hadrons collide, excited hadron matter, in some form or another, is created.
2) The excited matter propagates and decays.

So we have to make a model for the excitation

and a model for the decay.

We suggest that the excitation comes from the collision of two partons, one from each of the incoming hadrons. In such a collision there is a certain probability T that the two partons melt together into a fireball. There is also a certain probability that by this collision the two initial hadrons get excited. However, since we are only interested in the transverse momentum distribution at x = 0 we look away from the latter possibility for the moment.

The probability of creating a fireball with mass m and CM rapidity y is then given by

$$|T|^2 \, F\left(\frac{m\, e^{y}}{\sqrt{s}}\right) F\left(\frac{m\, e^{-y}}{\sqrt{s}}\right) dy \, \frac{dm}{m} \qquad (17)$$

where F again is the structure function. The fireball mass is bound below by m_π. We assume that the parton parton cross-section goes like $1/m^2$ as suggested by a very short range interactions between the partons.

More important for our main interest, the transverse momentum distributions, is our model of the decay of the fireball. This decay is supposed to occur by successive emission of pions. These pions are emitted statistically. That is, we assume that the fireball-fireball-pion coupling is independent of fireball mass and pion energy. The probability of emitting a pion from a fireball of mass m with a certain energy E_π is then proportional to the number of possible different final states.

If E_π is not too big, it follows from equations (7) and (16) that the number of fireball states having mass $m - E_\pi$ is approximately proportional to

$$e^{-E_\pi/T_H(m)} \tag{18}$$

So, when the fireball mass decreases from m to m $-\Delta$m the number of the emitted pions having momenta between $\vec{p}$ and $\vec{p} + d\vec{p}$ is given by

$$\frac{1}{T_H^4(m)} \left(e^{E_\pi/T_H(m)} - 1 \right)^{-1} \Delta m \, d^3p \tag{19}$$

It is now easy to compute the inclusive pion cross section. We find

$$\frac{d^3\sigma}{dp^2 dy} = \int_m^{\frac{dm}{3}} dy_1 F\left(\frac{me}{\sqrt{s}}\right) F\left(\frac{me}{\sqrt{s}}\right)^{y_1} \int \frac{dm'}{T_H^4(m')} \left(e^{\frac{E \cosh(y-y_1)}{E \cosh(y-y_1)/T_H(m')}} - 1 \right)^{-1} \tag{20}$$

where y is the rapidity and $E_\perp$ is the longitudinal mass $\sqrt{m_\pi^2 + p_\perp^2}$ of the pion measured in the CM system of the incoming hadrons.

The transverse momentum spectra calculated from the formula (20) seems to be in very good agreement with experiment. (See fig. 3). In fig. 4 we give the predicted y-dependence of the spectra.

In principle, apart from an overall normalization factor, our model is a zero parameter one. As input we used the universal slope α', the effective dimension D and the structure function F(x) was simply parametrized by

$$F(x) = \frac{1}{b} \theta(b-x) \tag{21}$$

with b = 0.75 which is somewhat above the value indicated by the deep inelastic scattering data. So effectively b was used as a free parameter.

Many other variants of the model have been consi-

dered especially concerning the connection between the inclusive spectrum and the level density. The one we have described here seems to agree best with data.

We hope however to put forward in a more detailed article how other proposals seem to fail together with other facets of our model, such as the multiplicity distribution, and a more detailed discussion of the connection between the Hagedorn spectrum and the one dimensionality of hadron matter.

Acknowledgement

Drs. Hans Bøggild, Gunnar Damgaard and Knud Hansen, all belonging to the experimental group at the Niels Bohr Institute, have given us invaluable help during this work. They have provided data, ideas and many instructive discussions. We also want to thank our colleagues at the high energy theoretical group for discussions.

Figure Captions

Fig. 1 Harmonic excitations in a string of partons. a) Unconstrained mode: $\lambda(\theta) > \pi a(\theta)$ everywhere. b) Constrained mode $\lambda(\theta) < \pi a(\theta)$ in the middle of the string.

Fig. 2 Hagedorn temperature as a function of mean mass. From Eq. (14) with D = 6.

Fig. 3 Predicted $p_\perp$ spectra and ISR data at y = 0 and at two values of s, s = 950 and s = 2850 GeV^2. (Data from ref. 1).

Fig. 4 Predicted dependence of the $p_\perp$ spectrum as y changes at fixed s. The central plateau is broken at large values of $p_\perp$.

References

1) CERN - Columbia - Rockefeller Collaboration, and Saclay - Strasbourg Collaboration, as reported by M. Jacob at the International Conference on high energy physics, Batavia (1972).

2) British - Scandinavian Collaboration

3) R. Hagedorn, Suppl. Nuovo Cimento 3, (1965) 147
R. Hagedorn, G. Ranft, Suppl. Nuovo Cimento 64A, (1969) 811
K. Bardakci, S. Mandelstam, Phys. Rev. 184, (1969) 1640

5) D. Gordon and G. Veneziano, Phys. Rev. D3, (1971) 2116
M. A. Virasoro, Phys. REv. D3, (1971) 2834
C. E. de Tar, K. Kang, C. I. Tan, J. H. Weis, Phys. Rev. D4, (1971) 425

6) H. B. Nielsen, L. Susskind, A. B. Kraemmer, Nucl. Phys. B28, (1971) 34
A. B. Kraemmer, H. B. Nielsen, Nucl. Phys. B41, (1971) 34
A. B. Kraemmer, H. B. Nielsen, Nucl. Phys. B41, (1972) 173

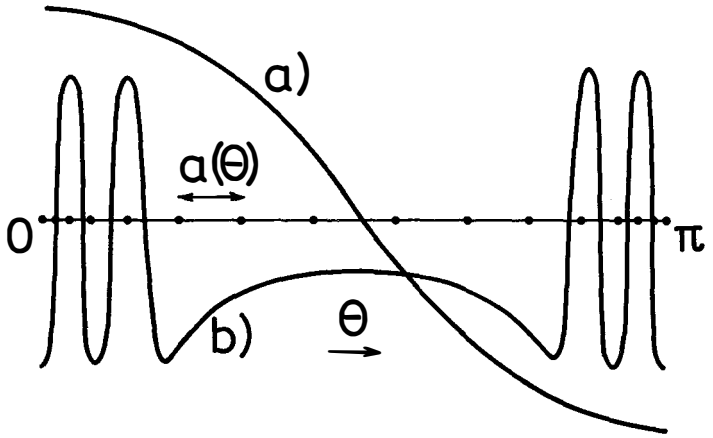


Fig. 1

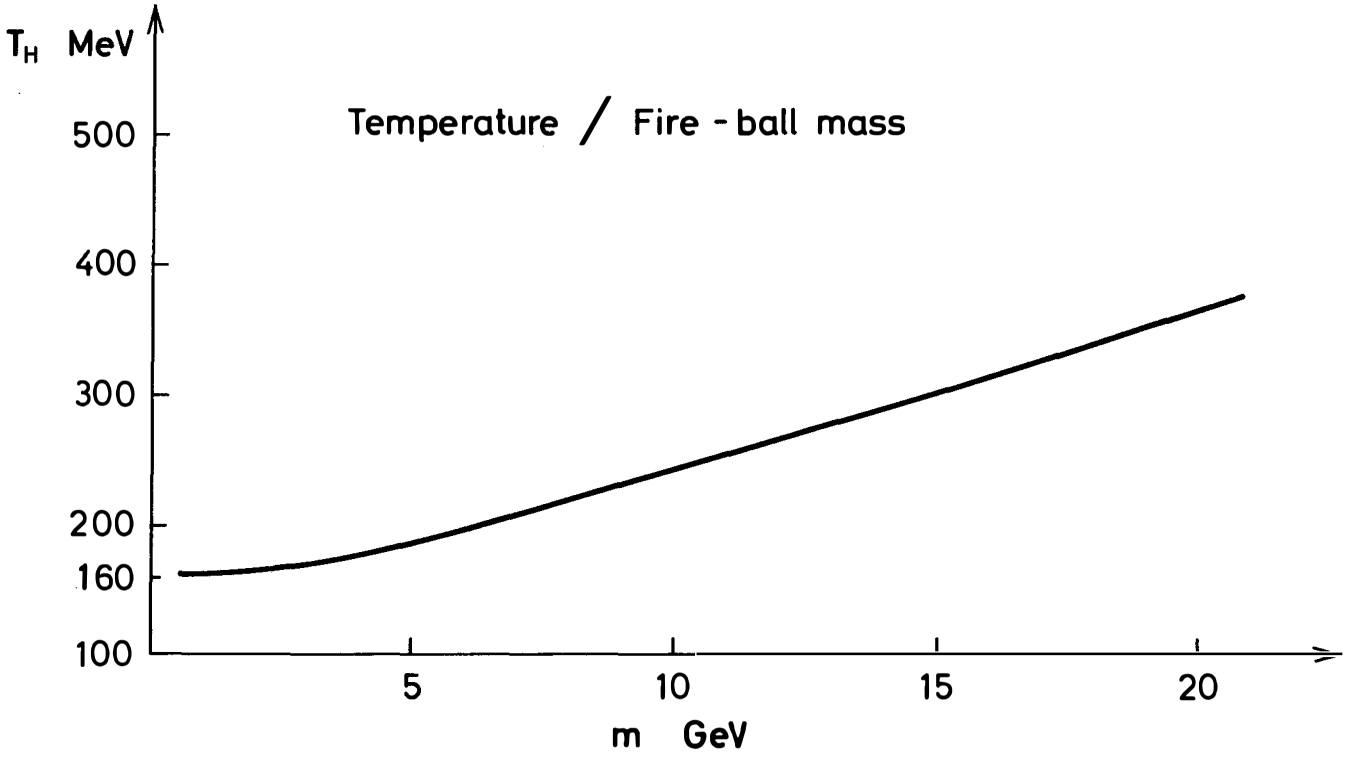

T_H MeV
Temperature / Fire - ball mass
500
400
300
200
160
100
5
10
15
20
m GeV

Fig. 2

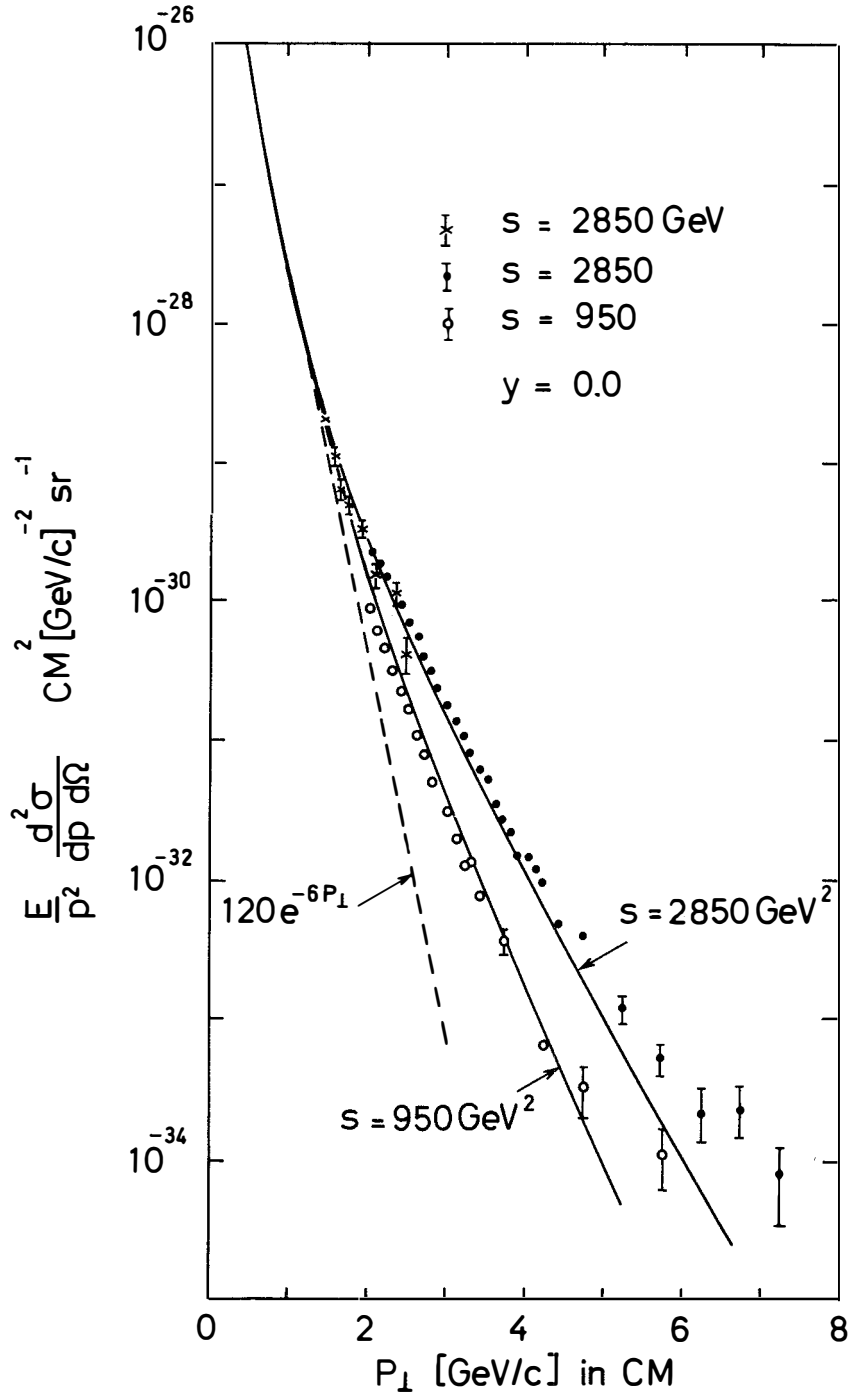

10^{-26}
10^{-28}
10^{-30}
10^{-32}
10^{-34}
$E\frac{d^2\sigma}{dp^2\,d\Omega}$ CM ^{2} [GeV/c] $^{-2}$ $^{-1}$ sr
s = 2850 GeV
s = 2850
s = 950
y = 0.0
$120\,e^{-6P_\perp}$
s = 2850 GeV^2
s = 950 GeV^2
0
2
4
6
8
$P_\perp$ [GeV/c] in CM

Fig. 3

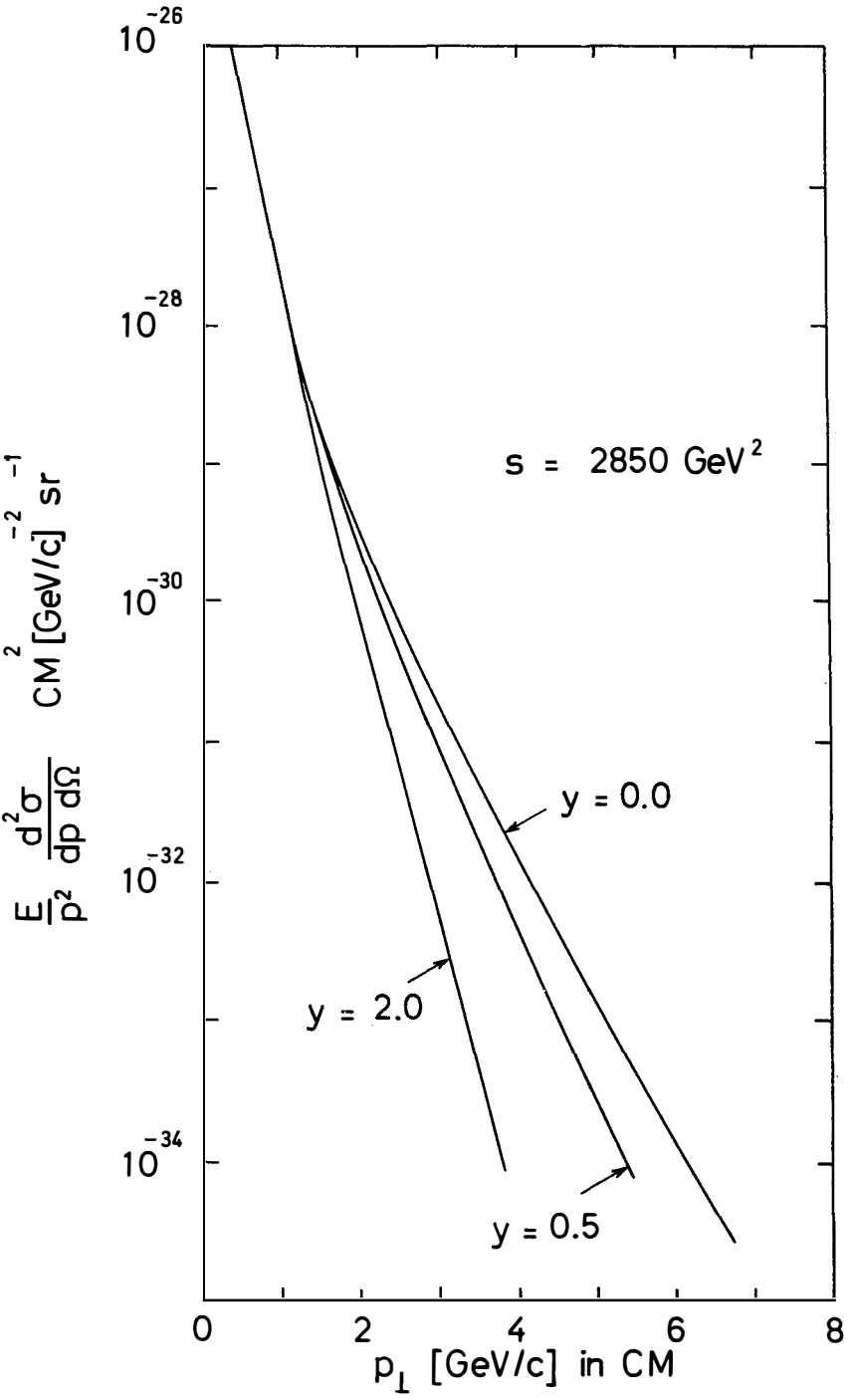

10^{-26}
10^{-28}
10^{-30}
10^{-32}
10^{-34}
$\frac{E}{p^2}\frac{d^2\sigma}{dp\,d\Omega}$ CM ^{2} [GeV/c] $^{-2}$ $^{-1}$ sr
s = 2850 GeV^2
y = 0.0
y = 2.0
y = 0.5
0
2
4
6
8
$p_\perp$ [GeV/c] in CM

Fig. 4

AVERAGE QUANTUM NUMBERS PER PARTICLE.

WHAT ARE THEY GOOD FOR ?

A.L.M. Mihul

Joint Institute for Nuclear Research

Dubna.

Abstract : Average per particle of the baryon, electric and strange quantum numbers is used for approximative analysis of leading properties of incident particles. A similar shape of the average baryon quantum number distribution as a function of $x = P_L / P_{L.max}$ is found for πp and pp inclusive reactions between 6 and 1500 GeV/c (Lab. mom.).

Résumé : On utilise la moyenne des nombres quantiques baryoniques, de charge ou d'étrangeté par particule pour analyser les propriétés directrices des particules incidentes. On trouve une forme similaire pour les distributions moyennes des nombres baryoniques en fonction de $x = p_L / p_{L\,max}$ pour les réactions inclusives pion nucleon et proton proton entre 6 GeV/c et 1500 GeV/c.



PAIR PRODUCTION AND QUANTUM NUMBER EXCHANGE IN MULTIPARTICLE PRODUCTION *)

by

Bengt PETERSSON

Laboratoire de Physique Théorique et Particules Elementaires, Université de Paris-Sud, Centre d'Orsay
91405 Orsay, France.





Abstract : We describe an investigation of the antiproton production, and extend the analysis to the production of K^-. In particular, we may in both cases explain the rise with energy of the yield and the shape of the rapidity spectra, without free parameters.

Résumé : Nous décrivons un travail sur la production des antiprotons, et étendons l'analyse à la production des K^-. En particulier, nous pouvons dans les deux cas décrire la dependance en énergie et la forme du spectre en rapidité, sans paramètres libres.

*) The following is based on a work together with R. Iengo and A. Krzywicki.

In this work we have investigated the production mechanism in $\bar{p}$ and K^- production, in light of the new results from ISR.

The motivations for our investigation are :

i) To understand the apparently spectacular rise with energy of the yield of these particles.

ii) To show that the experimental results can be used as evidence for the importance of quantum number exchange effects in multiparticle reactions.

The rise of the yield is quite difficult to describe by an asymptotic formalism. For example, the criterion of duality applied to the inclusive analysis of the reactions

$$pp \rightarrow \bar{p}, K^- \qquad (1)$$

leads one to expect early scaling, as these reactions are exotic in all subchannels [2]. Experimentally, the invariant cross section $E\frac{d\sigma}{d^3p}$ rises at fixed p^T by a factor of 20 for antiprotons and 7 for K^-, as the cms energy $\sqrt{s}$ grows from 7 to 53 GeV .

We will show that it is possible to understand this rise from a non-asymptotic formalism, taking into account the general features of multiparticle production.

We may then discuss the more important question of the effect of quantum number exchange. More precisely we may ask the question : is baryon number and strangeness conserved locally, i.e. is a proton-antiproton pair necessarily created within a small rapidity interval ?

Here we take advantage of the fact that the multiplicity of antiprotons and K^- is low even at the highest ISR energy ,

$$\langle n \rangle_{\bar{p}} = 0.2$$
$$\langle n \rangle_{K^-} = 0.4 \qquad (2)$$

for $\sqrt{s} = 53\text{GeV}$ [3]. Therefore, to a good approximation, at most one pair is created per event.

In describing the production of these pairs one may envisage two possibilities :

i) A "statistical hypothesis", in which there are no constraints due to strangeness and baryon number conservation, but the general features like leading particle effects are taken into account. This hypothesis is that the probability of creating a $N\bar{N}$ or $K\bar{K}$ pair is proportionnal to the production of a $\pi^+\pi^-$ pair in the same kinematical situation :

$$\frac{d^2\sigma}{(dq_p)\,(dq_{\bar{p}})} = C\,\frac{d^2\sigma}{(dK_+)\,(dK_-)} \qquad (3)$$

where the total four-momentum is the same,

$$K_+ + K_- = q_p + q_{\bar{p}} \qquad (4)$$

To uniquely determine the momenta we demand further

$$K_+^T = q_p^T$$
$$K_-^T = q_{\bar{p}}^T \qquad (5)$$
$$\text{sgn}\,[y(\pi^+) - y(\pi^-)] = \text{sgn}\,[y(p) - y(\bar{p})]$$

Equation (3) is true e.g. in the uncorrelated jet model. We will use the experimental pion spectra, and consider the equation as

giving the "effective phase space" for the creation of the pair.

ii) In the "exchange hypothesis", we include the effect of quantum number exchange, as it would result from e.g. a multi-peripheral model. This leads to the inclusion of a factor proportional to a power of the invariant mass of the pair. We observe that this power corresponds to the energy dependence of baryon or strangeness annihilation. Thus we expect :

$$\frac{d^2\sigma}{(d\,q_p)\,(d\,q_{\bar{p}})} = C'\left[\frac{(q_p + q_{\bar{p}})^2}{4\,m_N^2}\right]^{-\gamma} \frac{d^2\sigma}{(dK_+)(dK_-)}$$

where $\gamma = 1 - \alpha_\omega = \frac{1}{2}$, and the kinematical constraints are the same as above. Note that this reasoning breaks down when several pairs are produced.

We are thus in each case left with only one constant parameter, as far as the pion spectra are known. For the latter we use the fits of ref. 3,4 to the data with the approximation

$$\frac{d^2\,\sigma}{(dK_+)\,(d\,K_-)} = \frac{1}{\sigma_{inel}} \frac{d\sigma}{(dK_+)} \frac{d\sigma}{(dK_-)}$$

which is acceptable, because the rapidity separation between the pions are large in the above kinematical situation.

The results are presented in Fig. 1-3. For each set of curves, we use the free parameter to fix the 90° point at the highest energy. In Fig. 1, we present the result for the statistical model applied to antiprotons, in Fig. 2 the exchange model compared to the same data, and in Fig. 3 the exchange model compared with the experimental results on K^-.

From the comparison with data, we may draw the following conclusions:

i) The energy dependence and shape of the rapidity spectra are well described by the exchange model, both for $\bar{p}$ and K^-.

ii) The rise of the yield at 90° is also qualitatively correct in the "statistical" model, and may thus be a rather general feature. On the other hand, the cut-off factor in the invariant mass, typical for an exchange model, is crucial for the shape in the fragmentation region at ISR energies. The data are not yet good enough to establish the actual value of γ (A fit with $\gamma = 1$ is not significently worse). However, the superiority of the exchange model gives evidence for the importance of quantum number exchange effects.

REFERENCES

1. R. Iengo, A. Krzywicki and B. Petersson, Phys. Letters.

2. See e.g. Chan Hong-Mo, H.I. Miettinen, D.P. Roy and P. Hoyer, Phys. Letters 40 B, 406 (1972).

3. G. Damgaard and K.H. Hansen, "An estimate at the multiplicity of charged particles produced at the ISR", Contribution to the Zakopane Conference on Multiparticle Dynamics, Niels Bohr Institute report (1972).

4. H. Bøggild, K.H. Hansen and M. Suk, Nuclear Physics B27, 1 (1971)

5. E. Lillethun, "Charged particle production at ISR", Review at the XVI International Conference on High Energy Physics (Batavia 1972), Bergen Report Nº 47.

6. A. Bertin, P. Capiluppi, M. d'Agostino-Bruno, R.J. Ellis, G. Giacomelli, A.M. Rossi, G. Vannini, A. Bussière and R.T. Poe, Contribution to the XVI International Conference on High Energy Physics (Batavia 1972).

7. B. Alper, M. Bøggild, P. Booth, F. Bulos, L.J. Carroll, G. Damgaard, G. von Dardel, B. Duff, F.F. Heymann, J.N. Jackson, G. Jarskog, L. Jønsson, A. Klowning, L. Leistam, E. Lillethun, G. Lynch, M. Prentice, D. Quarris and J. Weiss, Contribution to the XVI International Conference on High Energy Physics (Batavia 1972).

8. M. Banner, J.L. Hamel, J.P. Pansart, A.V. Stirling, J. Teiger, H. Zaccone, J. Zsembery, G. Bassompierre, M. Croissiaux, J. Cresser, R. Morand, M. Riedinger and M. Schneegans, Contribution to the XVI International Conference on High Energy Physics (Batavia 1972)

9. J.V. Allaby, A.N. Diddens, R.W. Dobinson, A. Klowning, J. Litt, L.S. Rochester, K. Schlüpmann, A.M. Wetherell, U. Amaldi, R. Biancastelli, C. Bosio and G. Matthiae, Contribution to the 4th International Conference on High Energy Collisions, Oxford (1972).

FIGURE CAPTIONS

Fig. 1 - The invariant inclusive cross section for antiprotons at fixed p_T = 0.4 GeV/c, as a function of $y_{max} - y_{cm}(\bar{p})$ where $y_{max} = \ell n \sqrt{s} / m_N$. The data are from a compilation by Lillethun[5] :

$\sqrt{s}$ (GeV)	23.3	30.5	44.7	53.0
Ref. 6	◇	△	◆	▲
Ref. 7		o		•
Ref. 8	▼	▼	▼	▼

The dotted curve represents data at $\sqrt{s}$ = 7 GeV [9]. The full lines are the predictions of the "statistical" model, at 7 GeV, 23.3 GeV and 53 GeV.

Fig. 2 - The same as in Fig. 1, but the theoretical curves refer to the "exchange" model ($\gamma = \frac{1}{2}$).

Fig. 3 - The invariant inclusive cross section for K^-, compared with the "exchange"model ($\gamma = \frac{1}{2}$). The notations are the same as in Fig. 1.

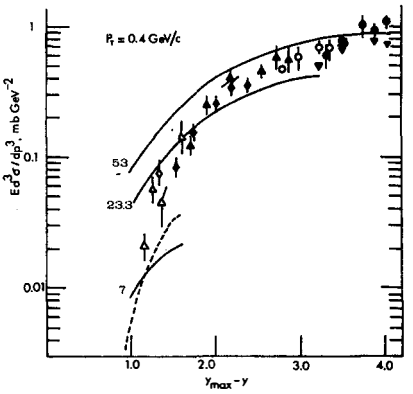

P_T = 0.4 GeV/c
53
23.3
7
1
0.1
0.01
1.0
2.0
3.0
4.0
$Y_{max} - y$
$E d^3\sigma/dp^3$, mb GeV^{-2}

Fig. 1

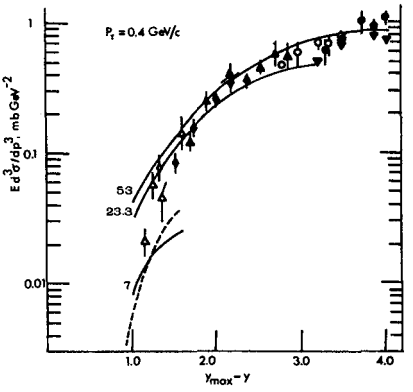

P_T = 0.4 GeV/c
53
23.3
7
1
0.1
0.01
1.0
2.0
3.0
4.0
$Y_{max} - y$
$E d^3\sigma/dp^3$, mb GeV^{-2}

Fig. 2

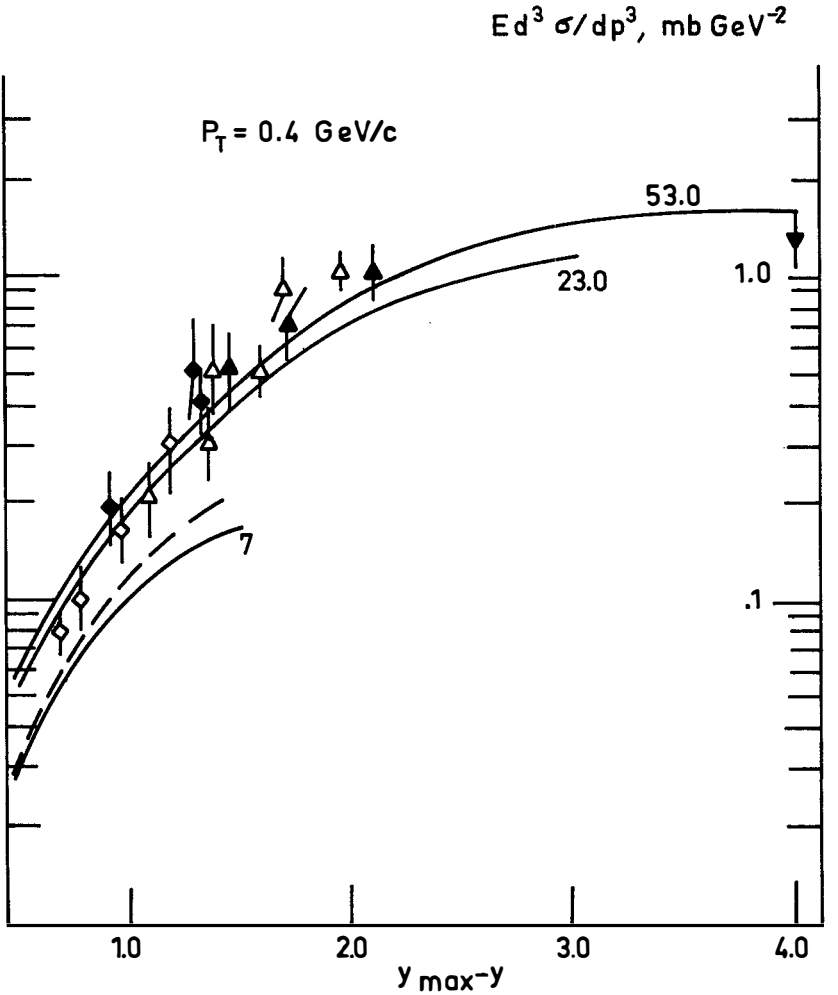


Fig.3

CLUSTERINGS IN HADRONIC PRODUCTION AND MARKOVIAN WALK*

Chung-I Tan
Brown University
Providence, Rhode Island 02912 (USA)

Abstract : The approach to the scaling limit of the inclusive cross sections in the central region is correlated with the local clustering effect in the rapidity distribution. An explicit model is constructed where the scaling limit can be approached from below. This is then explained from the point of view of Markovian walk in one-dimension.

Résumé : On établit une corrélation entre l'approche à la limite de scaling des sections efficaces inclusives dans la région centrale et l'effet de clustering local dans la distribution en rapidité. On construit un modèle explicite si la limite de scaling est approchée par en-dessous. Ceci est ensuite expliqué en considérant un chemin Markovien à une dimension.



(1) Introduction

The notion of duality depends crucially on the observation that all total cross sections approach their asymptotic limits from above. However, it has become clear that almost all inclusive cross sections approach their scaling limits in the central region from below. Although their energy dependences are consistent with the Mueller-Regge picture, the "negative" approach to scaling is somewhat puzzling. Since inclusive cross sections are generalized total cross sections, one would have guessed that the opposite were true.

We would like to elaborate on the role of secondary Regge singularities within the short-range co-relation (SRC) picture of hadronic productions. We show that their presence implies the existence of "local" clusterings in the rapidity distribution of a single event. The approach to the scaling limit is simply a manifestation of the "threshold" effect of cluster formations, and its "sign" depends on what the dominant clustering configuration is. To avoid the question of self-consistency, we adopt the modified SRC picture recently discussed by Frazer, Peccei, Pinsky and Tan[1], where diffraction was found to account for less than 20% of the p-p total cross section. We shall assume that the SRC component of the total cross section can be described by two Regge poles, one at $\alpha_p \simeq 1$, and another at $\alpha_M \simeq 1/2$.

(II) Multiperipheral Model

The Mueller-Regge picture is realized most naturally in the multiperipheral model (MPM). Since a single channel Chew-Pignotti[2] MPM contains only one output pole, and is known to lead to a Poisson multiplicity distribution, a more realistic model capable of producing a secondary Regge pole is the two-channel CP model.

Denote $A^{(a,b)}(Y)$, $Y = y_b - y_a > 0$, for the forward absorptive amplitude of the process $a + b \to a + b$. Let the input J-plane singularities be branch points β_0, β_1 (with $\beta_0 > \beta_1$)[3], and the internal coupling matrix be Λ, with $\Lambda_{00} = \lambda_0^2$, $\Lambda_{01} = \Lambda_{10} = \lambda^2$, $\Lambda_{11} = \lambda_1^2$, i.e., the n-particle absorptive part is proportional to

$$\ldots\Lambda_{00} e^{(\beta_0+1)x_i} \Lambda_{00} e^{(\beta_0+1)x_{i+1}} \ldots \Lambda_{01} e^{(\beta_1+1)x_j} \ldots \qquad (1)$$

where x_i's are rapidity separation between neighboring particles in the MP chain. In addition to λ_0^2, λ^2, λ_1^2, β_0, β_1, we need to specify an external coupling spinor for each external particle, e.g.

$$\psi_{(a)} = \begin{pmatrix} v_{0,a}^2 \\ v_{1,a}^2 \end{pmatrix} \qquad (2)$$

This model can be solved exactly by diagonalizing the "propagator function" $\alpha_{ij}(Y)$, defined by

$$A^{(a,b)}(Y) = \psi_{(a)}^T \alpha(Y) \psi_{(b)} \quad , \qquad (3)$$

and it satisfies the integral equation

$$\alpha_{ij}(Y) = \delta_{ij} e^{\beta_i Y} + \int_0^\infty dx\, e^{\beta_i x} \Lambda_{ik} \alpha_{kj}(Y-x) \quad . \qquad (4)$$

Let $\alpha'(Y) = U\, \alpha(Y) U^{-1}$ be diagonal, and we find

$$\alpha'(Y) = \begin{pmatrix} e^{\alpha_+ Y} & 0 \\ 0 & e^{\alpha_- Y} \end{pmatrix} \qquad (5)$$

where

$$\alpha_{\pm} = (\bar{\beta}_0 + \bar{\beta}_1)/2 \pm [(\bar{\beta}_0 - \bar{\beta}_1)^2/4 + \lambda^2]^{\frac{1}{2}} \tag{6}$$

and

$$\bar{\beta}_i = \beta_i + \lambda_i^2 \ , \ i = 0,1 \tag{7}$$

The matrix U can be chosen to be proper and orthogonal, and its elements can be read off from the "rotated" external coupling spinor

$$\psi'_{(a)} \equiv U \, \psi_{(a)} = \begin{pmatrix} G_+^{(a)} \\ G_-^{(a)} \end{pmatrix} \tag{8}$$

$$G_{\pm}^{(a)} = \pm [(\delta \pm \delta_0)/(2\delta)]^{\frac{1}{2}} V_{0,a}^2 + [(\delta \mp \delta_0)/(2\delta)]^{\frac{1}{2}} V_{1,a}^2 \tag{9}$$

where

$$\delta \equiv \alpha_+ - \alpha_- \ , \ \delta_0 \equiv \bar{\beta}_0 - \bar{\beta}_1 \ , \text{ and } \delta > \delta_0 \ . \tag{10}$$

The total cross section is now given by

$$\sigma^{(a,b)} = G_+^{(a)} G_+^{(b)} \, e^{(\alpha_+ - 1)Y} + G_-^{(a)} G_-^{(b)} \, e^{(\alpha_- - 1)Y} \ , \tag{11}$$

i.e., $G_+^{(a)}$ and $G_-^{(a)}$ are Regge couplings of the particle a to the output Regge poles α_+ and α_- respectively. To yield a nearly constant asymptotic total cross sections, we identify α_+ with $\alpha_p \simeq 1$ and to produce an average meson pole, we require $\alpha_- = \alpha_M \simeq 1/2$. We also interpret the duality constraint to mean that the contribution from α_- be always positive, i.e.,

$$G_-^{(a)} \, G_-^{(b)} \geq 0 \tag{12}$$

for any combination of particle pair (a,b).

The single-particle distribution is given by

$$\frac{d\sigma}{dy} = [e^{Y\,\sigma^{(a,b)}(Y)}]^{-1}\, B^{(a,b)}\,(y - y_a,\, y_b - y) \qquad (13)$$

where

$$B^{(a,b)}\,(x_a,x_b) = \psi_{(a)}^{\;T}\, \mathcal{A}(x_a) \wedge \mathcal{A}(x_b)\, \psi_{(b)} \qquad (14)$$

In (14), we have neglected contributions from two leading particles[4]. Let the internal Mueller double- Regge coupling matrix be

$$G = \begin{pmatrix} g_+ & g \\ g & g_- \end{pmatrix} = \begin{pmatrix} g_{PP} & g_{PM} \\ g_{MP} & g_{MM} \end{pmatrix}$$

It follows from (5), (8), and (14) that $G = U \wedge U^{-1}$, e.g.,

$$g_+ = (2\delta)^{-1}\,[(\lambda_0^{\,2})\,(\delta+\delta_0) + 4\lambda^2 + (\lambda_1^{\,2})\,(\delta-\delta_0)] \qquad (15)$$

$$g = (\delta)^{-1}\,(\lambda^2)\,(\beta_0 - \beta_1) \qquad (16)$$

We note that both g_+ and g are positive. Since the asymptotic approach to the scaling limit depends only on the sign of the $\alpha_P - \alpha_M$ term[5], we find that the limit is approached from <u>below</u> if $G_-^{(a)} < 0$, i.e., for all a,

$$(V_{0,a}^{\;2})\,(\delta-\delta_0)^{\frac{1}{2}} > (V_{1,a}^{\;2})\,(\delta+\delta_0)^{\frac{1}{2}} \qquad (17)$$

To understand this condition, let us next provide a statistical interpretation of the CP MPM.

(III) Random and Markovian Walks[6] in One-Dimension.

Since the multiparticle physics is equivalent to a one-dimensional many-body system, it is perhaps not surprising if we show next that a MPM is equivalent to a random walk problem in one-dimension. The one-channel CP model is known to lead to

a Poisson multiplicity distribution, and it can be shown that it corresponds to a random walk where each step length is controlled by a single probability density

$$w(x) = \ell^{-1} e^{-x/\ell} \theta(x) \tag{18}$$

The total rapidity Y is identified with the total distance travelled. Eq. (18) can also be shown to correspond to an "ideal Boltzmann gas", so that the distribution in the rapidity space is always uniform. Therefore, scaling holds at any value of Y. Note that the average step length, ℓ, is the only parameter given. All statistical averages can be calculated in terms of ℓ, e.g., the average multiplicity is

$$\langle n \rangle = (\ell^{-1}) Y + 2 \tag{19}$$

To produce non-uniformity in the rapidity distribution, we allow, for each step, two different probability densities

$$w_i(x) = \ell_i^{-1} e^{-x/\ell_i} \theta(x), \quad i=0,1 \tag{20}$$

where

$$\ell_0 > \ell_1 \tag{21}$$

To specify the problem uniquely, we need additional inputs:

(i) Let the probability for the initial (final) step being of the ith type be $r_i^{(a)}$ ($r_i^{(b)}$), i.e.

$$\sum_{i=0,1} r_i^{(a)} = \sum_{i=0,1} r_i^{(b)} = 1 \quad , \tag{22}$$

(ii) Let the probability of taking two steps of the ith type in succession be ν_i , $0 \leq \nu_i \leq 1$.

This is actually a special case of a Markovian walk problem.[6]

We have shown that this system is equivalent to our two-channel CP model discussed earlier if we identify[7]

$$\ell_i = (\alpha_+ - \beta_i)^{-1} \qquad i=0,1 \qquad (23)$$

$$\nu_i = \lambda_i^2 \, \ell_i \qquad i=0,1 \qquad (24)$$

and

$$r_0^{(a)} = \left[\left(\frac{\delta+\delta_0}{2\delta}\right)^{\frac{1}{2}}\right] (V_{0,a}^2) \; / \; G_+^{(a)} \qquad (25)$$

$$r_1^{(a)} = \left[\left(\frac{\delta-\delta_0}{2\delta}\right)^{\frac{1}{2}}\right] (V_{1,a}^2) \; / \; G_+^{(a)} \qquad (26)$$

Instead of enumerating all possible sequences for taking a fixed number of steps (there are 2^n possibilities for n steps), it is much simpler to visualize another situation where a "cluster" of steps of the same type are taken in succession, and then one alternates these two possible types of clusters. This procedure is equally adequate for calculating most of the statistical averages of the problem.

The probability density $W_i(z)$ for travelling a distance z via <u>any</u> number of steps of the ith type in successions is

$$W_i(z) = \sum_{n=1}^{\infty} (\nu_i)^{n-1}(1-\nu_i) \int_0^{\infty} dx_1 \, .. \int_0^{\infty} dx_n \, (\ell_i)^{-n} \, e^{-z/\ell_i} \, \delta(z - \sum_{j=1}^{n} x_j)$$

$$= L_i^{-1} \, e^{-z/L_i} \qquad (27)$$

where

$$L_i = \ell_i/(1-\nu_i) = (\alpha_+ - \bar{\beta}_i)^{-1} \, , \quad i=0,1 \qquad (28)$$

It follows from (27) that the average displacement of the type-i cluster is L_i. Within the type-i cluster, the average step length is still ℓ_i . (See Fig. 1)

To illustrate how we can go ahead to calculate probabilities, let us evaluate the probability density that, after N clusters of steps, the total distance travelled is Y. Assuming N is even, and assuming the first cluster is of the type-0, we find this probability density is

$$r_0^{(a)}\, r_1^{(b)} \int_0^\infty dz_1 \int_0^\infty dz_2 \cdots \int_0^\infty dz_N \, [W_0(z_1)W_1(z_2)]$$

$$\times \cdots [W_0(z_{N-1})\, W_1(z_N)]\, \delta\Big(Y-\sum_{i=1}^{N} z_i\Big)$$

$$= r_0^{(a)} r_1^{(b)} \frac{(L_0L_1)^{-N/2}}{[(N/2-1)!]^2} \int_0^Y dz \, [(z)(Y-z)]^{(N/2-1)} e^{-z/L_0}\, e^{-(Y-z)/L_1}$$

Before proceeding further, we shall give a few more useful relations

$$\frac{\delta+\delta_0}{2} = L_1^{-1} \tag{29a}$$

$$\frac{\delta-\delta_0}{2} = L_0^{-1} \tag{29b}$$

and

$$\lambda^2 = (L_0L_1)^{-\frac{1}{2}} \tag{29c}$$

(IV) Approach to Scaling Limit and Local Clustering

From the Mueller double-Regge analysis, the average multiplicity in the two-channel CP model is asymptotically[8]

$$\langle n \rangle = g_+ Y + (\delta)^{-1} \left(G_-^{(a)}/G_+^{(a)}\right) g + (\delta)^{-1} \left(G_-^{(b)}/G_+^{(b)}\right) g + 2 \,. \tag{30}$$

We would like to derive this same formula from our statistical analysis, thus elucidating origins of various factors in (30).

Within each pair of neighboring clusters, there exists two number densities

$$\rho_i = \ell_i^{-1} \quad , \quad i=0,1 \tag{31}$$

each describing the density of the type-i cluster. The total average density in a neighboring pair of clusters is

$$\rho = \frac{\rho_0 L_0 + \rho_1 L_1}{L_0 + L_1} = \frac{(L_0/\ell_0) + (L_1/\ell_1)}{L_0 + L_1} \tag{32}$$

so that the average number of particles produced, at large Y, is given by

$$\langle n \rangle \sim \rho Y \ . \tag{33}$$

Substituting $(\alpha_+ - \beta_i)^{-1}$, $(\alpha_+ - \bar{\beta}_i)^{-1}$ for ℓ_i, L_i respectively, we find

$$\rho = g_+ \quad , \tag{34}$$

thus justifying the first term in (30).

The second and the third terms in (30) reflect effects of local clusterings. Since we can always pair off any neighboring clusterings, the "net" deviation from the average density can only come from two "ends" of the Markov chain. Let us concentrate on the end labelled by a. The deviation of the density of the type-i cluster from the average density is

$$\Delta\rho_i = \rho_i - \rho = \begin{cases} -\left(\frac{L_1}{L_0+L_1}\right)\left(\ell_1^{-1} - \ell_0^{-1}\right) < 0 \quad i=0 \ . & \text{(35a)} \\ \left(\frac{L_0}{L_0+L_1}\right)\left(\ell_1^{-1} - \ell_0^{-1}\right) > 0 \quad i=1 \ . & \text{(35b)} \end{cases}$$

The probability for having the type-i cluster first is $r_i^{(a)}$, so that the average density deviation near the beginning end is

$$\Delta\rho^a = r_0^{(a)}\,\Delta\rho_0 + r_1^{(a)}\,\Delta\rho_1$$

$$= \left(-\frac{r_0^{(a)}}{L_0} + \frac{r_1^{(a)}}{L_1}\right)\left(\frac{L_0L_1}{L_0+L_1}\right)\left(\frac{1}{\ell_1} - \frac{1}{\ell_0}\right) \qquad (36)$$

This deviation extends over an average distance $(\alpha_+ - \alpha_-)^{-1} = \delta^{-1}$, so that the total deviation in average multiplicity is

$$(\delta)^{-1}\,(\Delta\rho^a)$$

Using relations between random walk parameters and that of CP model, we can show

$$(\delta)^{-1}\,(\Delta\rho^a) = (\delta)^{-1}\,(G_-^{(a)}/G_+^{(a)})\,(g) \qquad (37)$$

where

$$G_-^{(a)}/G_+^{(a)} = [-\,r_0^{(a)}\,(L_1/L_0)^{\frac{1}{2}} + r_1^{(a)}(L_0/L_1)^{\frac{1}{2}}]$$

$$= (L_0L_1)^{\frac{1}{2}}\,[-\,r_0^{(a)}/L_0 + r_1^{(a)}/L_1]$$

$$= (\lambda^{-2})\,[-\,r_0^{(a)}\,W_0(L_0) + r_1^{(a)}\,W_1(L_1)] \qquad (38)$$

and

$$g = \left(\frac{L_0L_1}{L_0+L_1}\right)(L_0L_1)^{-\frac{1}{2}}\,(\rho_1 - \rho_0)$$

$$= (\delta^{-1})\,(\lambda^2)\,(\beta_0 - \beta_1) \quad > 0 \qquad (39)$$

Eq. (37) again agrees with the second term of (30). The third term can similarly be provided.

Since the type-i cluster has an average length L_i, $r_i^{(a)}\,W_i(L_i)$ is then the relative weight for configurations that begin with the type-i cluster. When $G_-^{(a)}$, or (38), is positive, we shall speak of the configuration with the type-1 cluster at the end as the dominant production configuration; and conversely, when $G_-^{(a)}$ is negative, the type-0 configuration would

be dominant. When the latter happens, the particle number density near that end would be less than the asymptotic average. This precisely corresponds to the condition (17).

Since the single particle distribution is a measure of the particle number density, we find that, when (17) is satisfied, the central limit will be reached from below. In the context of the Mueller-Regge picture, this "threshold" behavior[9] is accomplished by the presence of a secondary trajectory, i.e., the contribution from the $\alpha_P - \alpha_M$ double-Regge term is negative. Unlike the total cross section where duality dictates that the contribution from α_- be positive, the sign of the $\alpha_P - \alpha_M$ term in inclusive density distribution depends on additional dynamical inputs. What we have attempted to do here is to indicate that a negative $\alpha_P - \alpha_M$ term is perfectly acceptable within the SRC picture, and it has a sensible statistical interpretation. Needless to say, our approach can be generalized to include productions of different particle types, and to include more trajectories so as to produce an exchange degenerate world. These considerations will be discussed elsewhere[7].

Footnotes and References

* Work supported in part by the U. S. Atomic Energy Commission. (Report No. COO-3130TA-280)

1) Frazer, Peccei, Pinsky, and Tan, Phys. Rev. (to be published)

2) Chew and Pignotti, Phys. Rev. 176, 2112 (1968).

3) Since we are leaving out the diffractive component, the leading cut, β_0, is no longer the P-P cut. We interpret β_0 and β_1 as two "effective" J-plane branch points for now.

4) Leading particles will give rise to triple-Regge behavior. In our model, it can be seen that they do not contribute. to the double-Regge limit in the central region.

5) In general, this is true only if the scaling limit in the central region has already been reached. If not, the $\alpha_M - \alpha_M$ term is also important. However, the latter can always be ignored whenever the corresponding α_M term in the total cross section becomes unimportant. When that is the case, the $\alpha_P - \alpha_M$ not only controls the transition from the fragmentation region to the central region, it also governs the asymptotic approach to the scaling limit in the central region.

6) See, for instance, Feller, An Introduction to Probability Theory and Its Applications, Vol. I, second edition (Wiley, N. Y., N. Y. 1957).

7) Brown Univ. Preprint COO-3130TA-282.

8) Eq. (30) yields the asymptote of $\langle n \rangle$, as a function of Y, of the form $aY + b$. The constant b normally depends on the inclusive distribution in the fragmentation region. In our picture, the leading particle effect always contributes two particles to $\langle n \rangle$, so that the rest of b comes from the approach to scaling in the central region. Since $\langle n \rangle = 2$ at Y=0 , the sign of (b - 2) determines the "curvature" of $\langle n \rangle$ as it approaches its asymptotic. (see Fig. 2).

9) This is not to be confused with the threshold effect due to the "short-range" repulsion, which can occur even at the one-channel CP model level. The latter type may be more relevant for the understanding of the $\bar{p}$ and k spectra where particles with masses much larger than that of the pion are produced. One simple way to incorporate this effect is to introduce a minimum rapidity gap, Δ, i.e., replacing (18) by $W_1(x) \propto e^{-x/\ell}\, \theta(x-\Delta)$. This is also discussed in Ref. 7.

Figure Captions

1) An average configuration for two pairs of neighboring clusters of steps. L_0, L_1 are average cluster lengths, and ℓ_0, ℓ_1 are average step lengths.
2) Shapes of the average multiplicity as a function of Y for various situations: (a) $g(G_-/G_+) > 0$, (b) $g(G_-/G_+) < 0$, and (c) ideal gas.

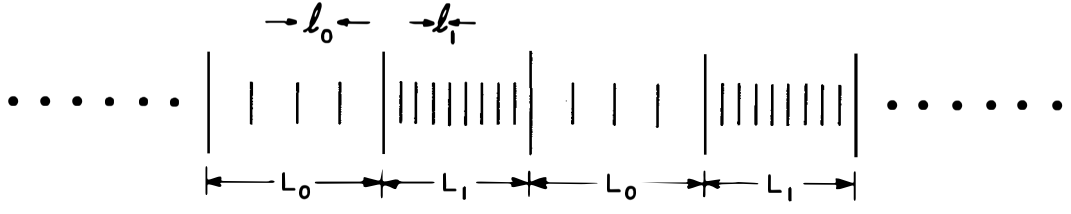
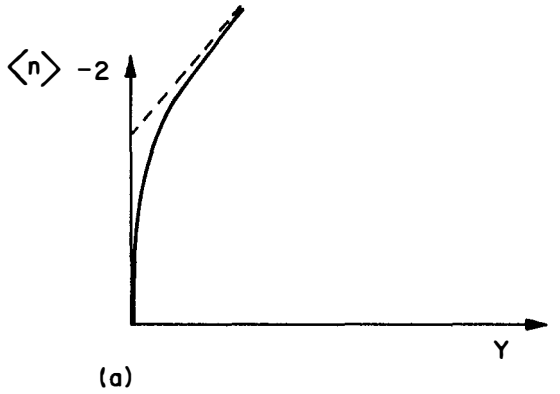
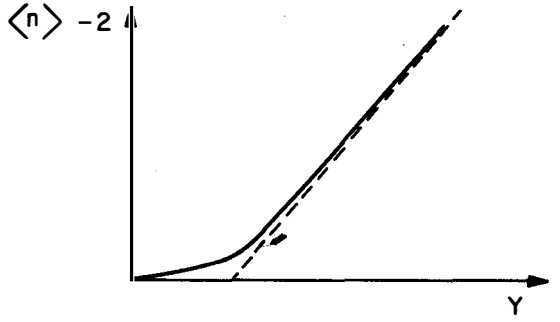


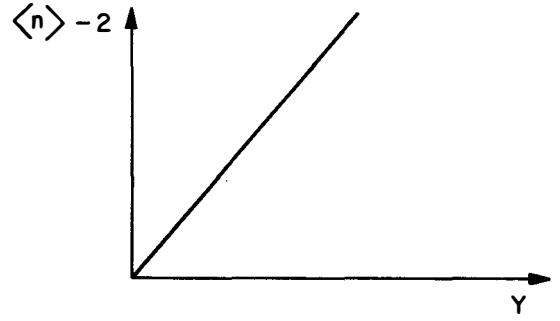
FIGURE 1



(a)



(b)



(c)

FIGURE 2

PRODUCTION IN THE CENTRAL REGION

Jiunn-Ming Wang*
Institute for Theoretical Physics
SUNY at Stony Brook, Stony Brook, N. Y. 11790

Abstract: Multiplicity distributions in a finite section of momentum space of the central region are discussed.

Résumé : On discute des distributions de multiplicité dans une région finie d'espace de moment de la région centrale.



The work I am going to describe is done in collaboration with K. S. Cheng of Stony Brook.

The question I am asking is as follows: If we set up a counter of finite size near the interaction region at ISR, what are the multiplicity distributions of the particles detected by the counter? In other words, consider a finite angular region Ω in the c.m. frame. What do the particle distributions in the region Ω look like regardless of what happens outside the region? The region Ω is assumed to exclude the forward and the backward directions.

Actually in the following we shall consider a fixed finite region D in the center of mass momentum space instead of the region Ω mentioned above. Because of the sharp cut off in the transversal momenta, the multiplicity distributions in D and Ω are very similar.

The advantages of considering such regions D or Ω are: (1) The contrast between independent emission models (IEM, the models for which the correlations are of short range) and the fragmentation models (FM) becomes much sharper than when we consider the whole phase space. (2) The diffractive tails of Wilson's two component models do not contribute to such regions at very high energies, and therefore we are testing the genuine "multiperipheral part" of such models.

The predictions are summarized in the following theorems for the probability $P_n^D(s)$ of finding n particles in the region D regardless of what happens elsewhere, and the moments

$$F_N^D = \langle n(n-1)\cdots(n-N+1)\rangle_D$$

$$= \sum_{n=N}^{\infty} n(n-1)\cdots(n-N+1)\, P_n^D(s) \qquad (1)$$

$$= \frac{1}{\sigma_{tot}} \int_D d^3p_1 \cdots \int_D d^3p_N \, \frac{d\sigma}{d^3p_1 \cdots d^3p_N} \,, \qquad (2)$$

where $\underline{p}_i$ are center of mass momenta of the final particles.

Theorem 1: In IEM, both $P_n^D(s)$ and $F_n^D(s)$ approach finite limits; and also $P_n^D(\infty)$ is bounded for large n by n^{-N} for any arbitrary N.

Theorem 2: As $s \to \infty$, FM predict the following behaviors:

(i) $F_N^D(s) = 0(\sqrt{s})^{N-1}$, $N \geq 1$

(ii) $P_0^D(s) = 1 - 0\left(\left(\frac{1}{\sqrt{s}}\right)^{\frac{1}{2}}\right)$.

In FM let us denote by $\nu(s)$ the maximum prong number for which σ_n behaves like $1/n^2$. In theorem 2, we took $\nu(s)$ to be proportional to $\sqrt{s}$. If we take $\nu(s)$ to be proportional to a smaller power[1] of s, (i) and (ii) will be modified. Although in FM the inclusive cross sections are non-vanishing in the central region, the two "fireballs" are separated in the sense of (ii). It is obvious that the smaller we take $\nu(s)$ to be, the more the two "fireballs" are separated and therefore the faster the probability $P_0^D(s)$ reaches the limit unity.

Now let's prove theorem 1. Eq. (2) and the fact that in IEM the inclusive cross sections $\frac{d\sigma}{d^3p_1 \cdots d^3p_n}$ reach finite limit, tells us immediately that in such models the $F_N^D(s)$ must reach finite limits. This in turn implies that the $P_n^D(s)$ must be finite at infinite energies. Note that

$$P_n^D(s) = \frac{1}{n!} \sum_{M=0}^{\infty} \frac{(-1)^M}{M!} F_{M+n}^D(s) \quad .$$

The convergence of the series (1) at infinite energies and for any N tells us that $P_n^D(\infty)$ must be bounded by any inverse power of n. This completes the proof of theorem 1.

Now we prove theorem 2. (i) is a straightforward result[2] of Eq. (2) and the fact that in FM $\frac{d\sigma}{d^3p_1 \cdots d^3p_n}$ is proportional to $(\sqrt{s})^{n-1}$. I shall not prove (ii) here. For the proof of (ii), I refer you to the paper I wrote with K. S. Cheng.[4]

For comparison, let me mention that in uncorrelated jet models, $P_n^D(s)$ are given at infinite energies by Poisson distributions, and therefore $P_0^D(\infty)$ is given by $e^{-\langle n \rangle_D}$.

We note then that a prong distribution in D which changes (falls and broadens) with energy is characteristic of FM, whereas a fixed and narrow prong distribution in D is characteristic of IEM.

Let's look at some experimental results. In Pisa-Stony Brook group experiments at ISR the central region coincides roughly with the so-called "L-Box" region which is comprised of twenty eight scintillation counters. Their results in the energy range $s = 480 \sim 2700\ \text{GeV}^2$ are: (1) $\langle n^2\rangle_{LB}/\langle n\rangle^2_{LB}$ remains constant, where LB stand for L-Box, (2) for each of the twenty eight counters the probability of an event contributing to the counter increases by about 50% as s increases in the above energy range. In other words $P_o(s)$ for each counter is decreasing instead of increasing with increasing s. These experimental results together with our earlier discussion force us to conclude that the fragmentation picture can not describe the multiparticle production in the central region.

I thank Professor G. Finocchiaro and Dr. R. Castaldi for making their experimental data available to me.

REFERENCES

1. See, for example, R. C. Hwa, to be published; H. D. I. Abarbanel and G. L. Kane, Phys. Rev. Letters 30, 67 (1973).

2. This follows from the results of ref. 3 and $\nu(s) \sim \sqrt{s}$. If $\nu(s)$ is not to be $\sim s^a$, $a<\frac{1}{2}$, then the results of ref. 3 tell us directly that $\frac{d\sigma}{d^3p_1 \cdots d^3p_n} \sim (s^a)^{n-1}$.

3. C. Quigg, Jiunn-Ming Wang and Chen-Ning Yang, Phys. Rev. Letters 28, 1290 (1972).

4. K. S. Cheng and Jiunn-Ming Wang, to be published in Physics Letters.

A COMPARISON OF MEDIUM ENERGY DATA WITH ISR RESULTS

R. Stroynowski

CERN, Geneva

INTRODUCTION

During the last year the flow of important results from the Intersecting Storage Rings at CERN has induced a change in terminology, namely the energy range of $10 \lesssim p_{LAB} \lesssim 30$ GeV/c which in the past 10 years was called "high energy" has become the "medium energy" range.

It has become of the greatest interest to compare medium and high energy results. The specific experimental situation at the ISR makes it rather difficult to find lower energy data which may be directly compared. Therefore one observes a tendency to discuss results from ISR separately from other data. In this talk I would like to contribute two comments which may be useful for future systematic studies of energy dependence of observed phenomena and present some comparison of ISR with the data coming from bubble chamber $\pi^+ p$ experiments at 8,16 and 23 GeV/c.

1. The first topic concerns the forward peak observed in the reaction

$$pp \to p + \text{anything} \qquad (1)$$

by the CERN-Holland-Lancaster-Manchester Collaboration [1,2]. In this experiment it was found that the spectrum of the proton reduced longitudinal momentum (presented in fig. 1) has a sharp peak near $x = +1$, then dips at $x = p^*_L/p^*_{MAX} \approx 0.85$ and rises again at $x \approx 0.6$. Furthermore, there are indications that the forward peak is independent of s, i.e. scales within the ISR energy range. This peak is usually associated at ISR energies with the recoil proton from the diffractively excited system at the other vertex (see fig. 2). It is also discussed in ref. [1] that when comparing ISR data with the results obtained at lower energies, the corresponding proton spectra do not scale as the lower energy results are higher than those from ISR. We want to remark that this is, however, not surprising, since at low energies there is a quite substantial production of resonances and the contribution from production mechanisms other than diffraction dissociation is not negligible. We would like therefore to ask the question of whether there is scaling when events coming from diffraction dissociation only are selected.

This problem was studied using the reaction

$$\pi^+ p \to \pi^+ + \text{anything} \qquad (2)$$

at 8,16 and 23 GeV/c. The data have come from Aachen-Berlin-Bonn-CERN-Cracow-Heidelberg-Warsaw Collaboration.

In figs. 3,4 and 5 the inclusive inelastic $x = p^*_L/p^*_{MAX}$ distribution of π^+ is presented together with the separate contributions arising from final states of different charged multiplicity. As can be seen, the forward peak developes with increasing energy and originates practically only from the 2- and 4- prong final states. The contributions from 6- prongs can be neglected in the region of $x \geq 0.8$.

The data are presented in the form of non-invariant cross section distributions. This is because the invariant $E^* \frac{d\sigma}{dx}$ distributions (fig. 6) contain the multiplicative energy factor which depresses the central region of $x \approx 0$, and hence may create the impression that the contribution of the leading peak to the total cross section is much larger than it actually is. The cross section for π^+ with momentum greater than $x = 0.8$ represents in all 3 experiments a fraction of about 3% of the total inclusive π^+ cross section. On the other hand since kinematics does not allow for more than one fast forward going particle per event, the events contributing to this region represent about 7% of the total inelastic cross section.

In the jargon of bubble chamber techniques, "2-prongs" represent events with 2 charged particles in the final state, irrespectively of the number of neutrals. In the 2-prong inelastic events however, the possible 3- body final states are only two and both are reactions well-identified in a bubble chamber.

$$\pi^+ p \rightarrow p\pi^+\pi^o \qquad (3)$$

$$\pi^+ p \rightarrow n\pi^+\pi^+ . \qquad (4)$$

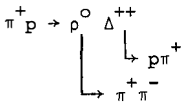
Similarly, with 4 prongs there is only one 4-body channel which is also very well identified in a bubble chamber

$$\pi^+ p \rightarrow p\pi^+\pi^+\pi^- . \qquad (5)$$

All other channels with 4- prongs are of higher multiplicity. The contributions of reactions (3), (4) and (5) to the distributions of π^+ from 2- and 4- prongs, respectively, are shown in fig. 7. It can be seen that in the region of $x \gtrsim 0.8$, the majority of the events come from the lowest multiplicity, i.e. 3- and 4- body final states. The final states of multiplicity greater than 4 contribute about 15% of the π^+ cross section in that region. This indicates that when studying the forward peak in the energy range of 8-23 GeV/c one can concentrate on only three well-identified reaction channels.

The next step is to separate different production mechanism in order to minimise the influence of resonance prodution. We shall try to select events which are predominantly produced by diffraction dissociation. This may be done by performing a kinematic selection of events in which π^+ is the only particle going forward in the c.m.s. all other particles going backward. This kind of kinematic selection is usually associated [3,4] with the selection of events dominated by diffraction dissociation (see fig. 8).

In figs. 9 and 10 the distributions of π^+ in the reactions (3), (4) and (5) are presented at the three energies studied. The thick lines represent distributions of positive pions coming from events in which the π^+ is the only particle going forward in cms. The hatched area in fig. 10 represents the distribution of the fastest π^+ coming from events in which the proton is the only particle going backward in the c.m.s., i.e. dominated by the diffraction dissociation of the incoming π^+. The events thus selected are presumably dominated by diffraction dissociation and the remaining events are mainly due to resonance production in reactions like,



whose cross section decreases strongly with increasing energy. As can be seen, for each of the reactions studied the percentage of the contribution to the forward peak coming from proton dissociation is increasing strongly with increasing energy.

The sum of the contributions of proton diffraction dissocation in the three reactions studied is compared in fig. 11 with the diffractive peak in the proton spectrum derived from the ISR results. The ISR data of Albrow et al. [1] at 22.5 + 22.5 GeV/c measured in the range $0.7 \lesssim p_\perp \lesssim 1.2$, were extrapolated to the low transverse

momentum region under the assumption of gaussian $p_\perp$ dependence

$$E\,\frac{d^3\sigma}{dp^3} = A(x)e^{-B(x)p_\perp^2}$$

and then integrated over the entire $p_\perp$ range. The forward peak in the proton spectrum at the ISR is presumably coming mostly from the proton diffraction dissociation at the other vertex (see fig. 2). Therefore, in order to make a qualitative comparison with the $\pi^+ p$ data, we have assumed factorisation of diffraction dissociation. The proton spectum was thus scaled down by the factor [5]

$$R = \left(\frac{\sigma^{TOT}_{asymptot\ (pp)}}{\sigma^{TOT}_{asymptot\ (\pi^+ p)}}\right)^2 = 3.08.$$

The error of the extrapolating procedure is quite large and is represented in fig. 11 by the hatched band. As can be seen, there is an indication that within 20-30% one can observe scaling of the forward peak in the energy range from $s = 31$ (P_{LAB} = 16 GeV/c) to $s = 1995$ GeV^2 (ISR 22.5 + 22.5 GeV/c). It should be noted that the contribution to the forward peak coming from the channels which were not considered in the present study (like e.g. five-body final states) may be estimated as 20-30% of the forward peak.

2. The second comment concerns recent results from the ISR on transverse momentum distribution. At the Oxford conference in April 1972 first results were presented [6] by the British-Scandinavian and CERN-Hamburg-Vienna Collaboration which indicated that in the region of small $p_\perp$ the invariant cross section for production of pions has an exponential behaviour as a function of transverse momentum, with a parameter equal to about 6.0 (GeV/c)$^{-2}$. Recently, new results have become available from the British-CERN-Columbia-Rockefeller Collaboration, Scandinavian Collaboration and many other groups [7,8,9]. They indicate that the invariant

cross section for pion production does not follow an exponential behaviour at higher $p_\perp$ values, a deviation towards power-like behaviour being observed starting at a value of $p_\perp \sim 2.5$ GeV/c (see fig. 12). This effect could not have been observed at low energies because of the limits imposed by phase space. It is not clear at the moment whether there is an energy dependence of the $p_\perp$ spectra within the ISR energy range. One may conjecture, however, that if scaling holds, the $p_\perp$ distribution also has a universal shape once the incident momentum becomes sufficiently high.

In fig. 13 the distribution of the invariant cross section as a function of transverse momentum is presented for the reaction

$$\pi^+ p \to \pi^+ + \text{anything}$$

at 8,16 and 23 GeV/c. The arrows indicate the kinematic limits at the three energies studied. As can be seen, there is some evidence that at 23 GeV/c incoming momentum the distribution starts to deviate from the sharp fall-off at the value of $p_\perp \sim 2.5$ GeV/c. This may be taken as an indication that phenomena well observed at the ISR start being visible already at about 20 GeV/c.

I am greatly indebted to Dr. D.R.O. Morrison for critically reading the manuscript. I wish to acknowledge the Aachen-Berlin-Bonn-CERN-Cracow-Heidelberg-Warsaw Collaboration for providing unpublished results.

REFERENCES

1. M.G. Albrow et al. Nucl. Phys. B51(1973) 388.

2. M.G. Albrow et al. Nucl. Phys. B.54(1973)6.

3. A. Bialas, A. Eskreys, W. Kittel, S. Pokorski, J.D. Tuominiemi and L.Van Hove, Nucl. Phys. B11(1969) 479.

4. W. Kittel, S. Ratti and L. Van Hove, Nucl. Phys. B30(1971) 333.

5. V. Barger and R.J.N. Phillips, Nucl. Phys. B32(1971) 93.

6. Contributed papers to the Fourth International Conference on High Energy Collisions, Oxford, April 1972 presented by E. Lillethun and W. Schmidt-Parzefall.

7. B. Alper et al, Production of High Transverse Momentum Particles in p-p Collisions in the Central Region at the CERN ISR, to be published in Phys. Letters.

8. B.J. Blumenfeld et al. - Contribution to the APS Meeting, New York (1973).

9. M. Banner et al. - Phys. Letters 41B (1972) 547.

FIGURE CAPTIONS

1. Longitudinal momentum spectra for π^+, K^+ and protons as functions of $x = 2\, p_L^*/\sqrt{s}$ for $p_\perp = 0.8$ GeV/c. The graph is taken from ref [1].

2. Diagram representing the exchange mechanism expected to dominate the forward peak in the proton X distribution at very high energy.

3. Inclusive and topological differential cross section distributions $d\sigma/dx$ as functions of the reduced longitudinal momentum x for the reaction (2) of 8 GeV/c.

4. As fig. 3 for 16 GeV/c.

5. As fig. 3 for 23 GeV/c.

6. Invariant inclusive distributions $E\, d\sigma/dx$ as a functions of the reduced longitudinal momentum x for the reaction (2) at 8 and 16 GeV/c.

7. Topological differential cross section distribution $d\sigma/dx$ as a function of x for the reaction (2) at 16 GeV/c for :

   a) Two charged particles in the final state (thin line). The thick line represents the contribution from the 3-body final states (3) and (4).

   (b) Four charged particles in the final state (thin lines). The thick line respresents the contribution from the 4-body final state (5).

8. Diagrams representing the exchange mechanisms expected to dominate the events. Selected as described in the text.

9. Differential cross section distribution $d\sigma/dx$ of π^+ produced at 8,16 and 23 GeV/c for a) reaction (3), b) reaction (4). The thick line represents the contribution coming from the events with the π^+ being the only particle going forward in the c.m.s.

10. Differential cross section distribution $d\sigma/dx$ of a) positive pions, b) protons produced in reaction (5) at 8,16 and 23 GeV/c. The solid line represents the contribution coming from the events with the π^+ being the only particle going forward in the c.m.s. The dashed area corresponds to the fastest π^+ when the proton is the only particle going backward in the c.m.s.

11. Comparison of the cross section distribution $d\sigma/dx$ of events with the π^+ being the only forward going particle in the reactions (3), (4) and (5) at 8,16 and 23 GeV/c with ISR data derived from ref [1] as described in the text.

12. Inclusive charged particle spectra averaged over charge at 90° in the c.m.s. for $\sqrt{s}$ = 53 GeV. Data taken from ref. [6,7].

13. Invariant cross section distribution as a function of transverse momentum for reaction (2) at 8,16 and 23 GeV/c.

Fig. 1

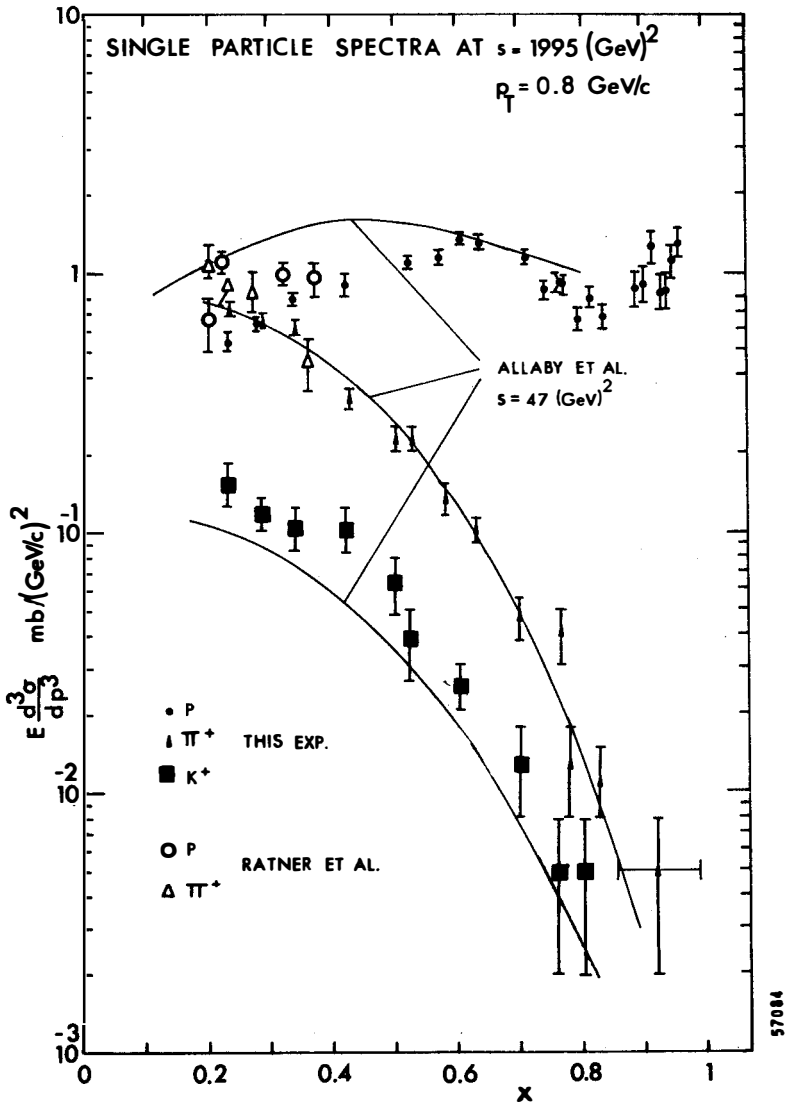

SINGLE PARTICLE SPECTRA AT s = 1995 (GeV)^2
P_T = 0.8 GeV/c
ALLABY ET AL.
s = 47 (GeV)^2
• P
▲ π$^+$
■ K$^+$
THIS EXP.
○ P
△ π$^+$
RATNER ET AL.
$E\frac{d^3\sigma}{dp^3}$ mb/(GeV/c)^2
x
10
1
10^{-1}
10^{-2}
10^{-3}
0
0.2
0.4
0.6
0.8
1
57084

Fig. 2

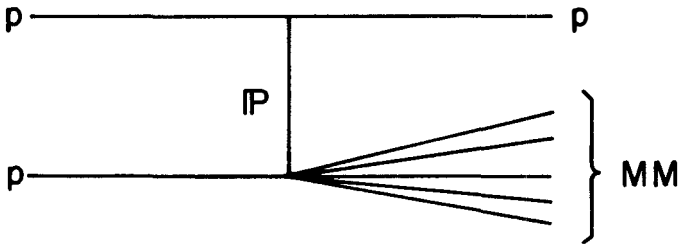


Fig. 3

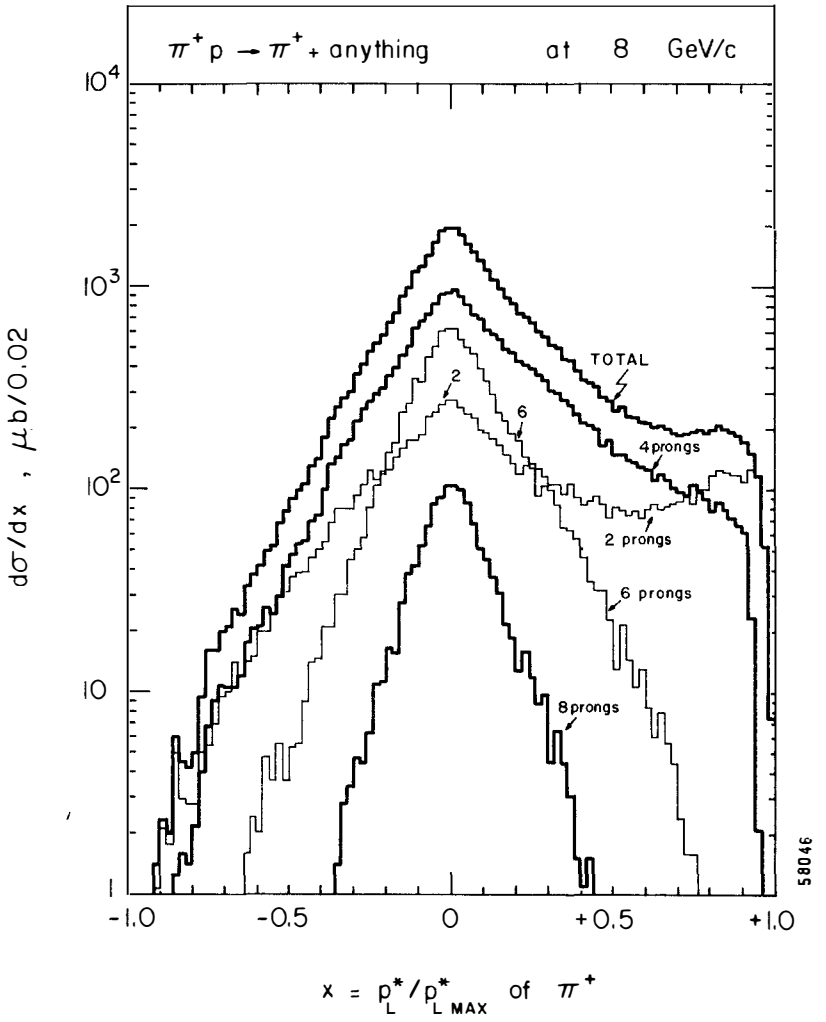

$\pi^+ p \rightarrow \pi^+ +$ anything at 8 GeV/c
10^4
10^3
10^2
10
1
$d\sigma/dx$, $\mu b/0.02$
TOTAL
2
6
4prongs
2 prongs
6 prongs
8prongs
-1.0
-0.5
0
+0.5
+1.0
$x = p_L^*/p_{L\,MAX}^*$ of π^+
58046

Fig. 4

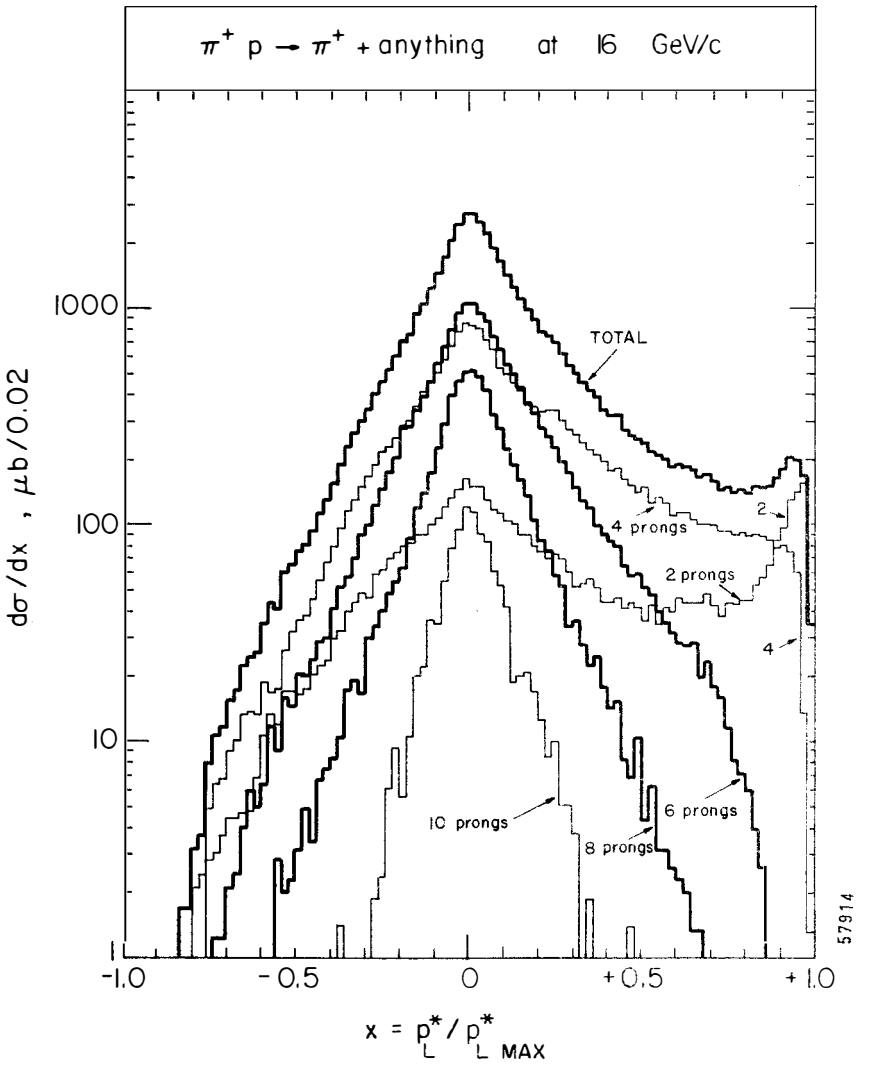

$\pi^+ p \rightarrow \pi^+ +$ anything at 16 GeV/c
1000
100
10
1
$d\sigma/dx$, $\mu b/0.02$
TOTAL
2
4 prongs
2 prongs
4
6 prongs
8 prongs
10 prongs
-1.0
-0.5
0
+0.5
+1.0
$x = p^*_L / p^*_{L\ MAX}$
57914

Fig. 5

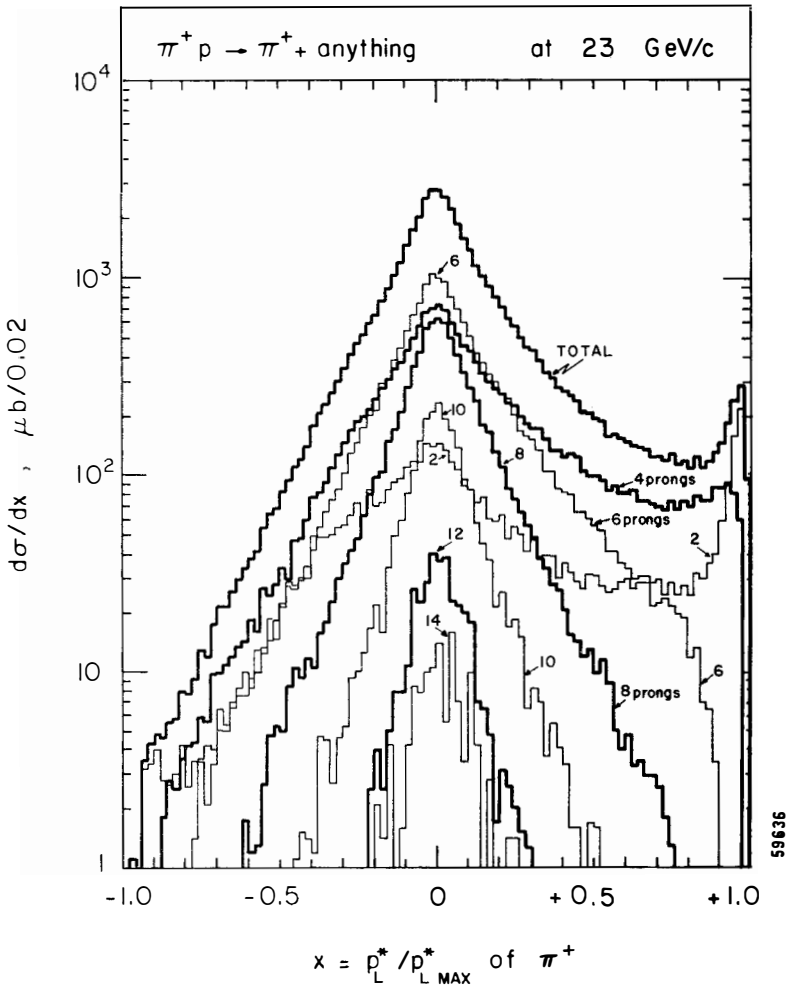

$\pi^+ p \rightarrow \pi^+ +$ anything at 23 GeV/c
10^4
10^3
10^2
10
1
$d\sigma/dx$, $\mu b/0.02$
TOTAL
4 prongs
6 prongs
8 prongs
2
6
10
8
2
12
14
10
6
-1.0
-0.5
0
+0.5
+1.0
$x = p_L^* / p_{L\,MAX}^*$ of π^+
59636

Fig. 6

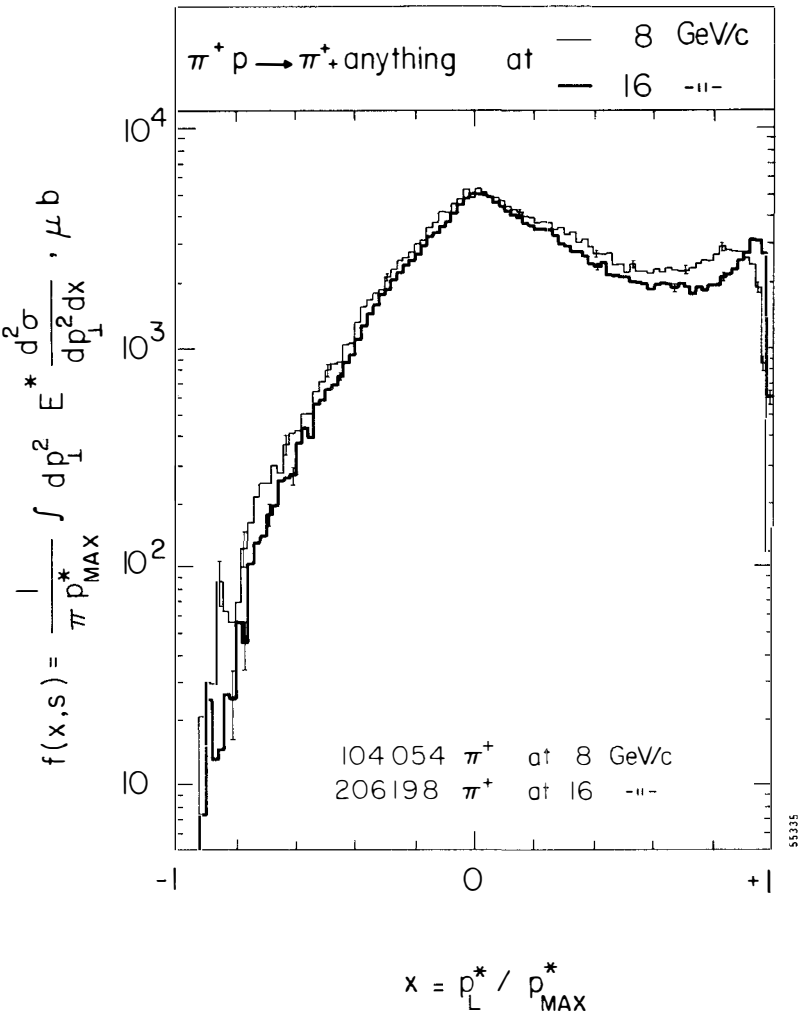
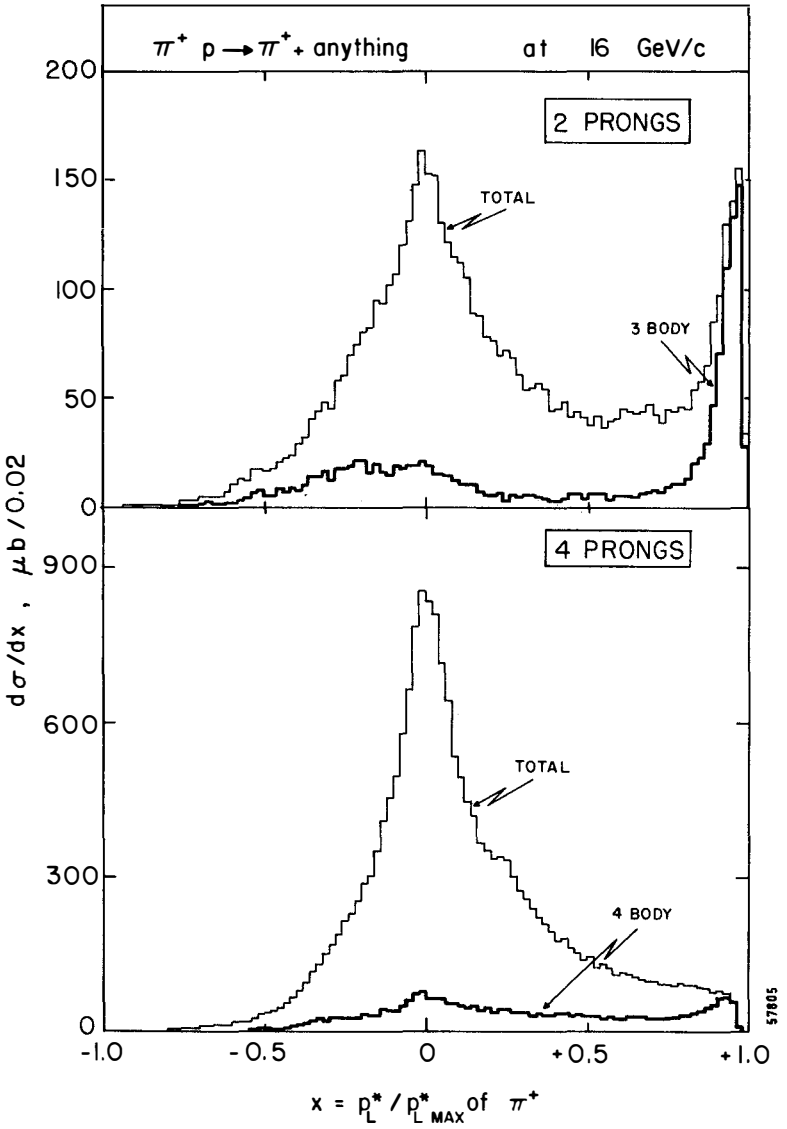
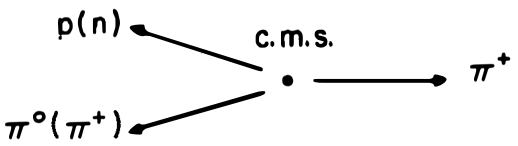
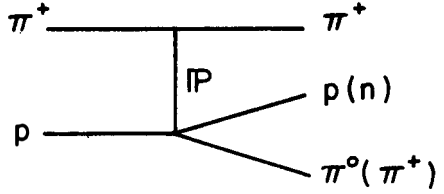

$\pi^+ p \longrightarrow \pi^+ +$ anything at
8 GeV/c
16 -"-
$f(x,s) = \frac{1}{\pi p^*_{MAX}} \int dp_T^2 \, E^* \frac{d^2\sigma}{dp_T^2 dx}$, μ b
10^4
10^3
10^2
10
104 054 π^+ at 8 GeV/c
206 198 π^+ at 16 -"-
55335
-1
0
+1
$x = p^*_L / p^*_{MAX}$

Fig. 7

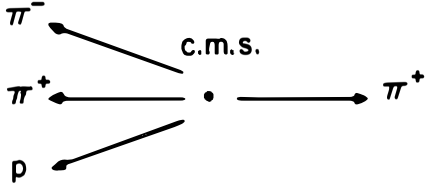

$\pi^+ p \rightarrow \pi^+ +$ anything at 16 GeV/c
2 PRONGS
TOTAL
3 BODY
4 PRONGS
TOTAL
4 BODY
200
150
100
50
0
900
600
300
0
-1.0
-0.5
0
+0.5
+1.0
$d\sigma/dx$, $\mu b/0.02$
$x = p_L^* / p_{L\,MAX}^*$ of π^+
57805

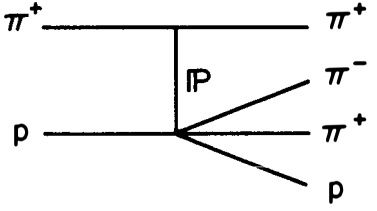
3 BODY

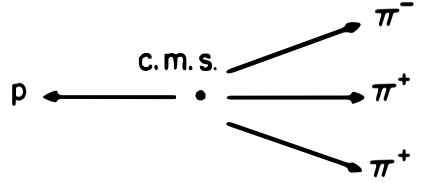




4 BODY







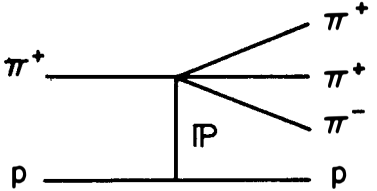


Fig. 8

Fig. 9

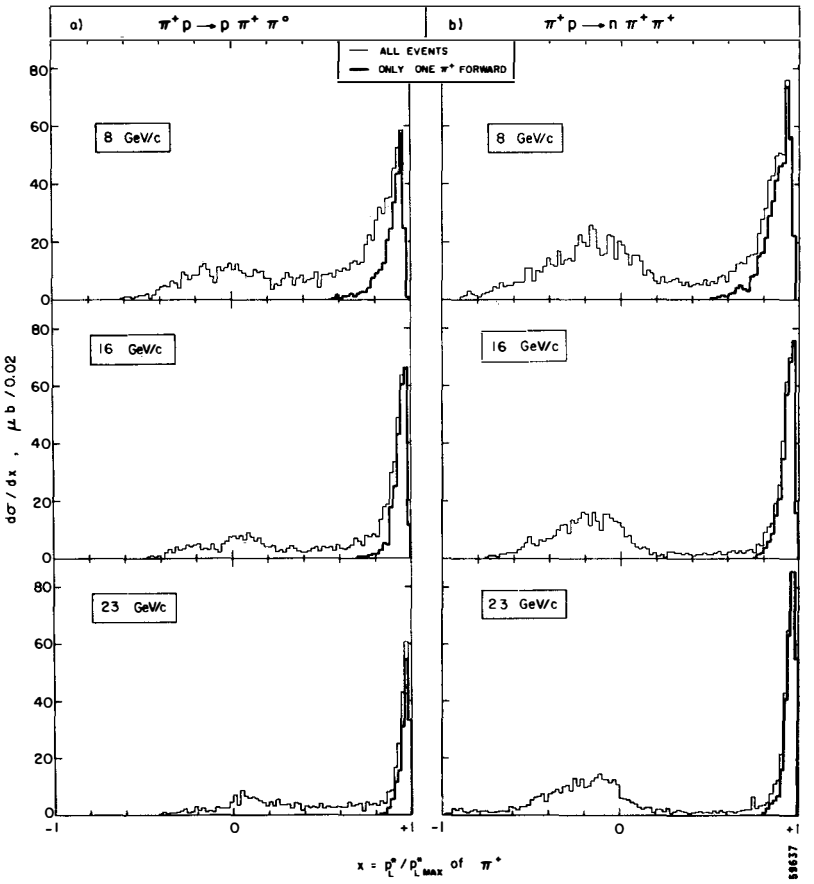

a) $\pi^+ p \rightarrow p\ \pi^+\ \pi^0$
b) $\pi^+ p \rightarrow n\ \pi^+\ \pi^+$
ALL EVENTS
ONLY ONE π^+ FORWARD
8 GeV/c
16 GeV/c
23 GeV/c
$d\sigma / dx$, $\mu b / 0.02$
$x = p_L^* / p_{L\,max}^*$ of π^+
89637

Fig. 10

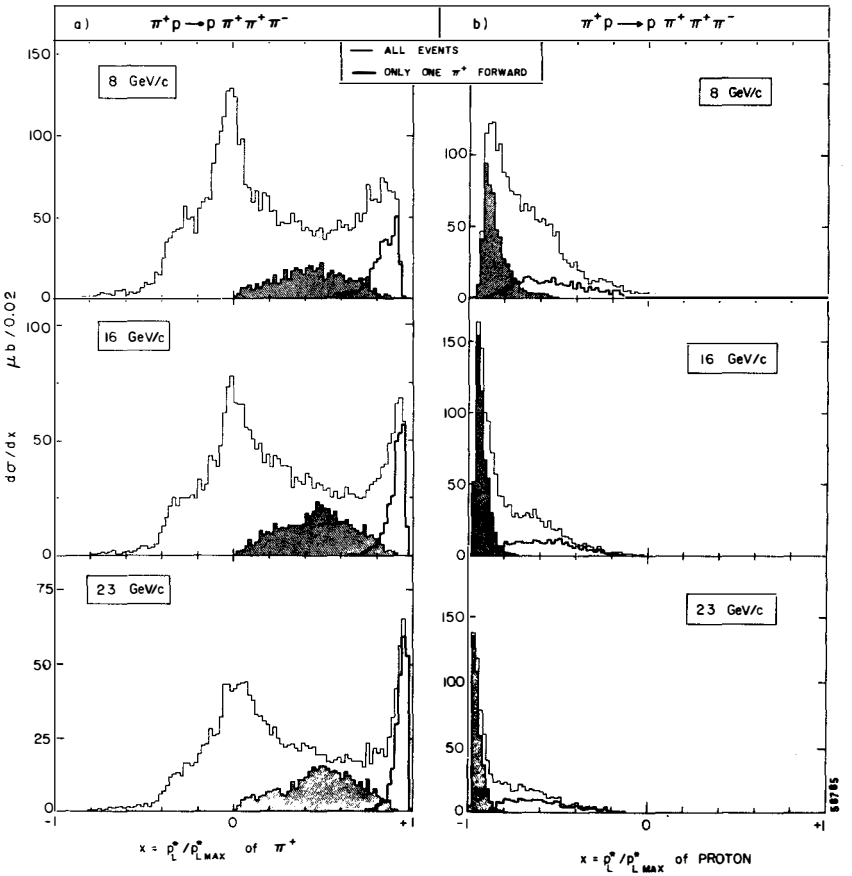

a) $\pi^+ p \rightarrow p\,\pi^+\pi^+\pi^-$
b) $\pi^+ p \rightarrow p\,\pi^+\pi^+\pi^-$
ALL EVENTS
ONLY ONE π^+ FORWARD
8 GeV/c
16 GeV/c
23 GeV/c
$d\sigma/dx$ $\mu b/0.02$
$x = p_L^* / p_{L\,MAX}^*$ of π^+
$x = p_L^* / p_{L\,MAX}^*$ of PROTON
68785

Fig. 11

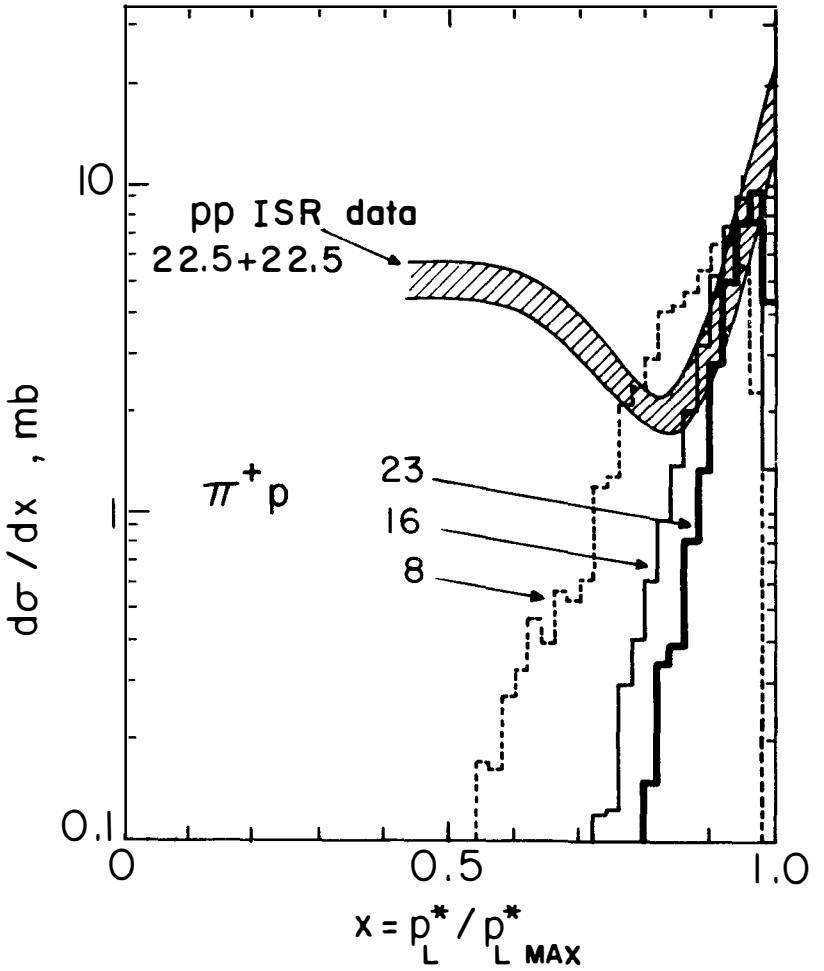
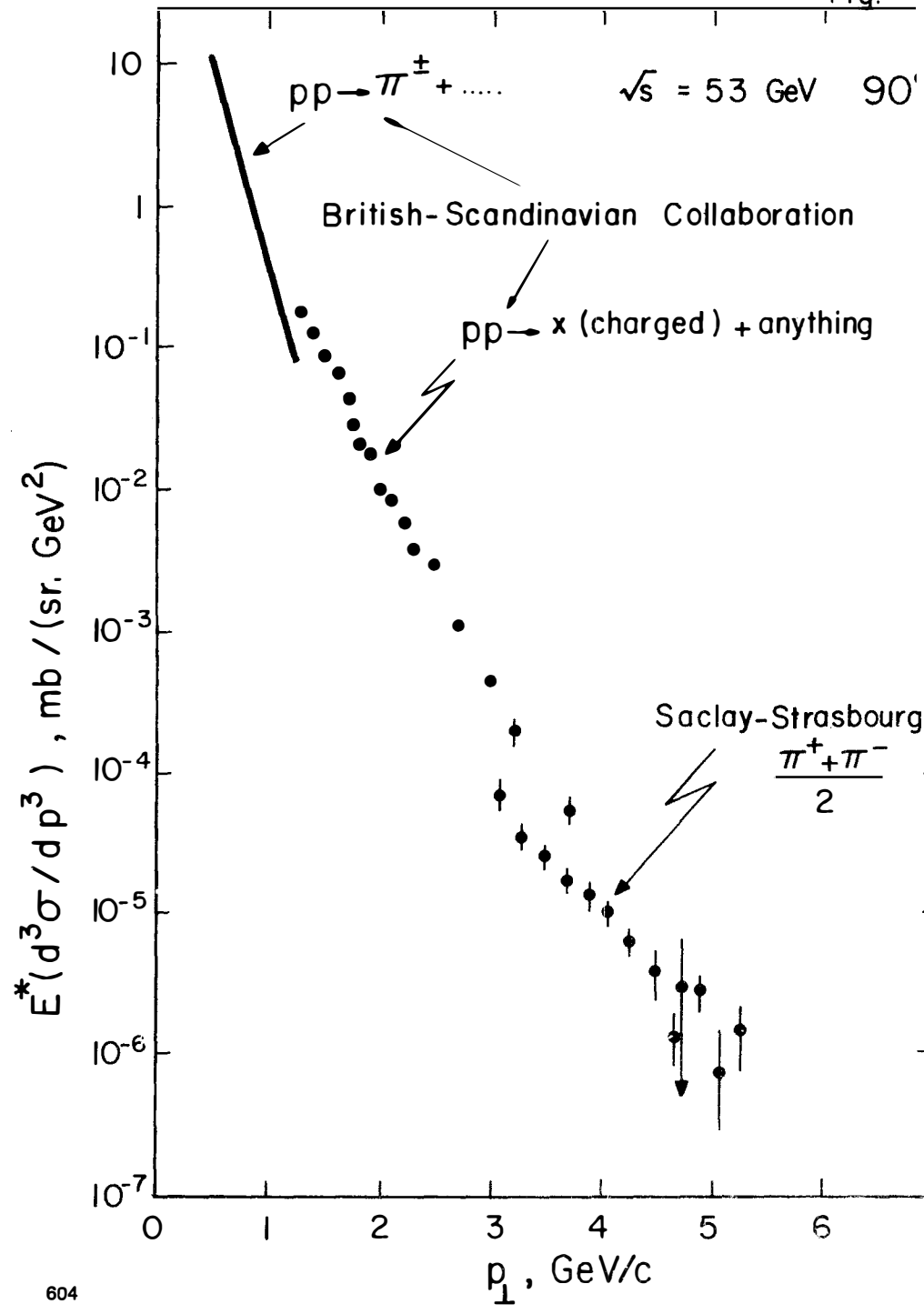
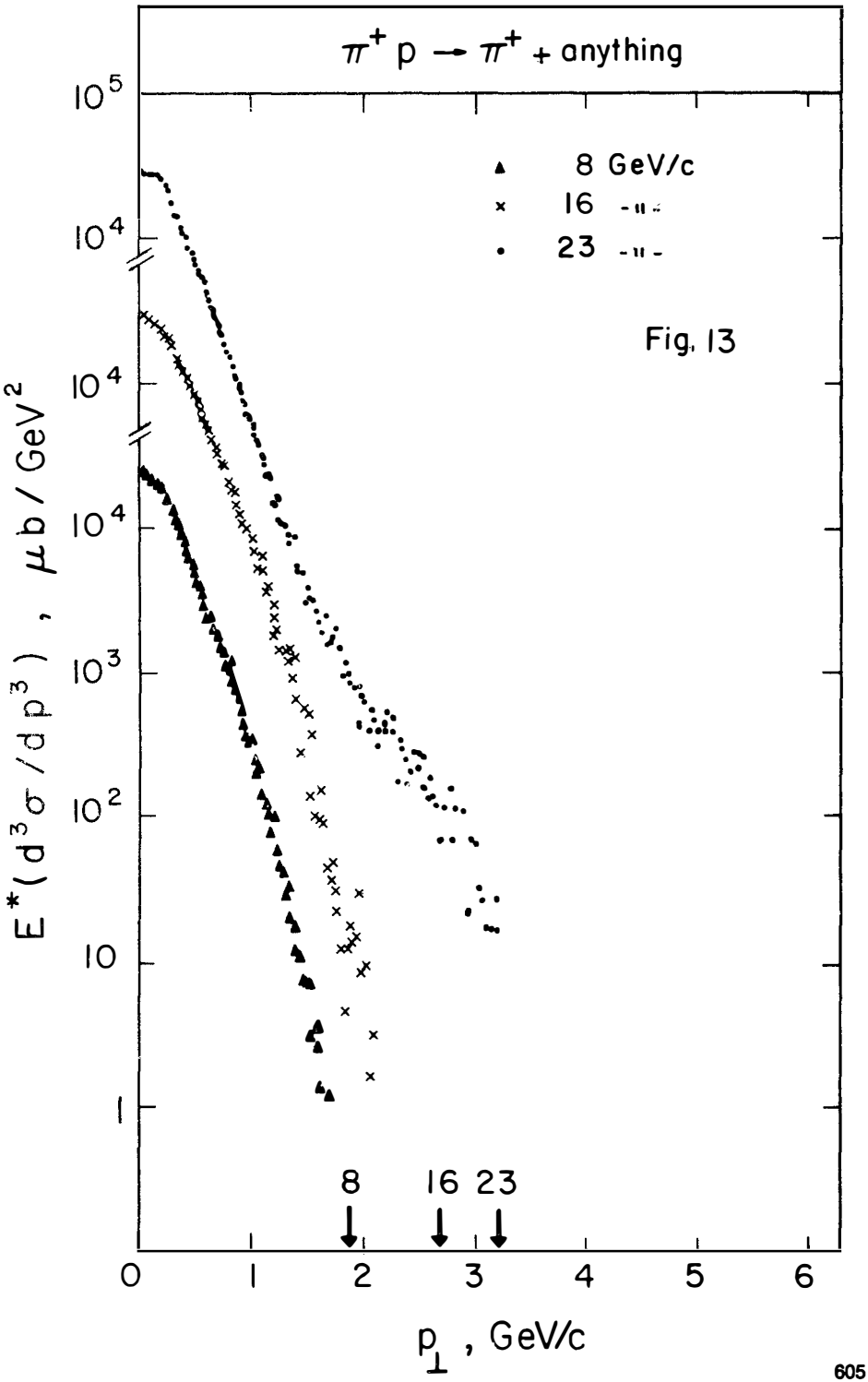

10
1
0.1
0
0.5
1.0
pp ISR data
22.5+22.5
$\pi^+ p$
23
16
8
$d\sigma / dx$, mb
$x = p_L^* / p_{L\ MAX}^*$

Fig. 12


pp → π± + ...
√s = 53 GeV 90°
British-Scandinavian Collaboration
pp → x (charged) + anything
Saclay-Strasbourg
π⁺+π⁻ / 2
E*(d³σ/dp³), mb/(sr. GeV²)
p⊥, GeV/c
10
1
10⁻¹
10⁻²
10⁻³
10⁻⁴
10⁻⁵
10⁻⁶
10⁻⁷
0
1
2
3
4
5
6

604


$\pi^+ p \rightarrow \pi^+ +$ anything
8 GeV/c
16 -"-
23 -"-
Fig. 13
$E^*(d^3\sigma/dp^3)$, $\mu b / GeV^2$
10^5
10^4
10^4
10^4
10^3
10^2
10
1
8
16
23
0
1
2
3
4
5
6
$p_\perp$, GeV/c

CONCLUSIONS FOR THE VIII^{e} MORIOND

ON THE POMERON

David W. G. S. Leith
Stanford Linear Accelerator Center, Stanford University
Stanford, California 94305 (USA)

Introduction:

We have enjoyed an interesting and stimulating week discussing the Pomeron and its properties. Our motivation for studying the Pomeron probably lies somewhere between two extremes --

(1) that the diffractive processes are not very fundamental in themselves, but that they cover up or conceal the remaining two-thirds of the cross section which is accounted for by a great variety of processes which exhibit a great deal of structure, and from which one is going to learn about the dynamics of two body strong interactions, and questions like possible internal structure of the nucleon; that is, one has to understand the one before being able to proceed to the other; or

(2) that diffraction is simply related to geometry, optics and absorption, and also represents the single largest cross section we deal with in particle physics; therefore, we should try to understand it before moving on to the more complex, smaller

cross section processes.

Wherever we derive our motivation, let's see what we have learned of the Pomeron.

Rising Total Cross Sections:

We have heard in some detail from Belletini about the ISR experiments on the p-p total cross section. The cross section is measured to rise about 4 mb through the ISR energy region, of (200-2000) GeV equivalent lab energy.

The experiments rely very heavily on the measurement of the luminosity of the circulating proton beams for the absolute normalisation and there has been much discussion of how reliable such measurements are. However, it seems that in recent months the stability of operation of the ISR has made the luminosity measurements much more reproducible. In addition, the agreement between the Cocconi group and the Belletini group results derived from very different techniques, is good confirmation of the effect. (Let me remind you that the Belletini group has a large--almost 4π-- scintillation counter hodoscope set up to measure multiplicity distributions in p-p scattering; they measure the total cross section by counting the secondaries and make a small correction for the losses due to particles which are emitted towards the beam holes or the cracks between the hodoscope counters: the Cocconi group make precision measurements of the forward elastic p-p scattering cross section with a counter hodoscope system and, using the

optical theorem, relate this to the total cross section. They also justify this use of the optical theorem in determining the total cross section by measuring the real part of the p-p scattering amplitude at several energies and showing that it is small and a negligible effect for the total cross section.)

It is interesting that using the two experiments described above, one could measure the total p-p scattering cross section independent of questions of the luminosity, L. This arises since the Cocconi experiment is sensitive to $\frac{\sigma_T^2}{L}$ (through the optical theorem), and the Belletini experiment measures $\frac{\sigma_T}{L}$, (through measurement of the secondary rate) -- thus the ratio of the two experiments measures the total cross section independent of L, $(\frac{\sigma_T^2}{L} \cdot \frac{L}{\sigma_T} \sim \sigma_T)$. Such an experiment, in which both sets of apparatus will measure σ_T in the same interaction region at the same time, is planned for this summer and should give good total cross section data quite independent of luminosity problems. Some data of this nature already exists, in which the two experiments were run in different interaction regions of the ISR; thus one has to make assumptions that the beam did not change shape between interaction regions. The results show a definite rise in σ_T of the same order as each experiment independently determined (i.e. ~ 4 mb).

This discovery has caused a great deal of interest and raised many questions. The simple Pomeron, as a single pole, is surely dead now -- but no one seems too sad (in fact, Andre Martin seemed positively gleeful at the prospect in his review talk). We have a puzzle about whether the total cross section will continue to

rise as the energy increases or will asymptotically approach a constant value from below. It will also be interesting to see whether the $\pi^{\pm}p$, $K^{-}p$ and γp cross sections will start to rise in the NAL energy region.

The elastic p-p scattering cross section has also been studied at ISR and has been shown to rise by the same amount as the total cross section, through the ISR energy range (i.e. ~ 10-12%). The ratio of elastic to total cross section is constant from ~ 60 GeV/c to 2000 GeV/c with a value of 0.175. A straightforward optical model calculation with a black disc would give this ratio as 0.5.

Differential Cross Sections and Shrinkage:

Another area of considerable interest during this week was the question of shrinkage in p-p scattering. We heard from the ISR experimenters (from Rubbia's group) and from Carrigan on the NAL U.S.-U.S.S.R. experiment. There is some controversy whether the small t region shrinks slowly much as the large t region but with a slope which is ~ 2 units steeper, or that there are two quite separate regions of shrinkage in p-p scattering -- the small t fast shrinking region and the large t slow shrinking region.

I presented the latter point of view in my introductory talk, where the p-p scattering data had been analyzed for all energies above 30 GeV/c and fit well with $\alpha' \sim .36$ GeV^{-2} for $t < 0.1$ GeV^2, and with $\alpha' \sim .1 \pm .1$ GeV^{-2} for $.15 \pm t \pm .5$ GeV^2. However, this

fit requires that the Serpukov data be renormalized in absolute value by $\sim \Delta b = -.4$ GeV^{-2}, (within their quoted systematic errors). Carrigan presented preliminary results of the NAL experiment which showed that the small t region ($t \leq .15$ GeV^2), does shrink with an $\alpha' \sim .4$ GeV^{-2} but that it saturates beyond 200 GeV -- that is, the p-p differential cross section for $t < .15$ GeV^2 shrinks with an $\alpha' \sim .4$ GeV^{-2} up to 200 GeV, beyond which there is little change of slope as the energy increases. This is an interesting result but we will have to wait for confirmation as it is (a) preliminary, (b) the effect is at end of the NAL experiment's range of measurement, and (c) systematic shifts in b completely change the interpretation -- the ISR experiments, NAL, and Serpukov all have problems in setting the absolute scale and these shifts can change the picture from continued shrinkage to the saturation case. This is a very interesting question which will receive a great deal of attention in the next months, especially from the new NAL data.

It has also been interesting to see the large t structure emerging in the p-p elastic scattering experiments at the ISR. The accelerator energy data have long shown a break in the slope of the differential cross section around $t \sim 1.2$ GeV^2; as the energy increases this break becomes a deep hole and a secondary scattering peak appears. The structure is observed to be only weakly dependent on energy and is well fit by optical models. It appears that one can identify the structure as a secondary diffraction peak.

K^+p Interactions:

It has been exciting to see many new and interesting features emerging from p-p interactions at the ISR --

-- σ_T rising with energy

-- small t structure in $d\sigma/dt$

-- shrinkage of $d\sigma/dt$ -- does the shrinkage saturate as σ_T begine to rise?

-- emergence of secondary diffraction peak

-- energy dependence of real part of the scattering amplitude, especially in the region where σ_T rises.

All of these interesting effects are rather difficult to study since they appear near the end of the available energy at the ISR. However, the K^+p system is also exotic in the s-channel and is already displaying the feature of a rising total cross section for energies in the neighborhood of 30 GeV. Through the Serpukov and NAL energy ranges where one has good separated secondary beams of K^+ mesons, the K^+p system should provide an ideal laboratory to study the new dynamical effects giving rise to the above listed phenomena.

Factorization:

We learned that factorization in diffractive processes -- elastic, diffraction dissociation and leading particle inclusive reactions -- is surprisingly good, holding to ~ 20 percent.

It would be interesting to have data on an even wider

variety of processes, and more importantly, with rather better accuracy. At intermediate energies, we know that non-leading effects such as cuts, are quite important and at high energies the observations of rising cross sections have killed any idea of simple single pole dominance of the interactions -- thus, we expect breaking of factorization to occur, maybe even at the 10% level. It would be very interesting to have experiments of sufficient accuracy to observe this breaking, and perhaps even see some s-dependence to the breaking of factorization.

Inelastic Diffraction Processes:

We have seen further evidence during the week that the inelastic (diffraction dissociation) processes have properties very similar to the elastic scattering reactions -- except for their spin structure:

-- the cross sections fall like a power law in momentum, $\sigma \propto p^{-n}$ where $n \sim 0.5$;

-- particle and antiparticle cross sections are approximately equal;

-- the differential cross section is sharply forward peaked, $d\sigma/dt \propto e^{at}$, and has a slope the same order (slightly steeper) as the related elastic slope;

-- the particle and antiparticle differential cross sections exhibit a crossover;

-- the cross sections factorize;

-- spin structure is not SCHC, nor TCHC.

We have not discussed the nature of these processes during this meeting. However, one of the interesting issues in the study of diffractive processes is whether these "diffraction dissociation states" are resonances or are kinematic in origin. I think that there is good evidence that a substantial contribution to these processes comes from kinematic enhancements, but there probably is some resonant production in addition. If this is indeed the situation it will be hard to sort it out experimentally since both contributions feed the same partial waves. One might hope to observe interference effects between the resonance and kinematic amplitudes (analogous to ω-ρ interference experiments), especially if the resonances are not too broad -- but these would be very difficult studies.

Spin Structure:

The spin structure in elastic scattering and vector meson photoproduction has been shown to be s-channel helicity conserving, in the main, but with a small ($\sim$ 15%) helicity flip amplitude. This helicity flip amplitude has natural parity, is isoscalar and displays almost no energy dependence, and is therefore associated with the Pomeron.

Coherent Multiparticle Production in Nuclei:

Yet another interesting feature of diffraction phenomena is the reporting of anomalous absorption of multiparticle states coherently produced in nucleii.

There have been several experiments in heavy liquid bubble chambers observing A_1 production by π's and Q production by K's. An optical model analysis of the data had implied that the A_1 and Q systems were absorbed in the nuclear matter with a cross section of order 20 mb. (i.e. not $3\sigma_\pi$ = 75 mb, nor $\sigma_\pi + \sigma_\rho \approx$ 50 mb, but $\sigma_A \sim \sigma_Q \sim \sigma_\pi$).

These results have been confirmed and greatly extended by an interesting spark chamber experiment at CERN. The coherent production of 3π and 5π final states by pions at 9, 12, and 15 GeV/c, and of $K\pi\pi$ final states by K^+ at 13 GeV/c have been studied with high statistics on a large number of nuclear targets. The absorption of the coherently produced multiparticle system was studied as a function of the size of the nucleus (i.e. how much nuclear matter it had to traverse) and the total cross sections deduced from an optical model analysis: they found

$$\sigma(3\pi) \sim (27 \pm 2) \text{ mb}$$

$$\sigma(5\pi) \sim (15 \pm 5) \text{ mb}$$

$$\sigma(K\pi\pi) \sim (22 \pm 3) \text{ mb}$$

New data on coherent production of $(N\pi\pi)$ final states at high energy and with many nuclear targets should be available shortly from a Rochester-Carnegie Mellon experiment at BNL. This is a very

interesting phenomenon, which is really not understood by the theorists. Hopefully, more progress will be made in understanding this phenomena in the near future.

Very High Energy:

Finally, we come to questions of the high energy behaviour of diffractive processes. It is interesting to ask whether diffraction persists at high energies; does it continue to compete with the other mechanisms, or does it die away, or does it dominate?

It seems that neither of the last two possibilities is true. Diffraction is important at high energy, but it is not the whole story. It accounts for about one-third of the total cross sections. Further it seems to dominate the low multiplicities.

From data on $pp \to px$ near $x = 1$ at the ISR there are now good indications of the cross section scaling in s and $1/M^2$ -- both of which would indicate a substantial triple pomeron contribution to this process -- confirming diffraction dominance at this extreme edge of phase space.

Another interesting question concerns the multiplicity distribution -- if diffraction only contributes to the small multiplicities then as the energy increases the average multiplicity due to other processes (the so-called multiperipheral component) will increase and the overall multiplicity distribution should eventually show the two components separated by a valley. Model dependent analysis of NAL data indicate that such a separation may

be expected at ISR energies.

Preliminary data from Belletini's ISR experiment does not show any sign of separation of the two components. This is not a definitive statement yet -- (a) the analysis of the experimental data is not yet complete, (b) it is not clear how converted electrons and positrons distribute themselves in multiplicity and whether the showers in the vacuum pipe could perhaps mask a valley between low multiplicity and high multiplicity events. We shall have to wait and see.

Final Comment:

One final question, which we should keep in mind when considering diffractive process --

we study diffraction in the following reactions:

-- elastic scattering

-- inelastic scattering - diffraction dissociation,

-- inelastic scattering - single particle inclusive,

Are all these processes really induced by the same t-channel mechanism?

PARTICIPANTS

First Session

ALTARELLI Guido, Istituto di Fisica "Guglielmo Marconi", Univ. di Roma, Piazalle delle Scienze, 5 ROMA (Italy).

ARTRU Xavier, Laboratoire de Physique Théorique et Hautes Energies, Bâtiment 211, Université de Paris-Sud, 91405 - ORSAY (France)

BERNARDINI Carlo, Istituto di Fisica "Guglielmo Marconi", Univ. di Roma, Piazalle delle Scienze, 5 ROMA (Italy)

BRISSON Violette, L.P.N.H.E., Ecole Polytechnique, 17 rue Descartes, 75230 - PARIS CEDEX 05

CARRIGAN Jr. Richard, National Accelerator Laboratory, P.O. Box 500 BATAVIA, IL 60510 (U.S.A.)

CONFORTO Gianni, Rutherford High Energy Laboratory, CHILTON, DIDCOT Berks (England) and I.N.F.N. ROMA (Italy)

CORDIER Alain, Laboratoire de l'Accélérateur Linéaire, Bâtiment 200, Université de Paris-Sud, 91405 - ORSAY (France)

DAR Arnon, M.I.T. Physics 6-406, CAMBRIDGE, MA 02139 (U.S.A.) and Physics Department, Technion Israël Institute of Technology, HAIFA (Israël)

FAYET Pierre, Laboratoire de Physique Théorique et Hautes Energies, Bâtiment 211, Université de Paris-Sud, 91405 - ORSAY (France)

GOURDIN Michel, Laboratoire de Physique Théorique et Particules Elémentaires, Université de Paris-Sud, Bâtiment 211, 91405 - ORSAY (France) and Laboratoire de Physique Théorique et Hautes Energies, Tour 16, 1er étage, Université de Paris VI, 4 place Jussieu, 75230 PARIS CEDEX 05 (France)

GRELAUD Brigitte, Laboratoire de l'Accélérateur Linéaire, Bâtiment 200, Université de Paris-Sud, 91405 - ORSAY (France)

GROSDIDIER Gilbert, Laboratoire de l'Accélérateur Linéaire, Bâtiment 200, Université de Paris-Sud, 91405 - ORSAY (France)

HAGUENAUER Maurice, L.P.N.H.E., Ecole Polytechnique, 17 rue Descartes, 75230 - PARIS CEDEX 05 (France)

HAIDT Dieter, Division TCL, C.E.R.N., 1211-GENEVE 23 (Suisse)

HENYEY Frank S., Randall Laboratory of Physics, University of Michigan, ANN ARBOR, MI 48104 (U.S.A.)

IENGO Roberto, Laboratoire de Physique Théorique et Hautes Energies, Bâtiment 211, Université de Paris-Sud, 91405 - ORSAY (France) and Istituto di Fisica, Univ. di TRIESTE (Italy)

ILIOPOULOS Jean, Laboratoire de Physique Théorique et Hautes Energies, Bâtiment 211, 91405 - ORSAY (France)

JEAN-MARIE Bernard, Laboratoire de l'Accélérateur Linéaire, Bâtiment 200, Université de Paris-Sud, 91405 - ORSAY (France)

KLUBERG-STERN Hannah, D. Ph. T., CEN-SACLAY, B.P. 2, 91190 - GIF-sur-YVETTE (France)

KRISCH Alan D., Randall Laboratory of Physics, University of Michigan, ANN ARBOR, MI 48104 (U.S.A.)

KUTI Julius, Department of Atomic Physics, Roland Eötvös University, Puskin utca 5-7, BUDAPEST VIII (Hungary)

LALANNE Dominique, Laboratoire de l'Accélérateur Linéaire, Bâtiment 200, Université de Paris-Sud, 91405 - ORSAY (France)

LAUTRUP Benni, Institut des Hautes Etudes Scientifiques, 91440 - BURES-sur-YVETTE (France)

LAYSSAC Jacques, Laboratoire de Physique Mathématique, Université des Sciences et Techniques du Languedoc, 34060 - MONTPELLIER CEDEX

LUTZ Anne-Marie, Laboratoire de l'Accélérateur Linéaire, Bâtiment 200, Université de Paris-Sud, 91405 - ORSAY (France)

LUTZ Pierre, Collège de France, Place Marcelin Berthelot, 75231 - PARIS CEDEX 05 (France)

MADARAS Ronald, Laboratoire de l'Accélérateur Linéaire, Bâtiment 200, Université de Paris-Sud, 91405 - ORSAY (France)

MASNOU Jean-Louis, Laboratoire de l'Accélérateur Linéaire, Bâtiment 200, Université de Paris-Sud, 91405 - ORSAY (France)

MEYER Henrich, DESY, Notkestieg 1, 2000 HAMBURG-52 (West Germany)

MEYER Philippe, Laboratoire de Physique Théorique et Hautes Energies, Bâtiment 211, Université de Paris-Sud, 91405 - ORSAY (France)

MIHUL Alexandru Mihai, J.I.N.R. (DUBNA) Head P.O. Box 79, Moscow, (U.R.S.S.)

MIHUL Mme, J.I.N.R. (DUBNA) Head P.O. Box 79, Moscow (U.R.S.S.)

MINE Philippe, L.P.N.H.E., Ecole Polytechnique, 17 rue Descartes, 75230 - PARIS CEDEX 05 (France)

MONTANET Lucien, Division TC, C.E.R.N., 1211 GENEVE 23 (Suisse)

NUYTS Jean, Université de Mons, Département de Physique Théorique, 19 avenue Maistriau, 7000 MONS (Belgique)

PEREZ-Y-JORBA Jean, Laboratoire de l'Accélérateur Linéaire, Bâtiment 200, Université de Paris-Sud, 91405 - ORSAY (France)

PETIAU Pierre, Ecole Polytechnique, Laboratoire de Physique Nucléaire des Hautes Energies, 17 rue Descartes, 75230 - PARIS CEDEX 05 (France)

PRENTICE Jim D., Phys. Dep., University of Toronto, TORONTO M55,1A7 Ontario (Canada)

PULLIA Antonio, Division TCL, C.E.R.N., 1211 GENEVE 23 (Suisse)

QUENZER Alain, Laboratoire de l'Accélérateur Linéaire, Bâtiment 200, Université de Paris-Sud, 91405 - ORSAY (France)

RENARD Fernand-Michel, Laboratoire de Physique Mathématique, Université des Sciences et Techniques du Languedoc, 34060-MONTPELLIER CEDEX

ROSNER John L., Division TH, C.E.R.N., 1211 GENEVE 23 (Suisse) and University of Minnesota, MINNEAPOLIS, MN 55455 (U.S.A.)

SCHILDKNECHT Dieter, DESY, Notkestieg 1, 2000 HAMBURG-52 (West Germany)

SCHILLING Klaus, Arbeitsstelle für Physik der Universität, D-48 - BIELEFELD, Herforder Str. 28 (Germany)

SILVESTRINI G. Vittorio, Laboratori Nazionali di Frascati, Casella Postale 70, 00044-FRASCATI (Italy)

SNOW George A., Laboratoire de Physique Théorique et Hautes Energies, Université de Paris VI, 4 place Jussieu, 75230 - PARIS CEDEX 05 (France) and University of Maryland, College Park, MD 20742 (U.S.A.)

SOURLAS Nicolas, Laboratoire de Physique Théorique et Hautes Energies, Bâtiment 211, Université de Paris-Sud, 91405 - ORSAY (France)

SONDEREREGGER Peter, Division NP, CERN, 1211 GENEVE 23 (Suisse)

STEINBERGER Jack, Division NP, CERN, 1211 GENEVE 23 (Suisse)

STERN Jan, Institut de Physique Nucléaire, Bâtiment 100, Université de Paris-Sud, 91405 - ORSAY (France)

SZKLARZ Geszon, Laboratoire de l'Accélérateur Linéaire, Bâtiment 200, Université de Paris-Sud, 91405 - ORSAY (France)

TESTA Massimo, Theoretical Study Division, CERN, 1211 GENEVE 23 (Suisse)

TRAN THANH VAN Jean, Laboratoire de Physique Théorique et Particules Elémentaires, Bâtiment 211, Université de Paris-Sud, 91405 - ORSAY (France)

VANDERHAGEN Regis, Ecole Polytechnique, 17 rue Descartes, 75230 - PARIS CEDEX 05 and Division NP, CERN, 1211 GENEVE 23 (Suisse)

VAN NIEUWENHUIZEN Peter, Laboratoire de Physique Théorique et Hautes Energies, Bâtiment 211, Université de Paris-Sud, 91405 - ORSAY (France)

VIVARGENT Marcel, Institut de Physique Nucléaire, Bâtiment 100, Université de Paris-Sud, 91405 - ORSAY (France)

WALKER James K., National Accelerator Laboratory, P.O. Box 500, BATAVIA, IL 60510 (U.S.A.)